Proceedings of CJJC2023

The 12th China-Japan Joint Conference on Material Recycling and Waste Management

Nov, 28-30 2023, Beppu, Oita, Japan

Organized by

Kyushu University

University of Science and technology Beijing

九州大学
KYUSHU UNIVERSITY

北京科技大学
University of Science and Technology Beijing

CONTENTS

Poster session p157-p228

Other papers p229-p270

MEASUREMENT OF AREAL TEMPERATURE DISTRIBUTION INSIDE CAPPING LAYER OF SOLID WASTE LANDFILL USING OPTICAL FIBER SENSOR

Rion Hamada[1], Takayuki Shimaoka[2], Teppei Komiya[2]
1 Graduate school of Engineering, Kyushu University, 744 Motooka, Nishi-ku, Fukuoka, JAPAN
2 Faculty of Engineering, Kyushu University, 744 Motooka, Nishi-ku, Fukuoka, JAPAN

1 INTRODUCTION

In order to close municipal solid waste final disposal sites and industrial solid waste management-type final disposal sites, it is necessary to meet the 11 criteria for closure[1)]. One of these criteria is that 'the interior of the landfill site is not abnormally hot compared to the surrounding temperature.' The current method for monitoring the temperature inside the landfill site involves measuring temperatures at limited points within the site. However, in large areas with vast landfill capacity, and in landfill sites where the solid waste is heterogeneous, it is not easy to appropriately select representative points. Therefore, there is a desire to comprehensively and three-dimensionally understand the temperature distribution within the landfill site.

Optical fiber sensors utilize the reflection and scattering of light, allowing for the measurement of physical quantities such as temperature[2)]. In recent years, this technology has also been utilized as a monitoring tool. It is believed that this technology can be used to understand the temperature distribution at the boundary between the landfill site and the surrounding environment. Additionally, it is expected that by performing inverse analysis based on the temperature distribution on the bottom and slopes of the landfill site, a three-dimensional temperature distribution within the landfill site can be estimated. The aim of this study was to investigate the potential of using optical fiber sensors to assess the temperature distribution at the boundary between the solid waste landfill site and the surrounding environment, and actual temperature distribution measurements were conducted within the capping layer of a real solid waste landfill site.

2 EXPERIMENTAL METHOD

2.1 Optical fiber and measurement equipment

A multi-mode optical fiber cable coated with resin (M-PAC(14/18)1GI-R(5.0HDPE) is used. The image is indicated as Figure 1. The optical fiber was connected to a Raman scattering light measurement instrument (OPTHERMO FTS3500, measurement interval 25 cm, spatial resolution 150 cm, number of accumulations 2^{22}),

Fig.1 The used optical fiber cable (M-PAC(14/18)1GI-R(5.0HDPE)

Fig.2 The used optical fiber measuring instrument (OPTHERMO FTS3500)

and an optical fiber sensor capable of measuring temperature distribution along the entire length of the optical fiber was constructed. The measurement interval refers to the spacing between temperature measurement points, and spatial resolution refers to the length over which measurements are taken with the temperature measurement point at the center. The temperature at the measurement point becomes the average temperature over the measured length. The image is indicated as Figure 2. The temperature measurement accuracy is stated as within ±1 °C in the product introduction[3)], but the temperature measurement accuracy confirmed through actual measurements in this study was ±0.4 °C.

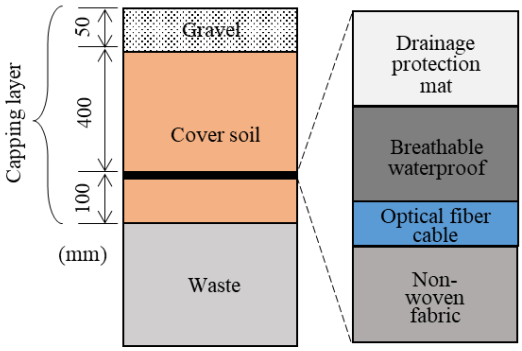

Fig.3 The structure of the capping layer

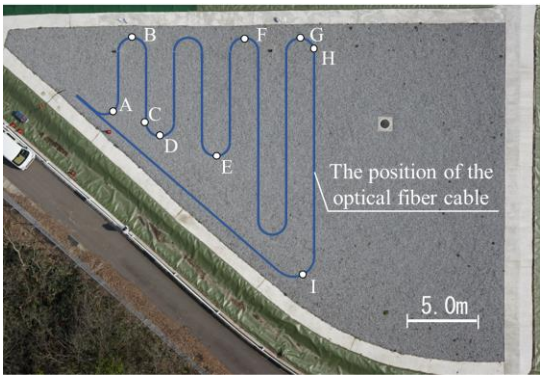

Fig.4 The position of the optical fiber cable

2.2 Solid Waste landfill

Experiments were conducted in the completed disposal section of the O Landfill in Shimane Prefecture. When applying the final cover soil, a capping is constructed for the purpose of covering the surface of the solid waste with a waterproof material to suppress rainwater infiltration into the solid waste layer and to control the release of landfill gas into the atmosphere. In this study, optical fiber cables were installed within the capping layer situated at the interface between solid waste and the natural environment, and measurements were conducted. The structure of the capping layer is shown in Figure 3. Optical fiber cables were routed on the upper surface of the non-woven fabric and secured with bundling bands. The positions of the optical fiber cable routing are shown in Figure 4. The routing starts from the upper left part of the landfill site and proceeds in a single stroke, with vertical routing spaced at 2.0 meters intervals. The total length of the optical fiber cables routed inside the capping layer was 115.6 meters. Points A to I were designated as representative points as shown in Figure 4.

2.3 Measurement conditions

On March 28, 2023, from 12:00 PM to 12:00 PM on March 29, temperature measurements were performed at 15-minute intervals using optical fiber sensors.

The measured values from the optical fiber sensors were calibrated using temperature measurements obtained from thermocouples adjacent to the optical fiber cables inside the capping layer.

3 RESULTS AND DISCUSSION

3.1 Estimation of two-dimensional temperature distribution within the capping layer

The temperature measurement results within the capping layer on March 28th at 2:00 PM using the optical fiber sensor are shown in Figure 5. Figure 5 depicts the cable length from the point where the optical fiber enters the ground (referred to as the position coordinate) on the horizontal axis, and the measured temperature on the vertical axis. Differences in temperature were observed based on the position coordinates, revealing a maximum temperature difference of 1.7°C. A two-dimensional temperature distribution was created using contour plotting software from the measurement data. Figure 6 illustrates the two-dimensional temperature distribution at 2:00 PM on the 28th, 11:00 PM on the 28th, and 8:00 AM on the 29th. At all times, there was a tendency for higher temperatures in the upper right section, while lower temperatures were observed in the left section. The variation in temperature within the capping layer is likely attributed to the fact that the landfill solid waste layer has a spatially varying temperature distribution. Additionally, differences in the thickness of the gravel and cover layers above the optical fiber cables at different locations may reflect variations in the impact of ambient temperature and surface temperature.

3.2 Temporal Changes in Temperature within the Capping Layer

Figure 7 presents the 24-hour temperature measurement results within the capping layer using the optical fiber sensor at points A to C. The temperature recorded by the optical fiber sensor shows an increase starting around 5:00 PM, followed by a decrease from around 7:00 AM the next morning. It was observed that temperatures tended to be higher at night compared to during the day. This indicates that the optical fiber sensor successfully captured the temperature variations within the capping layer over the course of 24 hours.

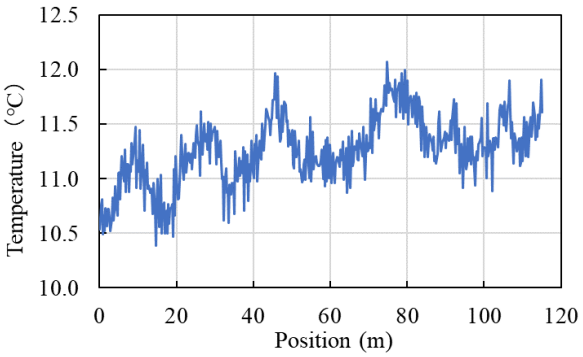

Fig.5 Example of temperature measurement results using an optical fiber sensor

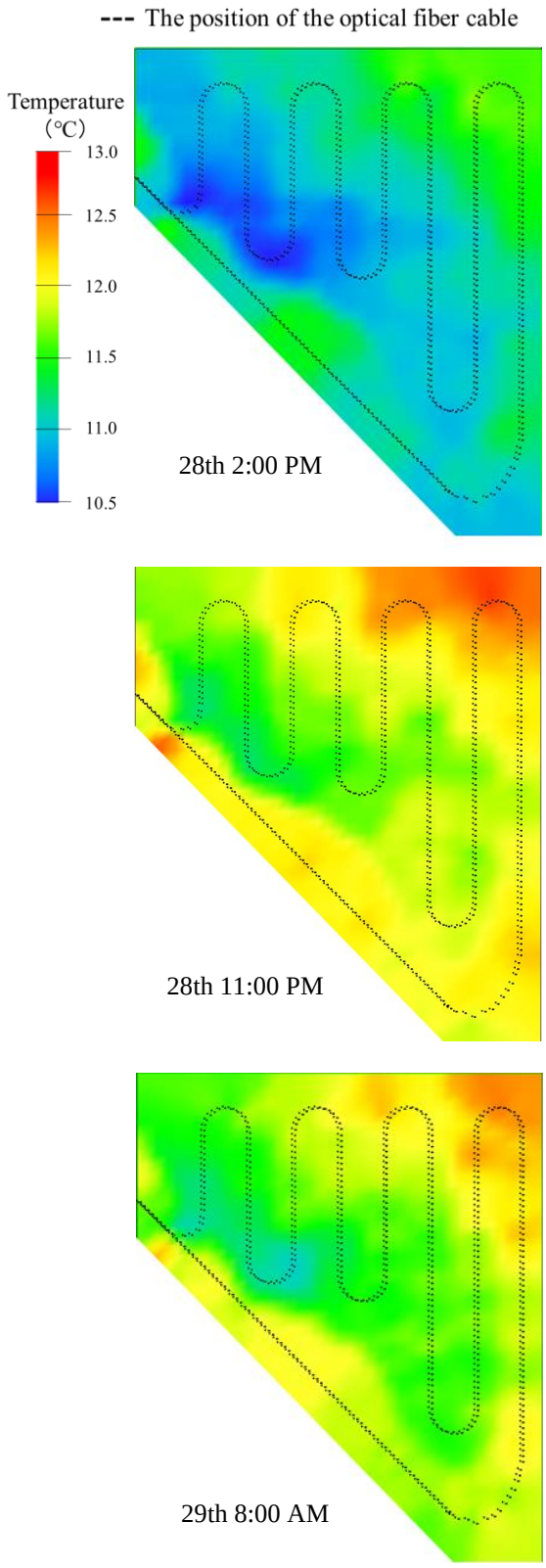

Fig.6 Two-dimensional temperature distribution within the capping layer

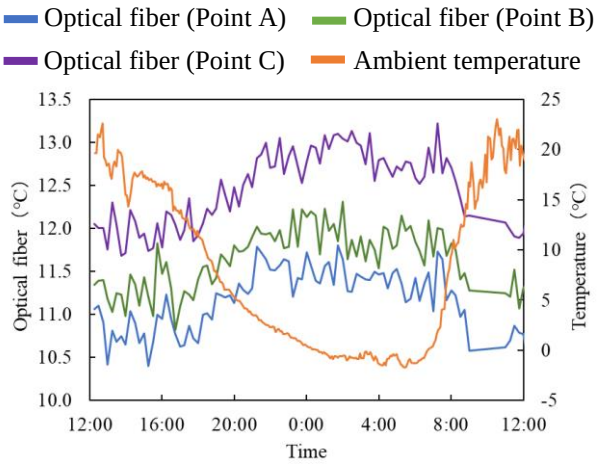

Fig.7 24-hour temperature measurement results within the capping layer

Next, to investigate the relationship between the temperature measurements by the optical fiber sensor and the ambient temperature, the correlation coefficient between the two was calculated by shifting the time of the temperature data. Table 1 shows the time shift and the corresponding correlation coefficient at which the maximum correlation was achieved. When the temperature data was shifted by 11 hours and 45 minutes to 12 hours and 40 minutes, the measurement data from the optical fiber sensor at points A to I exhibited a high positive correlation with the temperature data. It is inferred that the temperature at the depth where the optical fiber was installed varied approximately 11 hours and 45 minutes to 12 hours and 40 minutes after the temperature fluctuation.

Furthermore, the time lag between the temperature data obtained from the optical fiber sensor within the capping layer and the ambient temperature data was examined. In Figure 8, the measured temperature within the capping layer by the optical fiber sensor is presented with the 24-hour average value on the vertical axis and the time lag from the temperature variation in the ambient temperature on the horizontal axis. Assuming that the reason for the temperature difference within the capping layer was due to differences in the thickness of the gravel and cover layers at different locations, it can be expected that the greater the depth, the larger the time lag. Nevertheless, the 24-hour average temperature is expected to be nearly equal regardless of depth. However, in Figure 6, although there are differences in the time lag depending on the location, the 24-hour average temperatures ranged from 11.1°C to 12.5°C, varying by location. Based on these findings, it is considered that the primary factor causing the temperature difference within the capping layer was the difference in temperature within the landfill solid waste layer.

Table.1 The time lag of the capping layer temperature from the ambient temperature

	Point A	Point B	Point C	Point D	Point E	Point F	Point G	Point H	Point I
Time delay	+11h 45min	+12h	+12h 20min	+12h 10min	+12h	+11h 45min	+12h 40min	+12h 35min	+11h 45min
Correlation coefficient	0.820	0.836	0.809	0.788	0.794	0.836	0.865	0.863	0.748

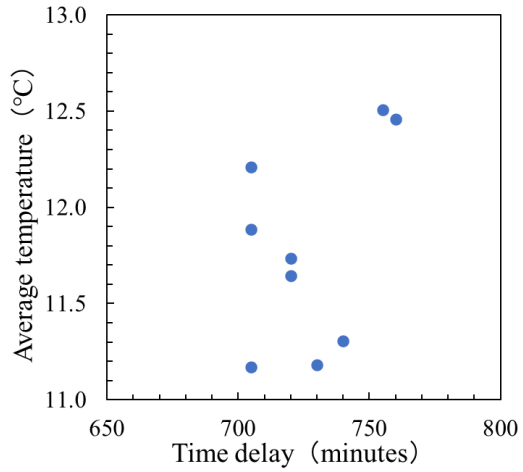

Fig.8 The relationship between the 24-hour average temperature within the capping layer and the time lag from the temperature variation in ambient temperature

4 CONCLUSIONS

The insights obtained in this study are summarized as follows.

1) The optical fiber sensors distributed on the surface of the capping layer revealed a temperature difference of up to 1.7°C within the capping layer.
2) It was confirmed that the temperature variation within the capping layer at a depth of 45 cm from the surface exhibits a time delay of approximately 11 hours and 45 minutes to 12 hours and 40 minutes relative to the ambient temperature.
3) The primary factor contributing to the temperature difference within the capping layer was believed to be the variation in temperature within the landfill solid waste layer.

As future tasks, further investigation into the factors contributing to the temperature distribution within the capping layer is warranted. Additionally, it is important to consider the installation method of optical fiber cables and determine appropriate spacing when implementing them in landfills. Furthermore, it is necessary to explore methods for estimating the three-dimensional temperature distribution within the landfill based on the temperature distribution at the boundary of the landfill obtained from measurements using the optical fiber sensor.

REFERENCES

1) Ministry of the Environment：Overview of criteria for the closure of final disposal sites, https://www.env.go.jp/recycle/kosei_press/h980616/h980616a-3.html (Date of viewing: June 14, 2023)
2) Non-Profit Organization for the Promotion of Optical Fiber Sensing: Introduction to Optical Fiber Sensors, p288, 2012
3) Sumitomo Electric Industries Ltd: Optical Fiber Temperature Distribution Measurement Device OPTHERMO, https://www.japantappi.org/wp-content/uploads/2022/11/SKC_catalog1.pdf (Date of viewing: June 14, 2023)

LOCALIZED INTENSIFICATION OF ARSENIC METHYLATION WITHIN LANDFILL LEACHATE-SATURATED ZONE

Lifang Hu[1], Yating Qian[1], Manting Ci[2], Yuyang Long[2], Ke Xu[1] and Yuqian Wang[1]
1 College of Quality and Safety Engineering, Institution of Industrial Carbon Metrology, China Jiliang University, Hangzhou 310018, China
2 Zhejiang Provincial Key Laboratory of Solid Waste Treatment and Recycling, School of Environmental Science and Engineering, Instrumental Analysis Center, Zhejiang Gongshang University, Hangzhou, 310012, China

ABSTRACT
Leachate-saturated zone (LSZ) of landfills is a complicated biogeochemical hotspot due to the continuous input of electron donors and acceptors from the top refuse layer with leachate migration. In this study, the methylation behavior of the arsenic (As) was investigated. The results indicate that As-methylation processes are influenced by temperature fields in LSZ. The dimethylarsinic acid biotransformation capability can be enhanced with an increase in temperature. Microbial diversity, quantification of functional gene (*arsM*), and co-occurrence network analysis further characterized the drivers of As methylation in LSZ. As-biogeochemical cycle pathways, as well as As-functional gene distribution among different temperature fields, were modeled on the basis of KEGG annotation. Binning analysis was further employed to assemble As-methylated metagenomes, enabling the identification of novel species for As methylation in landfills. Then, 87 high-quality draft metagenome-assembled genomes (MAGs) were reconstructed from LSZ refuse samples; nearly 15% (13 of 87) belonged to putative As-methylates functional MAGs. Combined with the model of the As-biogeochemical cycle, nine putative functional species could complete methylation processes alone. The findings of this study highlighted the temperature influence on the As-methylation behavior in LSZ and could facilitate the management of As contamination in landfills.
Keywords: Landfill leachate saturated zone; arsenic; methylation; temperature fields; draft metagenome-assebled genomes (MAGs).

1. INTRODUCTION
Landfills have been considered nonnegligible anthropogenic sources of arsenic (As). The As content of landfill leachate and refuse could reach 578 μg L^{-1} (Hu et al. 2019) and 38.4 mg kg^{-1}, respectively. These values are higher than the WHO's limit of 10 μg L^{-1} for potable water (WHO 2017) and the average As content in the earth's crust of 1.8 mg kg^{-1}(Mench et al. 2009). In landfills, the highest content of As fraction is inorganic arsenate [iAs(V)], followed by inorganic arsenite [iAs(III)], and various organoarsenicals such as monomethylarsonic acid (MMA) and dimethylarsinic acid (DMA). MMA and DMA are the main products of the As-methylation process (Hu et al. 2021, Hu et al. 2022).

Microbes have evolved multiple mechanisms for cellular defense against high As levels. As-related genes are taxonomically widespread and even subject to frequent horizontal gene transfer (Cai et al. 2009, Chen et al. 2017, Palmgren et al. 2017). In a previous study (Hu et al. 2021), we quantified some As biotransform functional genes, i.e., As(III) oxidase gene (*aioA*), As(V) reductase gene (*arrA* and *arrC*), and As-methylating genes (*arsM*). These functional gene distributions varied with changes in microbial diversity as the landfill process progressed, elucidating microbial feedback on As biotransformation in landfills. However, the As biotransformation pathway is still unknown in landfills.

As the landfill process progressed, as the predominant As species, As(V) tends to be reduced to a more mobile and toxic As(III) fraction under long-term anaerobic conditions (Hu et al. 2021, Hu et al. 2019, Hu et al. 2022). Then, As(III) can be methylated stepwise to MMA, DMA, and TMA by ArsM using S-adenosylmethionine (SAM) as the methyl donor (Ajees et al. 2012, Qin et al. 2006), and the volatile TMA(III) could be considered the final species of microbial methylation pathways (Huang et al. 2016, Qin et al. 2006, Zhang et al. 2015). The mechanism of As methylation is well-known, both at the biochemical and molecular levels. However, As biotransformation can be influenced by environmental factors, such as the As concentration and species, moisture content, redox potential, and temperature (Hu et al. 2019, Mestrot et al. 2009, Turpeinen et al. 2002, Vriens et al. 2014). As a huge complex human-made heterogeneous facility, the internal temperature gradually increases with depth (even up to 80°C) due to the biodegradation discrepancy (Hao et al. 2017). Meanwhile, the water

(leachate) content varies with depth. Frequently, landfill refuses at the bottom layer are always submerged by leachate to form a leachate-saturated zone (LSZ), a special landfill zone. A LSZ becomes a complicated biogeochemical hotspot due to the continuous input of electron donors and acceptors from the top refuse layer with leachate migration. Obviously, an LSZ with temperature fields will inevitably induce the discrepancy of microbial degradation.

To the best of our knowledge, the study of As-methylation processes in the LSZ has not been conducted. Therefore, in this study, the response of temperature fields in As methylation is proposed in an LSZ. The LSZ under typical temperature fields in landfills were simulated to (1) investigate As-methylation behavior and methylated As distribution, (2) profile the microbial community structure for As methylation, (3) analyze As-related genes and identify As biotransformation pathways, and (4) assemble putative As-methylated genomes. This study provides scientific proof for explaining the As migration and transformation mechanism in landfills.

2. METHODS

2.1. Municipal solid waste and leachate samples

Refuse samples were collected from simulated municipal solid waste bioreactor landfills in our laboratory, which had been stabilizing for 7 years. Before the mineralized refuse samples were crushed into pieces less than 1 cm, inert materials, such as stones, metal materials, glass, and plastics, were removed. Leachate samples were obtained from an equalizing reservoir of Hangzhou Tianziling landfill, Zhejiang Province, eastern China. The physicochemical properties of the refuse and leachate samples were determined as described previously (Hu et al. 2021), results were listed in **Table 1**.

Table 1 Physicochemical properties of refuse and leachate samples

Sample	Mineralized refuse (mg kg^{-1} dry weight)	Leachate (mg L^{-1})
Moisture content	71.9% ± 9.39%	/
pH	7.97	7.89
COD	/	2083.3
DOC	3691	4391.5
SO_4^{2-}	1610.7	477
Total As	16.62±1.57	0.028
As(III)	0.80	0.003
As(V)	14.89±2.09	0.016
MMA	NA	1.34×10^{-3}
DMA	NA	1.45×10^{-3}

2.2 Simulated landfill bioreactor experiments and diffusive gradient in thin-film deployment

2.2.1 Simulated landfill bioreactor preparation:

Tests were performed in four batch Plexiglas reactors (40 cm high by 24 cm outer diameter) under anaerobic conditions, where the solid–liquid ratio of refuse and leachate samples was set to 1:3 to simulate the landfill LSZ (**Fig. 1**). To maintain different temperature fields of the LSZ, hot water was recirculated around the reactor interlayer through a pump and PVC pipes, and the temperature gradient was set to 55℃, 45℃, 35℃, and 25℃ (room temperature). The reactors were continuously and synchronously operated in the dark.

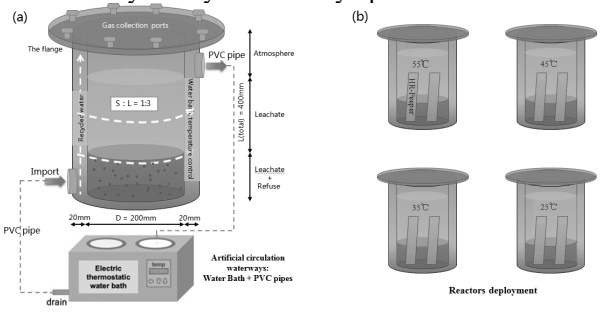

Fig. 1 Schematic diagram of bioreactors for LSZ with a temperature control system.

2.2.2 Preparation of diffusive gradient in thin-film sampler:

To obtain a dynamic mapping of As methylation over the LSZ in landfills, a passive sampling technique of diffusive gradient in thin-film (DGT) was employed. DGT provided a depletion zone to the adjoining membrane surface to achieve in situ measuring in the LSZ, including leachate and refuse released from the waste solid phase. An HR-Peeper pore-water sampler (EasySensor Ltd., www.easysensor.net) could realize vertical mapping at the LSZ, whose main structure was a plate with 30 sampling grooves (about 400-μL volume per groove), prefilled with water and sealed by a membrane (**Fig. 2**) (Ding et al. 2018, Pan et al. 2019, Sun et al. 2019).

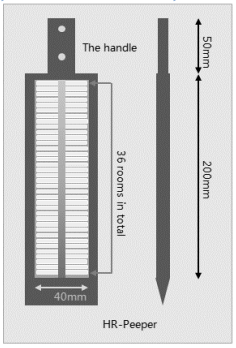

Fig. 2 Schematic diagram of HR-Peeper pore sampler.

2.2.3 Diffusive gradient in thin-film deployment:

To obtain dynamic profiles of MMA and DMA in the liquid–solid interface of the LSZ, the HR-Peeper sampler was vertically inserted into leachate-saturated refuses on days 3 and 21. After balancing for 24 h, the sampler was removed from the bioreactor, and its surface was rinsed thoroughly with ultrapure water. The member was carefully removed from the sampler, and the solution from each sampling groove was collected, which also realized stratified sampling in the vertical depth. Consequently, the concentration of MMA and DMA was analyzed by a high performance liquid chromatography - inductively coupled plasma mass spectrometry (HPLC-ICP-MS, NexION 300X, PerkinElmer, Inc., USA) with a PRP-X100 anion exchange column (Hamilton PRPX-100, 250 mm diameter, United Kingdom). The mobile phase was containing 20mM $NH_4H_2PO_4$ (pH 6.5) and the detection procedure was described as previously (Ding et al. 2016, Hu et al. 2019).

2.3 DNA extraction, 16S rRNA gene sequence, and *arsM* gene quantification

Total DNA was extracted from 0.5 g of each refuse sample (after 3- and 21-day incubation) using a FastDNA Spin kit (MP Biomedicals, Irvine, CA, USA) according to the manufacturer's protocol. The DNA concentration and purification were determined by NanoDrop 2000 UV-vis spectrophotometer (Thermo Scientific, Wilmington, USA), and DNA quality was checked by 1% agarose gel electrophoresis. Then, the DNA was applied as the template for polymerase chain reaction (PCR) to amplify the V4 hypervariable regions of the 16S rRNA gene using two universal primer pairs: 515F (5′ -GTGYCAGCMGCCGCGGTAA-3′) and 806R (5 ′ -GGACTACHVGGGTWTCTAAT-3 ′) (Walters et al. 2016). The thermal cycling conditions for the PCR have been previously described (Hu et al. 2022). The 16S rRNA gene for each sample was sequenced on the Illumina Miseqplat form (Illumina Inc., San Diego, CA, USA) at Majorbio (Shanghai, China). Sequences from 16S rRNA gene amplicon libraries were analyzed with QIIME 1.9.1. A total of 1,862,755 high-quality sequences were obtained, with an average depth of 476,932,364 bp for tested samples. All raw 16S rRNA amplicon sequence data in this study have been submitted to Sequence Read Archive (SRA) database of National Center for Biotechnology Information (NCBI) under accession numbers were SRP 334001.

The abundance of bacterial and archaeal 16S rRNA gene, as well as *arsM* gene, was quantified via quantitative real-time PCR (ABI7500, Applied Biosystems, USA). PCR amplification of 16S rRNA and *arsM* genes were applied the primers as previously reported (Hu et al. 2021, Jia et al. 2013, Suzuki et al. 2000). All analyses were performed in triplicate.

2.4 Metagenome sequence, assembly, gene prediction, and annotations

DNA extract from each refuse sample was fragmented to an average size of about 400 bp using Covaris M220 (Gene Company Limited, China) for paired-end library construction. Paired-end sequencing was performed on an Illumina Hiseq Xten platform (Illumina Inc., San Diego, CA, USA) at Majorbio (Shanghai, China). Clean data were obtained by trimming low-quality reads (<50 bp) using fastp v 0.20.0, resulting in a 79.7 Gbp sequence for an average of 11.4 ± 1.31 Gbp per sample; the raw Illumina datasets can be accessed at NCBI using the SRP accession number SRP 352692.

Clean reads were assembled using MEGAHIT v 1.1.2 based on the succinct de Bruijn graph method (Li et al. 2015). Then, assembled contigs (≥300 bp) were predicted from an open reading frame by MetaGene (Noguchi et al. 2006). Redundant genes were removed, a nonredundant gene catalog was clustered by CD-HIT at 90% identity and 90% coverage (Fu et al. 2012). SOAPaligner was adopted to map the clean data of each sample to the nonredundant gene catalog at 95% identity, and the abundance of each gene in each refuse sample was obtained (Li et al. 2009). Protein sequences translated from predicted genes were searched against the NR database (Altschul et al. 1997). The KEGG annotation was conducted using Diamond (Buchfink et al. 2015) against Kyoto Encyclopedia of Genes and Genomes database (version 94.2) with an E-value cutoff of 1×10^{-5}. These As related genes, including phosphate transporters (Pst/Pit), glycerol protein facilitator (GlpF) membrane proteins, arsenate reductase, arsenite permeases (ArsB and Acr3), arsenite S-adenosylmethyltransferase (ArsM) and etc., were further assigned to KO, Pathway, EC, and Module, and the corresponding abundances were calculated using KOBAS v 2.0 (Xie et al. 2011).

2.5 Binning analysis, genome annotation, and phylogenetic identification

Binning was performed by MaxBin2 (Wu et al. 2016) using contigs (≥1000 bp). The qualities of metagenome-assembled genomes (MAGs) were then assessed by CheckM (Parks et al. 2015): (i) marker genes in the MAG sequence were identified by HMM; (ii) HMMER v 3.1.2 was employed to compare these marker genes with common single-copy genes, and pplacer was used to place the MAGs into the reference evolutionary tree; (iii) specific genealogical marker sets were identified and quality assessments of MAGs were performed (Parks et al. 2015). The taxonomy of MAGs was assigned by AMPHORA2 according to the information of marker genes, as previously described (Wu and Scott 2012).

2.6 Statistical analysis

All analyses were performed using R v.3.6.1 (R Core Team, 2019) and pertinent packages. The methylated As (MMA and DMA) distribution in the LSZ was visualized by water–fall plot using the *ggplot2* package (version 3.2.1). The principal coordinate analysis (PCoA) plot indicated differences in microbial community structure under different temperature fields in different landfill stages (days 3 and 21). The correlations between *arsM* genes and microbes (at the phylum level) were evaluated through redundancy analysis (RDA). Both PCoA and RDA were performed using the *vegan* package (v.2.5-6) with the Bray–Curtis distance algorithm.

Network construction was performed based on operational taxonomic unit (OTU) abundance. Network analysis was performed using a molecular ecological network analysis pipeline (http://ieg4.rccc.ou.edu/mena/login.cgi) on OTU abundance based on random matrix theory. Networks were visualized by Cytoscape 3.7.0, as previously described (Nie et al. 2021, Shannon et al. 2003). The correlation matrix between the abundance of *arsM* gene and modules of co-occurred networks was constructed by psych package (version 1.6.6) (http://cran.r-project.org/package=psych) based on pairwise Spearman's correlation coefficients (r) and then visualized by *pheatmap* package (version 1.0.12).

3. RESULTS

3.1 As-methylation behavior variation with temperature fields

Combined DGT samplers were employed to investigate *in situ* profiles of MMA and DMA in landfill LSZ. The MMA and DMA distribution obviously varied with operational temperatures (**Fig. 3a**). Comparison of MMA pore-water profiles with DMA profiles revealed that DMA was the dominant methylated As in the aqueous phase at the early stage (Day 3). It seemed like MMA was prone to transform into DMA quickly. Moreover, both MMA and DMA distribution varied with temperature fields in the LSZ, although the MMA concentration was much lower than the DMA concentration. At room temperature, both MMA and DMA concentrations increased with depth from −6 to 0 mm below the liquid–solid interface, but they tended to decrease above the interface. As the temperature increased to 35°C, MMA concentration increased with depth (the highest value appeared in the range of 7.5–10 mm above the interface), whereas DMA concentration tended to be higher below the interface than above. The DMA concentration was much higher at 35°C than at room temperature, attributable to the increase in *arsM* gene abundance with temperature (**Fig. 4**). When the temperature was further increased to 45°C, the highest MMA concentration was approximately located at −1 mm below the interface, but MMA mass was less than that at 35°C, whereas DMA concentration was higher, increasing with depth at 45°C. However, there was no obvious difference in *arsM* abundance between DMA and MMA (**Fig. 4**); probably, the ArsM enzymeencoded by *arsM* genes strengthened with increase in environmental temperature. At 55°C, MMA concentration was higher than that at other temperatures (it varied slightly with depth), whereas DMA concentration was still higher than at room temperature, and the higher DMA concentration was located within the interface (−3 to 2.5 mm), although the *arsM* gene abundance was the lowest (**Fig. 4**). This also supports the claim that ArsM enzyme would strengthen with temperature increase.

The *arsM* abundance tended to increase on high temperatures (45°C and 55°C) and decrease at low temperatures (25°C and 35°C), although 16S rRNA abundance was lower at Day 21 than at Day 3 (**Fig. 4**), indicating that DMA concentration was much higher at 45°C and 55°C. Notably, both MMA and DMA concentrations were extremely low at 35°C, although the *arsM* gene abundance was similar to that at 55°C (**Fig. 4**). Combining the results of the total content of As species under different temperatures (**Fig. 3b**), arsenic removal mass reached the highest at 35°C. Probably, the bioreactor's reduced MMA and DMA concentration was due to its methylation efficiency to create TMA at 35°C. Similar study also indicated that Arsenic volatilization can be mediated via ArsM to dispose As-bearing wastes under anaerobic condition (Webster et al. 2016).

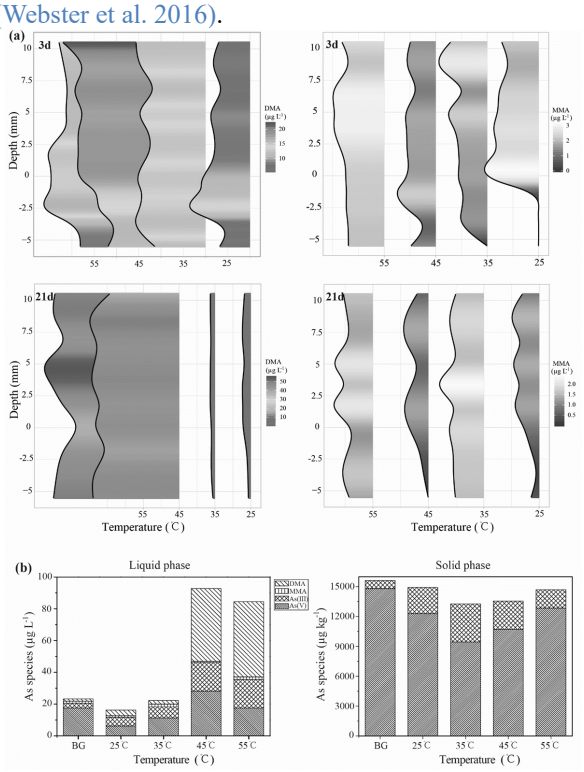

Fig. 3 Arsenic species distribution under different

temperature fields in LSZ of landfill. (**a**) DGT concentration profiles of MMA and DMA along depth in liquid-solid interface during different incubation stages, at Day 3 and Day 21, respectively. The zero horizontal lines showed the position of the liquid-solid interface. (**b**) As species distribution in leachate and solid phase under different temperature fields, respectively.

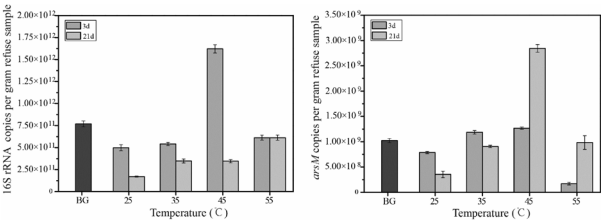

Fig. 4 Effect of temperatures on the absolute abundance of *arsM* and 16S rRNA genes present in refuse samples at different operational periods. Error bars indicate the standard deviation of three replicates. BG was the original refuse sample applied for the study.

3.2 Microbial communities shift influenced *arsM* gene distribution in different temperature fields

As-methylation behavior not only varied with different temperatures in the LSZ but also shifted along different operational stages, as mentioned above. Microbes were the main driver for As biotransformation in our previous studies (Hu et al. 2021, Hu et al. 2022), so microbial diversity was further analyzed to verify the mechanism of As methylation in LSZ. Alpha diversity was calculated to indicate the shift of microbial diversity at different temperatures and operational stages, as shown in **Fig. 5**. According to the Bray-Curtis distances, PCoA further showed the differences of microbial beta-diversity in the operational stages among different temperatures (**Fig. 6a**). Five groups were assembled, namely, 3d-25℃, 3d-35℃, 3d-45℃&55℃, 21d-25℃&35℃, and 21d-45℃&55℃. In addition, the microbial community structure shifted along axis PCoA1 across the operational stages and along axis PCoA2 from low- to high-temperature fields; we could infer that nutrients are the main factors for driving the microbial community structure in landfills because the content of nutrients decreased during operation (**Fig. 7**). RDA and a permutation test were also performed to determine the relationship between microbes and *arsM* gene distribution (**Fig. 6b**). The *arsM* gene abundance was significantly positively correlated with microbial community structure (r^2 = 0.271, p = 0.016) and was positively correlated with the abundance of Halobacterota, Chloroflexi, Actinobacteriota, Planctomycetota, Proteobacteria, Synergistota, Firmicutes, Bacteroidota, etc. Consequently, as shown in **Fig. 6c**, the microbial community structure not only shifted along different operational stages but also varied with different operational temperatures. By comparing days 3 and 21, the average abundance of Proteobacteria decreased from 27.3% to 6.9%, which was negatively correlated with *arsM* gene abundance (**Fig. 6b**). Meanwhile, the average abundance of Chloroflexi and Halobacterota increased from 2.4% and 0.17% to 9.1% and 13.7%, respectively. By comparing the low- and high-temperature groups at Day 21, Chloroflexi and Halobacterota increased with temperature. The average abundance of Actinobacteriota not only decreased from 13.0% on day 3 to 7.5% on day 21 but also decreased with temperature increase at the same operational stage.

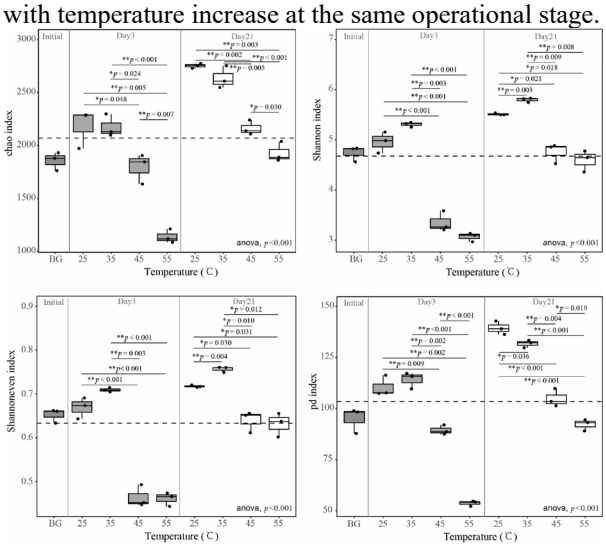

Fig. 5 Microbial alpha-diversity estimate calculations of taxa in LSZ under different operational temperatures. The Shannon index, Chao index, Shannoneven, and PD tree of the refuse sample microbiome are from different operational stages. Horizontal lines represent mean values $p < 0.05$ indicates statistical significance using a T-test.

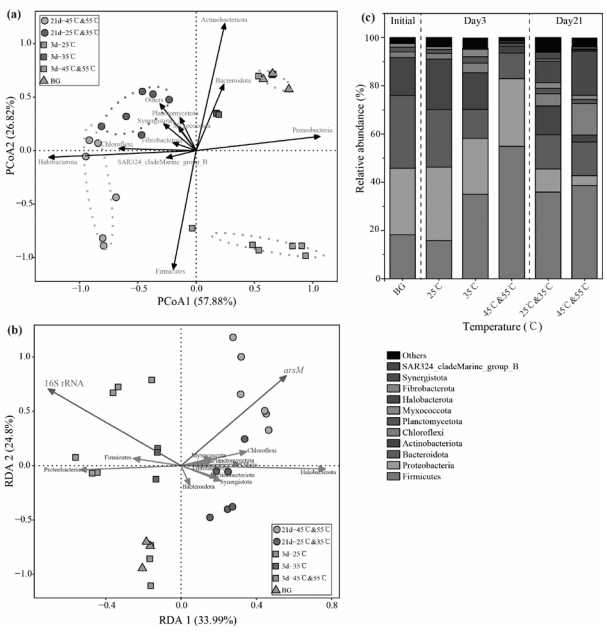

Fig. 6 Shifts in microbial communities influenced *arsM* gene distribution under different temperature fields across processes. Panel (**a**) was principal coordinate analysis (PCoA) of microbial communities in phylum level based on Bray-Curtis distances. The individual samples were shape coded to indicate as BG, Day3 and Day21 stage, respectively, while purple, green, blue, brown and red coded as the initial refuse sample and 3d-25℃, 3d-35℃, 3d-45℃&55℃, 21d-25℃&35℃ and 21d-45℃&55℃, respectively. Redundancy analysis (RDA) correlation biplot Panel (**b**) of *arsM* gene with microbial communities. Arrows indicated the director and magnitude of each microbial community in phylum level. Panel (**c**) indicated dominant bacterial phyla at different temperature fields and processing stages.

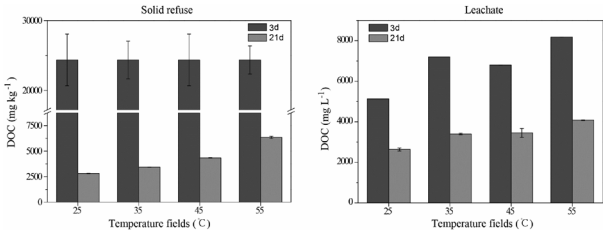

Fig. 7 The content of DOC varied with different temperature fields along processing. Panel (**a**) DOC for the solid refuse sample; Panel (**b**) DOC for leachate.

3.3 Methylation functional profiling of core–microbiome at different temperatures

Our previous studies showed that microbes drive arsenic methylation in landfills (Hu et al. 2021); moreover, as mentioned above, *arsM* gene distribution and microbial diversity varied with temperature in landfills. Co-occurrence network analysis further illuminated the details of interactions among the taxa at different operational stages (**Fig. 8a and 8b**) based on the significant nonparametric Spearman's correlations. Although the network size tended to decrease along with processing (**Table 2**), the correlation between taxa was prone to be excluded (negative correlations). The negative correlation only accounted for 8.9% on day 3, whereas it was up to 54.1% on day 21. It seemed to be the decrease in DOC that resulted in a more significant negative correlation between taxa in LSZ.

The modular composition of microbes not only varied with different temperatures (**Figs. 9 and 10**) but also influenced *arsM* gene distribution (**Fig. 9**), indicating that the *arsM* gene was significantly positively correlated with Modules 1#, 3#, 11#, and 20# ($r > 0.6$, $p < 0.05$) on day 3, and their relative abundance was nearly less than 1%, except for Module 1#. Particularly, for Module 1#, the abundance varied with temperature, and the highest value (8.53%) appeared at 35℃ field, and the second-highest value appeared at 45℃. Further, Firmicutes, Proteobacteria, and Bacteroidota were the dominant phyla (**Fig. 10**). It seemed that rare species constituted Module 3#, and Firmicutes dominated in this ecological cluster.

On day 21, Modules 1#, 9#, 15#, and 20# significantly co-occurred with *arsM* genes (**Fig. 9**). For Module 1#, the relative abundance tended to increase with an increase in LSZ temperature, up to 33.1% at 55℃, and the dominant phyla were Firmicutes, Proteobacteria, and Halobacterota (**Fig. 10**). Both size and abundance for the other three modules were extremely lower than those for Module 1#.

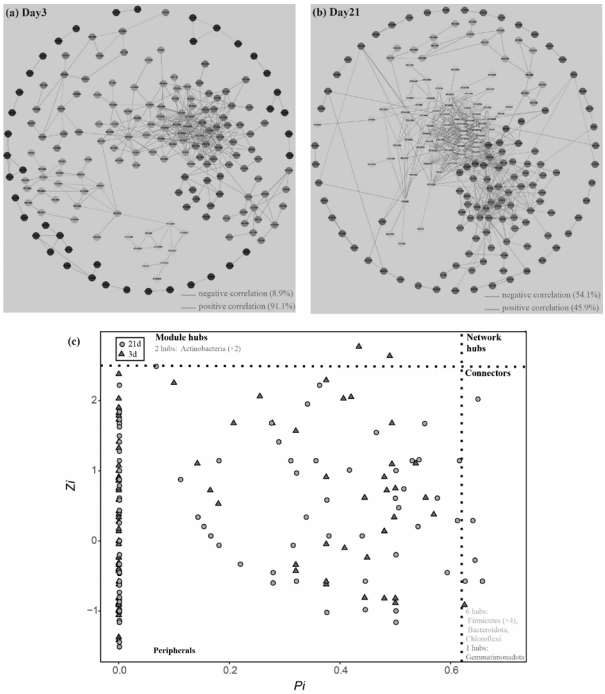

Fig. 8 Interaction relationships and core–microbiome

under different temperature fields at different operational stages. Panel (**a**) and (**b**) was overview of the microbial co-occurrence networks that were based on RMT and performed on OTU level. Nodes represented the OTUs, edges indicated significant correlation. The nodes of the same module were color coded randomly, and nodes in modules with less than 10 nodes were colored black. Panel (**c**) showed classification of nodes basing on *Zi* and *Pi* value to identify putative keystone species at different stages. The horizontal line was the *Zi* value 2.5, and modules hubs had *Zi* >2.5; the vertical line was *Pi* value =0.62, connectors had *Pi* >0.62.

Table 2 Topological properties of the co-occurrence networks of microbial communities at two different landfill process stages

Landfill stage	Day3	Day21
Total nodes	187	194
Total links	417	697
R square of power-law	0.851	0.757
Similarity threshold	0.95	0.98
Modularity	0.540	0.441
Module	22	21

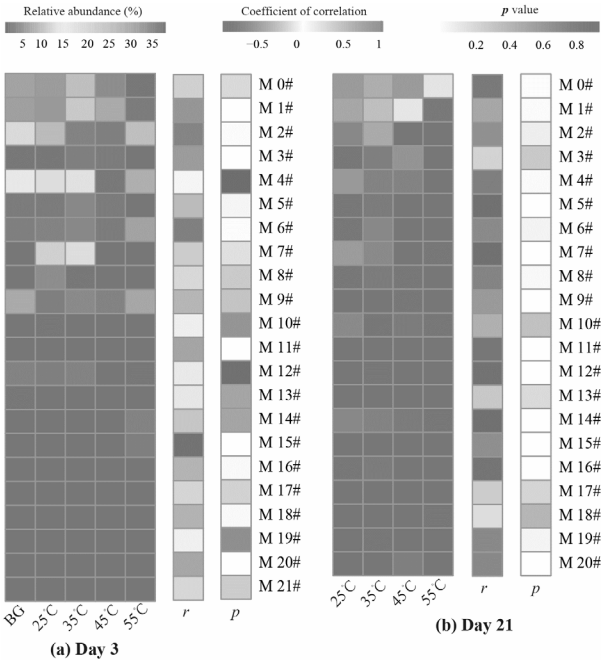

Fig. 9 Correlation between *arsM* gene abundance and the modules with different temperature fields along landfilling processes. Heatmaps indicated module compositions varied with temperature fields, the correlation coefficient and *p*-value between *arsM* gene and each module.

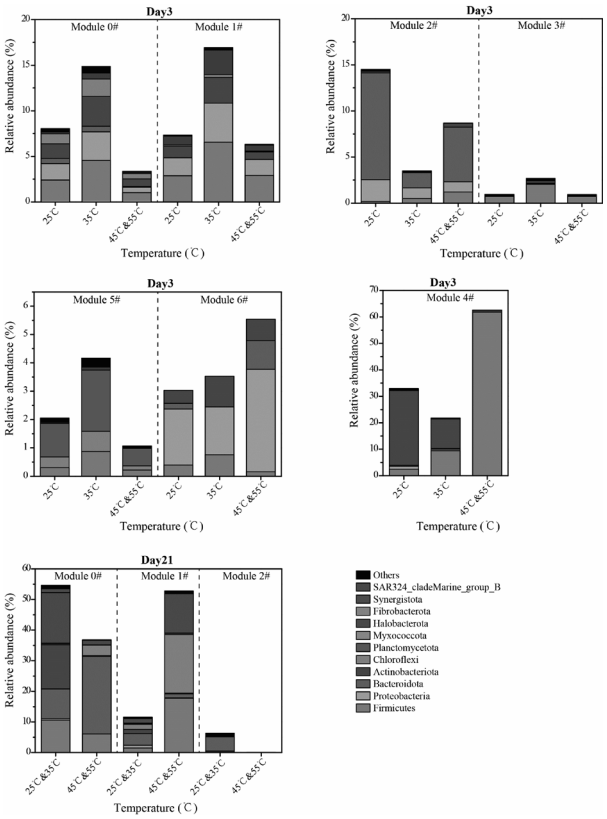

Fig. 10 Overview of modular distribution at different stages. It indicated the composition of ecological cluster (only showed modules with more than 10 nodes) in different temperature fields. Color indicated the phyla.

3.4 Gene sets underlying As-methylation processes and capability discrepancy at different temperatures

Microbes mediate As metabolism and play a paramount role in As biotransformation, participating in various metabolic functions, such as detoxification, anaerobic respiration, and methylation, which not only influence As mobility but also toxicity in the ecology of landfills (Hu et al. 2022). As shown in **Fig. 11**, the schematic of As-metabolic pathways and their functional genes within the context of pathways are summarized for landfill LSZ. Because arsenate might act as an analog of phosphate, As(V) enters the microbial cells via phosphate transporters (Pst/Pit), whereas arsenite was considered an analog of glycerol and entered into cells via glycerol protein facilitator (GlpF) membrane proteins (Mukhopadhyay et al. 2002). The Pst comprises periplasmic binding protein (PstS) (encoded by *pstS* genes) and the membrane-bound ABC-type transporter (PstCAB) (encoded by *pstCBA*) (Scanlan et

al. 2009). It indicated that the abundances of *pit* and *pst* genes were much higher than that of the *glpF* gene, and their abundance varied with different temperatures. Higher abundances of *pst* and *pit* genes were observed in 3d-35℃ and 21d-45℃&55℃ groups, whereas higher abundances of the *glpF* gene were observed in 3d-35℃, 21d-25℃&35℃, and 21d-45℃&55℃ groups. Consequently, the major mechanism for As transfer into microbial cells would be Pst/Pit. As illustrated in **Fig. 3b**, As(V) was the main species in the landfills; after transferring into cells, As(V) could be reduced to As(III) by arsenate reductase (ArsC) (encoded by the *arsC* gene). When As(III) was further extruded from the cells by efflux systems, two different families of arsenite permeases (ArsB and Acr3) were annotated in the LSZ, and the As resistance processes were characterized as arsenic detoxification in microbes. The abundance of the *arsB* gene was much lower than that of the *acr3* gene in the LSZ, and the abundance of the *acr3* gene seemed to decrease in the landfilling processes, namely, the highest value of the *acr3* gene abundance was observed in the BG refuse sample. Acr3 and ArsB showed no significant sequence similarity, although members of Acr3 were widespread in bacteria, archaea, and fungi, and those of ArsB in bacteria and archaea (Achour et al. 2007). The ArsM converted As(III) into MMA(V), DMA(V), and TMA(III), whereas glutathione S-transferase (GST) reduced MMA(V) and DMA(V) to MMA(III) and DMA(III) with oxidative methylation alternately using the Challenger Pathway (Bach 1945, Hayakawa et al. 2005, Rehman and Naranmandura 2012, Reimer et al. 2010). The volatile TMA is the final product in the As-methylation pathway, and it diffuses and will not accumulate in microbial cells (Qin et al. 2006). The certain abundance of the *arsM* gene was annotated in the LSZ samples; further, its abundance varied with different temperatures and landfill processes. The *arsM* gene tended to be more abundant as the landfill process progressed; in other words, the abundance of *arsM* on day 21 was much higher than on day 3. At the early stage (day 3), methylation reactions were more intense under the 35℃ condition, but a higher temperature intensified methylation at the later stage (day 21). Moreover, the *gst* gene was much more abundant than *arsM*, so GST (encoded by the *gst* gene) would not be the rate-limiting enzyme. Thus, the ArsM plays a significant role in arsenic cycles in landfills.

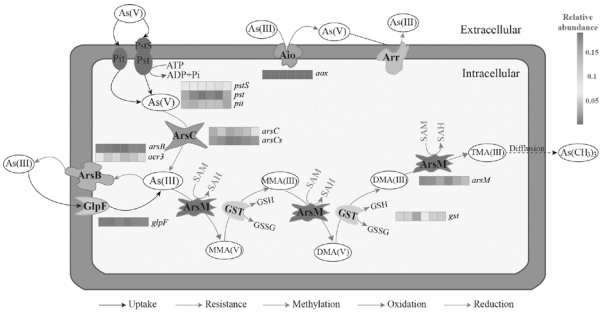

Fig. 11 Arsenic biotransformation pathways in the landfill and shift in abundance of the underlying genes among different temperature treatment metagenomes along processes. Heatmaps were ordered as: BG, 3d-25℃, 3d-35℃, 3d-45℃&55℃, 21d-25℃&35℃, and 21d-45℃&55℃.

3.5 Identification of As-methylated putative metagenome-assembled genomes

There were 87 MAGs with >70% and <10% contamination from the co-assembled metagenomes, and putative As-methylation microorganisms containing the genes for arsenite S-adenosylmethyltransferase (*arsM*) accounted for 15% of MAGs (13 of 87, **Fig. 12**). The 13 putative methylation MAGs of LSZ are detailed in **Table 3**, indicating that four MAGs were resolved to genus, namely, three strains (LSZ_MeAs_10, LSZ_MeAs_11, and LSZ_MeAs_12) to Syntrophomonas and one strain (LSZ_MeAs_13) to Anaerolinea. Two MAGs (LSZ_MeAs_8 and LSZ_MeAs_9) were resolved to Bacteroidales, one MAG (LSZ_MeAs_7) to Bacteroidetes, and the remaining six MAGs to Bacteria Domain.

The presence of arsenic functional genes was queried in the above MAGs and was deemed a response to As methylation for the existing *arsM* gene. LSZ_MeAs_1 MAG with 83.4% completeness identified both As(V) and As(III) uptake systems, namely, Pit/Pst for As(V) and GlpF for As(III), indicating that this species could complete As-methylation processes. Further, the expression of the *arsM* gene would be controlled by ArsR regulatory protein (encoded by the *arsR* gene), which is considered a member of the ArsR/SmtB family for metal/metalloid responsible repressors (Kostal et al. 2004, Rawle et al. 2021).

LSZ_MeAs_2 (74.8% completeness) also showed the existence of As(V) uptake system, resistance system, and ArsR repressors. By speculation, the arsenic metabolic processes could have started from the As(V) uptake system by Pst proteins; after cytosolic ArsC used thioredoxin (Trx) as a reductant to reduce As(V) to As(III), part of As(III) was excluded from cells by Acr3 (encoded by the *acr3* gene), and the other part was methylated by ArsM. The efflux system, Acr3, has arisen to cope with the more toxic arsenic form As(III),

indicating that this putative As-methylation functional species had higher tolerance to As. Moreover, the *arsR* gene for encoding repressor ArsR was queried in the MAGs that could adjust both arsenic resistance and methylation (Zhang et al. 2022). Two MAGs (LSZ_MeAs_3 and LSZ_MeAs_4) were identified by the *arsM* gene in their genome, but they have neither As(III) nor As(V) transporters, which might result in the impossibility for them to methylate arsenic alone. LSZ_MeAs_5 had Pst protein for As(V) transport, but lack the As reductase gene; thus, this species would not complete As methylation by itself.

The As uptake systems [both As(V) and As(III)], As(III) efflux system, and As(III) efflux carrier were also found in LSZ_MeAs_6 (99.2% completeness), and the *arsR* gene was found in this genome to adjust As-methylation processes. These MAGs seemed tolerant to be in the high As(III) environment.

LSZ_MeAs_7 (99.2% completeness) from Bacteroidetes identified the As(V) uptake system (Pit/Pst) and As resistance systems (ArsC and ArsAB). Notably, the ArsA ATPase (encoded by the *arsA* gene) could enhance the As(III) transport capability because ArsAB drives the active transport of As(III) through ATP, which is much faster than ArsB alone (Castillo and Saier 2010). The *arsR* gene was not identified in this genome; it could be ArsAB that adjusted As(III) levels via efflux out cells to realize As detoxification. Thus, this As-methylation species could also tolerate high levels of arsenic.

Both LSZ_MeAs_8 (98.7% completeness) and LSZ_MeAs_9 (77.6% completeness) were from Bacteroidales, although they had different As metabolic processes according to the organization of the As-related gene clusters. The former could accomplish As methylation alone because there were *pit* genes to regulate As(V) transport, *arsC* genes to reduce As(V) to As(III), and *arsM* genes for methylation. In comparison with LSZ_MeAs_8, the latter identified an As resistance system in its genome and would have a higher tolerance for arsenic.

Three strains were from the same genus Syntrophomonas, but only two MAGs (LSZ_MeAs_10 with 95.3% completeness and LSZ_MeAs_11 with 75.1% completeness) could accomplish methylation processes alone according to their As-related gene organization clusters, whereas LSZ_MeAs_12 (97.8% completeness) lacked either As(III) transport or As(V) reductase. LSZ-MeAs_10 identified the *arsAB* gene for an As resistant system, indicating that this strain could tolerate a higher As level than LSZ_MeAs_11. Further, the As(V) reductase of LSZ_MeAs_11 ArsCs (encoded by *arsCs*) was from a different family, which uses glutaredoxin (Grx) and GSH as reductants (Chrysostomou et al. 2015, Shi et al. 1999).

LSZ_MeAs_13 with 70.3% completeness, Anaerolinea sp., included both Pit/Pst and GlpF arsenic uptake systems and As(V) reductase system; a certain amount of As(III) would be accumulated in cells. On a purely protective purpose by conferring this host MAG resistance to both As(III) and As(V), more As(III), uptaken by GlpF and reduced by ArsC, seemed to be methylated, which then extruded the cellular compartment as TMA.

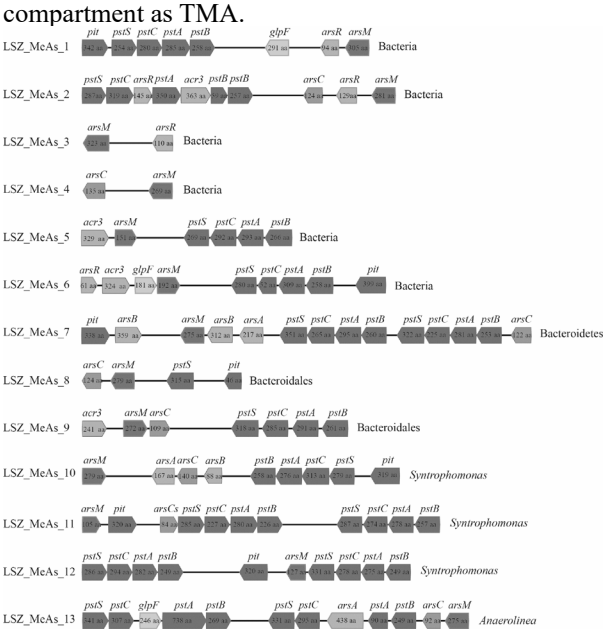

Fig. 12 Organization of As related gene clusters (**Table 3** for genes' description) observed in putative As methylation MAGs.

Table 3 Overview of all genome bins ≥ 70% complete and with ≤ 10% contamination

MAG name	Number contigs	Completeness (%)	Contamination (%)
LSZ_MeAs_1	1336	83.39	5.36
LSZ_MeAs_2	997	74.81	3.1
LSZ_MeAs_3	440	87.25	5.33
LSZ_MeAs_4	203	90.75	2.75
LSZ_MeAs_5	242	96.42	1.85
LSZ_MeAs_6	165	99.21	0
LSZ_MeAs_7	383	98.39	2.69
LSZ_MeAs_8	288	98.66	2.15
LSZ_MeAs_9	38	77.59	0
LSZ_MeAs_10	281	95.29	0.68
LSZ_MeAs_11	467	75.11	1.88
LSZ_MeAs_12	299	97.83	6.72
LSZ_MeAs_13	1336	70.34	4.55

4. DISCUSSION

4.1 Discrepancy in As methylation at different temperatures in LSZ

In previous studies (Hu et al. 2021, Hu et al. 2019), we pointed out that microbes would be the main driver to promote arsenic transformation in landfills, and environmental factors, such as moisture content, significantly affect arsenic species distribution. The refuse was immerged by retarded leachate in the LSZ, whereas the discrepancy in leachate migration was due to the permeability differences of landfill refuse; thus, the great heterogeneity of LSZ caused biogeochemistry differences in the LSZ (Jin et al. 2020a, Jin et al. 2020b). **Fig. 3a** indicates an obvious discrepancy in MMA and DMA distribution under different temperature fields in the LSZ. Notably, the capability of DMA biotransformation was prone to promote along with an increase in temperature; meanwhile, MMA distribution was much lower than DMA, although it varied with temperature and DMA. According to the microbial As-methylation pathway (**Fig. 11**), both MMA and DMA were intermediates for the final product, TMA(III), which is volatile in the classic Challenger Pathway (Huang et al. 2016, Qin et al. 2009, Qin et al. 2006, Wang et al. 2014, Zhang et al. 2015). **Fig. 3b** shows the differences in arsenic species distribution under different temperature fields, and the content of TAs varied with temperature. It was the TMA(III) biovolatilization that resulted in TAs discrepancy among different temperatures because methyl As intermediates [e.g., MMA(V) and DMA(V)] are nonvolatile (Mestrot et al. 2013). However, the shift of TAs with temperature was inconsistent with that of DMA; in addition, the lowest TAs content appeared at 35℃, whereas DMA tended to increase with an increase in temperature, indicating that more DMA was methylated to TMA(III) at 35℃ field, which caused a lower DMA distribution. There were two key functional enzymes in the As-methylation pathway: ArsM and GST (Chrysostomou et al. 2015, Qin et al. 2006). **Fig. 11** further shows that the abundance of both *arsM* and *gst* genes varied with temperature. Generally, **Fig. 4** indicates that more abundance of *arsM* gene was observed at higher temperatures (≥35℃). In particular, the highest abundance of the *arsM* gene appeared at 45℃. However, the highest methylation capacity was at 35℃ rather than 45℃, meaning that the GST enzyme for reducing pentavalent methylated As was profound because KEGG annotation results showed more abundance of the gst gene at the mesothermal field (around 35℃).

4.2 Contribution of microbial communities to As-methylation under different temperature fields

As shown in **Fig. 6**, microbial diversity significantly shifted in response to different temperatures in LSZ, which also influenced *arsM* gene distribution because ArsM protein was the key driver for As methylation (Hu et al. 2021, Yang et al. 2021). Particularly, RDA results elucidated the correlation between microbial community structure and *arsM* gene distribution, indicating that phyla, such as Halobacterota, Chloroflexi, Actinobacteriota, Planctomycetota, and Synergistota, were positively correlated with the *arsM* gene abundance.

Landfill refuse hosts complex communities of microbes, especially in LSZ (Jin et al. 2020a). Microbe–microbe interaction networks were further analyzed to unveil the discrepancy in patterns of biodiversity, community structure, and ecological functions under different temperature fields. **Fig. 8** presents the modular organization of the LSZ–microbiome network; the core–microbiome was driven by two main factors, landfilling processes (via biousable carbon source) and environment (via temperature), based on a similar phylogenetic origin of the refuse samples. Notably, an increase in negative correlation among taxa together with a decrease in DOC during the landfill process could be feedback into the evolution of metabolic capacity. However, competitive interactions are known as the key to maintaining a stable microbiome, whereas positive interactions are destabilizing in ecological communities (Katharine Z. Coyte 2015).

There is often a discrepancy between presence of As methylation genes and As methylation activity, especially for anaerobes (Viacava et al. 2020, Viacava et al. 2022), consequently, the relationship between As methylation capibility and modules of the core‐microbiome was further explored in the landfill. At the same landfill operational stage, the discrepancy in microbial modularity, which translated to predict functional capabilities among different modules of the core–microbiome, was a response to different temperature fields (**Fig. 9**), suggesting that temperature fields heavily influenced the assembly of LSZ microbial communities. Moreover, the abundance of modular could be associated with the As-methylated gene (*arsM* gene) distribution to some extent. Four core network modules had a significantly positive correlation ($r > 0.6$, $p < 0.05$) with As-methylated functions at the early landfill stage (day 3); there were also four core modules at the later stage (day 21). Besides, different temperature fields influenced the discrepancy in the abundance of the As-methylated modules; considering Module 1# at day21 for an example, the highest abundance appeared at 35℃, followed by 45℃. Regarding the composition of Module 1#, Firmicutes, Proteobacteria, and Halobacterota were the dominant phyla. It has been reported that Proteobacteria, Actinobacteria, Acidobacteria, and Choroflexi might play a paramount role in As methylation because these phyla constituted most of the carrying *arsM* gene microbial communities (Guo et al. 2020, Yan et al. 2020). In particular,

Proteobacteria plays an essential role in As methylation (Bennett et al. 2012). As mentioned before, Halobacterota positively affected the *arsM* gene distribution as well; thus, microbes in Module 1# would be further confirmed to influence the capability of As methylation indirectly (**Fig. 13**). As shown in **Fig. 13** (day21-M#1), *Methanosarcina* (Halobacterota) in Module 1# of day 21 was co-occurred with *Cryptanaerobacter* (Firmicutes), *Paenibacillus* (Firmicutes), *Proteiniclasticum* (Firmicutes), *Psychrobacillus* (Firmicutes), *Rhodococcus* (Actinobacteriota), and *Desulfobulbus* (Desulfobacterota). Therefore, these ecological clusters' positive correlation with the *arsM* gene abundance would contribute to As methylation in LSZ, which was also regulated by temperature fields.

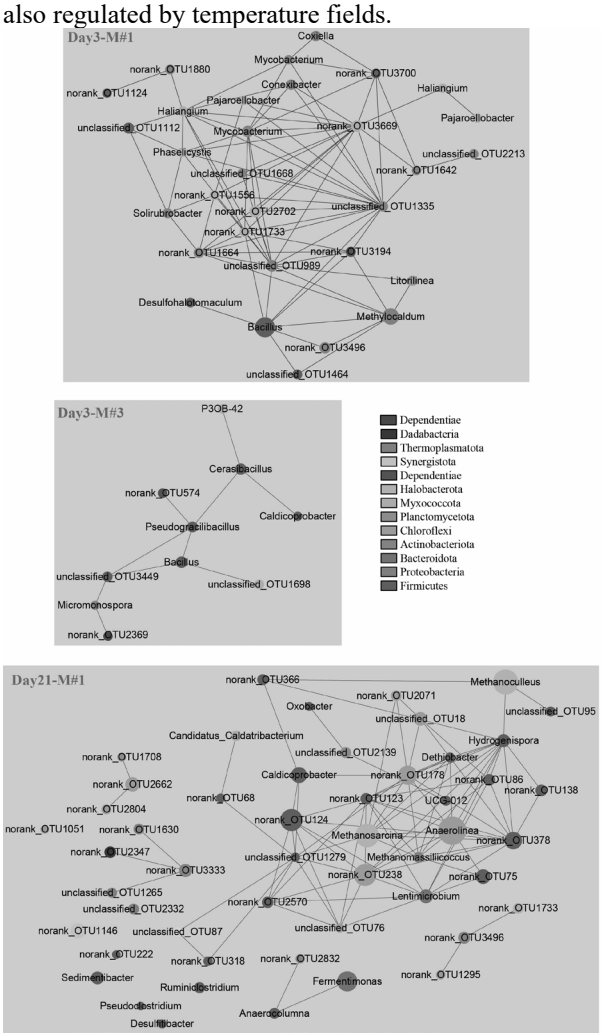

Fig. 13 Composition and positive interaction among putative keystone genera for As methylation and others in network modules. The network analysis was merged at genus level. Node sizes represented the node degree in the topological structure. The color was colored by phyla.

4.3 Putatively novel As-methylation functional species in LSZ

Identifying As-methylated functional species would help understand and even predict the future of arsenic in certain environments through reconstructing the genome of uncultured microbes (J ´er´emy Andres 2016). By annotating *arsM* and other As-related genes and attributing them to specific organisms, 13 MAGs were assembled and considered to play a crucial role in the underlying As-methylation processes (**Fig. 12**). Among them, four MAGs (LSZ-MeAs_3, LSZ-MeAs_4, LSZ-MeAs_5, and LSZ-MeAs_12) were identified to be impossible to complete As-methylation processes by themselves alone due to lack of either As transporters or As(V) reductase gene. For the other MAGs, seven of nine MAGs identified a*rsC*/*arsCs* genes in their genomes to encode the cytosolic As(V) reductase for conferring resistance to As(V) because the most common extracellular form of As was As(V) in the LSZ (**Fig. 3b**). Under anoxic conditions, most resistance mechanisms have arisen to cope with As(V) through reducing As(V) to As(III) and then excluding As(III) from cells via efflux systems or methylation by ArsM (Xiao et al. 2016). Notably, there were two independent and unrelated families of As(V) reductases in LSZ, one family, ArsC, used Trx as a reductant to reduce As(V) to As(III), and the other family, ArsCs, used Grx and GSH as reductants (Chrysostomou et al. 2015, Mukhopadhyay et al. 2002). Because of differences in As(V) reductases between LSZ_MeAs_10 and LSZ_MeAs_11, the two MAGs from the same genus Syntrophomonas would be two different species with inconsistent As resistance pathways (**Fig. 12**). Among the seven MAGs with *arsC*/*arsCs* genes, four MAGs identified As(III) efflux genes (*acr3* or *arsB*) to encode As(III) permeases, namely, LSZ_MeAs_2, LSZ_MeAs_7, LSZ_MeAs_9, and LSZ_MeAs_10. Both ArsB and Acr3 are widespread in bacteria and archaea (Chang et al. 2008). The ArsB functions as an As(III) /H^+ antiporter coupling the proton motive force (Cai et al. 2009), and the ArsB can associate with the ArsA (ATPase) to confer a higher ability of As(III) efflux than ArsB alone (Castillo and Saier 2010). Therefore, LSZ_MeAs_7 and LSZ_MeAs_10 would confer a higher level of arsenic resistance than LSZ_MeAs_2 and LSZ_MeAs_9.

Except for the LSZ_MeAs_2, LSZ_MeAs_2, and LSZ_MeAs_6 annotated *arsR* genes, ArsR was expressed to bind the operator/promoter DNA in the absence of inducing arsenic ion, and so may cause transcription repression. Upon binding As, ArsR could dissociate from the DNA and then result in derepression (Rawle et al. 2021). In other words, by controlling *arsM* gene expression, ArsR regular protein could regulate As detoxification in cells via As-methylation processes. Further, these three MAGs were only annotated to Bacteria, and there are still many

unknowns that need to be explored.

Notably, LSZ_MeAs_13, *Anaerolinea sp.*, identified neither ArsR nor As(III) efflux system; it would be As methylation that was sufficient to detoxify arsenic by converting As(V) into final TMA(III), which volatilizes as it is being formed (Qin et al. 2006). Thus, LSZ_MeAs_13 would confer a higher level of As methylation than other MAGs in LSZ-contaminated high As levels. This result is consistent with the results that Anaerolinea promotes As methylation in paddy soil (Yang et al. 2021).

5. CONCLUSION

Microbial As methylation processes are important components of As biogeochemical cycle in landfill, especially for As resistance and detoxification. The temperature fields obviously effected on As methyaltion in the LSZ, especially, mesothermal field (35°C) appeared to trigger the decrease of TAs content, as demonstrated the increasing the abundance of *arsM* gene. Basing on MRT, co-occurred networks further illuminated the details about influences of temperature fields on microbe-microbe interactions and ecological clusters. According to KEGG annotation and Challenger pathway (Bach 1945), arsenic biochemical cycle were modeled, where detailed the As methylation pathway in the landfil. Meanwhile, the temperature fields shifted As-related functional gene distribution. Then 13 As methylated functional MAGs (annotating *arsM* gene) were further reconstructed by Binning analysis, 9 putative functional species could complete methylation processes alone. This study provided a theoretical basis for management of As contamination in landfills: promoting the microbial As methylation to convert inorganic As to less toxic, methylated As species via temperature control.

ACKNOWLEDGMENTS

The work was supported by the National Natural Science Foundation of China (21876165 and 41977331), and the Fundamental Research Funds for the Provincial Universities of Zhejiang. The authors would like to thank Yupeng Lou from Shiyanjia Lab (www. shiyanjia.com) for the analysis.

REFERENCES

Achour, A.R., Bauda, P. and Billard, P. (2007) Diversity of arsenite transporter genes from arsenic-resistant soil bacteria. Research in microbiology 158(2), 128-137.

Ajees, A.A., Marapakala, K., Packianathan, C., Sankaran, B. and Rosen, B.P. (2012) Structure of an As(III) S-Adenosylmethionine Methyltransferase: insights into the Mechanism of Arsenic Biotransformation. Biochemistry 51(27), 5476-5485.

Altschul, S.F., Madden, T.L., Schaffer, A.A., Zhang, J., Zhang, Z., Miller, W. and Lipman, D.J. (1997) Gapped BLAST and PSI-BLAST: a new generation of protein database search programs. Nucleic acids research 25(17), 3389-3402.

Bach, S.J. (1945) Biological methylation. Biological reviews of the Cambridge Philosophical Society 20, 158-176.

Bennett, W.W., Teasdale, P.R., Panther, J.G., Welsh, D.T., Zhao, H. and Jolley, D.F. (2012) Investigating Arsenic Speciation and Mobilization in Sediments with DGT and DET: A Mesocosm Evaluation of Oxic-Anoxic Transitions. Environmental science & technology 46(7), 3981-3989.

Buchfink, B., Xie, C. and Huson, D.H. (2015) Fast and sensitive protein alignment using DIAMOND. Nature Methods 12(1), 59-60.

Cai, L., Liu, G., Rensing, C. and Wang, G. (2009) Genes involved in arsenic transformation and resistance associated with different levels of arsenic-contaminated soils. Bmc Microbiology 9.

Castillo, R. and Saier, M.H. (2010) Functional Promiscuity of Homologues of the Bacterial ArsA ATPases. International journal of microbiology 2010, 187373-187373.

Chang, J.-S., Ren, X. and Kim, K.-W. (2008) Biogeochemical cyclic activity of bacterial arsB in arsenic-contaminated mines. Journal of Environmental Sciences 20(11), 1348-1355.

Chen, S.-C., Sun, G.-X., Rosen, B.P., Zhang, S.-Y., Deng, Y., Zhu, B.-K., Rensing, C. and Zhu, Y.-G. (2017) Recurrent horizontal transfer of arsenite methyltransferase genes facilitated adaptation of life to arsenic. Scientific Reports 7.

Chrysostomou, C., Quandt, E.M., Marshall, N.M., Stone, E. and Georgiou, G. (2015) An Alternate Pathway of Arsenate Resistance in E. coli Mediated by the Glutathione S-Transferase GstB. Acs Chemical Biology 10(3), 875-882.

Ding, S., Chen, M., Gong, M., Fan, X., Qin, B., Xu, H., Gao, S., Jin, Z., Tsang, D.C.W. and Zhang, C. (2018) Internal phosphorus loading from sediments causes seasonal nitrogen limitation for harmful algal blooms. Science of the Total Environment 625, 872-884.

Ding, S., Wang, Y., Zhang, L., Xu, L., Gong, M. and Zhang, C. (2016) New holder configurations for use in the diffusive gradients in thin films (DGT) technique. Rsc Advances 6(91), 88143-88156.

Fu, L., Niu, B., Zhu, Z., Wu, S. and Li, W. (2012) CD-HIT: accelerated for clustering the next-generation sequencing data. Bioinformatics 28(23), 3150-3152.

Guo, T., Gustave, W., Lu, H., He, Y., Tang, X., Buchwalter, D.B. and Xu, J. (2020) Periphyton enhances arsenic release and methylation at the soil-water interface of paddy soils. Journal of Hazardous Materials 409, 124946-124946.

Hao, Z., Sun, M., Ducoste, J.J., Benson, C.H., Luettich, S., Castaldi, M.J. and Barlaz, M.A. (2017) Heat Generation and Accumulation in Municipal Solid Waste Landfills. Environmental science & technology 51(21),

12434-12442.
Hayakawa, T., Kobayashi, Y., Cui, X. and Hirano, S. (2005) A new metabolic pathway of arsenite: arsenic-glutathione complexes are substrates for human arsenic methyltransferase Cyt19. Archives of Toxicology 79(4), 183-191.
Hu, L., Nie, Z., Wang, W., Zhang, D., Long, Y. and Fang, C. (2021) Arsenic transformation behavior mediated by arsenic functional genes in landfills. Journal of Hazardous Materials 403, 123687-123687.
Hu, L., Wang, W., Long, Y., Wei, F., Nie, Z. and Fang, C. (2019) Fate and migration of arsenic in large-scale anaerobic landfill. Waste Management 87, 559-564.
Hu, L., Zhang, D., Qian, Y., Nie, Z., Long, Y., Shen, D., Fang, C. and Yao, J. (2022) Microbes drive changes in arsenic species distribution during the landfill process. Environmental Pollution 292, 1-12.
Huang, K., Chen, C., Zhang, J., Tang, Z., Shen, Q., Rosen, B.P. and Zhao, F.-J. (2016) Efficient Arsenic Methylation and Volatilization Mediated by a Novel Bacterium from an Arsenic-Contaminated Paddy Soil. Environmental science & technology 50(12), 6389-6396.
J ´er´emy Andres, P.N.B. (2016) The microbial genomics of arsenic. FEMS microbiology reviews 39, 1-24.
Jia, Y., Huang, H., Zhong, M., Wang, F.-H., Zhang, L.-M. and Zhu, Y.-G. (2013) Microbial Arsenic Methylation in Soil and Rice Rhizosphere. Environmental science & technology 47(7), 3141-3148.
Jin, Z., Ci, M., Yang, W., Shen, D., Hu, L., Fang, C. and Long, Y. (2020a) Sulfate reduction behavior in the leachate saturated zone of landfill sites. Science of the Total Environment 730.
Jin, Z., Zhang, S., Hu, L., Fang, C., Shen, D. and Long, Y. (2020b) Effect of substrate sulfur state on MM and DMS emissions in landfill. Waste Management 116, 112-119.
Katharine Z. Coyte, J.S., Kevin R. Foster (2015) The ecology of the microbiome: networks, competition, and stability. Science 350, 663–666.
Kostal, J., Yang, R., Wu, C.H., Mulchandani, A. and Chen, W. (2004) Enhanced arsenic accumulation in engineered bacterial cells expressing ArsR. Applied and environmental microbiology 70(8), 4582-4587.
Li, D., Liu, C.-M., Luo, R., Sadakane, K. and Lam, T.-W. (2015) MEGAHIT: an ultra-fast single-node solution for large and complex metagenomics assembly via succinct de Bruijn graph. Bioinformatics 31(10), 1674-1676.
Li, R., Yu, C., Li, Y., Lam, T.-W., Yiu, S.-M., Kristiansen, K. and Wang, J. (2009) SOAP2: an improved ultrafast tool for short read alignment. Bioinformatics 25(15), 1966-1967.
Mench, M., Schwitzguebel, J.-P., Schroeder, P., Bert, V., Gawronski, S. and Gupta, S. (2009) Assessment of successful experiments and limitations of phytotechnologies: contaminant uptake, detoxification and sequestration, and consequences for food safety. Environmental Science and Pollution Research 16(7), 876-900.
Mestrot, A., Planer-Friedrich, B. and Feldmann, J. (2013) Biovolatilisation: a poorly studied pathway of the arsenic biogeochemical cycle. Environmental Science-Processes & Impacts 15(9), 1639-1651.
Mestrot, A., Uroic, M.K., Plantevin, T., Islam, M.R., Krupp, E.M., Feldmann, J. and Meharg, A.A. (2009) Quantitative and Qualitative Trapping of Arsines Deployed to Assess Loss of Volatile Arsenic from Paddy Soil. Environmental science & technology 43(21), 8270-8275.
Mukhopadhyay, R., Rosen, B.P., Phung, L.T. and Silver, S. (2002) Microbial arsenic: from geocycles to genes and enzymes. FEMS microbiology reviews 26(3), 311-325.
Nie, Z., Hu, L., Zhang, D., Qian, Y., Long, Y., Shen, D., Fang, C., Yao, J. and Liu, J. (2021) Drivers and ecological consequences of arsenite detoxification in aged semi-aerobic landfill. Journal of Hazardous Materials 420.
Noguchi, H., Park, J. and Takagi, T. (2006) MetaGene: prokaryotic gene finding from environmental genome shotgun sequences. Nucleic acids research 34(19), 5623-5630.
Palmgren, M., Engstrom, K., Hallstrom, B.M., Wahlberg, K., Sondergaard, D.A., Sall, T., Vahter, M. and Broberg, K. (2017) AS3MT-mediated tolerance to arsenic evolved by multiple independent horizontal gene transfers from bacteria to eukaryotes. Plos One 12(4).
Pan, F., Guo, Z., Cai, Y., Liu, H., Wu, J., Fu, Y., Wang, B. and Gao, A. (2019) Kinetic Exchange of Remobilized Phosphorus Related to Phosphorus-Iron-Sulfur Biogeochemical Coupling in Coastal Sediment. Water Resources Research 55(12), 10494-10517.
Parks, D.H., Imelfort, M., Skennerton, C.T., Hugenholtz, P. and Tyson, G.W. (2015) CheckM: assessing the quality of microbial genomes recovered from isolates, single cells, and metagenomes. Genome Research 25(7), 1043-1055.
Qin, J., Lehr, C.R., Yuan, C., Le, X.C., McDermott, T.R. and Rosen, B.P. (2009) Biotransformation of arsenic by a Yellowstone thermoacidophilic eukaryotic alga. Proceedings of the National Academy of Sciences of the United States of America 106(13), 5213-5217.
Qin, J., Rosen, B.P., Zhang, Y., Wang, G., Franke, S. and Rensing, C. (2006) Arsenic detoxification and evolution of trimethylarsine gas by a microbial arsenite S-adenosylmethionine methyltransferase. Proceedings of the National Academy of Sciences of the United States of America 103(7), 2075-2080.
Rawle, R., Saley, T.C., Kang, Y.-S., Wang, Q., Walk, S., Bothner, B. and McDermott, T.R. (2021) Introducing

the ArsR-Regulated Arsenic Stimulon. Frontiers in Microbiology 12.
Rehman, K. and Naranmandura, H. (2012) Arsenic metabolism and thioarsenicals. Metallomics 4(9), 881-892.
Reimer, K.J., Koch, I. and Cullen, W.R. (2010) Organoarsenicals. Distribution and transformation in the environment. Metal ions in life sciences 7, 165-229.
Scanlan, D.J., Ostrowski, M., Mazard, S., Dufresne, A., Garczarek, L., Hess, W.R., Post, A.F., Hagemann, M., Paulsen, I. and Partensky, F. (2009) Ecological Genomics of Marine Picocyanobacteria. Microbiology and Molecular Biology Reviews 73(2), 249-+.
Shannon, P., Markiel, A., Ozier, O., Baliga, N.S., Wang, J.T., Ramage, D., Amin, N., Schwikowski, B. and Ideker, T. (2003) Cytoscape: a software environment for integrated models of biomolecular interaction networks. Genome research 13(11), 2498-2504.
Shi, J., Vlamis-Gardikas, A., Aslund, F., Holmgren, A. and Rosen, B.P. (1999) Reactivity of glutaredoxins 1, 2, and 3 from Escherichia coli shows that glutaredoxin 2 is the primary hydrogen donor to ArsC-catalyzed arsenate reduction. The Journal of biological chemistry 274(51), 36039-36042.
Sun, Q., Lin, J., Ding, S., Gao, S., Gao, M., Wang, Y. and Zhang, C. (2019) A comprehensive understanding of enhanced Pb mobilization in sediments caused by algal blooms. Science of the Total Environment 691, 969-980.
Suzuki, M.T., Taylor, L.T. and DeLong, E.F. (2000) Quantitative analysis of small-subunit rRNA genes in mixed microbial populations via 5'-nuclease assays. Applied and environmental microbiology 66(11), 4605-4614.
Turpeinen, R., Pantsar-Kallio, M. and Kairesalo, T. (2002) Role of microbes in controlling the speciation of arsenic and production of arsines in contaminated soils. The Science of the total environment 285(1-3), 133-145.
Viacava, K., Meibom, K.L., Ortega, D., Dyer, S., Gelb, A., Falquet, L., Minton, N.P., Mestrot, A. and Bernier-Latmani, R. (2020) Variability in Arsenic Methylation Efficiency across Aerobic and Anaerobic Microorganisms. Environmental science & technology 54(22), 14343-14351.
Viacava, K., Qiao, J., Janowczyk, A., Poudel, S., Jacquemin, N., Meibom, K.L., Shrestha, H.K., Reid, M.C., Hettich, R.L. and Bernier-Latmani, R. (2022) Meta-omics-aided isolation of an elusive anaerobic arsenic-methylating soil bacterium. Isme Journal.
Vriens, B., Lenz, M., Charlet, L., Berg, M. and Winkel, L.H.E. (2014) Natural wetland emissions of methylated trace elements. Nature Communications 5.
Walters, W., Hyde, E.R., Berg-Lyons, D., Ackermann, G., Humphrey, G., Parada, A., Gilbert, J.A., Jansson, J.K., Caporaso, J.G., Fuhrman, J.A., Apprill, A. and Knight, R. (2016) Improved Bacterial 16S rRNA Gene (V4 and V4-5) and Fungal Internal Transcribed Spacer Marker Gene Primers for Microbial Community Surveys. Msystems 1(1).
Wang, P.-P., Sun, G.-X. and Zhu, Y.-G. (2014) Identification and Characterization of Arsenite Methyltransferase from an Archaeon, Methanosarcina acetivorans C2A. Environmental science & technology 48(21), 12706-12713.
Webster, T.M., Reddy, R.R., Tan, J.Y., Van Nostrand, J.D., Zhou, J., Hayes, K.F. and Raskin, L. (2016) Anaerobic Disposal of Arsenic-Bearing Wastes Results in Low Microbially Mediated Arsenic Volatilization. Environmental science & technology 50(20), 10951-10959.
WHO (2017) Guidelines for drinking-water quality: fourth edition incorporating the first addendum, WHO, Geneva, Switzerland. .
Wu, M. and Scott, A.J. (2012) Phylogenomic analysis of bacterial and archaeal sequences with AMPHORA2. Bioinformatics 28(7), 1033-1034.
Wu, Y.-W., Simmons, B.A. and Singer, S.W. (2016) MaxBin 2.0: an automated binning algorithm to recover genomes from multiple metagenomic datasets. Bioinformatics 32(4), 605-607.
Xiao, K.Q., Li, L.G., Ma, L.P., Zhang, S.Y., Bao, P., Zhang, T. and Zhu, Y.G. (2016) Metagenomic analysis revealed highly diverse microbial arsenic metabolism genes in paddy soils with low-arsenic contents. Environmental Pollution 211, 1-8.
Xie, C., Mao, X., Huang, J., Ding, Y., Wu, J., Dong, S., Kong, L., Gao, G., Li, C.-Y. and Wei, L. (2011) KOBAS 2.0: a web server for annotation and identification of enriched pathways and diseases. Nucleic acids research 39, W316-W322.
Yan, M., Zeng, X., Wang, J., Meharg, A.A., Meharg, C., Tang, X., Zhang, L., Bai, L., Zhang, J. and Su, S. (2020) Dissolved organic matter differentially influences arsenic methylation and volatilization in paddy soils. Journal of Hazardous Materials 388.
Yang, S., Zhai, W., Tang, X., Gustave, W., Yuan, Z., Guo, T. and Shu, Y. (2021) The Effect of Manure Application on Arsenic Mobilization and Methylation in Different Paddy Soils. Bulletin of environmental contamination and toxicology.
Zhang, J., Cao, T., Tang, Z., Shen, Q., Rosen, B.P. and Zhao, F.-J. (2015) Arsenic Methylation and Volatilization by Arsenite S-Adenosylmethionine Methyltransferase in Pseudomonas alcaligenes NBRC14159. Applied and environmental microbiology 81(8), 2852-2860.
Zhang, J., Chen, J., Wu, Y.-F., Liu, X., Packianathan, C., Nadar, V.S., Rosen, B.P. and Zhao, F.-J. (2022) Functional characterization of the methylarsenite-inducible arsRM operon from Noviherbaspirillum denitrificans HC18. Environmental Microbiology 24(2), 772-783.

LEACHING RISK AND DECHLORINATION POTENTIAL OF PCDD/FS UNDER CO-LANDFILL SCENARIO OF STABILIZED FLY ASH AND MSW

Yingjie Sun[1] *, Mingxue Xin[1], Weihua Li[1]

1. School of Environmental and Municipal Engineering, Qingdao University of Technology, 777 Jialingjiang Road, Qingdao 266033, China

ABSTRACT

With the development of incineration technologies, incineration has become the most common treatment method of municipal solid waste in China. However, stabilized fly ash may enter landfills during the transition from landfill to incineration, which caused uncertain impact on landfill waste stabilization. Two simulated co-landfill columns were constructed based on different co-landfill methods (layer co-landfill and mixed co-landfill) to investigate the effect of stabilized fly ash co-landfilled municipal solid waste for bacterial community succession and change in metabolic pathways during hydrolysis-acidogenesis stage. The mixed co-landfill method resulted in higher degree of organic matter degradation, and the concentrations of volatile fatty acids (VFA) and chemical oxygen demand (COD) in leachate were higher. The dominant phyla were Firmicutes in the layered co-landfill column and Bacteroidetes in mixed co-landfill column. The dominant genera for the total bacterial composition and VFA production were different, Pseudomonas and Propionibacterium, Proteiniphilum and unclassified Bacteroides were the dominant genera responsible for VFA generation in the layered and mixed colandfill columns.

KEYWORDS

Municipal solid waste (MSW), Co-landfill, Stabilized fly ash, VFA production

1. INTRODUCTION

With urbanization and an increase in the urban population, the mass production of municipal solid waste (MSW) poses potential risks to human health and the environment **(Wijekoon et al., 2022)**. Owing to its low construction cost and simple operation, landfill treatment is important for the disposal of MSW. The stabilization process in landfills includes hydrolysis, acidogenesis and methanogenesis to remove degradable organic matter from MSW. The hydrolysis and acidogenesis stages of MSW degradation are long-term processes, which limit methanogenesis and restrict the stabilization process of landfill **(Kjeldsen et al., 2002)**. Therefore, determining the metabolic pathways of MSW degradation during the hydrolysis and acidogenesis stages is essential for landfill stabilization. By analyzing the bacterial community composition in actual landfill, **Wang et al. (2022)** elucidated the change in bacterial community structure and metabolic pathways in response to changes in landfill age. Although the microbial composition and metabolic pathways in landfills have been determined, some studies have indicated that changes in environmental factors affect their stability and the metabolic processes of landfills **(Xu et al., 2017)**.

Incineration has gradually been developed as another major treatment method because of its advantage of volume reduction and energy recovery. Fly ash (FA) generated through MSW incineration contains abundant heavy metals and dioxins, and is recognized as hazardous waste. However, the scenario of solidified/stabilized FA co-landfilled with MSW may occur because of inappropriate management of MSW landfills. Numerous microorganisms in landfills participate in the degradation of MSW. Previous studies have shown that landfill age has significant impact on leachate characteristics, for most leachate parameters, leachate concentration increases before middle age and then decreased away towards landfill maturity **(Gautam and Kumar, 2021)**. It is necessary to study

the potential threat of stabilized FA co-landfilled MSW for the stabilized process of MSW landfills. In this study, simulated co-landfill columns of stabilized FA and MSW based on different co-landfill methods were constructed. Change in the bacterial community and the relative abundance changes of genes related to VFAs production were explored. Moreover, changes in the metabolic pathways during the hydrolysis and acidogenesis stage and the dominant microorganism for VFA production at different stages were further elucidated.

2. MATERIALS AND METHODS

2.1 Materials

Raw MSW originated from a campus waste recovery site in Qingdao, China. All refuse was broken into pieces of <5 cm in size and homogeneously mixed before landfill. The moisture content of wet synthetic MSW was 70.10 % and the loss on ignition (LOI) was 18.99 %. Incineration FA was obtained from the reciprocating grate furnace of typical MSWI power plants in Qingdao. Chelating agent (sodium dietyldithiocarbamate; industrial grade) was always used to stabilize FA and inhibit the dissolution of heavy metals and dioxins. The stabilization treatment conditions and homogenization process of stabilized FA can be found in previous studies **(Xin et al., 2022)**.

2.2. Experimental device and operation procedure

Two co-landfill columns (Fig. 1) of stabilized FA and MSW were designed with the dimensions of 1.8 m (height) × 0.3 m (inner diameter). Layered co-landfill method (column L) and mixed co-landfill method (column M) were constructed to simulate possible scenarios of actual landfill. The specific details of the co-landfill columns were shown in Fig.1. The co-landfill column was composed of water distribution region, co-landfill region of stabilized FA and MSW and leachate storage region. 15 kg of stabilized FA and 150 kg of MSW were landfilled in the co-landfill region. The co-landfill region of column L included two MSW layers and stabilized fly ash layer which was placed in the middle of column L, whereas stabilized FA and MSW were landfilled in the co-landfill region of column M after mixed homogeneously. Two ports were installed on the top of the column to exhaust gas and inject distilled water. Another port was installed on the bottom of column to collect leachate. Before the experiment, 8 L of distilled water was injected into the two columns to attain an appropriate moisture content for refuse degradation. To simulate actual landfill scenarios, the total inflow was designed to conforms to the local annual rainfall in Qingdao. Using a peristaltic pump, 4 L of distilled water was added weekly to each column at a rate of 10 mL/min. Before injecting 4 L distilled water next week, leachate was collected and stored at a temperature of 4 ◦C. Columns L and M were operated at ambient temperature under anaerobic conditions.

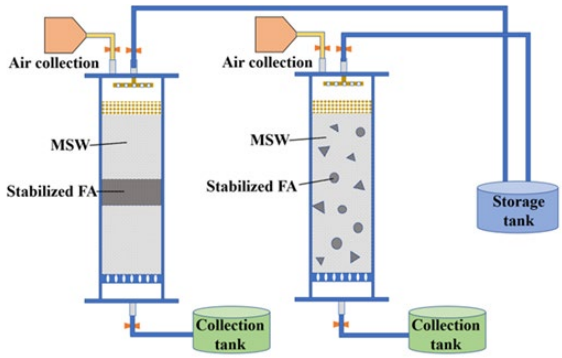

Fig. 1 The specific details of two co-landfill columns

2.3. Analytical methods

During operation of the anaerobic co-landfill columns, the leachate was collected in each column and filtered through 0.45 μm membrane before addition of each distilled water. The pH was measured using a pH meter (PHS–3C, Germany) and ORP was measured by ORP meter (WTW, Germany). VFA was determined by the distillation titration method. The COD concentration was measured using the potassium dichromate method (HACHDRB 200 Digestion Apparatus, USA). The concentration of acetate, propionate and butyrate in leachate were measured using gas chromatography (Agilent 6890-5975, USA). The solid samples were collected at 90d, 180d and

270d (L1, L2, L3 in column L and M1, M2, M3 in column M, respectively) and then storied at -80 ◦C.

3. Results and discussion

3.1. The change of leachate properties

Fig. 2 showed the trend of leachate properties during anaerobic co-landfill process. The initial pH of column M was approximately 10, which was significantly higher than that of column L (Fig. 2a). Eventually, the pH values in column M and L were maintained at approximately 6.3–6.5. The pH of column M was slightly higher than that in column L, indicating that the initial high pH still influenced the pH of the refuse system. The variation in the ORP was similar in column L and M, fluctuating at approximately -50 mV during the early stage and gradually decreasing to -300 mV. ORP between -200 to -400 mV is favorable for methanogenesis, and decrease in ORP increases the VFA evolution **(Ahmed et al., 2022)**. As shown in Fig. 2b, the initial VFA concentration was similar for column L and M. Subsequently, the VFA concentration significantly increased as anaerobic landfill progressed, and the maximum VFA concentration for column L and M reached 18,129 mg/L and 20,453 mg/L, respectively. The trend in the COD concentration was consistent with that of the VFA concentration. This result indicated that a higher degree of degradation was achieved in column M.

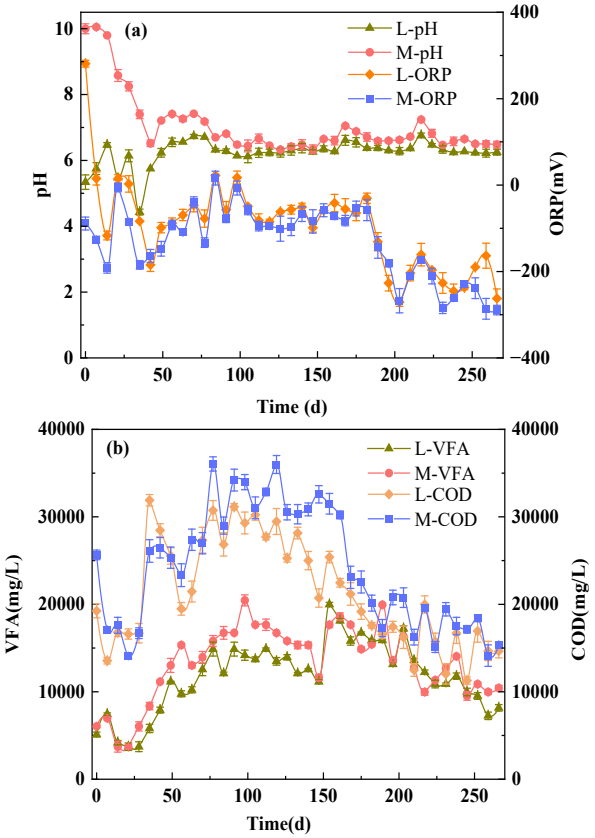

Fig. 2 The variation of leachate pH and ORP (a), VFA and COD (b) in each column (L and M represented the column that layered co-landfill way and mixed co-landfill way.)

Fig. 3 shows that the dominant VFAs was composed of acetate and butyrate at the initial stage of anaerobic co-landfill. The proportion of butyrate during this period was approximately 28–45 %, which was consistent with the result of the anaerobic degradation of lignocellulosic materials **(Li et al., 2020)**. After day 56, acetate was the main component and its proportion stabilized at approximately 42–55 % of the total VFAs. The percentage of propionate was low, and remained between 15 %–25 %. Acetate is important substrate for methane generation, and a low proportion of acetate in column L could inhibit methanogenesis and obstruct the stabilization of MSW.

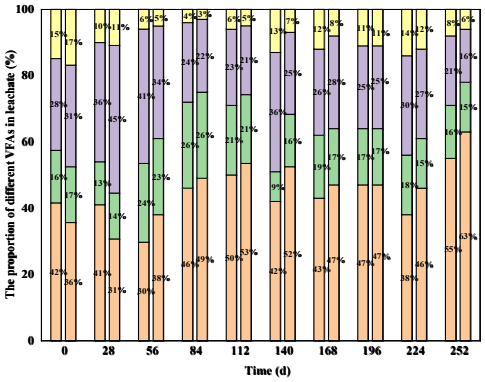

Fig. 3. The variations of acidification performance on proportion of VFAs (L and M represented the column that layered co-landfill way and mixed co-landfill way).

3.2. Dynamics succession of the bacterial community

3.2.1. Phylum level

The change in the bacterial community structure in each column at the phylum level was shown in Fig. 4. Firmicutes, Proteobacteria, Actinobacteria and Bacteroidetes were the main phylum during the anaerobic co-landfill process. The initial composition of the bacterial community was similar in columns L and M. The proportions of Firmicutes, Actinobacteria and Proteobacteria were 59.80 %, 22.31 % and 12.79 % in column L, which were 56.29 %, 23.93 % and 7.03 % in column M. Actinobacteria and Firmicutes released extracellular enzymes to accelerate the degradation of macromolecular organic matters and synthesize VFAs **(Zhou et al., 2022)**. During the middle stage, Proteobacteria and Bacteroidetes were the main phylum in column L, with proportion of 35.12 % and 48.42 %, respectively. However, Bacteroidetes was the predominant phylum in column M and its proportion increased to 85.56 %. Bacteroidetes contains abundant hydrolytic and acidogenic bacteria, which contribute to acidification and can survive at higher VFA concentration **(Zheng et al., 2022)**. In this study, Proteobacteria was closely related to hydrolysis, acidogenesis and acetogenesis process, whereas previous study indicated that Proteobacteria was important VFAs consumer. The low VFA concentration in column L may be related to the consumption by Proteobacteria. The bacterial community structure exhibited significant differences in columns L and M during the late stage. In column L, the bacterial community was primarily composed of Firmicutes, Proteobacteria and Bacteroidetes, whereas Bacteroidetes, Spirochaetes and Firmicutes were dominant in column M. The results indicated that the different co-landfill methods significantly changed the bacterial community structure during the co-landfill process, and the impact gradually increased as the landfill process advanced.

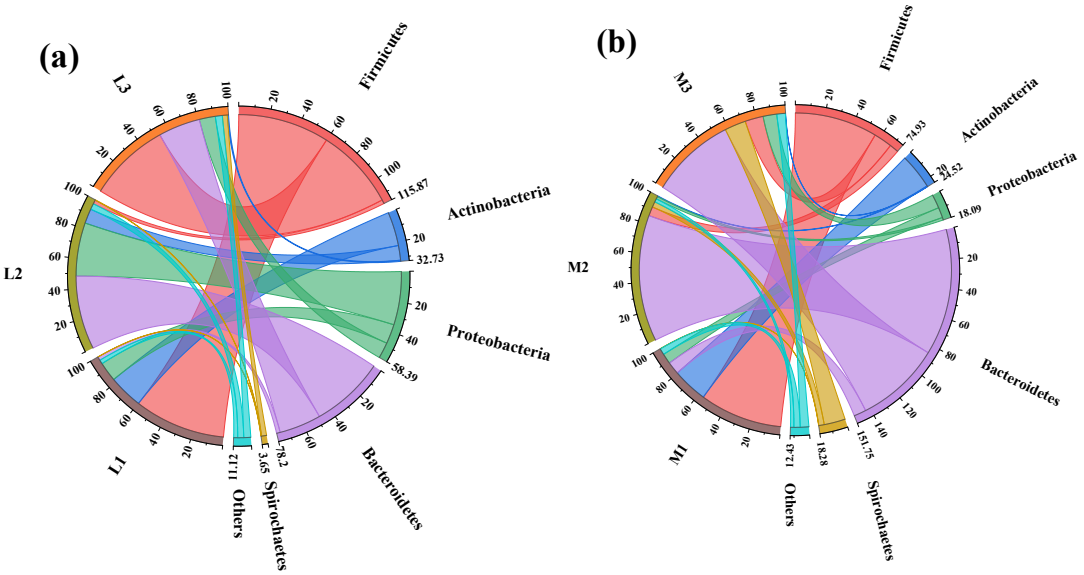

Fig. 4. Dynamics succession of bacterial community structure at the phylum level (L and M represented the column that layered co-landfill way and mixed co-landfill way.)

3.2.2. Genus level

As depicted in Fig. 5, the variations in bacterial community structure in each column were analyzed at the genus level during the entire co-landfill process. The dominant genus were Lapidilactobacillus, accounting for 26.63 %, followed by Propionibacterium (17.80 %), Amylolactobacillus (7.70 %) and Loigolactobacillus (4.54 %). Previous study indicated that Lapidilactobacillus and Amylolactobacillus always appeared with relatively high abundance in vegetable

environment **(Parente et al., 2023).** Lapidilactobacillus, Amylolactobacillus and Loigolactobacillus belong to the family Lactobacillaceae, which was the key player in starch degradation and are responsible for the production of acetate. Propionibacterium is well-known propionate producer, which actuates the enhancement of propionate production **(Atasoy et al., 2020)**. A higher abundance of Propionibacterium was observed in column M, accounting for 22.96 % at this stage. This result was consistent with the increase in the proportion of propionate during this period. Lapidilactobacillus (10.55 %) and Prevotella (7.26 %) were also the initial dominant genera in column M. Prevotella can degrade hemicellulose and starch to produce sugars, and further converted them to VFAs **(Ahmad et al., 2020)**. Although bacterial community structures at the phylum level were similar at the initial stage, difference at the genus level could be observed for the different co-landfill methods.

Significant difference at the genus level was observed in columns L and M during the middle and late stages. In the middle stage, unclassified Bacteroidales was most dominant genus, accounting for 25.92 % in column L and 46.44 % in column M. Bacteroidales could convert macromolecular organic matter to acetate and succinate, which was consistently the largest contributor across all organic load conditions in most anaerobic digestion **(Mercado et al., 2022)**. In the late stage, the relative abundance decreased to 17.02 % in column L, whereas that in column M maintained at 40.26 %. Previous study indicated that Bacteroidales and other genus in anaerobic digestion could enhance methane yield through synergistic interactions, which may promote methanogenesis **(Tukanghan et al., 2021)**. In the middle stage, Propionibacterium was the dominant genus, which accounted for 6.16 % in column L. However, Propionibacterium was replaced by unclassified Porphyromonadaceae (7.89 %) in column M, and propionate is the main product of Porphyromonadaceae **(Atasoy et al., 2020)**. With the progression of landfill process, the differences in microbial composition at the genus level for the two co-landfill methods significantly increased, indicating that the co-landfill method changed the microbial community structure during the landfill process. By comparing the microbial composition of the two co-landfill ways, higher organic matter degradation ability was observed in the mixed co-landfill method, which was consistent with the changes in leachate characteristics.

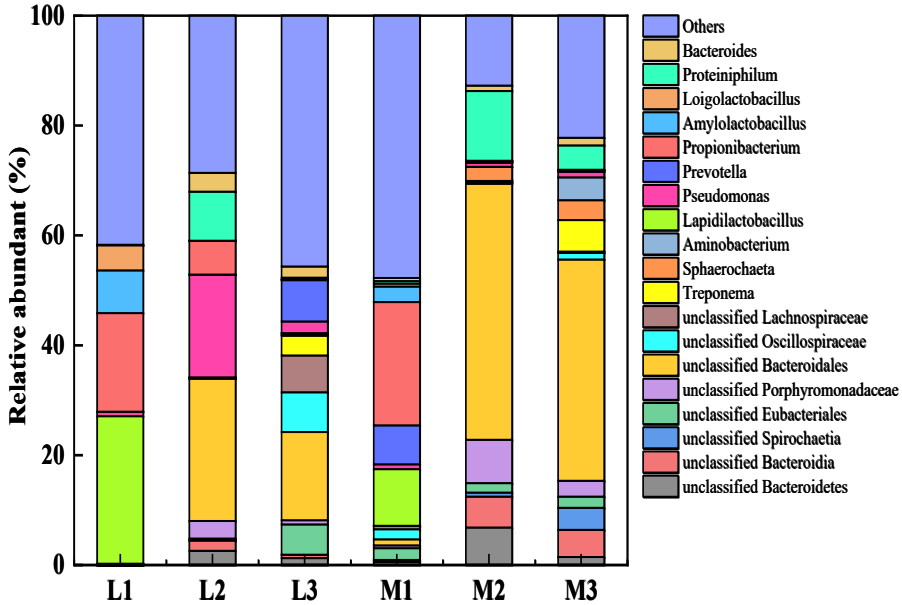

Fig. 5. Dynamics succession of bacterial community structure at the genus level (L and M represented the column that layered co-landfill way and mixed co-landfill way).

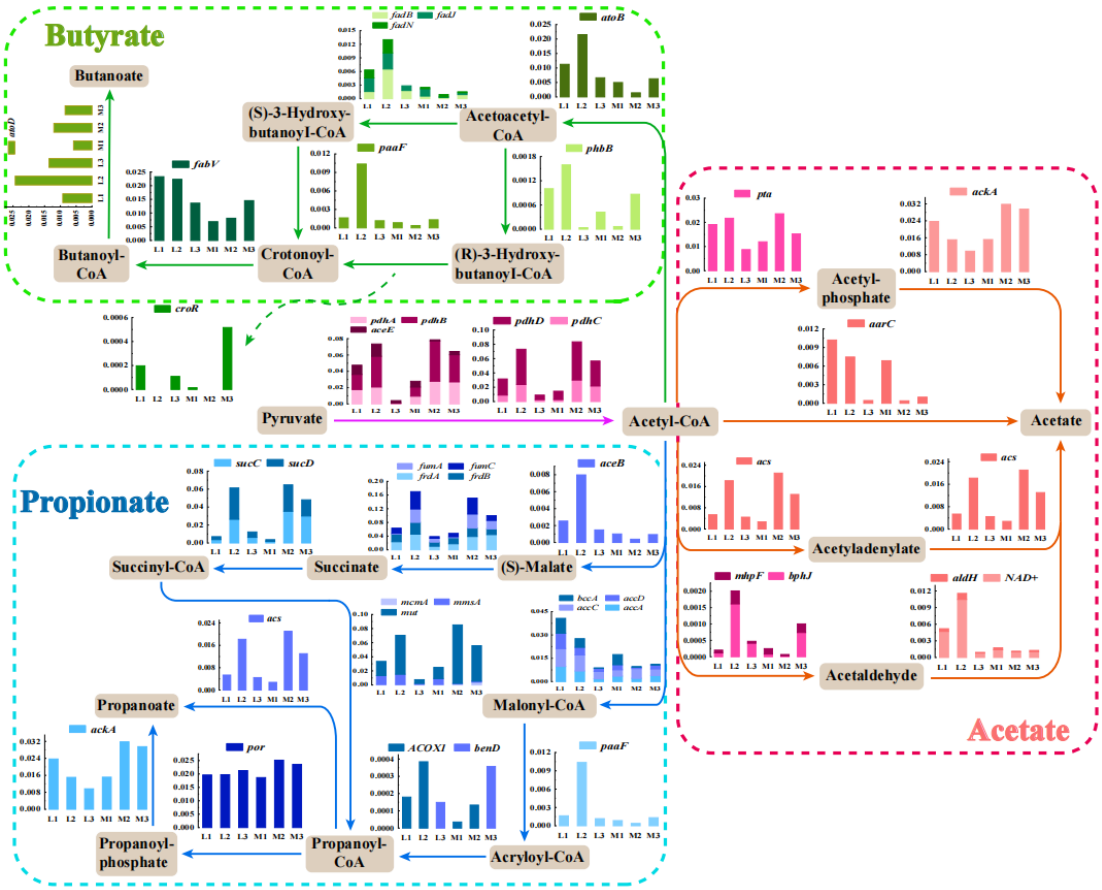

Fig. 6. Relative abundances of main genes encoding key enzymes for acetate, Propionate and butyrate production. The relative abundance of genes in each sample was shown in colored bar charts. (L and M represented the column that layered co-landfill way and mixed co-landfill way).

3.3. The variation in genes encoding key enzymes for VFA production

Acetate, propionate and butyrate are the most abundant VFAs produced by microorganisms and are the main substrates for subsequent methane production. The biosynthesis and metabolism of three VFAs are essential for anaerobic landfill stabilization process of refuse **(Wang et al., 2022)**. The variation in the relative abundance of the main genes encoding key enzymes for acetate, propionate and butyrate production was shown in Fig. 6. Glycolysis was the dominant metabolic pathway for VFAs production during the entire co-landfill process, and pyruvate was essential intermediate product for VFAs biosynthesis. The initial relative abundance of pdh encodes pyruvate dehydrogenase was higher in column L, whereas high relative abundant of pdh was observed in column M in the middle and late stages. These results suggested that the layered co-landfill method initially stimulated the degradation of organic matter and inhibited the activity of microorganisms in the late stage. The change in relative abundance of pdh may explain the low production of total VFA in column L. Previous studies indicated that pH is important factor affecting the abundance of pta and ack during anaerobic digestion process **(Liang et al., 2021)**. The acs encoding acetyl-CoA decarbonylase is a high affinity pathway for acetate anabolism **(Krivoruchko et al., 2015)**. The relative abundance of pta, ack and acs were high in the early stage of column L and low in the middle to late stages, which was opposite to the relative abundant variation of column M. The middle and late stage were

crucial for VFA production, high expression of acetate biosynthesis genes was consistent with the high proportion of acetate in column M. With regard to propionate production, aceB, benD and ACOX1 are crucial genes for propionate biosynthesis. However, the low relative abundance of aceB, benD and ACOX1 inhibited propionate production, which could lead to the low proportion of propionate in the total VFA concentration. For butyrate production, the relative abundance of genes related to butyrate synthesis in column L was significantly higher than that in column M during whole co-landfill process, which was consistent with the high proportion of butyrate in column L. Butyryl-CoA reacts with acetate to form butyrate, along with the regeneration of acetyl-CoA, which also decrease the percentage of acetate in column L **(Ding et al., 2010)**. Different co-landfill methods have a significant impact on the VFAs production. In general, the layered co-landfill method promoted the production of butyrate, while the mixed co-landfill method increased the proportion of acetate, which also caused different impacts on the refuse stabilization process. The result also indicated that the change in co-landfill methods influenced the metabolic pathways of organic matter during the early stage of co-landfill process.

4. Conclusion

In this study, the degradation process of organic matter was investigated for the co-landfill scenario of stabilized fly ash and MSW. Different co-landfill methods changed the microbial composition and metabolic pathways of VFAs production. High VFA concentration and acetic acid proportion can be observed in mixed co-landfill method. The initial microbial composition of the two co-landfill columns is similar, whereas subsequently dominant phylum in layered co-landfill column was Firmicutes and Bacteroidetes was dominant in mixed co-landfill column. Higher abundance of genes related to butyrate production was observed in the layered co-landfill column. For genus related to VFA production, Pseudomonas and Propionibacterium, Proteiniphilum and unclassified Bacteroide were dominant in the layered and mixed co-landfill columns. Layered co-landfill inhibited microbial metabolic activity in late stage, resulting in a significant decrease in the relative abundance of metabolic genes. During the landfill process, a large amount of stabilized FA should be prohibited from entering the landfill site.

REFERENCES

Ahmad, A.A., Yang, C., Zhang, J., Kalwar, Q., Liang, Z., Li, C., Du, M., Yan, P., Long, R., Han, J., 2020. Effects of dietary energy levels on rumen fermentation, microbial diversity, and feed efficiency of yaks (Bos grunniens). Front. Microbiol. 11, 625.

Ahmed, B., Tyagi, S., Rahmani, A.M., Kazmi, A.A., Varjani, S., Tyagi, V.K., 2022. Novel insight on ferric ions addition to mitigate recalcitrant formation during thermalalkali hydrolysis to enhance biomethanation. Sci. Total Environ. 829, 154621.

Atasoy, M., Eyice, O., Schnürer, A., Cetecioglu, Z., 2019. Volatile fatty acids production via mixed culture fermentation: revealing the link between pH, inoculum type and bacterial composition. Bioresour. Technol. 292, 121889.

Ding, H.B., Tan, G.Y.A., Wang, J.Y., 2010. Caproate formation in mixed-culture fermentative hydrogen production. Bioresour. Technol. 101, 9550–9559.

Gautam, P., Kumar, S., 2021. Characterization of hazardous waste landfill leachate and its reliance on landfill age and seasonal variation: a statistical approach. J. Environ. Chem. Eng. 9, 105496.

Kjeldsen, P., Barlaz, M.A., Rooker, A.P., Baun, A., Ledin, A., Christensen, T.H., 2002. Present and long-term composition of MSW landfill leachate: a review. Crit. Rev. Environ. Sci. Technol. 32, 297–336.

Krivoruchko, A., Zhang, Y., Siewers, V., Chen, Y., Nielsen, J., 2015. Microbial acetyl-CoA metabolism and metabolic engineering. Metab. Eng. 28, 28–42.

Li, Y., Xu, H.P., Hua, D.L., Zhao, B.F., Mu, H., Jin, F.Q., Meng, G.F., Fang, X., 2020. Two-phase anaerobic digestion of lignocellulosic hydrolysate: focusing on the acidification with different inoculum to substrate ratios and inoculum sources. Sci. Total Environ. 699, 134226.

Liang, J.S., Fang, W., Wang, Q.Y., Zubair, M., Zhang, G.M., Ma, W.F., Cai, Y.J., Zhang, P. Y., 2021. Metagenomic analysis of community, enzymes and metabolic pathways during corn straw fermentation with rumen microorganisms for volatile fatty acid

production. Bioresour. Technol. 342, 126004.
Mercado, J.V., Koyama, M., Nakasaki, K., 2022. Short-term changes in the anaerobic digestion microbiome and biochemical pathways with changes in organic load. Sci. Total Environ. 813, 152585.
Parente, E., Zotta, T., Giavalisco, M., Ricciardi, A., 2023. Metataxonomic insights in the distribution of Lactobacillaceae in foods and food environments. Int. J. Food Microbiol. 391–393, 110124.
Tukanghan, W., Hupfauf, S., Gomez-Brand ´ on, ´ M., Insam, H., Salvenmoser, W., Prasertsan, P., Cheirsilp, B., O-Thong, S., 2021. Symbiotic Bacteroides and Clostridium-rich methanogenic consortium enhanced biogas production of highsolid anaerobic digestion systems. Bioresour. Technol. Rep. 14, 100685.
Wang, Y.N., Xu, R., Wang, H.W., Shi, H., Kai, Y., Sun, Y.J., Li, W.H., Bian, R.X., Zhan, M. L., 2022. Insights into the stabilization of landfill by assessing the diversity and dynamic succession of bacterial community and its associated bio-metabolic process. Sci. Total Environ. 768, 145466.
Wiegel, J., Tanner, R., Rainey, F.A., 2006. An introduction to the family Clostridiaceae. Prokaryotes 4, 654–678.
Xin, M.X., Sun, Y.J., Wu, Y.K., Li, W.H., Yin, J.Q., Long, Y.Y., Wang, X.B., Wang, Y.N., Huang, Y.M., Wang, H.W., 2022. Stabilized MSW incineration fly ash co-landfilled with organic waste: leaching pattern of heavy metals and related influencing factors. Process Saf. Environ. Prot. 165, 445–452.
Xu, S., Lu, W.J., Liu, Y.T., Ming, Z.Y., Liu, Y.J., Meng, R.H., Wang, H.T., 2017. Structure and diversity of bacterial communities in two large sanitary landfills in China as revealed by high-throughput sequencing (MiSeq). Waste Manag. 63, 41–48.
Zhou, X., Lu, Y., Huang, L., Zhang, Q., Wang, X., Zhu, J., 2021. Effect of pH on volatile fatty acid production and the microbial community during anaerobic digestion of Chinese cabbage waste. Bioresour. Technol. 336, 125338.

LIFE CYCLE COST ASSESSMENT OF SOLIDIFICATION-TYPE LANDFILL SYSTEM FOR INCINERATION RESIDUES

Yuki Komori[1)] Hirofumi Nakayama[2)] Takayuki Shimaoka[2)]

1）GRADUATE SCHOOL OF ENGINEERING, KYUSHU UNIVERSITY, MOTOOKA744 FUKUOKA CITY, JAPAN

2）FACULTY OF ENGINEERING, KYUSHU UNIVERSITY, MOTOOKA744 FUKUOKA CITY, JAPAN

1. INTRODUCTION

In a solidification-type landfill system, incineration residue is mixed with cement and water, and then vibrationally solidified by the superfluid method to form a strong and environmentally safe ground. The authors have shown that solidification-type landfill system reduce life-cycle costs (LCC) because of smaller construction costs and shorter maintenance periods compared to conventional disposal systems. However, the conditions for calculating LCC, such as water

Table 1：Evaluation items at each life cycle stage

Life Cycle Stage / Landfill	Construction stage	Service period	Maintenance period	Abolition	Preparation for site use
Conventional landfill	・Landfill site civil works ・Leachate treatment facility construction	・Conventional reclamation work: Spreading, compaction, same-day soil covering, intermediate soil covering ・Leachate treatment ・Monitoring ・Maintenance and repair	・Leachate treatment ・Monitoring	Final soil covering	Ground improvement: dynamic consolidation method
Solidification-type landfill	・Landfill site civil works ・Leachate treatment facility construction ・Batcher plant construction	・Solidification-type disposal operations: Magnetic sorting, sifting, mixing of cement, water, and incineration residue, vibration compaction ・Surface water treatment ・Monitoring ・Maintenance and repair	・Surface water treatment ・Monitoring	Final soil covering	

Scope of this study

balance, the time required to meet water quality standards, and the number of equipment and heavy machinery required for solid waste landfill, were set based on pilot-scale experiments, and data based on demonstration tests that reproduced the construction and operation of a solid waste landfill under conditions similar to those of a full-scale landfill should be used to reexamine LCC It was necessary to reconsider the LCC using data based on demonstration tests that reproduced the construction and operation of a solid waste landfill under conditions close to those of a real landfill. Therefore, it was necessary to reexamine the LCCs based on the data from the demonstration test at the solid waste landfill in the F City landfill site. The objective of this study was to demonstrate the usefulness of the solidified landfill by reexamining the condition settings and calculating LCCs based on the data from the demonstration test at the solidification-type landfill at the F-city landfill site.

2. ESTABLISHMENT OF FINAL DISPOSAL SITE

Table 1 shows the evaluation items for each life cycle stage. The cost of each process was calculated and the LCCs of conventional and solidified landfills were compared and evaluated.

Scale of Final Disposal Site

Table 2 shows the various conditions of the final disposal sites set up. Two cases were set up for this study: a conventional landfill and a solidified landfill with an annual landfill capacity of 5,000 t/year (small) and 10,000 t/year (large) of

Table 2： Final Landfill Site Conditions

Item	Conventional type 100,000t	Solidification type 100,000t	Conventional type 1,000,000t	Solidification type 1,000,000t
Incineration residue landfilled per year (thousand tons/year)	5		50	
Years of landfill service (years)	20			
Total incineration residue landfilled (thousand tons)	100		1,000	
Volume of incineration residue and incineration residue solidified for landfill disposal (thousand m^3)	78.8	76.9	788	769
Volume of immediate and intermediate cover soil (thousand m^3)	15.8	0.0	158	0.0
Landfill volume (m^3)	94.6	76.9	946	769
Average depth of landfill (m)	20			
Landfill area (thousand m^2)	4.73	3.84	47.3	38.4
Number of landfill plots	1	5	5	10
Maintenance period (years)	15	3	15	3

incineration residue, respectively. The landfill depth was set at 20 m, and the service period was set at 20 years. Furthermore, the solidified landfill does not require a soil cover, and the volume of the landfill can be reduced by 23% compared to the conventional type because the volume is reduced by vibratory compaction using the superfluid method. The mixing ratio of solidified materials obtained from the demonstration test data is shown in Table 3. The unit volume weight of the solidified material was calculated as 1.50 t/m^3.

Setup Conditions for Water Balance and Water Treatment

The rainwater distribution rates for conventional and solidified landfills, assuming a rainfall rate of 1, are shown below. For the conventional landfill, surface water, evaporation rate, and leachate were calculated as 0.5, 0.28, and 0.22, respectively, for the landfill termination zone. For the landfill-in-progress section, no surface water was assumed to be generated, and calculations were performed assuming surface water 0, evaporation rate 0.28, and leachate 0.72. For the solidified landfill, calculations were made based on the data from the demonstration test4) , assuming 0.28 surface water, 0.72 evaporation rate, and 0 leachate for both the in-landfill and landfill-completed compartments. The demonstration tests showed that very little leachate is generated in the solidified landfill. It was also confirmed that a large amount of surface water is generated and that the quality of the surface water satisfies the standard after one year. Therefore, it was decided to provide water treatment for surface water for three years after the landfill is completed. In order to reduce the amount of surface water treatment, surface water generated from parcels during reclamation and within three years after reclamation was assumed to flow through an independent stormwater collection channel to the water treatment facility, while surface water from parcels three years after reclamation was completed was not treated and discharged.

Ground Improvement for Site Utilization

In conventional landfills, ground improvement is required for advanced utilization of the site after reclamation is completed. In this study, calculations were performed assuming dynamic consolidation as the ground improvement method. The cost of ground improvement was calculated by multiplying the estimated standard construction cost by the area where the site is to be utilized.

3. LCC CALCULATION RESULTS

Calculation Results of LCC Per Ton of Incineration

Table 3：Mixing ratio of solidified materials

Item	Incinerator ash	Fly ash	Cement	Water
Mixing ratio of mixing materials (%)	65.9	21.1	7.8	5.2

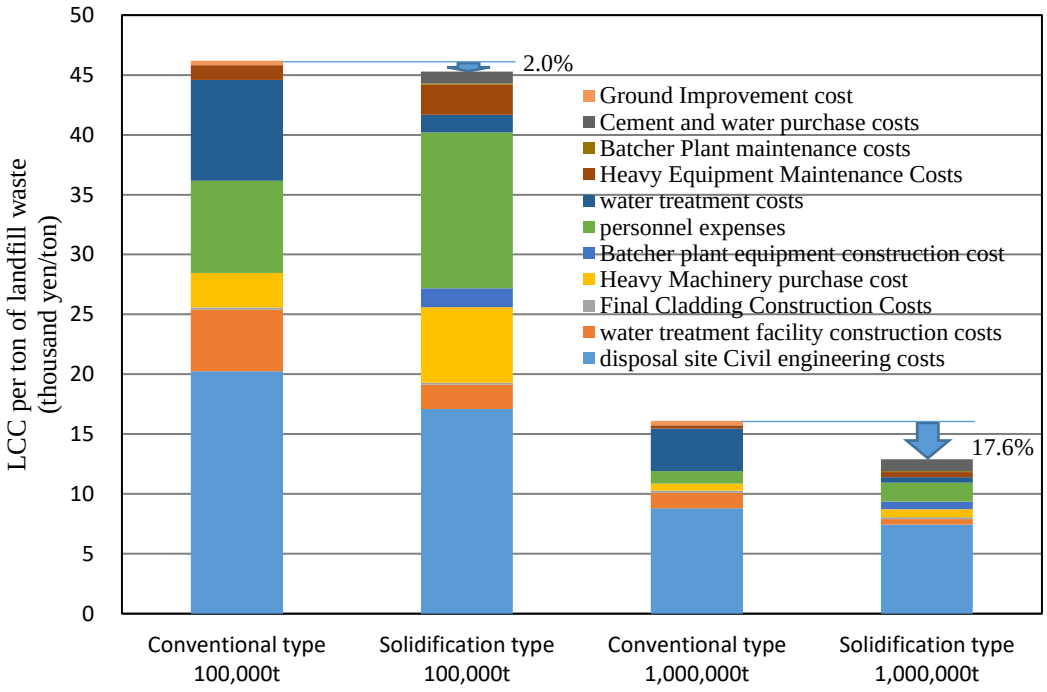

Figure 1 ：LCC from start of reclamation to ground improvement

Residue

Figure 1 shows the calculation results of LCC from the start of landfill to ground improvement for site utilization. The LCC per ton of landfill waste was 46.2 thousand yen/ton for the conventional type (100,000 tons) and 45.3 thousand yen/ton for the solidified type (100,000 tons), with the solidified type having an LCC approximately 2.0% lower than the conventional type. The LCC of the conventional type (1 million tons) was 16.1 thousand yen/t and that of the solidified type (1 million tons) was 12.9 thousand yen/t. The LCC of the solidified type was approximately 17.6% lower than that of the conventional type. The solidification type has lower costs for landfill site civil engineering, water treatment facility (conventional type: leachate treatment, solidification type: surface water treatment) construction, and treatment, while labor costs and heavy equipment purchase costs are higher.

LCC Calculation Results at Each Life Cycle Stage

Figure 2 shows the LCC calculation results for each life cycle stage. In the construction stage, the LCC is about 13.7% lower than that of the conventional type because the civil engineering costs for the landfill site and the water treatment facility construction costs for the solidification type are smaller than those for the conventional type. During the service period, the cost of leachate treatment for the solidification type was smaller than that for the conventional type, but the LCC was about 9.1% larger due to the higher cost of purchasing heavy equipment, labor, cement, and water. During the maintenance

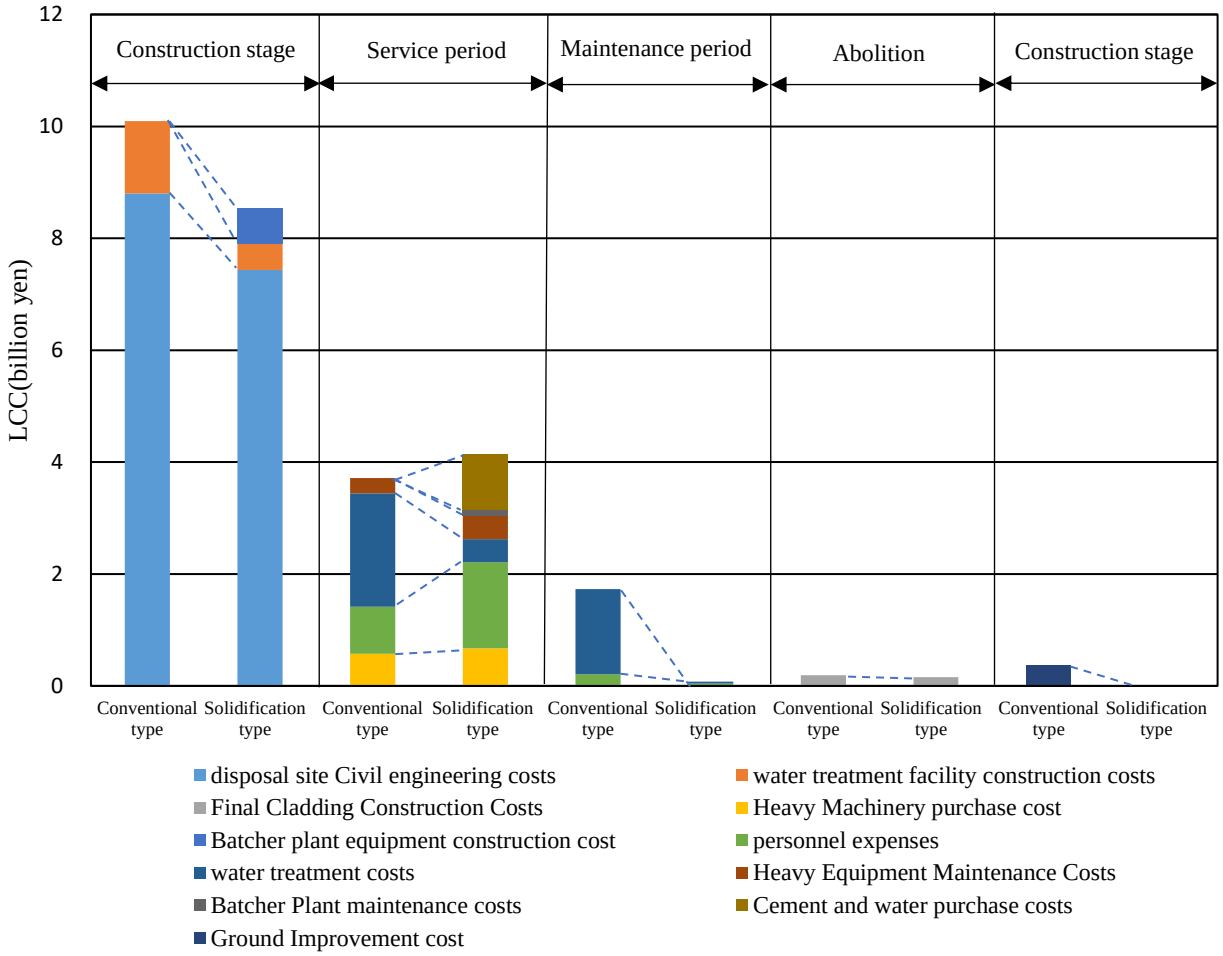

Figure 2：LCC calculation results for each life cycle stage

period, the solidification type requires a shorter maintenance period than the conventional type, and the leachate treatment cost can be significantly reduced.

4. CONCLUSION

・The LCC per ton of landfill waste was 49.0 thousand yen/ton for the conventional type (100,000 tons) and 45.3 thousand yen/ton for the solidification-type (100,000 tons), indicating that the solidification-type has an LCC about 2.0% smaller than the conventional type, and 18.9 thousand yen/ton for the conventional type (1,000,000 tons) and 12.9 thousand yen/ton for the solidified type The LCC of the solidification-type is about 17.6% lower than that of the waste disposal method.

・In the construction stage, the LCC of the solidification-type is about 13.7% lower than that of the conventional type, because the civil engineering cost for the landfill and the construction cost of the water treatment facility are smaller. During the service period, the cost of leachate treatment for the solidification-type was

smaller than that for the conventional type, but the LCC was about 9.1% larger because the cost of purchasing heavy equipment, labor, cement, and water was higher. In terms of maintenance period, the leachate treatment cost can be significantly reduced because the maintenance period of the solidification type is shorter than that of the conventional type.

REFERENCES

1) Takayuki Shimaoka, Teppei Komiya, Hirofumi Nakayama, Fuminori Hirosue, Hiroyuki Akita, Hiroyoshi Kasa, Isamu Sandanbata: Development of new technology for environmentally safe and robust final disposal site that can withstand a huge earthquake, Proceedings of the 26th Japan Society of Material Cycles and Waste Management, 2015, pp. 403-404, 2015.

2) Teppei Komiya, Daisuke Murakawa, Takayuki Shimaoka, Fuminori Hirosue, Hiroyuki Akita, Takahiro Aoki, Hirofumi Nakayama: Study on mass transport and pore space change associated with hygroscopic and tidal processes in solidification-type disposal ground of incinerated waste residue, Proceedings of the 12th Symposium on Environmental Geotechnics, pp.111-118, 2017,

3) Koh Kawasaki, Hirofumi Nakayama, Takayuki Shimaoka: Life cycle cost of waste Solidification Disposal System: A Study on the Life Cycle Cost of Solidification Disposal System, Presentation at the 2017 JSCE Western Branch Research Conference, 2018.03,

4) Takayuki Shimaoka: Social Implementation Study of Solidification Disposal System Contributing to the Resilience of Waste Disposal System, End of Research Report of the General Environmental Research Promotion Fund, 2023.

How can waste plastics be recycled? ～The Possibility of Recycling Non-woven Masks Using the Solvent Extraction Method～

Kazutoshi Ikenaga*

Sojo University, 4-22-1 Ikeda, Nishi-ku, Kumamoto, 860-0082, Japan

*corresponding author: ikenaga@nano.sojo-u.ac.jp

Keywords: purification, polyethylene, solvent extraction method

INTRODUCTION

The global recovery of waste plastics has reached about 400 million tons, including about 60% polyethylene (PE) and polypropylene (PP). From the perspective of carbon resource recycling and carbon resource conservation, it is critical to establish methodologies that enable the effective use of recovered waste plastics to be implemented on a wide scale. In many cases, however, the purity of optically sorted PE and PP from recovered waste plastics is about 80% due to waste plastics with different shapes and multilayered food packaging plastics, limiting the purity to high levels. In order to promote effective utilization of recovered plastics, the speaker's laboratory has been researching and developing a rapid and simple purity measurement method using IR measurement for the purity of recovered PE and PP obtained from optical sorting [1]. The sample preparation method used at that time was to prepare uniform film samples by preparing homogeneous solutions of PE and PP in toluene, and the results of screening experiments to search for solvents showed that many aromatic compounds with alkyl chains have the solubility of PE and PP. Among them, only PE and PP were successfully extracted selectively from recovered PE and PP using mesitylene or cumene as good solvents below 200°C [2]. Although there have been many reports on good solvent-poor solvent separation methods, this is the first report on the use of mesitylene or cumene.

METHODS

Experimental Operation of Solvent Extraction

1.0095 g of recovered PE in a cotton bag and 87.0 g of mesitylene were placed in a Nas flask and heated to reflux for 1 hour. After cooling, the cotton bag was removed and acetone, a poor solvent for PE, was added, and the extract was completely precipitated. The precipitate was filtered off as a white solid by suction filtration. After drying, 0.8434 g of white solid was obtained, whose IR measurement was PE, indicating a recovery of 84%. Acetone and mesitylene were distilled from the filtrate and 0.0584 g of solvent

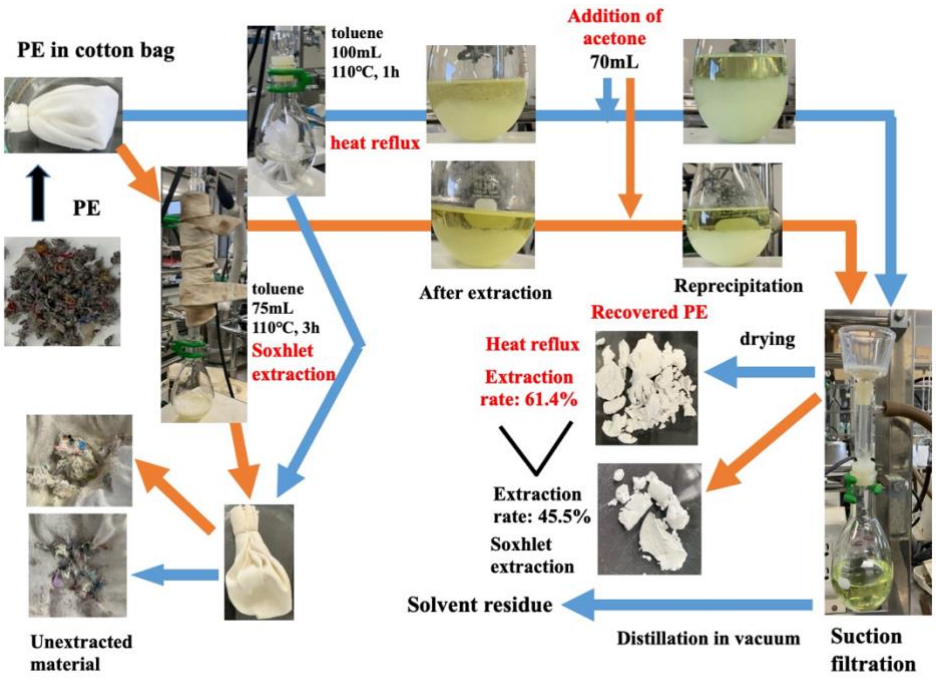

Figure 1. Extraction operation of PE using solvent extraction method

residue was yielded. In addition, 0.0691 g of unextracted material was recovered in a cotton bag (Figure 1).

RESULTS AND DISCUSSION

Aromatic compounds toluene, cumene, and mesitylene were used as extraction solvents to compare the extraction rates of recovered PE. Soxhlet extraction and in-flask extraction methods were used. In all experiments, the bags were removed after the extraction operation and acetone, a poor solvent for PE, was added to precipitate the extract. In the first experiment, the Soxhlet extraction method was performed using toluene, and the extraction rate was 49.1%. Since the temperature of the solvent receiver portion of the Soxhlet extractor was lower than the reflux temperature of toluene, a ribbon heater was used to maintain the temperature, but the extraction rate was low. On the other hand, the extraction rate increased to 60.5% when toluene was extracted in a cotton bag using the in-flask extraction method, which can receive sufficient heating. However, the extraction rate was still insufficient, so the use of cumene and mesitylene, which have high boiling points, increased the extraction rate to 84.4% and 83.5%, respectively. IR measurements of the recovered extract, the unextracted material remaining in the cotton bag, and the residue in the extraction solvent were performed. From those results, it was found that the recovered extract was mainly PE. However, since it is known that PP is also soluble in cumene and mesitylene, a separate purity measurement was performed, and it was also found to contain about 10% PP. On the other hand, the remaining unextracted material in the cotton bag was found to be PET and nylon; since acetone was used as a poor solvent for PE, the residue in the extraction solvent was found to contain ester compounds that may have been derived from polystyrene and printing inks. Very recently, we are starting to investigate the recovery of the waste non-woven PP disposable masks by this solvent extraction (Figure 2).

CONCLUSION

It was found that PE could be recovered efficiently from waste plastics by using this solvent extraction method. We plan to study solvent extraction of degraded PE in the future.

ACKNOWLEDGEMENT

The part of this study was supported to carry out by a Grant-in-Aid for Scientific Research (22K12452).

REFERENCES

[1] Patent 2019-506206; Kazutoshi Ikenaga, et al, 7th 3R International Scientific Conference on Material Circulation and Waste Management, Online, H-4, March 2021. [2] Kazutoshi Ikenaga, Yuki Morigami, 71st Annual Conference on Macromolecules, 3H07.

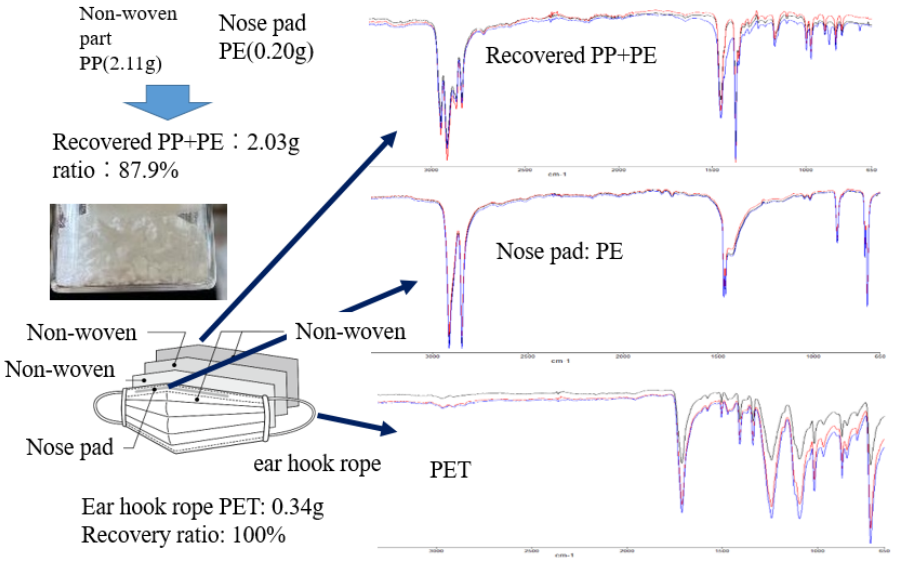

Figure 2. Recovery of PP (including PE) from PP non-woven "masks" using solvent extraction method

COMPARATIVE STUDY ON SURVEY METHODS FOR ESTIMATING THE AMOUNT OF PLASTIC FISHING GEAR DISCHARGED INTO THE OCEAN

Fumiya Ishibashi[1] Hirofumi Nakayama[2] Satoko Seino[2] Takayuki Shimaoka[2]

1）Graduate School of Engineering, Kyushu University, Motooka744, Fukuoka City, Japan

2）Faculty of Engineering, Kyushu University, Motoka744, Fukuoka City, Japan

1. INTRODUCTION

Marine plastics are recognised as an important issue that urgently needs to be resolved. Fisheries are considered to be one of the sources of marine plastic run-off and there is a need to establish a method to investigate the amount of plastic fishing gear discharged into the ocean. In this study, the amount of plastic fishing gear used and discharged by type was estimated and compared using two methods of surveying the amount of plastic runoff: a survey using logbooks kept by fishermen and a survey combining a questionnaire to fishermen and purchase records. The fishing method investigated was longline fishing1), which used a relatively high amount of plastic fishing gear per catch among the fishing boats. In estimating the amount of plastic gear discharged into the ocean using the two methods, plastic ocean discharge per tonne of catch, per day of operation and per kilometre of longline gear was calculated per management unit, per tonne of catch, per day of operation and per kilometre of longline gear trunk line. The unit volume of plastic marine runoff was calculated.

2. OVERVIEW OF LONGLINE FISHERIES, SCALE OF ACTIVITY AND VOLUME OF ACTIVITY SURVEYED

Figure 1 shows a diagram of a longline fishery. The trap consists of a trunk rope with a number of branch ropes attached to it and hooks attached to the ends of the branch ropes. In some cases, the entire trap may spill, while in other cases, a section of the trap may break, causing the float, trunk rope, branch rope, rope and other parts of the trap to spill. Information on the number of longline fisheries surveyed in this study, the scale of activity, including the number of longline fisheries, catch, number of days of operation and length of trunk rope, and the volume of activity is presented in Table 1. The

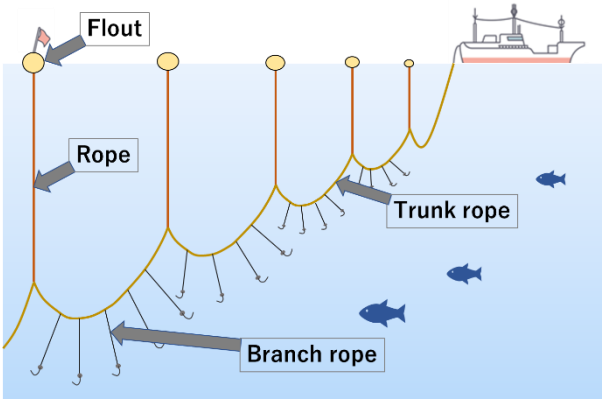

Figure 1: Diagram of longline fishing

number of days of operation and the length of the trunk rope are provided from the logbooks. The number of days of operation and the length of the mainline are the averages of the four operations that provided logbooks, while the catch. The catch was obtained from fishermen who were interviewed about their standard longline catch.

Survey method for recording gear spills in the logbooks

Four operators engaged in longline fishing were interviewed over a three-month period from January to March 2023. Four longliners engaged in longline fishing were asked to record details of spills of plastic fishing gear that occurred during their daily fishing for a period of three months from January to March 2023. The records were kept in a detailed operational diary of daily plastic gear spills during the three months from January to March 2023. The items recorded included: the type and quantity of gear used on the day, the type and quantity of gear spilled, and were set up to enable the calculation of the amount spilled, as described below. The record was set up to enable the calculation of the amount of gear spilled, which is described below. To convert the record of the quantity of gear spilled into weight. In order to convert the quantity records of spilled gear into weights, standard fishing gear actually used in longline fishing was provided (e.g. Figure 2), and weighed the gear by type. The amount of plastic fishing gear discharged at sea D1 (kg) in the period for which logbooks were recorded was estimated using equation (1) by multiplying the weight per unit of plastic fishing gear type i, $w_{1,i}$ (kg/piece or kg/m), by the number or length $n_{1,i}$ (piece or m) of each piece of fishing gear discharged at sea in the period.

$$D1 = \sum w_{1,i} \times n_{1,i} \ldots (1)$$

Table 1: Surveyed longline fishing activity Data on activity of longline fisheries surveyed

Survey method	Logbook survey	Questionnaire / purchase record survey
Number of operations surveyed	4	31
Annual catch	1.5～2.0 t	
Number of days in operation per year	21days	
Trunk line length per operation	36.8km	
Length of one pot	1.37km	
Number of stern lines per operation	27	

Questionnaire on fishing gear runoff rates and using fishing gear purchase records survey methodology

Data on the number and length of plastic fishing gear was extracted from fishing gear purchase records during the fishing season in a standard longline fishing operation and multiplied by the weight of each type of gear obtained through interviews with gear

Figure 2: Ropes used in longline fishing

manufacturers and actual measurements to estimate the weight of plastic fishing gear purchased. Here, the possible reasons for purchasing fishing gear are (i) to replace old gear with new ones, (ii) to replenish gear that has been lost at sea during operations, and (iii) to expand the scale of fishing operations. In this study, a questionnaire survey was conducted among 31 fishermen engaged in longline fishing, as it was necessary to ascertain the proportion of fishermen engaged in (ii). The questionnaire asked about each piece of fishing gear used in longline fishing, "the proportion of gear purchased to replenish gear that has been lost at sea". Finally, the weight $W_{2,i}$ (kg) of each plastic fishing gear estimated from the purchase records was multiplied by the proportion $p_{2,i}$ (-) of gear i purchased to replenish marine spills from the questionnaire survey to estimate the marine discharge of plastic fishing gear $D2$ using the following formula (2).

$$D2 = \sum w_{2,i} \times p_{2,i} \ldots (2)$$

3. RESULTS AND DISCUSSION

Plastic fishing gear use and marine runoff by type

Amount used: the weight breakdown of plastic fishing gear use by type according to the two methods is shown in Figure 3. The breakdown of usage in the four types of gear that could potentially be discharged into the ocean - trunk ropes, branch ropes, floats and ropes - was 47% for trunk ropes, 24% for floats, 16% for branch ropes and 13% for ropes in the logbook survey. In the questionnaire/purchase record survey, 60% of the trunk rope, 21.6% of the branch rope, 18% of the rope and 0.4% of the floats were used. The reason for the smaller proportion of floats used in the questionnaire/purchase record survey compared to the logbook survey is thought to be due to the very smallproportion of new purchases of floats in the longline fishing fleet.

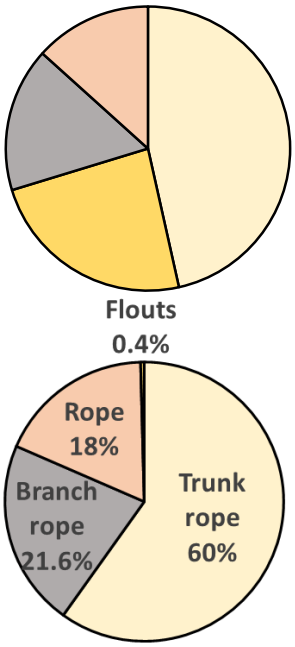

Figure 3: Breakdown of plastic fishing gear use by type (top) logbook survey (bottom) Questionnaire/purchase record survey

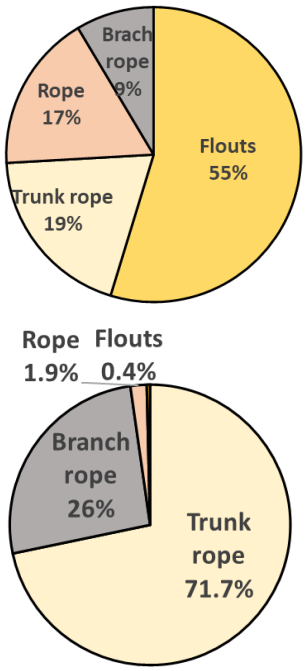

Figure 4: Breakdown of plastic fishing gear marine discharge by type (top) logbook survey (bottom) Questionnaire/purchase record survey

Marine spills: the weight breakdown of plastic fishing gear marine spills by type for the two methods is shown in Figure 4. The breakdown of the amount of spillage was 55% floats, 19% trunk ropes, 17% ropes and 9% branch ropes in the logbook survey. In the questionnaire and purchase record survey, 71.7% of the trunk rope, 26% of the branch rope, 1.9% of the rope and 0.4% of the floaters were found. The logbook survey resulted in a larger proportion of floats being lost, while the questionnaire and purchase record survey resulted in a larger proportion of trunk ropes being lost.

Marine discharge intensity of plastic fishing gear

The intensity of plastic gear marine run-off for the two methods of longline fishing investigated per operation, per tonne of catch, per day of operation and per kilometre of trunk rope (line) length is shown in Table 2. The average per unit of fishing effort per fishery was 32 kg/t (3.3-59 kg/t) for the logbook survey and 24 kg/t (9.5-38 kg/t) for the questionnaire and purchase record survey, respectively. Per tonne of catch, the logbook survey averaged 18 kg/t (1.9-34 kg/t) and the questionnaire/purchase record survey averaged 14 kg/t (5.4-21 kg/t). Comparing the intensity calculated by the logbook survey with the intensity calculated by the questionnaire and purchase record survey, the average values was slightly higher in the logbook survey, but there was no significant difference between the estimation results of the two survey methods.

Table 2: Intensity of each survey method (numbers are means, figures in brackets are based on standard deviations)

Survey method / Intensity	Logbook survey	Questionnaire/ purchase record survey
Per management unit (kg - plasticgear spills/management unit)	32 (3.3～59)	24 (9.5～38)
Per tonne of catch (kg - plastic gear spillage/t - catch)	18 (1.9～34)	14 (5.4～21)
Per day of operation (kg - plastic gear spilled/day - number of days in operation)	1.5 (0.18～2.8)	1.2 (0.46～1.8)
Per kilometre of line (kg - plastic gear spilled/km - length of line)	0.87 (0.076～1.7)	0.66 (0.26～1.0)

4. CONCLUSION

In this study, the amount of plastic fishing gear used and discharged into the sea in longline fisheries was estimated using two methods: a logbook survey and a questionnaire/purchase record survey. The average values were slightly higher in the logbook survey, but the values were generally close to each other.

(1) Hirofumi Nakayama, Fumiya Ishibashi, Katsushi Kuwamura, Satoko Seino, Takayuki Shimaoka: Doboku Gakkai Ronbunshu G (Kankyo), Vol. 78, No. 6, II_11-II_17 (2022) Study on input intensity of plastic products in fishing boats for fishing industry

THE STRESS RESPONSE OF TETRACYCLINE RESISTANCE GENES AND BACTERIAL COMMUNITIES UNDER THE EXISTENCE OF MICROPLASTICS IN TYPICAL LEACHATE BIOLOGICAL TREATMENT SYSTEM

Hong Li, Hongyuan Liu, Chengran Fang*
College of Civil Engineering, Zhejiang University of Technology, Hangzhou 310023, China

ABSTRACT

Landfill leachate is an important source of microplastics (MPs) and antibiotic resistance genes (ARGs). The A/A/O technology is a typical leachate biological treatment system. Under the action of PS and PE MPs, the nitrogen and phosphorus removal effect and sludge structure performance will be affected. The abundance of tetracycline resistance genes (*tet* genes) enriched on the biofilms of the two MPs was significantly higher than the aquatic phase and the sludge phase, and the load on PE was higher than PS due to its porous structure. The aging of MPs was related to the quality of leachate and acted on the structure of ARGs on MPs biofilm. In addition, the colonization of microorganisms and ARGs increased the risk of MPs pollution, and the exploration of potential degradation dominant bacteria was of great significance for MPs pollution control.

KEYWORDS: Microplastics, Antibiotic resistance genes, Emerging contaminants, leachate biological treatment, Bacterial community

1. INTRODUCTOIN

A world without plastics or synthetic organic polymers seems unimaginable today, yet their large-scale production and use have become an environmental issue of global concern.[1] The vast majority of the monomers used to make plastics, such as ethylene and propylene, are derived from fossil hydrocarbons, making them accumulate in landfills or natural environments rather than decompose.[1] Plastics with a particle size < 5 mm are considered as microplastics (MPs) as specified by the National Oceanic and Atmospheric Administration.[2] MPs are easily found in various aquatic ecosystems, including oceans, rivers, landfill leachate, and wastewater treatment plants (WWTPs). Among these environmental matrixes, Polystyrene (PS), Polyethylene (PE), Polyethylene terephthalate (PET), Polyvinyl chloride (PVC), and Polypropylene (PP) have been reported frequently.[2, 3, 4]

There is no doubt that polymer brings convenience to human life also push humans to another troubled abyss, antibiotic resistance (AR) is the same. The widespread occurrence of AR including antibiotic resistance genes (ARGs) and antibiotic resistant bacteria (ARB) in both natural and engineered ecosystems is a consequence of the extensive use of antibiotics.[5, 6] To make matter worse is the co-occurrence of such emerging contaminants. The hydrophobic surface of MPs is an ideal hotbed for ARB colonization and biofilm formation, representing a protective niche, the so-called 'plastisphere'.[7] The 'plastisphere' has attracted the attachment of pollutants and the selective enrichment of ARGs, which has become a hotspot for horizontal gene transfer (HGT).[8]

Landfill leachate is an important source of MPs and ARGs, and its complex composition brings more uncertainty to the environmental ecosystem.[8, 9] For example, metagenomic analysis was recently used to investigate the broad-spectrum characteristics of ARGs in landfill leachate from 12 cities in China, and identified 526 ARG subtypes belonging to 21 ARG types.[10] In addition, Xu et al. detected MPs (20-100 μm) in landfill leachate with the concentration of 291 ± 91 particles/L.[11] Therefore, seeking green and efficient landfill leachate treatment method has been given more far-reaching significance.

It is a convenient and economical treatment method to discharge leachate into WWTPs. Compared with conventional methods (such as recycling to landfills), physical and chemical methods, biological treatment has higher economic benefits and environmental friendliness. The WWTP is an anaerobic-anoxic-anoxic (A/A/O) process or directly called A/A/O technology, which is the basis of the operation of major WWTPs in China. However, there is currently no target technology for the treatment of emerging contaminants such as ARGs and MPs, hence it is necessary to systematically and comprehensively explore the stress effect and mechanism of such emerging contaminants in A/A/O system. In general, the objectives of the present study were to explore: (i) the stress effect of MPs on the operation of leachate biological treatment system; (ii) the interaction between MPs and ARGs; (iii) the microbial community participates in the operation of the system and the internal mechanism between the emerging contaminants.

2. MATERIALS AND METHODS

2.1. Materials and leachate composition

PS microplastic balls (φ=150 μm, density 1.282 g/cm^3) were purchased from Hongfu Plastic Materials

Co., Ltd. Ultra-high molecular weight PE microplastic powder (φ=150 μm, molecular weight of 450–500 w) were obtained from Shanghai Macklin Biochemical Co., Ltd. All MPs were cleaned with methanol in an ultrasonic cleaner for 15 min and dried at 40 ◦C for 5 h before use.

The composition of the synthetic leachate was as follows (per L): 6500 mg of NH_4Cl, 4500 mg of $NaNO_2$, 1250 mg of $KHCO_3$, 750 mg of acetic acid, 300 mg of $MgSO_4·7H_2O$, 250 mg of NaOH, 10 mg of KH_2PO_4, 5.6 mg of $CaCl_2·2H_2O$, 1.25 mL of trace element 1, and 1.25 mL of trace element 2. The trace element 1 composition was as follows (per L): 6000 mg of EDTA and 9000 mg of $FeSO_4·7H_2O$. The trace element 2 composition was as follows (per L): 14 mg of H_3BO_4, 990 mg of MnCl, 250 mg of $CuSO_4·7H_2O$, 430 mg of $ZnSO_4·7H_2O$, 190 mg of $NiCl_2·6H_2O$, and 220 mg of $NaMoO_4·2H_2O$.

2.2. A/A/O set-up and operating

The seed sludge was taken from Yuhang WWTP in Zhejiang Province and the geographic coordinate was 119.980134 E, 30.283285 N. The sludge was subjected to preliminary centrifugation and then suffocation exposed to the A/A/O system for three days, followed by culture and acclimation in the reactor. The A/A/O system was made of plexiglass, including anaerobic tank (A1, 6 L), anoxic tank (A2, 6 L), four aerobic tank (O, 6 L*4) and precipitation tank (25 L). An electric stirrer was equipped to control the dissolved oxygen (DO) in the A1 and A2 at 0.11-0.31 and 0.16-0.48 mg/L, respectively. The aerobic tank was oxygenated by a diffusion aerator to ensure that the content was 0.6-7.53 mg/L. The initial mixed liquid suspended solids (MLSS) and the hydraulic retention time was kept at 3500 mg/L and 4 days, respectively.

Both PE and PS MPs were set to 1 g/L in A1, A2, and O tanks. In order to facilitate the collection and analysis, each 1g MPs was wrapped with a 200-mesh filter, that is, each pool was uniformly suspended with 6 PE filter bags and 6 PS filter bags. A/A/O system and MPs were comprehensive detection every 10 days. The experimental treatment without MPs was expressed as CK.

2.3. ARGs extraction and quantification

DNA extraction included 0.2 g of freeze-dried sludge, 0.2 g of MPs, and a filter membrane of 0.22 μm passing through 100 mL of leachate. The sample DNA was obtained by DNeasy PowerSoil Pro Kit (Qiagen, Germany) and stored at -20 °C before real-time quantitative PCR (qPCR). Six tetracycline resistance genes (*tet* genes), including *tetA*, *tetB*, *tetM*, *tetO*, *tetQ*, and *tetT*, were widely reported in landfill leachate and identified as the target genes in this study. The qPCR reaction system and program settings could be referred to Liu et al.[12] Briefly, a 20 μL reaction system consisted of 10 μL TB Green Premix Ex Taq II (TaKaRa, Japan), 0.2 μL Primer 1 (20 μmol/L), 0.2 μL Primer 2 (20 μmol/L), 2 μL DNA extraction, and 7.6 μL double-distilled H_2O. The qPCR assay conditions were 30 s at 95 °C, 40 cycles of 30 s at 94 °C, 30 s at the annealing temperature, and 30 s at 72 °C.

2.4. Illumina sequencing and Bioinformatic analysis

Illumina MiSeq platform (Illumina, USA) was used to perform high-throughput sequencing of the V3-V4 region of the 16S rRNA gene of the sample, and the quality of the sequence was controlled and filtered. The sequencing database was constructed by Majorbio Ltd (Shanghai, China). Operational taxonomic units (OTUs) were performed at a similar level of 97% for biological information statistics and visual analysis.

3. RESULTS AND DISCUSSION

3.1. Effect of MPs on the operation of A/A/O

3.1.1. Nitrogen and phosphorus removal of the system

The physicochemical characteristics of the A/A/O leachate system were monitored whole process (Fig. 1). The influent concentrations of chemical oxygen demand (COD), total phosphorus (TP), total nitrogen (TN) and ammonia nitrogen (NH_3–N) were maintained at 844.56 ± 13.48, 6.45 ± 0.06, 691.50 ± 12.35, 339.27 ± 6.63 mg/L, respectively. Before adding MPs, a relatively high removal rate was maintained, such as COD remained above 86%. However, the addition of two MPs obviously affected the nitrogen and phosphorus removal of the system, and the removal rate of each physicochemical index reached the lowest on the 20th day. The results showed that the influence of MPs on the effluent was not linearly related to the residence time of pollutants, because of the slightly rebound at 30th day even 40th day, which might implied the process of tolerance in A/A/O.

3.1.2. Sludge structure performance of the system

MPs were cultured in A/A/O system for 40 days, and their stress also acted on activated sludge (Fig. 2). There were still abundant microbial communities in the sludge without MPs (Fig. 2 (a)) and in the first 10 days (Fig. 2 (b)), while after adding MPs, especially on the 40th day (Fig. 2 (c)), the zoogloea decreased and showed obvious filamentous structure. In addition, the proteins (PN) and polysaccharides (PS), as the main components of extracellular polymeric substances (EPS), account for about 70-80%, which is of great significance for the formation of bacterial aggregates and reactor performance.[13, 14] Generally, EPS can be divided into three parts: tightly bound EPS (TB-EPS), loosely bound EPS (LB-EPS), and soluble EPS (S-EPS), so that the sludge flocs form a gel-like structure.[15] Obviously, with the aging of MPs, the EPS content of sludge increased significantly ($p < 0.05$), which was in good agreement with the conclusion that MPs would lead to an increase of EPS.[16] Especially on the 40th day, the total amount of EPS in each reaction tank was 4 times higher than that CK experiment, and the growth rate of A1 was the highest, followed by A2, and O was the lowest, corresponding growth rate of 373.13% (Fig. 2 (d)), 346.11% (Fig. 2 (e)), and 313.66% (Fig. 2 (f)), respectively. The possible

explanation for the result is that MPs stimulate the secretion of EPS in activated sludge to buffer cell damage.[16] Meanwhile, the ratio of PN to PS in EPS presented a significant downward trend from an average of 2.46 in CK treatment to always less than 1 after adding MPs, and decreased to a minimum of 0.07 on the 40th day. Herein, it can be concluded that the stress response of sludge EPS to MPs may be that PS becomes a key component, while PN is the reason for dealing with MPs stress.

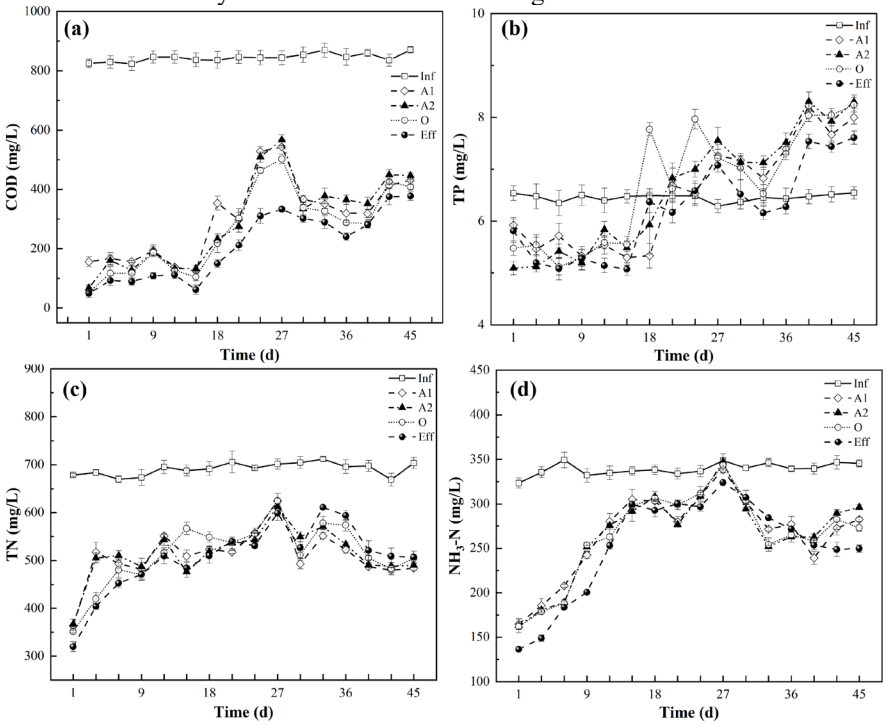

Fig. 1 Effects of MPs on COD, TP, TN and NH_3–N in A/A/O system.

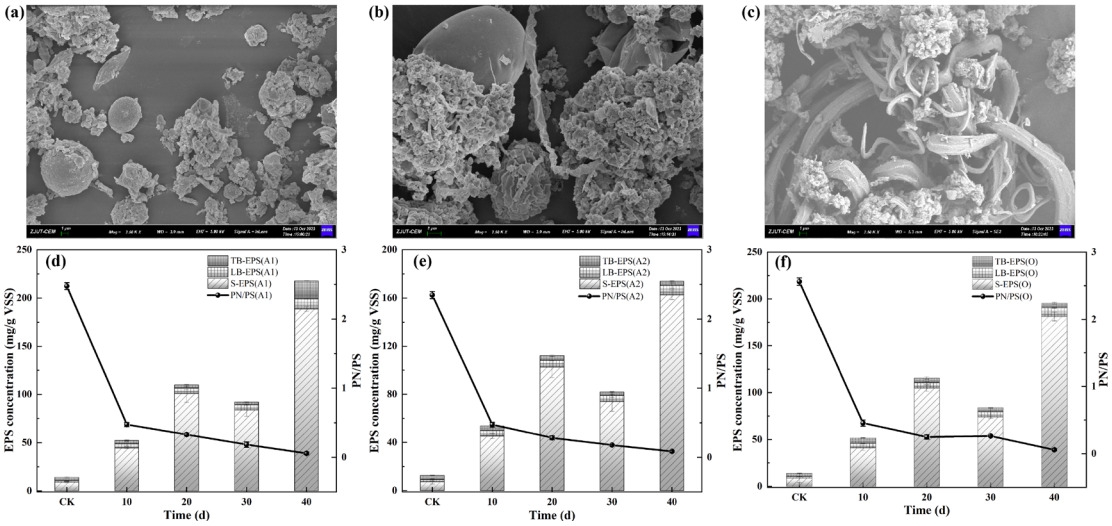

Fig. 2 Scanning electron microscopy (SEM) of the original sludge (a), the 10th day (b), and the 40th day (c). Variation of EPS concentration in A1 (d), A2 (e), and O (f).

3.2. Effect of MPs on the migration and propagation of *tet* genes

3.2.1. The distribution characteristic of *tet* genes in A/A/O

Six target ARGs were detected in raw leachate and activated sludge, and the average absolute abundance values in leachate and sludge were 6.47×10^{12} copies/L and 1.58×10^{7} copies/g, suggesting that landfill leachate and WWTPs were important reservoir for ARGs. Furthermore, to minimize the variance such as DNA extraction and qPCR efficiency, all target genes were normalized by 16S rRNA. The distribution characteristics of *tet* genes in A/A/O were shown in Fig. 3. Notably, the invasion of MPs significantly elevated the AR expression of the system. The target genes in the aqueous phase increased from 3.77×10^{-2} copies/L to

4.97×10^{-2} copies/L, while increased from 1.84×10^{-2} copies/g to 5.25×10^{-2} copies/g in the sludge phase. The consequence hinted that the stress response of ARGs to MPs in sludge was more significant than that in leachate.

During the operation of the system, the order of target gene abundance expression was *tetA* > *tetQ* > *tetO* > *tetB* > *tetT* > *tetM*, which was different from the previous beaker experiment.[8] The possible reason may be the simultaneous existence of PS and PE will reshape the profile of *tet* genes, as well as other environmental conditions, such as the obtained time of sludge, A/A/O operating conditions, etc. Interestingly, the common character in MPs environment was that the presence of MPs could exhibit a competitive advantage in the leachate activated sludge system, which was confirmed again in this study.[8] Similar conclusions also appeared in the estuarine environment, that is, the abundance of most target genes on plastics was higher than corresponding sediment samples and water samples.[17] In this study, the six target genes were 100% detected on both two MPs biofilms, and the expression level of *tetQ* was the highest, which was 4.75×10^{-1} copies/g (PS biofilm) and 1.22 copies/g (PE biofilm), respectively. Compared with PS biofilm, PE biofilm has an overwhelming superiority, with an ARG loading of 4.25×10^{-1} copies/g, while PS biofilm was only 2.22×10^{-1} copies/g. Moreover, the order of abundance of *tet* genes on PS biofilms was *tetQ* > *tetA* > *tetO* > *tetT* > *tetB* > *tetM*, and the order of abundance on PE biofilms was *tetQ* > *tetA* > *tetB* > *tetO* > *tetT* > *tetM*, demonstrating that *tet* genes were selectively enriched on different MPs.

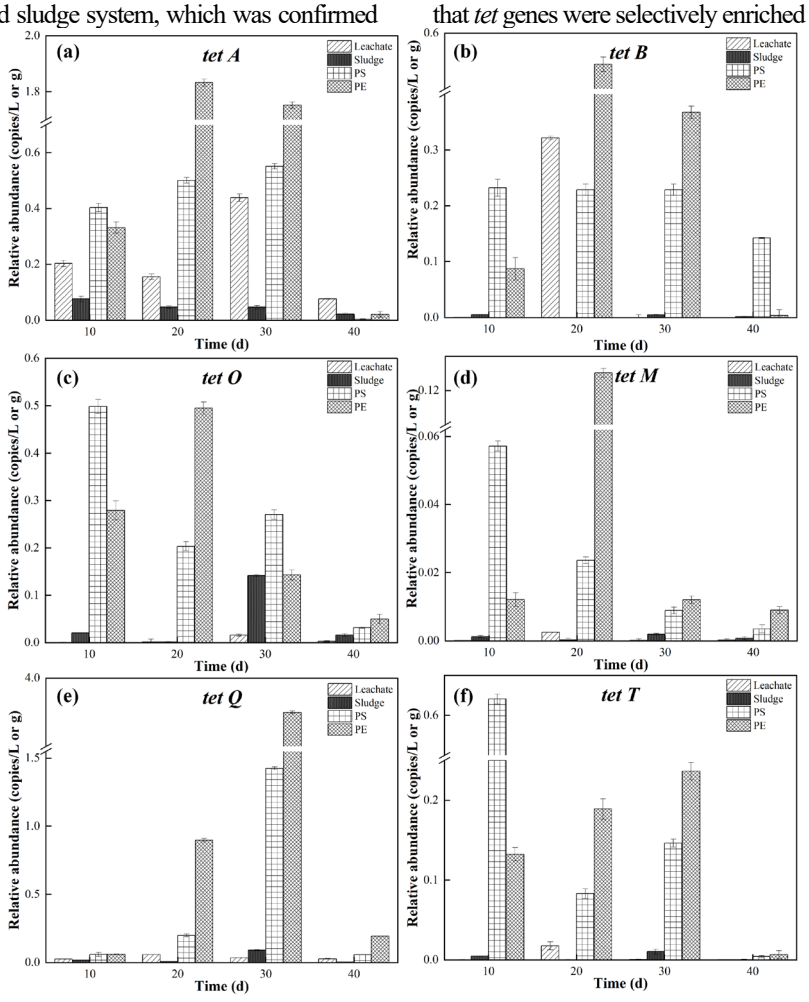

Fig. 3 The distribution characteristic of *tet* genes in A/A/O.

3.2.2. Interaction between *tet* genes and MPs in A/A/O

MPs are persistent in various environments and are susceptible to ultraviolet radiation, thermal degradation, biodegradation and oxidation reactions. These processes affect the properties of the polymer, including morphology, mechanical strength, oxygen content, molecular weight, etc., resulting in aging and degradation of the polymer.[18, 19] The Fourier transform infrared (FTIR) and SEM of the aging process of the two MPs were shown in Fig. 4. With the aging of PS in leachate activated sludge system, the transmittance intensity of (1780-1600 cm^{-1}) and methylene group (1490-1420 cm^{-1}) also showed an overall decreasing trend. The carbonyl index usually refers to the ratio of the peak area of the carbonyl group to the peak area of the methylene group, and its evolution is one of the

main indicators for monitoring the degree of polymer degradation.[18] The carbonyl index of PS decreased from 2.39 in virgin to 2.30 on the 40th day, but increased on the 20th day (2.42) and the 30th day (2.44), implying that there were multiple chemical reactions in the leachate environment (Fig. 4 (a)). Complex biochemical reactions accelerate the aging of MPs, making them more suitable for colonization of ARGs and ARB. The original PS exhibited a smooth spherical shape, but as the aging intensified, its surface gradually became rough and enriched more microorganisms (Fig. 4 (b) and (c)). The characteristic peaks of PE appeared at 2914, 2847, and 1471cm^{-1}, which were characterized by the antisymmetric stretching motion, symmetric stretching motion, and bending motion of methylene -CH_2-. The characteristic peak of 717cm^{-1} was mainly caused by plastic additives and the peak was [CH_2]n (n ≥ 4) (Fig. 4 (d)). Compared with PE, more carbonyl groups were formed on the surface of PS, indicating that PS was more easily oxidized in the aquatic habitat. In addition, from the perspective of physical structure and surface characteristics, the vital explanation for the enrichment of ARGs and ARB by PE might be attributed to the porous structure and hydrogen bonding (Fig. 4 (e) and (f)). In summary, leachate with complex composition and high contamination will accelerate the aging of MPs, and further aging of MPs will increase the migration and transformation of pollutants.

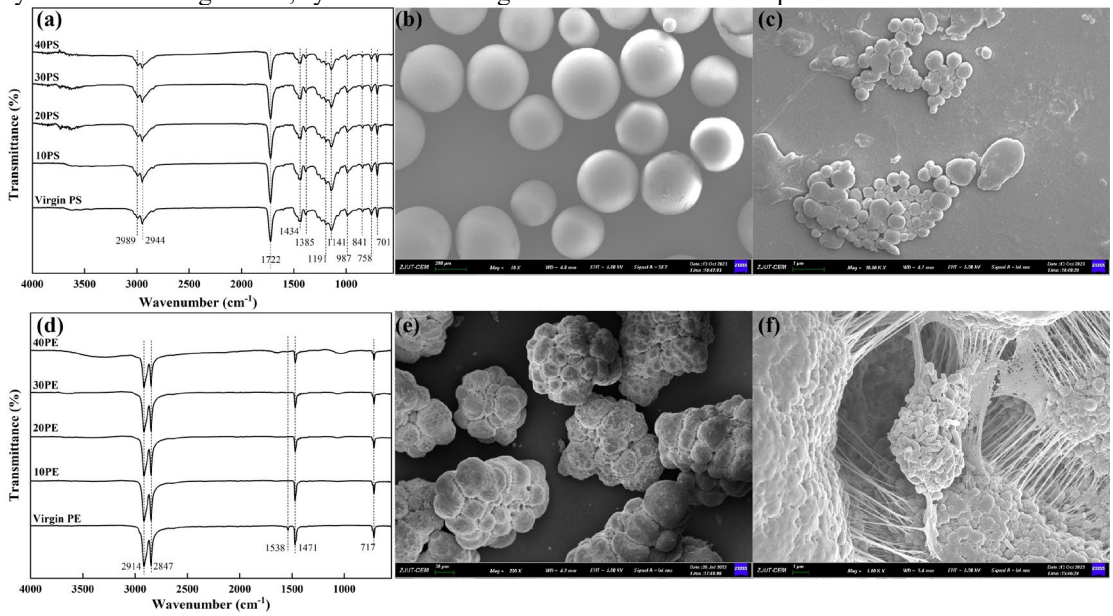

Fig. 4 The aging process of MPs. FTIR spectrometer of PS (a), SEM of original PS (b), and SEM of PS on 40th day (c); FTIR spectrometer of PE (d), SEM of original PE (e), and SEM of PE on 40th day (f).

The specific enrichment of *tet* genes on different MPs was not only linked to the structural properties of MPs, but also to the quality parameters of leachate during the operation of A/A/O system (Fig. 5). For example, almost all the *tet* genes on PS biofilm were closely associated with EPS, and most of them were negatively correlated, illustrating that the enrichment of ARGs on PS biofilm was closely related to the secretion of PN and PS in sludge. In addition, compared with other leachate quality parameters, TP showed more correlation with ARGs abundance on PS biofilm. Different from PS biofilm, the loading of ARGs on PE biofilm was more closely related to COD, TP, TN, NH_3–N, and pH, but not to EPS. The reason might be the porous structure of PE MPs increases the contact area with the leachate, which was more susceptible to hydrologic environmental conditions. Considering the microscopic size, strong hydrophobicity, potential additives and the ability to absorb contaminates, MPs shape the ARG profile while also affecting the entire functional modules of the A/A/O system (such as C fixation, C degradation, P cycling and N cycling). Hereby, it was urgent necessary to explore the mechanism among MPs, ARGs, and the system in typical leachate biological treatment systems.

(a)

	tet A	*tet B*	*tet O*	*tet M*	*tet Q*	*tet T*	COD	TN	TP	NH_3-N	pH	EPS
tet A	1.00											
tet B	0.96	1.00										
tet O	0.60	0.78	1.00									
tet M	0.37	0.62	0.90	1.00								
tet Q	0.56	0.36	0.05	-0.37	1.00							
tet T	0.30	0.54	0.94	0.94	-0.20	1.00						
COD	0.25	0.18	-0.30	-0.10	-0.26	-0.43	1.00					
TN	0.74	0.70	0.19	0.22	0.08	-0.06	0.83	1.00				
TP	-0.65	-0.80	-0.70	-0.81	0.27	-0.59	-0.46	-0.75	1.00			
NH_3-N	0.28	0.37	0.15	0.45	-0.56	0.11	0.83	0.78	-0.80	1.00		
pH	-0.33	-0.44	-0.25	-0.53	0.55	-0.20	-0.78	-0.78	0.86	-0.99	1.00	
EPS	-0.78	-0.89	-0.95	-0.75	-0.35	-0.80	0.27	-0.29	0.64	-0.05	0.15	1.00

(b)

	tet A	*tet B*	*tet O*	*tet M*	*tet Q*	*tet T*	COD	TN	TP	NH_3-N	pH	EPS
tet A	1.00	0.97	0.55	0.64	0.70	0.89	0.55	0.82	-0.35	0.28	-0.28	-0.30
tet B	1.00	0.72	0.82	0.50	0.80	0.74	0.93	-0.48	0.51	-0.50	-0.22	
tet O	1.00	0.91	-0.18	0.49	0.80	0.93	-0.90	0.94	-0.95	-0.32		
tet M	1.00	-0.08	0.40	0.97	0.93	-0.63	0.88	-0.85	0.04			
tet Q	1.00	0.73	-0.15	0.17	0.23	-0.48	0.48	-0.31				
tet T	1.00	0.22	0.70	-0.50	0.15	-0.20	-0.70					
COD	1.00	0.83	-0.46	0.83	-0.78	0.27						
TN	1.00	-0.75	0.78	-0.78	-0.29							
TP	1.00	-0.80	0.86	0.64								
NH_3-N	1.00	-0.99	-0.05									
pH	1.00	0.15										
EPS	1.00											

Fig. 5 Correlation analysis among the environmental factors, and *tet* genes loaded on PS biofilm (a) and PE biofilm (b).

3.3. The succession of microbial community in plastisphere and A/A/O

The SEM images of PS and PE confirmed the colonization of microorganisms. To gain insights into the

succession of microbial community structure on the surface of MPs, the bioinformatic analysis of A/A/O microorganisms was carried out (Fig. 6). In all samples, more than 40 phylum-level species were identified, and 1052 genus-level microorganisms were annotated. *Proteobacteria*, *Bacteroidota*, *Actinobacteriota*, *Firmicutes*, and *Chloroflexi* were the prevailing phyla on the two MPs biofilms and leachate activated sludge system, which was similar to previous study.[8, 17] Apparently, with the pressure of PS and PE, the *Proteobacteria* and *Bacteroidota* in the sludge dynamically grew, while the abundance of *Actinobacteriota*, *Firmicutes*, and *Chloroflexi* gradually decreased (Fig. 6 (a)), indicating that *Proteobacteria* and *Bacteroidota* have the potential strength to withstand the MPs poison. However, the activity and abundance of *Proteobacteria* and *Bacteroidota* in aerobic granular sludge were inhibited by PE MPs, which was different from our results. It was speculated that the sludge sources, the effects of various MPs and leachate conditions might be the reasons.[20] Moreover, despite there were specific differences in the relative abundance of various bacteria on PS biofilm and PE biofilm, the dominant bacteria on the two biofilms were concordance with the succession process of A/A/O environment, elucidating that the ambient environment could shape the MPs biofilm structure. Besides, NMDS (non-metric multidimensional scaling) analysis based on the OUT taxonomy level showed that the variation among the groups were small and had significant similarities ($p < 0.05$), which further proved the representativeness and rationality of the grouping in this study (Fig. 6 (b)).

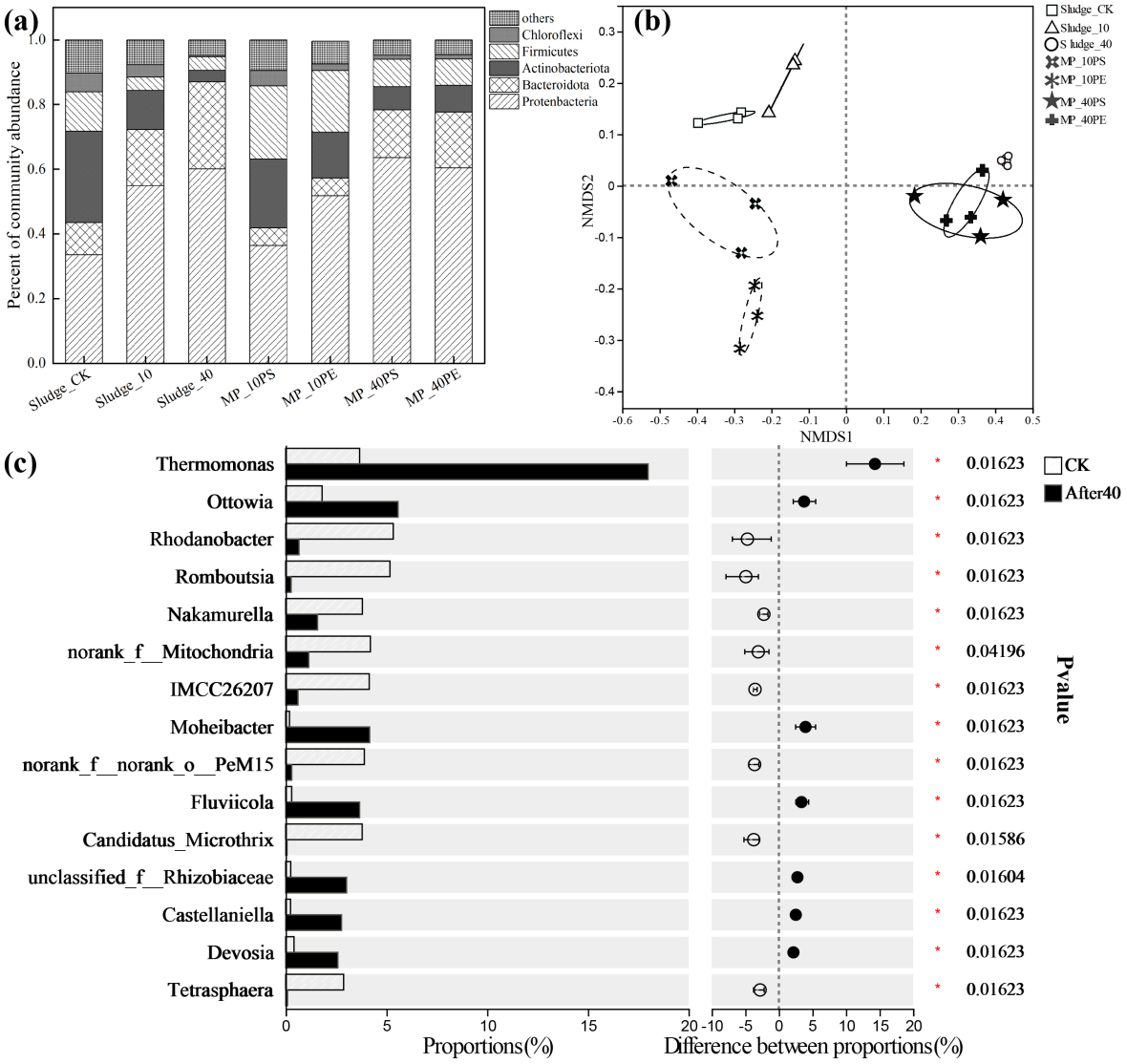

Fig. 6 The dynamic succession of the top 5 microbial groups on phylum leve (a). NMDS analysis based on OUT classification level (b). The points of different colors or shapes represent samples of different groups. The closer the two sample points are, the more similar the species composition of the two samples is. The horizontal and vertical coordinates represent the relative distance. Wilcoxon rank-sum test bar plot on genus level (95 % confidence intervals) (c). The X axis represents different groups, boxes of different colors represent different groups, and the Y axis represents the average relative abundance of a species in different groups.

Based on the community abundance data in the samples, statistical methods were used to detect specific species in the microbial community in different periods, conduct hypothesis tests, and evaluate the significance of the differences (Fig. 6 (c)). The results showed that the proportion of *Thermomonas* in all bacterial genera increased significantly from 3.67% in CK treatment to 17.99% after 40 days of MPs treatment ($p < 0.05$), which clarified the high adaptability of the predominant bacteria to PS and PE MPs. *Thermomonas* is related to nitrate reduction to achieve the purpose of nitrogen removal.[20] It also has been suspected as a potential host of *tetW* in previous studies.[8] Extensive studies have shown that there were significant correlation between ARG profile and bacterial community structure, indicating that these potential ARGs hosts could ultimately find their way to propagate among environmental microorganism.[21, 6] MPs are complex mixtures of chemicals. As a complex mixture of chemicals, MPs release organic and inorganic substances during aging, thereby changing the environmental microbial community and spreading pathogenic microorganisms on MPs. In addition, *Ottowia*, *Moheibacter*, *Fluviicola*, *unclassified_f_Rhizobiaceae*, *Castellaniella*, and *Devosia* were also potential MP-degrading genera. Among them, the enrichment of *Moheibacter* could promote organic matter degradation and nitrogen transformation, while *Rhodanobacter* was related to the role of phosphorus and has a highly differentiated copper-containing nitrite reductase (*nirK*) gene sequence.[22, 23] Furthermore, *Castellaniella* has been reported to have the ability to degrade highly resistant plastic polymers.[24] In summary, these bacteria were more or less related to nitrogen and phosphorus removal in the A/A/O system, and have the potentiality for the degradation of MPs. The colonization of ARGs and ARB on MPs not only increases the risk of pollution to the surrounding environment, but also further aggravates MPs pollution. Therefore, it is of great significance to research the mechanism of between MPs and ARGs in leachate, and the potential degradation dominant bacteria to reduce the MPs pollution risk in landfill leachate and WWTPs.

4. CONCLUSION

This study revealed the stress response of *tet* genes and microbial communities in typical leachate biological treatment system with the existence of MPs. The results showed that PS and PE MPs affected the nitrogen and phosphorus removal efficiency of A/A/O system, as well as the structure and performance of sludge. Under the stress of two MPs, activated sludge secretes more EPS to hinder cell damage. Compared with leachate and sludge, MPs have a competitive advantage over ARGs, especially PE MPs. The significant specific enrichment of *tet* genes on the two MPs and the succession of microbial community structure indicated that MPs have the superior performance of adsorbing ARGs and ARB, thereby increasing the risk of environmental pollution. This study is of great significance to the mechanism of action and pollution control of MPs.

ACKNOWLEGEMENTS

This work was funded by the National Natural Science Foundation of China (Grant Nos. 51878617, 51678531, 41977331, 51778579, and 21876165).

REFERENCES

1 Geyer, R., J.R. Jambeck, and K.L. Law, Production, use, and fate of all plastics ever made. *Sci Adv*, 2017. 3(7).

2 Xu, P., W. Ge, C. Chai, Y. Zhang, T. Jiang, and B. Xia, Sorption of polybrominated diphenyl ethers by microplastics. *Mar Pollut Bull*, 2019. 145: 260-269.

3 Ali, I., T. Ding, C. Peng, I. Naz, H. Sun, J. Li, and J. Liu, Micro- and nanoplastics in wastewater treatment plants: Occurrence, removal, fate, impacts and remediation technologies – A critical review. *Chem Eng J*, 2021. 423.

4 Lin, X., S. Zhang, S. Yang, R. Zhang, X. Shi, and L. Song, A landfill serves as a critical source of microplastic pollution and harbors diverse plastic biodegradation microbial species and enzymes: Study in large-scale landfills, China. *J Hazard Mater*, 2023. 457.

5 Guo, J., J. Li, H. Chen, P.L. Bond, and Z. Yuan, Metagenomic analysis reveals wastewater treatment plants as hotspots of antibiotic resistance genes and mobile genetic elements. *Water Res*, 2017. 123: 468-478.

6 Li, H., H. Liu, L. Qiu, Q. Xie, B. Chen, H. Wang, Y. Long, L. Hu, and C. Fang, Mechanism of antibiotic resistance development in an activated sludge system under tetracycline pressure. *Environ Sci Pollut Res Int*, 2023. 30(39): 90844-90857.

7 Gkoutselis, G., S. Rohrbach, J. Harjes, M. Obst, A. Brachmann, M.A. Horn, and G. Rambold, Microplastics accumulate fungal pathogens in terrestrial ecosystems. *Sci Rep*, 2021. 11(1): 13214.

8 Liu, H., H. Li, L. Qiu, Q. Xie, Y. Lu, B. Chen, H. Wang, Y. Long, L. Hu, and C. Fang, Alteration of the migration trajectory of antibiotic resistance genes by microplastics in a leachate activated sludge system. *Environ Pollut*, 2023. 333: 121981.

9 Shi, J., D. Wu, Y. Su, and B. Xie, Selective enrichment of antibiotic resistance genes and pathogens on polystyrene microplastics in landfill leachate. *Sci Total Environ*, 2021. 765:142775.

10 Zhao, R., J. Feng, X. Yin, J. Liu, W. Fu, T.U. Berendonk, T.

Zhang, X. Li, and B. Li, Antibiotic resistome in landfill leachate from different cities of China deciphered by metagenomic analysis. *Water Res*, 2018. 134: 126-139.

11 Xu, Z., Q. Sui, A. Li, M. Sun, L. Zhang, S. Lyu, and W. Zhao, How to detect small microplastics (20–100 μm) in freshwater, municipal wastewaters and landfill leachates? A trial from sampling to identification. *Sci Total Environ*, 2020. 733.

12 Liu, H., H. Li, L. Qiu, B. Chen, H. Wang, C. Fang, Y. Long, and L. Hu, The panorama of antibiotics and the related antibiotic resistance genes (ARGs) in landfill leachate. *Waste Manag*, 2022. 144: 19-28.

13 Yin, C., F. Meng, and G.-H. Chen, Spectroscopic characterization of extracellular polymeric substances from a mixed culture dominated by ammonia-oxidizing bacteria. *Water Res*, 2015. 68: 740-749.

14 Wang, H., C. Qiu, S. Bian, L. Zheng, Y. Chen, Y. Song, and C. Fang, The effects of microplastics and nanoplastics on nitrogen removal, extracellular polymeric substances and microbial community in sequencing batch reactor. *Bioresource Technol*, 2023. 379.

15 Chen, M., C. Hu, L. Wang, H. Sun, S. Xu, X. Ling, W. Bi, X. Li, and J. Deng, The novel application of polyoxometalates in sludge dewatering: Cells lysis and re-flocculation. *Chem Eng J*, 2023. 470.

16 Tang, S., J. Qian, P. Wang, B. Lu, Y. He, Z. Yi, and Y. Zhang, Exposure to nanoplastic induces cell damage and nitrogen inhibition of activated sludge: Evidence from bacterial individuals and groups. *Environ Pollut*, 2022. 306.

17 Guo, X.P., X.L. Sun, Y.R. Chen, L. Hou, M. Liu, and Y. Yang, Antibiotic resistance genes in biofilms on plastic wastes in an estuarine environment. *Sci Total Environ*, 2020. 745: 140916.

18 Su, Y., Z. Zhang, D. Wu, L. Zhan, H. Shi, and B. Xie, Occurrence of microplastics in landfill systems and their fate with landfill age. *Water Res*, 2019. 164: 114968.

19 Zhang, Y., J. Gao, Z. Wang, Y. Zhao, Y. Liu, H. Zhang, and M. Zhao, The responses of microbial metabolic activity, bacterial community and resistance genes under the coexistence of nanoplastics and quaternary ammonium compounds in the sewage environment. *Sci Total Environ*, 2023. 879: 163064.

20 Zheng, X., Z. Han, X. Shao, Z. Zhao, H. Zhang, T. Lin, S. Yang, and C. Zhou, Response of aerobic granular sludge under polyethylene microplastics stress: Physicochemical properties, decontamination performance, and microbial community. *J Environ Manage*, 2022. 323.

21 Lu, L., Y. He, C. Peng, X. Wen, Y. Ye, D. Ren, Y. Tang, and D. Zhu, Dispersal of antibiotic resistance genes in an agricultural influenced multi-branch river network. *Sci Total Environ*, 2022. 830.

22 Wang, N., X. Bai, D. Huang, M. Shao, Q. Chen, and Q. Xu, Insights into the influence of digestate-derived biochar upon the microbial community succession during the composting of digestate from food waste. *Chemosphere*, 2023. 316.

23 Xu, H., J. Lv, and C. Yu, Combined phosphate-solubilizing microorganisms jointly promote Pinus massoniana growth by modulating rhizosphere environment and key biological pathways in seedlings. *Ind Crop Prod*, 2023. 191.

24 Salinas, J., V. Carpena, M.R. Martínez-Gallardo, M. Segado, M.J. Estrella-González, A.J. Toribio, M.M. Jurado, J.A. López-González, F. Suárez-Estrella, and M.J. López, Development of plastic-degrading microbial consortia by induced selection in microcosms. *Front Microbiol*, 2023.

MICROPLASTIC, A POSSIBLE TRIGGER OF LANDFILL SULFATE REDUCTION PROCESS

Shuli Guo, Zixiao Wu, Xianghang Li, Dongsheng Shen, Jiali Shentu, Li Lu, Shengqi Qi, Min Zhu, Yuyang Long*

Zhejiang Provincial Key Laboratory of Solid Waste Treatment and Recycling, School of Environmental Science and Engineering, Zhejiang Gongshang University, Hangzhou, 310012, China

ABSTRACT

The environmental impact of microplastics (MPs) formed from landfill has not been gained enough attention. This research investigated the characteristics of the MPs occurrence in landfills through field sampling. It shows that the MPs abundance in the landfill surface soil and non-landfill areas can reach 3573 items·g^{-1} and 3041 items·g^{-1}, respectively. The vertical abundance of MPs increases significantly with depth, ranging from 387 to 11,599 items·g^{-1} with small size (≤10 μm, 65.61 %) and flake or wedge shape (38.48 %). The leachate movement in a longitudinal direction enables MPs to accumulate more easily in the landfill bottom layer with high moisture abundance. The abundance of MPs are significantly correlated with SO_4^{2-} and S^{2-} content, the two typical metabolic substrate and product of sulfate reduction process. In such heterogeneous environment, this significant correlation is not a random phenomenon in terms of the MPs have known substantial impact on biogeochemical processes. Microplastic is a possible trigger of landfill odor emission related with sulfate reduction. This research could serve as a reference for MPs and odor pollution management in landfills.

Keywords: Landfills, MPs, Emerging pollutant, Leachate, Sulfate reduction

INTRODUCTION

Plastics have become an indispensable material of modern human life due to their affordability, exceptional resistance to corrosion, and remarkable flexibility. They are widely used in various fields, and the output of plastic products has been increasing rapidly alongside the development of the economy and society. It is reported that the annual global plastic production has amounted to >390 million tons (PlasticsEurope, 2023). The current population growth trend and changes in consumption patterns suggest that plastic usage will continue to increase in the future. The annual global plastic production will escalate to 590 million tons by 2050, resulting in a cumulative global plastic production of 34 billion tons (Hoang, 2022; Rahul et al., 2023). China is currently the largest global producer of plastics and plastic products, reaching almost one third of the world's plastics production (PlasticsEurope, 2023). Obviously, it is a significant potential pollution risk.

The rapid growth in plastic production has resulted in an increasing amount of plastic waste that requires urgent disposal. Almost 21−42 % of global plastic waste ends up in landfills (Lin et al., 2023). Although plastic is known to be difficult to biodegrade, it undergoes a combination of physical, chemical, and biological processes in landfills that eventually result in the formation of microplastics (MPs). MPs are a relatively new type of pollutant with significant threat to the environment (Alimi et al., 2022; Lu et al., 2023). MPs are harmful due to the presence of toxic substances such as nonylphenol and phthalates (Hahladakis et al., 2018; Luo et al., 2022), as well as the accumulation of heavy metals, organic matter, and pathogenic microorganisms (Rai et al., 2022). They pose severe threat to both human health and the environment. Controlling the potential risk from MPs in landfills is urgent.

Currently, research about MPs abidance in ocean (Turan et al., 2021), marine sediments (Phuong et al., 2021), river (Lu et al., 2021), soil (Tunali et al., 2022), and other natural environments has been gained increasing interest. Related research on the MPs sources, degradation mechanisms, and biological effects has also been gradually conducted (Chen et al., 2023; Kumar et al., 2021; Möller et al., 2020). However, the occurrence of MPs in landfills has only recently gained attention (Gurjar et al., 2023; Lin et al., 2018; Nayahi et al., 2022; Su et al., 2019). It indicated that the size, shape, and type of these MPs were intricately linked to variables such as landfill composition, method, and duration (Su et al., 2019; Yu et al., 2022). Moreover, significant levels of MPs have been observed in both landfill leachate and groundwater (Bharath et al., 2021; Shen et al., 2022a). Due to the lightweight nature of MPs, they can migrate with leachate within landfills, eventually releasing into the surround environment (Bharath et al., 2021). Therefore, MPs in landfills can potentially be released into the surrounding environment through waste decomposition and leachate migration.

The landfilling process can last decades. It works as a

closed reactor that undergoes various dynamic fluctuations, including alterations in temperature (Sabrin et al., 2021), salinity (Makhadi et al., 2021), and microbial activity (Staley et al., 2018). These environmental factors can accelerate the physical changes of MPs in waste and affect their distribution throughout the landfill, disturbing the relevant biochemical reaction processes (Canopoli et al., 2020; Kjeldsen et al., 2002; Zha et al., 2022). Carbon, nitrogen, and sulfur are essential focuses in biogeochemistry (Chun, 2018). Studies have shown that MPs can alter the organic carbon storage in local environments, interfere with microbial structure and community, and influence the expression of functional genes, thereby impacting the carbon cycle in the environment (Sanz-Lazaro et al., 2021). Similarly, MPs can also affect the microbial composition in marine sediments and soil, thus influencing the nitrogen cycle process (Rong et al., 2021; Seeley et al., 2020). Furthermore, it has been demonstrated that the presence of MPs significantly can impact changes in microbial communities and gene pools related to the sulfur cycle. Moreover, biodegradable MPs have shown a greater influence on the sulfate reduction process compared to petroleum-based MPs (Pinnell et al., 2019; Wang et al., 2023). However, comparing with carbon and nitrogen, there has been relatively limited research on the association between MPs and sulfur, the typical source of "odor nuisance" (Jin et al., 2020; Ying et al., 2019). Sulfur metabolism and the carbon and nitrogen cycles are intertwined via various biological and geochemical processes. Therefore, the correlation between MPs and sulfur metabolism cannot be overlooked within such special artificial habitat like landfill.

In this study, the distribution and diffusion of landfill MPs were characterized through field sampling and analysis. The occurrence and behavior of MPs within landfills were examined and correlation between microplastics and the stability of the landfill was established. Especially, the relationship between MPs and odor related with sulfate reduction were evaluated. It aims to provide a scientific basis for MPs and related pollution processes controlling within landfills.

1. MATERIAOLS AND METOHDS

1.1. Study area

The tested landfill site with area of 80,000 m^2 is situated in Hangzhou, Zhejiang province in East China (Fig. 1A). It was operated in September 1995, accumulating approximately 1.35 million m^3 of landfill waste until now. The primary type of waste deposited in the landfill consists of domestic waste, with a more significant proportion accounting for lime soil, rubber, and plastic waste. The landfill leachate flows from the southern region to the northern side, where the leachate treatment station situated. It was lined by clay only. Almost 3/4 of the landfill reservoir was closed, while the left area is still undergoing service. The landfill body shows a higher elevation in the east and a lower elevation in the west. In addition, there is a higher elevation in the central region and lower elevations on the north and south sides. Farmland, settlements, and reservoirs are observed within a distance of just 500 m from the landfill.

1.2. Collection and processing of samples

Samples of waste and soil were collected from different depths both inside and outside the landfill. The sampling was conducted using a drilling rig (XY-1A, 90−110 mm). Four waste sampling wells were positioned within the landfill reservoir area, while three soil sampling points were situated outside to serve as control groups. The specific locations of the samples collection were shown in Fig 1B. The waste at FY-1 and FY-2 points were sampled at a depth of 20 m, while the waste at FY-3 and FY-4 points were sampled at depths of 12 m and 6 m, respectively. To account for the variations in landfill filling depths and waste samples, samples were taken at intervals of 3 m. Additionally, the soil samples were taken from the topsoil layer, which ranged in depth from 0 to 0.5 m. The weather of the whole week before sampling was sunny and dry. The waste and soil samples obtained were air-dried at room temperature in the laboratory, and then inert materials such as glass, stone, and wood were removed from them. Afterwards, each sample was gently turned for approximately 3 min using a flipping oscillator to ensure thorough mixing.

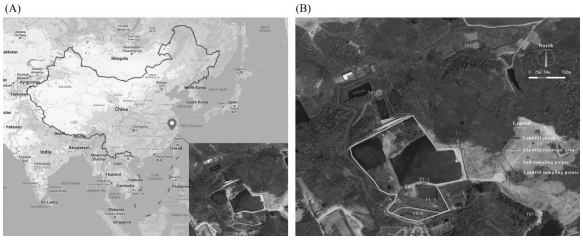

Fig. 1. Landfill location information (A) and sampling layout (B)

1.3. Measurement of MPs

1.3.1. Extraction of MPs: The method for extracting MPs from waste and soil samples were optimized (Li et al., 2022). Firstly, a 0.25 g of waste or soil sample was weighed and placed into a colorimetric tube, followed by the addition of saturated NaCl solution with a density of 1.2g·cm^{-3} to fix the volume to 25 mL. After swirling for 5 min, the matrix was inverted for 12 h. Next, the solid phase was removed via density separation, while the remaining solution was vacuumized using an aqueous filter membrane with pore size of 0.45 μm to trap the MPs. The captured MPs were then digested with 15 mL of H_2O_2 solution (30 %, v/v) at 60 ℃ for 24 h. Finally, the solution was filtered once again and rinsed at least three times with water.

1.3.2. Characterization of MPs: The MPs were suspended in 20 mL of dimethyl sulfoxide solution (50 %, v/v) with ultrapure water. The solution was then sequentially incubated at 25 ℃, 50 ℃, and 75 ℃, respectively. When each temperature was reached, 2 mL of Nile Red dye (10 $mg \cdot L^{-1}$) was added and left to stain for 10, 20, and 30 min, respectively. The cooled solution was subsequently vacuumed using 0.45 μm PTFE filter membrane. Finally, the samples were stored in glass petri dishes for further microscopic observation.

The MPs were characterized using a fluorescence microscope (DM2500, Lycra, Germany) with two levels of blue excitation light, and images were captured at 4× or 10× magnification. An efficient digital recognition software based on fluorescence label analysis was employed to identify the environmental MPs and subsequently calculate their abundance, particle size, and aspect ratio.

1.3.3. Quality assurance and quality control: The equipment used for the experiment consist of non-plastic materials, including glass and stainless steel. Prior to use, the items were thoroughly cleaned and rinsed three times with pure water. All exposed reagents and samples were covered with aluminum foil to prevent air contamination. The aforementioned operations were aimed at minimizing the contamination of MPs during the experiment. Furthermore, a blank control experiment was carried out, which ultimately revealed negligible contamination of MPs during the experimental process.

1.4. Physical and chemical analysis

The sample moisture content was determined by calculating the sample mass difference before and after drying under 105 ℃ for 24 h, while potential of hydrogen (pH) and electrical conductivity (EC) measurements were taken using the Series Meters-S20 pH meter and Five Easy Plus conductivity meter, respectively. Waste samples were also subjected for determination of sulfate (SO_4^{2-}) and dissolved organic carbon (DOC) by using ion chromatography (Metro-882 Compact IC Plus), and TOC analyzer (TOC-V CPN, Shimadzu, Japan), respectively. Additionally, S^0 and sulfide (S^{2-}) were determined through high-performance liquid chromatography (Waters e2895, USA) and methylene blue spectrophotometry, respectively (Higgins et al., 2006).

1.5. Statistical analysis

The MPs distribution of fixed points in the landfill obtained during the experiment was simulated by Surfer 15 software to obtain the MPs field characteristics basing on the sampling points in Fig. S1. SPSS 27 and Microsoft Excel 2019 were used for statistical analysis. Graphs were created using Origin 2018.

2. Results and discussion

2.1 Distribution and diffusion of MPs between landfill layers

The obtained samples from inside and outside the landfill were analyzed for MPs and correlated with their water content. A significant positive correlation was found between the two variables (P = 0.009**, R^2 = 0.7071) (Fig. 2A). To obtain a complete distribution of MPs in the landfill, measured values of MPs in the obtained samples and the theoretically calculated values of MPs, derived from the inverse regression of water content, were simulated by using the Surfer 15 software. The details of this process are described in Fig. 2B. Fig. 3 displayed the distribution of MPs found in and around the soil (0−0.5 m) in the landfill, highlighting significant differences (Fig. 3A). The MPs abundance within the landfill was significantly higher than that found outside, primarily because of the high levels of plastic waste generated. By contrast, the abundance of MPs in the surface soil adjacent to the landfill reservoir area was significantly higher than that of the distant soil, which fully indicated that MPs spread from the landfill to the outside.

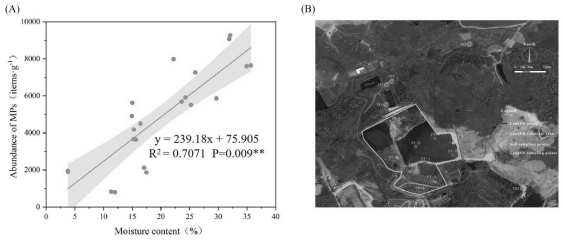

Fig. 2. Analysis of the correlation between MPs abundance and water content (A) and landfill contour simulation point bitmap (B)

The diffusion of MPs on the landfill surface was primarily influenced by surface runoff. The topography of the tested landfill was higher in the east and lower in the west, with a trough in the middle and high terrain on both sides. This created favorable conditions for high water levels to accumulate in the lower areas in the middle and west of the landfill reservoir area, resulting in the accumulation of MPs as surface runoff moves through this area. As shown in Fig. 3A. The highest measured abundance of MPs was 3573 $items \cdot g^{-1}$. Similarly, the eastern topography of the upper part of the landfill reservoir area was relatively low. As a result, high levels of MPs were present, up to 3041 $items \cdot g^{-1}$, much higher than the content found in surface soil at landfills in Iran (863−1544 $items \cdot kg^{-1}$) (Shirazi et al., 2023), Thailand (686−2278 $items \cdot kg^{-1}$) (Wang et al., 2020), and China (570−14,200 $items \cdot kg^{-1}$) (Wan et al., 2022). The prominent disparity can be largely attributed to variations in soil covering methods and approaches to leachate discharge management within each specific

landfill. This once again confirmed that the landfills are significant MPs sources, making them typical plastic fields. Simultaneously, it also can be serves as an obvious reminder of the amplified risk of MPs pollution related with the landfill. In addition, it was evident that numerous MPs were present in the soil beyond the confines of the landfill reservoir area. The theoretically calculated abundance of MPs in the soil can be as high as 1000 items·g^{-1}, which was considerably greater than those found in soils from agricultural (Zhou et al., 2020) or park areas (Fernandes et al., 2022). This suggested that there was a severe issue with horizontal migration and external diffusion of MPs in the surrounding areas of landfills. Therefore, the potential environmental risks caused by this phenomenon should not be underestimated.

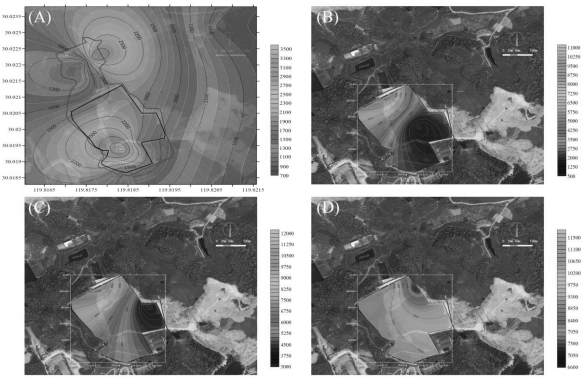

Fig. 3. Abundance distribution of MPs in surface (A), shallow (B), middle (C) and bottom (D) landfill

The vertical MPs occurrence characteristics in landfills, apart from horizontal distribution, were also determined. The distribution of MPs in the shallow layer (0−6 m), middle layer (6−12 m), and bottom layer (12−20 m) of the landfill was characterized. As shown in Fig. 3B-D. The MPs abundance distribution differed significant with depths across the entire landfill reservoir area. The shallow layer showcased a higher MPs abundance in the northwest. In the middle layer, there was a reduction in the area with low MPs abundance. Moving towards the southwest region, there was a gradual increase in the abundance of MPs. Furthermore, the high abundance area of MPs in the bottom layer was shifting from the northwest to the southwest. This phenomenon was likely due to the proximity of the northwest part of the landfill reservoir area to the leachate regulation tank, where MPs in the shallow layer tend to accumulate in low-lying areas due to leachate migration. Moreover, the west side of the landfill reservoir area was low, leading to the movement of the high MPs abundance area in the middle layer and the accumulation of MPs in the bottom layer. Hence, the topography and depth of landfills were crucial factors of MPs distribution, with significant emphasis on the differences in landfill depth.

In fact, at present, there is no definitive conclusion regarding the occurrence of MPs at different depths within landfills. Some studies have indicated that the abundance of MPs increased with landfill depth (Li et al., 2022; Yu et al., 2022; Su et al., 2019). However, from the tested landfill results (Fig. 3B-D), the highest abundance of MPs was observed in the bottom layer, ranging from 5606 to 11,679 items·g^{-1}. The middle layer showed a lower MPs abundance, ranging from 3009 to 11,575 items·g^{-1}, whereas the surface layer had the lowest one of 596−10,709 items·g^{-1}. It was noteworthy that the overall trend observed indicated an increase in MPs abundance with increasing landfill depth. Vertical and top-down migration of leachate in landfills can greatly impact the MPs distribution, often resulting in their greater abundance in deep areas. However, the potential for MPs to be trapped by landfill waste should not be overlooked, despite their generally low density and lightweight. Generally, the physical, chemical, and microbial activities within landfill waste undergo significant variations as the landfill age and depth increases. This is particularly true in deeper areas where there is often the presence of leachate saturation (Ci et al., 2022; Yang et al., 2022) and pressure (Shen et al., 2022b; Zhou et al., 2023), which can promote active microbial metabolism. Consequently, the possible reason behind the increase in MPs abundance with landfill depth could be that waste plastics present throughout the landfill degraded to varying degrees and formed MPs due to various processes that affected them during long-term accumulation. Despite being primarily non-biodegradable, the accumulation of MPs at the bottom of landfill is highly likely to have a close association with active microbial metabolic activities. This relationship deserves in-depth scrutiny and warrants significant attention.

2.2 Vertical occurrence characteristics of MPs in landfills

To further investigate the reasons behind the discrepancy in MPs abundance across various layers of the landfill, four sampling wells were selected for sampling and analyses. Generally, the landfill age is positively correlated with its depth. As observed from the MPs abundance (Fig. 4A), the MPs abundance within waste samples from FY-1, FY-2, FY-3, and FY-4 points were 1.92×10^{3}−1.16×10^{4}, 1.25×10^{3}−7.63×10^{3} items·g^{-1}, 1.63×10^{3}−3.99×10^{3} items·g^{-1}, and 3.87×10^{2}−8.06×10^{2} items·g^{-1}, respectively. However, an increasing trend was observed as the landfill depth increasing. The results showed that the MPs quantity was one or two orders of magnitude greater than those reported in relevant studies (5.90×10^{-1}−1.03×10^{2} items·g^{-1}) (Wan et al., 2022). This finding further emphasized that the environmental threat caused by MPs in landfills should not be overlooked. To provide a more intuitive visual relationship between MPs abundance and landfill depth, the abundance of

MPs in samples collected at four points was fitted to the landfill depth. As demonstrated in Fig. 4D, a significant linear positive correlation between MPs abundance and landfill depth was observed ($p < 0.05$). This pattern is also consistent with the distribution of MPs among the landfill layers throughout the previously mentioned landfill area.

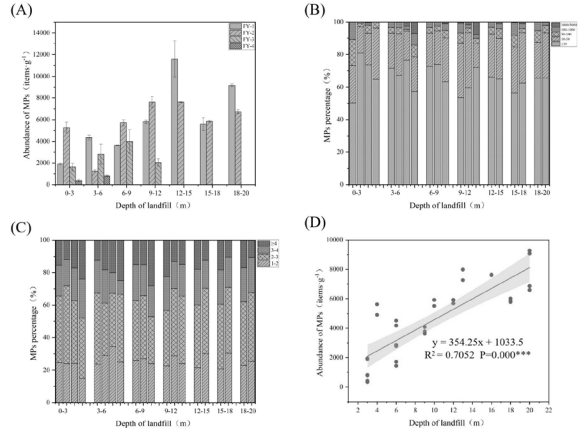

Fig. 4. Distribution of MPs abundance (A), particle size (B) and morphology (C) at different landfill depths, and correlation between landfill depth and MPs abundance (D)

According to the particle size characteristics of MPs found in FY-1, FY-2, FY-3, and FY-4 waste samples, the observed range of particle sizes was 1.20−4957.14 μm, 1.20−4930.12 μm, 1.20−4970.24 μm, and 1.20−4803.96 μm, respectively. There was no significant difference ($P > 0.05$) between the two sample sets, and the average particle size of MPs at different depths within the landfill is shown in Fig. 5. It can be observed that, apart from the upper layer's small average particle size of MPs, there was no significant difference in the average particle size of MPs among various waste samples with increasing years in landfills ($P > 0.05$), which differed from the conclusion drawn by previous studies (Li et al., 2022). The reason for this disparity could be related to the composition of landfill waste and inherent condition variances within the landfill. Furthermore, the upper layer of the landfill (approximately 4 m) consisted of overlying soil, which had fewer waste components. As a result, the abundance of MPs, especially those with larger particle sizes, was low. Additionally, applying soil cover could potentially increase the compaction degree and density of the upper layer of the landfill. This could make the MPs present within the layer more susceptible to extrusion and friction, leading to the fragmentation of large MP particles into smaller ones.

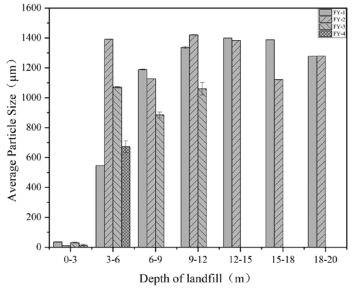

Fig. 5. Mean particle size distribution of MPs at different landfill depths

To evaluate the particle size distribution of MPs in landfills of different ages, the MPs sizes were classified into five groups: A (≤ 10 μm), B (10−50 μm), C (50−100 μm), D (100−1000 μm), and E (1000−5000 μm). The MPs particle size distribution in FY-1, FY-2, FY-3, and FY-4 waste samples showed no significant difference, as displayed in Fig. 4B. Among the different classes of MPs, Class A tiny particle size MPs accounted for the highest proportion at 65.61 %. Class B particles with a tiny particle size followed next, accounting for 24.19 % of the total. The proportion of Class C small MPs was significantly lower at 4.87 %, while Class D medium MPs and Class E large MPs were even less prevalent at 3.52 % and 1.81 %, respectively. These results suggested that MPs in landfill had undergone considerable aging. Moreover, the vertical distribution of MPs in landfills could not be entirely attributed to leachate migration since the proportion of MPs of various sizes did not exhibit significant changes with increasing landfill depth. Therefore, physical, chemical, and biological processes leading to MPs formation might play a vital role.

The morphology of MPs has a significant impact on their behavior and biotoxicity in the environment. The aspect ratio can be used to describe the morphology of MPs to some extent. MPs with an aspect ratio of 1−2 appeared mostly granular or pellet-shaped. Those with an aspect ratio of 2−3 were typically flake or wedge-shaped, MPs with an aspect ratio of 3−4 showed rod-shaped morphology, while MPs with an aspect ratio of ≥4 had fibrous structure. According to Fig. 4C, there were no significant differences between MPs' forms in waste at FY-1, FY-2, FY-3, and FY-4, and their proportion in different forms showed no significant variation with landfill depth increment. The most common forms of MPs found in landfills were flake and wedge (Li et al., 2022; Su et al., 2019; Sholokhova et al., 2023; Wan et al., 2022), accounting for 38.48 % of the total. This finding was consistent with the results of most landfill studies. Following closely behind was the granular and pellet form at 24.33 %, while fibrous and rod-shaped MPs accounted for 18.72 % and 18.47 %, respectively. The primary contributors to plastic pollution may be the bags,

bottles, and containers that are commonly used in daily life.

In conclusion, as landfill depth increased, there was a significant increase in the abundance of MPs within the landfill. However, there was no significant difference in the particle size and form of MPs. It was inferred that the occurrence of MPs within landfills was related to landfill depth but might also be influenced by other environmental factors.

2.3 Relationship between MPs distribution and key metabolic processes in landfills

Landfills are highly dynamic microbial systems, and the varying internal environmental conditions play an inevitable role in the distribution of MPs through direct or indirect effects on microbial metabolism. This study analyzed the relationship between basic survival factors such as moisture content, pH, EC, and DOC, and the abundance of MPs in landfills. As depicted in Fig. 6A, the MPs abundance was found to be positively correlated with basic survival factors, including water content, EC, and DOC, in addition to pH value. Notably, there was a significant positive correlation between water content and the abundance of MPs ($P = 0.009^{**}$, $R^2 = 0.7071$) (Fig. 2A). Thus, it can be deduced that variations in water content within the landfill had a crucial impact on the distribution and transfer of MPs. Obviously, the active microbial activity under high-water content conditions may also be related to MPs distribution.

In addition to the basic survival factors of microorganisms, this study also conducted a detailed correlation analysis between MPs and specific microbial metabolic processes. Compared with the carbon and nitrogen metabolism involved in the above-mentioned basic survival factors, this study chose sulfur metabolism, a widely criticized H_2S odor generation metabolic process, as the target for analysis. From the perspective of the distribution of sulfur metabolites and products, with the increase of landfill depth, the content of SO_4^{2-}, the main metabolic substrate that produced H_2S odor, presented a trend of gradual increase at first and then slow decreased. The reason for this had been preliminarily identified. That is, SO_4^{2-} was enriched during landfill and consumed by strong sulfate reduction behavior deep in the landfill (Long et al., 2016). Similarly, the contents of sulfur metabolism intermediate S^0 and end product S^{2-} also increased with the increase of landfill depth. Further, the MPs abundance was fitted with the contents of sulfur metabolizing substrate SO_4^{2-}, intermediate S^0, and end product S^{2-}. As shown in Fig. 6B-D, the overall abundance of MPs showed a significant linear relationship with the content of SO_4^{2-}, S^0, and S^{2-} ($P = 0.000^{***}$, $P = 0.001^{**}$, and $P = 0.000^{***}$). The results showed that the existence of MPs in landfill had an inseparable relationship with sulfur metabolism. That was, MPs showed the same frequency fluctuation regardless of SO_4^{2-} consumption (S^{2-} increase) or decay (S^{2-} decrease). Thus, the presence of MPs might affect the sulfate reduction process throughout. Therefore, it was speculated that the concerned H_2S odor generation process in landfills was also secretly coupled with the occurrence of new pollutant MPs. However, this was only a general rule of static characterization, and perhaps the dynamic process would show a clearer process, which needs further attention.

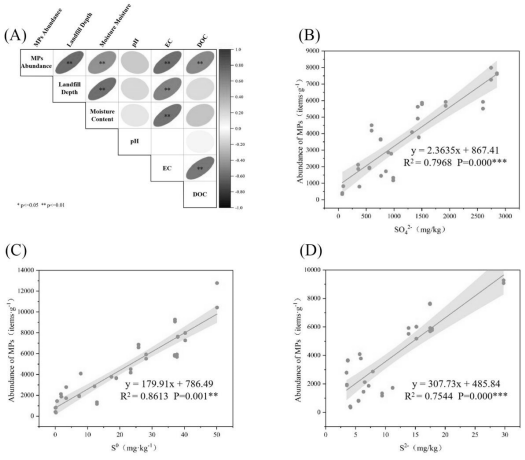

Fig. 6. Thermal map (A) of the correlation between MPs abundance and environmental factors, and analysis of the correlation between MPs abundance and SO_4^{2-} (B), S^0 (C) and S^{2-} (D)

Previous studies have shown that the presence of MPs significantly impacts microbial communities and gene pools associated with sulfate reduction. Among them, biodegradable MPs can be degraded by microorganisms, serving as a carbon source, leading to increased microbial activity in the environment. On the other hand, the unique microbial communities attached to the surfaces of petroleum-based MPs with higher environmental content may have a significant impact on sulfate reduction (Pinnell et al., 2019; Wang et al., 2023) and forming "plastisphere" (Zettler et al., 2013). MPs can interact with co-existing natural organic matter to form biofilm layers or eco-corona (Ali et al., 2022; Shi et al., 2023). It can be speculated that the presence of MPs may reshape the biodiversity of landfills, including the sulfate-reducing microorganisms. Therefore, there is an urgent need for long-term experiments to explore the associations between MPs and sulfate reduction, in order to gain a better understanding of the impact of MPs on odor release from landfills and promote the development of practical solutions to address the issues of MPs and odor pollution in landfills.

3. CONCLUSIONS

The landfill MPs risk is obvious. The landfill surface

layer with high abundance of 3573 items·g^{-1}, leading to severe pollution of the surrounding environment. The prevalence of MPs in landfill generally increased with landfill depth, featuring small-sized particles (65.61 %) measuring ≤10 μm along with flake/wedge shapes (38.48 %). The presence of MPs was more pronounced in deep layers with high-water content and rich microbial viability. Significantly, the levels of SO_4^{2-}, a common metabolic substrate for sulfate reduction, and S^{2-}, a metabolite, were positively correlated with MPs abundance inside landfill. Microplastic is a possible trigger of landfill odor emission related with sulfate reduction.

REFERENCES

Ali I., Tan X., Li J.Y., et. al., 2022. Interaction of microplastics and nanoplastics with natural organic matter (NOM) and the impact of NOM on the sorption behavior of anthropogenic contaminants - a critical review. J. Clean. Prod. 376:134314.

Alimi O.S., Claveau-Mallet D., Kurusu R.S., et. al., 2022. Weathering pathways and protocols for environmentally relevant microplastics and nanoplastics: what are we missing? J. Hazard. Mater. 423:126955.

Bharath K.M., Natesan U., Vaikunth R., et. al., 2021. Spatial distribution of microplastic concentration around landfill sites and its potential risk on groundwater. Chemosphere. 284:131376.

Canopoli L., Coulon F., Wagland S.T., 2020. Degradation of excavated polyethylene and polypropylene waste from landfill. Sci. Total Environ. 698: 134125.

Chen BF., Zhang Z.Y., Wang T.Z., et. al., 2023. Global distribution of marine microplastics and potential for biodegradation. J. Hazard. Mater. 451:131198.

Chun S., 2018. Mass balance analysis on the behavior of major elements disposed at a waste landfill site. Waste Manag. 71:233-243.

Ci M.T., Yang W.Y., Jin H.H., et. al., 2022. Evolution of sulfate reduction behavior in leachate saturated zones in landfills. Waste Manag. 141:52-62. .

Fernandes E.M.S., de Souza A.G., Barbosa R.F.D., et. al., 2022. Municipal park grounds and microplastics contamination. J. Polym. Environ. 30(12):5202-5210.

Gurjar U.R., Xavier K.A.M., Shukla S.P., et. al., 2023. Seasonal distribution and abundance of microplastics in the coastal sediments of north eastern Arabian Sea. Mar. Pollut. Bull. 187:114545.

Hahladakis J.N., Velis C.A., Weber R., et. al., 2018. An overview of chemical additives present in plastics: migration, release, fate and environmental impact during their use, disposal and recycling. J. Hazard. Mater. 344(1):179-199.

Higgins M.J., Chen Y.C., Yarosz D.P., et. al., 2006. Cycling of volatile organic sulfur compounds in anaerobically digested biosolids and its implications for odors. Water Environ. Res. 78(3):243-252.

Hoang T.C., 2022. Plastic pollution: where are we regarding research and risk assessment in support of management and regulation?. Integr Environ Assess Manag(Integrated Environmental Assessment and Management). 18(4): 851-852.

Jin Z.Y., Ci M.T., Yang W.Y., et al., 2020. Sulfate reduction behavior in the leachate saturated zone of landfill sites. Sci. Total Environ. 730:138946.

Kjeldsen, P., Barlaz M.A., Rooker, A.P., et al., 2002. Present and long-term composition of MSW landfill leachate: a review. Crit. Rev. Environ. Sci. Technol. 32(4):297-336.

Kumar R., Sharma P., Manna C., et. al., 2021. Abundance, interaction, ingestion, ecological concerns, and mitigation policies of microplastic pollution in riverine ecosystem: a review. Sci. Total Environ. 782:146695.

Li N.Y., Han Z.Y., Guo N.F., et. al., 2022. Microplastics spatiotemporal distribution and plastic-degrading bacteria identification in the sanitary and non-sanitary municipal solid waste landfills. J. Hazard. Mater. 438:129452.

Lin L., Zuo L.Z., Peng J.P., et. al., 2018. Occurrence and distribution of microplastics in an urban river: a case study in the Pearl River along Guangzhou City, China. Sci Total Environ. 644:375-381.

Lin X., Wang S., Ni R., et. al., 2023. New insights on municipal solid waste (MSW) landfill plastisphere structure and function. Sci Total Environ. 888:16382.

Long Y.Y., Fang Y., Shen D.S., et. al., 2016. Hydrogen sulfide (H_2S) emission control by aerobic sulfate reduction in landfill. Sci. Rep. 6:38103.

Lu H.C., Ziajahromi S., Ziajahromi S., et. al., 2021. A systematic review of freshwater microplastics in water and sediments: recommendations for harmonisation to enhance future study comparisons. Sci Total Environ. 781:146693.

Lu X.H., He H.P., Wang Y., et. al., 2023. Masses and size distributions of mechanically fragmented microplastics from LDPE and EPS under simulated landfill conditions. J. Hazard. Mater. 445:130542.

Luo H., Liu C., He D., et. al., 2022. Effects of aging on environmental behavior of plastic additives: migration, leaching, and ecotoxicity. Sci. Total Environ. 849:157951.

Makhadi R., Oke S.A., Ololade O.O., 2021. The influence of non-engineered municipal landfills on groundwater chemistry and quality in bloemfontein, South Africa. Molecules 25(23):5599.

Möller J.N., Löder M.G.J., Laforsch C., 2020. Finding microplastics in soils: a review of analytical methods. Environ Sci. Technol. 54(4):2078-2090.

Nayahi N.T., Ou B.L., Liu Y.Y., et. al., 2022. Municipal solid waste sanitary and open landfills: contrasting

sources of microplastics and its fate in their respective treatment systems[J]. J. Clean Prod. 380(2):135095.
Phuong N.N., Fauvelle V., Grenz C., et. al., 2021. Highlights from a review of microplastics in marine sediments. Sci. Total Environ. 777:146225.
Pinnell L.J., Turner J.W., 2019. Shotgun metagenomics reveals the benthic microbial community response to plastic and bioplastic in a coastal marine environment. Front. Microbiol. 10:1252.
PlasticsEurope., 2023. Plastics – the Facts 2022: An analysis of the latest data related to plastics production, demand, conversion and waste management in Europe.
Rahul T., Numanuddin A., Deblina D., et. al., 2023. A critical review and future perspective of plastic waste recycling. Sci. Total Environ. 881: 163433.
Rai P.K., Sonne C., Brown R.J.C., et. al., 2022. Adsorption of environmental contaminants on micro- and nano-scale plastic polymers and the influence of weathering processes on their adsorptive attributes. J. Hazard. Mater. 427:127903.
Rong L.L., Zhao L.F., Zha L.C., et al., 2021. LDPE microplastics affect soil microbial communities and nitrogen cycling.Sci Total Envirvon. 773:145640.
Sabrin S., Nazari R., Karimi M., et. al., 2021. Development of a conceptual framework for risk assessment of elevated internal temperatures in landfills. Sci. Total Environ. 782:146831.
Sanz-Lazaro C., Casado-Coy N., Beltran-Sanahuja A., 2021. Biodegradable plastics can alter carbon and nitrogen cycles to a greater extent than conventional plastics in marine sediment. Sci. Total Environ. 756:143978.
Seeley M.E., Song B., Passie R., et al., 2020. Microplastics affect sedimentary microbial communities and nitrogen cycling. Nat. Commun. 11(1):21-28.
Shen M.C., Xiong W.P., Song B., et. al., 2022a. Microplastics in landfill and leachate: occurrence, environmental behavior and removal strategies. Chemosphere. 305:135325.
Shen D.S., Zhou H.M., Jin Z.Y., et. al., 2022b. Sulfate reduction behavior in pressure-bearing leachate saturated zone. J. Environ. Sci. 126:545-555.
Shi X.D., Chen Z.J., Wei W., et. al., 2023. Toxicity of micro/nanoplastics in the environment: roles of plastisphere and eco-corona. Soil Environ. Health. 1:100002.
Shirazi M.M.G.F., Shekoohiyan S., Moussavi G., et. al., 2023. Microplastics and mesoplastics as emerging contaminants in Tehran landfill soils: the distribution and induced-ecological risk. Environ. Pollut. 324:121368.
Sholokhova A., Denafas G., Ceponkus J., et. al., 2023. Microplastics in landfill bodies: abundance, spatial distribution and effect of landfill age. Sustainability. 15(6):5017.
Staley B.F., de los Reyes F.L., Wang L., et. al., 2018. Microbial ecological succession during municipal solid waste decomposition. App. Microbiol. Biotechnol. 102(13):5731-5740.
Su Y.L., Zhang Z.J., Wu D., et. al., 2019. Occurrence of microplastics in landfill systems and their fate with landfill age. Water Res. 164:114968.
Tunali M.M., Myronyuk O., Tunali M., et. al., 2022. Microplastic abundance in human-influenced soils in recreational, residential, and industrial areas. Water Air Soil Pollut. 223(11):433.
Turan N.B., Erkan H.S., Engin G.O., 2021., Current status of studies on microplastics in the world's marine environments. J. Clean. Prod. 327:129394.
Wan Y., Chen X., Liu Q., et. al., 2022. Informal landfill contributes to the pollution of microplastics in the surrounding environment. Environ Pollut. 293:118586.
Wang W., Ge J., Yu X., et. al., 2020. Environmental fate and impacts of microplastics in soil ecosystems: progress and perspective. Sci. Total Environ. 708:134841.
Wang H.L., Yang Q., Li D., et. al., 2023. Stable isotopic and metagenomic analyses reveal microbial-mediated effects of microplastics on sulfur cycling in coastal sediments. Environ. Sci. Technol. 57:1167-1176.
Yang W.Y., Ci M.T., Hu L.F., et. al., 2022. Sulfate-reduction behavior in waste-leachate transition zones of landfill sites. J. Hazard. Mater. 428:128199.
Ying L.Y., Long Y.Y., Yao L.H., et. al., 2019. Sulfate reduction at micro-aerobic solid – liquid interface in landfill. Sci. Total Environ. 667:545-551.
Yu F., Wu Z., Wang J., et. al., 2022. Effect of landfill age on the physical and chemical characteristics of waste plastics/microplastics in a waste landfill sites. Environ. Pollut. 306:119366.
Zettler E.R., Mincer T.J., Amaral-Zettler L.A., 2013. Life in the "plastisphere": microbial communities on plastic marine debris. Environ. Sci. Technol. 47(13):7137-7146.
Zha F.G., Shang M.X., Ouyang Z.Z.,et. al, 2022. The aging behaviors and release of microplastics: a review. Gondw. Res. 108:60-71.
Zhou B.Y., Wang J.Q., Zhang H.B., et. al., 2020. Microplastics in agricultural soils on the coastal plain of Hangzhou Bay, east China: Multiple sources other than plastic mulching film. J. Hazard. Mater. 388:121814.
Zhou H.M., Guo S.L., Hui C.,et. al, 2023. Sulfate reduction behavior in response to changing of pressure coupling with temperature inside landfill. Waste Manag. 171:491-501.

HYDROTHERMAL PRETREATMENT ENHANCED ENZYMATIC HYDROLYSIS OF WASTE TISSUE PAPER FOR BIOETHANOL PRODUCTION

Pin Lv [1,2], Hongzhi Ma [1, 2*], Yueyao Wang [1,2] and Qunhui Wang [1,2]
1 Department of Environmental Science and Engineering, University of Science and Technology Beijing 100083, China
2 Beijing Key Laboratory of Resource-oriented Treatment of Industrial Pollutants, Beijing 100083, China
* Corresponding author:
E-mail: mahongzhi@ustb.edu.cn

ABSTRACT
In this study, four types of different waste paper were selected for hydrolysis and ethanol fermentation. And tissue paper (TP) was adopted as a representative waste paper and high-pressure hydrothermal with various solvents (water, 1% w/v NaOH, or DES) were performed.With 68.42 ± 3.42% carbohydrates (cellulose+ hemicellulose) present, TP shows potential as a renewable biomass for bioethanol production. SEM, EDS and 3DEEM results showed that the structure of TP could be effectively destroyed under the optimal pretreatment conditions while removing the additive components on the surface.The optimum process conditions of high pressure hydrothermal pretreatment of TP were determined by single factor test. These conditions included a duration of 50 minutes in a high-pressure reactor with pure water as the solvent at 160°C. The biomass-to-water ratio was maintained at 1:25 (w/v), and the optimum severity factor (SF) was determined to be 3.47. The resulting pretreated TP exhibited a 72-hour reducing sugar yield of 0.61 g sugar/g paper, which was 38.64% higher than untreated TP.

INTRODUCTION
Waste paper constitutes a major fraction of municipal solid waste, comprising over 35% of total lignocellulosic waste. Annually, more than 400 million tonnes of waste paper is generated worldwide, but only about 50-65% is recycled[1]. Waste paper typically consists of 60-70% cellulose, with lower amounts of hemicellulose (10-20%) and lignin (5-10%)[2]. The composition of waste paper make it feasible for conversion to bioethanol due to its widespread availability, low cost and high carbohydrate content. However, most of the current research on the ethanol fermentation of waste paper is centred around office paper, and not much research has been done on the effect of different types of paper on ethanol fermentation, which is needed to determine the best substrate.
In this study, paper types were screened and analysed for their properties, followed by hydrothermal solvent screening and pre-treatment optimisation. These findings provide a theoretical basis for the efficient yield of reducing sugars and subsequent ethanol fermentation.

BASIC QUANTITATIVE COMPOSITIONAL ANALYSIS OF THE MATERIAL
Analysis of raw material components:Cellulose represents glucose content, while hemicellulose represents xylose content in the following enzymatic process. The analysis of raw cellulose, hemicellulose, and lignin from the five varieties of waste paper is depicted in Table 1. Tissue paper features the highest cellulose content of all waste paper types at 59.60±2.98%, followed by newspaper and kraft paper, at percentages of 51.47±2.57% and 49.45±2.47%. Another benefit of waste tissue paper is that it is non-recyclable waste, which can provide greater environmental and economic benefits if utilized properly. Thus TP was selected in this study as the raw materials for following hydrolysis.

Table 1: Quantitative compositional analysis of tested types of the waste paper

Type of paper	Cell-(%)	Hem-(%)	Lig-(%)
Tissue paper	59.60	8.82	29.93
Cardboard paper	46.50	9.27	20.39
Kraft paper	49.45	6.76	25.71
Office paper	44.55	7.43	19.74
Newspaper	51.47	10.29	16.08

Effect of different hydrothermal solvent pretreatments: The findings from the evaluation of TP subsequent to hydrothermal pre-treatment using three distinct solvents are showed in Fig 1. It showed after hydrothermal treatment using varying solvents, the overall cellulose (comprising cellulose and hemicellulose) in the TP was

enriched. Total cellulose was enriched in ascending order by 1% NaOH, water, DES. Specifically, with 1% NaOH used as the solvent, the whole cellulose was enriched up to 95%(94.0 ± 4.62%), was observed in comparison to 68.42 ± 3.42% in the control group, representing an increase of 40.22%. The lignin content was reduced to 5.66 ± 0.28% from 29.93 ± 1.50% in the control group, which represents an 81.09% reduction. The best enrichment of total cellulose by 1% NaOH may be attributed to its efficient disruption of lignocellulosic biomass structure thereby enhancing the solubilisation of lignin fractions.NaOH disrupts the connection between hemicellulose and lignin through solubilisation and saponification reactions, which destroys and separates the lignin due to the disruption of the ester bond[3].

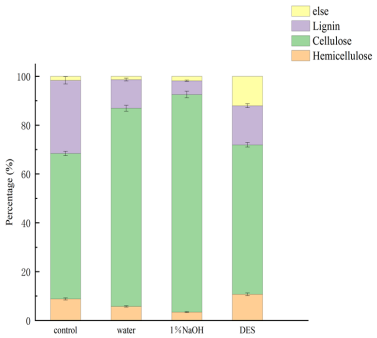

Fig 1: Percentage of material composition of TP after different pretreatment

CHARACTERIZATION OF TP

The XRD of waste paper with and without hydrothermally treatment with different solvents were shown in Fig. 2a. The diffraction peaks with 2θ in the range of 16°-17° were attributed to the crystalline plane of (101) of cellulose I_β, representing the amorphous region of cellulose, and the diffraction peaks with 2θ in the range of 22°-23° were attributed to the crystalline plane of (002) of cellulose I_β, representing the crystalline region of cellulose[4]. The diffraction peaks of 2θ in the range of 34°-35° are attributed to the crystallographic plane of (004) of cellulose I_β, indicating the presence of cellulose type I in tissue paper[5]. The diffraction peaks in the amorphous and crystalline regions of TP after hydrothermal pretreatment with different solvents were similar, but the peak areas were different. As shown in Fig. 2(b-e), the crystallinity (CrI) of cellulose in the samples was calculated by the peak deconvolution method (PDM) using Jade software[6]. The CrI in the untreated TP was 47.92%, whereas it was reduced to 33.66% after hydrothermal pretreatment with water as solvent, 34.27% with 1% NaOH and 29.28% with DES as solvent. The various degrees of reduction in CrI, indicated that the crystalline zone in the tissue paper was disrupted.The variation of crystallinity of materials after hydrothermal pretreatment with different solvents also explains the mechanism of total cellulose enrichment. That is, the dissolution of lignin is increased by destroying the crystalline zone of the material.

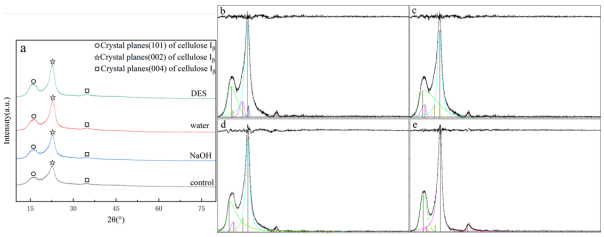

Fig 2: XRD patterns(a) and jade images(b-e) of Tissue paper with different hydrothermal solvent: (b)control; (c) water; (d)NaOH; (e) DES

3DEEM ANALYSIS OF PRETREATMENT HYDROLYSATE

The hydrothermal pretreatment efficiently exposed cellulose to biodegradation by eliminating a portion of the hemicellulose and lignin fractions. However, the degradation of these components also generates compounds that are challenging to decompose. The dehydration of pentose monomers acquired by the degradation of hemicellulose results in furfural, while the degradation of hexose (glucose) obtained from degraded cellulose can produce hydroxymethylfurfural (HMF). Inhibitors present in the hydrolysis products derived from waste tissue paper that had undergone hydrothermal pretreatment with varying solvents were analysed using 3DEEM. The findings are presented in Figure 3 (a-c). Only phenolic substances representing lignin were detected in the hydrolysate, and furfural representing cellulose and 5-HMF representing hemicellulose were not detected, which indicated that the influence of hydrothermal pretreatment materials was mainly concentrated on the solubilization of lignin, but almost did not decompose cellulose and hemicellulose. This also explains that the lignin content of the materials decreased to varying degrees after pretreatment, resulting in an increase in the ratio of cellulose to hemicellulose in the materials.The analysis of the hydrolysate explains the mechanism of hydrothermal pretreatment, including the decomposition of lignin in the material into soluble phenolic substances to release the structural binding of the material.

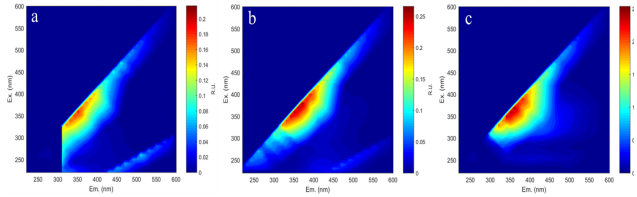

Fig 3: 3DEEM images(a-c) of Tissue paper hydrolysate with different hydrothermal solvent: (a)water; (b) NaOH; (c) DES

EFFECT OF VARIOUS HYDROTHERMAL CONDITIONS ON THE ENZYMATIC PROPERTIES OF TP

The hydrothermal results for various solvents are presented in Figure 4(a,d). Hydrothermal temperature was fixed at 160°C, hydrothermal time was 50 minutes, and SF's calculated value was 3.47. Pretreatment with water as a solvent produced the highest enzyme accessibility of the biomass. The resulting enzyme hydrolysis yield of the pretreated waste tissue paper was 0.61 g sugar/g paper, which is a 38.64% increase compared to the yield of 0.44 g sugar/g paper in the blank control group. Pretreatment using 1% NaOH as a solvent resulted in an enzyme hydrolysis yield of 0.58 g sugar/g paper, a 31.82% increase. The pretreatment using DES as a solvent resulted in an enzyme hydrolysis yield of 0.38 g sugar/g paper, which was 13.64% lower than the yield of the blank control. Organic acid-based DES disrupts the hydrogen bonding network between lignocellulosic components, while selectively solubilising specific components of the feedstock. However, it has the highest pKa of all tested solvents and ionises the largest amount of hydrogen ions to attack lignocellulose during pretreatment[7]. This accounts for the 13.64% decrease in enzymatic hydrolysis results for tissue paper pretreated with hydrothermal-assisted organic acid-based DES compared to the blank control group. Meanwhile, hydrothermal pretreatment using 1% NaOH improved the results by 31.82%, also compared to the control group.The findings indicate that higher sugar yields can be achieved for waste tissue paper through pre-treatment with pure water at appropriate temperatures without the addition of solvents or acidic and alkaline substances. This approach is deemed more economically and practically viable compared to the expense of other chemicals. Therefore, it is suggested that hydrothermal pretreatment presents an effective and environmentally friendly method for treating waste paper.

Several studies have also shown that the increase in saccharification yield of pretreated substrates is a result of significant removal of hemicellulose, enhancing fibre porosity and increasing enzyme accessibility to cellulose fractions[8].The ideal hydrothermal pretreatment condition for TP was established through one-way optimization experiments, identifying pure water as solvent, and a temperature of 160°C maintained for 50 minutes, with an optimum SF of 3.47. The resulting reducing sugar yield after 72 hours was 0.61g of sugar per paper, indicating a 38.64% increase when compared to TP that was untreated.

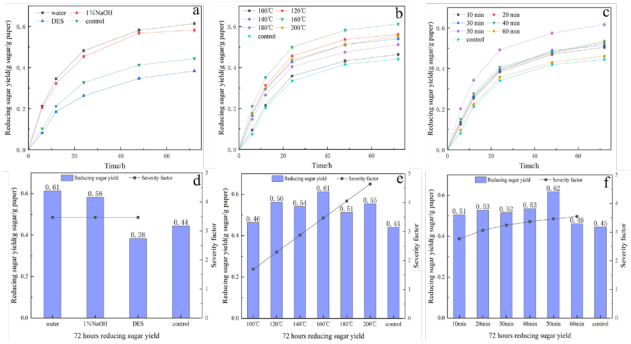

Fig 4: Enzyme hydrolysis images(a-f) of Tissue paper with different hydrothermal pretreatment conditions:
(a,d) solvent; (b,e) temperature; (c,f) time

CONCLUSION

1) Five different waste paper materials were analysed for their cellulose, hemicellulose, and lignin composition. The waste paper towel with the highest holocellulose content (68.42%) was identified for resource utilisation.

2) After hydrothermal pretreatment with water as solvent, the total cellulose of TP was enriched from 68.42±3.42% to 92.67±4.35%, while the crystallinity decreased from 47.92% to 33.66%. According toXRD and 3DEEM, the influence mechanism of hydrothermal pretreatment on the material includes ionizing solvent ions and high pressure physical action to destroy the structure of lignocellulosic biomass.

3) The optimal hydrothermal pretreatment condition for TP was established as holding at 160°C for 50 minutes with pure water as the solvent and an optimal SF of 3.47. The resulting 72-hour reducing sugar yield was 0.61 g sugar/g paper, representing a 38.64% increase when compared to the untreated waste TP.

ACKNOWLEDGEMENTS

This research was supported by National key R & D program of China (2022YFE0105700)

REFERENCES

[1] Annamalai N, Sivakumar N, Oleskowicz-Popiel P. Enhanced production of microbial lipids from waste office paper by the oleaginous yeast Cryptococcus curvatus [J]. Fuel, 2018, 217: 420-6.

[2] Kumar V, Pathak P, Bhardwaj N K. Waste paper: An underutilized but promising source for nanocellulose mining [J]. Waste Manag, 2020, 102: 281-303.

[3] Gandam P K, Chinta M L, Pabbathi N P P, et al.

Second-generation bioethanol production from corncob – A comprehensive review on pretreatment and bioconversion strategies, including techno-economic and lifecycle perspective [J]. Industrial Crops and Products, 2022, 186.
[4] Dubey A K, Gupta P K, Garg N, et al. Bioethanol production from waste paper acid pretreated hydrolyzate with xylose fermenting Pichia stipitis [J]. Carbohydrate Polymers, 2012, 88(3): 825-9.
[5] French A D. Idealized powder diffraction patterns for cellulose polymorphs [J]. Cellulose, 2014, 21(2): 885-96.
[6] Park S, Baker J O, Himmel M E, et al. Cellulose crystallinity index: measurement techniques and their impact on interpreting cellulase performance [J]. Biotechnology for biofuels, 2010, 3: 1-10.
[7] Tang W, Huang C, Ling Z, et al. Enhancing cellulosic digestibility of wheat straw by adding sodium lignosulfonate and sodium hydroxide to hydrothermal pretreatment [J]. Bioresource Technology, 2023, 379: 129058.
[8] Jeoh T, Ishizawa C I, Davis M F, et al. Cellulase digestibility of pretreated biomass is limited by cellulose accessibility [J]. Biotechnology and bioengineering, 2007, 98(1): 112-22.

Development of Melting Furnace to Achieve Resource Circulation

Yasumasa Hirato[1], Yuto Onuma[1], Motohiro Sakamoto[1], Fumiki Hosho[1], Shigenori Inoue[1], Eiichi Tsuji[2]
1 Water and Environment R&D Dept.I, Kubota Corporation,
1-1, Hama 1-chome, Amagasaki, Hyogo ,661-8567 Japan
2 Incineration and Melting Engineering Dept., Kubota Corporation,
1-1, Hama 1-chome, Amagasaki, Hyogo ,661-8567 Japan

ABSTRACT

In our long term vision GMB2030, Kubota aims to build solutions of resource circulation. The Kubota Surface Melting Furnace (KSMF) is one of the core technologies, and this report describes on the fuel cost reduction of KSMF and recovery of metals from slag produced from KSMF by using a metal separator. As for reduction of fuel cost, a series of tests were conducted to change fuel from kerosene to RPF (Refuse Paper & Plastic Fuel). We achieved self-sustaining combustion (fossil fuel-free) operation for more than 84 hours continuously. Regarding the recovery of metals, as a result of tests using a metal separator, 92% of the copper in the raw materials could be recovered. The precious metal concentration was 10 to 89 times more concentrated, and it was confirmed the high potential value of the recovered material.

1. INTRODUCTION

In recent years, the demand for resource circulation has been increasing worldwide due to the concept of SDGs and the declaration of carbon neutrality by many countries. In the field of waste treatment, the 2021 revision of the Basel Convention restricts the import and export of waste plastics. Due to these circumstances, countries, local governments, and businesses are required to take more concrete and realistic action. Kubota's long-term vision GMB2030 calls for “building resource recovery solutions” and positions melting technology as one of its core technologies. We are currently developing technologies to effectively utilize waste plastics that are difficult to recycle, and to recover valuable metals contained in residue from recycle process for automobiles, electrical and electronic products, etc. This report introduces the current development status.

2. OUTLINE OF THE TECHNOLOGY

2.1. Features of Kubota Surface Melting furnace

Kubota surface melting furnace (KSMF) is a device that thermochemically separates and concentrates the elements in the material to be treated by melting it at high temperatures. It has a double cylindrical structure with an outer cylinder and an inner cylinder, and the waste is put between these two cylinders. The waste is supplied into the furnace by rotating the outer cylinder and the integrated floor. The inside of the furnace is maintained at approximately 1,250-1,350°C using a fuel burner. The waste is melted and flows towards the center of the furnace and falls through the slag port into the water tank. The melted waste rapidly cooled in the water tank is discharged outside the furnace as sandy slag (Fig. 1). The slag can be used as civil engineering materials. And also, the slag contains valuable metals (containing gold, copper, etc., hereinafter referred to as metals) derived from waste. If metals are separated from slag, metals that are more concentrated than ore can be extracted. It can be recovered and recycled as a raw material for refining non-ferrous metals, making it possible to achieve resource circulation. In addition, heavy metals with low boiling points such as lead and cadmium contained in the processed material are removed by volatilization in a high-temperature furnace and recovered as fly ash from melting furnace. These heavy metals can also be reused by non-ferrous refinery.

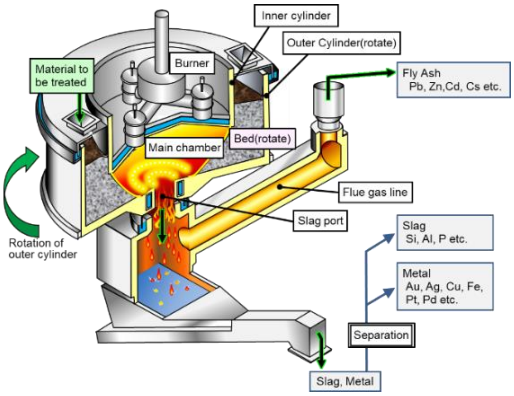

Fig.1 Schematic Diagram of
Kubota Surface Melting Furnace (KSMF)

2.2. Issues of the technology

Various efforts are necessary to realize resource circulation that takes advantage of the separation and recovery performance of melting technology. The most

pressing issues are as follows. The first issue is the reduction of fuel costs. Due to the recent rise in crude oil prices, fuel costs account for one-third of the life cycle costs of melting processing facilities, and reducing them is essential to ensure customer business viability. The second issue is the improvement of recovery rate of precious metals from recycling residues such as mixtures of waste plastics, metals, glass, etc.. The recovery involves recovering trace amounts of precious metal components contained in recycling residues such as shredder residue (SR). This is an initiative to promote resource circulation and contribute to society by recovering low-concentration metals that are disposed of in landfills in high-concentration and high-grade materials. This report will discuss the above two points.

3. OVERVIEW OF THE DEVELOPMENT

3.1. Concept of the development

3.1.1. Reduction of fuel costs: The reduction of fuel costs will be achieved by a fuel conversion from kerosene to waste plastic. [1] The waste plastic is inexpensive compared to kerosene in terms of cost per heating value, which not only contributes to lower fuel costs, but also can contribute to solving the global problem of waste plastic disposal. In the test, RPF was used and mixed with the material to be processed and supplied to the melting furnace. RPF is a solid fuel made from waste plastic and waste paper, which are difficult to recycle, and is used as an alternative to fossil fuels such as coal and coke.

3.1.2. Precious metal recovery from recycling residue: A metal separator is used to separate and recover valuable metals from the molten slag produced in the melting furnace. Separation of metals is performed by wet specific gravity separation. [2] The metal separator is a machine that has a proven track record in resource recovery from about 1 million tons of illegal dumped waste in Teshima-island, Japan, which Kubota conducted in the 2000s.

3.2. Development objectives

3.1.1. Reduction of fuel costs: The development objectives were to achieve self-sustaining operation (zero kerosene usage) and to maintain self-sustaining operation for 72 hours. Self-sustaining operation is an operation in which the temperature inside the furnace is maintained above the melting temperature of the material to be processed (approximately 1,300°C) using only the combustion heat of the RPF without using any kerosene burner. 72 hours continuous operation is set as an indicator of the stability of self-sustaining operation.

3.1.2. Precious metal recovery from recycling residue: The amount and recovery rate of precious metals recovered from SR were used as evaluation indicators. We evaluated the technology of separation and concentration. In addition, we evaluated the economic potential of recovered metals.

3.3. Overview of the test

3.1.1. Reduction of fuel costs: A series of test was conducted with the cooperation of “Clean Park Saga”, an industrial waste treatment facility of the Saga Prefecture, Japan. The flow diagram, equipment outline, and RPF specifications are shown in Fig. 2, Table 1, and Table 2. The test was conducted six times in total from November 2021 to December 2022, with each test was conducted for approximately two consecutive weeks.

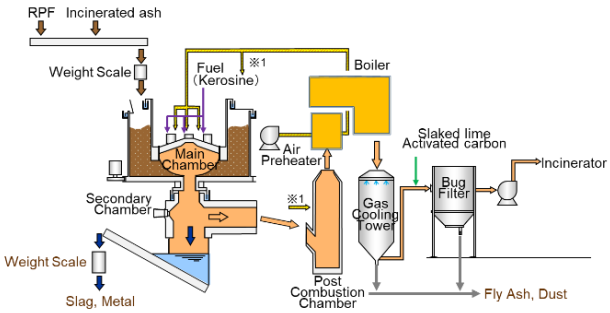

Fig.2 KSMF Flow Chart of Clean Park Saga

Table1 Facility Outline

Name of facility	Clean park Saga
Location	Karatsu-city, Saga
Operation start	April, 2009
Processing object	Industrial waste
Incinerator	Rotary kiln furnace 84t/day(42t×2 Furnace)
Melting furnace	Surface melting furnace 23.3t/day

Table2 Property of RPF

Size	φ10mm×20mm
Ash	4.4%
TVS	95.6%
Water content	1.0%
LHV	31.8MJ/kg (Kerosene : 43.3MJ/kg)
Price per LHV	0.63 ¥/MJ (Kerosene : 2.31 ¥/MJ)

Fig.3 RPF Used for the Test

3.1.2. Precious metal recovery from recycling residue: Melting tests and metal separation tests using SR were conducted at Kubota Shin-Yodogawa Environmental Plant Center (Osaka Prefecture, Japan).

For SR, we used a sample provided by Hoshiyama Shoten Co., Ltd.. Waste glass was mixed and melted with SR as a simulated incineration ash. Waste glass is suitable for the test because it does not contain precious metals and thus does not effect to the metal recovery we are planning to evaluate. As shown in Fig. 4, the metal separator separates the target material by specific gravity while stirring it inside a rotating drum. A mixture of slag and metal mixed with water is introduced from the top of the drum, and water is also introduced from the bottom of the drum. The heavy materials (metal, specific gravity 6-8) that overcomes the water flow from the bottom are collected at the bottom, and the light materials (slag, specific gravity 3) is discharged from the top along with the water, then this allows the metal and slag to be separated.

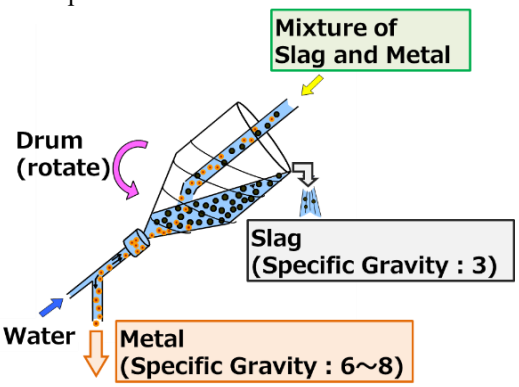

Fig.4 Schematic Diagram of Metal Separator

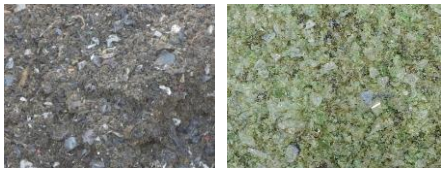

Fig.5 Photos of SR and Glass for the Test

4. RESULTS

4.1. Reduction of fuel costs

In a test conducted in September 2022, Continuous self-sustaining operation was succeeded for 84 hours, exceeding the target of 72 hours (Fig. 6). The RPF mixing ratio was 32% of processed material (Table3). Regarding the reduction of fuel costs, it was evaluated that the running costs (fuel costs, chemical costs for exhaust gas treatment, disposal costs of fly ash) that are affected by the fuel change, and was found that 33% reduction compared to conventional ash melting. If waste plastic itself is used as fuel instead of RPF, the cost of purchasing RPF can be further reduced, and the reduction is expected to be approximately 65%. These results have been highly evaluated by customers, and actual implementation is planned on January 2024. Furthermore, the exhaust gas properties during the test were below regulation values, and the results of the slag elution and content tests were also below standard values, confirming that there were no problems with facility operation.

During the test, an infrared camera was inserted into the furnace, and the furnace was operated while checking the conditions inside the furnace. This camera can withstand the high temperature of 1,300°C inside the furnace, and can visualize the situation inside the furnace, moreover it can also measure the temperature field like a thermography. Fig.7 shows a comparison between good and bad conditions inside the furnace. Red color indicates high temperature, 1,400°C, and blue color indicates 500°C. It is captured that in the good condition on the left, the processed material with RPF (yellow: low temperature material at 1,050°C) is being supplied ON the melting surface, but in the bad condition on the right, the material has sunk BENEATH the melting surface.

This state is shown in Fig. 8 as a cross-sectional schematic diagram. In good conditions, RPF is fed onto the melting surface and burns properly due to the heat and oxygen in the furnace. On the other hand, in a bad condition, there is a fixed objects in the supply section, RPF is supplied so as to sneak under the molten surface, and it cannot react with the oxygen in the furnace, making it difficult for the RPF to burn. It is thought that the fixed objects in the supply section is caused by carbonization of the RPF before it enters into the furnace. It was confirmed that in such a bad condition, the temperature inside the furnace would drop and self-sustaining operation would no longer be possible.

As a solution, in order to suppress carbonization of the RPF, we monitored the temperature at the bottom of the supply cylinder and operated to prevent the RPF from heating up before entering the furnace. It was confirmed that this method can suppress carbonization. In addition, as mentioned earlier, the condition of the supply can be detected using images from an infrared camera. Therefore, we have developed a program that processes the video to automatically determine whether the supply is good or bad. This program is used for furnace operation adjustments.

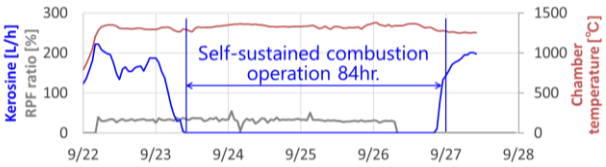

Fig.6 Time Trend of Operation

Table3 Evaluation of Processing Amount

RPF mixing ratio	0%	32%
Evaluation time	33Hr	39Hr
Input amount of ash	1.01t/h	0.63t/h
Input amount of RPF	0.00t/h	0.29t/h
Input amount	1.01t/h	0.92t/h
Kerosene	216L/h	0L/h
Produced amount of slag	1.02t/h	0.71t/h

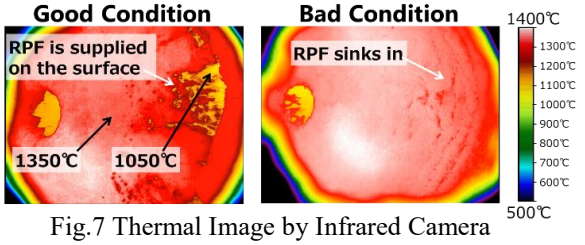

Fig.7 Thermal Image by Infrared Camera

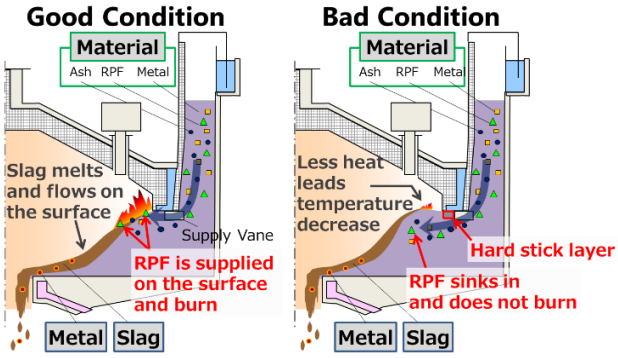

Fig.8 Comparison of Supply Condition

4.2. Precious metal recovery from recycling residue

Table 4 shows the three components of SR used in the test and the concentrations of precious metals contained in SR. Gold and platinum were below the detection limit, but trace amounts of precious metals were confirmed, with silver at 2.8 mg/kg, copper at 1.11%, and palladium at 0.33 mg/kg. However, due to its low concentration, it cannot be used as a raw material for non-ferrous refining in the SR state.

The molten slag processed by melting SR was passed through a metal separator, and the recovered metal was analyzed. Table 5 shows the results. The precious metal concentrations in the recovered metals were all higher than in SR, with the concentration ratio being over 65 times higher for gold and 89 times higher for silver. The recovery rate of precious metals in SR, for example, was 92.2% for copper. The remaining 7.8% is thought to be incorporated into the slag as oxides or small metal particles. Additionally, the potential value of the recovered metal was 11,972 JPY per ton of molten slag (estimated based on October 2022 bullion prices).

From the above, it was confirmed that the melting furnace and metal separator were able to concentrate and recover precious metals in SR to a high concentration, and that the recovered metals had high potential value.

Table4 Property of SR

Ash	25.3%			
TVS	74.7%			
Water content	10.2%			
Metal concentration				
Au	Ag	Cu	Pt	Pd
<0.2mg/kg	2.8mg/kg	1.11%	<0.2mg/kg	0.33mg/kg

Table5 Result of Metal Recovery

	SR (A)	Collected Metal (B)	Concentration ratio =B/A
Au	<0.2mg/kg	13mg/kg	>65
Ag	2.8mg/kg	249mg/kg	89
Cu	1.11%	53.9%	49
Pt	<0.2mg/kg	2mg/kg	>10
Pd	0.33mg/kg	5mg/kg	17

5. CONCLUSIONS

In order to realize resource circulation by using Kubota Surface Melting Furnace, we conducted tests to reduce fuel costs of KSMF and recover precious metals from the molten slag.

5.1. Reduction of fuel costs

A test was conducted in which the fuel of KSMF was changed from kerosene to RPF (waste plastic), and the target of 72 hours of the self-sustaining operation was achieved (actual result: 84 hours). The effect of reducing fuel costs was confirmed.

In the future, in order to utilize not only highly granulated RPF but also wastes such as raw waste plastic, recycling residue, etc. as fuel, we will develop a simple granulation system that can transform waste into a shape suitable for KSMF's fuel.

5.2. Precious metal recovery from recycling residue

As a result of melting SR and collecting the metal by applying the metal separator, it was able to recover 92% of the copper in SR. The precious metal concentration was 10 to 89 times more concentrated compared with raw SR, and it was confirmed the recovered material have a high potential as an urban mining resourcing.

In the future, in order to recover metals that cannot be recovered at present, we will improve the metal recovery rate, including the operation adjustment of KSMF.

ACKNOWLEDGMENTS

We would like to express our gratitude to the Saga Prefecture Environmental Clean Foundation for the demonstration test of fuel cost reduction, and Hoshiyama Shoten Co., Ltd. for the precious metal recovery test using SR, in developing the technology in this report.

REFERENCES

[1] Y.Hirato, F.Hosho, S.Inoue, E.Tsuji, "Development of energy-saving techonology for a melting furnace using RPF as a combustion improver." *The 34th Annual Conference of JSMCWM*, 2023

[2] M.Sakamoto, K.Akasaka, Y.Onuma, S.Okaichi, F.Hosho, S.Inoue, D.Higashi, F.Watanabe, K.Hoshiyama, "Development of Technology for Recycling Thermal Energy and Valuable Metals from Industrial Waste by Using the Surface Melting Furnace" *The 33rd Environmental Technology Symposium of JSME*, 2023

Enhanced chloride removal from MSWI fly ash using an accelerated wet-carbonation process

Yunmei Wei*[1], Xiaoqi Du[1], Sijie Liu[1], Yi Wen[1], Qin Liao[1], Gangzhen Jiao[2]

1 Key Laboratory of Three Gorges Reservoir Region's Eco-Environment, Ministry of Education, College of Environment and Ecology, Chongqing University, Chongqing, 400045, P.R. China

2 Department of Environmental Science and Safety Engineering, Tianjin University of Technology, Tianjin, 300384, P.R. China

*Corresponding author: Yunmei Wei (Tel./fax: +86-023-65120750)
E-mail: wym_1982@cqu.edu.cn; creansr@126.com

ABSTRACT: This study evaluated three wet-based pretreatment methods (water-washing, CO_2-aided washing, and flue gas-aided washing) to remove chlorides using MSWI fly ashes from 13 incineration plants in China. Water washing was suitable for removing Cl^- from MSWI fly ash containing a limited amount of less-soluble Cl^-containing salts. However, for fly ash with a significant proportion of these less-soluble Cl-containing salts, injection of CO_2/flue gas during washing promoted their decomposition and increased the chloride removal rates by 2–12%. Compared with chloride, the removal rate of sulfate was lower under all treatment scenarios and ranged from 7% to 47%. Therefore, caution should be taken when exploring techniques for the deep removal of chloride from MSWI fly ash, as sulfates may be the limiting factor in fly ash samples with low chloride contents when utilizing the fly ash for cement clinker production. This study confirmed that CO_2/flue gas injection during washing promoted the removal of the less-soluble harmful components of fly ash, expanding the applications of ash materials.

KEYWORDS: MSWI fly ash; carbonation; chloride; salt removal; recycling; cement clinker

INTRODUCTION

Washing with water or acid/alkaline solutions is the most frequently adopted method to remove chloride salts and other soluble components from fly ash, which increases its replacement percentages in cement kilns. Water washing is an effective pretreatment approach for chloride removal, but the chloride removal ratio varies widely from 40% to 90% [1–3]. For fly ash samples with lower chloride removal efficiencies, acid washing may improve chloride removal. However, the high alkalinity of the fly ash residues, mainly caused by the high content of Ca-containing compounds in fly ash, can make it challenging to improve the concentration of target constituents leached by acids[4,5]. A high acid consumption will also be economically disadvantageous.

CO_2-aided washing is a potential alternative for enhancing chloride removal from MSWI fly ash. This work adopted fly ash samples from 13 waste incineration plants to examine the effect of different wet pretreatment methods on chloride removal, including water washing, CO_2-aided washing, and flue gas-aided washing. Due to the high cost of pure CO_2 and the potential of utilizing waste/flue gas from an incineration plant as the CO_2 source, simulated flue gas (containing 20% CO_2 and 80% N_2) has been used. Theoretically, CO_2 injection during ash washing pretreatment should enhance chloride removal and also capture CO_2, thus reducing CO_2 emissions into the atmosphere, which is particularly important for China's "Dual Carbon Target Strategy" [6]. This research aims to promote the mass recycling of MSWI fly ash by reducing the chloride content of fly ash. The focus of current study is to evaluate the impact of CO_2 injection on the removal efficiency of Cl^- by using MSWI fly ash samples from 13 waste incineration plants. Because MSWI fly ash shows significant potential to be used to produce cement clinker, this study further evaluated the effect of pretreatment on the ash blending ratio to partially replace traditional raw materials.

EXPERIMENTAL DESIGN TO REMOVE CHLORIDE FROM MSWI FLY ASH

MSWI fly ash samples were collected from 13 incineration plants in China, namely CQ-A, CQ-B, CQ-C, BJ-A, AH-A, AH-B, AH-C, TJ-A, SZ-A, SZ-B, SZ-C, SZ-D, and SH-A incineration plant. Three sets of experiments were used to determine the critical factors influencing the removal efficiency of chloride from MSWI fly ash. In the first set of experiments, water-washing pretreatment was performed to determine the chloride removal efficiency of all ash samples from 13 incineration plants. Based on the results of the first set of experiments, CO_2-aided washing was also conducted for the ash samples with lower chloride removal rates. In the second set of experiments, the ash was washed with distilled water under continuous CO_2 bubbling at a flow rate of 80 ml/min. To improve the utilization rate of CO_2 in the flue gas, flue gas-aided washing was also evaluated at different gas flow rates (100 mL/min, 300 mL/min, and 400 mL/min) using simulated flue gas (CO_2: air = 1:4). During each washing experiment, the liquid-to-solid ratio was maintained at 10:1 by mixing 5 g ash sample with 50 ml extraction solution. The mixed sample was shaken for 5–45 min in a horizontal oscillator at a rate of 180 rad/min. At pre-determined time intervals, the ash suspension was separated by a vacuum filter to obtain an ash residue and extraction solution. The ash residue was oven-dried, weighed, and then ground to obtain a homogeneous sample for further analysis.

RESULTS AND DISCUSSION

As shown in Fig. 1, a significant percentage of Cl was removed by water-washing treatment at a liquid-to-solid ratio of 10 for 30 min. However, the removal rate varied, reaching 85% for CQ-A, 74% for CQ-B, 85% for CQ-C, 92% for BJ-A, 89% for AH-A, 96% for TJ-A, 91% for SZ-A, 94% for SZ-B, 92% for SZ-C, 91% for SZ-D, 92% for AH-B, 94% for AH-C, and 83% for SH-A, respectively. The large discrepancies in Cl^- removal rate among the fly ash samples from different incineration plants reveal that water-washing did not always lead to the satisfactory removal of Cl^-. Thus, for fly ash samples with lower Cl^- removal efficiencies, namely CQ-A, CQ-B, AH-A, SZ-A, SZ-D, AH-B, and SH-A, which accounted for approximately half of the total number of all ash samples, CO_2-aided washing was also performed.

The fly ash samples from CQ-A, CQ-B, AH-A, SZ-A, SZ-D, AH-B, and SH-A incineration plants, which displayed lower Cl^- removal rates, were selected for the CO_2-aided washing experiment. The results for each incineration plant are shown in Fig. 2. CO_2-aided washing increased the Cl^- removal rate by approximately

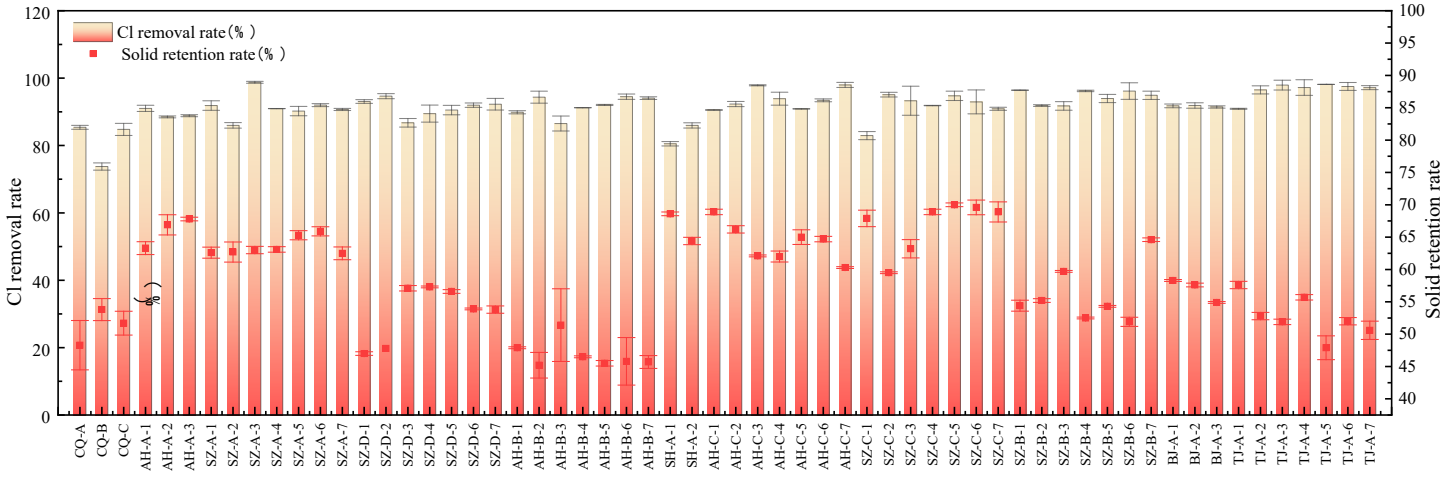

Fig.1 Chlorine removal and solid retention rate for the 60 ash samples from 13 incineration plants in water washing treatment

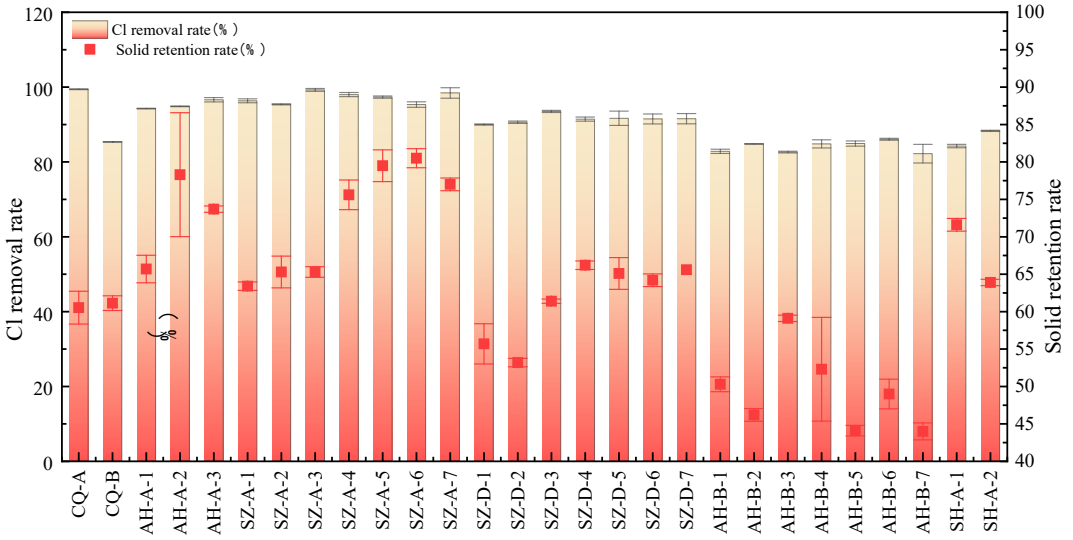

Fig.2 Chlorine removal and solid retention rate for the 28 ash samples from 7 incineration plants in CO_2-aided washing treatment

10% for CQ-A and CQ-B. For the other ash samples, the Cl^- removal rate increased from 89% to 95% for AH-A ash, 91% to 97% for SZ-A ash, 91% to 92% for SZ-D ash, and from 83% to 86% for SH-A ash. These results support the effectiveness of CO_2 injection on Cl^- removal, but for AH-B fly ash, the Cl^- removal rate decreased from 91% to 84%, possibly due to the newly-formed more-insoluble Cl-bearing compounds.

Due to the negative effect of CO_2 injection on AH-B ash, flue gas-aided washing was performed for the ash samples, except for AH-B ash. The results reveal that flue gas-aided washing exhibited almost an equivalent Cl^- removal effect as that of the CO_2-aided washing system. However, for sulfate, the situation was much more complex, especially for ashes from CQ-A and CQ-B. In these samples, CO_2 injection decreased the sulfate removal percentage, but flue gas injection resulted in almost equivalent sulfate removal as water washing.

CONCLUSIONS

The resource utilization of fly ash as an alternative material for cement clinker production has attracted attention, but harmful components in fly ash limit its resource utilization capacity, especially chloride and sulfate. Water washing treatment resulted in a great disparity in the Cl^- removal rates among the fly ash samples from 13 different incineration plants, ranging from 73% to 96%. This reveals that water-washing did not always lead to the satisfactory removal of Cl^-. For fly ash samples with a relatively low Cl^- removal efficiency after water washing (CQ-A, CQ-B, AH-A, SZ-A, SZ-D, and SH-A), the calculated ash blending ratios were in the range of 0.3–1.5%. CO_2 injection during washing promoted Cl^- removal from these fly ashes from 74–92% to 84–99%. Flue-gas-aided washing showed almost equivalent Cl^- removal as that of CO_2-aided washing.

REFERENCES

[1] Jiang Y, Xi B, Li X, et al. Effect of water-extraction on characteristics of melting and solidification of fly ash from municipal solid waste incinerator[J]. Journal of Hazardous Materials, 2009, 161(2-3):871-877.

[2] Colangelo F, Cioffi R, Montagnaro F, et al. Soluble salt removal from MSWI fly ash and its stabilization for safer disposal and recovery as road basement material[J]. Waste Management, 2012, 32(6):1179-1185.

[3] Kinnarinen T, Huhtanen M, Penttila M, et al. Removal of chloride from fly ash produced in

hazardous waste incineration by leaching and displacement washing in a vertical filter press[J]. Waste Manage Res, 2013, 31(2):178-186.

[4] Hu HY, Liu H, Shen WQ, et al. Comparison of CaO's effect on the fate of heavy metals during thermal treatment of two typical types of MSWI fly ashes in China[J]. Chemosphere, 2013, 93(4):590-596.

[5] Zhang Y, Cetin B, Likos WJ, et al. Impacts of pH on leaching potential of elements from MSW incineration fly ash[J]. Fuel, 2016, 184:815-825.

[6] Sarmiento LM, Clavier KA, Paris JM, et al. Critical examination of recycled municipal solid waste incineration ash as a mineral source for portland cement manufacture – A case study[J]. Resources, Conservation and Recycling, 2019, 148:1-10.

State-of-the-art on recycling of municipal solid waste incineration residues in Japan

Hirofumi Sakanakura[1]
1 Division of Material Cycles and Waste Management / National Institute for Environmental Studies / 16-2 Onogawa, Tsukuba city, Ibaraki, Japan

ABSTRACT
This paper elucidates the current status of recycling of the thermal treatment residues in Japan in the solution level of city, ward, town and village based on the data reported by the Ministry of the Environment[1]. The result showed that although the recycling rate reaches 30%, nearly half of Japan's municipalities still dispose 100% of the residues in landfills. Recycling trends are strongly affected by population of municipality and thermal treatment method being applied.

INTRODUCTION
In Japan, about 80% of municipal solid waste (MSW) are thermally treated by incineration and gasification – melting, mainly, and thermal treatment residues such as incineration bottom ash (IBA), incineration fly ash (IFA), and MSW slag are generated in more than 3 million tons in total annually. The current flow of thermal treatment residues is shown in Figure 1[1]. Although the thermal treatment residues are being recycled in some municipalities, in most municipalities they seem to be disposed of in landfills. It is important to accurately grasp the status of recycling/landfilling of such thermal treatment residues to evaluate the status of MSW treatment strategy in Japan. Therefore, we organized the data from the survey by Ministry of the Environment (MOE's survey, FY 2018 version[1]) to clarify the factors that affect the recycling of thermal treatment residues.

METHOD

Linking municipality data and facility data
In Japan, municipality (city, ward, town, village) is responsible for MSW treatment. Small municipalities often form union. The status of recycling might depend on thermal treatment facility and landfill capacity of each municipality and union. Since the MOE's survey are divided into data by municipality (not association) and data by facility (Figure 2), it is necessary to connect both data. In addition, because of merger history, one municipality may belong to different unions. The areas covered by each association in one municipality are investigated using municipality's MSW treatment plans. Amount of MSW transferred to a union's facility was calculated from the ratio of the area's population to the entire municipality. The throughput of each municipality was calculated from the population proportion of each municipality in one union and the throughput of the facility of that union.

Judgment of outsourcing
Melting processes include not only ash melting and gasification-melting those are carried out by municipalities and unions themselves, but also ash

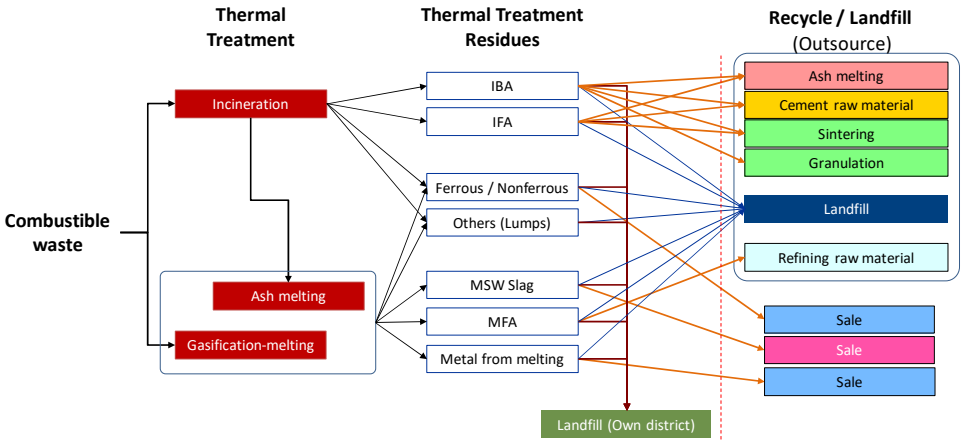

Figure 1. Current flow of thermal treatment residues in Japan.
IBA: Incineration bottom ash, IFA: Incineration fly ash, MFA: Melting furnace fly ash

Data by city, ward, town, village (garbage processing status)	Data by facility (Maintenance status by facility)
Population **Collection amount** Type (Combustible, Incombustible, etc.) **Carrying amount** Type (Combustible, Incombustible, etc.) Facility (Incineration, Crushing, etc.) **Treated amount** Type (Combustible, Incombustible, etc.) Facility (Incineration, Crushing, etc.) Incineration (Directly, Others) Landfilled (Directly, Incineration residues, Non-incineration residues) Stock (by facility) **Recovered amount** - Paper, Metals, Glass, PET bottles, Fertilizers, Feed, MSW Slag, Fuel, Cement raw material, Refining raw material, etc.) - by facility (Incineration, Crushing, etc.)	**Incineration facility (n=1134)** Facility name, Processed amount, Recovery amount, Waste type, Facility type, Process, Furnace type, Number of furnaces, Start year, Residual heat amount, Power generation capacity, Ash processing equip., Operation system, Revision/abolition, Proportion of industrial waste, Waste composition, Reuse/repair items **Bulky waste facility (n=625)** ... **Landfill (n=1695)** Facility name, Capacity, Landfilled amount, Remaining capacity, Waste type, Location, Start year, Area, Volume, End year, Seepage control, Leachate treatment, Operation system, Status, Proportion of industrial waste, Structure, Management status, etc.

Figure 2. Items of a survey on waste treatment related to thermal treatment residue. Colored text indicates items used. Red text: numeric value that can be compared between the two, blue text: numerical value, green text: facility information.

melting that is carried out outsourced to private sectors. Also, landfilling is not only carried out at a facility owned by the municipality itself, but also outsourced to the private sector. To distinguish them, several points were checked: the type of facility is gasification-melting or not, ash processing equipment is melting or not, and recycling of MSW slag has been reported or not. Regarding landfill, if the landfilled waste amount based on the data by municipality definitely exceeds the amount calculated from the data by facility, it is determined that the municipality is outsourcing landfilling partially at least.

RESULTS

Landfill capacity (overall)

The remaining capacity of landfill ranged from approximately 0.01 to 10 m^3/person (Figure 3). There seems unclear negative and positive correlation with the population below and above 100,000 people, respectively. Of the total 1,719 municipalities, 465 municipalities do not have their own landfill (Tokyo Special Wards were counted as 1 ward in this study). From Figure 4, a positive correlation was observed between the remaining capacity and the landfilled amount (including waste other than thermal treatment residue), although there was a large variation. The landfilled amount for 90 municipalities was 0 kg/person/year. From Figure 5, it is difficult to find a correlation between the remaining capacity and the resource recovery rate of thermal treatment residue. Of the 1,641 municipalities where thermal treatment is conducting, the number of municipalities with a resource recovery rate of 0% and 100% was 829 (50.5%) and 185 (11.3%), respectively.

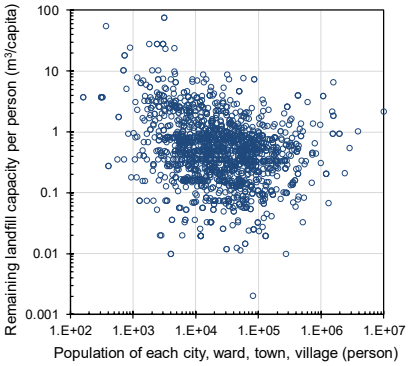

Figure 3. Relationship between population and residual capacity

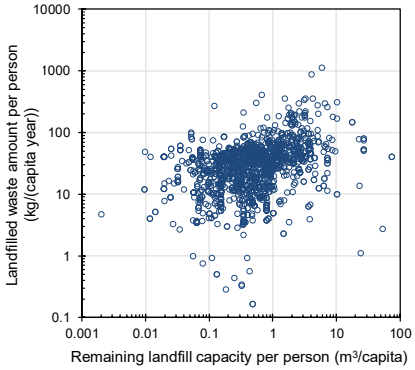

Figure 4. Relationship between residual capacity and total disposal amount

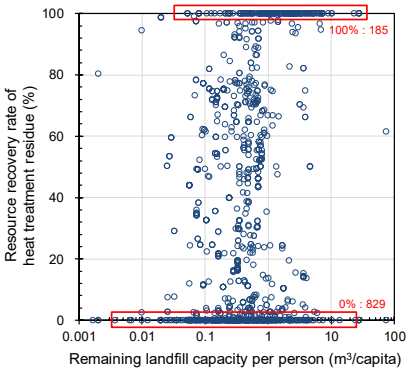

Figure 5. Relationship between residual capacity and resource recovery rate

Locality

From Figure 6, many municipalities from Kanto to Kinki districts, as well as parts of Shikoku and Kyushu districts, have determined that the landfill of thermal treatment residues is outsourced. Municipalities that recycle all thermal treatment residues are scattered in small populations. Looking at the distribution of the most applied recycling methods in each municipality (Figure

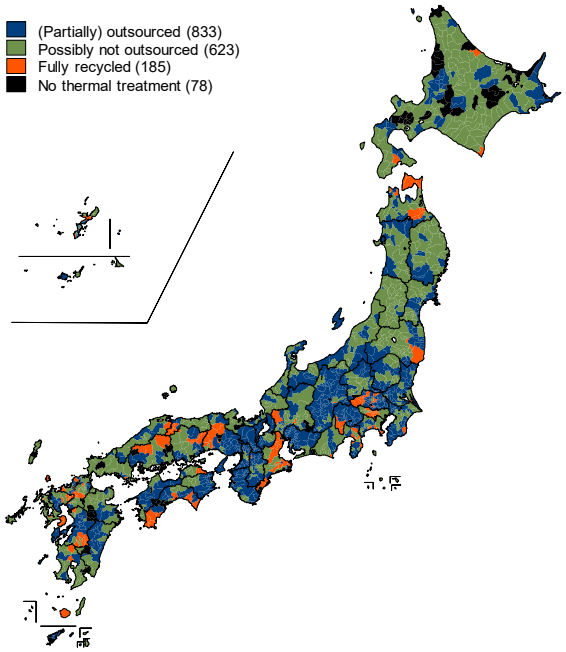

Figure 6. Distribution of outsourcing of landfill of thermal treatment residues. The numbers in parentheses are the number of municipalities.

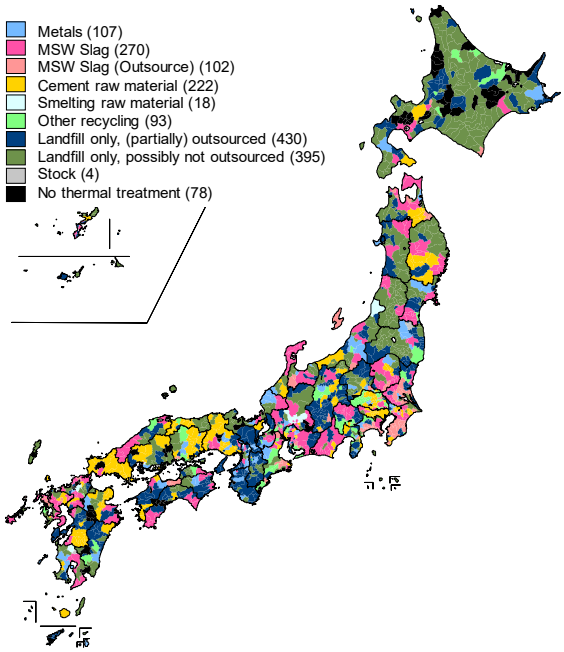

Figure 7. Distribution of the most common resource recovery methods for thermal treatment residues. The numbers in parentheses are the number of municipalities.

7), Melting is slightly more common in middle of Honshu. In particular Ibaraki, Chiba, and Kanagawa prefectures, there are many municipalities that have outsources melting. Cement raw materials are prominent large cities such as Sapporo and Tokyo, and also many cities near cement factories especially Chugoku and Kyushu districts.

Difference in thermal treatment method

Figure 8 shows the status of resource recovery for each thermal treatment method – (a) Mechanical grate incineration, (b) Fluidized bed incineration, (c) Gasification-melting. Facilities are arranged in descending order of recovery rate. The diagram is limited to municipalities with only one facility (note that many large cities are therefore not covered). Incineration facilities tend to apply cement raw material mainly. As for "Other recycling" in MoE's survey, most of them are turned into sintering, granulation, and crushing. Gasification – melting facilities mainly produce MSW slag and metals. In the case of a shaft type gasification – melting, the metals are molten metal, and in the case of fluidized bed gasification – melting, the main materials are steel and aluminum recovered from below the gasification furnace.

Difference in population, landfill capacity and treatment method

Figure 9 shows the proportion of recycling and/or landfill. Figure 9(a) shows over all proportion. Figure 9(b) shows the influence of population of municipality. The largest recycling ratio is found between 100,000 and 300,000 people, and it gradually decreases for both

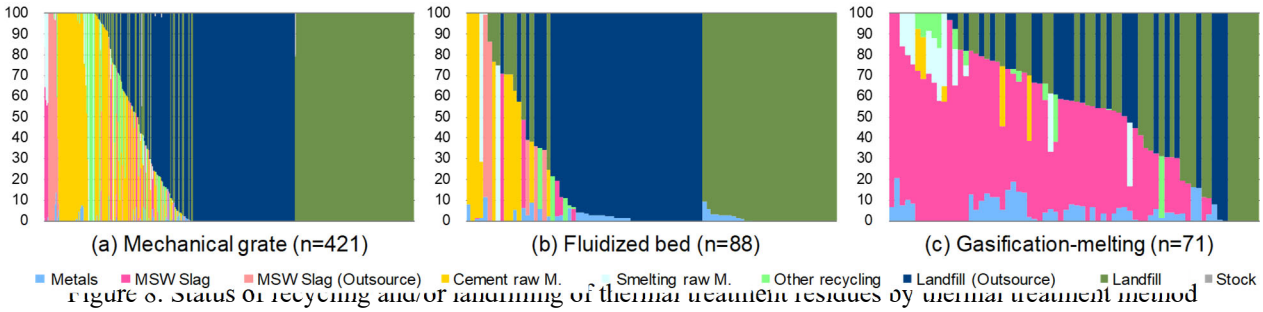

Figure 8. Status of recycling and/or landfilling of thermal treatment residues by thermal treatment method (horizontal axis: each facility)

larger and smaller populations, with the lowest values being 1 million or more and less than 10,000. In particular, outsourced landfill is extremely rare in municipalities with more than 1 million people. One of the reasons is thought to be that large cities with populations of 1 million or more often have sea area landfill sites. Compared to Figure 9(b), Figure 9(c) population density did not show as clear a trend. Figure 9(d) remaining landfill capacity showed the most obvious trend that the recycling rate for 0 to 0.35 m^3/person was as high as 46%, while it was only 11% for 1 m^3/person or more.

Although there are many municipalities with a resource recovery rate of 0% or 100% (Figure 5), we can conclude that differences in recycling rate can be summarized by population (Figure 9(b)) and remaining landfill capacity per capita (Figure 9(d)). Municipalities that generate a certain big amount of residue and have relatively little landfill capacity are doing their best to recycle the residues. However, landfill-free municipalities are not the most committed to recycling. It is assumed that the residues are outsourced to a low-cost private landfill site. Furthermore, when sorted by thermal treatment method (Figures 9(e) to (g)) these differences became even more pronounced. Gasification – melting recycles the most, and the fluidized bed incinerator the least.

CONCLUSION

Recycling rate differs depending on the size of municipality, remaining capacity of landfill, thermal treatment method, regional characteristics, etc. More than half of municipalities still do not recycle thermal treatment residue. Recycling status of each type of residue such as IBA and IFA might be significantly different. In order to develop an effective recycling strategy, it is expected to investigate the type and amount of each residue generated and outsourced or not in the MoE's survey.

ACKNOWLEDGEMENT

This research is supported by the Environmental Research Promotion Fund JPMEERF20183002, ``Establishment of ``Green Improvement Technology for Incineration Bottom Ash" Combining Physical Sorting and Aging" and the Waste/3R Technology Breakthrough Promotion Project, ``Resources of Incineration Bottom Ash According to Regional Characteristics." The project was implemented under the theme of ``Establishment of a Scheme for Recycling and Recycling".

REFERENCE

1) Ministry of the Environment (2020) FY2018 general waste treatment status survey, https://www.env.go.jp/recycle/waste_tech/ippan/h30/index.html (accessed November 1, 2020)

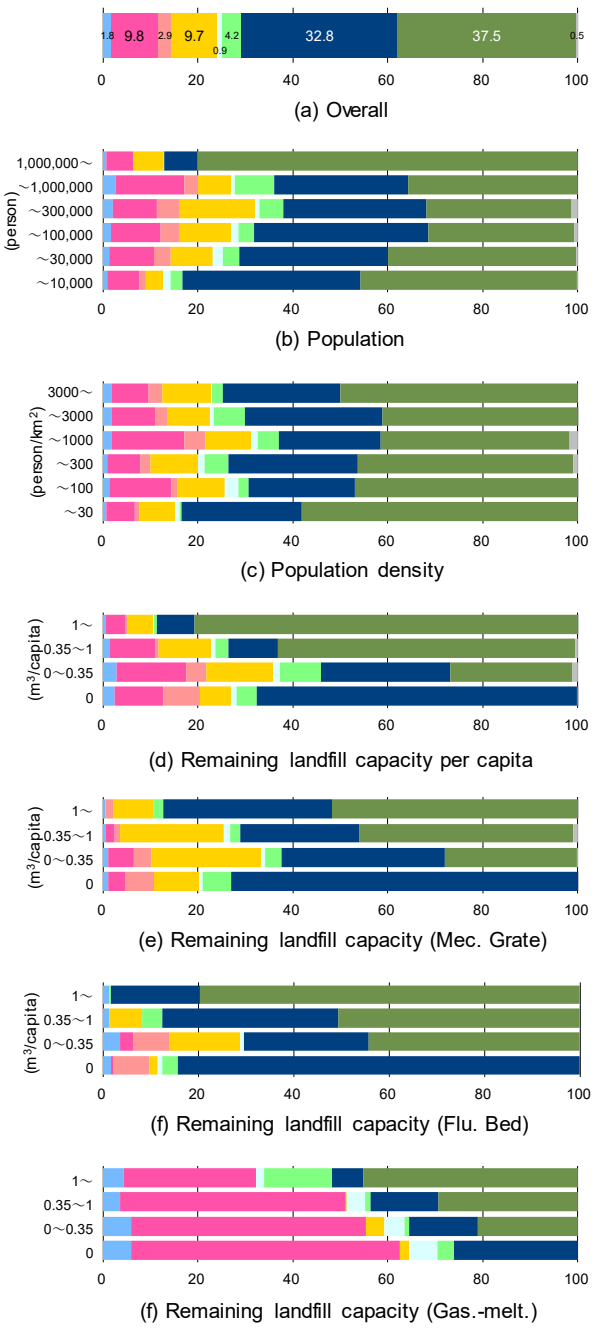

Figure 9. Proportion of recycling by each factor (Legends: see Figure 8)

SYNTHESIS OF ALKALINE MODIFIED COAL FLY ASH FOR SOIL AMENDMENT: IMPACT OF INITIAL MOISTURE ON EVAPORATION MITTIGATION CAPACITY (EXTENDED TIME)

Pu Yang[1], Hao Xu[1], Fumitake Takahashi[1]*
1 Department of Transdisciplinary Science and Engineering, Tokyo Institute of Technology
G5-610, Tokyo Institute of Technology, Suzukake, 4259, Nagatsuta, Midori-ku, 226-8503, Yokohama, JAPAN

INTRODUCTION

During the process of power generation, million tons of coal burning residue are produced. Coal fly ash (CFA) accounts for 60% - 90% of coal burning residue, and the utilization of CFA is insufficient[1]. In addition, arable land was polluted with utilization of CFA; underground water was contaminated with the storage of CFA; air was polluted with the long-distance transportation of CFA. Consequently, CFA should be disposed with safety or utilized with high added values.

Different technologies have been investigated for CFA treatment, such as landfill and utilized as construction materials[2]. However, these available technologies are accompanied by soil, water, and soil pollution, low value-added product generation, and human health risk. It is therefore extremely attractive to develop a new technology to overcome these limitations.

Arid and semi-arid areas are important areas on the earth, where food crop farms are exposed to water deficient problems with poor productivity and diversity. Thus, water holding capacity of the soil there needs to be improved for the plant growth. CFA is mainly composed of silica and alumina, making it potentially to be used as adsorbents for pollutant reduction and water amelioration[3, 4]. A previous work reported that raw CFA gave a positive impact on soil water holding capacity[3], but this effect didn't lead to significant improvement. Therefore, any attempts should be made to further improve the ability of CFA in increasing soil water holding capacity. From the viewpoint of practical application, the utilization of CFA in soil amendment solves both solid waste problem and poor soil water retention capacity problem. In arid and semi-arid area, the main water loss way is water evaporation, therefore, water evaporation mitigation capacity (EMC) was often measured to confirm water retention capacity of soil. In this study, a new method was developed to modify CFA aiming at improve EMC.

MATERIALS AND METHODS

Before treatment, CFA was dried in an oven at 105 °C for 24 h. Then, KOH and CFA were mixed at different ratios, and deionized water was also added into the mixture. After 10 min standing time, mixtures in crucibles were calcinated in a muffle furnace at 500 °C for 1 h, and the calcinated residue was collected for further analysis.

Akatama soil was used in this study, which was crushed and sieved smaller than 75 μm. Before EMC test, CFA, KOH modified CFA and soil were dried in an oven at 105 °C for 24 h to eliminate moisture inference. Then soil was mixed with raw CFA (R-CFA), calcinated-CFA (C-CFA), calcinated KOH-modified CFA (KOH:CFA=1:1 (KC11), KOH:CFA=2:1 (KC21), and KOH:CFA=3:1 (KC31)) respectively. EMC was tested at 3 initial moistures (10%, 20% and 40%) under 6 conditions (Only Soil (OS), Raw CFA (R-CFA), C-CFA, KC11, KC21 and KC31) with 1 hour interval.

RESULTS AND DISCUSSION

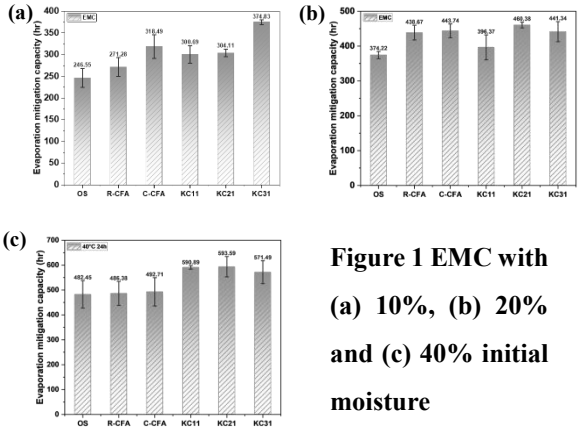

Figure 1 EMC with (a) 10%, (b) 20% and (c) 40% initial moisture

Figure 1 shows that at all initial moisture conditions, the addition of CFA and modified CFA improved the EMC of soil. Adding KC31, KC21, and KC21 led to most

significant improvement of EMC at 10%, 20%, and 40%, respectively. KOH modification enhanced the promotion effect of CFA on EMC. However, the addition of KC11 yielded weaker promotion effect on EMC compared to R-CFA and C-CFA. The inconsistent effects of CFA and modified CFA on EMC improvements at different initial moistures indicated that initial moisture influenced the promoting extent of CFA and modified CFA on EMC.

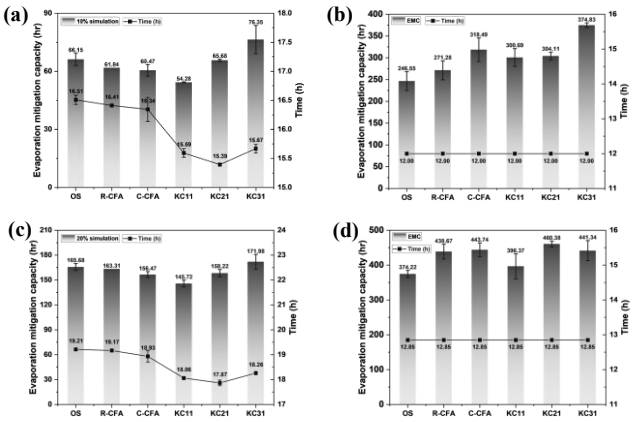

Figure 2 (a) Simulated and (b) real EMC with 10% initial moisture; (c) Simulated and (d) real EMC with 20% initial moisture

Based on data of 40% initial moisture condition, EMC with 10% and 20% initial moisture was simulated. In this work, EMC was measured for 24 hours with 40% initial moisture to ensure maximum soil water evaporation. Correspondingly, EMC was measured for 12 and 12.85 hours with 10% and 20% initial moisture, respectively. When soil water content dropped to half and one quarter with 40% initial moisture, EMC data was captured and calculated to simulate the EMC with 10% and 20% initial moisture. As indicated in **Figure 2 (a)** and **(c)**, the addition of KC11, KC21, and KC31 resulted in a shorter remaining EMC measurement time within controlled period compared to OS, R-CFA, and C-CFA. This indicates that KOH modification endowed CFA with a stronger suppressing effect on soil water evaporation than OS, R-CFA, and C-CFA.

As shown in **Figure 2**, the values of simulated EMC are lower than those of real EMC at 10% and 20% initial moisture after 24 h observation, which agrees with the results obtained under 14 h measurement of EMC. In addition, the blending of KC31 led to the best improvement in both real EMC and simulated EMC under 10% initial moisture. However, the optimal conditions for the best EMC improvement were different between real EMC and simulated EMC with 20% initial moisture. Furthermore, the promoting extent of additives on EMC (either real or simulated) varied a lot when the initial moisture content increasing from 10% to 20%.

Figure 3 (a) shows that KOH modification produced $K_4(CO_3)_2(H_2O)_3$ at the expense of SiO_2 and aluminum silicate. As shown in **Figure 3 (b)**, increasing addition of KOH led to the accumulation of angular particles, conversely the smooth ball-like particles were disappeared in R-CFA and C-CFA, confirming the appearance of $K_4(CO_3)_2(H_2O)_3$.

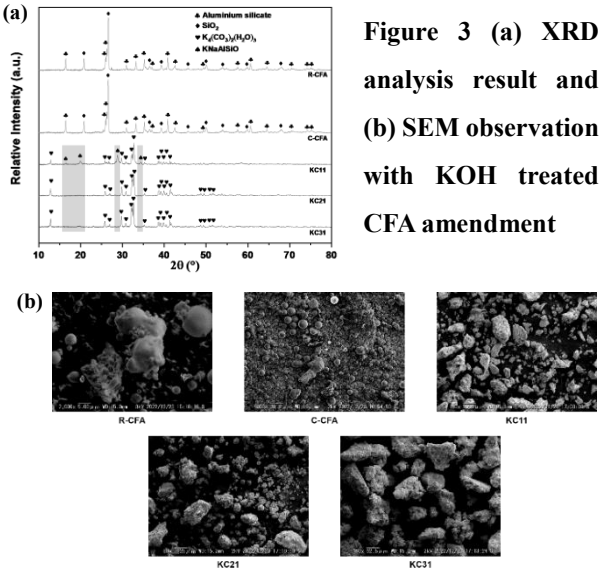

Figure 3 (a) XRD analysis result and (b) SEM observation with KOH treated CFA amendment

CONCLUSIONS

The modified CFA increased the EMC more significantly than raw CFA regardless of the initial moisture content. However, at different initial moistures, the results were inconsistent, suggesting that initial moisture influenced the EMC extent of treated CFA.

ACKNOWLEDGMENT

This work was supported by JST SPRING, Grant Number JPMJSP2106. Japan.

REFERENCES

(1) Dindi, A.; Quang, D. V.; Vega, L. F.; Nashef, E.; Abu-Zahra, M. R. M. Applications of fly ash for CO2 capture, utilization, and storage. Journal of CO2 Utilization 2019, 29, 82-102.

(2) Zhou, Z.; Sofi, M.; Liu, J.; Li, S.; Zhong, A.; Mendis, P. Nano-CSH modified high volume fly ash concrete: Early-age properties and environmental impact analysis. Journal of Cleaner Production 2021, 286.

(3) Song, M.; Lin, S.; Takahashi, F. Coal fly ash amendment to mitigate soil water evaporation in arid/semi-arid area: An approach using simple drying focusing on sieve size and temperature. Resources, Conservation and Recycling 2020, 156.

(4) Kaewmee, P.; Song, M.; Iwanami, M.; Tsutsumi, H.; Takahashi, F. Porous and reusable potassium-activated geopolymer adsorbent with high compressive strength fabricated from coal fly ash wastes. Journal of Cleaner Production 2020, 272.

MSW INCINERATION FLY ASH STABILIZATION BY UTILIZING POZZOLANIC BOTTOM ASH

Mitali Nag[1], Takayuki Shimaoka[1], Hirofumi Nakayama[1] and Teppei komiya[1]
[1]Department of Urban and Environmental Engineering, Faculty of Engineering, Kyushu University, 744 Motooka, Nishi-ku, Fukuoka, 819-0395, Japan

ABSTRACT
Fly ash (FA) produced during the incineration of municipal solid waste (MSW) has a significant potential for leaching harmful elements. Calcium silicate hydrate (C–S–H) is the main hydration product of cement and can immobilize the leaching of toxic metals, formed by the reaction of Ca with pozzolanic Si in a highly alkaline environment. Toxic metals can be immobilized by the addition of pozzolan to FA residues (in lieu of cement), which is a source of Ca and provides an alkaline condition. The current study proposed a new approach of reusing the fine-fraction of MSW incineration bottom ash (BA), which contains amorphous silica, known as pozzolan for immobilization of lead (Pb) and zinc (Zn) in FA. The dissolved amorphous silica and alumina emerged from the BA, with available Ca ions and in an extremely alkaline condition owing by FA, stimulate the pozzolanic reaction, resulting the formation of cementitious compounds of C–S–H gel and calcium aluminate hydrates (C-A-H) that can immobilize the heavy metals leaching from FA. The existence of calcium hydroxide promotes the carbonation process, reducing pH, and consequently immobilizing heavy metals. The method involves the simple mixing of BA and FA with water. The leaching concentrations of Pb and Zn significantly reduced in the stabilized FA samples followed by standard Japanese leaching test (JLT- 46). Pb stabilization efficiency was reached >99.9% after 16-days of settling periods with 10% dosage of BA at room temperature. 20% moisture and 30% of BA dosage enhance the Pb immobilization nearly 100%. The added BA to FA residues reacted with $Ca(OH)_2$ and CaClOH produced the C–S–H gel. pH, XRD, and SEM-EDX analyses evaluated the carbonation and pozzolanic reactions that promoted the immobilization of Pb and Zn. Immobilization of heavy metals by using fine-fraction of BA seems to be very effective and technically feasible. The technology can save original material, produce inert material and avoids landfilling of incineration residues.

INTRODUCTION
Municipal solid waste incineration (MSWI) is a common technology used in developed countries for waste treatment. In Japan, about 90% of solid waste generated was processed using incineration technology. The total amount of incineration residues was 8.03 mt/y, including 20 – 30% of fly ash (FA) and 70 – 80% of bottom ash (BA) (MOE, 2022). FA is considered hazardous waste due to the presence of high concentrations of leachable heavy metals such as Zn and Pb. Common treatments for FA stabilization are melting, sintering, cement solidification, acid extraction, and chelating reagents, which is also stipulated by Japan's law. Most of the techniques are efficient but require raw materials and energy consumption. BA which is also MSWI residue that is either disposed in landfills or reused in civil engineering applications. BA in coarse particles contains crystalline silica oxide (mainly quartz), which is non-reactive and suitable for reuse in the construction field. This makes BA, particularly in larger particles, reused as bulk fill for road construction, but the residual or finer fraction of BA is unused and usually disposed in landfills. Due to the essential components contained in BA, it is feasible to reuse BA for heavy metal immobilization. Fine particle of BA is rich in pozzolans, such as amorphous silica and alumina, and with the presence of calcium ions can promote heavy metals immobilization involving carbonation and pozzolanic reaction. Pozzolanic product, i.e., calcium silicate hydrates (C-S-H) gel, is able to adsorb or entrap heavy metals, while carbonation reaction produces pH reduction with consequent heavy metal immobilization in FA (Ouhadi et al., 2014; Mostafa et al., 2001).
In the present study, fine fractions of BA are used for heavy metal immobilization in FA. The simplicity of the proposed technology, which only requires wastes produced from the same incineration plant, has objectives: (1) to investigate the role of pozzolans in fine fraction of BA to immobilize heavy metals in FA; (2) reuse residual or fine fraction of BA; (3) obtain a new simple method for FA stabilization, with cost-effective and environmentally-friendly materials; (4) produce new material that is suitable for safe disposal; (5) reduce the amount of MSWI waste going to the landfill; (6) produce new material that may be reused for other purposes such as filler.

MATERIALS AND METHODS
Sample preparation
Untreated BA and FA were collected from incineration

plant R1 and R2 located in the city of Fukuoka, Japan. To remove the moisture, FA was oven dried at 60ºC for 24 hours, while bulk BA was dried at room temperature. BA was sieved into the particle size fraction of < 250µm and ground by a mechanical milling machine for about 3 minutes till it reached homogenous size with FA. The experiment was performed as shown in Table 1, by mixing ratio of FA: BA: Water = 10:1:10, mixed for 25 minutes with a magnetic stirring device. Each prepared sample was divided into two halves, one half was placed in the oven for 4h at 120ºC (oven-dry), while the other half was dried at room temperature (air-dry). For analysis, the samples were kept open at room temperature and settled for 4, 8, 16, 30, and 60 days after mixing.

Table 1. Experiment condition

BA and FA samples	BA fraction (µm)	FA :BA:H_2O	Mixing time (mins.)	Drying condition	
				Air-dry (A)	Oven-dry (O) (4h 120° C)
R1 R2	< 250	10:1:10	25	1/2	1/2

Sample characterization:
The initial condition of raw FA and BA were determined by X-ray fluorescence (XRF) for their elemental composition, by X-ray diffractometry (XRD) for their mineral phase, by inductively coupled plasma optical emission spectroscopy (ICP-OES) for Pb and Zn concentration in their leachate using standard Japanese leaching test (JLT-46). After FA is stabilized by BA, Pb and Zn immobilization were analyzed by ICP-OES, XRD, and SEM-EDX.

RESULTS AND DISCUSSION

Characteristics of raw FA and BA

The collected FA samples were in a dry state and tested by freeze-drying condition, while the collected BA samples were in a wet state (Table 2). Initial leaching concentrations of Pb and Zn in FA and BA are also provided in Table 2.

Table 2. Physical and chemical characteristics of raw FA and BA

	Raw FA		Raw BA	
	R1	R2	R1	R2
MC (%)	5.49 ± 0.27	21.70 ± 0.35	34.94 ± 0.12	5.49 ± 0.09
LOI (%)	1.32 ± 0.41	0.35 ± 0.01	7.40 ± 0.09	1.74 ± 0.09
pH (-)	12.62 ± 0.5	12.08 ± 0.01	11.50 ± 0.01	11.61 ± 0.02
Pb (mg/L)	113.5 ± 0.5	6.60 ± 0.3	0.12 ± 0.05	0.86 ± 0.23
Zn (mg/L)	7.4 ± 0.02	1.30 ± 0.02	0.26 ± 0.25	0.24 ± 0.06

Chemical composition of raw FA and BA:
According to XRF result in Table 3, Si, Ca, and Cl were the major elements in FA, the contents of which were over 10 wt.%. In BA, Si, Ca, and Al were the major elements. Among heavy metals, Zn and Pb are the most abundant elements. Considering the environmental toxicity, these two metals were selected as the main target in this study. Similar to Pb^{2+}, Zn^{2+} may react with substances like oxygen or acids to form potentially toxic compounds, but Zn in metallic form is relatively harmless.

Table 3. Chemical composition of raw FA and BA

Composition (wt%)													
Sample	SiO_2	Al_2O_3	Fe_2O_3	TiO_2	MnO	P_2O_5	CaO	MgO	Na_2O	K_2O	Cl	S	F
FA - R1	11.7	2.35	0.69	0.58	0.03	0.54	40.0	2.46	6.53	2.99	24.52	2.13	0.07
FA - R2	8.54	3.06	1.19	0.88	0.07	1.38	19.4	2.74	13.3	7.72	26.12	2.48	0.09
BA - R1	23.5	9.82	3.90	2.29	0.14	2.77	42.5	2.46	1.85	0.75	2.88	0.59	0.03
BA - R2	21.8	9.12	3.56	2.20	0.13	2.55	43.1	2.44	1.88	0.77	3.03	0.68	0.03
Composition (ppm)													
Sample	Zn	Cu	Pb	Cr	Ni	Ba	Sb	Sn	Sr	As	V	Cd	Co
FA - R1	14820	1060	3595	120	40	930	1235	10	180	20	0	225	0
FA - R2	77120	5190	22100	220	30	1735	11580	0	330	150	2	580	6
BA - R1	6730	5560	1480	560	240	2830	140	80	410	10	5	120	10
BA - R2	6800	4620	130	520	165	2760	150	95	410	9	5	120	10

Leaching test of stabilized FA:
The effects of BA on Pb and Zn immobilization were investigated under air-dry and oven-dry with settling times until 60 days as shown in Figure 1. The highest efficiency was achieved using BA (<250 µm) with air-dry treatment. In R1 sample, more than 99% and 96% of Pb and Zn immobilization were achieved after 16 days, respectively. Oven-dry could accelerate the prompt initiation of carbonation, but air-dry exhibits better immobilization of Pb and Zn in a relatively longer settling time accords with previous studies.

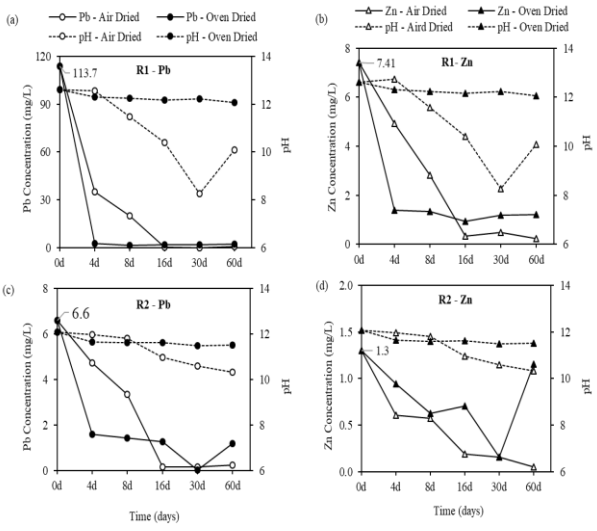

Figure 1: Pb and Zn leaching concentration with time in R1 and R2 samples

Mineralogy of stabilized FA:

The mineral phases of raw FA and BA identified by XRD are shown in Figure 2(a). In FA sample, halite, sylvite, and calcium chloride hydroxide were the major mineral phases. In BA sample, quartz and Ca-rich minerals such as calcite, lime, and hydrocalumite were the major mineral phases. However, in the stabilized sample shown in Figure 2(b), the peaks originally found in raw ashes such as lime, portlandite, and calcium chloride hydroxide disappeared, while new calcite peaks appeared, suggesting that phases have reacted with CO_2, and silica and/or alumina contained in the BA, thus carbonation reaction occurred. The main reaction formulas involved are listed as follows Assi et al., 2019; Rao & Meena, 2017):

Carbonation reactions:

$$CaO + H_2O \rightarrow Ca(OH)_2 \quad (1)$$

$$Ca(OH)_2 + CO_2 \rightarrow CaCO_3 + H_2O \quad (2)$$

$$2CaClOH + CO_2 \rightarrow CaCl_2 + CaCO_3 + H_2O \quad (3)$$

$$C\text{-}S\text{-}H + CO_2 \rightarrow CaCO_3 + SiO_2 + H_2O \quad (4)$$

Pozzolanic reactions:

$$Ca(OH)_2 \rightarrow Ca^{+2} + 2OH^- \quad (5)$$

$$Ca^{+2} + 2OH^- + SiO_2 \rightarrow C\text{-}S\text{-}H \quad (6)$$

$$Ca^{+2} + 2OH^- + Al_2O_3 \rightarrow C\text{-}A\text{-}H \quad (7)$$

New aluminosilicate minerals (i.e., kozulite, stilbite) appeared, which may be formed from reactions that occur in an amorphous matrix. A small peak of hydrocalumite ($Ca_2Al(OH)_6Cl(H_2O)_2$) and ettringite ($Ca_6Al_2(SO_4)_3(OH)_{12}\cdot 26H_2O$) is identified in the stabilized sample. These phases are commonly present in cement systems, as it forms through the reaction of calcium and alumina, and these phases prevent heavy metal from leaching out.

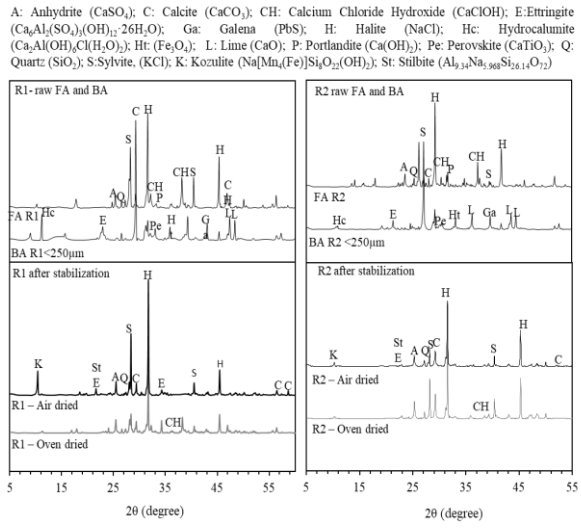

Figure 2: XRD pattern of raw and after stabilization in R1 and R2 samples

Microstructural of stabilized FA:

As shown in Figure 3 (a) and (b), a clear difference between FA before and after stabilization can be seen by FA round particle covered with new structures of C-S-H after stabilization. In the same sample, fibres structures with approximately 1 – 2 μm long and flake structures were found in the stabilized sample shown in Figure 3(c). It is suggested that C-S-H in fibres or needle shape crystals exhibited with a size of 0.5–2 μm long and <0.2 μm wide. At a lower magnification, C-S-H with dense structure or assembled grains-like seems to be easily identified in the same observed sample as shown in Figure 3(d). Calcium silicate hydrate (C-S-H) gel observed by scanning electron microscopy (SEM) is not uniformly distributed on the microscopic scale and exists in various shapes such as fibres, flakes, honeycombs, and tightly assembled grains, which also accords in this study. C–S–H has a large number of structural sites available for cations and anions to bind. Therefore, after hydration occurred and prompted the heavy metals in FA to combine with silicate or be wrapped in C–S–H gel, thus preventing leaching.

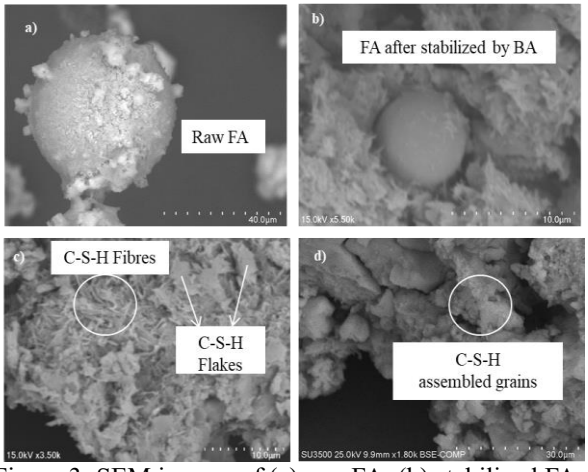

Figure 3: SEM images of (a) raw FA; (b) stabilized FA by BA; (c) C- S -H in stabilized FA 3500 ×; and (d) C-S-H in stabilized FA 5500 × magnification

OPTIMIZATION OF L/S AND FA/BA RATIOS TO IMMOBILIZE HEAVY METAL IN FA

Two approaches are taken to optimize the moisture and utilization of BA amount for heavy metal immobilization in MSWI FA by using fine fraction of BA, which was different liquid-to-solid (L/S) ratios and different FA/BA ratios. R1-FA and fine fraction BA (d< 250μm) with air-dry treatment was selected as the representative in this studies. As shown in Figure 4 (a), it is indicated that the lower L/S condition (20% of moisture) can effectively immobilized the Pb and Zn in FA. Water is required to drive the CO2 reaction, but too much water limits the reaction due to the blockage of the pores in the solid (Fernández Bertos et al., 2004). A higher amount of BA

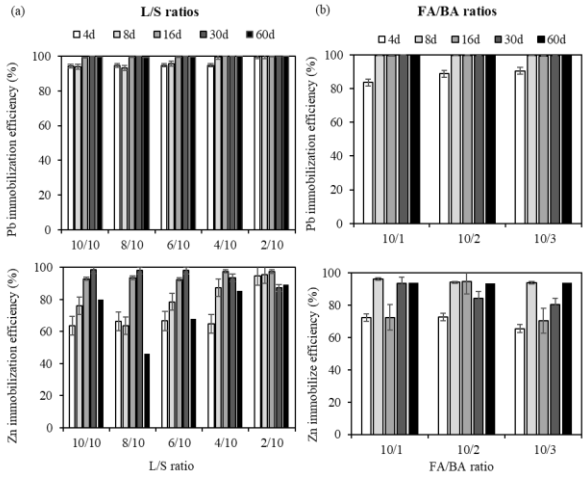

Figure 4: Immobilization efficiency of a) Pb and Zn by different L/S ratios; b) Pb and Zn by different FA/BA ratios

addition (FA/BA=10/3) resulted in higher immobilization of Pb which was shown significantly at day-4 (Figure 4 (b)). It proved the hypothesis that increasing the BA amount would increase the pozzolanic activity due to an addition of Si and Al contents and the amorphous nature of the major phases in BA.

CONCLUSION

MSWI BA has the potential to immobilize heavy metals in FA, particularly Pb and Zn, as it contains pozzolans. The highest Pb and Zn immobilization was achieved by using BA in air-dry condition. Oven-dry could accelerate the initiation of immobilization, but air-dry exhibits better immobilization of Pb and Zn in a relatively longer settling time. Carbonation and pozzolanic reactions are thought to be heavy metals immobilization mechanisms. Carbonation occurred, as evidenced by pH reduction in the leaching solution and formation of calcite ($CaCO_3$). Pozzolanic reaction product, and structures of C-S-H gel, was identified by SEM-EDX analysis. For further optimizations, FA stabilization using BA (d<250µm) and air-dry, as well as under lower water amount (L/S = 2/10) and higher BA amount (FA=BA 10/3) resulted in higher Pb and Zn immobilization efficiency. Therefore, this technology can avoid bottom ash becoming a residue and minimize water resources.

The technology can save original material, produce inert material and avoids landfilling of incineration residues.

REFERENCES

Assi, A., Federici, S., Bilo, F., Zacco, A., Depero, L. E., & Bontempi, E. (2019). Increased sustainability of carbon dioxide mineral sequestration by a technology involving fly ash stabilization. Materials, 12(7). https://doi.org/10.3390/ma12172714

Fernández Bertos, M., Simons, S. J. R., Hills, C. D., & Carey, P. J. (2004). A review of accelerated carbonation technology in the treatment of cement-based materials and sequestration of CO2. In Journal of Hazardous Materials (Vol. 112, Issue 3, pp. 193–205). Elsevier. https://doi.org/10.1016/j.jhazmat.2004.04.019

MOE (Ministry of The Environment), G. of J. 2022. (2022). Waste treatment and current status, Japan, 2022. https://www.env.go.jp/recycle/waste_tech/ippan/r2/index.html

Mostafa, N.Y., El-Hemaly, S.A.S., Al-Wakeel, E.I., El-Korashy, S.A., Brown, P.W., 2001. Characterization and evaluation of the pozzolanic activity of Egyptian industrial byproducts:I: silica fume and dealuminated kaolin. Cement Concr. Res. 31, 467e474. https://doi.org/10.1016/S0008-8846(00)00485-3.

Ouhadi, V.R., Yong, R.N., Amiri, M., Ouhadi, M.H., 2014. Pozzolanic consolidation of stabilized soft clays. Appl. Clay Sci. 95, 111e118. https://doi.org/10.1016/J.CLAY.2014.03.020.

Rao, N. V., & Meena, T. (2017). A review on carbonation study in concrete. IOP Conference Series: Materials Science and Engineering, 263(3). https://doi.org/10.1088/1757-899X/263/3/032011

ASSESSING THE METAL RECOVERY VALUE OF MUNICIPAL SOLID WASTE INCINERATION RESIDUES: IMPACT OF PRETREATMENT ON FLY ASH AND BOTTOM ASH

Pengfei LI[1] and Takayuki Shimaoka[2]
1 Department of Civil Engineering, Graduate School of Engineering, Kyushu University, Fukuoka, Japan
2 Department of Civil Engineering, Faculty of Engineering, Kyushu University, Fukuoka, Japan

ABSTRACT

This paper focuses on evaluating the metal recovery potential of Municipal Solid Waste Incineration (MSWI) residues, with particular emphasis on the influence of pretreatment methods on MSWI fly ash and bottom ash. We assess the effectiveness of these pretreatments in enhancing the concentration of valuable metals and compare the metal content before and after treatment. Our findings reveal that water washing significantly enhances fly ash's zinc and copper content, surpassing the minimum industrial-grade requirements. Mechanical sieving is an efficient pretreatment method for bottom ash, with copper content peaks in the 1 - 2 mm particle size range for both bottom ash samples. These results provide valuable insights into the potential for metal recovery from MSWI residues. They hold significance for relevant research, engineering practices, and policy formulation.

Keywords
Water-Washing, Mechanical Sieving, Zinc, Copper, Lead

INTRODUCTION

The incineration method has become widely adopted for the disposal of municipal solid waste (MSW) in Japan and China due to its advantages in energy recovery and reduction in mass and volume of MSW (Hjelmar, 1996). In Japan, approximately 80% of MSW is treated using incineration, while in China, the utilization of this method has steadily increased in recent years, with around 50% of MSW being disposed of through incineration as of 2019 (Wei *et al.*, 2022). However, the incineration process generates two types of residue: bottom ash and fly ash. Fly ash is classified as a hazardous material due to its content of toxic heavy metals and organic pollutants. Therefore, proper treatment of fly ash before final disposal is imperative. In contrast, bottom ash can be directly sent to municipal waste landfills (Zhang *et al.*, 2021; Shunda Lin *et al.*, 2022).

These waste residues, however, contain valuable metal resources, including zinc, copper, lead, antimony, and potassium (Tang and Steenari, 2016; Tang *et al.*, 2018, 2019, 2022). Unfortunately, conventional landfilling practices do not facilitate the recovery of these precious resources. Consequently, the recovery of metals from fly ash and bottom ash has emerged as a pivotal concern within waste incineration, leading to the development of pertinent engineering practices in various countries.

For example, Switzerland employs an acid-leaching method to recover zinc from approximately 60% of its fly ash (Weibel *et al.*, 2018). At the same time, China utilizes a water-washing technique to extract potassium chloride and sodium chloride. Furthermore, fly ash and bottom ash offer the distinct advantage of not requiring mining operations or long-distance transportation, making them more environmentally advantageous than traditional ore.

However, before embarking on metal recovery efforts, it is essential to ascertain the intrinsic value of fly ash and bottom ash. The metal content within these residues is intricately linked to the composition of the waste materials and the specific types of metals present (Jung *et al.*, 2004). In the case of Fukuoka City, waste is categorized into combustible refuse, non-combustible refuse, glass and PET bottles, and bulky refuse. As depicted in **Fig. 1**, the Seibu incineration plant processes both combustible refuse and combustibles segregated from non-combustible refuse and bulky refuse. The combustible refuse accounts for 93.9% of the total, with combustibles separated from non-combustible refuse and bulky refuse making up 6.1%. In contrast, the Rinkai incineration plant exclusively receives combustible refuse as its waste input. Furthermore, both plants employ grate-type furnaces.

This study aims to assess the potential for metal recovery from fly ash and bottom ash generated by two incineration facilities in Fukuoka City, Japan, particularly considering different waste compositions used as input materials for incineration. We will also investigate the effectiveness of two pretreatment methods in enhancing the concentration of valuable metals in these incineration residues. For fly ash, known for its high soluble salt content, we will

emphasize the effect of the water-washing method in concentrating valuable metals (Wang *et al.*, 2001). Additionally, we will explore the relationship between particle size and heavy metal content in bottom ash, necessitating mechanical sieving as a pretreatment method (Chimenos *et al.*, 1999). This research is expected to offer valuable insights and guidance for relevant industries and policy formulation.

1. MATERIALS AND METHODS

1.1 Materials

The fly ash sample obtained from the Rinkai incineration plant has been designated as fly ash R. In contrast, the fly ash sample from the Seibu incineration plant is denoted as fly ash S. The pH of the leachate for fly ash R is about 11.8, and for fly ash S, it is about 10.3. Similarly, the bottom ash sample derived from the Rinkai incineration plant is labeled as bottom ash R, and the corresponding sample from the Seibu incineration plant is identified as bottom ash S. These samples were collected using established protocols. Subsequently, the samples were meticulously preserved in hermetically sealed containers to against contamination before analysis.

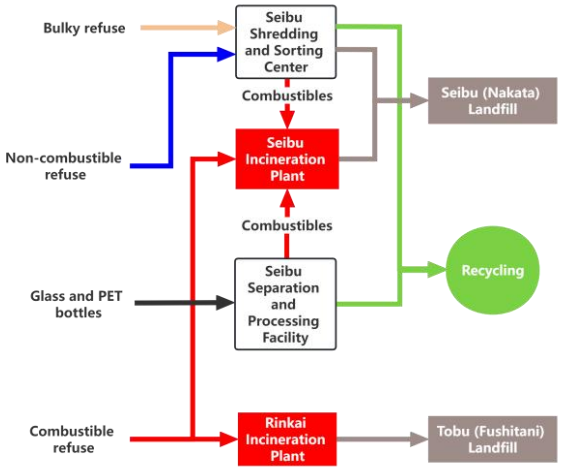

Fig. 1 Sources of waste input for Seibu and Rinkai incineration plants.

1.2 Water-washing experiment

A plastic bottle with a volume of 250 mL was used for the experiment. Initially, 30 grams of fly ash were placed inside the bottle, and this was followed by the addition of 180 mL of deionized water. To facilitate mixing, a magnetic stir bar was introduced into the bottle, and the mixture was stirred for a duration of 10 minutes at a speed of 200 rpm. After this stirring period, the sample was subjected to centrifugation at 3000 rpm for 20 minutes. This washing procedure was repeated once for thorough purification. Subsequently, the solid phase obtained from the centrifugation was carefully dried at 105°C for a period of 12 hours before undergoing further measurements and analysis.

1.3 Mechanical sieving experiment

A specific quantity of bottom ash, approximately 1000 grams, was placed in a tray and dried at 105°C for 24 hours. After drying, the bottom ash was subjected to sieving using screens with apertures of 2mm, 1mm, 0.5mm, and 0.25mm. Following the sieving process, the mass of bottom ash Rt each particle size was measured to calculate its mass distribution.

1.4 Sample characterization

The elemental composition of both samples was determined using Energy Dispersive X-ray Fluorescence Analysis (ED-XRF), employing a Spectro Xepos spectrometer with matrix-adjusted calibration. The measurements were conducted on pressed powder pellets with a diameter of 32 mm.

Qualitative identification of mineral phases of fly ash samples before and after leaching was performed by the X-ray diffraction (XRD) technique. Before the analysis, samples were manually ground to powder with a mortar. Analyses were conducted in a Rigaku Multiflex diffractometer by CuKα radiation under the 2-theta range of 2–75◦ and scanning step of 0.02◦ at the beam current of 30 mA and the voltage of 44 kV. Jade (v. 9.0) and PDXL (v. 2.1.2.0) software packages were used for the phase identification.

2. RESULTS AND DISCUSSION

2.1 Characterization of the fly ash samples

2.1.1 Characteristics of the raw fly ash samples

As indicated in **Table 1**, the fly ash samples R and S exhibit distinct elemental compositions. Specifically, fly ash R contains 1.58% Zn, 0.36% Cu, 0.36% Pb, 0.18% Sb, and 2.00% K. In contrast, fly ash S demonstrates significantly higher levels of Zn at 5.09%, with 0.40% Cu, 1.11% Pb, 1.45% Sb, and 5.28% K.

By Chinese geological and mineral industry standards, the Zn content in fly ash R falls within the prescribed cut-off grade range of 1.5-2.0%, while the Zn content in fly ash S comfortably exceeds the minimum industrial grade range of 3.0-6.0% (DZ/T 0214-2020). Additionally, the Pb content in fly ash S meets the specified cut-off grade range of 0.5-1.0%, and the Sb content in fly ash S also conforms to the prescribed cut-off grade range of 0.5-0.7% (DZ/T 0201-2020; DZ/T 0214-2020). It is worth noting that the Cu contents in both fly ash samples closely approach the cut-off grade of 0.5% (DZ/T 0214-2020). Furthermore, the K contents in both fly ash samples surpass the minimum industrial grade threshold of 2% (DZ/T 0212.2-2020). As shown in **Fig. 2** (a) and (b), the crystal phases of fly ash R are primarily $CaSO_4$,

$CaCO_3$, CaClOH, NaCl, and KCl. In comparison to fly ash R, fly ash S does not exhibit the presence of CaClOH in its crystal phases, which corresponds to its relatively lower pH value.

Table 1
The concentration of valuable metals in fly ash samples.

Sample	Concentration (wt. %)				
	Zn	Cu	Pb	Sb	K
Fly ash R	1.58	0.36	0.36	0.18	2.01
Fly ash S	5.09	0.40	1.11	0.95	5.28
Washed ash R	3.61	0.72	0.34	0.49	0.53
Washed ash S	7.75	0.60	1.61	1.45	0.52
Bottom ash R	0.30	0.21	0.14	-	-
Bottom ash S	0.92	0.75	0.22	-	-
Cut-off grade	1.5-2.0[a]	0.5[a]	0.5-1.0[a]	0.5-0.7[b]	0.5[c]
Minimum industrial grade	3.0-6.0[a]	0.7[a]	1.5-2.0[a]	1.0-1.5[b]	2.0[c]

a: DZ/T 0214-2020: Specifications for copper, lead, zinc, silver, nickel, and molybdenum mineral exploration. b: DZ/T 0201-2020: Specifications for tungsten, tin, mercury, and antimony mineral exploration. c: DZ/T 0212.2-2020: Specifications for salt mineral exploration—Part 2: Present saline lake mineral.

2.1.2 Characteristics of the water-washed fly ash samples

The mass of washed fly ash R and S constitutes 37.87% and 48.47% of the raw fly ash. After water-washing, the concentration of zinc in washed fly ash R and washed fly ash S reached 3.61% and 7.75%, respectively, meeting the minimum industrial-grade requirements (DZ/T 0214-2020). In the case of copper, the content increased to 0.72% in washed fly ash R and 0.60% in washed fly ash S. The copper content in washed fly ash R exceeded the minimum industrial grade, while in washed fly ash S, it reached the cut-off grade (DZ/T 0214-2020). Comparatively, there was no significant change in Pb content in washed fly ash R compared to the original ash. This could be attributed to its higher pH value, as under high pH conditions, Pb forms complex ions and dissolves in the leachate (Zhang, Jiang and Chen, 2008). In contrast, washed fly ash S showed an increased Pb concentration, reaching 1.61%, meeting the minimum industrial grade (DZ/T 0214-2020). After water washing, both washed fly ash samples exhibited increased Sb content. In washed fly ash R, the Sb content approached the cut-off grade, while in washed fly ash S, it reached the minimum industrial grade (DZ/T 0201-2020). As shown in **Fig. 3** (a) and (b), after water washing treatment, peaks corresponding to $Cu_2(OH)_2CO_3$ and $ZnCO_3$ were observed in both samples. And, NaCl and KCl disappeared in both samples. Furthermore, in fly ash R, CaClOH transformed into $Ca(OH)_2$.

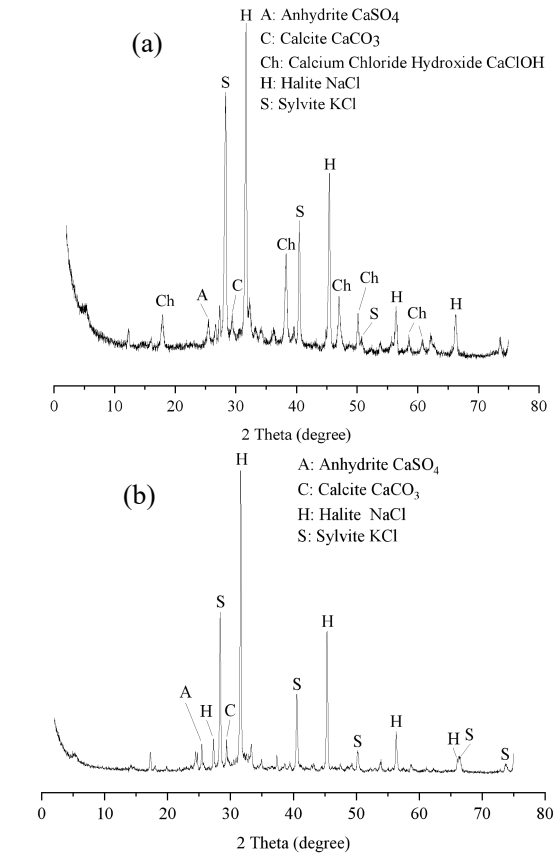

Fig. 2 XRD pattern of fly ash samples: (a) fly ash R, (b) fly ash S.

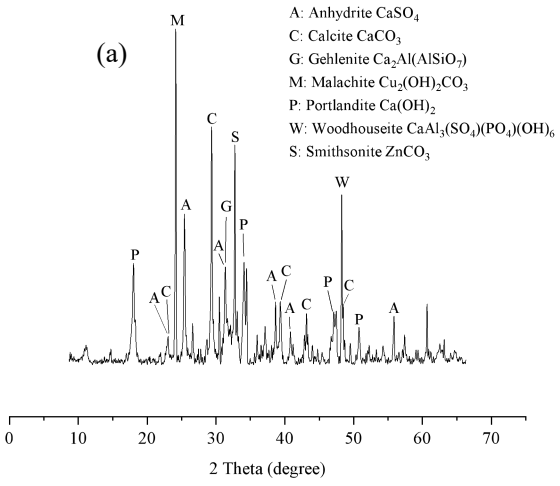

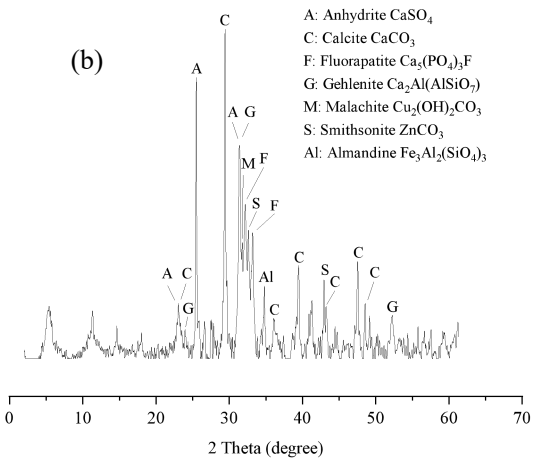

Fig. 3 XRD pattern of washed fly ash samples: (a) washed ash R, (b) washed ash S.

2.2 Relationship between particle size and heavy metal concentrations in bottom ash

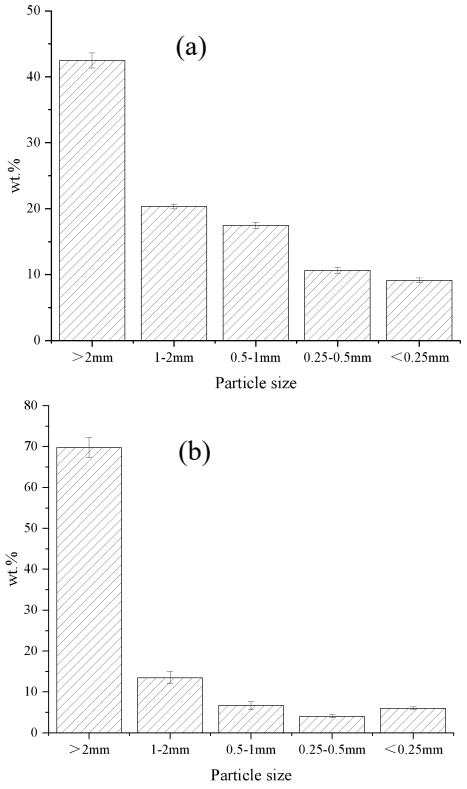

Fig. 4 The distribution of bottom ash mass with particle size after sieving: (a) Bottom ash R; Bottom ash S.

Table 1 indicates that the concentrations of Zn and Pb in two bottom ash samples are below the specified cut-off grade (DZ/T 0214-2020). However, the Cu concentration in bottom ash S exceeds the minimum industrial grade (DZ/T 0214-2020). **Fig. 4** displays the mass distribution for these two samples at various particle sizes.

As illustrated in **Fig. 5**, the copper concentration in both samples peaks when the particle size ranges between 1-2mm and decreases as the particle size decreases. Because of copper's low volatility, its concentration varying with the bottom ash particle size is likely related to the sizes of copper-containing waste components, such as copper wires and metal pieces, for instance. For bottom ash R, none of the samples at different particle sizes meet the cut-off grade for copper(DZ/T 0214-2020). In the case of bottom ash S, the ash with particle sizes larger than 2mm meets the cut-off grade, while samples with particle sizes in the ranges of 1-2mm, 0.5-1mm, and 0.25-0.5mm all exhibit copper concentrations surpassing the minimum industrial grade (DZ/T 0214-2020). However, the concentration falls below the cut-off grade when the particle size is less than 0.25mm.

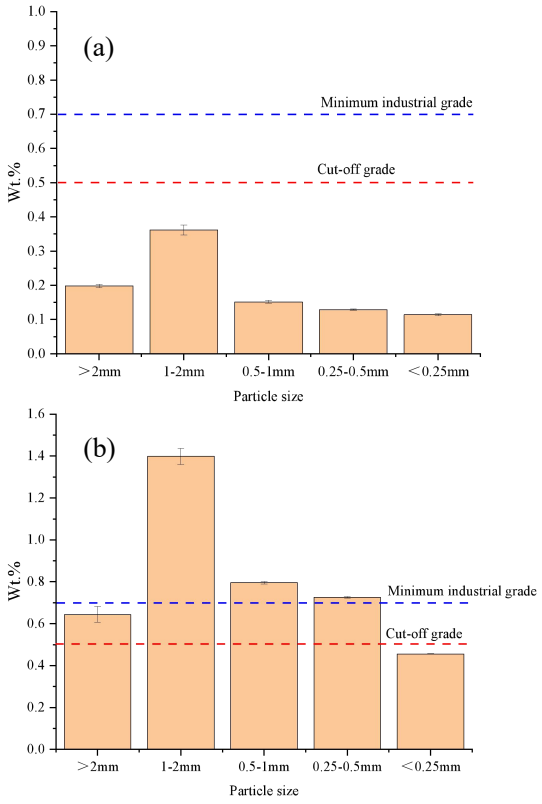

Fig. 5 Variation of Zn and Cu content in bottom ash R after sieving with particle size: (a) Bottom ash R; Bottom ash S.

3. CONCLUSION

Water washing is an effective method for increasing the concentration of heavy metals in fly ash. Following water washing pre-treatment, the zinc and copper content in both fly ash samples significantly increased and exceeded the corresponding industrial standards. $Cu_2(OH)_2CO_3$ and $ZnCO_3$ were detected in the post-washing samples.

Mechanical sieving is an effective pre-treatment method for bottom ash. In the case of bottom ash, the copper content is highest in the 1-2mm particle size range and decreases as the particle size decreases. In Sample B, copper concentrations in samples with particle sizes of 1-2mm, 0.5-1mm, and 0.25-0.5mm exceed industrial standards, while in Sample A, the copper content falls short of meeting the cut-off grade.

The assessment of recovery value for solid waste incineration residues in this study is based on the boundaries of ore grades and the minimum industrial standards. However, it is important to note that solid waste incineration residues significantly differ from ores. Firstly, they do not require mining and transportation, which is a notable advantage. Additionally, the influence of elemental aluminum present in solid waste incineration residues on metal recovery should not be overlooked. Research suggests that during the acid leaching process of fly ash, elemental aluminum can form alloys with copper and lead, making the extraction of these two metals challenging (Weibel *et al.*, 2018). Furthermore, copper in bottom ash is likely to exist in alloy form, making its recovery different from that of copper ores. Therefore, it is reasonable to assert that the application of ore standards to assess the recovery value of waste incineration residues warrants further research.

ACKNOWLEDGEMENTS

We gratefully acknowledge the support provided by Nishihara Cultural Foundation and JST SPRING (Grant Number JPMJSP2136). We would also like to express our appreciation to the operators of the MSWI plants for their provision of sample materials. Additionally, we sincerely thank Yuki Kajino and Dania Labira for their analytical support.

REFERENCES

Chimenos, J.M. et al. (1999) 'Characterization of the bottom ash in municipal solid waste incinerator', Journal of Hazardous Materials, 64(3), pp. 211–222. Available at: https://doi.org/10.1016/S0304-3894(98)00246-5.

DZ/T 0201-2020: Specifications for tungsten, tin, mercury, and antimony mineral exploration.

DZ/T 0212.2-2020: Specifications for salt mineral exploration—Part 2: Present saline lake mineral.

DZ/T 0214-2020: Specifications for copper, lead, zinc, silver, nickel, and molybdenum mineral exploration.

Jung, C.H. *et al.* (2004) 'Metal distribution in incineration residues of municipal solid waste (MSW) in Japan', *Waste Management*, 24(4), pp. 381–391. Available at: https://doi.org/10.1016/S0956-053X(03)00137-5.

Shunda Lin *et al.* (2022) 'Disposal technology and new progress for dioxins and heavy metals in fly ash from municipal solid waste incineration: A critical review', *Environmental Pollution*, 311, p. 119878. Available at: https://doi.org/10.1016/j.envpol.2022.119878.

Tang, J. *et al.* (2018) 'Assessment of copper and zinc recovery from MSWI fly ash in Guangzhou based on a hydrometallurgical process', *Waste Management*, 76, pp. 225–233. Available at: https://doi.org/10.1016/j.wasman.2018.02.040.

Tang, J. et al. (2019) 'Highly efficient recovery and clean-up of four heavy metals from MSWI fly ash by integrating leaching, selective extraction and adsorption', Journal of Cleaner Production, 234, pp. 139–149. Available at: https://doi.org/10.1016/j.jclepro.2019.06.198.

Tang, J. et al. (2022) 'Optimizing critical metals recovery and correlative decontamination from MSWI fly ash: Evaluation of an integrating two-step leaching hydrometallurgical process', Journal of Cleaner Production, 368, p. 133017. Available at: https://doi.org/10.1016/j.jclepro.2022.133017.

Tang, J. and Steenari, B.-M. (2016) 'Leaching optimization of municipal solid waste incineration ash for resource recovery: A case study of Cu, Zn, Pb and Cd', Waste Management, 48, pp. 315–322. Available at:

https://doi.org/10.1016/j.wasman.2015.10.003.

Wang, K.-S. et al. (2001) ‘Effects of a water-extraction process on heavy metal behavior in municipal solid waste incinerator fly ash’, Hydrometallurgy, 62(2), pp. 73–81. Available at: https://doi.org/10.1016/S0304-386X(01)00186-4.

Wei, Y. et al. (2022) ‘Removal of harmful components from MSWI fly ash as a pretreatment approach to enhance waste recycling’, Waste Management, 150, pp. 110–121. Available at: https://doi.org/10.1016/j.wasman.2022.06.041.

Weibel, G. et al. (2018) ‘Extraction of heavy metals from MSWI fly ash using hydrochloric acid and sodium chloride solution’, Waste Management, 76, pp. 457–471. Available at: https://doi.org/10.1016/j.wasman.2018.03.022.

Zhang, Y., Jiang, J. and Chen, M. (2008) ‘MINTEQ modeling for evaluating the leaching behavior of heavy metals in MSWI fly ash’, Journal of Environmental Sciences, 20(11), pp. 1398–1402. Available at: https://doi.org/10.1016/S1001-0742(08)62239-1.

Zhang, Yuying et al. (2021) ‘Treatment of municipal solid waste incineration fly ash: State-of-the-art technologies and future perspectives’, Journal of Hazardous Materials, 411, p. 125132. Available at: https://doi.org/10.1016/j.jhazmat.2021.125132.

STUDY ON REDUCTION OF COD LOAD IN FLY ASH BY USING CHEMICAL DOSAGE MANAGEMENT DEVICE

Takeshi Yamasaki[1], Hirotaka Fujiwara[1], Takayuki Mizunari[1]
1 Resource Circulation Technology Department Circular Economy Business Development Group
KURITA WATER INDUSTRIES LTD. ,Kurita Innovation Hub 3993-15,Haijimacho,Akishima-shi,Tokyo,Japan

1.INTRODUCTION

In Japan, heavy metal such as lead is often leached from fly ash generated from municipal solid waste incinerators, and chelate agents are generally used to immobilize heavy metal.

To immobilize heavy metal, it is necessary to use a required and enough amount of chelate agent.

However, since the heavy metal content fluctuates, the dosage rate is set excessively considering the safety treatment.

On the other hand, since chelate agents contain persistent COD components, excessive dosage increases the COD load on a landfill site and affect its closure period. We have developed a chemical dosage managing device that can easily measure the required addition rate of chelate agent on site. This article describes the results of its application to reducing the COD load caused by fly ash.

2.MATERIALS AND METHOD

2.1 Fly ash sample

An evaluation test was conducted using fly ash from facility A shown in Table 1.

Table1 Facility A overview

Index	Specifications
waste	municipal waste
Incinerator model	stoker furnace
acidic gases treatment prosess	dry scrubbing process
acidic gases neutralization agent	slaked lime
heavy metal immobilization agent	organic chelate agent

Figure 1 shows the analysis results of heavy metal content and leaching amount at facility A raw fly ash. The leaching tests were conducted according to Japan Leaching Test 13th method (JLT13). The Pb contents were fluctuated from 580 to 1410 mg/kg. pH values of eluates were high alkalinity above12, and Pb concentration exceeded the standard value (0.3 mg/l) .

This trend is the same as that of general municipal waste incineration facilities in Japan. At this facility, the chelate addition rate was set at 4% (constant dosage rate).

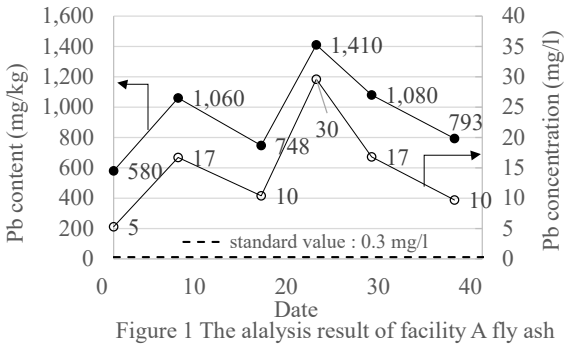

Figure 1 The alalysis result of facility A fly ash

2.2 Heavy metal immobilization agent

Chelate agent containing piperazine dithiocarbamate, which is commonly used in Japan, was used. Table 2 shows the analysis results.

Table 2 Overvew of the organic chelate agent

Index	Specification
product name	ASHNITE® S-803※
pH	13～14(25℃)
specific gravity	1.25
COD contents	195,000 mg/kg

※This product name is used in Japan

2.3 Table test method

2.3.1 Examination on chelate dosage rate

20 g of raw fly ash were weighed into a beaker, a predetermined amount of humidifying water and a chelate agent were added, and the mixture were stirred uniformly with a spatula. After curing this treated ash for one day, leaching tests were conducted based on the JLT13 method, and leachate were analyzed.

The chelate agent dosage rate when the Pb concentration in the leachate was lower than the standard value (0.3 mg/l) was set as the required dosage rate.

2.3.2 Leaching test method of chelate treated fly ash

The Pb and COD concentration in the treated ash were measured based on the JLT13 method.

2.4 Examination about chelate dosage rate and residual chelate concentration on fly ash by using chemical dosage management device

The chemical dosage management device "S.sensing® AS" shown in Figure 2 was installed at facility A site, and the required chemical dosage rate to the raw ash and the residual chelate concentration in the treated ash were measured. S.sensing® AS is a device that can measure the concentration of chelate agents in about 30 minutes using absorbance analysis.

Figure 2 S.sensing® AS

3.RESULTS AND DISCUSSION

3.1 Chelate dosage rate for fly ash at table test

As shown in Figure 3, the chelate agent dosage rate to satisfy the Pb standard value were in the range of 1.5 to 2.5%, which is 1.5 to 2.5% lower than the 4% addition rate set in facility A actual machine.

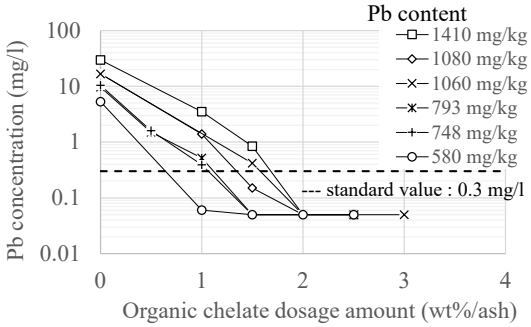

Figure 3 JLT13 test result of facility A fly ash

3.2 Correlation between chelate dosage rate and COD leaching concentration at table test

As shown in Figure 4, the COD concentration increased in the case the chelate agent was further added after the Pb leaching concentration decreased.

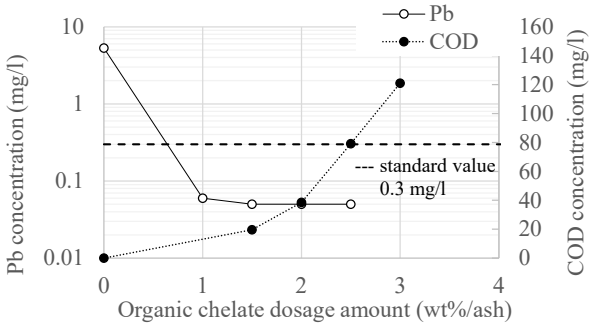

Figure 4 JLT13 test result of facility A fly ash

3.3 Examination result about dosage management device (on site evaluation)

As shown in Figure 5, the chelate dosage rate to raw fly ash guided by the chemical dosage management device S.sensing® AS correlates with the required dosage rate obtained by table test, confirming that this device can guide the required addition rate of chelate agent on site.

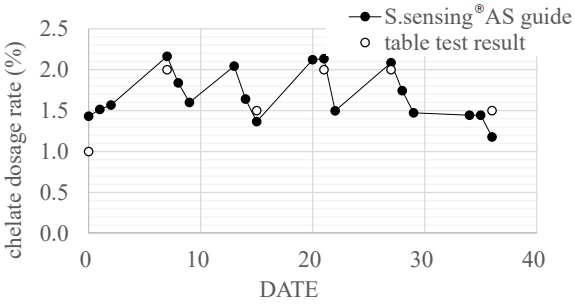

Figure 5 The correlation between the guide dosage rate by S.sensing® AS and table test result

3.4 Examination about COD reduction

Figure 6 shows the COD concentration from treated ash with using S.sensing® AS to reduce the chelate agent dosage rate from 4 % to 3 % in the actual machine.

As shown in the figure 6, a reduction in COD concentration was confirmed. Additionally, at facility A, the amount of chelate agent used per month decreased from 8.7 tons to 6.7 tons. It was estimated that the amount of COD derived from chelate agent was reduced by 390 kg-COD/month.

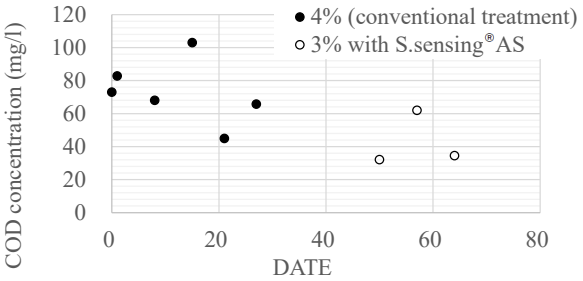

Figure 6 The correlation between JLT 13 COD concentraion by conventional treatment and S.sensing® AS treatment

4. CONCLUSION

Through this study, we found that COD components derived from chelate agent can be reduced by monitoring the properties of fly ash on-site and controlling its dosage rate.

As future effort, we will consider the measurement frequency that follows changes in fly ash properties, and also work to optimize the amount of acid gas treatment agents used, which will have an impact on reducing the treatment load of leachate at landfill sites.

CONSTRUCTION AND EVALUATION OF A RECOVERED PAPER SORTING SUPPORT SYSTEM USING DEEP LEARNING

Naoya Kojo[1], Takayuki Shimaoka[1], Yasuhiro Sugisaki[1]
1 Kyushu University, 744 Motooka Nishi-ku, Fukuoka, Japan

1.INTRODUCTION

The recycling of wastepaper greatly contributes not only to securing raw materials for paper products but also to reducing waste and maintaining forest resources. In Japan, the collection and utilization rate of wastepaper is around 65%, which is one of the highest in the world. Although it is difficult to expect further expansion of wastepaper utilization, considering recent global warming and the need for waste reduction, the promotion of recycling is still necessary.

In increasing Japan's wastepaper collection rate, the focus is currently on wastepaper generated in offices. Unlike the collection of households wastepaper in communities, it is collected by companies or building management companies that contract regional collection and transport operators. As for the current state of office wastepaper, there are problems with the low collection rate of mixed paper and the fact that recycling of mixed paper in small business sites with a few employees is not progressing very much[1)].

Recent trends in waste sorting have seen notable efforts in utilizing IT technology, particularly artificial intelligence, which is being applied across many fields due to its versatility, including in the area of resource recycling.

Convolutional Neural Networks (CNNs) are one type of image recognition technology that uses deep learning. They extract local features of images through convolutional layers and summarize these features in pooling layers, which are stacked in multiple layers. Through this process, CNNs can learn by repeatedly extracting object features, enabling highly accurate image recognition.

In this research, we develop a wastepaper sorting system using image recognition and object detection technology by AI, designed for practical use scenarios to support the separation of commercial wastepaper. By evaluating this system, we will examine the feasibility of using an AI-based wastepaper sorting system within the current regulatory framework.

2.DATASET AND MODELS

In the system developed in this study, we sort eight types of paper products. The settings for the eight sorting classes, with each product type considered as one class, and the learning-related settings are shown in Table.1. Among the eight sorting classes and the eight types of paper products, four types can be disposed of as wastepaper, while the other four types cannot be discarded as wastepaper because they contain materials other than paper. These types of paper products can be easily mistaken for paper at first glance, which often leads to them being incorrectly thrown away as wastepaper. They have been designated as prohibited items that require special attention during wastepaper sorting.

Table. 1 Settings of training.

	Class	Number of images		Pixel	Epoch
		Training	Validation		
1	envelope	50	10	1600 x 1064	300
2	juicepack	50	10		
3	milkpack	50	10		
4	paperbag	50	10		
5	papercup	50	10		
6	postcard	50	8		
7	receipt	50	8		
8	slip	50	10		

As a method of evaluating object detection, we use the mean Average Precision (mAP). The criteria for assessing object detection are 'whether the position of a specific object within the image has been correctly detected' and 'whether the predicted label of the detected object matches the correct label'. The results are aggregated for each detected bounding box as a successful detection with a correct prediction (True Positive, TP), a successful detection with an incorrect prediction (False Positive, FP), and a missed detection

despite the object's presence (False Negative, FN). Using these values, Precision and Recall are calculated as follows.

$$Precision = \frac{TP}{TP + FP}$$

$$Recall = \frac{TP}{TP * FN}$$

By taking Precision on the vertical axis and Recall on the horizontal axis and plotting points with the aggregated values for each bounding box, the Average Precision (AP) is calculated through integration for each precision level. By calculating this AP for all classes being classified and then averaging it, the mean Average Precision (mAP) can be determined. The closer this value is to 1, the higher the accuracy of the model. Generally, a model is considered to have a good level of accuracy if the value is above 0.5.

3.RESULTS

We conducted training with the above settings and evaluated the performance of the model. The results of the training are shown in Table.2. mAP50 represents the mean Average Precision mAP when the overlap between the detected area and the actual area by the bounding box exceeds 50%. mAP50-95 is the average of the mAP values when the threshold for the area overlap is varied from 50% to 95% in increments of 5%. The closer these metrics are to 1.0, the better the model applies to the validation data. The experimental results showed that the accuracy of mAP50-95 for the overall validation data was 0.760, and the accuracy of mAP50 was 0.972, indicating that detection was possible with an accuracy of over 90% under the assumed conditions. Looking at the results for each class, high precision, recall, and mAP scores are demonstrated for many classes. However, the recall for the 'milkpack' class was 0.72, and the recall for the 'slip' class was 0.8, which is relatively low, missing about 20% of the instances. The possible causes include the object blending in with the background color, making it difficult to detect, or photos taken from a distance where the object is too small to be recognized. In addition, the precision for the 'postcard' class was 0.719, which is lower compared to other classes, indicating it was often misidentified as another class. This is thought to be due to its resemblance to the 'receipt' or 'slip' classes at a glance, leading to misrecognition, suggesting a need for augmenting the diversity of the training data.

Table. 2 Results of validation.

Class	Precision	Recall	mAP50	mAP50-95
all	0.93	0.9211	0.972	0.76
envelope	1	0.97	0.995	0.782
juicepack	1	0.978	0.995	0.793
milkpack	1	0.72	0.986	0.667
paperbag	0.925	0.9	0.915	0.548
papercup	0.948	1	0.995	0.837
postcard	0.719	1	0.995	0.879
receipt	0.874	1	0.995	0.859
slip	0.97	0.8	0.898	0.717

4.CONCLUSION

In conclusion, this research implemented a wastepaper sorting system utilizing image recognition technology based on deep learning as a measure to assist in the sorting of wastepaper and verified its accuracy. The findings obtained from this research are as follows:

1) The precision of mAP50-95 for all validation data was 0.760, and the accuracy of mAP50 was 0.972, indicating that under the assumed conditions, recognition is possible with high accuracy of over 90%.

2) Analysis of paper products that were misrecognized revealed that data with objects blending into the background color or images of objects taken from a distance that appear small have lower recall rates. It is necessary to increase the dataset for paper products with similar appearances to improve differentiation.

Among these, particularly for data with small images of objects, there is a tendency to miss detections due to the characteristics of Yolo. Therefore, it is considered necessary in practical applications to limit the distance from which photographs are taken to avoid capturing images from too far away.

ACKNOWLEDGEMENTS

The authors are grateful to the Fukuoka City Project to Support Demonstration and Research on Technology for Recycling Business-Related Waste for support on the research.

References

1) Jigyoukei gomi no shigenka suishin kentou iinkai. Efforts to promote recycling of commercial waste as a resource. 2010.
2) Lau Chun Tat. (2021). Construction of trash classification support system based on deep learning. Forum on Information technology, 20, CO-003.

RESEARCH ON TAG RECEPTION PERFORMANCE IN DETECTING LITHIUM-ION BATTERIES(LIBs) USING RFID TAG

Koji Sakakibara[1], Eriko Aibara[1], Takayuki Shimaoka[1]
Kenji Ito[2], Haruichi Kanaya[2]
[1]Department of Urban and Environmental Engineering, faculty of Engineering,
Kyushu University,744 Motooka, Nishi-ku, Fukuoka, Japan
[2]Department of Electronics Graduate School of Information Science and Electrical Engineering,
Kyushu University,744 Motooka, Nishi-ku, Fukuoka, Japan

ABSTRACT

There have been many incidents of ignition caused by lithium ion batteries (hereinafter referred to as "LIBs") mixed in noncombustible waste and other materials. In this study, we conducted basic research on a method to detect products containing LIBs mixed in waste, based on the premise that RFID (Radio Frequency Identification) tags, which are widely used as automatic identification technology, are attached to LIBs. The tag used in the experiment is unidirectional RFID tag antenna under development, which can receive radio waves from a reader/writer(hereinafter referred to as R/W) even when the tag is attached to a metal product. In this study, the performance of the tag alone was verified, and the reception strength and distance under obstructions (several types of waste) and general environmental conditions were measured. Experimental results show that if the distance between the tag and R/W is approximately 2.5 m or less, detection is possible even in the presence of obstacles such as metal. This result suggested the possibility of LIB detection using unidirectional RFID tag antenna, although there is a limit to the tag and R/W distance.

1. Introduction

In recent years, there have been many incidents of smoke and fire caused by lithium ion batteries (hereinafter referred to as LIBs) mixed in with noncombustible waste, etc. If LIBs are present at the loading ports of packer trucks or crushing equipment at recycling facilities, they may ignite due to excessive compression or crushing of the LIBs. The fire accident is a serious problem. Currently, countermeasures against such fire accidents include early detection of abnormal temperature rise of waste and smoke/fire and introduction of automatic fire extinguishing systems, but these are only post-detection. In order to reliably reduce the number of accidents, it is necessary to take pre-detection and remove LIBs mixed in refuse before it is collected and processed.

This study aims to construct a LIBs detection system that can be implemented in society, based on the premise that RFID (Radio Frequency Identification) tags, which are widely used as an automatic identification technology, can be attached to LIBs. However, since general FRID tags cannot transmit radio waves when attached to metal products such as LIBs. So in this study, we used RFID tags under development at the Kyushu University. We have confirmed in an anechoic chamber that the RFID tag works properly when attached to a LIBs, and clarified the relationship between the reception strength depending on the distance between the tag and the reader/writer (hereinafter referred to as R/W) and the tag's orientation. It was also found that the presence of obstacles such as water and metal between the tag and the R/W made it difficult to read the tag.

Furthermore, for the purpose of practical application of this detection system, tag reading experiments were conducted when tags were placed not only in an anechoic room but also in a general living environment to confirm the effect on reception.

2. Materials and methods

2.1 RFID tags

Two types of RFID tags were used in the experiment. The RFID tags used were a unidirectional RFID tag antenna developed by Ito et al.[1)] (called A tag) and a commonly used conventional RFID tag antenna used on the back of price tags on clothes. (called B tag) In the case of B-tags, if the tag is in contact with metal or liquid, the reflected waves from the antenna are
canceled out or absorbed. This makes reception difficult by the reader/writer. (hereafter referred to as R/W) which transmits radio waves to the tag and receives the reflected waves from the tag On the other hand, A-tags have "unidirectional directivity," meaning that radio waves do not propagate in the direction of the tag's installation surface. (Table 1)

Table1 Comparison of the performance of the two tags, unidirectional RFID tag antenna(A-tag) and conventional RFID tag antenna tag(B-tag)

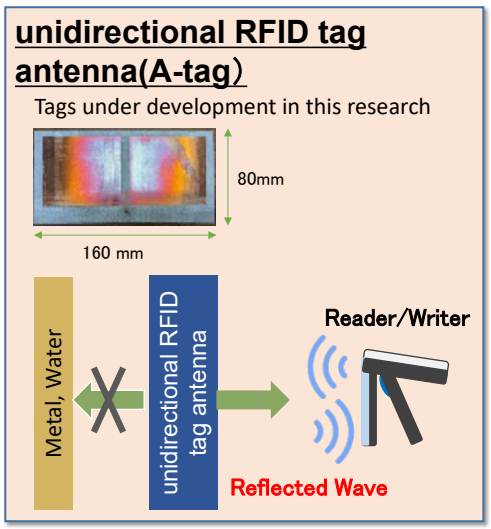

2.2 Experimental Methods

An overview of the experimental apparatus is shown in Figure1. The experiment was conducted in an anechoic chamber, where the entire room was lined with radio wave absorbers that block the effects of external radio waves in order to eliminate the influence of radio waves present in the general environment.

The R/W and the tag were placed at the same height. Received strength was measured by changing the distance between the tag and the R/W and by changing the reception angle by rotating the tag clockwise and counterclockwise. Receiving strength is indicated by the received signal strength indicator (RSSI) value. The higher the RSSI value, the more stable the reception.

Based on the results in the anechoic room, the same method was used to check reception in general environments where WiFi radio waves are present or metal products are nearby.

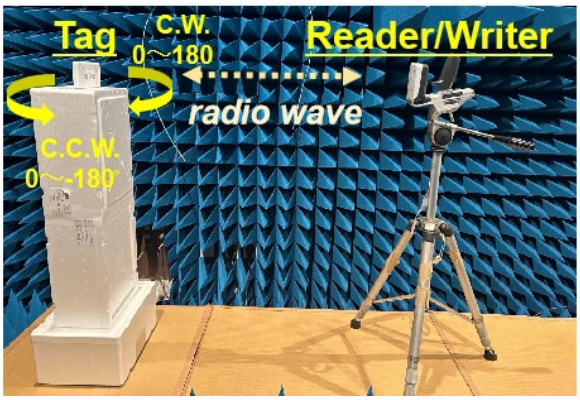

Figure1 Experiments in an anechoic chamber

3. Results and discussions

Experimental results and discussion are presented for the following items.

(1) Confirmation of the unidirectional directivity performance of the A-tag

(2) Influence of obstacles that are assumed to be mixed with the A-tag on the reception status

(3) Confirmation of reception status in general environment

The reception strength in each experiment was the average of RSSI values (dBm) measured five times consecutively. Reception strength and reception range are shown in the radar chart. Reception range is shown from 0 to 180 degrees clockwise and from -180 to 0 degrees counterclockwise.

3.1 Confirmation of the unidirectional directivity performance of the A-tag

Mobile batteries are the largest cause of fires caused by rechargeable batteries. We affixed A and B tags to a mobile battery and compared the results with those obtained with the tag alone. When the A tag was affixed to the mobile battery, the reception strength of the A tag was equal to or greater than that of the tag alone, but when the B tag was affixed to the mobile battery, it could not be received. This confirmed the unidirectional directional performance of the A-tag.(Figuer2)

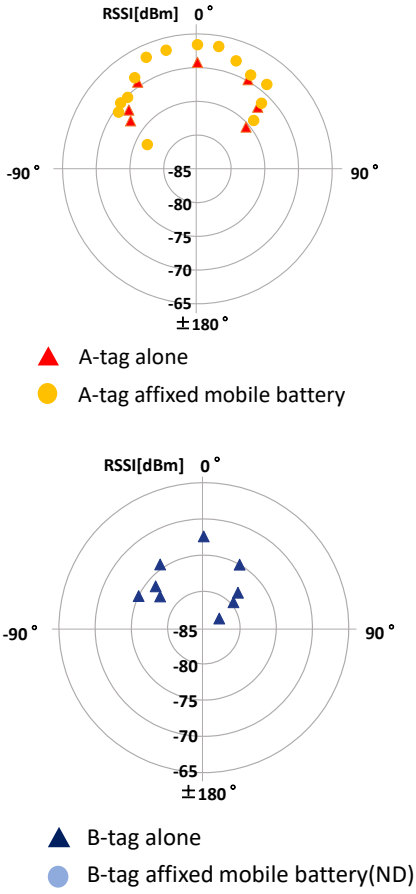

Figure2 Comparison of RSSI and reception range of A and B-tag between tag alone and tag affixed to mobile battery

3.2 Influence of obstacles that are assumed to be mixed with the A-tag on the reception status

Assuming that LIBs containing products are disposed of mixed with various types of waste, an obstacle in a 45L trash bag was prepared. Four types of obstacles were selected: plastic bottles, plastic bottles filled with water, empty cans, and timbers. The obstacles were placed between the tag and the R/W at 0.5 m from the tag, and the reception status at each obstacle was measured. (Figure 3)

The results are shown in Figure 4. It can be seen that the reception strength of the PET bottle is the same as that of the case with no obstruction, while the PET bottle filled with water has a lower reception strength of 5 dBm and a narrower reading range. The timbers was easy to read with an RSSI value about 1 dBm larger. Empty cans could not be read at any angle.

Further experiments were conducted for empty cans by moving the receiving distance closer. As a result, as shown in Figure 5, even empty cans could be received when the receiving distance was moved closer to 2.5 m or 1 m.

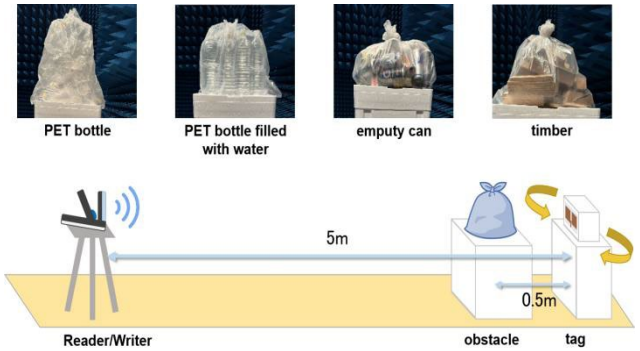

Figure3 Four types of obstacles and experimental condition

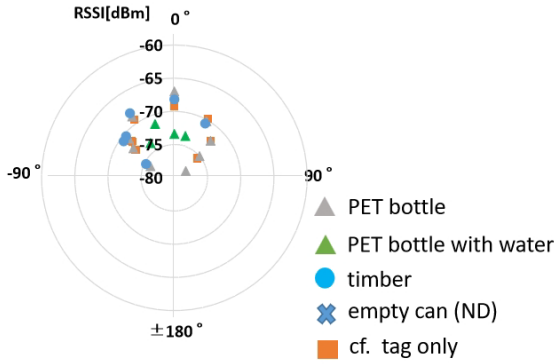

Figure4 Comparison of RSSI and reception range due to obstruction

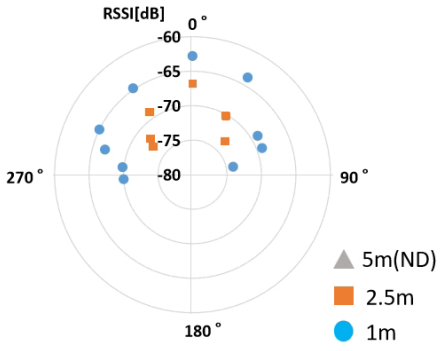

Figure5 Comparison of RSSI and reception range for each reception distance in empty cans

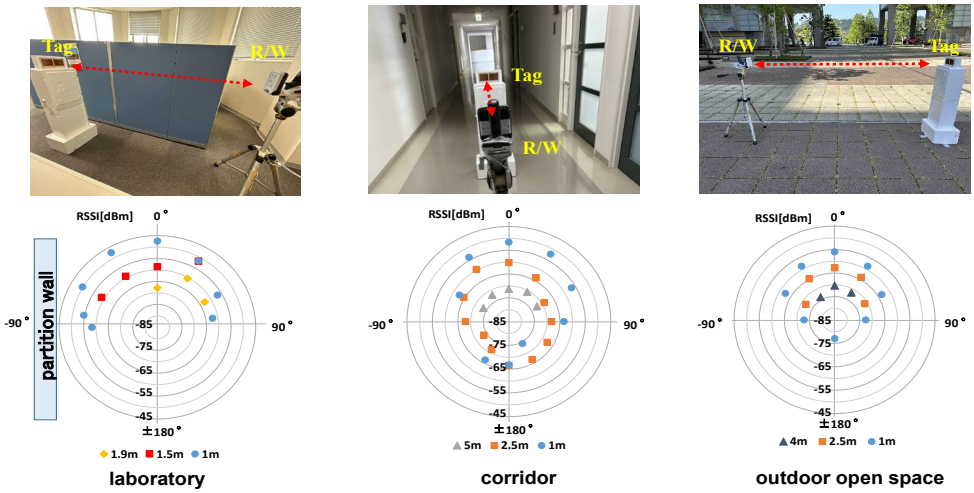

Figure6 Comparison of RSSI and reception range under general environment

3.3 Confirmation of reception status in general environment

In addition to the previous measurements in an anechoic chamber, the detection was also checked in a general environment where other radio waves, such as Wi-Fi, were present. We chose laboratories, corridors, and outdoor plaza on the university campus. The distance between the tag and R/W was set at 5 m, the maximum reception distance for A-tags, and varied in three steps. The results are shown in Figure 6.

In the laboratory, the maximum reading distance was only 1.9 m. However, at a distance of 1 m, the maximum reading distance was ±90 degrees, as in the anechoic chamber. At a reception distance of 1 m, the counterclockwise (-90 to 0 degrees) reception strength was 4 to 8 dB greater than the clockwise (0 to 90 degrees). The reason why the counterclockwise direction was easier to read is that there is a divider in this direction, we expect that the metal inside the divider affected the reception. In the corridor, the results of reception conditions were equivalent to those in the anechoic chamber. Furthermore, even when the tag was set at a reception distance of 2.5 meters and 1 meter, and the tag was facing backward, it could be read within a range of ±90 to 180 degrees. This may be due to the fact that the corridors and walls of the building are made of steel, which allows the R/W to read radio waves reflected from all angles by the metal. Finally, outdoors, the reception distance was only up to 4 m, but at 2.5 m and 1 m, the reception results were equivalent to those in an anechoic chamber.

4. Conclusion

The purpose of this study is to construct a system to detect LIBs containing products mixed in waste by attaching the unidirectional RFID tag antenna to LIBs. Using the tag antenna which under development, measurements of the tag's reception status in various situations were conducted. As a result, the following findings were obtained.

(1) Due to the tag's unidirectional directivity, the tag could be detected even if it was attached to a product containing metal objects that weaken radio waves, such as a mobile battery.

(2) Reception strength weakened when water or metallic objects were between the tag and the R/W. However, stable reception was achieved when the reception distance was reduced to 2.5 m.

(3) Even in general environments where other radio waves such as Wi-Fi exist, reception performance equivalent to that in an anechoic chamber was confirmed at a reception distance of 1 m or less in the laboratory and 2.5 m or less outdoors. On the other hand, in a corridor, reception was confirmed to be possible in all 360° directions.

These results suggest that unidirectional RFID tag antennas can be used to pre-detect LIBs mixed in waste. We plan to continue our research on the following points for practical application.

(1) Develop tags that can be miniaturized and bent, and confirm the performance of these tags.

(2) Demonstrate practical detection methods. For example, the detection of refuse bags containing LIBs by R/W set on a packer truck or by refuse collection workers with the R/W.

Reference

1)Kenji Ito, Haruichi Kanaya,Design of 900 MHz band metal-available compact dipole antennaProc.IEEE Electronics Packaging Technology Conference, 6pages,Dec.5-8th, 2023.(in press),https://www.eptc-ieee.net/

A study on a method for detecting large landfills by unsupervised learning using sentinel-2

Taiki Kamitaki[1], Yasuhiro Sugisaki[2], Takayuki Shimaoka[2]

1 Dept. of Faculty of Engineering, Kyushu University

West3 room916 744 Motooka, Nishi-ku, Fukuoka City, Japan

2 Dept. of Urban and Environmental Engineering, Faculty Engineering, Kyushu University

West2 room1010 744 Motooka, Nishi-ku, Fukuoka City, Japan

Abstract

It is assumed that there are many illegal dump sites, especially in developing countries. These unmanaged dump sites have negative impacts on environment, such as untreated leachate. Therefore, their location and size need to be detected and managed. In this study, we try to detect landfill site (illegal dump sites) using satellite remote sensing data which have visible light to short-wavelength infrared information. As a method, we use hierarchical clustering, unsupervised learning. As a result, we obtain a proposed method for detection. And we also found that it is difficult to distinguish between slums and landfill sites.

1. Introduction

In developing countries such as Asia and Africa, there are many areas where waste is not collected. It makes illegal dumpsites. It is difficult to assess the location and number of these illegal dumpsites. Illegal dumpsites can cause leachate to flow out and contaminate the environment, which is considered harmful to human health. In addition, the emission of greenhouse gases such as CO_2 and CH_4, especially CH_4, is high, which has an impact on global warming. For these reasons, it is important to know number, location, and size of illegal dumpsites.

In this study, satellite remote sensing data, specifically Sentinel-2 satellite data, was used to perform land use and land cover classification by unsupervised learning. It classified landfills (illegal dumpsites), cities, forests, rivers, oceans, and bare ground. By comparing the results with data from high-resolution satellite images, we aimed to identify a method for detecting landfills.

2. Materials and Methods

2.1. Target area

The target area for this study was downtown Mumbai, India (Fig.1.).

Figure1. Target area of this Study.
@2022 Google

India has the second largest population in the world, almost the same number as China in 2022, and Mumbai City is the second most populous city in India. In addition, its GDP is the largest in India. It is assumed to have a large amount of waste emissions.

The target area was defined as the area shown by the red frame in Fig.1. (8.94 km x 11.88 km). This area includes landfill sites (blue circle in Fig.1.) and various landforms such as urban areas, forests, and rivers.

2.2. Outline of Landfill Sites

The landfills analyzed in this study are Deonar Landfill, located in the lower middle of the analysis area in Fig.1., and Kanjurmarg Landfill, located in the upper right. Deonar Landfill is the oldest landfill in India, built in 1927. The site covers an area of approximately 132 ha, with approximately 5500 tons of waste is loaded daily. Kanjurmarg Landfill was established in 2015. The site extends over an area of about 141 ha and is the largest landfill in the city. Approximately 4,000 tons of waste is loaded daily.

2.3. Satellite remote sensing data

In this study, we used Sentinel-2/MSI in satellite remote sensing data, which has 11 bands ranging from visible to shortwave infrared. In addition to these data, NDVI, GRVI, NDMI, NDWI, and MNDWI were also used. The method of obtaining the data is as follows.

$$\mathrm{NDVI} = \frac{\mathrm{B8} - \mathrm{B4}}{\mathrm{B8} + \mathrm{B4}} \quad \mathrm{GRVI} = \frac{\mathrm{B3} - \mathrm{B4}}{\mathrm{B3} + \mathrm{B4}}$$

$$\mathrm{NDMI} = \frac{\mathrm{B8} - \mathrm{B11}}{\mathrm{B8} + \mathrm{B11}} \quad \mathrm{NDWI} = \frac{\mathrm{B4} - \mathrm{B11}}{\mathrm{B4} + \mathrm{B11}}$$

$$\mathrm{MNDWI} = \frac{\mathrm{B3} - \mathrm{B11}}{\mathrm{B3} + \mathrm{B11}}$$

B3: Visible(green), B4: Visible(red),
B8: Near infrared, B11: Short wavelength infrared

These data were standardized. Date of the data is December 3, 2022.

2.4. Methods

Used analysis method was hierarchical clustering, which is unsupervised learning. This method makes clusters in order from the most similar data or clusters. In this study, Euclidean distance was used as the distance measurement method between data and Ward's method as the distance measurement method between clusters. A dendrogram of the analysis results and a map of the results were used to confirm how the landfill sites were classified.

3. Results and Discussion

A dendrogram of the analysis results is shown in Fig.2. From this dendrogram, landfill sites can be identified if they are classified in the same class. Therefore, we find for the maximum number of classes in which two landfills can be divided into a single cluster. As a result (right side of Fig. 2.), it was found that when all area was divided into five classes, the landfill sites were identified as class 3. This result is displayed on a map in Fig. 3. In this figure, place which classified as number 3 are colored red. Airport. (Chhatrapati Shivaji Maharaj International Airport) and slums are classified in the same class as landfill sites. Table 1 shows the percentage of the extent of each class in the areas of landfills 1 and 2, slums, and airports. In this study, a land use and land cover kind was determined when at least 70% of its area was classified into the same class. As a result, landfill site, slums, and airports were same class for this classification, and landfill site could not be classified alone.

Next, we compared the satellite remote sensing data values (radiance values) for the landfill, the slum, and the airport respectively. Comparing the landfill and the airport, the mean values of B1-B5 were found to be higher for the airport, with values in the low 70s for the airport and values between 50 and 65 for the landfill (see Table2). Table3 shows the differences for landfill site2, airport, and slums from landfill site1 in the average values of B1 to B5. It shows that in B5, the difference between landfills is small, but the difference between landfill site1 and the airport and between landfill site1 and the slum area is large. Therefore, it is possible to distinguish between landfills, airports, and slums by comparing the mean value of B1 to B5 and the value of B5.

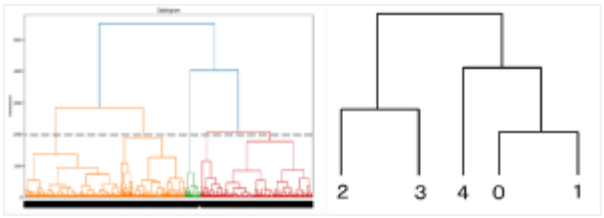

Figure 2. Classification results dendrogram

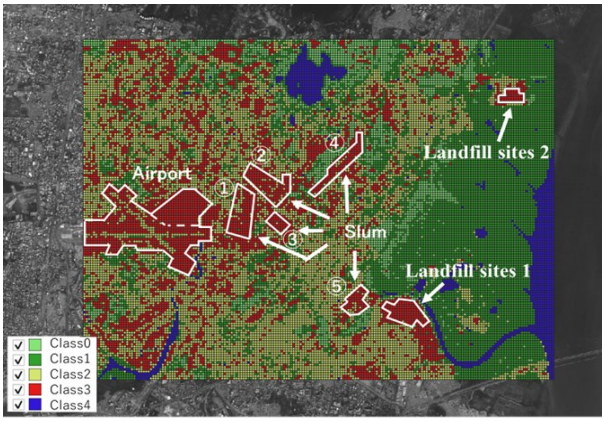

Figure 3. Classification results (classified into five classes) and region at each location map.

Table 1: Percentage of classes at each location (%)

	Class0	Class1	Class2	Class3	Class4
Landfill site1	0.0	0.0	1.5	98.5	0.0
Landfill site2	0.0	0.0	0.0	100.0	0.0
Slum	0.0	0.6	14.4	85.0	0.0
Airport	0.0	1.0	18.0	81.0	0.0
Airport (Terminal area)	0.0	0.0	0.4	99.6	0.0

Table 2: Average of remote sensing data per band

	B1	B2	B3	B4	B5
Landfill site1	51.1	53.5	57.1	60.9	64.0
Landfill site2	61.2	60.7	62.0	65.1	65.1
Slum	63.5	62.3	60.1	60.8	58.6
Airport	72.1	70.8	72.9	71.6	72.0

Therefore, we performed the classification again in the same way as above, using two types of data, the average value of B1 to B5 and the value of B5, for place with class number 3 as the previous classification result. The results are shown in Figure 4. Table 4 shows the percentage of the extent of each class in the areas of landfills 1 and 2, slums, and airports. Landfills and airports (terminal area) could be distinguished, but landfills and slums could not be distinguished.

4. Conclusion

The conclusions of this study can be summarized as follows.

(1) Hierarchical clustering was used to classify the Mumbai area in India using Sentinel-2 data. As a result, when the entire area was classified into five classes, landfill sites could be classified into one class. However, this class included airports and slums in addition to landfills.

(2) The respective average values of B1 to B5 (B1 to B4 are visible light and B5 is the near-infrared spectrum) were higher at the landfill and at the airport.

(3) There was a difference in B5 (visible light spectrum) values between the landfill, the airport, and the slum area. Further analysis of this showed a clear distinction between the landfill and the airport (terminal area), but not between the landfill and the slum area.

(4) In order to establish a method for detecting landfill sites using satellite remote sensing data in the future, the method used in this study, the detection of land elevation change using SAR data, and land temperature using thermal infrared data could be combined.

Table 3: Differential values which is average of remote sensing data from landfill site1 at each location.

	B1	B2	B3	B4	B5
Landfill site2	-10.1	-7.2	-4.9	-4.1	-1.1
Slum	-12.4	-8.8	-3.0	0.1	5.5
Airport	-21.0	-17.3	-15.8	-10.7	-8.0

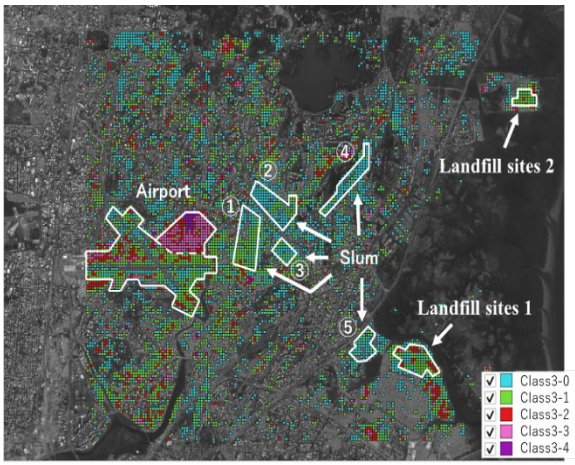

Figure 4 Classification results map (additional analysis)

Table 4: Percentage of classes at each location (additional analysis) (%)

	Class3-0	Class3-1	Class3-2	Class3-3	Class3-4
Landfill site1	20.3	53.4	24.8	1.5	0.0
Landfill site2	6.0	90.0	4.0	0.0	0.0
Slum	67.3	32.4	0.3	0.0	0.0
Airport	18.1	38.6	20.6	19.5	3.1
Airport (Terminal area)	2.1	3.7	27.4	56.4	10.4

GREENHOUSE GAS EMISSIONS FROM WASTE SECTORS IN CHINA: IMPLICATIONS FOR CARBON MITIGATION

Rongxing Bian[1*], Shudan Gao[1], Xiao Teng[1], Tingxue Zhang[1], Yingjie Sun[1]

1 Qingdao Solid Waste Pollution Control and Resource Engineering Research Center, Qingdao University of Technology, School of Environmental and Municipal Engineering, Huangdao District, Qingdao, China

ABSTRACT

Reducing carbon emissions has been the consensus among countries worldwide. As an important anthropogenic source of greenhouse gas (GHG), however, the GHG emission pattern from the waste sector in China's cities and counties is unclear which hinders the development of an effective strategy for GHG reduction. In this study, the GHG emissions from the waste sector of China during 2006–2019 were studied based on the Intergovernmental Panel on Climate Change (IPCC) inventory models. The total GHG emissions from the waste sector increased from less than 55.38 million metric tons (Mt) in 2006 to 178.06 Mt in 2019, with landfills accounting for the majority of GHG emissions. The proportion of GHG emissions from municipal solid waste (MSW) incineration increased rapidly from 7.8% in 2006 to 22.4% in 2019. The GHG emissions increased rapidly from less than 2.67 Tg in 2006 to 55.64 Mt in 2019, with the contribution increasing from 4.8% to 31.2%, as more MSW was landfilled. Among the seven regions of China, Eastern China contributed the most to GHG emissions. Therefore, there is a significant GHG mitigation potential in the MSW disposal sector. These findings indicate that GHG mitigation strategies should be based on the MSW generation and disposal situation, economic level, and operational management level of each region and province.

1 INTRODUCTION

Global climate change and ecological problems caused by the greenhouse effect have become a severe threat to humanity in the 21st century. The global carbon dioxide (CO_2) concentration in the atmosphere reached its highest level (411.4 ppm) in 2019, and the total global greenhouse gas (GHG) emissions were approximately 52.4 Gt CO_2-eq (Olivier and Peters, 2020). CO_2, methane (CH_4), and nitrous oxide (N_2O) are the main GHGs, accounting for 72%, 19%, and 6% of the total GHG emissions, respectively (Olivier and Peters, 2020). CO_2 emission in China have rapidly increased at an average annual rate of 7.73% during 2000–2014 (Wang and Jiang., 2019) due to rapid industrialization, and the country's total GHG emissions accounted for 26.0% of the total global GHG emissions (Olivier and Peters, 2020). China has the second-largest economy after the United States and is the largest GHG emitter; as such, the country is under great pressure to mitigate CO_2 emissions, especially since it signed the 2015 Paris Agreement. Furthermore, China has set an ambitious target to reach the GHG emission peak by the end of 2030 or earlier and achieve carbon neutrality by 2060. Therefore, corresponding GHG emission mitigation strategies are necessary to attain this target.

The waste sector is an important source of GHG emissions with its estimated GHG emissions increasing from 0.36 to 72.4 Mt CO_2-eq from 1949 to 2013 (Lou et al., 2017), and reaching 76.6 Mt CO_2-eq in 2017 (Zhao et al., 2019). Among the municipal solid waste (MSW) disposal sectors, landfills are the third-largest anthropogenic source of CH_4 emissions, accounting for 12% of the total anthropogenic CH_4 emissions (EPA, 2013). The total CH_4 emissions from the waste sector

are expected to reach almost 800 Mt CO_2-eq by 2015 (Chai et al., 2016). China, as the largest emitter, has undergone an unprecedented increase in MSW production, from 148 Mt in 2006 to 242 Mt in 2019 (NBSC, 2006; NBSC, 2020). Therefore, mitigating GHG emissions from waste sectors would be a highly cost-effective method of reducing GHG emissions, even though it accounts for less than 3% of the total anthropogenic GHG emissions (Bogner et al., 2008).

Efforts have been devoted to mitigating GHG emissions from the waste sector in China. MSW sorting, which can reduce the amount of MSW generated at the source and facilitate recycling, has been implemented in many regions of China (Wang and You, 2021; Zhou et al., 2019). Liu et al. (2021) demonstrated that the GHG emission intensity of incineration was lower than that of landfilling and composting. Liu et al.(2017) reported that landfilling with biogas recovery scenarios emitted more GHGs (117kg CO_2-Eq/t) than MSW incineration (-124 kgCO_2-Eq/t). Thus, changing the main MSW disposal method from landfilling to incineration is an effective measure to reduce the total GHG emissions. The proportion of MSW incineration exceeded that of landfilling for the first time in 2019 (NBSC, 2020). However, for many less-developed counties and towns in China, landfilling remains the principal waste disposal method. Among the waste sector, landfilling contributed to 65.8% of the overall GHG emissions in 2017 (Zhao et al., 2019). Many efforts such as the selection of aged refuse and compost as functional cover soil to improve the CH_4 oxidation efficiency, have been devoted to mitigating CH_4 emissions from landfills Sadasivam and Reddy, 2013). Improving the landfill gas (LFG) collection efficiency and achieving CH_4 resource utilization via the LFG-to-Energy project is another effective measure to mitigate landfill CH_4 emissions.

Comprehensive and accurate estimation of GHG emissions should be a precondition for designing a proper GHG emission reduction strategy. There has been great progress in quantifying CH_4 emissions from MSW landfills in China (Cai. et al., 2014;Cai et al., 2018; Du et al., 2017; Lou et al., 2017; Peng et al., 2016; Zhang and Chen, 2014; Zhao et al., 2019). Large discrepancies still exist in these studies due to insufficient data regarding MSW generation and disposal in landfills, MSW composition, LFG collection, and CH_4 oxidation efficiency. Previous studies have been conducted based on the city level, while GHG emissions from counties in China have not been studied (Lou et al., 2017; Zhao et al., 2019). The composition characteristics, disposal mode, disposal scale, operation and management level of landfills and incinerators at the county level are significantly different to those at the city level. According to the China Urban Rural Statistical Yearbook, landfilling remains the principal MSW disposal method for most counties in China, with MSW landfilling accounting for a total proportion of 77.9% in 2019 which was significantly higher than that of cities (45.6%). Owing to the limitation of the serviced population, the scale of landfills is less than 500 t/d, and their depth is less than 5 m. Therefore, the CH_4 generation and emission characteristics are quite different to those of

Table 1 Composition of municipal solid waste in different regions of China

Regions	Food waste	paper	Plastics	Textile	Woods	Rubber and leather	metal	glass	Others
NC	50.76	11.57	11.77	4.18	4.29	1.6	2.75	3.92	0.92
NE	58.87	7.24	11.14	2.69	5.94	5.5	1.08	3.00	6.31
EC	64.50	8.65	12.45	2.30	1.77	0.8	0.65	2.92	2.02
SC	51.18	11.81	13.49	3.71	2.03	0.9	0.74	1.86	5.85
NW	51.93	6.85	9.41	2.72	1.75	1.6	1.21	2.89	4.25

SW	52.22	9.98	12.61	2.81	2.50	4.1	1.16	1.62	7.11
MC	49.42	3.12	8.61	4.04	4.75	1.5	0.76	0.81	8.30

Note: NC: North China, NE: North East, EC: East China, MC: Middle China, SC: South China, SW: South West and NW: North West.

larger-scale landfills in cities. Notably, the GHG emission inventory of waste disposal units reported in the above literature cannot reflect the changing trend over recent years since many strategies, such as MSW classification, and zero-waste city construction, have emerged (Lou et al., 2017; Song et al., 2015).

In this study, GHG emissions from waste sectors including landfills, incinerators and others (compost/fermentation), were evaluated using the inventory models recommended by the IPCC. The objective of this study was to estimate the trends and patterns of GHG emissions from the waste disposal sector in the cities and counties of China, by considering the variation in MSW disposal methods from 2006 to 2019. The contribution of regional GHG emissions was also evaluated in five-year intervals. The results obtained will help determine the contribution and responsibilities of various national and regional GHG mitigation strategies which will be helpful in achieving the carbon emission peak and carbon emission neutrality.

2 MATERIALS AND METHODS

2.1 Coverage area and data source

In this study, GHG emission estimation data for the waste sector covered 31 provinces in mainland China, with the exception of Taiwan, Hong Kong, and Macau. The spatial distribution of GHG emissions is presented in the following seven regions of China: North East (NE), North China (NC), East China (EC), South China (SC), Middle China (MC), North West (NW), and South West (SW). The provinces in the seven regions are listed in Table S1.

The MSW collection and disposal quantities of landfill, incineration, and other methods (compost and fermentation) used in this study were acquired from the China Statistical Yearbooks, China Environmental Statistics Yearbooks, and Statistics Yearbooks of the Ministry of Housing and Urban–Rural Development of PRC (MHDC). Waste composition data (Table 1) for the seven regions during 2006 - 2019 were derived from published papers and official statistical yearbooks (Cai et al., 2018; Gu et al., 2017; Lou et al., 2017).

2.2 Methods for estimating greenhouse gas emissions

(1) CH4 emissions from landfills: Estimation of CH_4 emissions from landfills using the IPCC first order delay (FOD) method is described as follows (Palut and Canziani, 2007):

$$G_{CH4}(t) = \sum_{i=1}^{n} MSW_{ti} * MSW_{fi} * L_{0i}(1 - e^{-k}) * e^{-k(n-i)} \quad (1)$$

$$L_{0i} = MCF * DOC_i * DOC_{fi} * F * \frac{16}{12} \quad (2)$$

$$E_{CH4}(t) = G_{CH4}(t) * (1 - R) * (1 - OX) \quad (3)$$

where G_{CH4} is the total CH_4 generation yield in a particular year (Gg/y); E_{CH4} is the total CH_4 emissions in a particular year (Gg/y); MSW_{ti} is the total MSW generated in year *i*; *t* is the inventory year; MSW_{fi} is the fraction of MSW disposed in landfills in year *i*; L_0 is the potential CH_4 production capacity (m^3/Mg); *MCF* is the CH_4 correction factor (dimensionless); *DOC* is the fraction of degradable organic matter; DOC_f is the fraction of dissimilated *DOC*; *F* is the fraction of CH_4 in the LFG; *R* is the recovery rate of LFG; *OX* is the CH_4 oxidation factor; *k* is the rate of the reaction constant; and n = (year of calculation) – (initial year of waste acceptance). The values of the input parameters of the IPCC FOD model are listed in Table 2. Because

disparities existed in the scale and management level of landfills, the input values of *MCF*, *OX*, and *R* were different, and based on the default values recommended by the IPCC and expert judgment (Table 3) (IPCC, 2013).

(2) GHG emissions from MSW incineration: The GHG emissions from MSW incinerators included CO_2 and N_2O by the combustion of fossil carbon and combustion of nitrogenous components, respectively. The CO_2 emissions were calculated as follows (Zhao et al., 2019):

$$I_{CO2} = MSW * \sum_j (WF_j * dm_j * CF_j * FCF_j * OF_j) * 44/12 \quad (4)$$

where: I_{CO2} represents the CO_2 emissions in an inventory year (Gg/yr); *MSW* is the total amount of MSW as incinerated wet weight (Gg/yr); WF_j is the fraction of waste type of component *j*; dm_j is the dry matter content in component *j;* CF_j is the fraction of carbon in the dry matter of component *j*; FCF_j is the fraction of fossil carbon; and OF_j is the oxidation factor. The input parameter values are presented in Table S2.

As recommended by the IPCC, the N_2O emission rate was set to 50 g N_2O/t wet MSW for evaluating the total N_2O emissions from MSW incineration (Lou et al., 2017).

(3) GHG emissions from MSW composting: Following the method used by Lou et al., 2017, the CH_4 and N_2O emission rate for composting were set to 4 g CH_4/kg wet MSW and 0.3 g N_2O/kg wet MSW.

(4) Total GHG emissions from the MSW disposal sector: The overall GHG emissions from the waste disposal sector were aggregated based on the sum of the individual values (normalized to a CO_2-equivalent value) estimated in each treatment process (landfill, incineration and compost) by applying the respective emission estimation methods described above. The established GWP values for CH_4 and N_2O are 25 and 298 times higher than that of CO_2, respectively (IPCC, 2013).

Table 2 Parameter input values for the FOD model

Parameter	Food waste	Paper	Wood	Textiles	Reference
DOC	0.11	0.24	0.33	0.24	Cai et al., 2018
DOC_f	0.5				Default value
k(1/y)	0.18	0.06	0.03	0.06	Default value
Delay time (month)	6				Default value
F	0.5				Default value

Table 3 Parameter input values for the FOD model

Parameter	MCF	R	OX
City	0.96	0.24	0.1
County	0.92	0	0.1

3 RESULTS AND DISCUSSION

3.1 Variations in MSW generation and treatment

The changes in MSW transportation and harmless treatment amounts are presented in Fig. S1. An average rate of increase of 5% per year from 148.41 Mt in 2006 to 242.06 Mt in 2019 is observed in MSW transportation volume in cities due to the rapid economic growth and urbanization. In contrast, the MSW volume transported at the county level was different, ranging from 60 to 80 Mt during this period. Furthermore, the transportation amount was stable over the past five years, which is mainly attributed to the

migration of people from counties to cities, even though MSW from small villages had been treated by the county system due to the implementation of the "Integration of Urban and Rural Sanitation" management. China has made great progress in harmless MSW treatment. The proportion of harmless treatment increased from less than 53.0% to 98.9% at the city scale and from less than 7.0% in 2006 to 96.2% in 2019 at the county level.

MSW disposal and treatment in China has transformed from unmanaged open dumps, simple landfills, and open burning to modern sanitary landfills and MSW incineration plants over the last two decades (Lou et al., 2017). In 2019, there were 652 landfills, 389 incinerators and 141 other harmless treatment facilities operating in cities, whereas there were 1233 landfills, 111 incinerators and 34 other harmless treatment facilities in counties. Landfilling and incineration are the principal harmless MSW treatment methods in China (Fig. 1). Landfilling is the main disposal method for MSW treatment in cities. However, the percentage decreased from over 81.0% in 2006 to less than 45.6% in 2019, and the contribution of MSW incineration increased from less than 15.0% in 2006 to 50.7% in 2019. Notably, in 2019, the proportion of MSW incineration exceeded that of landfilling for the first time and became the main method of MSW disposal at the city level in China. China has set an ambitious target to reach 50% MSW incineration at the national level and 60% in the eastern developed regions by 2020. The implementation of "Zero Waste City" and "Zero landfilling of Raw Waste" will also help to reduce the amount of MSW landfilling.

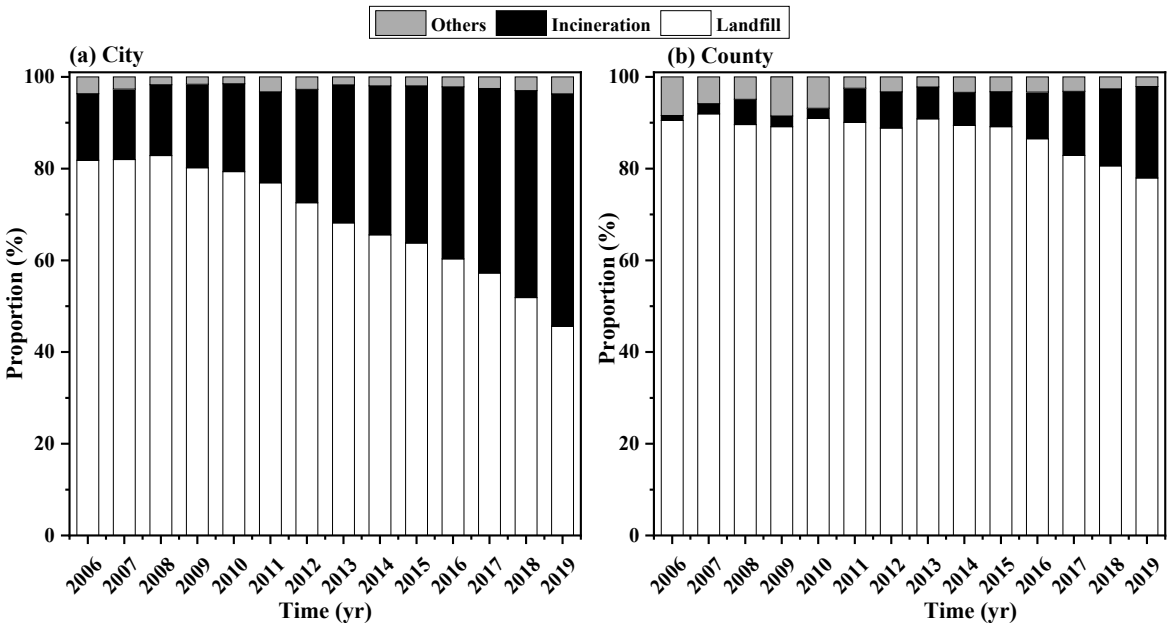

Fig. 1 Variations in the proportion of different MSW treatment methods in China during 2006-2019.

Thus, a continuous increase in MSW incineration is expected in the future. In contrast to cities, landfilling accounted for more than 80% of MSW disposal in counties and the treatment proportion of MSW incineration has rapidly increased during the last three years owing to the construction of small-sized MSW incineration plants in developed provinces in Eastern China. The Chinese government has proposed that new landfills should not be built in cities after 2021 and raw MSW should not be sent to landfills. Many regions in

China have implemented MSW classification, particularly for kitchen or wet waste, which account for the highest proportion of MSW, are treated using anaerobic fermentation. As a consequence, the percentage of MSW landfilling will decrease over time, while the percentage of MSW incineration and fermentation will increase.

3.2 GHG emission patterns from the MSW disposal sector

The GHG emission patterns from the MSW disposal sector from 2006 to 2019 are shown in Fig. 2. The overall GHG emission from the waste sector increased rapidly from 55.38 Mt in 2006 to 178.06 Mt in 2019, with the expansion of urbanization and population and improved MSW harmless treatment efficiency (Fig. S1). A rapid increase in the estimated GHG emissions from 52.71 Mt in 2006 to 122.42 Mt in 2019 was observed in cities owing to rapid urbanization and economic development. However, the GHG emissions increased from less than 2.67 Mt in 2006 to 55.64 Mt in 2019, during this period at the county level (an increase of almost 20 times), owing to the improved harmless MSW treatment efficiency.

Notably, GHG emissions from cities accounted for most of the GHG emissions in the MSW sector. The contribution of the city MSW sector decreased from 95.2% in 2006 to 70.6% in 2015. After 2015, the contribution of GHG emissions from the MSW sector remained relatively stable at 70% for cities and 30% for counties. The improved harmless MSW treatment efficiency and landfilling, as the main MSW treatment methods at the county level (Fig. 1b), were the main reasons for the improved share of GHG emissions from the MSW sector. Among the GHGs, the contribution of CH_4 was generally the highest, and decreased from 91.4% in 2006 to 70.4% in 2019 at the city level in China (Fig.3a). At the county level, CH_4 accounted for more than 90% of the overall

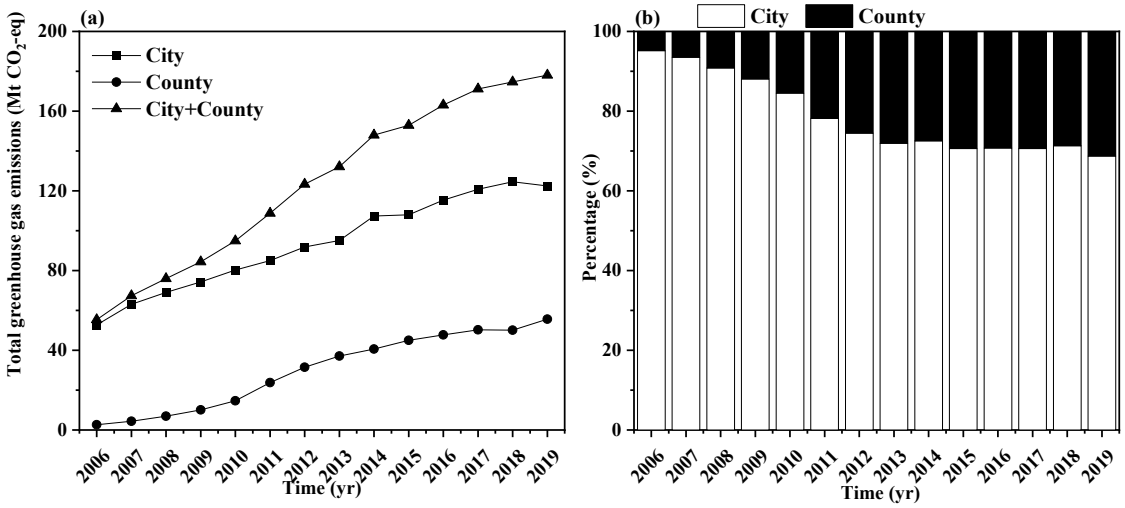

Fig. 2 Variations in the (a) total GHG emission patterns and (b) percentage of GHG emissions from MSW disposal in the cities and counties of China during 2006-2019.

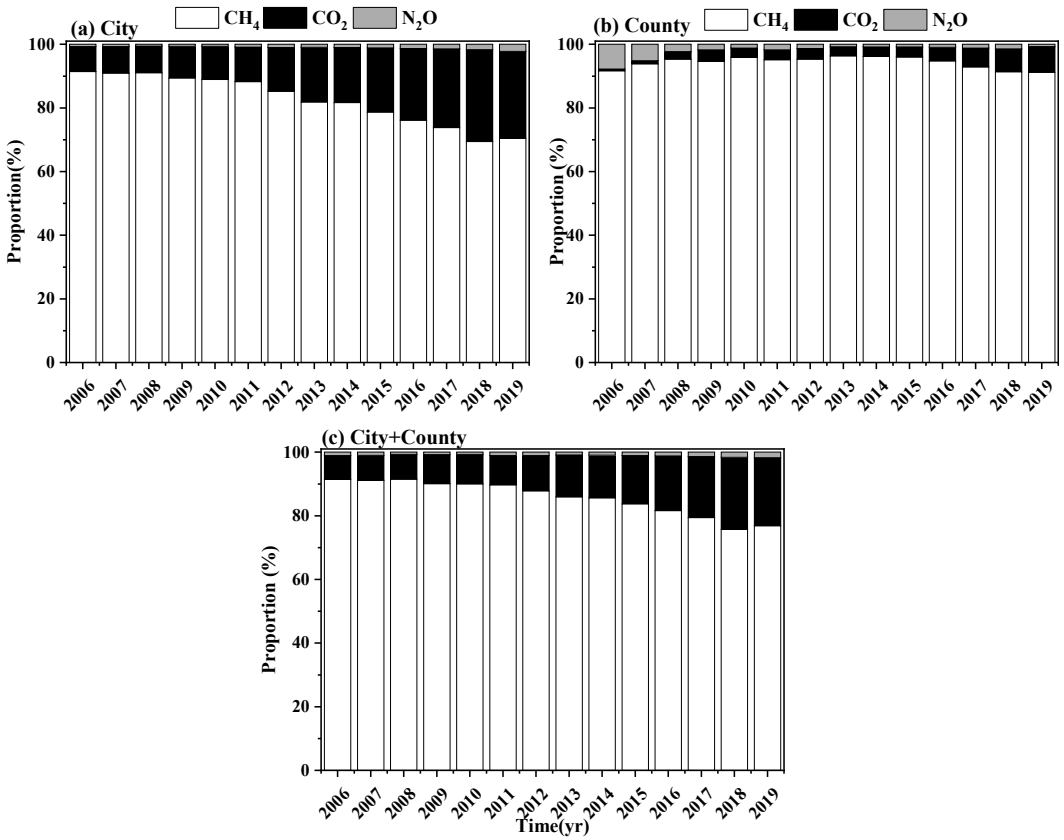

Fig. 3 Variations in the CH_4, CO_2 and N_2O emission proportions from the waste sector during 2006-2019.

GHG emissions during the study period (Fig.3b). CO_2 was the second-highest contributor to GHG emissions in the waste sector, with contributions of 27.3% and 8.1% in cities and counties during 2019, respectively Fig.3a and Fig.3b. Overall, the contribution of CH_4 decreased from 91.5% in 2006 to 76.9% in 2019, and that of CO_2 increased from 7.5% in 2006 to 21.3% in 2019 (Fig.3c). The contribution of N_2O was less than 2% during the study period.

3.3 Contributions of GHG emissions from different MSW sectors

Landfilling, incineration and composting/anaerobic fermentation are the main MSW treatment technologies in China. GHG emissions from different MSW disposal sectors and their proportions are shown in Fig. 4. Landfills contributed the most to the total GHG emissions from the waste sector. For cities, the share of GHG emissions was relatively stable during 2006–2011 ranging from 88.7% to 91.0%. After 2011, the contribution of GHG emissions from landfills decreased rapidly from 88.7% in 2010 to 69.5% in 2019. Moreover, the contribution of GHGs from MSW incineration increased from 8.2% in 2006 to 28.8% in 2019, owing to the rapid development of MSW incineration capacity. At the county level, landfills accounted for more than 90%of the total GHG emissions from the waste sector during the study period. CO_2 emissions from MSW incineration accounted for less than 10% of the total GHG emissions owing to the small treatment capacity of MSW incinerators, which was a result of the high

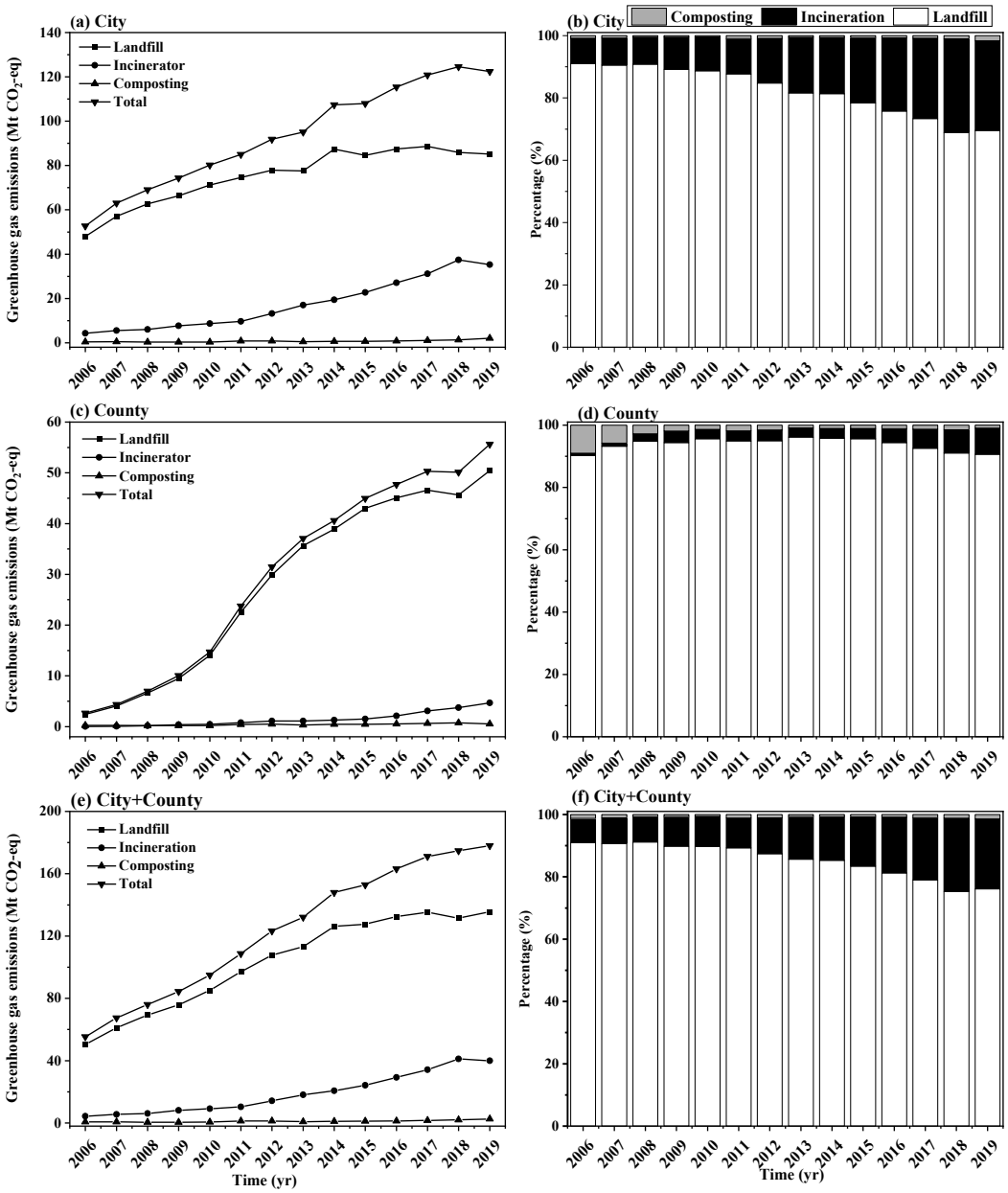

Fig. 4 Variations in GHG emissions and the proportions of different harmless treatment methods during 2006-2019.

investment cost of MSW incinerator plants. Overall, landfills contributed the most to the GHG emissions from the MSW sector, even though its share decreased from 91.0% in 2006 to 76.2% in 2019. This was followed by MSW incineration, which accounted for 22.4% of the total GHG emissions in 2019. The overall percentage of GHG emissions from MSW composting/fermentation was less than 2.0% during this period, owing to the closure of composting plants without an acceptable end-use for composted products (Lou et al., 2017).

3.4 Spatial distribution of GHG emissions from different regions of China

Owing to geographical location, population, industrial

layout, and other factors, there is a great difference in economic and social development between Eastern and Western China. This difference is also reflected in the MSW management level and disposal methods in the eastern and western regions. Understanding the spatial distribution of GHG emissions is essential for decision-makers to develop GHG mitigation strategies. The spatial distribution of GHG emissions from seven regions of China in 2008, 2013, and 2018 is shown in Fig. 5. During this period, governments, private enterprises, or their consortium invested and constructed many modern sanitary landfills and incinerators because of the tremendous pressure from the rapid increase in MSW generation, especially in the developed eastern coastal areas of China. Compared to the baseline year of 2006 at the city level, the GHG emissions increased by 2.3 and 3.3times in the NW regions during 2013 and 2018, respectively, and by 3.01 and 3.3 times in the MC and SC regions during 2018, respectively. The rapid rise in GHG emissions from the NW, MC, and SC regions was caused by an increase in MSW disposal treatment facilities during the study period, which was ascribed to the basic requirement that the non-hazardous waste disposal rate was over 80% for the grant title of the state healthy city for the local governments (Lou et al., 2017). Furthermore, a more rapid increase in the GHG emissions from the county MSW sector was observed in different regions of China. For example, the GHG emissions from NC, NE, and NW in 2018 were 113.7, 42.4, and 28.7 times higher than the baseline year of 2006. The remarkable increase in GHG emissions from the county MSW sectors for these regions was attributed to the development and implementation of the "integration of urban and rural sanitation". Consequently, more sanitary landfills and incinerators have been constructed in the counties of China.

A regional discrepancy was observed in GHG emissions from landfills and incinerators. The proportion of GHG emissions from landfills decreased from more than 86.0% and 79.3% in 2008 to 50.6% and 56.1% in 2018 for the EC and SW regions, respectively, in the MSW disposal sector at the city level. Moreover, the proportion of GHG emissions from MSW incineration increased sharply from less than 13.6% and 20.6% in 2012 to 48.4% and 43.7% in 2018, respectively. However, for the NE and NW regions, landfilling accounted for more than 90% of the total GHG emissions from the MSW sector. At the county level, landfilling remained the most significant contributor to GHG emissions, with a contribution of more than 92.0% in 2018; however, in the regions of EC, the proportion of GHG emissions from MSW incineration increased sharply from 4.7% in 2008 to 18.2% in 2018, due to the developed economy, which facilitated investments and construction of MSW incinerators.

Among the seven regions of China, EC had the largest GHG emission contribution during the study period owing to a more developed economy and larger population. However, the corresponding contributions of GHG emissions from EC decreased from 34.9% in 2008 to 29.6% in 2018, which may be attributed to the increased GHG emissions from other regions and rapidly increasing incineration applications in EC regions, as MSW incineration emits less CO_2 than landfilling when treating an equal amount of MSW (Liu et al., 2017; Wang et al., 2017). Conversely, NW had the smallest GHG emissions of the seven regions, but its contribution increased from 5.1% in 2008 to 7.7% in 2018. The contribution of GHG emissions from the seven regions followed the order of EC > NC > SW > MC > SC > NE > NW in 2008, which was changed to EC > NC > SC > MC > SW > NE > NW in 2018.

In addition to the difference in regional GHG emissions, GHG emissions also presented significant differences at the provincial scale. From the perspective of the city level, GHG emissions in some provinces, such as Shanghai, Zhejiang, Beijing, Tianjin, and Chongqing, decreased owing to the increasing contribution of MSW incineration. Furthermore, GHG emissions from MSW

incineration exceeded MSW landfilling in these provinces in 2019. However, in provinces such as Jiangxi, Shannxi, Liaoning, and Shanxi, landfills still accounted for more than 80% of the overall GHG

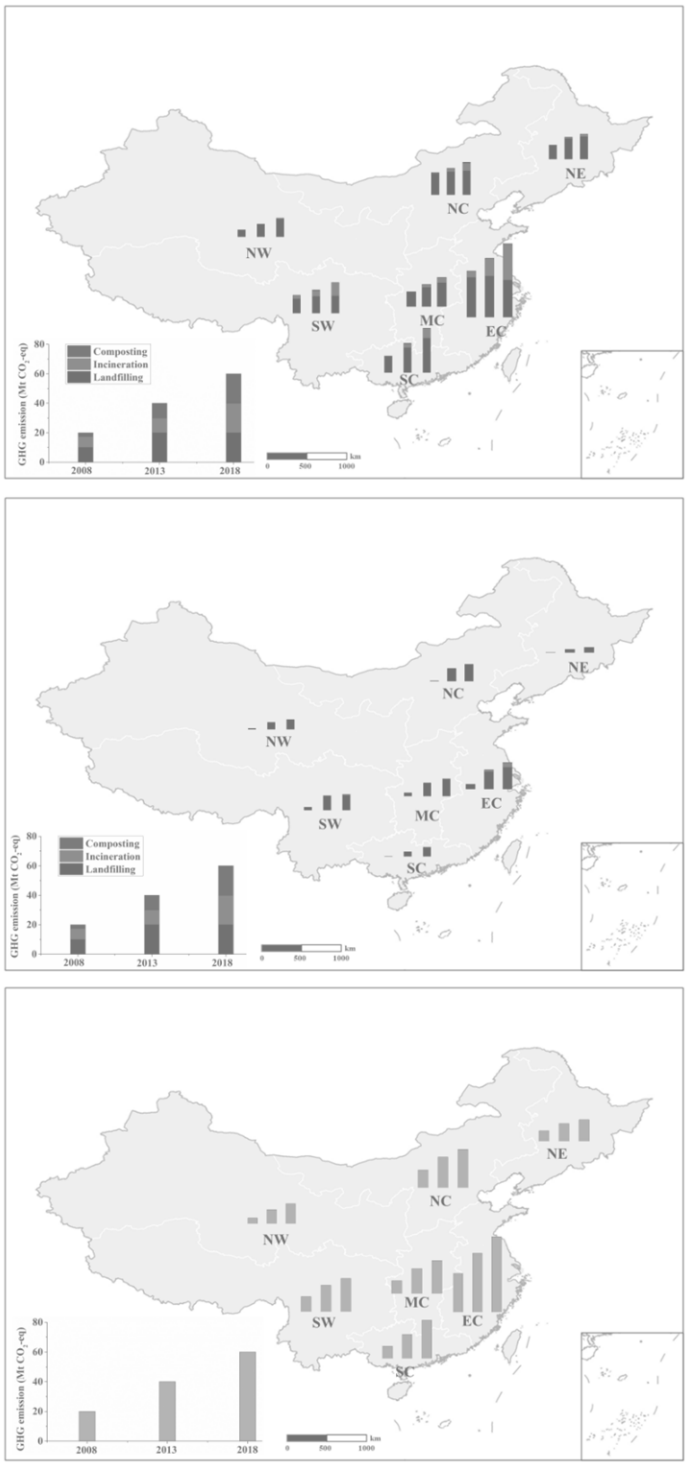

Fig. 5 Changes in the spatial distribution of GHG emission from seven regions of China for (a) City, (b) county, and (c) city + county. Legend description: the first, second, and third column from left to right present the GHG emissions in the year of 2008, 2013, and 2018, respectively. The columns consist of three sub-columns with different

colors, which signify the GHG emissions from landfill (black), incineration plant (red), composting (blue), and total GHG emissions (dark yellow). Note: NC: North China, NE: North East, EC: East China, MC: Middle China, SC: South China, SW: South West, and NW: North West.

emissions. At the county level, landfills remained the main GHG emission source, accounting for more than 80%, except in Shandong province (67% in 2019). This could be attributed to the small incinerators constructed in recent years in small counties and towns in Shandong.

3.5 Uncertainty analysis

The estimated GHG emissions from the waste sector in China are summarized in Table 4. Our estimated CH_4 emissions were significantly higher than those reported in other studies excluding that of Zhang and Chen. (2014), despite these studies using the same inventory methods. Cai et al. (2014) used the IPCC Tier 1 methodology to estimate CH_4 emissions, omitting the LFG collection efficiency and oxidation efficiency of cover soil, which was the main reason for the higher CH_4 emission estimation. The higher CH_4 emission estimates in our study than those of comparative studies could be due to the following: (a) the discrepancy in MSW composition between different regions, particularly that of food waste, which is the main component of MSW, was higher in this study than those in other comparative studies, even though they used the same IPCC-FOD methods (Cai et al.,2014; Zhao et al., 2019); (b) uncertainty existed in the input parameters. Generally, 10% uncertainty associated with the parameters can generate up to 20% uncertainty in the results, and 20% uncertainty associated with the parameter can lead to 40–50% uncertainty in the results (Du et al., 2017). The *OX* and *R* parameters are key factors affecting the accuracy of the evaluation results. In this study, the values of these two parameters were constants for all regions (Table 3), and, in the studies by Lou et al. (2017) and Cai et al.(2014), the values of *OX* and *R* were determined by

Table 4 Gap between CO_2 emissions from waste sectors found in comparative studies

Time (yr)	CH_4 emissions from landfills (Mt)	CO_2-eq emissions from MSW incinerator (Mt)	Total GHGs (Mt)	Reference
	3.157	/	/	Zhang and Chen., 2014
	1.254	5.895	/	Lou et al., 2017
2007	1.186	/	/	Cai et al., 2014
	1.323	4.762	37.855	Zhao et al., 2019
	2.289(2.446)	2.425 (2.767)	63.047 (63.992)	This study
	1.638	7.412	/	Zhao et al., 2019
	1.621	/		Lou et al., 2017
2010	2.243	/	/	EPA., 2013
	2.000		/	Peng et al., 2016
	2.848 (3.410)	6.636 (7.057)	77.826 (92.299)	This study
	1.800	/	/	Cai et al., 2018
2012	1.792	11.231	56.034	Zhao et al., 2019
	3.115 (4.310)	13.173 (14.267)	123.294	This study
2013	1.859	/	/	Du et al., 2017

2017	1.779	14.522	58.995	Zhao et al., 2019
	3.102(4.527)	16.999 (18.104)	132.117	This study
	2.017	23.926	74.361	Zhao et al., 2019
	3.545 (5.408)	27.780 (30.747)	116.418(165.955)	This study

Note: The data presented in the table are the GHG emissions from the waste sector at the city scale in China, and the data in ( ) present the total GHG emissions from the waste sector in cities and counties.

the type of MSW landfill which is the main reason for the lower estimated CH_4 emissions.

Fossil carbon emissions from MSW incineration have rarely been reported. Owing to the higher proportion of food waste in the waste composition, our estimated results are lower than those of previous reports despite the same estimation method being used. Overall, our estimated GHG emissions from the waste sector were generally higher than those in previous reports. Some uncertainties exist in our estimated results. Therefore, it is important to collect real activity data for the estimation process of the waste sectors, especially for waste composition and MSW operation conditions.

3.6 GHG mitigation potential from the MSW sector

Carbon emissions are closely related to the population, energy intensity and income/economic development levels (gross domestic product (GDP)) (Du et al., 2017;Wang et al., 2018) , such that provinces with a high GDP and large population, such as Shandong, Shanghai, Guangdong, and Zhejiang, produce the highest GHG emissions, while provinces, such as Qinghai, Hainan, and Tibet, exhibited the opposite trend. Fig. 6 presents the relationship between GHG emissions, population, and GDP at the city and county levels. For cities, a significant positive correlation between GHG emissions and population was found. However, there was no significant correlation between GHG emissions and population at the county level. However, the overall GHG emissions from the waste sector of cities and counties indicated that the GHG emission intensity was closely related to the population and GDP, implying that a higher population and GDP induce higher human activity, leading to more GHG emissions in the waste sector. China has set an ambitious target to reach the GHG emission peak by the end of 2030 or earlier.

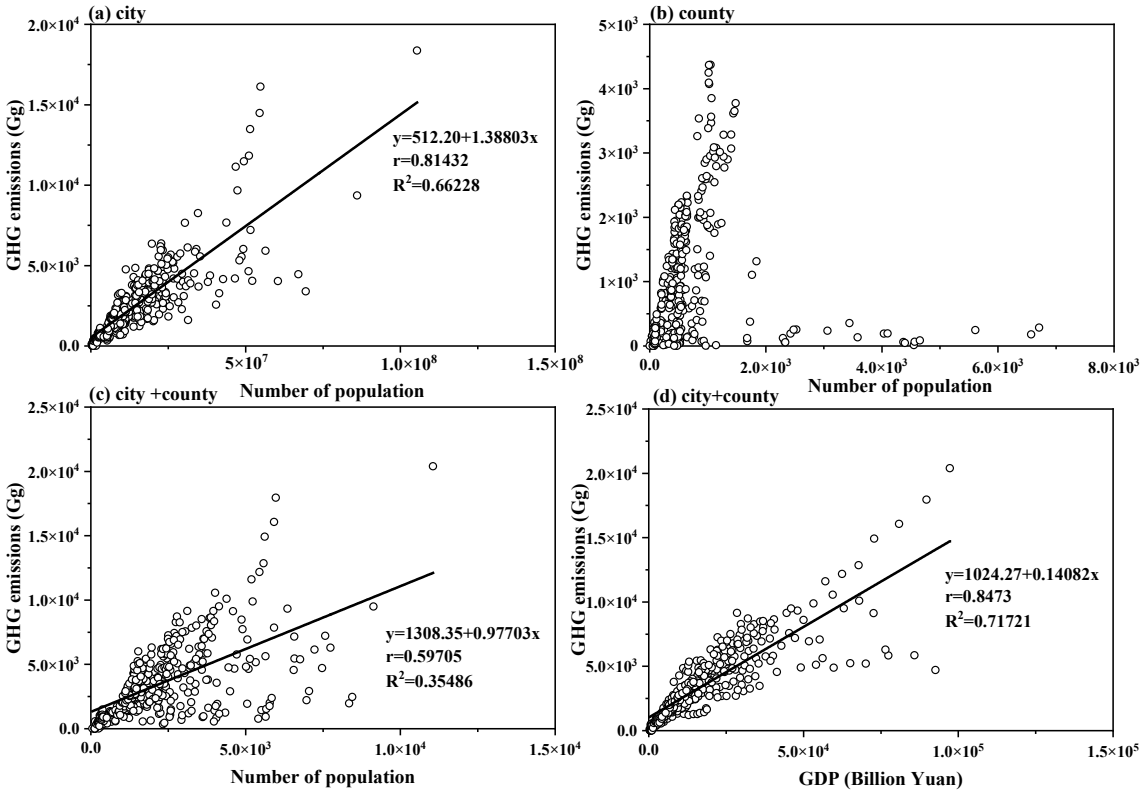

Fig. 6 Regression curves for GHGs emissions by waste sector, population and GDP in China from 2006 to 2019.

Compared with 2005, CO_2 emissions per unit of GDP decreased by 60%. Decoupling carbon emissions from economic growth is crucial for implementing the "Intended Nationally Determined Contributions" (Wang and Zhang.,2019), and weak decoupling was observed during 2005-2014 in China (Wang and Jiang.,2019). In our estimation, the CO_2 emissions per unit of GDP decreased by 20% in 2018 compared with that in 2006 and the CO_2 emissions per person increased from 112.6 kg/p·a in 2006 to 261.3 kg/p·a in 2018. Thus, taking measures to reduce GHG emissions from waste sectors is necessary to assist China in achieving its carbon peak and carbon neutrality targets.

Many measures have been implemented to reduce GHG emissions from the waste sector (Cai et al., 2018; Lou et al., 2017). MSW classification is helpful in reducing the disposal amount of landfilling and incineration owing to the utilization of recyclable waste. The practice in Zhejiang Province and Shanghai has proven that MSW classification can reduce the total MSW generation. Furthermore, according to the regulations on waste classification management in different cities, kitchen waste, which accounts for the largest proportion of MSW, will be treated by anaerobic fermentation; thus, the amount of MSW landfilling will be decreased in the future as the terminal treatment facilities are completed. Landfill is an important source of CH_4 emission, accounting for 12% of the total CH_4 emissions (EPA, 2013). For landfills, improving the LFG collection system efficiency and LFG utilization by constructing LFG-to-energy projects would be an effective measure to reduce GHG emissions. Unfortunately, more than 50% of landfills in China do not install LFG collection systems (Chai et al.,2016), and the collection efficiency is generally lower; thus, a

large amount of fugitive CH_4 is emitted to the atmosphere from landfills (Bian et al., 2021a). Cover soil, as the last barrier between MSW and the atmosphere, plays a key role in CH_4 mitigation through methane oxidation in the soil environment (Frasi et al., 2020; Pecorini and Iannelli, 2020). Clay, which is a commonly used cover material, has a lower CH_4 oxidation efficiency. Choosing functional cover soil, such as compost, and aged refuse, could improve the CH_4 oxidation rate in the cover soil as they have high organic matter contents and microbial abundance (Bian et al., 2019b; Niemczyk et al., 2021).CH_4 oxidation in the cover soil depends on the cover soil type, water content, organic matter, nitrogen nutrients, and climatic conditions (Bian et al., 2019b; Bian et al., 2021b). Thus, the CH_4 emissions in each landfill, especially parameter *OX* in the inventory model should be specialized based on actual landfill conditions.

GHG mitigation strategies in the waste sector must be adapted to local conditions. New sanitary landfills and incinerators should be constructed in less developed counties and towns to improve the efficiency of MSW treatment. As landfilling contributes the most to GHG emissions, landfill CH_4 mitigation should focus on improving the landfill management level and LFG collection efficiency (Bian et al., 2021a; Zhao et al., 2019). Additionally, the government should encourage more MSW incinerator construction in counties and towns as it emits lower GHG than MSW landfilling for the same amount of MSW (Liu et al., 2017; Wang et al., 2017), and MSW incineration would even become a GHG sink (Liu et al., 2017). Moreover, using functional materials as the cover soil to reduce CH_4 emissions is also necessary for small-sized landfills in counties and towns. For cities, improving LFG collection, utilization efficiency, and oxidation efficiency of cover soil have been widely recognized by landfill managers. Furthermore, anaerobic digestion of food waste with CH_4 to produce electricity could also be an effective measure for mitigating GHG emissions (Chen et al., 2020). In addition to these measures, new carbon sequestration and carbon fixation technologies should be encouraged in MSW incineration because incineration also accounts for a large amount of GHG emissions in the waste sector (Fan et al., 2021; Hu et al., 2021; Xu et al., 2021).

4 CONCLUSIONS AND POLICY IMPLICATIONS

4.1 Conclusions

The MSW disposal sector is an important source of GHG emissions. The emission pattern from 2006 to 2019 in China was estimated from the perspective of cities and counties in this study. The main findings are as follows: (1) the estimated results showed that the total GHG emissions from the waste sector increased from 55.38 Mt CO_2-eq in 2006 to 178.06 Mt CO_2-eq in 2019; (2) A rapid increase in the estimated GHG emissions from 52.71 Mt in 2006 to 122.42 Mt in 2019 was observed in cities, and from less than 2.67 Mt in 2006 to 55.64 Mt in 2019 was observed in counties; (3) CH_4 emissions from MSW landfilling contributed the most to GHG emissions, but the contribution of GHG emissions from incineration has increased rapidly in recent years and accounted for 22.4% of the total GHG emissions in 2019; (4) GHG emissions from the waste sector exhibited clear regional differences: the region of East China contributed 29.6% of the overall GHG emissions in 2019, followed by NC (15.6%), and SC (15.5%), NW contributed the least to GHG emissions.

4.2 Policy implications

The waste sector has a large GHG mitigation potential. MSW classification and resource reduction are the most promising strategies for mitigating GHG emissions. Improving the LFG collection and utilization efficiency and operation management level of landfills are necessary for mitigating landfill CH_4 emissions. Changing the MSW disposal method from landfilling to incineration is also an effective strategy for GHG reduction, particularly for regions with a relatively lower proportion of MSW incineration.

This study presented the GHG emission situation in China from the waste disposal sector during 2006–2019 and provides essential information to understand the changing trends of GHG emissions caused by the conversion of waste disposal methods from the perspectives of cities and counties. The results obtained will not only be helpful to China, but also for some developing countries with an urgent need for carbon emission mitigation to understand the potential of reducing GHG emissions from the MSW disposal sector.

REFERENCE

Bian, R.X., Chen, J.H., Li, W.H., Shi, W., Lin, Y.F., Chai, X.L., Sun, Y.J., 2021a. Methane emissions and energy generation potential from a municipal solid waste landfill based on inventory models: A case study. Environ. Prog. Sustain.Energ. e13654 https://doi.org/10.1002/ep.13654

Bian, R.X., Chen, J.H., Li, W.H., Sun, Y.J., Chai, X.L., Wang, H.W., Wang, Y.N., Zhao, J.W., 2021b. Numerical modeling of methane oxidation and emission from landfill cover soil coupling water-heat-gas transfer: Effects of meteorological factors. Process Saf. Environ. Prot.146, 647-655. https://doi.org/10.1016/j.psep.2020.11.052

Bian, R.X., Komiya, T., Shimaoka, T., Chai, X.L., Sun, Y.J., 2019a. Simulative analysis of vegetation on CH_4 emission from landfill cover soils: Combined effects of root-water uptake, root radial oxygen loss, and plant-mediated CH_4 transport. J. Clean. Prod. 234, 18-26. https://doi.org/ 10.1016/j.jclepro.2019.06.139

Bian, R.X., Shi, W., Duan, Y.B., Chai, X.L., 2019b. Effect of soil types and ammonia concentrations on the contribution of ammonia-oxidizing bacteria to CH_4 oxidation. Waste Manage. Res. 37(7), 698-705. https://doi.org/ 10.1177/0734242X19843988

Bogner, J., Pipatti, R., Hashimoto, S., Diaz, C., Mareckova, K., Diaz, L., Kjeldsen, P., Monni, S., Faaij, A., Gao, Q., Zhang, T., Ahmed, M.A., Sutamihardja, R.T., Gregory, R., Intergovernmental Panel on Climate Change Working, G., III, 2008. Mitigation of global greenhouse gas emissions from waste: conclusions and strategies from the Intergovernmental Panel on Climate Change (IPCC) Fourth Assessment Report. Working Group III (Mitigation). Waste Manag. Res. 26(1), 11-32. https://doi.org/ 10.1177/0734242X07088433

Cai, B. F., Liu ,J.G,, Gao, Q. X., Nie, X.Q., Cao, D., Liu, L. C., Zhou,Y., Zhang, Z.S., 2014. Estimation of Methane Emissions from Municipal Solid Waste Landfills in China Based on Point Emission Sources. Adv Clim Chang Res. 5(02), 81-91. https://doi.org/10.3724/SP.J.1248.2014.081

Cai, B., Lou, Z., Wang, J., Geng, Y., Sarkis, J., Liu, J., Gao, Q.X., 2018. CH_4 mitigation potentials from China landfills and related environmental co-benefits. Sci. Adv. 4(7), eaar8400. https://doi.org/ 10.1126/sciadv.aar8400

Chai, X., Tonjes, D.J., Mahajan, D., 2016. Methane emissions as energy reservoir: Context, scope, causes and mitigation strategies. Prog. Energ Combust Sci. 56, 33-70. https://doi.org/ 10.1016/j.pecs.2016.05.001

Chen, S., Huang, J., Xiao, T., Gao, J., Bai, J., Luo, W., & Dong, B. (2020). Carbon emissions under different domestic waste treatment modes induced by garbage classification: Case study in pilot communities in Shanghai, China. Science of The Total Environment, 717, 137193. https://doi.org/10.1016/j.scitotenv.2020.137193

Du, M., Peng, C., Wang, X., Chen, H., Wang, M., Zhu, Q., 2017. Quantification of methane emissions from municipal solid waste landfills in China during the past decade. Renew. Sust. Energ.Rev. 78, 272-279. https://doi.org/ 10.1016/j.rser.2017.04.082

EPA, 2013. Global Mitigation of Non-CO_2 Greenhouse Gases: 2010–2030. United States Environmental Protection Agency (EPA) Washington DC (2013).

Fan, Y., Feng, J.Q., Yang, M., Tan, X., Fan, H.J., Guo, M.J., Wang, B.J., Xue, S., 2021. CO_2(aq) concentration-dependent CO_2 fixation via carboxylation by decarboxylase. Green Chem. 23(12), 4403-4409. https://doi.org/ 10.1039/d1gc00825k

Fei, F., Wen, Z., De Clercq, D., 2019. Spatio-temporal estimation of landfill gas energy potential: A case study in China. Renew. Sust. Energ.Rev. 103, 217-226.

https://doi.org/ 10.1016/j.rser.2018.12.036

Frasi, N., Rossi, E., Pecorini, I., Iannelli, R., 2020. Methane oxidation efficiency in biofiltration systems with different moisture content treating diluted landfill gas. Energies 13(11), 15. https://doi.org/ 10.3390/en13112872

Gu, B., Jiang, S., Wang, H., Wang, Z., Jia, R., Yang, J., He, S., Cheng, R., 2017. Characterization, quantification and management of China's municipal solid waste in spatiotemporal distributions: a review. Waste Manage. 61, 67-77. https://doi.org/ 10.1016/j.wasman.2016.11.039

Hu, C.M., Wang, M.Q., Lapointe, B.E., Brewton, R.A., Hernandez, F.J., 2021. On the Atlantic pelagic Sargassum's role in carbon fixation and sequestration. Sci. Total Environ. 781, 7. https://doi.org/ 10.1016/j.scitotenv.2021.146801

IPCC, 2013. The final draft Report, dated 7 June 2013, of the Working Group I contribution to the IPCC 5th Assessment Report. In: Climate Change 2013: the Physical Science Basis.

Liu, Y., Sun, W., Liu, J., 2017. Greenhouse gas emissions from different municipal solid waste management scenarios in China: Based on carbon and energy flow analysis. Waste Manage. 68, 653-661. https://doi.org/ 10.1016/j.wasman.2017.06.020

Liu Y,J., Chen S.Q., Chen AJ. Y., Lou Z.Y., 2021 .Variations of GHG emission patterns from waste disposal processes in megacity Shanghai from 2005 to 2015. Journal of Cleaner Production, 30, 886-902. https://doi:10.1016/J.JCLEPRO.2021.126338.

Lou, Z., Cai, B. F., Zhu, N., Zhao, Y., Geng, Y., Yu, B., Chen, W., 2017. Greenhouse gas emission inventories from waste sector in China during 1949–2013 and its mitigation potential. J. Clean. Prod. 157, 118-124. https://doi.org/ 10.1016/j.jclepro.2017.04.135

National Bureau of Statistics of China (NBSC), 2006. China Statistical Yearbook.China Statistics Press, Beijing (in Chinese). http://www.stats.gov.cn/tjsj/ndsj/

National Bureau of Statistics of China (NBSC), 2020. China Statistical Yearbook.China Statistics Press, Beijing (in Chinese). http://www.stats.gov.cn/tjsj/ndsj/

Niemczyk, M., Berenjkar, P., Wilkinson, N., Lozecznik, S., Sparling, R., Yuan, Q.Y., 2021. Enhancement of CH_4 oxidation potential in bio-based landfill cover materials. Process Saf. Environ. Prot. 146, 943-951. https://doi.org/ 10.1016/j.psep.2020.12.035

Olivier, J.G., Peters, J.A.H.W., 2020. Trends in global CO_2 and total greenhouse gas emissions: 2020 Report. PBL Netherlands Environmental Assessment Agency.

Pecorini, I., Iannelli, R., 2020. Landfill GHG reduction through different microbial methane oxidation biocovers. Processes 8(5), 12. https://doi.org/ 10.3390/pr8050591

Peng, S., Piao, S., Bousquet, P., Ciais, P., Li, B., Lin, X., Tao, S., Wang, Z., Zhang, Y., Zhou, F., 2016. Inventory of anthropogenic methane emissions in mainland China

from 1980 to 2010. Atmos. Chem. Phys. 16(22), 14545-14562. https://doi.org/10.5194/acp-16-14545-2016

Reddy, K.R., Yargicoglu, E.N., Chetri, J.K., 2021. Field-scale performance of biochar-amended soil covers for landfill methane oxidation. Biomass Convers. Biorefinery, 16. https://doi.org/10.1007/s13399-021-01487-w

Sadasivam, B.Y., Reddy, K.R., 2013. Landfill methane oxidation in soil and bio-based cover systems: a review. Reviews in Environmental Science and Bio/Technology 13(1), 79-107. https://doi.org/10.1007/s11157-013-9325-z

Song, Q., Li, J., Zeng, X.J., 2015. Minimizing the increasing solid waste through zero waste strategy. J. Clean. Prod. 104, 199-210. https://doi.org/10.1016/j.jclepro.2014.08.027

Wang, Q., Jiang, R., 2019. Is China's economic growth decoupled from carbon emissions?. J. Clean. Prod. 234,225, 1194-1208. https://doi.org/10.1016/j.jclepro.2019.03.301

Wang, W.J., You, X. Y., 2021. Benefits analysis of classification of municipal solid waste based on system dynamics. J. Clean. Prod. 279, 123686. https://doi.org/10.1016/j.jclepro.2020.123686

Wang, Q., Zhang, F., 2021. The effects of trade openness on decoupling carbon emissions from economic growth–evidence from 182 countries. J. Clean. Prod. 279, 123838. https://doi.org/10.1016/j.jclepro.2020.123838

Wang, Q., Zhao M,M., Li, R., Su, M.,2018. Decomposition and decoupling analysis of carbon emissions from economic growth: A comparative study of China and the United States. J. Clean. Prod. 197,178-184. https://doi.org/10.1016/j.jclepro.2018.05.285

Xu, S.Y., Qiao, Z.H., Luo, L.W., Sun, Y.Q., Wong, J.W.C., Geng, X.Y., Ni, J., 2021. On-site CO_2 bio-sequestration in anaerobic digestion: Current status and prospects. Bioresour. Technol. 332, 14. https://doi.org/ 10.1016/j.biortech.2021.125037

Selection of particle size of municipal solid waste incineration bottom ash used as raw material for artificial aggregate

Yuqing DENG[1], Teppei KOMIYA[2], Takayuki SHIMAOKA[2], Takayuki NURUYU[3], Daizo FUKUOKA[3]
1 Department of Civil Engineering, Graduate School of Engineering, Kyushu University, Fukuoka, Japan
2 Department of Urban and Environmental Engineering, Faculty of Engineering, Kyushu University, Fukuoka, Japan
3 FKG Corporation, Yatsushiro, Kumamoto, Japan

Abstract: Municipal solid waste incineration (MSWI) is the main method of waste disposal in Japan, which generates a substantial amount of incineration bottom ash every year, but the utilisation rate of incineration ash is still quite low.In order to improve the utilisation of incineration bottom ash and to promote the reuse of resources, the main purpose of this paper is to investigate the most suitable particle size for the production of artificial aggregate material from incineration bottom ash by classifying bottom ash into 12 particle sizes. The incineration bottom ash was subjected to a toxic substance content test (Ministry of the Environment of Japan Notification No.19), a toxic substance leaching test (Environment Agency of Japan Notification No.46), and X-ray fluorescence(XRF)analysis. The results of the experiments showed that there is a relationship of Pb content exceeding the standard by 2-3 times for incineration bottom ash with a particle size dimension of less than 2mm. It is necessary to consider the problem of excessive Pb content in the production of artificial aggregate materials, so that the adjustment of stabiliser and fixative ratios can be carried out.

1. INTRODUCTION

According to a study by the Japan Waste Management Corporation, Japan's waste emissions in 2020 were 41.669 million tons, of which 80%(33.466 million tons) were be used for incineration and the remaining for recycling（20%）and landfill (1%)）[1].The incineration process reduces the mass of the waste by about 70% and the volume by 90%.[2-3] Between 80%~90 % of the residue produced is bottom ash (BA), with the remainder being fly ash (FA) and other air pollution control residues[4].The recycling rate of general waste bottom ash, which constitutes a large proportion of final disposal waste, is still very low; although recycling is being promoted through its use as a raw material for cement and the recovery of iron content, it is hoped that the application of recycling will be further expanded.

The physical composition of waste bottom ash includes ash, metals, glass and crystals, and oxides that are difficult to melt[5].Although it may contain potentially harmful heavy metal elements, the level of leaching potential is relatively low, and bottom ash is considered a benign material that can be used in construction, road base materials and other civil engineering works[6-7]. With regard to the use of bottom ash,various European countries have implemented and enacted legal regulations at an earlier date[8]. Particularly in Germany and Denmark, the use of bottom ash is upwards of 80%[9-11].

Therefore, the aim of this study is to achieve the objective of making artificial aggregates from bottom ash for civil engineering applications such as construction and road paving materials by classifying the incineration ash into 12 particle sizes, testing the physical properties of each particle size category such as leaching concentration of toxic substances and content of toxic substances and investigating the most suitable particle size category for the production of artificial aggregates.

2. MATERIALS AND METHODS

2.1 MATERIALS

Municipal solid waste bottom ash (particle size less than 40 mm) from two waste incineration plants(Western incineration plant and Eastern incineration plant) of Japan.The bottom ash was sized into 12 size fractions in order to investigate the particle size categories that could be used as artificial aggregate, taking into account both environmental safety (e.g. effect of specific surface area on heavy metal content) and resourcefulness (e.g. useful metal content).

2.2 METHODS

Since the objective of this experiment is mainly to use artificial aggregates for road paving material, the standard of this experiment is to adopt the Japanese standard for soil material for the experiment.

2.2.1 Hazardous Substances Content Test (Ministry of the Environment of Japan Notification No.19[12])

The collected bottom ash was dried in the air (impurities such as small and medium-sized stones, wood chips, etc),then were removed and screened through a non-metallic 2mm sieve to obtain a well-mixed sample.Every catagory sample will produce 3 parallel samples.9g sample of each size was weighed (6g for some samples due to insufficient mass) and the sample was mixed thoroughly with 1mol/L hydrochloric acid solution at a ratio of 3% by mass to volume.The prepared sample solution is continuously shaken for 2 hours using an oscillator (pre-adjusted to approximately 200 oscillations per minute with an amplitude of between 4 cm and 5 cm) at room temperature (generally about 25°C) and atmospheric pressure (about 1 atm). The shaking vessel should be made of polyethylene or a vessel that will not adsorb or leach the substance to be measured, and the volume of the vessel should be at least 1.5 times the volume of the solvent.The samples obtained by oscillation were centrifuged after standing for about 10 to 30 minutes, and the filtrate was collected by filtering the supernatant through a membrane filter with a pore size of 0.45 μm. The required amount is then accurately weighed and used as a test solution for measurement.The final sample solution was subjected to ICP testing.

2.2.2 Hazardous Substances Leaching Test (Environment Agency of Japan Notification No.46[13])

The samples were air-dried for 24h and then sieved into different sizes.Every catagory sample will produce 3 parallel samples.For each sample,15 g of each size was taken and 150

g of ultrapure water was added to make a sample mix (10% by weight-volume ratio).The samples were shaken horizontally for 6 hours at 200 cycles/min at an amplitude of 4-5 cm. The sample was left to stand for 10-30 minutes, centrifuged at 300 gravitational acceleration for 20 minutes and filtered through a 0.45 μm pore size, 90 mm diameter membrane filter to obtain the sample.

Acid digestion: Take 50 ml of the sample, add 5 ml of HNO_3(60％) and heat for about 2 hours until the volume of the solution becomes about 10 ml. Then, add more 5 ml of HNO_3(60％) and heat for 2-3 hours covered with a glass plate to concentrate the volume to 5 ml. The sample is transferred to a 50 ml volumetric flask and the volume is fixed with HNO_3(1 ％) to make a sample solution.The final samples obtained will be tested for ICP.

2.2.3 Method of Element Composition (XRF)

The samples were air-dried for 24h and then sieved into different sizes,then powdered the samples.10g of oven-dried ash samples were further heated at 600 °C for 2h to calculate the Loss on Ignition (LOI).Preparing the samples for XRF test after pressing the powdered sample in circular disced shaped containers in pressing machine.The samples were ready to apply XRF test to get the samples chemical composition for each particle sizes of incineration plants.

3. RESULTS AND DISCUSSION

3.1 Moisture content

The samples were dried, weighed and tested for moisture content. The moisture content of the Eastern incineration facility was slightly higher than that of the Western sample.

Table 1 Moisture content

Sample name	average	Maximun	minimum
Western BA	13.2%	14.0%	12.0%
Eastern BA	14.5%	17.3%	12.3%

3.2 particle size distribution

In actual operations, since incineration ash particle sizes larger than 37.5 mm do not exist, the actual particle size classification is 11.More than 60% of the samples particle sizes above 2 mm.

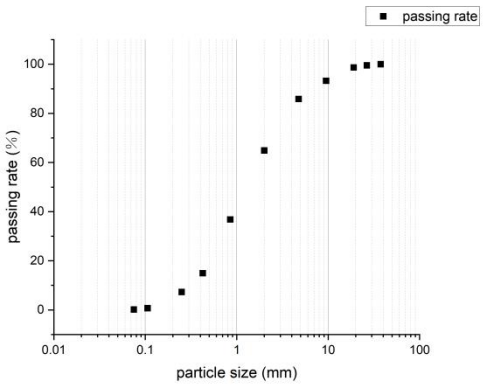

Figure 1 Western samples passing rate

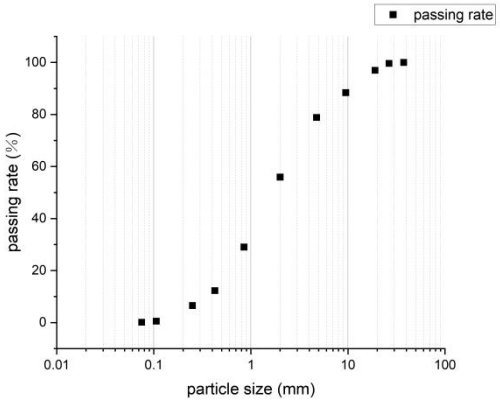

Figure 2 Eastern samples passing rate

3.3 Hazardous Substances Content Test

According to the test results, there is a decreasing trend in the content of harmful substances as the particle size of the bottom ash increases.It is noteworthy that the ash particles have an approximately spherical shape, and smaller diameter particles exhibit a larger specific surface area. This may lead to an increased affinity for adsorption or encapsulation of harmful substances, resulting in higher levels of such substances in the incineration ash with smaller particle sizes.The experiment is conducted in accordance with the standards outlined in Notification No.19 by the Japanese Ministry of the Environment.In some samples, the Pb content exceeded the specified standard values, while other elements remained below their respective standard values. Of particular concern is the observation that the Pb content in the incineration ash with a particle size below 2mm surpassed the standard values.Within the particle size range of 0.85mm-2mm, the content of harmful substances reached its peak, with the over-limit phenomenon being most pronounced for Pb, approximately 2-3 times the standard value.

These experimental findings suggest that the particle size of bottom ash significantly influences the content of harmful substances in the process of artificial aggregate material preparation, with Pb being particularly affected. This provides valuable insights for further optimizing the manufacturing process.

Table 2 Hazardous Substances content of Western samples

Particle Size(mm)	Content (mg/kg)			
	Cd	Cr	Pb	B
＜0.075	1.2	30.3	95.6	1.4
0.075-0.106	3.4	78.0	**352.9**	3.1
0.106-0.25	3.8	40.1	**245.0**	1.6
0.25-0.425	2.3	67.2	**422.6**	2.2
0.425-0.85	1.9	74.4	**424.7**	2.1
0.85-2	1.0	49.0	**507.5**	2.4
2-4.75	0.7	73.7	121.1	3.9
4.75-9.5	5.5	49.5	73.8	2.8
9.5-19	5.5	32.1	93.7	1.4
19-26.5	0.4	14.1	133.8	9.6
26.5-37.5	10.7	161.5	117.4	3.2
Standard value	45	250	150	4000

Table 3 Hazardous Substances content of Eastern samples

Particle Size(mm)	Content (mg/kg)			
	Cd	Cr	Pb	B
＜0.075	3.4	84.3	**154.8**	2.1
0.075-0.106	3.3	91.7	**166.5**	2.3
0.106-0.25	2.4	88.0	**162.3**	2.3
0.25-0.425	2.2	90.4	**195.9**	2.4
0.425-0.85	1.9	74.4	**210.7**	2.2
0.85-2	1.4	79.4	**517.3**	2.8
2-4.75	1.0	77.8	71.4	2.6
4.75-9.5	1.0	122.3	73.8	3.2
9.5-19	2.5	77.4	63.2	11.6
19-26.5	0.6	95.5	87.2	10.8
26.5-37.5	3.5	67.0	97.7	2.3
Standard value	45	250	150	4000

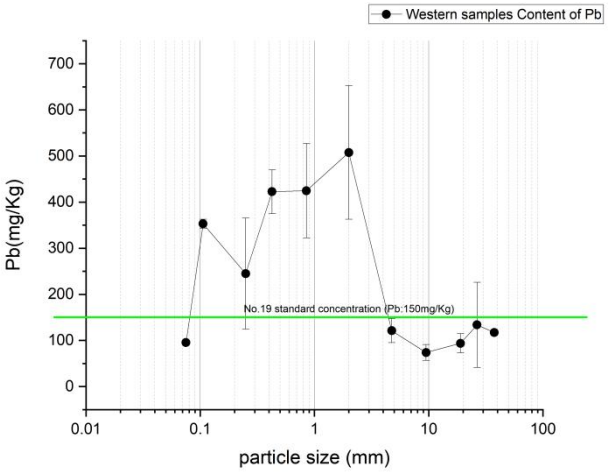

Figure 3 Western samples Pb content

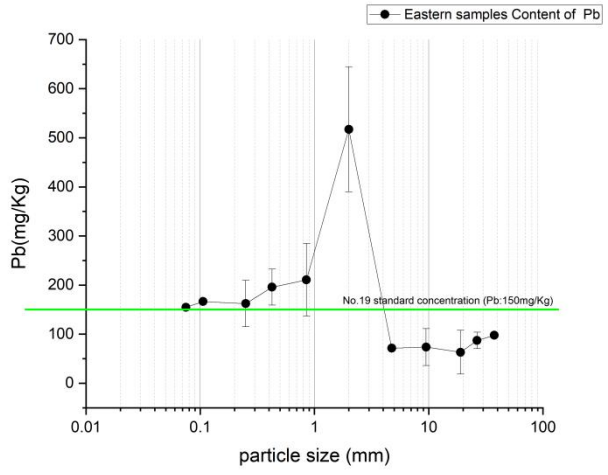

Figure 4 Eastern samples Pb content

3.4 Hazardous Substances Leaching Test

Due to the difficulty in obtaining a sufficient sample quantity for complete leaching experiments for some incineration bottom ash with particle sizes below 0.106mm, and the presence of large metal chunks in some larger particle-sized incineration bottom ash unsuitable for leaching experiments (particle sizes above 9.5mm), we opted to conduct leaching experiments on the main particle-sized incineration bottom ash. Following the standards outlined in Environment Agency of Japan Notification No.46, the results revealed an over-limit phenomenon for chromium and boron elements. The total chromium concentration mostly exceeded the specified hexavalent chromium concentration in JLT46. However, the actual hexavalent chromium concentration may be lower than the standard set by JLT46.

Overall, as the particle size increased, there was a decrease in the concentration of leached heavy metals, consistent with the trend observed in the content of harmful substances. While there were instances of Pb element content exceeding the limits in the samples, the leaching experiment results essentially did not exhibit over-limit conditions.

Additionally, in the production of artificial aggregate material using bottom ash, other binders will be added, resulting in a decrease in the leached concentration of harmful substances in the final artificial aggregate material. Therefore, the assessment of whether the particle size of incineration bottom ash is suitable for producing artificial aggregate material based solely on leaching experiments has certain limitations and requires a comprehensive consideration of other factors.

Table 4 leaching concentration of Western samples

Particle Size(mm)	leaching concentration (mg/L)			
	Cd	Cr	Pb	B
0.106-0.25	＜0.01	0.24	＜0.01	0.79
0.25-0.425	＜0.01	0.18	＜0.01	1.43
0.425-0.85	＜0.01	0.13	＜0.01	0.80
0.85-2	＜0.01	0.09	＜0.01	1.54
2-4.75	＜0.01	0.07	＜0.01	1.50
4.75-9.5	＜0.01	0.01	＜0.01	1.42
9.5-19	＜0.01	0.02	＜0.01	1.58
Standard value	0.003	0.05(Cr^{6+})	0.01	1

Table 5 leaching concentration of Eastern samples

Particle Size(mm)	leaching concentration (mg/L)			
	Cd	Cr	Pb	B
0.106-0.25	＜0.01	**0.37**	＜0.01	0.39
0.25-0.425	＜0.01	**0.29**	**0.03**	0.40
0.425-0.85	＜0.01	**0.21**	＜0.01	0.38
0.85-2	＜0.01	**0.13**	＜0.01	0.31
2-4.75	＜0.01	**0.11**	＜0.01	0.25
4.75-9.5	＜0.01	**0.05**	＜0.01	**1.36**
9.5-19	＜0.01	0.01	＜0.01	**1.24**
Standard value	0.003	＜0.05(Cr^{6+})	0.01	1

3.5 Element Composition (XRF)

The detailed information on the chemical composition of samples comes from XRF testing analysis performed on samples of different particle sizes. The average content of each chemical element/component was calculated based on samples of different particle sizes. According to the XRF results, it is revealed that the highest content in the incineration bottom ash is associated with calcium, potassium,

and aluminum elements. Additionally, three rare metals are present, with barium showing a relatively high concentration. The results for Pb content are consistent with previous tests, indicating a trend of higher content with smaller particle sizes.

Furthermore, the concentration of heavy metals in the incineration bottom ash is generally highest in the particle size range of 0.85 mm to 4.75 mm. This suggests a significant influence of particle size range on heavy metal content. Combining the XRF results, we have drawn comprehensive conclusions regarding the distribution of chemical components in samples of different particle sizes, providing crucial academic references for further research.

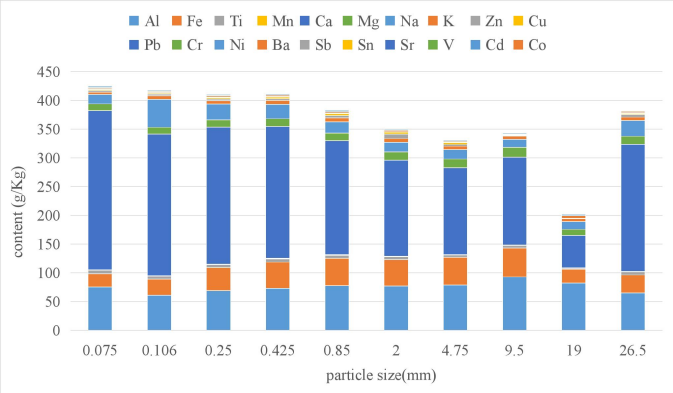

Figure 5 Elemental content of Western samples

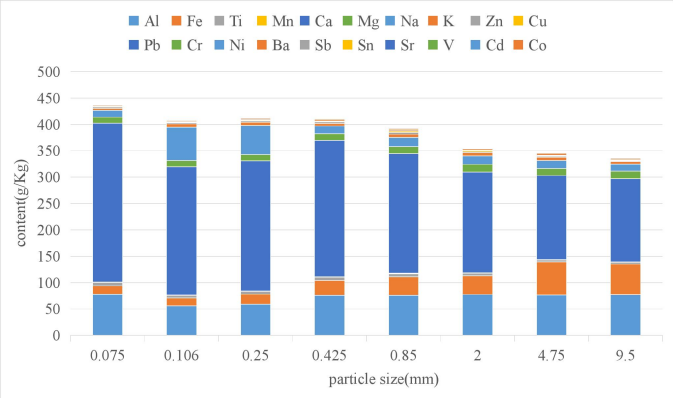

Figure 6 Elemental content of Eastern samples

4.Summary and Future Considerations

In the process of producing artificial aggregate materials, various binders and stabilizers will be added,which can also reduce the leaching of harmful substances.However,the harmful substances content of bottom ash seems will not be changed.Against this backdrop, the results of content testing emerge as a crucial indicator for evaluating the properties of bottom ash.Based on the results of content testing, it is evident that the concentration of heavy metals in incineration bottom ash increases as the particle size decreases.Particularly concerning is the observation that bottom ash with a particle size below 2mm exhibits Pb levels exceeding the standard by 2-3 times. However, since the portion with a particle size below 2mm constitutes over 60% of the total mass of bottom ash, solely utilizing particles larger than 2mm for the production of artificial aggregate material would result in under-utilization of the incineration bottom ash resource.To enhance the utilization rate, a plan is underway to employ finer sieves, especially within the 0.85mm-2mm range, to pinpoint the peak location of Pb content while simultaneously maximizing utilization.

In addressing the concern of elevated Pb content when using incineration bottom ash for the production of artificial aggregate material, adjustments to the ratio of bottom ash raw material to other binders are deemed necessary. This ensures that the artificial aggregate material adheres to environmental standards while maintaining optimal physical properties. While there is a slight excess of certain heavy metal elements in the leaching process, current levels are deemed acceptable. Mitigation strategies, including the addition of heavy metal stabilizers and solidification methods during the production of artificial aggregate material, are envisaged to bring the heavy metal content within environmental standards.

Given XRF results indicating valuable metals in bottom ash of different particle sizes, consideration is being given to extracting metals from particles below 2mm, while particles above 2mm are earmarked for use in the production of artificial aggregate material. This research direction holds promise for achieving positive outcomes in resource utilization and environmental protection.

REFERENCES

[1] Ministry of the Environment :Waste management in Japan https://www.env.go.jp/recycle/waste_tech/ippan/r2/data/disposal.pdf

[2] Xiaomin Dou, Fei Ren, Minh Quan Nguyen, Ashiq Ahamed, Ke Yin, Wei Ping Chan, Victor Wei-Chung Chang,Review of MSWI bottom ash utilization from perspectives of collective characterization, treatment and existing application,2017

[3] Audrius Vaitkus, Judita Gražulytė, Ovidijus Šernas, Viktoras Vorobjovas, Rita Kleizienė,An algorithm for the use of MSWI bottom ash as a building material in road pavement structural layers,2019

[4] Ciarán J. Lynn, Gurmel S. Ghataora, Ravindra K. Dhir OBE,Municipal incinerated bottom ash (MIBA) characteristics and potential for use in road pavements,2017

[5] P. Stabile, M. Bello, M. Petrelli, E. Paris, M.R. Carroll, Vitrification treatment of municipal solid waste bottom ash,2019,

[6] Y. Lu, A. Tian, J. Zhang, Y. Ang, P. Shi, Q. Tang and Y. Huang, "Physical and Chemical Properties, Pretreatment, and Recycling of Municipal Solid Waste Incineration Fly Ash and Bottom Ash for Highway Engineering: A ,2020.

[7]M. Van Praagh, M. Johansson, J. Fagerqvist, R. Grönholm, N. Hansson, H. Svensson,
Recycling of MSWI-bottom ash in paved constructions in Sweden – A risk assessment,2018

[8]Cho, B.H.; Nam, B.H.; An, J.; Youn, H. Municipal Solid Waste Incineration (MSWI) Ashes as Construction Materials—A Review. Materials 2020.

[9]Astrup, Thomas; Christensen, Thomas Højlund.Waste incineration bottom ashes in Denmark:Status and development needs by 2003, 2005.

[10]Chen D, Zhang Y, Xu Y, Nie Q, Yang Z, Sheng W, Qian G. Municipal solid waste incineration residues recycled for typical construction materials-a review. 2022.

[11]Olaf Holm, Franz-Georg Simon,Innovative treatment trains of bottom ash (BA) from municipal solid waste incineration (MSWI) in Germany,2017

[12]Announcement Law No.19 of the Ministry of Environment. https://www.env.go.jp/hourei/06/000029.html

[13]Announcement Law No.46 of the Ministry of Environment. https://www.env.go.jp/kijun/dt1-1.html

VEGETATION REMODELS THE CHARACTERISTIC BIOREACTIVE ZONE OF THE COVER AND THUS INFLUENCES METHANE OXIDATION AND CHLOROBENZENE DEGRADATION PROCESSES

Shangjie Chen, Zhilin Xing, and Tiantao Zhao
1 College of Chemistry and Chemical Engineering, Chongqing University of Technology
No. 69, Hongguang Avenue, Huaxi Street, Banan District, Chongqing, China

ABSTRACT
vegetation, particularly trees such as Paulownia tomentosa and Ricinus communis, enhances oxygen transport within landfill cover layers, influencing the distribution of oxygen and creating distinct biotic reaction zones. This, in turn, strengthens the degradation efficiency of methane and chlorobenzene in the cover layer. The findings underscore the importance of vegetation in optimizing landfill cover layers for effective CAH removal and ecological restoration.

KEY WORDS: plants, microorganisms, methane oxidation, chlorobenzene degradation, landfill cover

INTRODUCTION

In landfill sites, a substantial amount of chlorinated waste, when subjected to anaerobic conditions, generates landfill gas. Under anaerobic conditions, the produced landfill gas is predominantly composed of methane (CH_4), with an annual release reaching up to 50 million tons, exhibiting a global warming potential over 80 times that of CO_2 over a 20-year timeframe (IPCC, 2014; Maria et al., 2023). Consequently, landfill sites have emerged as the third-largest anthropogenic source, following agriculture and coal mining (Du et al., 2017; Lou et al., 2017). Furthermore, landfill sites contribute significantly to the annual production of 1.6 × 10^7 m^3 of gaseous chlorinated hydrocarbons, constituting approximately 20% of the overall environmental gas emissions, thereby establishing them as a primary anthropogenic source of chlorinated hydrocarbon pollutants (Aghdam et al., 2019; Jafari et al., 2017; Tan et al., 2017). Despite chlorinated hydrocarbons in landfill gas exhibiting concentrations much lower than those of methane, they pose a latent "triple-threat effect" (teratogenic, carcinogenic, mutagenic effects) and environmental genetic toxicity, presenting a severe threat to ecological safety and human health (Majumdar et al., 2014; Carriero et al., 2018).

Numerous studies indicate that microorganisms within landfill cover layers play a pivotal role in methane emission reduction and chlorinated hydrocarbon degradation (Chuan et al., 2018; Hermon et al., 2018; Barul et al., 2017). Research demonstrates that CH_4, under the influence of methane-oxidizing bacteria, undergoes aerobic oxidation to CO_2. However, the diffusion limitations of oxygen confine this process primarily to the top layer of the landfill cover (Chi et al., 2015; Xu and Zhang, 2022). Parsaeifard et al. (2020) confirmed anaerobic methane oxidation as another crucial process for methane removal. Methane-oxidizing bacteria, as typical co-metabolic microorganisms, utilize methane monooxygenase (MMO), produced during methane degradation, as a significant catalyst for co-metabolic degradation of chlorinated organic compounds (Schmidt et al., 2014; Leu et al., 2020). Nevertheless, aerobic co-metabolism fails to achieve the complete degradation of chlorinated organic compounds. Chlorinated hydrocarbons under anaerobic conditions tend to undergo dechlorination reactions, with degradation rates increasing with the degree of substitution (Cappelletti et al., 2012; Arora and Bae, 2014). Susarla et al. (1996) confirmed that chlorinated organic compounds such as PCE and chlorobenzene undergo dechlorination in the reduction process, forming low-chlorinated intermediates or mineralizing to produce CO_2 and CH_4. Hence, the processes of methane oxidation and chlorinated hydrocarbon biodegradation coexist in close association within the landfill cover layer.

The methane oxidation process and chlorinated hydrocarbon biodegradation within landfill cover layers are influenced by various factors, including soil moisture content, soil porosity, pH, temperature, and organic carbon content (Chanton et al., 2009; Chen et al., 2023). In recent years, research emphasis has shifted towards optimizing soil parameters within the cover layer to enhance the activity of functional microorganisms. This optimization, relying on biological processes and environmental influences, aims to achieve methane emission reduction and removal of landfill gas (Zhang et al., 2020; Shuai et al.,

2018). It is essential to note that the presence of vegetation in the cover layer introduces a certain degree of disparity between simulated landfill sites and actual landfill sites. Studies indicate that, apart from providing carbon sources and energy for microorganisms through root exudates and litter decomposition, the existence of vegetation significantly alters the community structure of rhizosphere microorganisms through the formation of secondary pores resulting from root expansion (Bian et al., 2020; Lee et al., 2017; Ben-Noah and Friedman, 2018). Vegetation roots actively participate in soil respiration by transporting O_2 into the soil and facilitating lateral diffusion, thereby inducing the settlement of aerobic microorganisms in the rhizosphere microhabitat. Powell et al. (2014) observed that the rhizospheres of vegetation such as *Scripus Atrovirens* and *Carex Comosa* significantly enriched methane-oxidizing bacteria, effectively enhancing the co-metabolic degradation rates of c-DCE and TCE. Tawney et al. (2008) confirmed that the roots of Phragmites Australis could moderately facilitate oxygen penetration into the soil, creating favorable gas conditions for the biological oxidation process of c-DCE.

The joint phytomicrobial remediation technique has become a focal point of research for achieving methane emission reduction and pollutant removal in landfill cover layers. However, the prevailing emphasis has largely centered on the reinforcing effects of root exudates on rhizospheric microorganisms (Kim et al., 2016; Kuzyakov and Razavi, 2019). The objective of this study is to investigate the impact of vegetation root-mediated gas transport on the biological reaction zone within landfill cover layers, providing new insights into the patterns of methane oxidation and chlorinated hydrocarbon degradation under plant influence. Given the diversity of plant species in cover layers, we selected adaptable and widely applicable herbaceous, shrub, and tree vegetation as experimental materials. Our investigation aims to elucidate the changes in gas distribution, microbial community structure, and biometabolic characteristics within the cover layer influenced by these vegetation types. The obtained results contribute to enhancing our understanding of how vegetation promotes methane reduction and chlorinated hydrocarbon removal in cover layers, offering theoretical guidance for ecological restoration efforts in landfill sites.

MATERIALS AND METHODS

Soil samples

The soil samples for this study were obtained from the Changshengqiao landfill site in Nanan District, Chongqing City, China (29° 30′ 45.31″ , 106° 37′ 9.87″). The landfill site, designed with a burial capacity of up to 2.1 × 10^7 m^3, has been in stable operation for nearly 28 years since its establishment in 1994, processing approximately 3000 tons of waste per day during peak periods. Soil samples were extracted using a rock coring method from a depth of 0.1-0.3 m within the cover layer. The burial duration of the samples exceeded 2 years, and the collected soil samples were transported on ice to the laboratory.

Upon arrival, the soil samples underwent manual removal of stones, followed by sieving through a 2 mm soil sieve, and manual mixing for homogenization. The processed soil samples were divided into three portions: one underwent acclimatization for simulating the conditions of the landfill cover layer, another was stored at -80°C for subsequent DNA extraction, and the remaining portion, after air-drying, underwent physicochemical property analysis.

Plant-cover coupled systems

The plant-cover coupling system was constructed primarily using PVC as the main material. The main body of the plant-cover coupling system consists of two reaction columns, each with a height of 140 cm and an internal diameter of 30 cm. On the side of the reaction column, there are bio-gas and soil sampling ports, positioned at intervals of 15 cm along the column, starting 5 cm above the reactor's bottom and extending upward. The upper and lower ends of the reaction column are connected via flanges and sealed with rubber rings. At the bottom center, there is an inlet for the mixed gas, while on the upper end, there are side ports for air intake and exhaust gas discharge. The reaction column is filled with a 5 cm thick layer of coarse sand and gravel, isolated by wire mesh, providing support for the cover soil and ensuring a more uniform transfer of the mixed gas. The height of the cover soil filling is approximately 90 cm, leaving the remaining space for vegetation growth.

Previous studies have indicated that vegetation in landfill cover layers can be categorized into herbaceous, shrub, and woody plants (Chen et al., 2023). In this study, representative species, namely Trifolium repens (white clover), Ricinus communis (castor bean), and Paulownia tomentosa (princess tree), were selected as experimental materials, along with a control group. In the initial stage of reactor assembly, high-purity nitrogen was introduced through the bottom inlet, and the oxygen concentration was monitored under different gradients simulating cover layers. Once the overall oxygen concentration distribution stabilized, a biogas mixture of CH_4 and CO_2 (volumetric ratio of 1) was introduced to acclimate the microbial community structure and biological activity within the simulated cover layers. The acclimatization period lasted approximately 15 days. Following acclimatization, the vegetation was transplanted to the surface of the simulated cover layer soil column, establishing the plant-cover coupling system, with a stabilization period of 15 days. During the stabilization period, the system

received 8 hours of daily illumination and appropriate watering.

Using acclimatized active landfill cover soil as the biological medium, a simulated landfill gas was generated by introducing CH_4 (50%) and CO_2 (50%) into a CB (chlorobenzene) pollution generator. The simulated landfill gas was then directed into the plant-cover coupling system through an inlet, maintaining a constant simulated landfill gas flux throughout the process. Throughout the system's operation, continuous sampling and analysis were conducted for the biogas components (CH_4, O_2, and CO_2) and pollutant (CB) under different gradients. Two parallel samples were collected for each gradient. The operational conditions of the system maintained a temperature range of 22-27°C and an air humidity level between 45% and 78%.

Gas Detection

The gas sampling was conducted using a YW11 vacuum pump (ZiRun Electrical Appliance Factory, Jieyang, Guangdong, China) that automatically extracted 1 ml of gas from the system's gas sampling port. Immediately following, gas analysis and detection were performed using an SC-6000A gas chromatograph (ChuanYi Spectrograph Instrument Co., Ltd., Chongqing, China) equipped with a TCD detector. Chromatographic conditions included a stainless-steel chromatographic column (TDX8-12-25, 2m); the temperatures of the column oven, injection port, and detector were set at 80°C, 120°C, and 120°C, respectively. The carrier gas consisted of a mixture of hydrogen and nitrogen, with a flow rate of 25 $mL \cdot min^{-1}$, and a sample injection volume of 500 μL.

CAHs (Chlorinated Aromatic Hydrocarbons) were analyzed and detected using an SC-8000 gas chromatograph (ChuanYi Spectrograph Instrument Co., Ltd., Chongqing, China) equipped with an ECD detector. The chromatographic conditions were as follows: a stainless-steel chromatographic column (GDX-104, 2m); the temperatures of the column oven, injector, and detector were set at 80°C, 200°C, and 200°C, respectively. The carrier gas consisted of a mixture of argon and nitrogen, with a flow rate of 40 mL·min-1, and a sample injection volume of 500 μL. The split flow rate was 10 $mL \cdot min^{-1}$, and the baseline compensation was set at 0.00 nA.

RESULTS AND DISCUSSION

Cover gas distribution under vegetation

Under the influence of atmospheric pressure and natural diffusion, a counter-diffusion process occurs between oxygen and landfill gas within the cover layer of a landfill. In the presence of vegetation, oxygen not only undergoes natural diffusion but is actively transported into the landfill cover layer, altering its longitudinal distribution in the landfill (Figure S1). The methane concentration decreases with decreasing cover layer depth, while the oxygen concentration exhibits the opposite trend, confirming the role of the cover layer soil in methane biodegradation. Under the influence of vegetation, the oxygen concentration at different gradients within the cover layer changes, thereby altering the distribution of aerobic zones (O_2 > 0.5 mg/L), hypoxic zones (0.5 mg/L > O_2 > 0.01 mg/L), and anaerobic zones (0.01 mg/L > O_2) in the biological reaction bands (as shown in Figure 1) (Xing et al., 2023).

In the absence of vegetation cover, the landfill cover layer exhibits three biological reaction bands (aerobic zone: 0 cm to -30 cm; hypoxic zone: -30 cm to -45 cm; anaerobic zone: -45 cm to -90 cm), with the anaerobic zone dominating. Compared to the scenario without vegetation cover, the herbaceous plant Trifolium repens and the shrub Ricinus communis significantly expand the hypoxic zone. Under the cover of Trifolium repens, the hypoxic zone extends from 0 cm to -75 cm, while under the cover of Ricinus communis, the hypoxic zone ranges from -30 cm to -75 cm. The oxygen concentrations at various layers under the cover of Ricinus communis are generally higher than those under the cover of Trifolium repens, while the methane concentrations show the opposite trend. This indicates that the process of methane biodegradation is accompanied by oxygen consumption. Additionally, the tree vegetation Paulownia tomentosa can transform the entire simulated landfill cover into an aerobic environment, causing the methane concentration along its distribution to be significantly lower than in the simulated landfill cover layer without vegetation cover.

Please do not write print page numbers.

The impact of vegetation on soil O_2 content is regulated by a variety of physical, chemical, and biological processes, with O_2 being transported into the rhizosphere by plant roots and permeating into the deeper soil layers (Feng et al., 2017; Bian et al., 2020). Previous reports have indicated that plant transpiration is one of the primary mechanisms regulating the rhizospheric gas environment. Additionally, different root system configurations, including parabolic, uniform, exponential, and triangular types, along with the secondary voids formed by root growth, can also facilitate the entry of air into the deep soil layers (Bohn et al., 2011; Feng et al., 2017). Ng et al. (2015) confirmed significant differences in soil moisture content induced by different root system configurations, playing a crucial role in the distribution of oxygen in the soil profile.

The typical vegetation, root system configurations, and physicochemical properties of rhizospheric soil in the landfill cover layer are presented in Table S1. The root system configurations of Trifolium repens, Ricinus communis, and Paulownia tomentosa are triangular, exponential, and parabolic, respectively, with

Paulownia tomentosa exhibiting the longest average root system length. Ricinus communis follows with the second-longest average root system length. It is inferred that both root system configuration and length collectively influence the distribution of O_2 in the landfill cover layer, thereby shaping different biological reaction bands. The parabolic root system is most conducive to root oxygen transport, and root system length is positively correlated with O_2 profile concentrations. This finding aligns with the results of Bian et al. (2020).

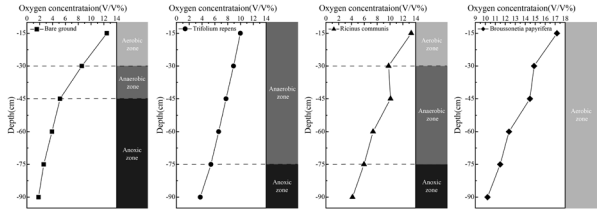

Fig. 1 Response zone distribution of simulated cover under bare soil and vegetation cover

Methane oxidation efficiency and chlorobenzene degradation capacity

Vegetation reshapes the methane oxidation efficiency and chlorobenzene degradation capability of the landfill cover layer, as illustrated in Figure 2. Concerning methane oxidation, the simulated landfill cover layer under the influence of Trifolium repens exhibits slightly lower methane oxidation efficiency compared to bare soil. In contrast, the other two vegetation types enhance the methane oxidation efficiency of the cover layer, with Paulownia tomentosa having the highest methane oxidation efficiency, reaching 80.87%. The presence of Trifolium repens does not favor the methane biodegradation process in the cover soil, a phenomenon that appears inconsistent with previously reported research results (Hilger et al., 2000; Reichenauer et al., 2011; Xin et al., 2016). Studies by Éliane et al. (2015) indicate that herbaceous vegetation, due to generally shorter root systems, only begins to impact soil microecology after four years of vegetation establishment. It is inferred that herbaceous vegetation is not initially conducive to the diffusion of air into the soil environment, forcing the original aerobic zones to transition into hypoxic zones, thereby reducing the average methane oxidation efficiency of the soil column.

In comparison to herbaceous vegetation, the root systems of shrubs and trees are generally longer, promoting the diffusion of O_2 into deeper soil layers (Bian et al., 2020). The O_2 concentration in the landfill cover layer is a critical factor limiting the rate of CH_4 oxidation (Chi et al., 2012). Thus, as Ricinus communis and Paulownia tomentosa introduce O_2 deeper into the soil, the biological reaction bands in the cover layer undergo changes, significantly enhancing the methane oxidation efficiency of the cover layer.

Research indicates that the degradation capability of chlorobenzene (CB) in the cover layer under vegetation is superior to that in the bare cover layer, with the strengthening effect ranking as follows: *Paulownia tomentosa* > *Ricinus communis* > *Trifolium repens*. In landfills, due to the limitation of O_2, the CB biodegradation pathways primarily include aerobic co-metabolism and anaerobic dechlorination processes, with the efficiency of aerobic co-metabolism degradation significantly higher than that of anaerobic dechlorination (Field and Sierra-Alvarez, 2008; Nelson et al., 2014; Gholami et al., 2019). Thus, Ricinus communis and Paulownia tomentosa enhance the CB degradation capability of the cover layer by increasing the O_2 concentration, promoting the aerobic co-metabolism pathway during CB biodegradation.

It is noteworthy that the methane oxidation rate in the cover layer under Trifolium repens is lower than that in the bare soil cover layer. However, its CB degradation capability is slightly higher than that of the bare soil cover layer, and the expansion of the hypoxic zone may be the main reason for this situation. Xing et al., through continuous monitoring, droplet digital PCR, and multi-omics techniques, investigated the degradation mechanisms of trichloroethylene (TCE) in the landfill cover layer. The results indicate that all six biodegradation pathways of TCE in the cover layer occur in the hypoxic zone. The regulation of the proportion of aerobic co-metabolism and anaerobic dechlorination pathways in the hypoxic zone significantly affects the efficiency of chlorinated hydrocarbon biotransformation.

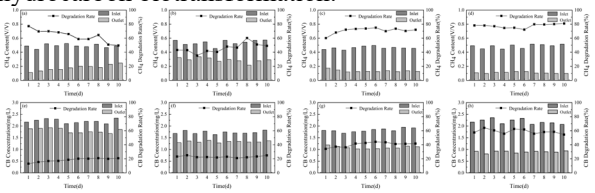

Fig. 2 Methane oxidizing capacity and chlorobenzene degradation capacity of simulated mulches under bare soil and vegetation cover

CONCLUSIONS

In the process of chlorobenzene degradation, all four distinct cover layers established stable aerobic, anaerobic, and hypoxic zones. Different vegetation root systems exert varying influences on the oxygen distribution within the cover layer, with the root system of the tree species Paulownia tomentosa having a predominant impact on the overall oxygen content in the cover layer. The order of oxygen transport capacity is as follows: tree species *Paulownia tomentosa* > shrub species *Ricinus communis* > herbaceous species *Trifolium repens*. The average methane degradation rates for bare soil, Trifolium repens, Ricinus communis,

and Paulownia tomentosa cover layers are 63.4%, 37.2%, 70.81%, and 77.81%, respectively. Similarly, the average chlorobenzene degradation rates are 18.48%, 23.05%, 40.65%, and 59.15%, respectively.

Under the influence of Ricinus communis and Paulownia tomentosa, there is a notable enhancement in the cover layer's capacity for degrading chlorobenzene and methane. In the case of Trifolium repens, there is an improvement in the cover layer's ability to degrade chlorobenzene, although the enhancement is not statistically significant. The different responses of these vegetation types underscore the complex interplay between plant root systems and the dynamics of oxygen distribution, contributing to variations in the degradation efficiency of chlorobenzene and methane within landfill cover layers.

REFERENCE

IPCC. Climate Change 2014: Mitigation of Climate Change. Contribution of Working Group III to the Fifth Assessment Report of the Intergovernmental Panel on Climate Change [M]. Cambridge University Press, 2014.

Maria O., Andris P., Paul B. 2023. A global review of methane policies reveals that only 13% of emissions are covered with unclear effectiveness. One Earth. 6(5), 519-535.

Du, M., Peng, C., Wang, X., Chen, H., Wang, M., Zhu, Q., 2017. Quantification of methane emissions from municipal solid waste landfills in China during the past decade. Renew. Sustain. Energy Rev. 78, 272–279.

Lou, Z., Cai, B.-F., Zhu, N., Zhao, Y., Geng, Y., Yu, B., Chen, W., 2017. Greenhouse gas emission inventories from waste sector in China during 1949–2013 and its mitigation potential. J. Cleaner Prod. 157, 118–124.

Aghdam E F, Scheutz C, Kjeldsen P. Impact of meteorological parameters on extracted landfill gas composition and flow. Waste Management, 2019, 87: 905-914.

N.H. Jafari, A.M. Asce, T.D. Stark, F. Asce, T. Thalhamer Progression of elevated temperatures in municipal solid waste landfills. J. Geotech. Geoenviron. Eng., 143 (2017), pp. 1-16.

H. Tan, Y. Zhao, Y. Ling, Y. Wang, X. Wang. Emission characteristics and variation of volatile odorous compounds in the initial decomposition stage of municipal solid waste. Waste Manag., 68 (2017), pp. 677-687.

D. Majumdar, S. Ray, S. Chakraborty, P.S. Rao, A.B. Akolkar, M. Chowdhury, A. Srivastava. Emission, speciation, and evaluation of impacts of non-methane volatile organic compounds from open dump site emission, speciation, and evaluation of impacts of non-methane volatile organic compounds from open dump site. J. Air Waste Manag. Assoc., 64 (2014), pp. 834-845.

G. Carriero, L. Neri, D. Famulari, S. Di, D. Piscitelli, A. Manco, A. Esposito, A. Chirico, O. Facini, S. Finardi, G. Tinarelli, R. Prandi, A. Zaldei, C. Vagnoli, P. Toscano, V. Magliulo, P. Ciccioli, R. Baraldi. Composition and emission of VOC from biogas produced by illegally managed waste landfills in Giugliano (Campania, Italy) and potential impact on the local population. Sci. Total Environ., 640–641 (2018), pp. 377-386.

Chuan D, Liu J M, et al. Assessment of the health risks and odor concentration of volatile compounds from a municipal solid waste landfill in China. Chemosphere: Environmental toxicology and risk assessment, 2018, 202(7): 1-8

Hermon L, Denonfoux J, Hellal J, et al. Dichloromethane biodegradation in multi-contaminated groundwater: Insights from biomolecular and compound-specific isotope analyses. Water Research, 2018, 142(10): 217-226

Barul C, Fayossé A, Carton M, et al. Occupational exposure to chlorinated solvents and risk of head and neck cancer in men: a population-based case-control study in France. Environmental Health, 2017, 16(1): 77

Z. Chi, W. Lu, H. Wang. Spatial patterns of methane oxidation and methanotrophic diversity in landfill cover soils of southern China. J. Microbiol. Biotechnol., 25 (4) (2015), pp. 423-430.

Xu S, Zhang H. First evidence for anaerobic oxidation of methane process in landfill cover soils: Activity and responsible microorganisms[J]. The Science of the total environment, 2022, 841:156790.

N. Parsaeifard, M. Sattler, B. Nasirian, V.C.P. Chen. Enhancing anaerobic oxidation of methane in municipal solid waste landfill cover soil. Waste Manag., 106 (2020), pp. 44-54.

Schmidt M, Lege S, Nijenhuis I. Comparison of 1,2-dichloroethane, dichloroethene and vinyl chloride carbon stable isotope fractionation during dechlorination by two Dehalococcoides strains. Water Research, 2014, 52: 146–154.

A.O. Leu, C. Cai, S.J. McIlroy, G. Southam, V.J. Orphan, Z. Yuan, S. Hu, G.W. Tyson. Anaerobic methane oxidation coupled to manganese reduction by members of the methanoperedenaceae. ISME J., 14 (4) (2020), pp. 1030-1041

Cappelletti M, Frascari D, Zannoni D, Fedi S. Microbial degradation of chloroform. Applied Microbiology and Biotechnology, 2012, 96(6): 1395–1409.

Arora PK, Bae H. Bacterial degradation of chlorophenols and their derivatives. Microbial Cell Factories, 2014, 13(1): 31

Susarla S, Masunaga S, Yonezawa Y. Reductive dechlorination pathways of chloro organics under

anaerobic conditions. Water Science and Technology, 1996, 34(5/6): 489–494.

J.P. Chanton, D.K. Powelson, R.B. Green. Methane oxidation in landfill cover soils, is a 10% default value reasonable? J. Environ. Qual., 38 (2009), pp. 654-663.

Chen SJ, Wang YQ, Xu FQ, Xing ZL, Zhang XP, Su X, Li J, Zhao TT, Wan SB. 2023. Synergistic effects of vegetation and microorganisms on enhancing of biodegradation of landfill gas. Environmental Research, 227, 115804.

H. Zhang, Z. Xing, J. Wang, T. Zhao. Advances in microbial degradation of chlorinated hydrocarbons. Chin. J. Biotechnol., 36 (2020), pp. 1083-1100.

L. Shuai, T.T. Zhao, Z.L. Xing, X. Yang, E.Y. Wang. Advances in biotic and abiotic mutual promoting mechanism for chlorinated aliphatic hydrocarbons degradation. Chin. J. Biotechnol., 34 (2018), pp. 510-524

R. Bian, W. Shi, X. Chai, Y. Sun. Effects of plant radial oxygen loss on methane oxidation in landfill cover soil: a simulative study. Waste Manag., 102 (2020), pp. 56-64.

E.H. Lee, K.E. Moon, K.S. Cho. Long-term performance and bacterial community dynamics in biocovers for mitigating methane and malodorous gases. J. Biotechnol., 242 (2017), pp. 1-10.

I. Ben-Noah, S.P. Friedman. Review and evaluation of root respiration and of natural and agricultural processes of soil aeration. Vadose Zone J., 17 (2018), pp. 1-47

C.L. Powell, M.N. Goltz, A. Agrawal. Degradation kinetics of chlorinated aliphatic hydrocarbons by methane oxidizers naturally-associated with wetland plant roots. J. Contam. Hydrol., 170 (2014), pp. 68-75

I. Tawney, J. Becker, A. Baldwin. A Novel Dual-Compartment, continuous-flow wetland microcosm to assess cis-dichloroethene removal from the rhizosphere. Int. J. Phytoremediation, 10 (2008), pp. 455-471

G.W. Kim, A. Ho, P.J. Kim, S.Y. Kim. Stimulation of methane oxidation potential and effects on vegetation growth by bottom ash addition in a landfill final evapotranspiration cover. Waste Manag., 55 (2016), pp. 306-312

Y. Kuzyakov, B.S. Razavi. Rhizosphere size and shape: temporal dynamics and spatial stationarity. Soil Biol. Biochem., 135 (2019), pp. 343-360

Chen SJ, Wang YQ, Xu FQ, Xing ZL, Zhang XP, Su X, Li J, Zhao TT, Wan SB. 2023. Synergistic effects of vegetation and microorganisms on enhancing of biodegradation of landfill gas. Environmental Research, 227, 115804.

Xing, Z.L., Chen, S.J., Xu, F.Q., Su, X., Gou, F., Shi, Y.C., Chen, H., Xiang, J.X., Li, J., Zhao, T.T., 2023. Quantitative analysis of TCE biodegradation pathway in landfill cover utilizing continuous monitoring, droplet digital PCR and multi-omics sequencing technology. J. Environ. Manage. 344, 118509.

Feng, S., Leung, A., Ng, C., Liu, H., 2017. Theoretrical analysis of coupled effects of microbe and root architecture on methane oxidation in vegetated landfill covers. Sci. Total Environ. 599, 1954-1964.

Bian, R.X., Shi, W., Chai, X.L., Sun, Y.J., 2020. Effects of plant radial oxygen loss on methane oxidation in landfill cover soil: A simulative study. Waste Manage. 102, 56-64.

Bian, R., Xin, D., Chai, X., 2018. A simulation model for methane emissions from landfills with interaction of vegetation and cover soil. Waste Manage. 71, 267-276.

Bohn, S., Brunke, P., Gebert, J., Jager, J., 2011. Improving the aeration of critical fine-grained landfill top cover material by vegetation to increase the microbial methane oxidation efficiency. Waste Manage. 31, 854-863.

Ng, C.W.W., Liu, H.W., Feng, S., 2015. Analytical solutions for calculating pore-water pressure in an infinite unsaturated slope with different root architectures. Can. Geotech. J. 52(12), 1981-1992.

Bian, R.X., Shi, W., Chai, X.L., Sun, Y.J., 2020. Effects of plant radial oxygen loss on methane oxidation in landfill cover soil: A simulative study. Waste Manage. 102, 56-64.

Hilger, H.A., Wollum, A.G., Barlaz, M.A., 2000. Landfill methane oxidation response to vegetation, fertilization, and liming. J. Environ. Qual. 29(1), 324-334.

Reichenauer, T.G., Watzinger, A., Riesing, J., Gerzabek, M.H., 2011. Impact of different plants on the gas profile of a landfill cover. Waste Manage. 31 (5), 843–853.

Xin, D., Hao, Y., Shimaoka, T., Nakayama, H., Chai, X., 2016. Site specific diel methane emission mechanisms in landfills: a field validated process based on vegetation and climate factors. Environ. Pollut. 218, 673–680.

Éliane, M.N., Robert, L.B., Alexandre, R.C., 2015. Does vegetation affect the methane oxidation efficiency of passive biosystems? Waste Manage. 38, 240-249.

Chi, Z.F., Lu, W.J., Li, H., Wang, H.T., 2012. Dynamics of CH4 oxidation in landfill biocover soil: Effect of O2/CH4 ratio on CH4 metabolism. Environmental Pollution. 170, 8-14.

Field, J.A., Sierra-Alvarez, R., 2008. Microbial degradation of chlorinated benzenes. Biodegradation. 19(4), 463-480.

Nelson, J.L., Jiang, J.D., Zinder, S.H., 2014. Dehalogenation of Chlorobenzenes, Dichlorotoluenes, and Tetrachloroethene by Three

Dehalobacter spp. Environmental Science & Technology. 48(07), 3776-3782.
Gholami, F., Mosmeri, H., Shavandi, M., Dastgheib, S.M.M., Amoozegar, M.A., 2019. Application of encapsulated magnesium peroxide (MgO2) nanoparticles in permeable reactive barrier (PBR) for naphthalene and toluene bioremediation from groundwater. Sci. Total. Environ. 655, 633-640.
Xing, Z.L., Chen, S.J., Xu, F.Q., Su, X., Gou, F., Shi, Y.C., Chen, H., Xiang, J.X., Li, J., Zhao, T.T., 2023. Quantitative analysis of TCE biodegradation pathway in landfill cover utilizing continuous monitoring, droplet digital PCR and multi-omics sequencing technology. J. Environ. Manage. 344, 118509.

Ministry of Science and Technology China/Japan Cooperation Research Project: Research on Carbonization Resource Utilization Technologies for Agricultural and Livestock. (EFCaR ® System)

Sijia Zheng, Ryoichi Sakamoto, Kozo Ueda
Circular Economy Business Innovation Department, Hitachi Zosen Corporation,7-89, Nanko-kita1-chome, Suminoe-ku, Osaka, Japan

1. INTRODUCTION

Known as a finite and dwindling resource, phosphate rocks have been mined in large quantity to produce phosphate-based fertilizers in order to meet the demands of an ever-growing global population. Approximately 20 Mt phosphorus is annually extracted from the earth.[1)] the estimates for depletion of phosphate rocks reserves range from 40 to 400 years[2)]. Therefore, the recovery of phosphorus resources will become critical in the food production value chain.

According to a study conducted by the Organization for Livestock Environment and Development, the percentage of phosphorus in the excretion of livestock manure is 97% for dairy cows, 95% for beef cattle, 75% for fattening pigs, and 100% for chickens, based on the amount excreted by each livestock species fed standard feed[3)]. Thus, effective utilization of phosphorus derived from livestock waste would allow for the sustainable sourcing of phosphorus and the recycling of livestock manure.

In parallel, with the rapid development of animal husbandry in China, the total amount of livestock waste has increased dramatically, which has a greater impact on the ecologies capacity to naturally absorb such waster. Therefore, proper treatment and recycling of livestock waste reduce the volume of waste and odor decomposition is under pressure. Using biochar that was heat treated by carbonization from livestock wastes into fertilizers is an effective way to solve this waste resource utilization problem.

However, existing hydrothermal carbonization technology in China is less applicable to livestock waste with higher moisture content. It has not only strict requirements on the water content of raw materials, but it is a complex process, with high energy consumption and large investment in capital equipment.

The EFCaR ® System developed by Hitachi Zosen Corporation had already been successfully verified in Japan and been proven to be a viable solution for phosphorus recycling and waste management in the livestock sector. It was adopted in the Ministry of Science and Technology China/Japan Cooperation Research Project to improve carbonization resource utilization technologies for agricultural and livestock in China.

2. MATERIALS AND METHODS

2.1 Technical principle

The outline of Energy Free Carbonizing for Resource Recovery (EFCaR®) System is shown in the Fig.1 below.

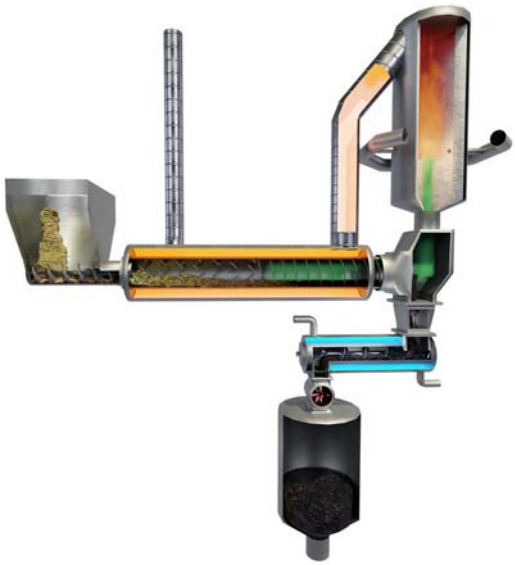

Fig.1 Outline of EFCaR® System

In this process flow, dried raw materials (approx. 40% moisture content) are fed into such an indirect-heating rotary kiln to produce biochar. The kiln consists of an inner cylinder and an outer cylinder. In the inner cylinder where air is almost totally cut-off, the material is heated to a certain temperature by indirect heat transfer while being rotated, so that the organic matter in the material undergoes pyrolysis, generating pyrolysis gas and biochar. The pyrolysis gas is sent into the combustion chamber, where it mixed with air, and combusted to a temperature of approximately 850°C. The combustion gas is then sent to the outer cylinder of the kiln, where it flows along the circumference of the rotating inner cylinder and is used as a heat source to uniformly heat the inner cylinder of the kiln. The biochar is cooled and stored as the main raw material

for the subsequent production of biochar-based fertilizer. The greatest feature of this system is that it can continuously produce biochar at a uniform temperature without the use of fuel, except during start-up.

2.2 Project scheme

The objective of Ministry of Science and Technology China/Japan Cooperation Research Project is to introduce Japanese technology to China and to apply and industrialize the technology through demonstration test. One of the ten projects adopted in 2021, "Research on Carbonization Resource Utilization Technologies for Agriculture and Livestock (EFCaR ® System)" has embarked on a three-year demonstration from October 2021 to September 2024. During the three years of project implementation, tasks must be established each year and an interim report must be submitted to the Ministry of Science and Technology of China after each task completed.

The tasks are shown below:

1.Production of carbonization equipment, using various raw materials at different temperatures to produce 9 types of biochar.

2.Analyzing both the biochar mentioned above and biochar-based fertilizers made from these 9 types of biochar, evaluating in terms of carbon fixation and nutrient content to select the most valuable biochar.

3. Using the same process as the biochar selected in task2, manufacture the biochar and biochar-based fertilizer in bulk and conduct field tests to confirm their properties and fertilizer effectiveness.

The program involves a total of four units(Fig.2). Hitachi Zosen Corporation, serving as the Japanese responsible party, provides technical support of carbonization and guides the demonstration operation of carbonization equipment. Shenyang Agricultural University, as the Chinese responsible party, manages the project, analyzes and evaluates the biochar and biochar-based fertilizer. CSSC Luzhou Environment Protection (Nanjing) Co. LTD conducts engineering, procurement, construction work and participates in the commissioning. Shenyang Longtai Bioengineering Co. Ltd. produces biochar-based fertilizer with other ingredients such as. Nitrogen and Potassium

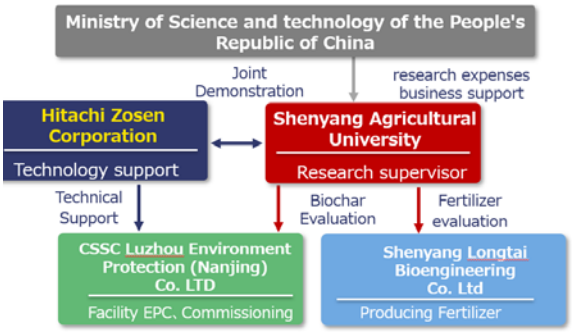

Fig.2 Project Organizational Structure

3. RESULTS AND DISCUSSION

As we officially concluded biochar production in September of this year, subsequent growth tests and field tests are currently ongoing, and experimental data are not yet available. Instead, the results of a domestic demonstration project in Japan where the similar experimental process was carried out will be introduced below.

3.1 Soluble phosphorus

The ease with which phosphorus can be absorbed by the roots of plants is indicated by the water-soluble P_2O_5 (hereafter abbreviated as WP) and the citric acid-soluble P_2O_5 (hereafter abbreviated as CP). Meanwhile, all phosphorus contained in the fertilizer is total P_2O_5 (hereafter abbreviated as TP). The degradation rate (CP/TP x 100) is used as an indicator to consider productivity.

Both the Biochar produced by EFCaR ® System and burned ash from the same hog manure were analyzed to check the TP, WP, CP and CP/TP. The result is shown in the Table1 below.

Table1 Phosphorus leaching properties

Unit (%))

Material	TP	CP	WP	CP/TP
Biochar	10	6.9	0.49	69
Burned ash	22.9	13.3	0.19	58.1

From the Table 1, Biochar had a lower concentration of TP and CP than burned ash, but CP/TP of Biochar is higher than burned ash. The higher phosphate concentration in burned ash compared to biochar is due to differences in the carbon content in the substrates. Unlike biochar, burned ash did not contain organic carbon and thus a higher content of TP was shown. However, the decomposition rate, CP /TP, is over 10% higher in biochar compered to burned ash. This suggests that incineration reduces the amount of soluble phosphoric acid in the raw material and plants can absorb P_2O_5 effectively from biochar compared to burned ash.

3.2 Growth tests

In order to verify the effectiveness of using biochar as a fertilize, Growth tests of Japanese mustard spinach were conducted using a Wagner pot. The experimental method is to apply chemical fertilizer, biochar, and steamed bone meal with the same amount of phosphoric acid, nitrogen, and potassium, respectively.

Japanese mustard spinach's growth results are shown below(Fig3), and it proves that biochar is a viable alternative to not only conventional chemical fertilizers but also steamed bone meal which is known as an animal-based organic fertilizer characterized by its high

phosphoric acid content and long fertilizing effectiveness.

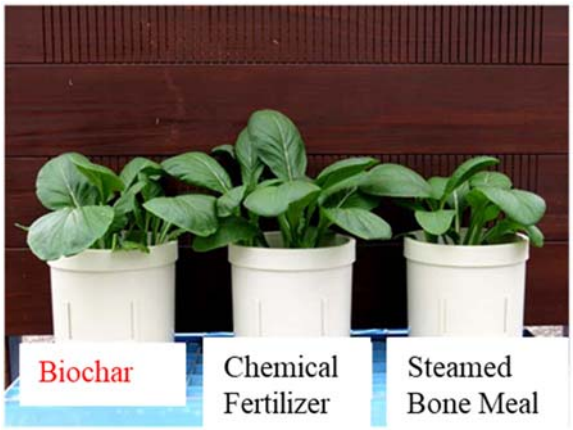

Fig.3 Result of Growth Test

3.3 Field test

With the cooperation of Katakura & Co-op Agri Corporation and Osaka Prefectural Research Institute of Environment, Agriculture and Fisheries, Hitachi Zosen Corporation conducted field tests to study the efficacy of biochar-based fertilizer. Fertilizer for the fields was produced by mixing biochar from pig manure and raw materials (nitrogen and potassium, etc.) The form of the fertilizer was granular for easy-handling. Biochar and other raw materials were blended at a ratio of 1:9 (N:P:K=12:12:12). The fertilizer was applied in cultivation trials of Cabbage (*Brassica oleracea var. capitata*) (Fig.4) and Rice (*Oryza sativa*) (Fig.5) in different regions.

Table2 the result of Cabbage field test

Mixed biochar	Fertilizer Reduction Rate	yield※1		yield
		t/10a	index	standard deviation
0%	-	7.7	100	1.2
5%	-	7.3	95	0.9
10%	-	7.0	92	1.0
10%	5%	7.4	97	1.0
-	-	2.2	28	0.7
average※2		5.1	67	

※1：adjusted weight×Number of plants planted: 2,900 plants/10a

※2： Yield of Ibaraki cabbage in 2014,spring [4)]

As the result shown in the Table2 & Table3, the yield of the area where the fertilizer mixed with the biochar was the same as that of the area where no biochar was applied. Even with a 5% reduction of fertilizer amounts applied, the fertilizer maintained the same effects as conventional fertilizers.

Fig.4 Cabbage just before harvest

Table3 the result of rice field fest

Mixed biochar	Fertilizer Reduction Rate	(milled) brown rice yield		
		kg/10a	index	standard deviation
0%	-	407	100	19
5%	-	349	86	42
10%	-	388	95	26
10%	5%	405	100	22
-	-	339	83	29
average※3		508	125	

※3： of the 2015 harvest (Kinki area average) [5)]

Fig.5 Rice just before harvest

3.4 Antibiotics

Antibiotics are usually used in the piggery to prevent disease and promote growth, which was administrated with feed and injection, remain in manure. There is high possibility to arouse Antibiotic pollution, if the compost produced from the manure was used in the farmland. EFCaR® System succeeded in producing antibiotic-free biochar. In Hitachi Zosen Corporation's antibiotics analysis of biochar showed that the biochar-based fertilizer met the Japanese quality standards.

Pig manure, compost and biochar from the same

source were analyzed to confirm the value of general antibiotics: tetracycline (TC), oxytetracycline (OTC), chlortetracycline (CTC) and doxycycline (DOXY). Each kind of general antibiotics is shown in the Table4. And Sum of individual antibiotics, shown as total tetracycline antibiotics were 24,973 ng/dry-g of the hog manure, 2,117 ng/dry-g of the compost, ND of the biochar. From Table4 Antibiotics in biochar were proved to be completely degraded by EFCaR® system.

Table 4 Analysis results of antibiotics[6)]

Unit (ng/dry-g)

Material	TC	OTC	CTC	DOXY	TOTAL
Pig manure	880	93	12,000	12,000	24,973
Compost	67	180	900	970	2,117
Biochar	ND	ND	ND	ND	ND

4. FUTURE OUTLOOK

On September 22th, 2020, Chinese President Xi Jinping announced at the 75th session of the United Nations General Assembly that China is striving to peak its greenhouse gas emissions by 2030 and become climate neutral by 2060. In response to President Xi Jinping's statement, in August 2022 China's Ministry of Science and Technology, the National Development and Reform Commission and nine other authorities issued the *Implementation Plan for Science and Technology to Support Carbon Peak and Carbon Neutrality (2022-2030)*,which co-ordinates scientific and technological innovation actions to support the realization of carbon peak by 2030. China now is demonstrating an increased determination to a profound low-carbon transformation of its economy and society. One of the best examples is that China launched its national emissions trading system (ETS), on 16 July 2021, which so far covers only one sector: power generation.

While not so long ago in May 2019, Improved IPCC Guidelines were approved at the 49th Session of the Intergovernmental Panel on Climate Change (IPCC), in which add a method for calculating carbon stocks associated with biochar inputs to agricultural and grassland soils. The reason was that the carbon C bonds making up biochar are strong and not easily decomposed by soil microorganisms, which can remain in the agricultural land for more than 100 year. And the next year, 2020, biochar was recognized by the Japanese government's J-Credit System as an effective method of long-period carbon sequestration in the soil. It is calculated that 1 ton of biochar can store 905 kg of carbon dioxide. J-Credit Scheme is designed to certify the amount of greenhouse gas emissions reduced and removed by sinks within Japan. It is said that Chinese government is now preparing the national standard related to biochar manufacturing, and we have reason to believe that biochar will be included in the China's national emissions trading system in the near future.

5. CONCLUSION

The biorchar made by EFCaR® System developed by Hitachi Zosen Corporation has already been proven to be effective in the aspects below. It has a higher solubility than burning ash and it is a viable alternative to both chemical fertilizers and steamed bone meal. In the field test, replacing chemical fertilizers with a portion of biochar can cut down on some of the chemical fertilizers while maintaining their effectiveness. Furthermore, antibiotics in biochar were completely degraded. The same results could be expected in the undergoing Ministry of Science and Technology China/Japan Cooperation Research Project. While promoting EFCAR® equipment in China, Hitachi Zosen is working with project partners Shenyang Agricultural University and CSSC Luzhou Environment Protection (Nanjing) Co. LTD to accelerate the development of standards for biochar production and facilitate the entry of biochar into China's national emissions trading system.

References

1) O. Gantner, W. Schipper and J. J. Weigand, in *Sustainable Phosphorus Management*, ed. R. W. Scholz, A. H. Roy, F. S. Brand, D. T. Hellums and A. E. Ulrich, Springer, Dordrecht, 2014, pp. 237–242
2) S. J. van Kauwenbergh, World Phosphate Rock Reserves and Resources, 2010.
3) Kiyonori HAGA, Effective use of livestock wastes as phosphorus resources, *Journal of Arid Land Studies*32-4, 149-155 (2023)
4) w-Stat Portal Site of Official Statistics of Japan, http://www.e-stat.go.jp/SG1/estat/List.do?lid=000001141603
5) Ministry of Agriculture, Forestry and Fisheries http://www.maff.go.jp/j/tokei/kouhyou/sakumotu/sakkyou_kome/pdf/syukaku_suiriku_15.pdf
6) Kozo Ueda, Energy-Effective Carbonization Technology, *Phosphorus Recovery and Recycling*, Chapter 25
7) Ministry of Agriculture, Forestry and Fisheries, Environmental Policy Office, *Methodology for the application of biochar to agricultural land* https://www.maff.go.jp/j/kanbo/kankyo/seisaku/climate/forum/attach/pdf/biochar-1.pdf

ENHANCEMENT OF ANAEROBIC DIGESTION FROM FOOD WASTE VIA INERT SUBSTANCES BASED ON METAGENOMIC ANALYSIS: OXIDATIVE PHOSPHORYLATION AND METABOLISM

Xiupeng Jiang [a], Zongsheng Li [a], Kunsen Lin [a], Youcai Zhao [a,c], Lianghu Su [b], Tong Wu [d], Tao Zhou [a,c*]

[a] *The State Key Laboratory of Pollution Control and Resource Reuse, School of Environmental Science and Engineering, Tongji University, 1239 Siping Road, Shanghai 200092, China*

[b] *Nanjing Institute of Environmental Sciences, Ministry of Ecology and Environment, 8 Jiangwangmiao Street, Nanjing 210042, P.R. China*

[c] *Shanghai Institute of Pollution Control and Ecological Security, 1515 North Zhongshan Rd. (No. 2), Shanghai 200092, PR China*

[d] *School of Chemical Science and Engineering, Tongji University, 1239 Siping Road, Shanghai 200092, China*

Abstract: The application of anaerobic digestion (AD) in the treatment of food waste (FW) has become widespread. However, the presence of inert substances, such as bones, ceramics, and shells, within FW introduces a degree of uncertainty into the AD process. To clarify this intricate issue, this study conducted an in-depth investigation into the influence of inert substances on AD. The results revealed that when inert substances were present at a concentration of 0.08 g/g VSS, methane productivity in the AD process was significantly augmented by 86%. Subsequent investigations suggested that this positive effect was primarily evident in various biochemical processes, including solubilization, hydrolysis acidification, methanogenesis, and the accumulation of extracellular polymeric substances. Metagenomic analysis showed that inert substances enhance the relative abundance of hydrolytic bacteria and have a pronounced impact on hydrogenotrophic methanogens (*Methanosarcina*) and acetotrophic methanogens (*Methanobacterium*). Additionally, inert substances significantly increased the relative abundance of functional genes in oxidative phosphorylation, a pivotal pathway for ATP synthesis. Furthermore, inert substances had a substantial effect on the functional genes related to the metabolic pathways associated with methanogenesis (both hydrogenotrophic and acetotrophic). This comprehensive study sheds light on the substantial impact of inert substances on the AD of food waste, contributing to an enhanced understanding of the underlying mechanisms of anaerobic fermentation.
Keywords: Food Waste; Methane Production; Inert Substances; Microbial Community; Metabolic Pathways

1 INTRODUCTION

The annual generation of municipal solid waste in China is consistently increasing at a rate of 5-7%, in which food waste (FW) constitutes approximately 50~60% (Wang et al., 2016; Du et al., 2021; Meng et al., 2022; Sailer et al., 2022). The FW amount in Asia was expected to significantly increase to 4.16 billion tons by 2025 (Wang et al., 2021; Ren et al., 2018). If not adequately treated during the collection, transportation, and storage processes, FW will seriously pollute the air, water, and soil, which would pose threat to the sustainable development and realization of the strategic objectives of "Carbon Peak and Carbon Neutralization" (Tang et al., 2019). It is urgent to find the suitable way to treat FW.

Anaerobic fermentation was considered as an effective method for the FW treatment. It can degrade carbohydrates and other organic wastes, simultaneously, convert them into valuable products such as volatile fatty acids (VFAs), hydrogen and methane (Alvarado et al., 2022; Bu et al., 2022; Luo et al., 2022; Wang et al., 2019), which has advantages in energy saving and low secondary pollution, and possesses immense market potential based on the current development of carbon neutral society. Among them, methane, an environmentally-friendly and high-quality energy, is being vigorously promoted by the government (Qin et al., 2022; Luo et al., 2020). Meanwhile, the popularization of methane plays an essential role in the improvement of regional energy structure and sustainable development (Liu et al., 2020; Reshmy et al., 2021a, Ren et al., 2022; Valenca et al., 2021). Thus, anaerobic digestion (AD) is a great potential method for resource treatment of FW.

However, FW is usually mixed with inert substances, like bones, shells and ceramics, which are typical inert substances commonly present and have a high content in FW (Zhang et al., 2022; Morris et al., 2020). They would be broken in the main pretreatment process of AD engineering, and then enter into the AD system. Researches on anaerobic digestion of FW until now mainly focused on the influence of operating conditions and pretreatment methods, such as ultrasound and microwave (Yue et al., 2021); hydrothermal and ionizing radiation (Fei et al., 2022); biochar and race metals (Deena et al., 2022); temperature and moisture content (Wainaina et al., 2019; Wang et al., 2021); The impacts of multiple inert substances on anaerobic digestion of FW, and its potential mechanism based on metagenome (especially microbial community characteristics and metabolic pathway) remain unclear. It was worthy noted that the main components of bones and shells are $CaCO_3$ and $Ca_3(PO_4)_2$, while SiO_2 take greatest account to ceramic's compositions. The presence of these inert substances introduces a degree of uncertainty regarding the AD of FW. On the one hand, Chen et al compared the effects of different alkalinity sources (including eggshell waste containing $CaCO_3$) on methane production in the process of AD, and proposed that the presence of eggshell has a positive impact on pH adjustment (Chen et al., 2015). It was pointed out that the presence of $CaCO_3$ can alleviate the acidity in the anaerobic fermentation system (Luo et al., 2020). Trace elements such as Ca^{2+} are essential nutrients for the normal metabolism of microorganisms (Sanjaya et al., 2021). On the other hand, Wang et al found that low concentrations of CaO_2 which contains calcium had no significant effect on hydrolysis and acid producing microorganisms, but had a significant inhibitory effect on methanogens (Wang et al., 2019).

Therefore, this study aims to discuss the effect of the typical inert substances (bones, ceramics and shells) on AD of FW and clarify its influence mechanism. To be exactly, the impact of inert substances on each stage of AD was comprehensively analyzed, and the changes of microbial population characteristics and related enzyme activities were revealed in the presence of inert substances. In addition, metagenome was also employed

to further reveal its influence on microbial functions and metabolic pathways in the AD. This study was expected to provide data and theoretical support for optimizing the AD performance of FW in the project and a new and alternative idea for exploring the mechanisms of the role of complex and difficult to be degraded substances in the process of AD.

2 MATERIALS AND METHODS

2.1 Characteristics of FW, inert substances and WAS inoculums

According to the composition analysis of FW produced by the canteen, rice, green vegetables, noodles and eggs were selected to simulate FW, which were then crushed into pulp for further utilization. The final characteristics of simulate FW are shown in Table 1. Waste activated sludge used for inoculation mainly was obtained from the secondary sedimentation tank of a municipal wastewater treatment plant in Shanghai, China, and its main characteristics are shown in Table 1.

Table 1 Characteristics of FW and WAS

Parameter	FW	WAS
pH	6.6±0.2	6.8±0.2
Total suspended solid (TSS)	68.2±1.7 g/L	37.9±1.6 g/L
Volatile suspended solid (VSS)	66.8±1.1 g/L	20.1±1.4 g/L
Total COD (TCOD)	95.7±1.8 g/L	31.2±1.6 g/L
Soluble COD (SCOD)	9.2±1.2 g/L	0.32 g/L

Inert substances (bones, ceramics and shells) were purchased from a vegetable market in Shanghai. Bone was cooked, and then removed external meat, fat and internal bone marrow. Shells were taken from oysters cooked without meat, and ceramic was a bowl. Bones and shells treated were washed many times and dried in the oven. All the inert substances were broken to less than 1mm respectively, and then they were mixed in a certain proportion as the object of this study. According to Table S1, Table S2, Table S3 and Fig. S1, its main components are $CaCO_3$, SiO_2, $Ca_{10}(OH)_2(PO_4)_6$. Due to the low VSS/TSS (0.05 ± 0.01), the content of organic matter in inert substances can be ignored compared with that in FW.

2.2 Experiments evaluating the effect of inert substances on anaerobic digestion

Reactors in this experiment were 250 mL glass serum bottles, in which 150 mL mixture of FW and WAS were added (the ratio of sludge VSS / FW VSS was 10%). Six levels of inert substances (0 (control), 0.05, 0.1, 0.2, 0.5 and 1 g) were dosed into each reactor, respectively. Then, the dose of the inert substances in each reactor was respectively 0, 0.02, 0.04, 0.08, 0.2 and 0.4 g/gVS FW. The acid-base reagent was adopted to adjust the pH of the reactors to 7.0, and then 99.98% nitrogen was blown for 2 min to discharge the air and sealed with rubber stoppers to ensure an anaerobic environment. The testes were operated in an air bath shaker (37 °C, 175 rpm) for anaerobic digestion at pH 7.0. The yield of methane in reactors was determined every two days to explore the impact of inert substances on anaerobic digestion of FW. After the phenomenon was stable, 50 mL samples were withdrawn and stored immediately in the -80 ℃ refrigerator for further microbial and metagenomic analysis. Simultaneously, the remaining samples in the reactors were used for other mechanism studies (eg: enzyme activities, synthetic water, EPS, etc.).

2.3 Effects of inert substances on each stage during anaerobic digestion

Under the condition of pH 7.0, solubilization, hydrolysis, acidification, and methanogenesis were contained during FW anaerobic fermentation for methane. Mixed FW samples were taken from the reactors after stable operation to centrifugate, and supernatant was used to determine concentrations of soluble protein and carbohydrates in order to explain the effect of inert substances on solubilization.

The hydrolysis of anaerobic fermentation from reactors with inert substances was explored by measuring the hydrolysis efficiency of synthetic wastewater, which consisted of 1.5 g bovine serum albumin (BSA, Mw 67,000), 2 g dextran (Mw 23,800), 135 mL tap water and 15 mL FW fermentation broth as inoculum. Besides, the pH was adjusted to 7.0, and the temperature was set to 37℃. Samples were taken from the synthetic wastewater of every reactor to determine the concentration of BSA and dextran daily. The hydrolysis efficiencies of BSA and dextran were expressed by the following Equation (2-1):

$$\text{Hydrolysis efficiency (\%)} = (C_0\text{-}C)/C_0 \times 100\% \quad (2\text{-}1)$$

Where C_0 and C represent the initial and residual concentrations (mg/L), respectively.

The experimental design for the investigation of inert substances' effect on the acidification of sludge fermentation was similar to the above hydrolysis except for the substrate, which was replaced by 1.5 g L-glutamate and 2 g glucose, and then VFAs concentration in reactors was determined daily.

Methanogenesis was divided into two types which include acetic acid as substrate and hydrogen and carbon

dioxide as substrate. Due to different substrates used, this study explored the influence of inert substances from two aspects. Acetic acid as substrate: mixed fermentation broth was transferred to a 250 mL serum bottle containing 0.72 g sodium acetate, 135 mL tap water and 15 mL FW fermentation broth from reactors as inoculum. After nitrogen blowing and sealing, reactors were placed into an air-bath shaker at 150 rpm and 37 °C. Samples were taken daily to determine methane, and pH was adjusted to maintain at 7.0. Carbon dioxide as substrate: the experimental design for the investigation was the same as above, except that the substrates were replaced by 80 % hydrogen and 20 % carbon dioxide. Methane production was measured to explore the effect of inert substances on methanogenesis.

2.4 Analytical methods

The methods of TSS, VSS, TCOD, SCOD, protein, carbohydrate, VFAs and activities of key enzymes adopted the previously published (Federation et al., 2005; Jiang et al., 2021; Xiao et al., 2013). The concentration of extracellular polymeric substances (EPS) was determined by Wang et al (Wang et al., 2009), and the extraction method of ESP was shown in the supplementary material. Samples were taken from the reactors and sent to the biological company to determine the activity of related enzymes. 50 mL samples were withdrawn from FW reactors and rapidly quick-frozen with liquid nitrogen. Then treated samples were transported to Majorbio laboratory (Shanghai) in dry ice for metagenomic analysis. The detailed description of metagenome was shown in supplementary materials.

3 RESULTS AND DISCUSSION

3.1 Performance of methane production stimulated by inert substances

The data in Fig. 1 a) showed changes in methane production in different reactors within 26 days when the concentrations of inert substances were 0-0.4 g/g VSS FW (0-1g). Obviously, inert substances have a positive impact on methane production with the concentration range of 0.02-0.2 g/g VSS FW. When the concentration was 0.02-0.2 g/g VSS FW, the promotion of inert substances on the methane production gradually enhanced with the increase of concentration, and the methane production was 130.0-199.2 mL/g VSS, especially with a concentration of 0.08 g/g VSS FW, the performance of food waste AD was markedly improved, and the methane production in the reactor was 199.2 mL/g VSS, which was 1.9 times that of control (106.8 mL/g VSS). However, when the concentration was more than 0.08 g/g VSS FW, the positive effect began to weaken, and it showed a weak inhibitory effect with the concentration of 0.4 g/g VSS FW. It was speculated that because the components of these inert substances were mainly inorganic substances, their high content would lead to the low VSS/TSS in the reactors, thus inhibiting microorganisms from using limited organic substances in the anaerobic system. Therefore, samples in reactors with a concentration of 0.08 g/g VSS FW and control were selected for further mechanism studies, which were defined as inert substances and control. In summary, AD of FW was significantly enhanced with the concentration of inert substances in a certain range.

AD of FW mainly includes solubilization, hydrolysis acidification and methanogenesis (Fig. 1 b)). Usually, solubilization of FW is a physical process without the direct participation of microorganisms, while hydrolysis, acidification and methanogenesis are all directly participated by microorganisms, which mainly play an important role in the fermentation system through their enzymes with specific functions (Jiang et al., 2020). Due to microorganisms producing methane in the reactor being too active, substrate accumulated in the acidification was also used by inoculated microorganisms for methane, resulting in the depletion of the acid accumulated in the acidification. Therefore, the accurate effect of inert substances on acidification was analyzed by measuring the activity of enzymes related to acid production in this experiment. The data in Fig. 1 c) revealed that proteins and carbohydrates in the solubilization were apparently affected by inert substances. The concentration of proteins and carbohydrates in control were 337.2 mg/L and 79.9 mg/L respectively, while 417.0 mg/L and 92.6 mg/L in reactors with inert substances, which were both 1.2 folds of control, indicating that inert substances improved solubilization AD of FW. Due to the existence of inert substances, more shear forces were generated, which accelerated the destruction of EPS, thus dissolving many macromolecular organics, such as carbohydrates and proteins. Hence, it can be estimated that the improvement of inert substances on CH_4 production can be achieved by promoting the solubilization of FW.

Hydrolysis is regarded as the rate-limiting step of anaerobic fermentation (Luo et al., 2016). As shown in Fig. 1 c), there was no significant difference in the hydrolysis efficiency of BSA between the inert material and control (50.1% versus 47.5%), while the hydrolysis efficiency of dextran in the reactors with inert substances was 66.7%, which was 1.2 times that of control (57.0%). Furthermore, it can be seen from Fig. 1 f), the activities of α-glucosidase and protease in control were 182.4 and 45.4 U/ug protein, respectively, while 225.2 and 49.1 U/ug protein in the presence of inert substances, which were 1.2 times and 1.1 times of that in control respectively. It is universally known that protease and α-glucosidase hydrolysis stage are two essential hydrolases in hydrolysis (Xie et al., 2019), the improvement of the activities of which can improve

hydrolysis. In summary, inert substances promoted the hydrolysis of carbohydrates and proteins in FW, thus providing more intermediates for subsequent methane production.

Small molecular organics such as glucose and amino acids were transported inside through the cell membrane, and converted into VFAs by complex enzymes system in the cell, which are the substrates for methane. Meanwhile, the activities of acetate kinase (AK) and phosphotransacetylase (PTA), which are the key enzymes of decarboxylation of pyruvate to acetic acid (Jiang et al., 2021), were 61.3 and 56.0 U/ug protein in the reactors with inert substances, which were improved compared with control (57.2 and 46.4 U/ug protein). It can be concluded that inert substances can significantly promote the acidification of AD of FW.

Methanogenesis mainly contains two metabolic pathways for methane production from FW: acetic acid trophic pathway (decarboxylation of acetic acid into methane and CO_2) and hydrogen trophic pathway (H_2 and CO_2 as substrates to synthesize methane through oxidation-reduction). The data in Fig. 1 d) and Fig. 1 e) indicated that inert substances markedly enhanced methanogenesis both in the acetic acid trophic pathway and the hydrogen trophic pathway. When sodium acetate was used as the substrate, the production of methane in the reactors with inert substances (0.07 mL-50.9 mL) was much higher than that in the control (0.02 mL-34.3 mL). Simultaneously, when H_2/CO_2 was used as the substrate, the production of methane in the presence of inert substances (0.9 mL-8.8 mL) was also increased compared with the control (0 mL-3.5 mL). Moreover, it was found that the activity of F_{420}, a specific enzyme in methanogens, in the reactors with inert substances and control were 11.4 U/ug and 9.5 U/ug protein, which indicated that inert substances have a positive effect on the production of methane.

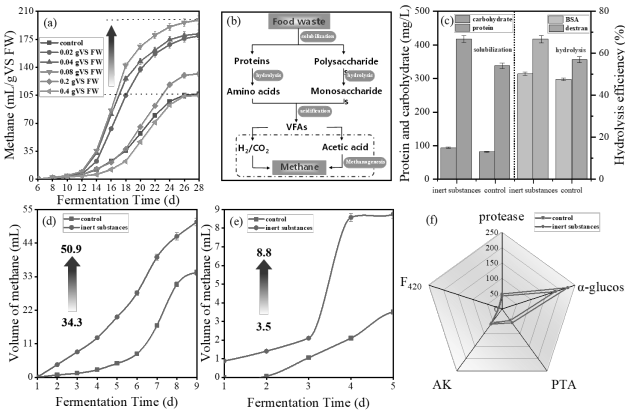

Fig. 1 Improvement of methane production, solubilization, hydrolysis, acidification, and methanogenesis in FW fermentation reactors with different concentration of inert substances

3.2 Responses of EPS to the presence of inert substances

The main components of EPS in FW are protein and carbohydrate, which are essential for the growth and metabolism of microorganisms and the integrity of cell structure (Basuvaraj et al., 2015; Van Dierdonck et al., 2012). Besides, EPS can protect microorganisms from external damage and be substrates for methane fermentation. In this study, three-dimensional excitation-emission matrix fluorescence spectroscopy (EEM) was used to characterize the effects of inert substances on LB-EPS and TB-EPS in the fermentation broth, which was shown in Fig. 2. It can be seen from the figure that EPS extracted from reactors mainly has a same characteristic fluorescence peak (Peak A), the Ex and Em wavelengths of which were 250-300 nm and 300-375 nm, respectively. According to previous studies, Ex and Em wavelengths of peaks at 270-290 nm and 320-370 nm, respectively, belonged to proteins such as tryptophan and tyrosine (Leenheer & Croue, 2003; Zeng et al., 2021). Obviously, characteristic peaks of LB-EPS and TB-EPS with inert substances had higher fluorescence intensity compared with control, indicating that the presence of inert substances promoted the release of organic substances from FW and increased the content of protein in EPS. It is worth noting that when Ex/Em was (375-425 nm) / (450-500 nm), there was an obvious characteristic fluorescence peak (Peak B) of LB-EPS (Fig. 2 b)) in the existence of inert substances. It is recorded that peaks at Ex and Em wavelengths of 250-450 and 380-550 nm, respectively, were related to humic acid (Chen et al., 2003).

Furthermore, carbohydrate content in EPS was presented in Fig. S2, which were 23.1 and 28.9 mg/L in LB-EPS and TB-EPS with inert substances respectively, while were 22.3 and 25.4mg/L respectively in control, indicating that inert substances had no significant effect on the carbohydrate concentration in EPS. In conclusion, the presence of inert substances improved the concentration of protein in EPS, which can provide more substrates for methane production. In addition, studies have shown that microorganisms can produce more TB-EPS in a comfortable environment (Ye et al., 2011), implying that methanogens survive in a relatively comfortable environment in the presence of inert substances, which was more conducive to microbial methane production.

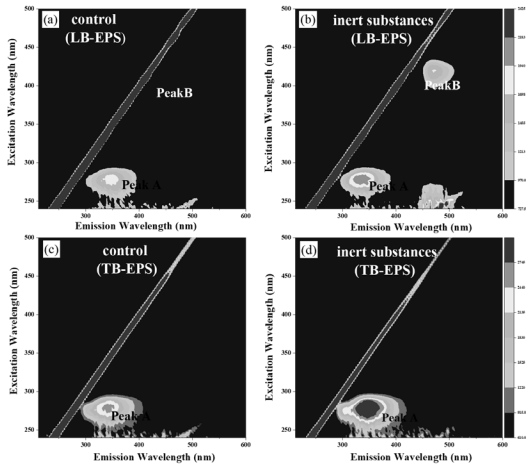

Fig. 2 Effects of inert substances on EEM fluorescence spectra of LB-EPS and TB-EPS

3.3 Changes of microbial community with inert substances

It is reported that AD is a very complex process related to different microbial consortia (archaea and bacteria), including solubilization, hydrolysis acidification and methanogenesis. Organic substances in FW were degraded in the phase of microbial growth and metabolism, during which CH_4 was produced. Hence, changes in microbial population distribution at the phylum-level, order-level and genus-level were mainly analyzed to discover the internal reason for the improvement of AD biotransformation performance caused by inert substances in this study.

As shown in Fig. 3 a) and Table S4, both in inert substances reactor and control, the dominant bacteria in the anaerobic fermentation system are *Firmicutes*, *Euryarchaeota*, *Bacteroidetes*, *Proteobacteria*, *Actinobacteria*, *Tenerictes*, *Chloroflex*, accounting for more than 90% of all microbial consortia. It was reported that microorganisms contained in these phyla generally exist in the AD system, which can degrade organic matter (Mamindlapelli et al., 2022). *Firmicutes*, which accounted for the most significant proportion, was reported to participate in the hydrolysis of complex organic substances such as lipids, proteins and carbohydrates (Zhou et al., 2020). The relative abundance of *Firmicutes* in the reactor with inert substances was much higher than that in the control (49.8% versus 43.7%), which improved the hydrolysis efficiency of organic matter and provided sufficient intermediate products for methane production. It is more noteworthy that the relative abundance of *Euryarchaeota* in the inert substance reactor was significantly higher than that in control, reaching 2.8 times (25.0% versus 8.9%). Previous studies have shown that microorganisms in this phylum are mainly involved in methane production (Magdalena et al., 2021), and its increase directly improved the accumulation of methane. *Proteobacteria*, which utilize acetic acid to grow normally (Lu et al., 2012), decreased in abundance from 17.7% in control to 5.7% with inert substances, contributing to the accumulation of acetic acid. It is reported that acetic acid is the substrate for microbial decarboxylation reaction to produce methane, which is an important metabolic pathway for methane production by anaerobic fermentation. Meanwhile, *Tenericutes* were also significantly enriched in the reactor with inert substances (5.1%), which was 10 times that of the control (0.5%). It was reported that many microbes in *Tenericutes* have the ability to ferment glucose and other sugars into acid (Braz et al., 2018). Therefore, the enrichment of this phylum was conducive to acid accumulation and finally strengthened anaerobic fermentation for methane production.

Further analysis was conducted at the order-level (Fig. 3 b)) and Table S5). The relative abundances of *Methanosarcinales*, *Methanobacteriales*, and *Methanomicrobiales* belonging to Archaea were all increased with inert substances compared with control (20.9%, 1.2%, 1.7%, versus 5.3%, 1.1%, 0.3%), which include important methanogens in the fermentation system (Cai et al., 2022). Moreover, *Methanosarcinales* can not only take up acetic acid, but also H_2/CO_2 and methyl compounds to synthesize methane (Shin et al., 2010). Besides, the relative abundances of *Bacillales* and *Acholeplasmatales* belonging to *Firmicutes* and *Tenerictes*, respectively were also higher than those of control (1.9% and 4.6% versus 1.1% and 0.2%. As mentioned above, microbial consortia in these phyla are advantageous to the degradation of organic matter and acid production during fermentation, which can provide more intermediates for methane production.

Finally, the microbiome was identified at the genus level to explore the enhancement of inert substances on AD (Fig. 3 c) and Table S6). In the presence of inert substances, methanogens that use acetic acid, H_2/CO_2 or methylamine and formic acid to produce methane also had apparent changes. The percentage of *Methanosarcina* was found a threefold increase with inert substances (from 5.3% to 20.8%), which was reported to produce methane using H_2/CO_2, methyl compounds or acetic acid (Magdalena et al., 2021; Liu et al., 2021). Furthermore, *Methanobacterium* which was considered as strict hydro-genetic methanogen in the existence of inert substances, was significantly higher than that of control (Liu et al., 2021). What's more, the relative abundance of unclassified_p__*Firmicutes* with inert substances was raised from 19.4% to 5.0% compared to control, which contains hydrolysis bacteria.

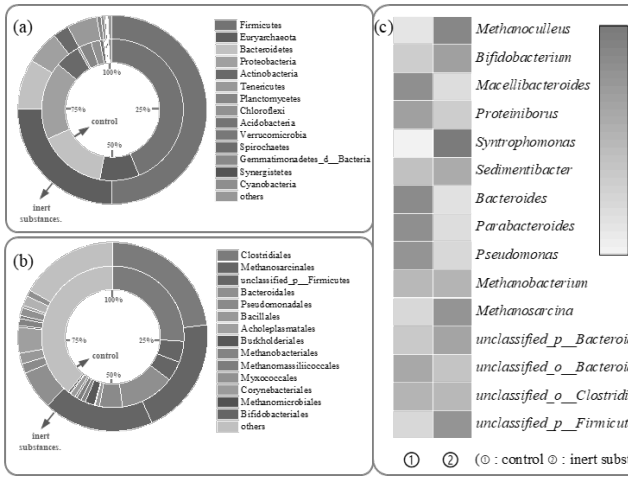

Fig. 3 Influence of inert substances on microbial community structure at phylum (a), order (b), genus (c) levels based on metagenomics analysis

3.4 Enhancement of metabolic functions of microbial community by inert substances

According to the above analysis, inert substances significantly impacted on the microbial community, which have different functions in the fermentation system, and cooperate to produce methane. This study applied metagenomics sequencing technology to explore changes in microbial functions and metabolic pathways based on KEGG databases. Fig. S3 shows the difference analysis from pathway level 3. In the presence of inert substances, the relative abundance of metabolic pathways, glycolysis/gluconeogenesis, methane metabolism, pyruvate metabolism, butanoate metabolism, oxidative phosphorylation and aminoacyl-tRNA biosynthesis was significantly higher than that of control, which led to the enhancement of methane production. As mentioned above, the production of methane by anaerobic fermentation of microorganisms was mainly through the enzymes with specific functions in their cells in the fermentation system. Therefore, further analysis about the influence of inert substances was conducted in terms of the changes of enzymes in these pathways.

3.4.1 Oxidative phosphorylation (ATP biosynthesis):

Oxidative phosphorylation is an important pathway of ATP synthesis. According to the above analysis, oxidative phosphorylation was evidently enhanced in the presence of inert substances, which indicated that ATP synthesis was enhanced. ATP widely exists in all microorganisms and performs an important role in cell metabolism and various biochemical reactions requiring energy supply. As shown in Fig. 4 a), oxidative phosphorylation for synthesis of ATP mainly includes five parts. It can be seen from Fig. 4 b) and Fig. S4 that except for complex II, the other four parts were all improved in the presence of inert substances. Complex I: the relative abundance of the three NADH dehydrogenases (*ND*, *NDUFS8*, *nuoEFG*) in the inert substances reaction system was significantly higher than that in control, which can catalyze the oxidation of NADH, transfer electrons to CoQ, and pump out H^+ into membrane space. Complex III: both *MQCRB* and *MQCRC* belong to cytochrome c reductase complex, which was both an electron transporter and a proton translocator catalyzing the transfer of electrons from CoQ to cytochrome c and concurrently pumped out H^+ into membrane space. Complex IV: in the presence of inert substances, the relative abundance of *COX1*, *COX2*, *ccoNO* and *cydB* was remarkablly up-regulated, which promoted the synthesis of H_2O and the release of H^+ into the membrane space. Complex V: this part, a key step of ATP synthesis, was the most obviously up-regulated part affected by inert substances. It can be seen from the figure that the abundances of most ATP synthetases (*ATPF1ABEG*, *ATPF0ABC*, *ATPeF0A*, *ATPVABCDEFIK*, *PMA1*, *ppa*) were significantly increased, which directly promoted the biosynthesis of ATP, while the improvement of ATP production was conducive to promoting the production of methane by anaerobic fermentation of microorganisms.

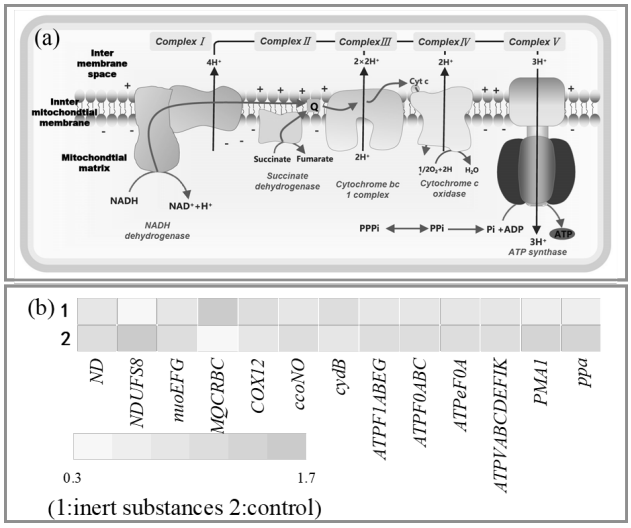

Fig. 4 Significant improvement of enzymes in the metabolic pathway of oxidative phosphorylation(a) and relative abundance of improved functional gene (b) in the presence of inert substances.

3.4.2 Substrate metabolism and methane biosynthesis:

Acetic acid trophic pathway (Fig. 5:

decarboxylation of acetic acid to produce methane and CO_2) and hydrogen trophic pathway (Fig. 6 a)): H_2 and CO_2 are used as substrates to synthesize methane through redox) were mainly analyzed in this study.As shown in Fig. 5 a), the red background during metabolism indicated the related enzymes were up-regulated in the presence of inert substances. Firstly, glucose was transported into the cell membrane, and glucose-6 phosphate was generated under the action of glucokinase (*pfkc*). It can be seen from Fig. 5 b) and Fig. S5 that in the presence of inert substances, the relative abundance of *pfkc* was 0.7898%, 1.7 times that of the control (0.4642%). Glucose-6 phosphate generates pyruvate through Embden-Meyerhof Pathway (EMP), which provided more substrates for pyruvate metabolism to produce acetic acid. It can be seen from the figure that the metabolism of pyruvate to produce acetic acid mainly included 7 ways. Affected by inert substances, the relative abundances of enzymes involved in these pathways had an obvious upward trend. The specific analysis was as follows. As an acetaldehyde dehydrogenase, *adhE* acts on the aldehyde or carbonyl group of the donor and takes NAD^+ or $NADP^+$ as the acceptor. It is related to the conversion of acetyl CoA to acetaldehyde, whose upregulation increased the acetaldehyde yield in the inert substance system. *PorA*, *porB*, *porC* and *porD*, pyruvate ferredoxin oxidoreductase, can directly convert pyruvate to acetyl CoA with iron-sulfur protein as the receptor, and their relative abundance was obviously increased in the inert substance system. *PoxL* is a pyruvate oxidase, which can convert pyruvate into phosphoric acid, and its relative abundance with inert substance was 0.3785%, which was 3.8 times that of the control (0.0999%). *AcdB* is related to the conversion of acetyl CoA to acetic acid and the synthesis of ADP. The relative abundance of *acdB* in the inert substance system and control was 0.2575% and 0.1537%, respectively. *AckA* (acetic acid kinase) is a phosphotransferase with a carboxyl group as its receptor. Acyp is an acyl phosphatase. The upregulation of these two enzymes improved the yield of acetic acid synthesized by acetyl phosphate. In the butanoate metabolism, *atoA* and *atoD* are both coenzyme A transferases, which are important for the conversion of butyric acid to butyryl CoA; *ptb* is a phosphate butyryl transferase; *crt* is a carbon-oxygen lyase; these enzymes are related to the conversion of butyric acid to acetyl coenzyme, and their relative abundance in the presence of inert substances was significantly higher than that in control. *CdhC*, *cdhD* and *cdhE* are acetyl CoA decarboxylases, and their relative abundances in the inert substances system and control were 0.01898%, 0.0114%, 0.0244% and 0.0035%, 0.0080% and 0.0107%, respectively, which are higher than those in control. *MtrABCDEFGH* belong to tetrahydromethanopterin S-methyltransferase and are related to the synthesis of methyl coenzyme A, whose total relative abundance was 0.1550% with inert substances, higher than that in control (0.04949%). Both *fdhA* and *fdhB* belong to formate dehydrogenase and act on CH or CH_2 group and sulfur group donors; *hdrA1B1C1A2B2C2DE* belongs to reductase, which acts on the sulfur group donor with ferrithioprotein as the receptor, and their relative abundance was higher than that of control in the presence of inert substances. *McrABDG* belongs to methyl coenzyme M reductase and can synthesize methyl coenzyme into methane. The total relative abundance of *McrABDG* was higher than that of control (0.2237% versus 0.0944%) in the presence of inert substances, which was conducive to improving methane production. In conclusion, the increase in the abundance of the enzymes as mentioned above promoted acetic acid trophic methanogenesis, ultimately leading to the improvement in the total production of methane.

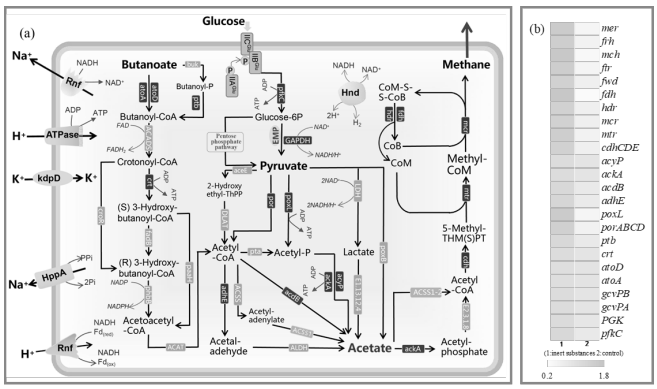

Fig. 5 Significant improvement of enzymes in the acetic acid trophic pathway(a)and relative abundance of improved functional gene (b) in the presence of inert substances (red background indicates improvement enzymes).

Fig. 6 a) showed the methane production pathway with CO_2 as substrate involved in the upregulated pathway. The increased abundance of *pfkC*, *mtr*, *mcr*, *fdh* and *hdr* belong to the enzymes involved in the public pathway in the methanogenesis, which had been analyzed in detail in the mentioned acetic acid trophic methanogenesis. *PGK* is a phosphoglycerate kinase related to the conversion of glucose to pyruvate, which can transfer phosphate groups with the carboxyl group as the receptor and is a related enzyme. *GcvPA* and *gcvPB* belong to glycine dehydrogenase, which generates CO_2 with disulfide as the acceptor. Their relative abundance in the presence of inert substances was 1.3 times that of the control and their upregulation can increase the production of CO_2 and ultimately led to the improvement of methane production (Fig. 5 b) and Fig. S5). *Fwd* is a formylmethanofuran dehydrogenase, which acts on the aldehyde or carbonyl group with iron-

sulfur protein as the receptor to generate formylmethanofuran; *ftr* belongs to acyltransferases; *mch* belongs to methenyl tetrahydromethanopterin cyclohydrolase; *mer* belongs to reductase; The improvement of these enzymes improved the yield of intermediate products during the conversion of CO_2 to methane. *Frh* is important for the relevant conversion between F420 and $F420H_2$, which is coenzyme F420 oxidoreductase. When inert substances were present, the abundance of *frh* was improved (0.1154% versus 0.03793%). The changes in these enzymes eventually led to the increase of methane accumulation.

As is known to all, the microbial reducing power which was usually manifested by the mutual conversion of two forms of nicotinamide adenine dinucleotide (reduced NADH and oxidized NAD^+) was closely related to substrate metabolism and methanogenesis, especially in carbon source metabolism. As shown in Fig. 6 b-c), in the presence of inert substances, the content of NADH and NADH/NAD^+ in the microorganism were significantly increased, and the content of NAD^+ was significantly decreased, which indicated that extensive NAD^+ was reduced to NADH. Besides, NADH was further oxidized to release electrons and transferred to intracellular energy storage materials or methanogenic activities in the organic matter metabolism and methanogenesis. What's more, NADH performed a direct role in providing hydrogen in the production of methane.

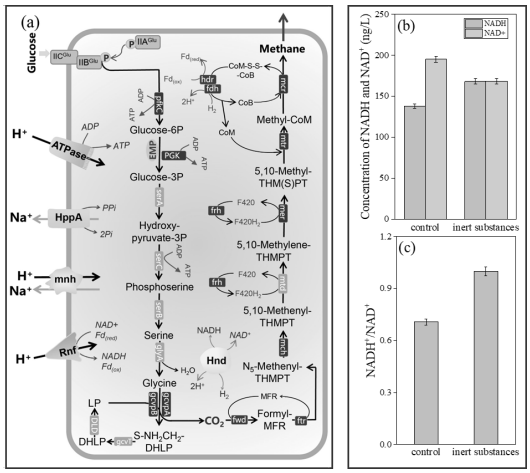

Fig. 6 Significant improvement of enzymes in the hydrogen trophic pathway(a), changes between NADH and NAD^+ (b-c) in the presence of inert substances (red background indicates improved enzymes).

4 CONCLUSION

In this study, inert substances were found to show a positive effect on methane production during anaerobic fermentation of FW, and enhanced fermentation stages and EPS were responsible for the improvement of methane production. Interestingly, metagenomics analysis was applied to unravel the fundamental mechanisms of how inert substances enhanced the activity of methanogenic bacteria, enzyme synthesis and substrate metabolism. It has shown that inert substances improved total methanogens and functional bacteria. Most notably, metagenomics analysis has revealed that enzyme synthesis in the metabolic pathway of glycolysis/gluconeogenesis, pyruvate metabolism, butanoate metabolism, methane metabolism and oxidative phosphorylation were promoted by inert substances.

ACKNOWLEDGMENTS

The work is financially supported by Tongji University (2022-4-YB-12) and the Social Development Program of Science and Technology Committee Foundation of Shanghai (No. 21DZ1209501).

APPENDIX A SUPPLEMENTARY DATA

E-supplementary data associated with this article can be found in the online version.

REFERENCE

1. Alvarado, V., Hsu, S.C., Wu, Z.Y., Zhuang, H.C., Lee, P.H., Guest, J.S., 2022. Roadmap from Microbial Communities to Individuality Modeling for Anaerobic Digestion of Sewage Sludge. Environ Sci Technol. 56, 6596-6607.
2. Basuvaraj, M., Fein, J., Liss, S. N., 2015. Protein and polysaccharide content of tightly and loosely bound extracellular polymeric substances and the development of a granular activated sludge floc. Water Res. 82, 104-117.
3. Braz, G.H.R., Fernandez-Gonzalez, N., Lema, J.M., Carballa, M., 2018. The time response of anaerobic digestion microbiome during an organic loading rate shock. Appl Microbiol Biotechnol. 102, 10285-10297.
4. Bu, J., Wei, H.L., Wang, Y.T., Cheng, J.R., Zhu, M.J., 2021. Biochar boosts dark fermentative H_2 production from sugarcane bagasse by selective enrichment/colonization of functional bacteria and enhancing extracellular electron transfer. Water Res. 202, 117440.
5. Cai, M.W., Yin, X.R., Tang, X.Y., Zhang, C.J., Zheng, Q.F., Li, M., 2022. Metatranscriptomics reveals different features of methanogenic archaea among global vegetated coastal ecosystems. Sci Total Environ. 802, 149848.

6. Chen W., Westerhoff P., Leenheer J.A., Booksh K., 2003. Fluorescence Excitation -- Emission Matrix Regional Integration to Quantify Spectra for Dissolved Organic Matter. Environ Sci Technol. 37(24), 5701-5710.
7. Chen, S.J., Zhang, J.S., Wang, X.K., 2015. Effects of alkalinity sources on the stability of anaerobic digestion from food waste. Waste Manage. Res. 33, 1033-1040.
8. Deena, S.R., Vickram, A.S., Manikandan, S., Subbaiya, R., Karmegam, N., Ravindran, B., Chang, S.W., Awasthi, M.K., 2022. Enhanced biogas production from food waste and activated sludge using advanced techniques-A review. Bioresour Technol. 355, 127234.
9. Du, M.T., Liu, X.R., Wang, D.B., Yang, Q., Duan, A.B., Chen, H., Liu, Y.W., Wang, Q.L., Ni, B.J., 2021. Understanding the fate and impact of capsaicin in anaerobic co-digestion of food waste and waste activated sludge. Water Res, 188, 116539.
10. Federation, W.E., Association, A.P.H., 2005. Standard methods for the examination of water and wastewater. American Public Health Association (APHA), Washington, DC, USA.
11. Fei, X.H., Jia, W.B., Chen, T., Ling, Y.S., 2022. Life cycle assessment of food waste anaerobic digestion with hydrothermal and ionizing radiation pretreatment. J Clean Prod. 338, 130611.
12. Jiang, X.P., Qin, Z.Y., Feng, L.Y., Chen, Y.G., Chen, J.G., Zhang, X.Z., Zhang, Z.G., Guo, Y.Q., Sun, J., 2020. Volatile fatty acids production from waste activated sludge during anaerobic fermentation: The effect of superfine sand. Bioresour Technol. 319, 124249.
13. Jiang, X.P., Yan, Y.Y., Feng, L.Y., Wang, F., Guo, Y.Q., Zhang, X.Z., Zhang, Z.G., 2021. Bisphenol A alters volatile fatty acids accumulation during sludge anaerobic fermentation by affecting amino acid metabolism, material transport and carbohydrate-active enzymes. Bioresour Technol. 323, 124588.
14. Leenheer, J.A & Croue J.P., 2003. Characterizing Dissolved Aquatic Organic Matter. Environ Sci Technol. 37(1), 18A.
15. Liu, C., Huang, H.N., Duan, X., Chen, Y.G., 2021. Integrated Metagenomic and Metaproteomic Analyses Unravel Ammonia Toxicity to Active Methanogens and Syntrophs, Enzyme Synthesis, and Key Enzymes in Anaerobic Digestion. Environ Sci Technol. 55, 14817-14827.
16. Lu, L., Xing, D.F., Ren, N.Q., 2012. Pyrosequencing reveals highly diverse microbial communities in microbial electrolysis cells involved in enhanced H-2 production from waste activated sludge. Water Res. 46, 2425-2434.
17. Luo, J.Y., Chen, Y.G., Feng, L.Y., 2016. Polycyclic aromatic hydrocarbon affects acetic acid production during anaerobic fermentation of waste activated sludge by altering activity and viability of acetogen, Environ. Sci. Technol. 50 (13), 6921–6929.
18. Luo, T.Y., Xu, Q.X., Wei, W., Sun, J., Dai, X.H., Ni, B.J., 2022. Performance and Mechanism of Fe3O4 Improving Biotransformation of Waste Activated Sludge into Liquid High-Value Products. Environ Sci Technol. 56, 3658-3668.
19. Magdalena, J.A., Greses, S., Gonzalez-Fernandez, C., 2021. Valorisation of bioethanol production residues through anaerobic digestion: Methane production and microbial communities. Sci Total Environ. 772, 144954.
20. Mamindlapelli, N.K., Arelli, V., Jukanti, A., Maddala, R., Anupoju, G.R., 2022. Anaerobic Co-digestion of Biogenic Wastes Available at Palm Oil Extraction Factory: Assessment of Methane Yield, Estimation of Kinetic Parameters and Understanding the Microbial Diversity. BioEnergy Res. 16(1), 213-227.
21. Meng, Q.C., Liu, H.B., Zhang, H.D., Xu, S.Y., Lichtfouse, E., Yun, Y.B., 2022. Anaerobic digestion and recycling of kitchen waste: a review. Environ Chem Lett. 20, 1745-1762.
22. Morris, J.P., Backeljau, T., Chapelle, G., 2019. Shells from aquaculture: a valuable biomaterial, not a nuisance waste product. Rev Aquacult. 11(1), 42-57.
23. Qin, Y., Yang, J.N., Wu, Y.X., Wang, D.B., Liu, X.R., Du, M.T., He, D.D., Yi, N., 2022. The degradation of allyl isothiocyanate and its impact on methane production from anaerobic co-digestion of kitchen waste and waste activated sludge. Bioresour Technol. 347, 126366.
24. Ren, Y.Y., Wang, C., He, Z.A., Qin, Y., Li, Y.Y., 2022. Enhanced biomethanation of lipids by high-solid co-digestion with food waste: Biogas production and lipids degradation demonstrated by long-term continuous operation. Bioresour Technol. 348, 126750.
25. Ren, Y.Y., Yu, M., Wu, C.F., Wang, Q.H., Gao, M., Huang, Q.Q., Liu, Y. 2018. A comprehensive review on food waste anaerobic digestion: Research updates and tendencies. Bioresour Technol. 247, 1069-1076.
26. Sailer, G., Eichermueller, J., Empl, F., Poetsch, J., Pelz, S., Kuptz, D., Oechsner, H., Mueller, J., 2022. Improving the energetic utilization of household food waste: Impact of temperature and atmosphere during storage. Waste Manag. 144, 366-375.
27. Sanjaya, E.H., Cheng, H., Qin, Y., Kubota, K., Li, Y.Y., 2021. The impact of calcium supplementation on methane fermentation and ammonia inhibition of fish processing wastewater. Bioresour Technol. 337, 125471.
28. Shin, S. G., Lee, S., Lee, C., Hwang, K., Hwang, S.,

2010. Qualitative and quantitative assessment of microbial community in batch anaerobic digestion of secondary sludge. Bioresour Technol. 101, 9461-9470.
29. Tang, J.L., Pu, Y.H., Wang, X.C.C., Hu, Y.S., Huang, J., Ngo, H.H., Pan, S.W., Li, Y.Y., Zhu, N.M., 2019. Effect of additional food waste slurry generated by mesophilic acidogenic fermentation on nutrient removal and sludge properties during wastewater treatment. Bioresour Technol. 271(294), 122218.
30. Valenca, R.B., dos Santos, L.A., Firmo, A.L.B., da Silva, L.C.S., de Lucena, T.V., Santos, A.F.D.S., Juca, J.F.T., 2021. Influence of sodium bicarbonate ($NaHCO_3$) on the methane generation potential of organic food waste. J Clean Prod. 317, 128390.
31. Van Dierdonck, J., Van den Broeck, R., Vervoort, E., D'haeninck, P., Springae, D., Impe, J.V., Srnets, I., 2012. Does a change in reactor loading rate affect activated sludge bioflocculation? Process Biochem. 47 (12), 2227-2233.
32. Wainaina, S., Lukitawesa., Awasthi, M.K., Taherzadeh, M.J., 2019. Bioengineering of anaerobic digestion for volatile fatty acids, hydrogen or methane production: A critical review. Bioengineered. 11, 437-458.
33. Wang, D.B., He, D.D., Liu, X.R., Xu, Q.X., Yang, Q., Li, X.M., Liu, Y.W., Wang, Q.L., Ni, B.J., Li, H.L., 2019. The underlying mechanism of calcium peroxide pretreatment enhancing methane production from anaerobic digestion of waste activated sludge. Water Res. 164, 114934.
34. Wang, J.F., Zhao, Z.Q., Zhang, Y.B., 2021. Enhancing anaerobic digestion of kitchen wastes with biochar: Link between different properties and critical mechanisms of promoting interspecies electron transfer. Renew. Energy. 167, 791-799.
35. Wang, P., Wang, X.Z., Chen, X.T., Ren, L.H., 2021. Effects of bentonite on antibiotic resistance genes in biogas slurry and residue from thermophilic and mesophilic anaerobic digestion of food waste. Bioresour Technol. 336, 125322.
36. Wang, Y.Y., Bing, Z., Li, G.X., Liu, Y., 2016. Evaluation the anaerobic hydrolysis acidification stage of kitchen waste by pH regulation. Waste Manage. 53, 62-67.
37. Wang, Z., Wu, Z., Tang, S., 2009. Extracellular polymeric substances (EPS) properties and their effects on membrane fouling in a submerged membrane bioreactor. Water Res. 43 (9), 2504–2512.
38. Xiao, N., Chen, Y., Ren, H., 2013. Altering protein conformation to improve fermentative hydrogen production from protein wastewater. Water Res. 47 (15), 5700–5707.
39. Xie, J., Duan, X., Feng, L.Y., Yan, Y.Y., Wang, F., Dong, H.Q., Jia, R.Y., Zhou, Q., 2019. Influence of sulfadiazine on anaerobic fermentation of waste activated sludge for volatile fatty acids production: Focusing on microbial responses. Chemosphere. 219, 305-312.
40. Ye, F.X., Peng, G., Li, Y., 2011. Influences of influent carbon source on extracellular polymeric substances (EPS) and physicochemical properties of activated sludge. Chemosphere. 84 (9), 1250-1255.
41. Yue, L.C., Cheng, J., Tang, S.Q., An, X.X., Hua, J.J., Dong, H.Q., Zhou, J.H., 2021. Ultrasound and microwave pretreatments promote methane production potential and energy conversion during anaerobic digestion of lipid and food wastes. Energy. 228, 120525.
42. Zeng Y., Tang X., Fan C., Tang，L., Zhou，M., Zhang，B., Wang，R., Li, G., 2021. Evaluating the Effects of Different Pretreatments on Anaerobic Digestion of Waste Activated Sludge Containing Polystyrene Microplastics. ACS ES&T Wat. 2, 117-127.
43. Zhang, H.D., Zhang, C.Y., Zheng, Q.X., Zeng, X., 2022. Extraction of Calcium Phosphate Nanoparticles from Cooked Bone Wastes by Supercritical Water. Waste Biomass Valori. 13(4), 2287-2294.
44. Zhou, L.J., Gao, Y., Yu, K., Zhou, H., De Costa, Y.G., Yi, S., Zhuang, W.Q., 2020. Microbial community in in-situ waste sludge anaerobic digestion with alkalization for enhancement of nutrient recovery and energy generation. Bioresour Technol. 295, 122277.

MAGNETIC DIATOMITE MEDIATED ANAEROBIC DIGESTION OF KITCHEN WASTE: PERFORMANCE AND METAGENOMIC ANALYSIS

Dong Li[1] and Xiaoli Chai[1, 2]
1 College of Environmental Science and Engineering, Tongji University
1239 Siping Road, Shanghai 200092, China
2 Shanghai Institute of Pollution Control and Ecological Security
1239 Siping Road, Shanghai 200092, China

ABSTRACT

A large amount of kitchen waste (KW) brings environmental pollution and sanitation problems. Anaerobic digestion (AD) is an effective technology to treat kitchen waste and generate biogas energy.

Diatomite is widely used as an adsorbent, filter aid, and construction material because of its high permeability, high porosity, small particle size, large surface area, low thermal conductivity, and chemical inertness. Diatomite has the characteristics of high porosity and large surface area provides a favorable habitat for microbial growth and reproduction, so the application of diatomaceous earth in wastewater biological treatment has also received wide attention. Considering the good biophilicity of diatomite, it was hypothesized that diatomite might be a good carrier additive to promote the performance of anaerobic digestion of organic solid waste for methane production. Meanwhile, magnetization modification of diatomite is thought to serve both biophilic and electron transfer functions.

This study investigated the effect of natural diatomite (DE) and magnetic diatomite (MDE) on anaerobic digestion performance of kitchen waste. Results showed that the cumulative methane yield increased by 3.18-11.76% and 8.07-15.15%, respectively, and the lag time decreased significantly with DE and MDE. The peak of cumulative methane yield was achieved at 580.04 ± 1.61 mL/g VS with 3 g/L MDE, which is close to the theoretical methane production. Besides, DE and MDE reduced the inhibition of NH_4^+-N and volatile fatty acids accumulation, and it could improve the system stability. The metagenomic analysis of key microorganisms and related metabolism pathways involved in AD system was further investigated. The results suggested that DE and MDE contributed to strengthen methanogenesis through enriching the various predominant methanogenic pathways and activating most enzymes related to methane metabolism. DE and MDE could improve the AD system function and provided a better AD performance by shifting the microbial communities and altering functional genes. This study provided a theoretical basis for DE and MDE applications and improvements in AD process of KW.

KEYWORDS

Magnetic diatomite; Metagenomic analysis; Methane yield; Anaerobic digestion; Kitchen waste

HIGHLIGHTS

- Adding MDE improved the methane production.
- The functional gene abundance and activity of enzymes were related to MDE.
- MDE stimulated acetate and CO_2 of the methane metabolism pathways.

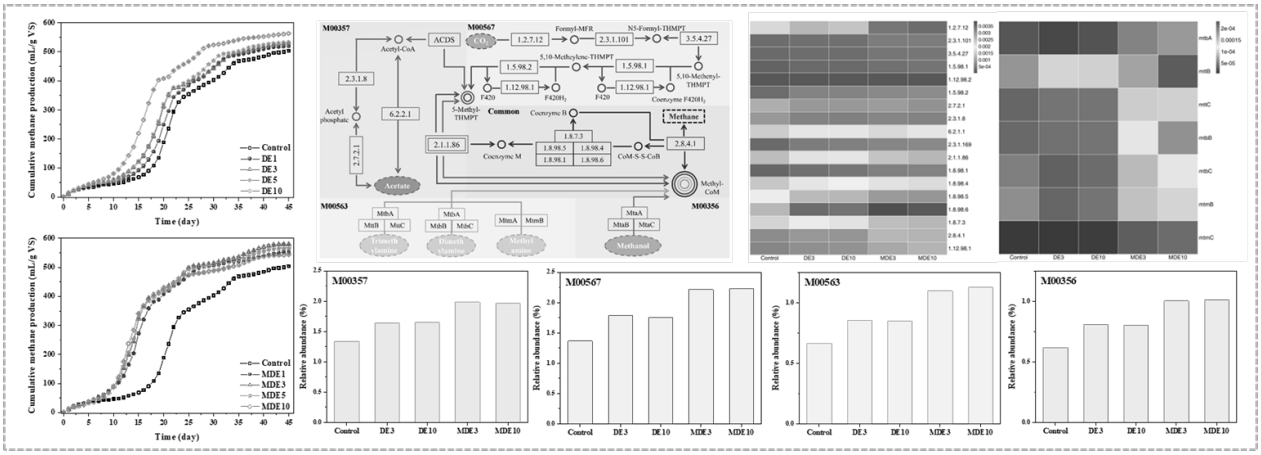

PHOTOSYNTHETIC BACTERIA TREATMENT OF FOOD WASTE

Huize Liu[1], Jizheng Zhang[1], Guangming Zhang[1*]
1 School of Energy & Env. Engr., Hebei University of Technology
Tianjin, China

INTRODUCTION

Food waste is produced in large amount and the normal treatment method is anaerobic digestion to produce biogas or aerobic fermentation to produce fertilizer. This paper proposed a novel strategy, food waste hydrolysis combined with photosynthetic bacterial (PSB) treatment to produce valuable PSB biomass rich in protein and poly-β-hydroxybutyrates. This work can provide a novel solution to food waste resourificaiton.

EXPERIMENTS

Food waste was collected from the school kitchen, crushed and mixed, and then hydrolyzed naturally for 72 h till the pH dropped below 4.5. Then the supernatant was separated for PSB treatment. The PSB inoculum was cultured in lab. The initial COD was around 4500 mg/L, the PSB dose was 20%, the pH was 8.5, the lighting conditions were 2000 lux and 24 h unless stated otherwise. All indexes were measured according to standard methods.

RESULTS

The food waste supernatant was effective treated by the PSB, the COD and NH_4-N removal efficiency reached 80% and higher under all conditions. The PSB biomass increased continuously during treatment.

Impact of light intensity

Clearly 2000 lux was the best for PHB synthesis and reached 44% at D14. This was also the optimal for protein synthesis, however, the protein content decreased continuously, which might be caused by insufficient macro-elements and complex byproducts during fermentation.

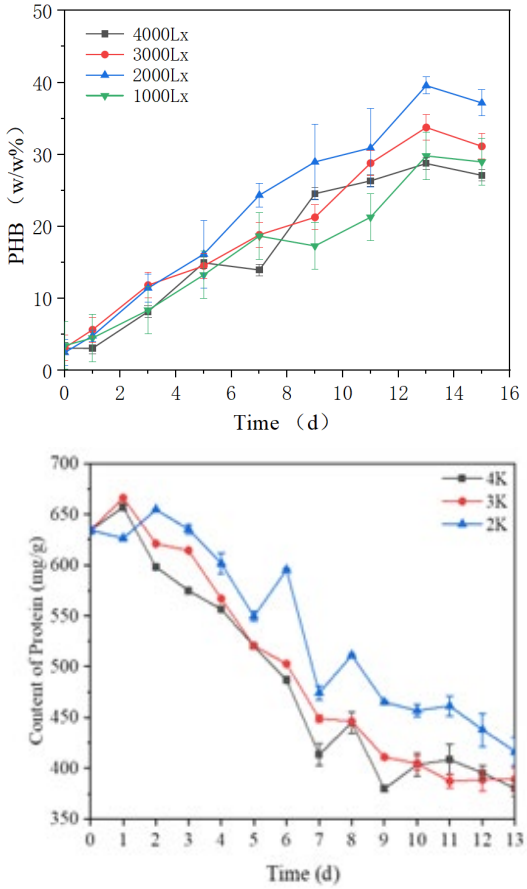

Fig. 1 Impact of light intensity on PHB and protein

Impact of lighting cycle

Lighting cycle was reported to impact the biomass growth and components synthesis. Further, it can reduce lighting energy compared to continuous lighting. Fig. 2 showed that the lighting cycle did affect the PHB and protein synthesis. Interesting, the 6h:6h cycling was the best for PHB synthesis while the 3h:3h cycling was the optimal for protein. No significant differences in the biomass growth or pollutants removal were find among various lighting cycles. Thus, the interim lighting strategy can be adopted to save energy.

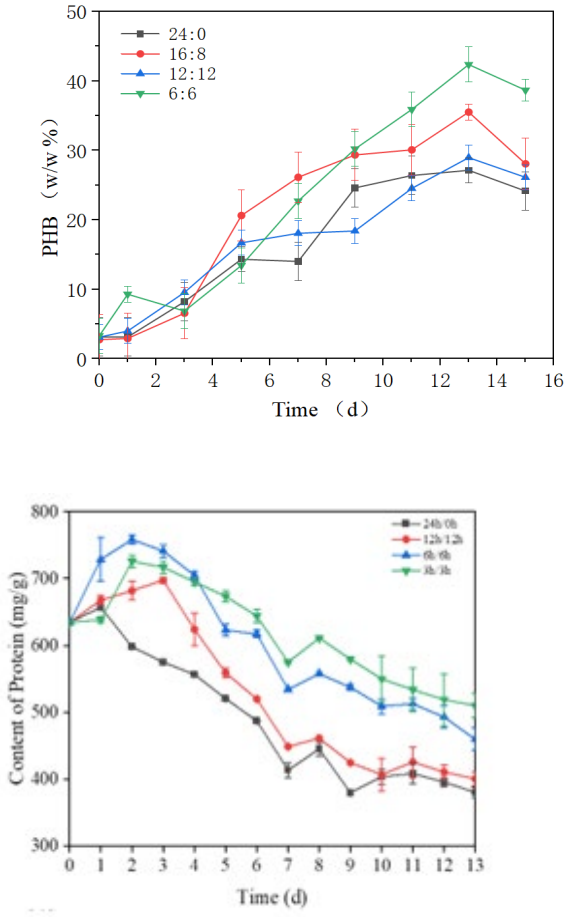

Fig. 2 Impact of lighting cycle on PHB and protein

Impact of weak magnetic field

A weak magnetic field has been reported to improve biomass growth and accelerate pollutant removal. However, in the work PSB showed negative response to the implementation of weak magnetic field in terms of both biomass and COD and removals. On the other hand, magnetic field did alleviate the dropping trend of protein content in PSB. As for the PHB content, no significant difference was obtained with the introducing of magnetic field.

Fig. 3. Impact of magnetic field on PHB and protein

STRENGTHEN HIGH-LOADING OPERATION OF WASTEWATER TREATMENT PLANTS BY COMPOSITE MICRON POWDER CARRIER: MICROSCALE CONTROL OF CARBON, NITROGEN AND SULFUR METABOLIC PATHYWAY

Chengxian Wang[1], Bin Lu[1], and Xiaoli Chai[1,2]
1 State Key Laboratory of Pollution Control and Resource Reuse, College of Environmental Science and Engineering, Tongji University, 1239 Siping Road, Shanghai 200092, China
2 Shanghai Institute of Pollution Control and Ecological Security, Shanghai 200092, China

ABSTRACT

The concentration of activated sludge is a crucial factor influencing the capacity and efficiency of sewage wastewater treatment plants (WWTPs). However, high sludge concentrations can lead to sludge loss in the secondary sedimentation tank, resulting in reduced processing capacity, particularly during low-temperature stages and sludge bulking. This study investigated the impact of adding composite micron powder carriers (CMPC) in high-concentration powder carrier biofluidized bed (HPB) technology to the biochemical units of WWTPs on sludge concentration and settling performance. For the traditional activated sludge method (ASM), its hydraulic retention time (HRT) was 8 h, with an average effluent total nitrogen (TN) of 15.14 mg/L. Sludge bulking was prone to occur in low-temperature environments, resulting in a high average sludge volume index (SVI) of 560 mL/g. Conversely, with a CMPC dosage of 4 g/L, the HRT of HPB technology was 4.8 hours, and the average effluent TN was 11.40 mg/L, with a removal efficiency of 67.43%. During operation of HPB technology under high sludge concentration conditions (8 g/L), the average SVI remained at 85 mL/g, indicating excellent settling characteristics. Moreover, in the sequencing batch reactor (SBR), the SVI value of bulking sludge decreased from the original 695 to 111 mL/g by the 9th day of operation with the CMPC dosage of 2 g/L. At the same time, the filamentous bacteria almost disappeared, suggesting that CMPC inhibit the growth of filamentous bacteria. Metagenomic analysis demonstrated that CPMC enhance the utilization of small molecular fatty acids in activated sludge and promote electron transfer between nitrate and nitrite, thereby improving wastewater treatment capacity. Additionally, CMPC enhanced the relative abundance of Saprospiraceae in sludge, which accelerate the degradation of polysaccharides in extracellular polymeric substances, weaken sludge's hydrophilic properties, and improve sludge's settling performance. Overall, these findings suggested that CMPC effectively strengthen the high-loading operation of WWTPs by improving sludge concentration and sedimentation performance.

KEYWORDS

HPB technology, micro-size powder carrier, settling performance, extracellular polymeric substance, metagenomic analysis

HIGHLIGHTS

- Composite micron powder carrier (CMPC) enhanced the settling performance.
- Settleability of sludge was correlated to the PS and PN distribution in total EPS.
- CMPC enhanced small-molecule fatty acid utilization for electron transfer.
- The abundance of Thiothrix genus was positively correlated with SV30 and SVI value.
- Settling property optimized by CMPC was revealed via C, N and S metabolic pathways.

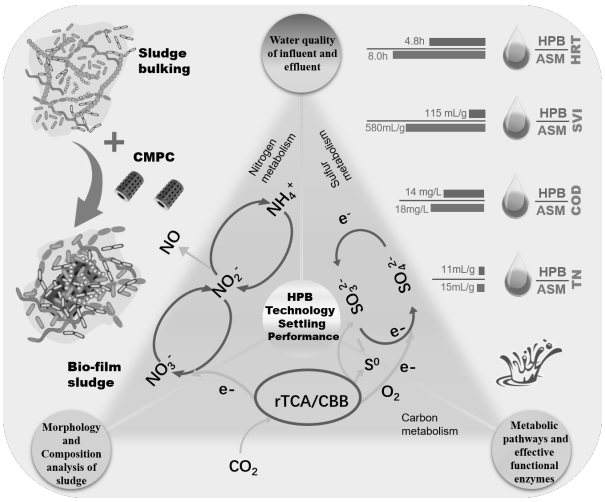

Graphical Abstract

EFFICIENT NITROGEN REMOVAL FROM RURAL WASTEWATER IN HUMUS BIOCHEMICAL SYSTEM WITH LOW DISSOLVED OXYGEN CONDITIONS: SLUDGE AND MICROBIAL CHARACTERISTICS

Zhengliang Du [1, 2], Bin Lu [1], and Xiaoli Chai [1, 2]
1 College of Environmental Science and Engineering, Tongji University, Shanghai, Cina
2 Shanghai Institute of Pollution Control and Ecological Security, Shanghai, China

ABSTRACT
Along with the rapid social development and population growth, plenty of rural wastewater rich in organic matter, nitrogen, phosphorus, and various pathogens is generated in rural areas in China. Due to restricted local budgets, complex geographical conditions, and incomplete treatment facilities, the rural wastewater treatment rate is still less than 35%, while the remaining untreated rural wastewater is discharged directly into the surrounding environment, posing a substantial threat to the natural environment and public health. Currently, some advanced biological technologies have been introduced to treat rural wastewater instead of traditional ecological technologies with lower treatment efficiencies. However, the biotreatment reactors were complicated in operation and required professional maintenance, making them difficult to apply in remote rural areas. In addition, the aerobic zone in biological treatment systems typically requires high-flow aeration to support the oxidative degradation and nitrification reactions, which is incompatible with the carbon neutrality purpose. It is of great significance to develop efficient, simple, and low-energy technology for rural wastewater treatment, which is conducive to improving the social and economic benefits in rural areas.
Humus bio-functional material is a biomaterial made from natural humus soil, which can complement biological treatment technologies to further improve the strengthen their removal capacity for nitrogen and phosphorus, while improving sludge settleability and reducing waste sludge yield and odour. Notably, the humus soil microorganisms introduced into sludge return systems were generally cultured under low dissolved oxygen (DO) levels of $\leqslant$ 0.5 mg/L. Accordingly, if these facultative anaerobes can be cultured and domesticated directly in the reactor to replace conventional activated sludge for rural wastewater treatment, this would greatly save the total energy consumption. In this study, therefore, a humus biochemical system (HBS) process was constructed using humus bio-functional materials as inoculum to treat synthetic rural wastewater under low DO conditions, and the removal performance, sludge physicochemical properties, and microbial community structures of the HBS process were investigated. The results indicated that the HBS showed commendable performance for wastewater treatment, where the removal efficiencies of COD, NH_4^+-N, and TN reached 97.0%, 95.9%, and 87.2%, with corresponding stable effluent concentrations of 11.0, 1.7, and 5.1 mg/L, respectively. Furthermore, HBS sludge contained more humus-like substances and was characterized by higher settleability and stability, compared to conventional activated sludge. Illumina sequencing revealed that the HBS had a relatively high microbial abundance and diversity, with recognizable genera dominated by *Dechloromonas*, *Flavobacterium*, *Propionicicella*, *Thiobacillus*, and *Propionicimonas*, which were involved in the processes of nitrogen in HBS. The study provides a new solution for rural wastewater treatment with lower operating costs.

KEYWORDS
Rural wastewater; Nitrogen removal; Humus biochemical system; Microbial community; Humus bio-functional materials

EXOGENOUS DISSOLVED ORGANIC CARBON SPURS BACTERIAL-ALGAL COMPETITION AND PHOSPHORUS-PAUCITY ADAPTATION: BOOSTING MICROCYSTIS' PHOSPHORUS UPTAKE CAPACITY

Tingting Li, Xiaoli Chai, Boran Wu
College of Environmental Science and Engineering, Tongji University
1239 Siping Road, Shanghai, China

ABSTRACT
Dissolved organic carbon (DOC) can alter the availability of background nutrients by affecting the proliferation of heterotrophic bacteria, which exerts a notable influence on algal growth and metabolism. However, the mechanism of how exogenous DOC (eDOC) precipitates shifts in bacterial-algal interactions and modulates the occurrence of cyanobacteria blooms remains inadequately elucidated. Therefore, this study investigated the relationship between bacteria and algae under eDOC stimulation. We found that excess eDOC triggered the breakdown and reestablishment of the equilibrium between Microcystis and heterotrophic bacteria. The rapid proliferation of heterotrophic bacteria led to a dramatic decrease in soluble phosphorus, and thereby resulted in the inhibition of the Microcystis growth. When the organic carbon was depleted, the rapid death of heterotrophic bacteria released large amounts of dissolved phosphorus, which provided sufficient nutrients for the recovery of Microcystis. Notably, Microcystis rejuvenated and showed higher cell density compared to the carbon-absent group. This phenomenon can be ascribed that Microcystis regulated the compositions of extracellular polymeric substance (EPS) and the expression of relevant proteins to adapt to a nutrient-limited environment. Using time of flight secondary ion mass spectrometry (TOF-SIM) and proteomic analysis, we observed an enhancement of the signal of organic matter and metal ions associated with P complexation in EPS. Moreover, Microcystis upregulated proteins related to organic phosphorus transformation to increase the availability of phosphorus in various forms. In summary, this study emphasized the role of DOC in algal blooms, revealing the underestimated enhancement of Microcystis nutrient utilization through DOC-induced heterotrophic competition and providing valuable insights into eutrophication management and control.

KEYWORDS
Exogenous organic carbon, Microcystis, Phosphorus availability, Algal bloom, Ion micro distribution

CONCLUSIONS
DOC leads to inhibition of Microcystis due to competition from heterotrophic bacteria resulting in phosphorus restriction, with an inhibition rate of 98%. However, after the competition, organic carbon enhanced the growth adaptability of algae to limited nutrition. Microcystis increased the biomass per unit phosphorus utilization by 25%. This was due to that the rapid death of heterotrophic bacterium provided biologically available phosphorus as organic carbon was consumed, approximately 75% of the phosphorus was transferred from bacterial cells to algal cells. Moreover, eDOC increased calcium-phosphorus complexed organic matters in EPS, resulting in the release of metal-bound phosphorus. Furthermore, eDOC driven the co-evolution of bacteria and algae. Microcystis exhibited various regulatory strategies during mutualistic reconstruction, such as enhanced photosynthesis, optimized the expression of metal transporters, and the production of specific polysaccharides, which facilitated the construction and attachment of the heterotrophic bacterial community. After the reconstruction of the symbiotic relationship, Microcystis experienced a more vigorous growth momentum. Therefore, eDOC was intimately associated with the waxing and waning of algal bloom.

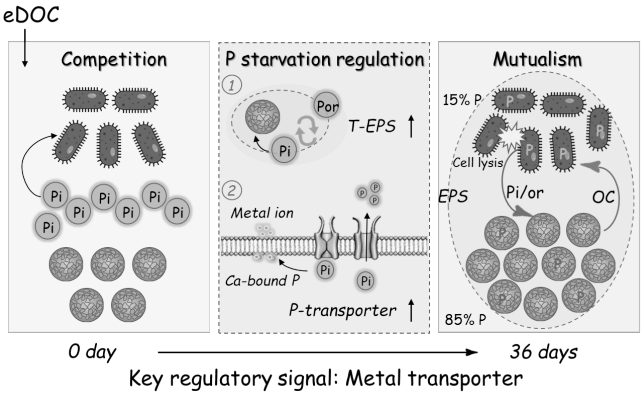

Graphical Abstract

THE ADAPTIVE REGULATION MECHANISM OF ANAMMOX GRANULE SLUDGE UNDER CALCIUM IONS STRESS: DEFENSE MODES TRANSFORMATION

Pengcheng Wang[1], Bin Lu[1], and Xiaoli Chai[1,2]
1 State Key Laboratory of Pollution Control and Resource Reuse, College of Environmental Science and Engineering, Tongji University, 1239 Siping Road, Shanghai 200092, China
2 Shanghai Institute of Pollution Control and Ecological Security, Shanghai 200092, China

ABSTRACT
Anammox granular sludge (AnGS) has received considerable attention due to its low carbon footprint (less aeration energy and carbon source consumption), but growth rate and stability are still the bottlenecks of AnGS process. Calcium ion (Ca^{2+}) is essential for the growth of anaerobic ammonium oxidation bacteria (AnAOB) and plays an important role in the formation and stability of AnGS. Response of AnGS to Ca^{2+} under different concentrations was comprehensively investigated by multi-spectral and metagenomics analysis in four aspects: nitrogen removal performance, surface morphology, extracellular polymeric substance (EPS) composition and characterization, and microbial community. The nitrogen removal efficiency was significantly enhanced at appropriate Ca^{2+} concentration (2 mmol/L). However, the nitrogen removal performance of AnGS declined with the Ca^{2+} concentration increased from 2 to 8 mmol/L, due to the negative effects of excess Ca^{2+} on EPS, mass transfer efficiency, and functional microorganisms. Meanwhile, an unexpected slight "rebound" of nitrogen removal efficiency was observed (Ca^{2+} = 6 mmol/L) and attributed to the defense mode transformation of AnGS (from "ion stabilization" to "precipitate shield" modes) against excess Ca^{2+} stress. Based on the findings, the response mechanism of AnGS to Ca^{2+} was established, which is valuable for filling the theoretical gap in enhancing the granulation and stability of AnGS and providing a reference for the operation of the AnGS process.

KEYWORDS
anammox, anammox granule sludge, calcium ion, extracellular polymeric substances, functional microbial community, ion stabilization, precipitate shield

HIGHLIGHTS
- 2 mmol/L Ca^{2+} significantly enhances the nitrogen removal performance of AnGS.
- Mode switching theory of AnGS to defend against excess Ca^{2+} was proposed.
- "Precipitate shield" protects AnGS from the stress of high concentration Ca^{2+}.
- "Precipitate shield" has poor mass transfer efficiency (NH_4^+-N, NO_2^--N, etc.).

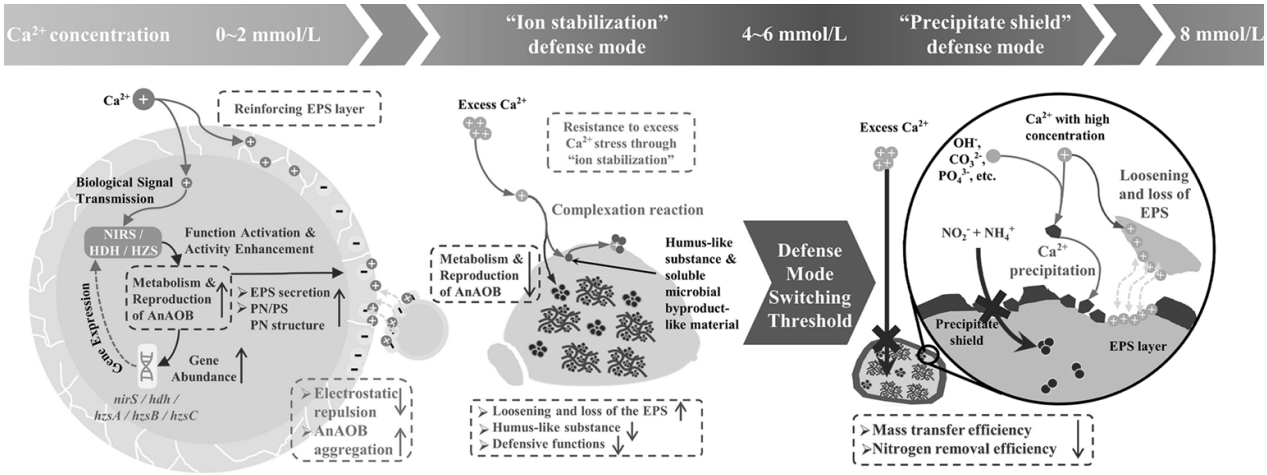

EFFECT OF SEEPAGE PATH OF INVADED AQUEOUS PHASE ON THE LEACHING CHARACTERISTICS OF HEAVY METALS IN LANDFILL STABILIZED FLY ASH

Weihua Li [1 *], Meng Li [1], Shuxia Cai [1], and Yingjie Sun [1]

1 Qingdao Solid Waste Pollution Control and Resource Engineering Research Center, School of Environmental and Municipal Engineering, Qingdao University of Technology, 777 Jialingjiang East Road, Qingdao 266520, China
*Corresponding author: liweihua@qut.edu.cn; Tel.: +86-157-6398-9110

ABSTRACT

The column leaching experiment of stabilized fly ash was established by simulating acid rain with "sulfuric acid + nitric acid" extractant to study the influence of acid rain seepage path on the leaching behavior of heavy metals in fly ash under the condition of damaged fly ash ton bags in the landfill. The results showed that the six seepage paths all promoted the leaching of Pb, Zn, Cu, Cd, Cr, and Ni in stabilized fly ash to varying degrees. Compared with the horizontal seepage path of "upper left inflow - lower right outflow", the vertical seepage path of "upper inflow - lower outflow" was more likely to promote the leaching of heavy metals in fly ash due to the double influence of gravity potential energy and matrix potential. Under the mode of "dynamic scouring + static soaking + dynamic scouring", the cumulative leaching amount of heavy metals was higher. Under the seepage path of "upper left inflow - upper right outflow", the fluctuation of pH value of leachate was the smallest, the cumulative leaching amount of heavy metals was the lowest, and the stability of heavy metals in fly ash matrix was the best. The research results can provide a scientific basis for the evaluation of the leaching behavior of heavy metals from stabilized fly ash in extreme acid rain environment and the environmental risk management and control when the fly ash ton bag in the actual landfill was damaged.

KEYWORDS

fly ash landfill; broken ton bag; acid rain; seepage path; heavy metal leaching

1. INTRODUCTION

Incineration is currently the preferred method for treating MSW in China. However, the secondary pollutant fly ash generated from MSW incineration, due to its rich diversity of heavy metals, has always been a pain point of concern in the industry for its safe disposal.

Chelating agent stabilization, such as widely used dithiocar-bamate (DTC), has a better low compatibilization ratio and stabilization effect, making it the main fly ash pretreatment method nowadays **(Kyung-Jin et al., 2000; Ma et al., 2019)**. It is worth noting that heavy metal pollutants still exist in fly ash, whether it is pretreated using solidification or stabilization. When stabilized fly ash encounters complex landfill environmental conditions, there are still varying degrees of potential leaching risks for the heavy metals it contains **(Li et al., 2022, 2021, and 2020)**.

In China, stabilized fly ash requires bagging and packaging (also known as “ton bagging”) before landfill disposal, but there are no special requirements for the material and quality of “ton bags” (such as seepage prevention or not, sealing or not, etc.). Therefore, in practice, considering the differences in material quality of ton bags, due to the standardization of operations and management, there are some phenomena of varying degrees of damage to ton bags filled with fly ash during loading, transportation, stacking, and landfill processes. Once the ton bags filled with fly ash are damaged to varying degrees, the unfavorable liquid phase invading it will form diverse percolation paths. To the best of our knowledge, exploring the impact of unfavorable liquid phase invasion on the leaching behavior of heavy metals in landfill stabilized fly ash under diversified percolation paths can provide important theoretical references for the standardization of the ton bagging, landfill disposal, and management processes of fly ash.

In this study, the leaching behavior of heavy metals (Pb, Zn, Cu, Cd, Cr, Ni) from landfill stabilized fly ash under six percolation paths with simulated acid rain (SAR) were investigated via column leaching experiments. Especially, the evolution laws of mineral structure and surface morphology of residual fly ash matrix were analyzed simultaneously.

2. MATERIALS AND METHODS

2.1. Stabilized fly ash samples

Fly ash samples stabilized with DTC chelating agent were collected from a large MSWI power plant equipped with three 750 t/d mechanical grate furnaces in Qingdao city, China. Crush the stabilized fly ash sample until it passes through a 10 mesh sieve, and then homogenize it through the quartering method before sealing and storing it at room temperature. The contents of target heavy metals (unit: mg/kg) and main chemical constituents (unit: %) are in the following order of Zn (4473.8) > Pb (1322.0) > Cu (434.0) > Cd (166.5) > Cr (112.5) > Ni (26.3) and CaO (49.1) > Cl (17.5) > K_2O (11.2) > SO_3 (8.8) > SiO_2 (3.1) > Fe_2O_3 (2.8) > Na_2O (2.1) > MgO (0.8) > TiO_2 (0.7) = Al_2O_3 (0.7) > P_2O_5 (0.4), respectively.

2.2. Preparation of invading SAR

According to the Chinese national standard "Solid Waste Leaching Toxicity Leaching Method - Sulfuric Acid and Nitric Acid Method" (HJ/T 299-2007), a simulated acid rain was prepared. This standard assumes the acidic leaching process of harmful components in waste under non-standard landfill conditions. The specific preparation parameters of SAR are as follows: add sulfuric acid and nitric acid mixed with 2:1 (mass ratio) to deionized water, and adjust pH=3.2 ± 0.05.

2.3. Percolation path tests

The design of the percolation path for invasive SAR was based on the damage scenario of fly ash ton bag in landfills. In this study, 6 possible breakage scenarios of fly ash ton bags in landfills were assumed, and 6 corresponding percolation paths were designed in the form of column percolation tests (**Table 1**). Six Plexiglas columns (**Fig. 1**) with a height of 350 mm and an inner diameter of 50 mm were used to simulate the column percolation system. Each column was loaded with 441.3 g (dry weight) homogenized stabilized fly ash samples. The upper and lower layers of fly ash layer were filled with 50 mm fine sand respectively, for well influent distribution and effluent drainage. Plastic sheets were used to separate the fly ash layer from the fine sand layer to prevent their mixing.

A stage inflow mode was adopted to simulate the discontinuous SAR invasion environment in reality, with a 25 day interval between the operating cycles of each stage (S1~S3). The operating time of each stage was based on the experimental design of USEPA Method 1314, with a cumulative liquid-solid ratio (L/S) of 10 as the end point for each stage. The sampling time of leachate in the S1, S2, and S3 stages was set when the cumulative L/S reached 0.2/0.5/1.0/1.5/2.0/4.5/5.0/9.5/10, 0.2/0.5/1.0/2.0/5.0/10, and 0.2/2.0/10, respectively. After each stage, residual fly ash samples inside the column were sampled and analyzed for the solid phase index.

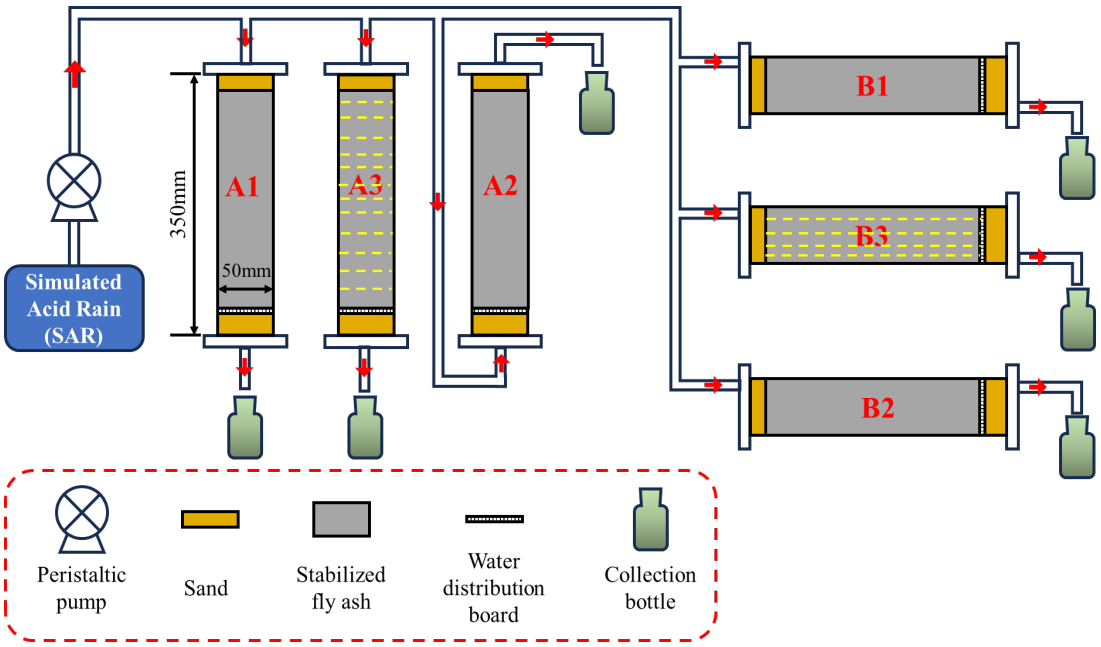

Fig. 1. Schematic diagram of the experimental device.

2.4. Analytical methods

Effluent characteristics were analyzed for pH, electrical conductivity (EC), and heavy metal concentration. pH value was measured using a pH meter (PHS-3 C; Germany). EC value was measured using a EC meter

(DDS-307A). The concentration of heavy metals (Cr, Cd, Pb, Zn, Cu, Ni) was measured using ICP-OES (iCAP 7000 SERIES, USA). All determinations were repeated at least once to ensure the reproducibility of results, and the average values were used for data analysis.

Table 1 Experimental designs for simulating the percolation paths of invading acid rain

Number of simulated columns	Types of percolation paths	Scenario of ton bag break
A1	top in and bottom out	The top and bottom of the ton bag were damaged: invading SAR entered from top and flowed out from bottom.
A2	top in and bottom out after immersion	The top of the ton bag was first damaged, and the invading SAR entered and gradually accumulated until it breaked through the bottom of the ton bag and flowed out.
B	bottom in and top out	The top and bottom of the ton bag were damaged, and the bottom leachate drainage system was blocked: invading SAR seeped in from bottom and overflowed from top.
C1	top left in and bottom right out	The top left and bottom right of the ton bag were damaged: invading SAR entered from the top left and flowed out from the bottom right.
C2	top left in and bottom right out after immersion	The top left of the ton bag was damaged, and the invading SAR entered and gradually accumulated until it breaked through the bottom right of the ton bag and flowed out.
D	top left in and top right out	The top left and top right of the ton bag were damaged (the bottom was not damaged): invading SAR entered from the top left and overflowed from the top right.

3. Results and discussion

3.1. Changes in pH, EC, and major elements of fly ash leachate

During the initial leaching of SAR in S1, the increase in the effluent pH and EC reflected the strong acid neutralization ability (ANC) of the landfill stabilized fly ash samples. Generally, the effluent pH and EC showed fluctuating and continuous decreasing trends in S1~S3, respectively.

Interestingly, the percolation path of B2 with "top left in and top right out" (the only scenario where the bottom of the ton bag is not damaged) shows lower pH values and higher EC values, which is related to the fact that the landfill fly ash in B2 always remains in a soaked state.

Cl, K, and Na in the landfill fly ash were fully leached in S1, and their leaching behaviors were generally similar to the influence of seepage paths.

Ca exhibited a long-term leaching pattern, with on peak at each stage.

Overall, A1 showed the highest cumulative leaching amount, while A3 and B3 showed the faster leaching rates, B2 (the bottom is not damaged) showed a slower leaching rate.

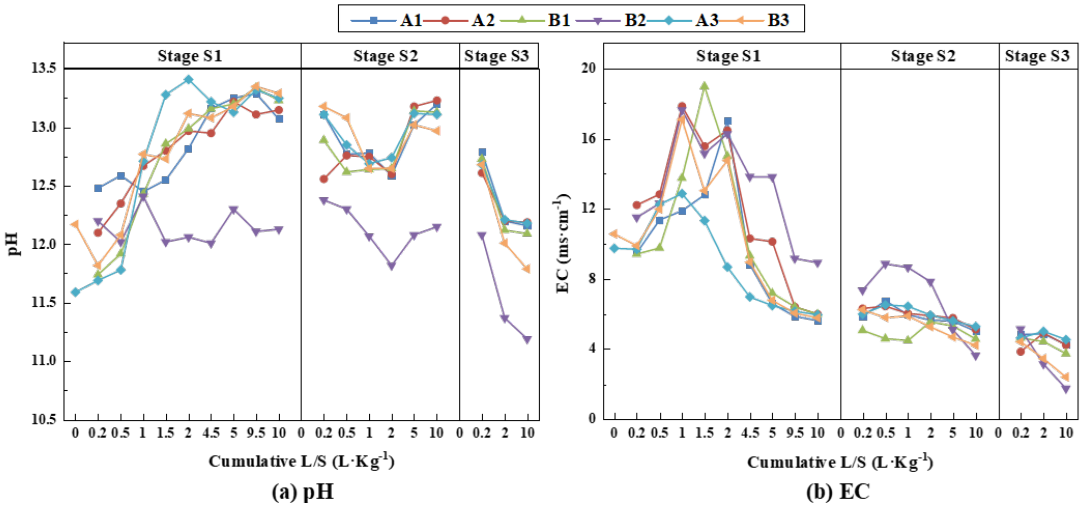

Fig. 2. Changes in pH and EC of fly ash leachate under different seepage paths.

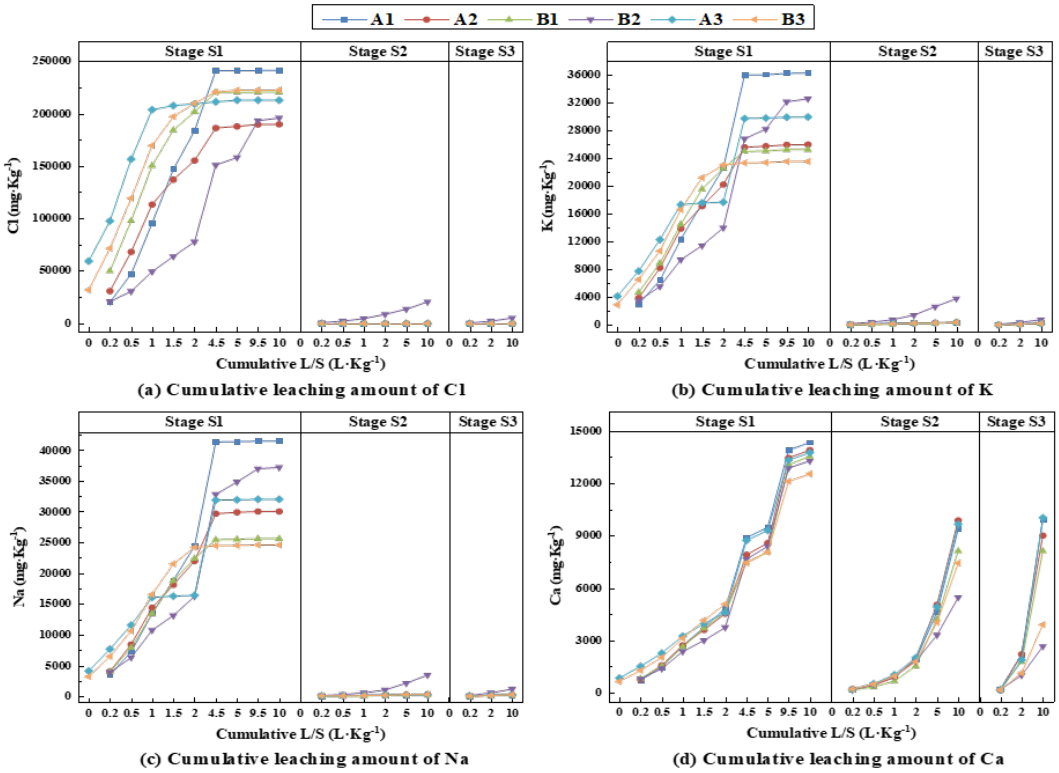

Fig. 3. Changes in the cumulative leaching amount of main elements (Cl, K, Ca, Na) in fly ash leachate under different seepage paths.

3.2. Changes in heavy metal leaching behavior

The leaching behavior of Pb/Cr/Ni (S1~S3), Cu (S2~S3) and Zn/Cd (S1~S3), Cu (S1) was significantly influenced by the conditions of "dynamic leaching" (A1, A2, B1) and "dynamic leaching + static immersion + dynamic leaching" (A3, B3), respectively.

Generally, the longitudinal seepage path was more likely to promote the short-term leaching of heavy metals in landfill fly ash, while their long-term stability under the transverse seepage path was greatly affected.

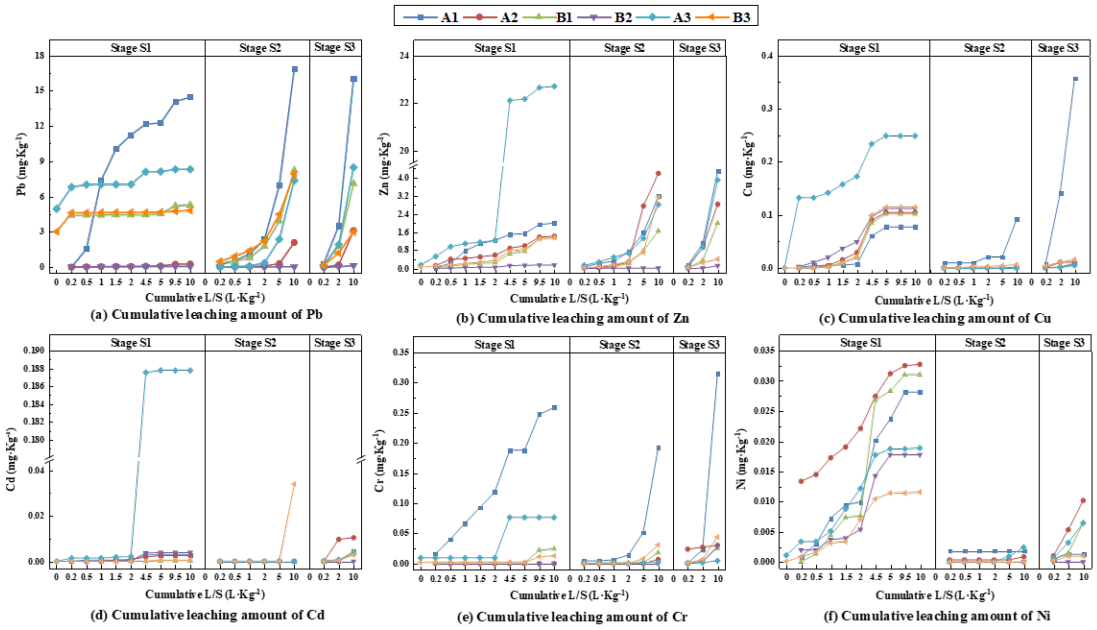

Fig. 4. Changes in the cumulative leaching amount of heavy metals (Pb, Zn, Cu, Cd, Cr, Ni) in fly ash leachate under different seepage paths.

3.3. Changes in mineral structure and surface morphology of solid fly ash matrix

With the dissolution of a large amount of soluble salts (NaCl, KCl, etc.) in fly ash during SAR intrusion, peaks of some trace mineral components (such as Ca-Al-Si-O) were detected.

The enhancement of $CaCO_3$ peak was due to the large washing out of Cl-based soluble salts in fly ash and the carbonation reaction of CaClOH during the stagnation period (25d) in S1~S2 and S2~S3.

Overall, the changes in mineral structure of residual fly ash matrix were mainly influenced by intermittent SAR leaching, and were relatively less affected by changes in seepage paths.

In S1, a large amount of soluble salts (NaCl, KCl, etc.) in fly ash were dissolved, resulting in a decrease in surface cluster like structures and the appearance of angular rod-shaped or columnar structures.

With the continuous SAR leaching in S2~S3, $CaCO_3$ and $CaSO_4$ became the main mineral phases in residual fly ash, and the surface rod-shaped structure significantly increased.

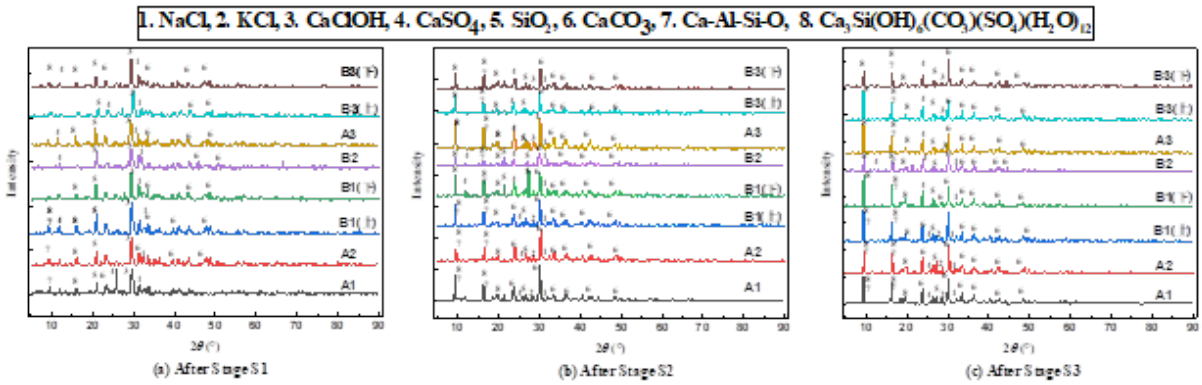

Fig. 5. XRD patterns of residual solid phase fly ash after leaching at different stages under different seepage paths (note: B1 (upper), B3 (upper) and B1 (lower), B3 (lower) are solid phase fly ash samples obtained from above and below B1 and B3 columns, respectively.).

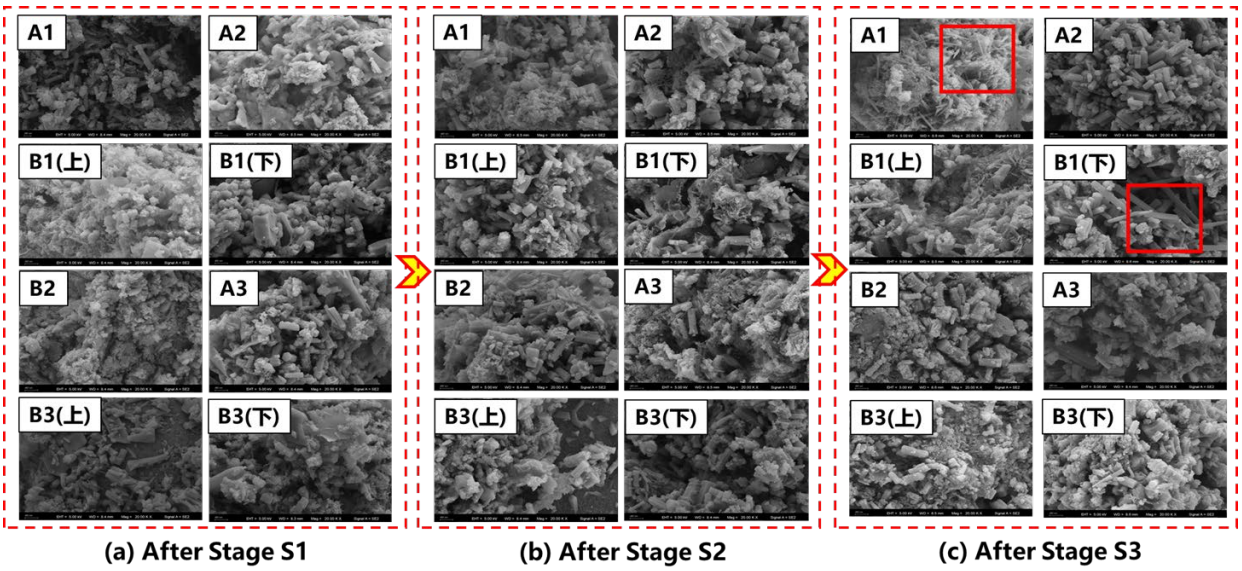

Fig. 6. Surface morphology of residual solid phase fly ash after leaching at different stages under different seepage paths (note: B1 (upper), B3 (upper) and B1 (lower), B3 (lower) are solid phase fly ash samples obtained from above and below B1 and B3 columns, respectively.).

4. Conclusions

The periodic SAR invasion with various seepage paths can affect the stability of heavy metals in fly ash to varying degrees, especially in the early stages of

each rainfall.

In the early stages of SAR invasion, the “top in and bottom out” mode (A1 and A3) was more likely to leach heavy metals from landfill fly ash compared to the “top left in and bottom right out” mode (B1 and B3).

The “dynamic leaching + static immersion + dynamic leaching” mode (A3 and B3) can quickly dissolve heavy metals in the early leaching stage of SAR, especially for Zn and Cd. Under the single “dynamic leaching” mode (A1 and B1), heavy metals in fly ash exhibited a long-term continuous leaching trend, especially for Pb, Cr, and Ni. The leaching of Cu was significantly affected by “dynamic leaching + static immersion + dynamic leaching” mode in stage S1, while it was significantly affected by “dynamic leaching” mode in stages S2 and S3.

The “top left in and top right out” mode (B2) was the only scenario where there was no damage to the bottom of the fly ash ton bag. The pH of the fly ash leachate was relatively low, and the stability of heavy metals in landfill fly ash was the best.

Enhancing the anti-seepage performance of fly ash ton bags (especially at the bottom of the bag) and standardizing the landfill operation process of fly ash play an important role in reducing the leaching risk of heavy metals in landfill fly ash. In addition, from the perspective of environmental risk management for landfill fly ash, special attention should also be paid to the long-term stability of heavy metals in landfill stabilized fly ash.

References:

Kyung-Jin, H., Shuzo, T., Toshio, K., 2000. Extraction of heavy metals from MSW incinerator fly ashes by chelating agents. J Hazard Mater. 75, 57-73.

Li, W., Gu, K., Yu, Q., Sun, Y., Wang, Y., Xin, M., Bian, R., Wang, H., Wang, Y.N., Zhang, D., 2021. Leaching behavior and environmental risk assessment of toxic metals in municipal solid waste incineration fly ash exposed to mature landfill leachate environment. Waste Manag. 120, 68-75.

Li, W., Sun, Y., Xin, M., Bian, R., Wang, H., Wang, Y.N., Hu, Z., Linh, H.N., Zhang, D., 2020. Municipal solid waste incineration fly ash exposed to carbonation and acid rain corrosion scenarios: Release behavior, environmental risk, and dissolution mechanism of toxic metals. Sci Total Environ. 744, 140857.

Li, W., Yu, Q., Gu, K., Sun, Y., Wang, Y., Zhang, P., Zheng, Z., Guo, Y., Xin, M., Bian, R., 2022. Stability evaluation of potentially toxic elements in MSWI fly ash during carbonation in view of two leaching scenarios. Sci Total Environ. 803, 150135.

Ma, W., Chen, D., Pan, M., Gu, T., Zhong, L., Chen, G., Yan, B., Cheng, Z., 2019. Performance of chemical chelating agent stabilization and cement solidification on heavy metals in MSWI fly ash: A comparative study. J Environ Manage. 247, 169-177.

STUDY ON NEUTRALIZATION OF INCINERATION ASH LAYER USING HIGHLY DISSOLVED CARBON DIOXIDE SOLUTION

Kentaro Miyawaki[1], Tomohiro Kishi[2], Ayana Matsumoto[3]
1 Department of Interdiciplinary Science and Engineering, Meisei University
2-1-1 Hodokubo, Hino-city, Tokyo, Japan
2 Meisei University (Graduated), 2-1-1 Hodokubo, Hino-city, Tokyo, Japan
3 Graduate School of Science and Engineering, Meisei University,
2-1-1 Hodokubo, Hino-city, Tokyo, Japan

INTRODUCTION

Incinerator residues in landfill retain alkalinity for long periods of time. Depending on landfill conditions and leachate collection and drainage conditions, leachate may have a high pH over a long period of time.

The neutralizing effect of atmospheric carbon dioxide (CO_2) on high pH leachate in the vicinity of collection pipes and after runoff has been investigated. And being studied is the inflow of CO_2 gas into the incinerator ash layer for the purpose of heavy metal fixation. There are several examples of the use of oxygen and ozone ultrafine bubbles (UFB) as leachate treatment to removal organic pollutants such as COD[1)]. However, there are no examples of studies of neutralization treatment of leachate or incineration residues with CO_2-dissolved UFB. Incineration residue-dominated landfill layers have complex voids.

The authors have been investigating the use of CO_2 as ultra-fine bubbles (UFBs) in solution and flowing down the incinerator ash layer, with the goal of slowly delivering CO_2 to the microscopic space.

METHODS

Sample and column influent

In the experiment, incinerated ash collected on December 8, 2022 at a municipal solid waste combustible waste processing facility was used. The incinerated ash was sealed and stored for a short period of time before use. The moisture content was 19.8%. CO_2-UFB water (CO_2 dissolution device: UFB generation loop type OK nozzle + pump) and pure water were used as the inflow water to the column.

Incinerator ash layer neutralization test (column)

A plastic column with an inner diameter of 53.8 mm and a total length of 200 mm was packed with three layers of incinerator ash 50 mm each (150 mm total). The packing density was 1.14 kg/m^3 under the CO_2-UFB condition and 1.20 kg/m^3 under the pure water condition. CO_2-UFB water and pure water were dropped into the incinerator ash layer to neutralize and wash out the ash. Inflow water was dripped at a rate of 500 mL/h (rainfall equivalent 220 mm/h) and the experiment was continued for 6 hours. Leachate from the bottom was collected every 30 minutes to measure pH, EC, ORP, and inorganic carbon (IC) concentrations, as well as TC and metals. Due to time constraints, water flow was stopped after 6 hours per day (L/S approximately 7.5), and water flow was continued for 6 hours the next day as well, for a total of 18 hours over 3 days.

Leaching test (sample after neutralization test)

The incinerator ash in the column after the neutralization test was divided into three parts: upper, middle, and lower. Leaching tests for each incinerator ash were conducted in accordance with JLT No.13 test. The pH, EC, and ORP of the solutions obtained were measured.

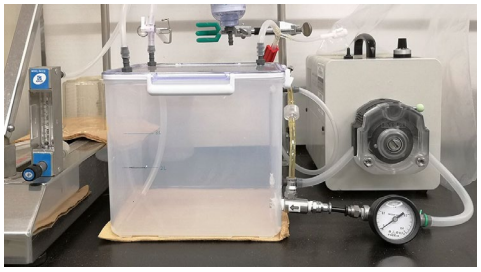

Photo 1 CO_2 dissolution equipment

Photo 2 Column test equipment

RESULT AND DISCUSSION

Incinerator ash layer neutralization test (column)

In the incinerator ash layer neutralization test (column test), the inlet water was flowed for 6 hours and stopped for 18 hours under the test conditions. This was repeated 3 times. Therefore, each measured value fluctuated significantly when water flow was resumed.

Figure 1 shows the pH change of the effluent with the water flow rate as the liquid/solid ratio L/S. Initially, the pH of the leachate was about 13 under all conditions, but at L/S 20, the pH dropped to 9.4 under the CO_2-UFB condition and to 11.8 under the pure water condition, indicating that the CO_2-UFB water supply can significantly reduce the leachate pH.

Figure 2 shows inorganic carbon (IC) changes of the effluent. IC was measured as a measure of dissolved CO_2. The initial IC was high. After L/S 15, the IC concentration increased under conditions where CO_2-UFB water was supplied (CO_2-UFB). This increase in IC occurred at the same time as the rapid decrease in pH (Figure 1).

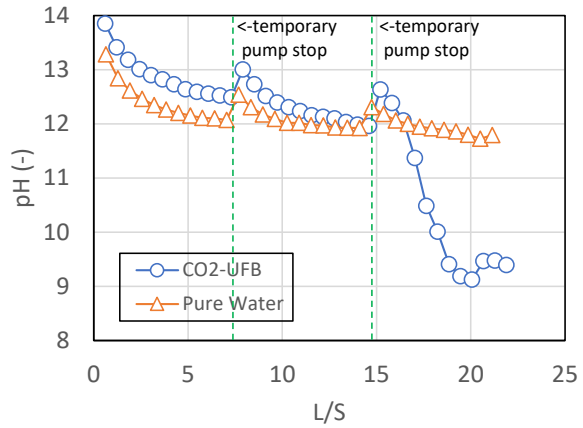

Figure 1 pH change of effluent

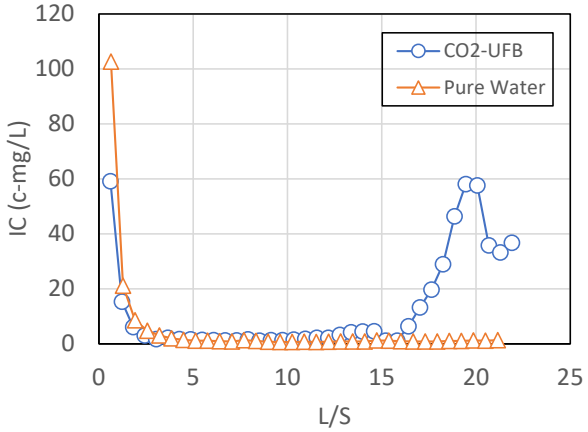

Figure 2 IC change of effluent

It was inferred that neutralization on the incinerator ash surface had progressed, allowing some of the incoming CO_2 to pass through unreacted. Assuming that inflow IC - outflow IC = CO_2 absorption, the value for L/S20 was 0.83 mmol/incinerator ash-g.

Figure 3 shows the calcium (Ca) concentration change. Since it is expected that Ca contained in incinerator ash reacts with absorbed CO_2 to form $CaCO_3$, we focused on the change in Ca concentration. In the CO_2-UFB condition, Ca began to be leached earlier than in the pure water condition and showed a decreasing trend after L/S 10. In the pure water condition, Ca was leached at a constant concentration from L/S 8 to 20.

Figure 4 shows the change in electrical conductivity (EC), which was similar for both the CO_2-UFB and pure water conditions, and the EC value was 1/10 by the initial L/S2, confirming the progress of washing out soluble salts. No particular CO_2 effect was observed.

Figure 5 shows the change in oxidation-reduction potential (ORP), which was not significantly different between the CO_2-UFB and pure water conditions for a certain period of time, although the CO_2-UFB condition tended to be more affected by the pause.

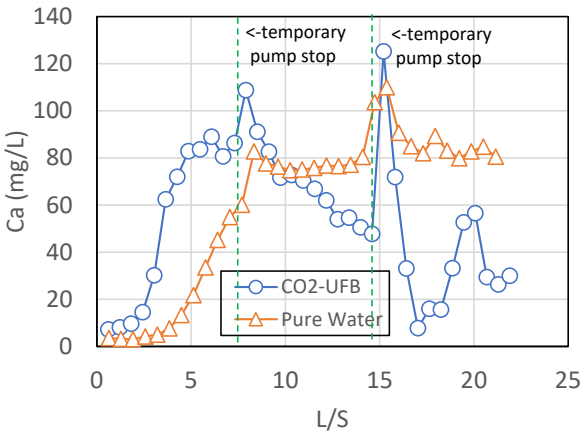

Figure 3 Ca concentration change of effluent

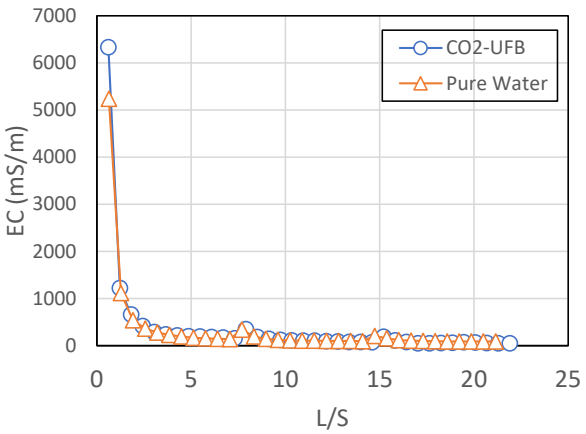

Figure 4 EC change of effluent

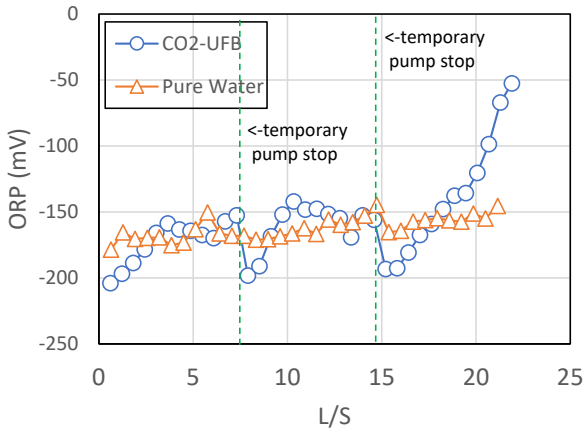

Figure 5 ORP change of effluent

Figure 6 shows changes in chromium Cr as an example of other metals in the effluent. The concentration was slightly higher in the initial period and decreased rapidly. The concentration of Cr remained higher in the CO_2-UFB condition than in the pure water condition, except in the initial period.
Chromium elution was also observed in the case of CO_2 gas ventilation[2)], and a similar trend was inferred.

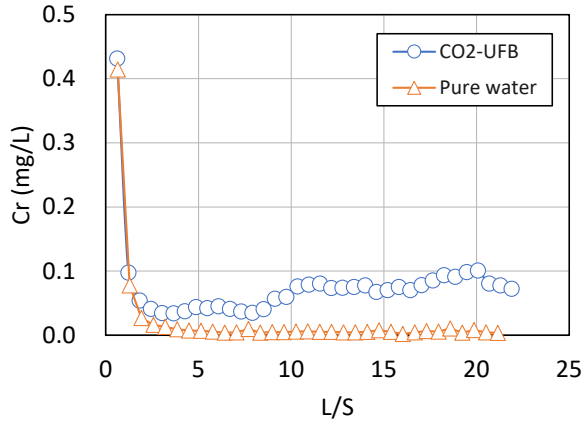

Figure 6 Cr change of effluent

Leaching test (sample after neutralization test)
The results of the leaching test on the incinerator ash after the column test are shown. Figure 7 shows the pH of the leaching tests for the upper, middle, lower, and pre-watering incinerator ash. under the CO_2-UFB condition, neutralization was observed to be progressing from the upper layer. Neutralization of the incinerated ash surface could be inferred. The results of the pure water condition confirmed that it is difficult to lower the pH by washing out alone. Figure 8 shows the EC, and it can be said that soluble salts can be reduced to 1/5 after washing out about L/S20. In addition, the CO_2-UFB condition tended to increase the dissolution of soluble salts.

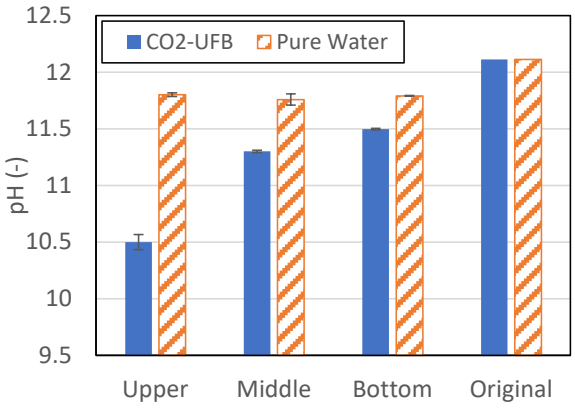

Figure 7 pH of leaching test

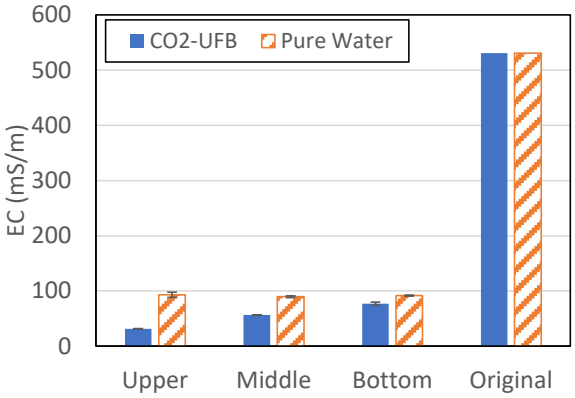

Figure 8 EC of leaching test

Surface Observation
Surface observations were made on the incinerator ash at the top of the column. Photo 3 shows the incinerator ash particles and Photo 4 shows the enlarged portion.

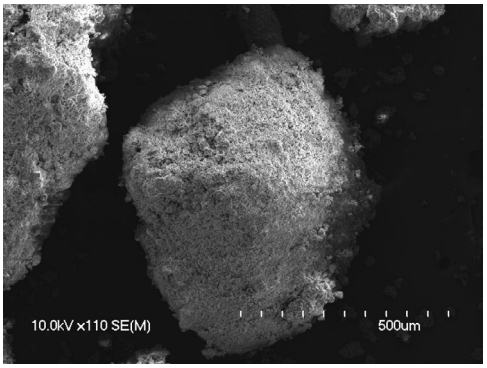

Photo 3 SEM image (Ash after column test)

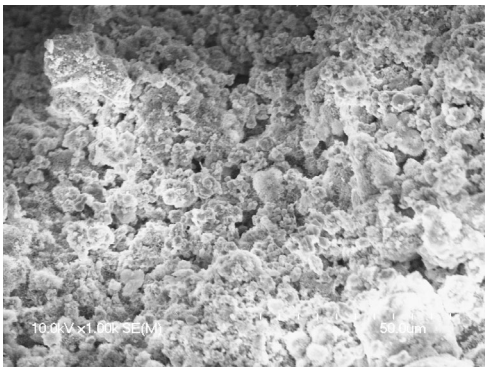

Photo 3 SEM image (Ash after column test)

SUMMARY
When a high carbon dioxide dissolved solution (CO_2-UFB water) was passed through the incinerator ash landfill layer, slow neutralization progressed, and the leachate pH decreased from 13 to 9.4 at about L/S20. Result of leaching test indicated that the incinerator ash was neutralized from the upper area.
Related tests are currently ongoing.

REFERENCES
1) for example: Mei Bai, Zhibin Liu, Liangtong Zhan, Zhu Liu & Zhanhuang Fan, A comparative study of removal efficiency of organic contaminant in landfill leachate-contaminated groundwater under micro-nano-bubble and common bubble aeration, Environmental Science and Pollution Research volume 29, pages87534–87544 (2022)
2). Koga Shigeizumi, Hiroshi Kubota, Haruna Kochi, Kenichi Sato, Takuro Fujikawa, Yosuke Nagayama, Hirofumi Sakanakura, Daigo Fujita, Elution and Mechanical Characteristics of Municipal Solid Waste (MSW) Incineration Bottom Ash that has Undergone Accelerated Carbonation Treatment using CO2 Recovered from Incineration Plant Exhaust, Journal of the Japan Society of Material Cycles and Waste Management, Vol. 31, PP 116-130 (2020)

ACKNOWLEDGEMENT
This research was supported by JSPS Grant-in-Aid for Scientific Research JP20K12227.

ETHANOL AND BIO-BASED PRODUCTS CO-PRODUCTION FROM WASTE MATERIALS VIA MICROBIAL FERMENTATION

Yongsheng Li[1], Haishu Sun[1], Yuanchun Zhang[1], Shuya, Duan[1], Dayi Qian[1,2], Xiaona Wang[1] and Qunhui Wang[1]

1 School of Energy and Environmental Engineering, University of Science and Technology Beijing, 30 Xueyuan Road, Haidian District, Beijing, 100083, China;
2 School of Chemistry and Environmental Science， Yili Normal University，Xinjiang Yining 835000，China.

INTRODUCTION

With the increase of global warming and other environmental problems, countries have established the goal of reducing carbon emissions. Ethanol, a representative of bioenergy, is now being added to gasoline as a supplement to automotive fuels because of its inherently high octane rating, good resistance to detonation, and low pollution [1].

The first generation of fuel ethanol relies mainly on food crops such as corn and sugarcane, whose production technology is mature and the ethanol yield is considerable. However, the development of fuel ethanol industry based on food crops as raw material may also cause national food security problems. In addition, conventional bioconversion to energy is based on the production of a single product, but due to thermodynamic and biological limitations, this does not maximize the use of the energy contained in biomass and is not economical [2]. Therefore, co-production of ethanol and biobased products from wastes not only reduces the use of food crops, but also fully utilizes the energy contained in biomass and enhances the profitability of ethanol production with the economic benefits of "by-products".In order to study the co-production of ethanol and biobased products from waste through microbial fermentation, this paper conducted a literature search and analysis based on the Web of science database, reviewed the research hotspots of ethanol co-production of biobased products, and outlined the challenges of the current co-production and the strategies for improvement.

MATERIALS AND METHODS

The data were searched in the core collection of Science Citation Index Expanded (SCI-E) – Clarivate Analytics' ISI – Web of Science© (WoS) for co-production of ethanol and biobased products. The type of search applied was "advanced search" applying the following logic operation: TS= (*ethanol or "*ethyl alcohol" or *alcohol) AND TS= co$produc* AND TS= (fermen* or yeast*).

RESULT AND DISCUSSION

Ethanol, as an important bioenergy source, has a wide range of co-production potential to generate a variety of valuable biobased products. Fig. 1 provides an overview of ethanol and biobased product co-production.

Fig. 1. The overview of ethanol and biobased product co-production.

The co-production of ethanol and bioenergy such as hydrogen can be widely used in automotive fuels, fuel cells, household natural gas, aviation kerosene, etc., to maximize the use of energy resources by making full use of the energy in biomass. In practical research, there are various process methods for ethanol and bioenergy

cogeneration, and Fig. 2 is an example of ethanol and methane cogeneration to introduce the process pathway used in the research process.

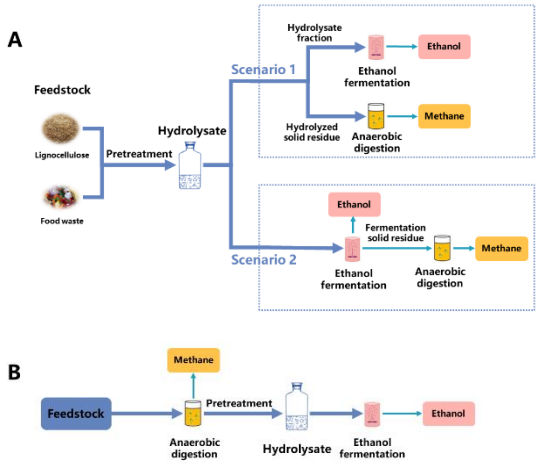

Fig. 2. Process flow diagram of ethanol and methane co-production. (A) Adapted from [3]. (B) Adapted from [4].

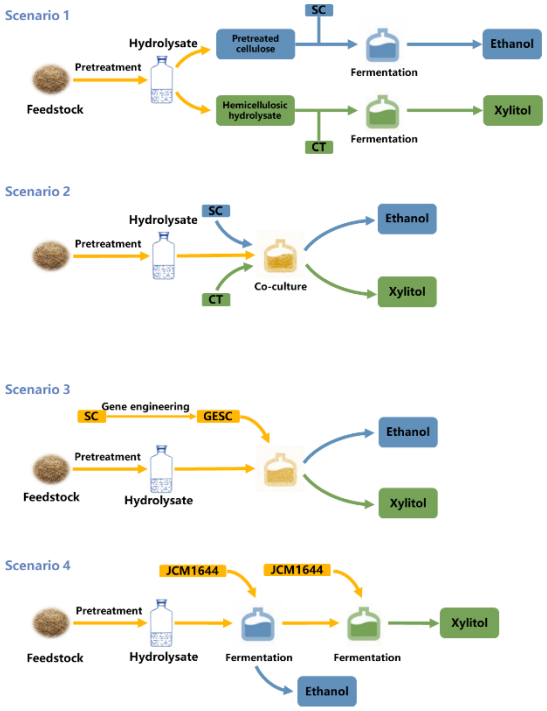

Fig. 3. Schematic diagram of the process flow of ethanol and xylitol co-production. Note: SC: Saccharomyces cerevisiae; CT: Candida tropicalis; GESC: Gene engineering Saccharomyces cerevisiae; JCM1644: Candida sojae JCM 1644

In addition, ethanol can be co-produced with high value-added products such as xylitol, and these co-produced products have a wide range of prospects for application in the fields of sweeteners, new environmentally friendly materials, pharmaceutical products, etc., which can improve the economic returns and increase the added value of the industry. Ethanol and these high value-added products co-production also has a variety of process pathways (Fig. 3).

Through the strategy of multi-product co-production, ethanol production can achieve efficient utilization of resources and enhance the sustainable development of the bioenergy industry. However, pretreatment of higher amount of lignocellulose in wastes, improvement of fermentation process and removal of inhibitory components during metabolism are challenges that need to be addressed urgently. Development of better and more environmentally friendly pretreatment processes, genetic modification and metabolic engineering of fermentation strains are good options.

CONCLUSION

In the current study, the yield of co-production of feedstocks has not reached the optimal target, and it is necessary to synthesize the advantages of the existing pretreatment technologies to study more advanced pretreatment technologies as well as to adopt some genetic technologies for strain improvement. Despite some challenges, the future of ethanol co-production is promising based on the advantages of co-producing ethanol with biobased products.

ACKNOWLEGEMENT

This work was supported by Special Fund for Key Science & Technology Program in Xinjiang Province（2022B02021-1) and the National Key R&D Program of China (Grant NO. 2022YFE0105700).

REFERENCE

[1] Göktaş M., Kemal Balki M., Sayin C., et al. An evaluation of the use of alcohol fuels in SI engines in terms of performance, emission and combustion characteristics: A review. Fuel, 2021, 286:119425

[2] Unrean P., Ketsub N. Integrated lignocellulosic bioprocess for co-production of ethanol and xylitol from sugarcane bagasse. Industrial Crops and Products, 2018, 123:238-246

[3] Wu, C.F., Wang, Q.H., Xiang, J., Yu, M., Chang, Q., Gao, M., Sonomoto, K., 2015. Enhanced Productions and Recoveries of Ethanol and Methane from Food Waste by a Three-Stage Process. Energy & Fuels 29, 6494-6500.

[4] Kaur, M., Kumar, M., Singh, D., Sachdeva, S., Puri, S.K., 2019. A sustainable biorefinery approach for efficient conversion of aquatic weeds into bioethanol and biomethane. Energy Conversion and Management 187, 133-147.

RECENT PROGRESS AND TRENDS IN MICROBIAL LIPID PRODUCTION FROM BIOMASS WASTES

Haishu Sun[1], Zhen Gao[2], Xiaona Wang[1] and Qunhui Wang[1]
1 School of Energy and Environmental Engineering, University of science and technology Beijing, 30 Xueyuan Road, Haidian District, Beijing, China
2 Foshan Gaoming District No.1 Senior High School, 68 Xinghe Road, Gaoming District, Foshan, Guangdong, China

ABSTRACT
Microbial lipids have attracted attention as an intriguing alternative for the biodiesel and oleochemical industries to achieve sustainable energy generation. However, large-scale production is hindered by high processing costs. As multiple variables affect lipid synthesis, an up-to-date overview that will benefit researchers studying microbial lipids is necessary. In this review, the most studied keywords from bibliometric studies are first reviewed. Based on the results, the hot topics in the field were identified to be associated with microbiology studies that aim to enhance lipid synthesis and reduce production costs. The research updates and tendencies of microbial lipids were then analyzed in depth. In particular, feedstock and associated microbes, as well as feedstock and corresponding products, were analyzed in detail. Strategies for lipid biomass enhancement were also discussed, including feedstock adoption, value-added product synthesis, selection of oleaginous microbes and cultivation mode optimization. Finally, the environmental implications of microbial lipid production and possible research directions were presented.

KEYWORDS: Single cell oil; Feedstock; Oleaginous microbe; Cultivation mode; Environmental implications

INTRODUCTION

Global climate change and other environmental problems resulting from the excessive consumption of fossil fuels are urgent concerns. Faced with a shortage of petrochemical petroleum, the contradiction of food for oil, and deteriorating environmental problems, it is urgent to develop renewable, clean, and environmentally friendly energy sources. Microbial lipids have emerged as promising substitutes for the oleochemical industry in a move toward renewable and sustainable energy production. However, large-scale microbial lipid development is limited by high processing costs. Therefore, the exploration of cost-effective feedstocks, combined with the use of waste substrates, which are environmentally and economically sustainable, might be a feasible alternative for reducing costs [1].

Oleaginous microbes can efficiently utilize low-cost biomass wastes for lipid production. Certain species of oleaginous microbes possess inherent oleaginous properties. Identifying excellent oleaginous strains is crucial for industrializing microbial lipids. Industrial production strains should be stable, highly productive, with the ability to assimilate diverse carbon (C) sources and be tolerant to a wide range of inhibitors in complex substrates. In addition to using inexpensive raw materials, co-producing microbial lipids with valuable compounds like pigments and polyunsaturated fatty acids can improve the economics of microbial lipids [2].

To enhance the economic competitiveness of microbial lipid production, cultivation modes have been optimized. While microorganisms have inherent pathways for lipid synthesis, the theoretical yield is limited to around 0.2-0.3 g/g, which hampers industrial production. Biomass growth is dominant when C and nitrogen are abundant, but lipid synthesis requires limited nutrients and sufficient C. Therefore, optimizing cultivation modes is crucial to meet the distinct nutrient demands of these two stages. Maximum lipid yield is achieved when minimal carbon flux is directed towards biomass growth [3].

Owing to the crucial role of microbial lipids in promoting environmental and economic sustainability, more than 3000 articles have been published over the last 2 decades. However, most review papers on this topic focus on limited factors and lack comprehensive recommendations for improving lipid biosynthesis. To address this gap, this review provides a comprehensive overview of key research areas in microbial lipids. Recent advancements and trends in the most studied keywords related to microbial lipids are thoroughly discussed, along with an overview of cultivation modes optimization to maximize lipid production. The review also explores the environmental implications of microbial lipid production and suggests potential research directions. Overall, this study aims to inspire further innovation in the microbial lipid production.

RESEARCH TENDENCIES ANALYSIS

Research on microbial lipids was initially limited, with only a few publications per year until 2008 (Fig.1). However, since 2010, the number of articles has substantially increased, likely due to factors such as active clinical and safety trials and the establishment of organizations focused on microbial lipid production. Notably, over 300 papers were published in 2021 alone, indicating a significant increase in researchers' interest in this topic. The keywords associated with research on microbial lipids include feedstocks, oleaginous microbes, products, research methods, cultivation modes, and products. Among these, oleaginous microbes and products have received the most attention.

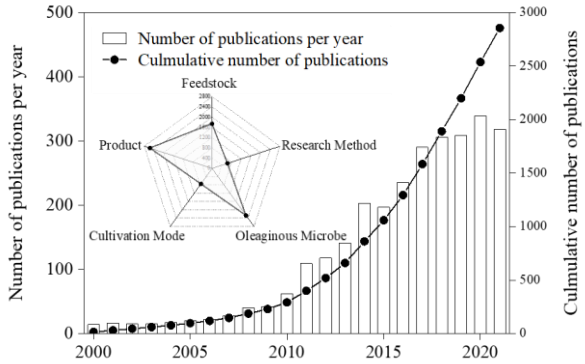

Fig.1 Number of publications and keywords analysis on microbial lipids during the past 21 years.

FEEDSTOCKS

Feedstocks and associated oleaginous microbes

In terms of feedstock, the most frequently used carbon source is glucose. Recently, the utilization of low-cost materials such as food waste and lignocellulosic biomass for the production of microbial lipids has attracted widespread attention (Fig.2). Additionally, glucose-based wastes such as molasses have been utilized for lipid production. Oleaginous microorganisms have garnered significant attention due to their abundant resource availability, high lipid content, short generation time, and broad carbon source utilization. Among the oleaginous microbes, yeast had the highest occurrences, followed by microalgae, molds, and bacteria.

Oleaginous yeasts, such as *Lipomyces*, *Rhodotorula*, and *Rhodosporidium*, are extensively studied for their ability to produce lipids from a wide range of low-cost materials. These yeasts are known for their rapid consumption of diverse organic materials and stable lipid production, making them popular choices for microbial lipid production. *Lipomyces*, for example, can convert hemicellulosic hydrolysate sugars into lipids without detoxification, making it promising for lipid generation in the presence of toxic components. *Rhodotorula* is commonly used for natural carotenoid production, while *Rhodosporidium* species can convert lignocellulosic biomass into lipids. *Yarrowia lipolytica*, a preferred yeast for lipid production, has its genome sequenced, enabling synthetic biology and genetic engineering applications to enhance lipid production [4].

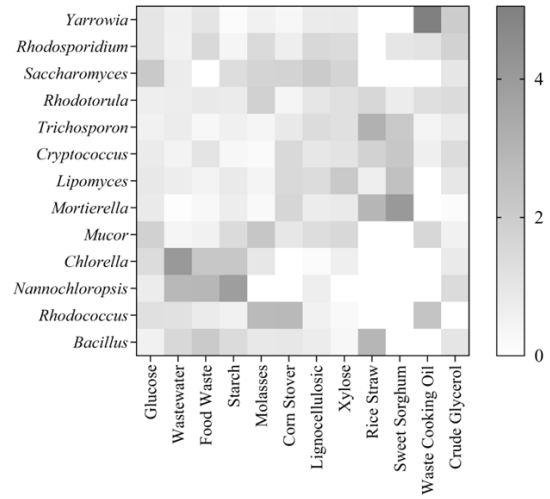

Fig.2 Frequently studied feedstocks and their associated microbes for lipid production.

Feedstocks and corresponding products

Research on microbial lipid from numerous raw materials is mainly focused on biodiesel (Fig.3), because the FA compositions of microbial lipid are comparable to vegetable oils commonly used for the synthesis of first-generation biodiesel. The utilization of microbial sources for biodiesel production has been considered the most reliable and appropriate strategy to meet the productive, technical, and environmental demands. However, the high cost of raw materials is a key factor that limits the popularity and application of microbial lipid. Therefore, the development of low-cost and easily available raw materials is one of the hot spots for research into products derived from microbial lipid. In addition, it is worth noting that small amounts of microbial lipid can also be very valuable. The valorization of low-cost raw materials towards the production of value-added PUFAs such as GLA, EPA, ARA, and DHA are attracting increasing interest [5].

EPA, particularly ethyl esters, are commercialized for hypertriglyceridemia treatments. Lignocellulosic biomass is a frequently studied source that can be utilized as a low-cost C source for PUFA synthesis, not only because lignocellulosic biomass is a renewable supply of sugars for the production of value-added products but also because it is a plentiful waste stream.

DHA is essential for correct brain and visual development in newborns. *Crypthecodinium cohnii* is well-known for producing high amounts of DHA-

enriched lipids, with DHA content typically ranging from 30-50%. To achieve efficient DHA production, lignocellulosic hydrolysates are often used as feedstocks for *C. cohnii* [6].

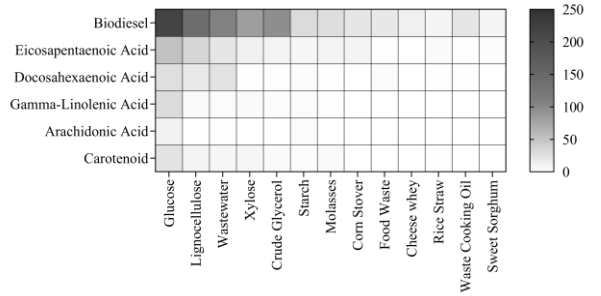

Fig.3 Frequently studied feedstocks and the corresponding products.

CULTIVATION MODES

The culture mode can affect the yield and productivity of microbial lipid. The primary culture modes may be categorized into batch, fed-batch, and continuous based on the various nutrient amendment methods (Fig.4). To obtain high cell density and product yield, fed-batch mode is preferred over other cultivation strategies. Owing to the different needs of oleaginous microbes at different stages, two-stage fermentation or two-stage fed-batch cultivation have received substantial attention in recent years [7].

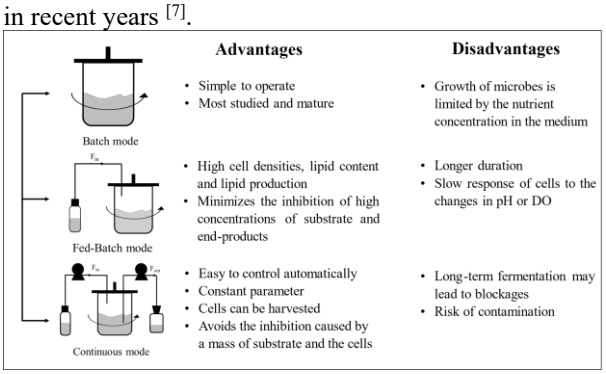

Fig.4 Comparison of several common cultivation modes utilized for lipid production

Microbial lipid production consists of two stages, in which the biomass first grows, and then lipid accumulation occurs. The cell proliferation phase requires a rich medium, whereas the lipid accumulation requires only a carbon source. The difference in nutritional demand between biomass growth and lipid yield presents a dilemma. Two-stage cultivation is used to separate the cell proliferation and lipid accumulation phases, thereby creating an environment suitable for biomass growth and lipid accumulation. This mode allows oleaginous microbes to increase biomass under suitable conditions and then transfer to another system for lipid accumulation, which has been demonstrated to improve lipid production. Two-stage fermentation can be implemented in both fed-batch and continuous modes and allows easy adjustment of the two stages by modifying the nutrient input. Two-stage fermentation is not limited to nutrients; other factors, such as pH, C/N ratio, DO, and temperature, could be adjusted to ensure that the culture conditions are more targeted for both phases [8].

Our group developed a two-stage fermentation mode: *ex situ* and *in situ*. As we found that lactic acid can promote cell proliferation but inhibit lipid accumulation, a two-stage fermentation was developed using *R. toruloides* in different systems with high and low lactic acid concentrations. After 4 days of cell proliferation in 100 mL of saccharified food waste liquid (lactic acid concentration of 8.3 g/L), the yeast was transferred to 100 mL of saccharified liquid (lactic acid concentration of 0.3 g/L) prepared from fresh food waste for 6 days for lipid accumulation. Compared to traditional one-stage fermentation, this *ex situ* two-stage fermentation resulted in a total lipid concentration of 9.19 g/L and a lipid yield of 0.204 g/g total sugar, which increased by 44.27% and 60.63%, respectively [9].

In addition, as an acidic environment (pH 4.0) can promote the cell proliferation of *R. toruloides* and an alkaline environment (pH 11.0) can promote lipid accumulation, an *in situ* two-stage fermentation mode based on pH in the same medium was developed; that is, after adjusting the pH of the hydrolysate to 4.0, sterilization and inoculation for acid stage fermentation was conducted for 1 day. The pH value was then adjusted to 11.0, and the yeast was fermented in an alkaline stage for 5 days, in which the maximum lipid production was 6.94 g/L, which was 84.6% higher than that in the traditional single stage fermentation [10]. In conclusion, the *ex situ* two-stage fermentation mode can tolerate greater lactic acid concentrations in the substrate, whereas the *in situ* fermentation mode enables greater lipid production and has potential for practical use.

ENVIRONMENTAL IMPLICATIONS AND FUTURE DIRECTIONS

Several environmental issues have arisen as a result of the use of fossil fuels, such as global warming caused by greenhouse gas emissions produced during the combustion of fossil fuels to generate electricity. The swift rise of renewable energy sources is in line with the concept of “more energy, less C emissions”. Microbial lipid has been identified as an attractive possibility for biochemical production. Biodiesel produced from microbial lipids presents a number of benefits over traditional petroleum-based diesel, such as being a safer and cleaner alternative for the environment. A recent study indicated that converting global food waste into biodiesel could potentially replace around 27.9 million

tonnes of mineral diesel, leading to a reduction of roughly 0.31 million tonnes of CO_2 emissions [11]. Also, microbial lipid can be generated by biomass wastes, and part of it solves the problem of waste disposal.

Large-scale microbial lipid production has been extensively studied, but the high costs associated with commercial application remain a major challenge. On the other hand, microbial conversion processes have low product concentrations, which increase downstream processing costs. To address these challenges, several approaches need to be considered. First, it is crucial to further explore low-cost, substantial, and sustainable feedstocks for lipid synthesis. Waste streams for lipid production need to be identified and adopted, such as lignocellulosic biomass, which is the most abundant for energy recovery. However, lignin is difficult to degrade. The future studies should focus on the structural characterization of lignocellulosic waste, mechanisms of degradation, and process development for valorization. The pretreatment of raw substrates is also necessary to enhance the efficiency of the process. Second, selecting or encoding new strains will definitively improve the lipid generation from wastes. Although several key genes have been identified through genetic engineering and the effects of these genes have been studied independently, future research should explore theories that explain how two or more genes interact in the process. Furthermore, a systems biology technology based on omics and computational models will aid in the design and reconstruction of superior strains for lipid production enhancement. Third, the fermentation process is quite important to the total cost. Developing two-stage fermentation modes might promote high lipid production while supplying nutrients at the appropriate fermentation phase. Additionally, studying the kinetics of the system allows for a better understanding of the fluxes and interactions between important factors, enabling the prediction of different conditions. Eventually, the co-production of high value-added products is required for economic viability. More attention should be paid in future research to the regulation of the C flow in the co-production process, which will aid in achieving a maximum theoretical yield of multiple products.

CONCLUSION

Microbial lipids, as renewable energy sources, may be a promising approach to tackle the problems of fossil fuel depletion, environmental contamination, and climate change. However, large-scale microbial lipid production is still limited owing to high processing costs. The main opportunity is to study feedstock supply and cultivation mode optimization to produce high value-added products. However, to actualize this progress, low-cost, substantial, and sustainable raw materials must be explored. Highly effective oleaginous strains must be selected or encoded, and the involvement of two or more genes in lipid biosynthesis must be clarified. In a single study, focusing on a particular feedstock and examining its fermentation using a group of oleaginous bacteria as both novel candidates and controls were preferred. Simultaneously, exploring and stabilizing the synthesis route of high-value-added products could expand the commercial applications of microbial lipids.

REFERENCES

[1] Tan X, Zhang Y, Zhao X, Yang L, Yangwang S, Zou Y, Lu J (2022) Anaerobic digestates grown oleaginous microalgae for pollutants removal and lipids production. Chemosphere 308: 136177.

[2] Chaturvedi S, Bhattacharya A, Nain L, Prasanna R, Khare SK (2019) Valorization of agro-starchy wastes as substrates for oleaginous microbes. Biomass Bioenerg 127: 105294.

[3] Das M, Patra P, Ghosh A (2020) Metabolic engineering for enhancing microbial biosynthesis of advanced biofuels. Renew Sust Energ Rev 119: 109562.

[4] Brandenburg J, Blomqvist J, Shapaval V, Kohler A, Sampels S, Sandgren M, Passoth V (2021) Oleaginous yeasts respond differently to carbon sources present in lignocellulose hydrolysate. Biotechnol Biofuels 14:124.

[5] Tomas-Pejo E, Morales-Palomo S, Gonzalez-Fernandez C (2021) Microbial lipids from organic wastes: outlook and challenges. Bioresour Technol 323:124612.

[6] Jakhwal P, Biswas JK, Tiwari A, Kwon EE, Bhatnagar A (2022) Genetic and non-genetic tailoring of microalgae for the enhanced production of eicosapentaenoic acid (EPA) and docosahexaenoic acid (DHA)-A review. Bioresour Technol 344: 126250.

[7] Polburee P, Limtong S (2020) Economical lipid production from crude glycerol using *Rhodosporidiobolus fluvialis* DMKU-RK253 in a two-stage cultivation under non-sterile conditions. Biomass Bioenerg 138: 105597.

[8] Zhang X, Chen J, Wu D, Li J, Tyagi RD, Surampalli RY (2019) Economical lipid production from *Trichosporon oleaginosus* via dissolved oxygen adjustment and crude glycerol addition. Bioresour Technol 273: 288-296.

[9] Ma X, Gao Z, Gao M, Wu C, Wang Q (2019) Microbial lipid production from food waste saccharified liquid under two-stage process. Bioresour Technol 289: 121626.

[10] Gao Z, Ma YQ, Ma XY, Wang QH, Liu Y (2019) A novel variable pH control strategy for enhancing lipid production from food waste: Biodiesel versus docosahexaenoic acid. Energy Convers Manage 189: 60-66.

[11] Gao Z, Ma Y, Liu Y, Wang Q (2022) Waste cooking oil used as carbon source for microbial lipid production: Promoter or inhibitor. Environ Res 203: 111881.

EFFICACY OF ORGANIC CHELATORS IN STABILIZING HEAVY METALS WITHIN MUNICIPAL SOLID WASTE INCINERATION FLY ASH

Ze Zhang [1], Zhongli Luo [2], Amirhomayoun Saffarzadeh [3], Chuanfu wu [1]

1 Department of Environmental Engineering, School of Energy and Environmental Engineering, University of Science and Technology Beijing, 30 Xueyuan Road, Haidian District, Beijing 100083, China

2 Organic Materials Research Laboratory, Tosoh Corporation, Shunan,746-8501, Japan

3 Department of Urban and Environmental Engineering, Graduate School of Engineering, Kyushu University, West 3, 744 Motooka, Nishi-ku, Fukuoka 819-0395 Japan

INTRODUCTION

Domestic waste incineration power generation technology is the most effective way to realize the resourcefulness and harmlessness of municipal solid waste, and has been more widely applied and promoted (Soltanian et al., 2022; Tian et al., 2023; Zhang et al., 2023). Currently, the total amount of municipal solid waste incinerated in China has exceeded 100 million tons per year, with incineration accounting for more than 60 percent of the overall solid waste, and continues to show an upward trend (Wang et al., 2020). Municipal solid waste incineration fly ash (MSWI FA) from the incineration process accounts for 3-5 percent of the total amount of waste generated, and its annual production has exceeded 10 million tones in China. (C et al., 2020; Phua, 2019). MSWI FA is recognized as a hazardous waste (coded HW18) due to its high content of leachable heavy metals (HMs) and chlorides and persistent organic pollutants (Chen et al., 2022; Ma et al., 2021). Nowadays, landfilling is considered the main disposal method for MSWI FA, but direct landfilling may cause serious groundwater and soil contamination due to the easily leachable toxic HMs. Therefore, harmless pre-treatment of MSWI FA is required before landfilling (Liu et al., 2018; Wang et al., 2021).

MSWI FA can currently be disposed of through separation and solidification/stabilization (S/S). Some researchers have used the pre-washing method to extract the highly soluble hazardous elements from MSWI FA in an effort to lessen the impact of the substance on the environment. However, this method uses a lot of water or acid and produces a lot of hazardous waste liquids, which, if handled improperly, can lead to secondary pollution (Han et al., 2023; Wei et al., 2022; Yan et al., 2022). Some research has concentrated on the S/S of MSWI FA using cement-based binders such cement and slag, but this approach has a high volume growth ratio, poor heavy metal solidified capacity, and poor long-term stability of the solidified body (Jiang et al., 2022; Tian et al., 2021; Wang et al., 2023). When MSWI FA is heated to high temperatures during the vitrification process, although hazardous substances can be effectively immobilized (Huang et al., 2022; Jiang et al., 2022), The process must be used at a high temperature of 1100–1500°C, and its applicability is hampered by its high energy consumption (Song et al., 2023). In contrast, chemical stabilization of MSWI FA is a highly effective and eco-friendly pretreatment technique (Zhu et al., 2022).

Chemical stabilizers are classified into inorganic and organic stabilizers. Inorganic stabilizers (e.g., sulfides, phosphates, and molybdates) have been widely evaluated and used in previous studies (A et al., 2020; C et al., 2021). It has been shown that Na_2S and sodium NaH_2PO_4 do not stabilize HMs in MSWI FA, even at levels higher than 5% (Zhu et al., 2020). Researchers have suggested alternate techniques of stabilization that include organic chelating agents (CAs), such as thiourea derivatives, chitosan, and dithiocarbamate (DTC) formate, to get around the drawbacks of inorganic stabilizers (Li et al., 2019; Ma et al., 2019). These organic CA chelate HMs in the form of covalent and ligand bonds, have high stability properties, and are virtually unaffected by environmental conditions. The amount of organic CA used in the MSWI FA chelating stabilization procedure is lower than that of inorganic stabilizers, but it has a better stabilizing impact on HMs (particularly Pb and Cd) (Zhang et al., 2020). Previous studies have shown that DTC-based CAs have better treatment effects than other organic CAs due to the formation of stable macromolecular complexes of sulfur groups with HMs (Sun et al., 2018; Tian et al., 2016). However, due to various production techniques and raw ingredients, the DTC-based CAs available on the market have quite diverse effects. Piperazine chelators (piperazine dithiocarbamates) and SDD (dithiocarbamates) are now the two most common DTC-based chelators.

In order to stabilize heavy metals in MSWI FA, two piperazine chelators and one SDD chelator were used in this investigation, the research mainly consists of: i) Comparison of the stabilization effects of three CAs at different addition levels, stabilization times, and extracts ; ii) Environmental risk assessment of HMs in MSWI FA before and after chelation ; iii) The MSWI FA before and after chelation was characterized in order to better understand the mechanism of action of DTC chelators in stabilizing HMs.

MATERIALS AND METHODS

Materials

The MSWI FA used in this study was obtained from Chengdu and the incinerator was of grate type. The MSWI FA was sieved through 40 mesh.

Heavy metal organic CAs include piperazine dithiocarbamate (TS300) from Japan, dithiocarbamate (SDD) from China and piperazine dithiocarbamate (PD) from China.

Stabilization Experimental Methods

The 50g of MSWI FA was weighed using an electronic balance after the original MSWI FA had dried completely. CAs and ultrapure water were then added in accordance with a specific weight percentage to make sure that the water-ash ratio was 0.25 (wt%). The mixture was then stirred for 10 minutes before being sealed and stored.

Leaching Tests

(1) Leaching of heavy metals under mixed landfill conditions

With reference to the requirements of the Chinese standard < *Solid Waste-Leaching Toxicity Leaching Method-Acetic Acid Buffer Solution Method* > (HJ/T 300-2007), the leaching of MSWI FA before and after stabilization was simulated in the environment of a mixed landfill of domestic waste after leaching by refuse leachate, the leaching solution was acetic acid with pH = 2.64. Finally, the HMs concentrations in the leaching solution were analyzed by an inductively coupled plasma-atomic emission spectrometer (ICP-AES) according to the Chinese standard method < *Solid Waste-Determination of 22 metallic elements-Inductively coupled plasma emission spectrometry* > (HJ 781-2016).

(2) Leaching of heavy metals under compartmentalized landfill conditions

With reference to the standard < *Solid Waste-Leaching Toxicity Leaching Method-Sulfuric Acid Nitric Acid Method* > (HJ/T 299-2007), simulating the leaching of MSWI FA before and after its stabilization in a partitioned landfill environment after acid rain drenching, with leaching agent pH = 3.20 ± 0.5 (H_2SO_4 : HNO_3 = 2:1). Finally, the HMs concentrations in the leaching solution were analyzed by an inductively coupled plasma-atomic emission spectrometer (ICP-AES) according to the Chinese standard method < *Solid Waste-Determination of 22 metallic elements-Inductively coupled plasma emission spectrometry* > (HJ 781-2016).

(3) Total amount of heavy metals

The total amount of HMs in the original MSWI FA was determined using the microwave digestion method in < Solid Waste-Determination of 22 metallic elements-Inductively coupled plasma emission spectrometry > (HJ 781-2016). According to the standard method in (HJ 781-2016), the concentration of HMs in the digested solution was detected and analyzed using an inductively coupled plasma-atomic emission spectrometer (ICP-AES).

Environmental risk assessment

The Risk assessment code (RAC) is used to assess each heavy metal's independent potential environmental risk under various disposal scenarios. Based on the readily bioavailable portion of the solid-phase matrix HMs fractions (the ratio of the acid-soluble state to the total amount of heavy metals in the BCR method), which is calculated as shown in Equation 1, the RAC independently determines the potential environmental risk level of various HMs. The classification of the environmental risk level of HMs is shown in Table 1.

$$RAC(\%)=\frac{F1}{F1+F2+F3+F4}\times 100 \quad (1)$$

Where: F1, F2, F3 and F4 represent the acid-soluble, oxidizable, reducible and residual fractions, respectively; F1 represents the content of components with high bio-efficacy of heavy metals, mg/kg.

Table 1 Classification of Heavy Metal Environmental Risk Levels by RAC Method

RAC index	Environmental risk level
RAC≤1%	Safety
1%＜RAC≤10%	Low risk
10%＜RAC≤30%	Medium risk
30%＜RAC≤50%	High risk
RAC＞50%	Extremely high risk

RESULT AND DISCUSSION

Heavy metals contents and leaching characteristics of MSWI FA

Table 2 shows that the raw MSWI FA had a Zn value of 4770 mg/kg, followed by a Pb concentration of 740 mg/kg. Zn is mainly sourced from galvanizing , smelting , machinery manufacturing , organic synthesis , mine, Pb is mainly sourced from gasoline additives , ammunition , solder , paint , pesticide (Fan et al., 2018). Zn was only leached at a concentration of 0.345 mg/L, though. The leaching concentration of other heavy metals in the ash, with the exception of Pb, was

Table 2 Total content and leaching concentration heavy metals in raw municipal solid waste incineration fly ash

Items	Heavy metals						
	As	Zn	Pb	Ni	Cd	Cr	Cu
Total content (mg/kg)	170	4770	740	350	220	10	405
Leaching concentration (mg/L)	0.005	0.345	0.461	0.004	0.013	0.021	0.03
GB16889-2008 (mg/L)	0.3	100	0.25	0.5	0.15	4.5	40

evidently far lower than the limit value of the < *Landfill Pollution Control Standard* > (GB 16889-2007). The leaching concentration of Pb was 0.461mg/L, which was higher than the specified 0.25mg/L. Therefore, Pb was the focus of this study to screen the best stabilizer and the optimal amount of additive.

Leaching of heavy metals from MSWI FA before and after chelation stabilization (mixed landfill)

As shown in Figure 1(a), under the mixed landfill condition, all the three CAs have good stabilizing effect on Pb, and the leaching concentration of Pb is 0.073 mg/L, 0.194 mg/L, and 0.127 mg/L, respectively, which is already lower than the limit of the regulations of GB 16889-2007 when the addition amount is 0.3%. The reason for this is that the organic CA contains coordination atoms like S, N, and O that combine with heavy metal ions to form cyclic complexes through coordination and ionic bonds. The resulting macromolecular organic CAs also have an adsorption effect on heavy metal ions, which further lessens the toxicity of Pb leaching. The leaching concentration of zinc under the acetic acid leaching condition was substantially lower than the standard limit of 100 mg/L, and the stabilizing effect of the three CAs on zinc was not immediately apparent. The leaching concentration of Cd increased noticeably and beyond the standard of 0.15 mg/L with the addition of a minor dose of chelating agent (0.3%–1.0%). This might be as a result of the inclusion of CAs, which raised the pH of the leaching environment and increased Cd leaching. When the CAs was added at 1.5%, the leaching concentration of both Pb and Cd had a decreasing trend and was lower than the standard limit value, which might be due to the fact that the CA preferentially reacted with Pb^{2+} to generate macromolecular complexes of Pb, and when the CA was added in excess, it reacted with Cd^{2+} to generate complexes of Cd. From Fig. 1 (a), it can be seen that TS300 has the best stabilization effect, when the addition amount of TS300 is 0.3%, the Pb leaching concentration is 0.073 mg/L, and the stabilization rate is more than 84.16% ; when the addition amount is 1.5%, the Pb leaching concentration is 0.009 mg/L, and the chelation rate is more than 98%. This is because the TS300 has a piperazine fraction that is greater than 40% and contains more DTC groups.

The leaching concentration of the three CAs showed a decreasing and then increasing trend of the three HMs in 28 days at the addition of 0.3% (Fig. 1(b)). This could be because the reaction between the HMs and DTC groups was incomplete on day 0, so there was a decreasing trend in the leaching of the HMs from day 0 to day 3, and with the passage of time, the complexes were gradually oxidized, causing the HMs to be re-released, an increasing trend. The MSWI FA of 0.3%-TS300 had the lowest leaching concentrations of Pb and Zn after 28 days of maintenance, at 0.083 mg/L and 0.138 mg/L, respectively, as shown in Fig. 1(b). The leaching concentrations of Pb and Zn were still below the standard limits after 28 days of sequestration. Although the leaching of Cd in the raw MSWI FA did not exceed the requirement (as shown in Table 1), it did so with the addition of the CAs.

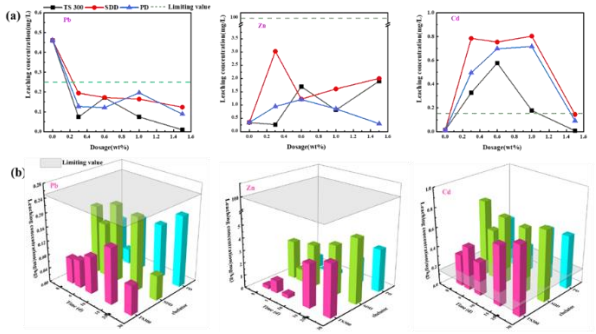

Figure 1: (a) Leaching of Pb, Zn, and Cd under mixed landfill conditions; (b) Trends in leaching concentrations of Pb, Zn, and Cd under mixed landfill conditions over 28 days.

Leaching of heavy metals from MSWI FA before and after chelation stabilization (compartmentalized landfill)

Pb in the raw MSWI FA leached at a rate of 3.096 mg/L under acid rain conditions, which was 12.4 times the specified limit value, and at a rate of 6.7 mg/L under acetic acid conditions. The leaching concentration of other metals was within the prescribed limit value. The leaching concentration of Pb can meet the standard when the additions of TS300 are 1.5%, and it is 0.066 mg/L, and the stabilization rate reaches 97.87% (as shown in Fig. 2(b)). The leaching concentration of Pb can meet the standard when the additions of SDD and PD are 6.0% and 8.0%, and they are 0 mg/L and 0.026 mg/L, respectively. The TS300 group exhibited the lowest leaching concentration, which increased somewhat at 3% addition but remained significantly below the regulatory limit. Contrary to acetic acid leaching, sulfuric acid-nitric acid leaching had nil Cd leaching, suggesting that acid rain leach is less capable of leaching Cd and that Cd in the chelated MSWI FA is more stable in the environment of acid rain. Overall, TS300 provided the best stabilization of the three CAs, with only 1.5% required to bring all metal leaching concentrations up to standard after chelation.

From Fig. 2(b), it can be seen that using 1.5%-TS300 stabilized MSWI FA, the leaching concentration of Pb in acid rain environment was 0.066 mg/L for 0 days, the leaching concentration of Pb exceeded the standard of 0.32 mg/L after seven days, and reached 0.993 mg/L after 28 days, which was about four times of the standard limit. The leaching concentration of Zn did not exceed the standard in 28 days, but its leaching concentration of 28 days was 0.568 mg/L, which was

higher than that of the raw MSWI FA of 0.3915 mg/L. It was presumed that the ion exchange reaction occurred in the chelating and stabilizing system as the maintenance time became longer, resulting in the leaching concentration of Zn in the chelated MSWI FA higher than that of the original MSWI FA.

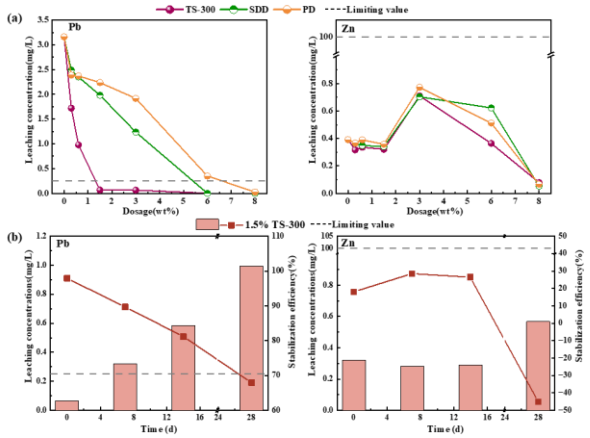

Figure 2: (a) Leaching concentrations of Pb, Zn under compartmentalized landfill; (b) Trends of leaching concentration and stabilization rate of Pb, Zn under compartmentalized landfill conditions over 28days

Environmental risk assessment

The risk assessment code (RAC) index approach was used to assess the environmental risk of Pb, Zn, and Cd in MSWI FA both before and after chelation treatment. As shown in Fig. 3, the environmental risk of Pb in raw MSWI FA is extremely high risk. After chelation, the environmental risk of Pb in 1.5%-TS300 and 6%-SDD group turn to low risk. The environmental risk of Zn in raw MSWI FA is low risk. After chelation, the environmental risk of Zn in 1.5%-TS300 and 6%-SDD group turn to safety. Cd has been in the safe range despite its minor leaching. Based on what we discussed above, we can certainly know that 1.5%-TS300 can effectively harmless HMs in MSWI FA.

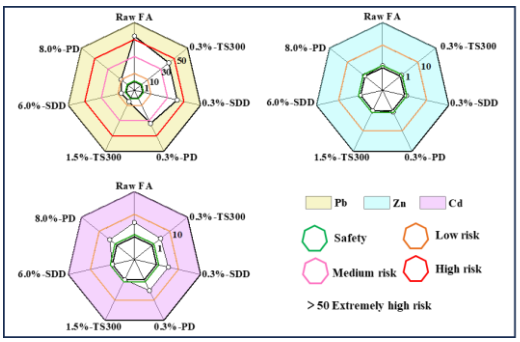

Figure 3: RAC risk indices of Pb, Zn and Cd in MSWI FA before and after chelation.

XRF Elemental Analysis

The elemental comparison of MSWI FA before and after chelation is shown in Table 3. The predominant elements found in MSWI FA are Ca and Cl, with Ca being the most abundant and typically exceeding 20% in Cl content within MSWI FA. After chelation, there is a notable reduction in the concentration of HMs such as Zn, Pb, and Cd. This decrease is attributed to the introduction of elements like C, H, O, and N by CA.

Table 3 Comparison of elements in raw MSWI FA and TS 300 chelated MSWI FA

	Ca	Cl	Na	K	S	Si	Zn	Mg	Fe	Al	Pb	Cu	Cd
Raw MSWI FA	24.063	21.774	10.016	5.777	3.547	1.408	0.769	0.499	0.426	0.305	0.168	0.062	0.06
1.5%TS300-MSWI FA	21.526	25.74	6.569	7.57	2.755	0.945	0.658	0.353	0.398	0.283	0.166	0.063	0.038

Changes in XRD

The XRD spectra of the pristine MSWI FA and 1.5%-TS300 treated MSWI FA are shown in Fig. 4. The raw MSWI FA was found to contain various minerals such as CaClOH, KCl, NaCl, CaCO3, CaSO4, etc. However, the crystal structures of HMs were not detected, indicating that the heavy metal substances in the MSWI FA were primarily present in amorphous forms, which is in agreement with the results of some previous studies

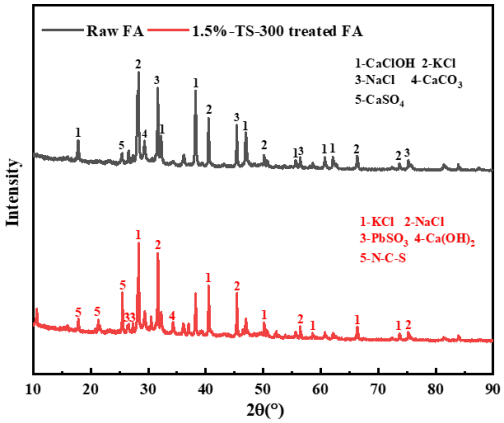

Figure 4: XRD patterns of raw and 1.5% TS300 treated MSWI FA

The peak shape of the 1.5%-TS300-treated MSWI FA has undergone a notable transformation, marked by the disappearance of the original $CaCO_3$ and $CaSO_4$ minerals and the emergence of a novel crystalline phase comprising Ca, Pb, and DTC compounds. $Ca(OH)_2$ is formed as a result of the hydrolysis of hydrophilic TS300, which generates a considerable amount of OH^- and precipitates with Ca^{2+}. The intensity of the characteristic peaks of mineral salts in the stabilized system was significantly reduced, which was attributed

to the agent's hydrolysis, complexation, and cross-linking of the characteristic functional groups to promote compound solubilization and element migration. The distinct and sharp characteristic peaks observed at 2ɵ=26.1° and 27.3° can be attributed to the lead sulfite phase, providing evidence for the reduction of Pb^{4+} by TS300. Additionally, the appearance of a new N-C-S phase within the range of 2ɵ=17.5° to 24.8° provides confirmation of the chelation between the DTC group in TS300 and MSWI FA.

AFM characterization of Treated MSWI FA

AFM images depict the three-dimensional structure of chelation products formed by TS300 and SDD. It can be seen from plan Fig. 5 (b_1) and 5 (c_1) that the TS300 chelation product is denser and more homogeneous compared to the SDD chelation product. The 3D Fig. 5 (b_2) illustrates the dense and uniform three-dimensional structure of fly ash chelated with TS300, suggesting the existence of macromolecular chelates that encapsulate Pb within these structures. In the 3D Fig. 5 (b_4), we observe the presence of agglomerated macromolecular chelates on a smaller scale, in which an insoluble substance connects two particles. This structural arrangement promotes expansion into larger chelates, rendering them less vulnerable to acid or base attack and reducing the leaching potential of HMs into the environment.

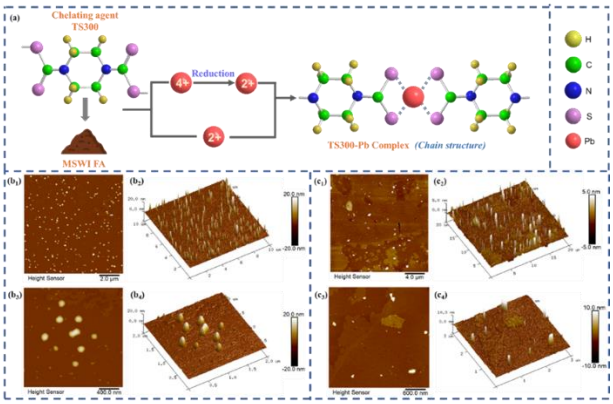

Fig 5: (a) Illustration of the mechanism of TS300 and Pb chelation process; (b_1, b_3) plane view of TS300 treated FA; (b_2, b_4) 3D view of figure b_1 and b_4; (c_1, c_3) plane view of SDD treated FA; (c_2, c_4) 3D view of figure b_1 and b_4

Fig. 5 (a) illustrates the stabilization mechanism of the CA TS300 for Pb, which primarily involves the reduction of the unstable Pb^{4+} in a high-valence state and the synthesis of macromolecular chelates.

Based on the above analysis, the stabilization mechanism can be attributed to the following aspects: (i) the reducing nature of TS300 facilitates the conversion of easily leachable Pb^{4+} to the more stable Pb^{2+} by reducing its valence state; (ii) DTC groups within the CA TS300 react with HMs, forming stable macromolecular complexes; (iii) These chelates also exhibit an encapsulation function, which effectively reduces the leaching rate of lead.

CONCLUSION

This study comparatively investigates the stabilization effects of three DTC CAs on HMs in MSWI FA. Under both mixed landfill and partitioned landfill conditions, the addition of TS300 at a dosage of 1.5% effectively reduced the leaching concentration of HMs to meet standard limits. Environmental risk assessment of MSWI FA was conducted both before and after chelation. It was observed that the environmental risk of chelated MSWI FA, was reduced from a state of serious pollution to a safe condition when compared to the raw MSWI FA. Additionally, tests of AFM confirmed the presence of new substances and the introduction of sulfur groups in the chelated MSWI FA. It also revealed that the macromolecular chelates formed in the 1.5% TS300 treated FA possessed a three-dimensional structure, which contributed to the stabilization of Pb and reduced its susceptibility to leaching in both acidic and alkaline environments.

ACKNOWLEGEMENT

The study was supported by the National Key Research and Development Program of China (2021YFE0112100) and the Fundamental Research Funds for the Central Universities (QNXM20220055).

REFERENCE

A XC, A RM, A QZ, A WW, A QL, B SSA, et al. The factors influencing sludge incineration residue (SIR)-based magnesium potassium phosphate cement and the solidification/stabilization characteristics and mechanisms of heavy metals - ScienceDirect. Chemosphere 2020; 261

C ZYA, C WLA, C ZPA, C LZAB, B SBA, B WXA, et al. Experimental study on the stabilization of heavy metals in fly ash from municipal solid waste incineration by N-30 alkaline silica sol - ScienceDirect. Process Safety and Environmental Protection 2021; 148: 1367-1376

Chen J, Lin X, Li M, Mao T, Li X, Yan J. Heavy metal solidification and CO_2 sequestration from MSWI fly ash by calcium carbonate oligomer regulation. Journal of cleaner production 2022: 359

Fan C, Wang B, Zhang T. Review on Cement Stabilization/Solidification of Municipal Solid Waste Incineration Fly Ash. Advances in Materials Science and Engineering 2018; 2018: 1-7 https://doi.org/10.1155/2018/5120649.

Han SY, Ju TY, Meng FZ, Lin L, Li JL, Chen KL, et al. Comprehensive study of recycling municipal solid waste incineration fly ash in lightweight aggregate with bloating agent: Effects of water washing and bloating

mechanism. Science of the Total Environment 2023; 881 https://doi.org/10.1016/j.scitotenv.2023.163267.

Huang B, Gan M, Ji Z, Fan X, Zhang D, Chen X, et al. Recent progress on the thermal treatment and resource utilization technologies of municipal waste incineration fly ash: A review. Process Safety and Environmental Protection 2022; 159: 547-565

Jiang G, Min X, Ke Y, Liang Y, Yan X, Xu W, et al. Solidification/stabilization of highly toxic arsenic-alkali residue by MSWI fly ash-based cementitious material containing Friedel's salt: Efficiency and mechanism. Journal of hazardous materials 2022: 425

Li R, Zhang B, Wang Y, Zhao Y, Li F. Leaching potential of stabilized fly ash from the incineration of municipal solid waste with a new polymer. Journal of Environmental Management 2019; 232: 286-294

Liu X, Zhao X, Yin H, Chen J, Zhang N. Intermediate-calcium based cementitious materials prepared by MSWI fly ash and other solid wastes: hydration characteristics and heavy metals solidification behavior. Journal of Hazardous Materials 2018; 349: 262-271

Ma W, Chen D, Pan M, Gu T, Zhong L, Chen G, et al. Performance of chemical chelating agent stabilization and cement solidification on heavy metals in MSWI fly ash: A comparative study. Journal of Environmental Management 2019; 247: 169-177

Ma Y, Wang P, Lin X, Chen T, Li X. Formation and inhibition of Polychlorinated-rho-dibenzodioxins and dibenzofurans from mechanical grate municipal solid waste incineration systems. J Hazard Mater 2021; 403: 123812 https://doi.org/10.1016/j.jhazmat.2020.123812.

Phua Z, ApostolosDong, Zhi-LiLisak, GrzegorzNg, Wun Jern. Characteristics of incineration ash for sustainable treatment and reutilization. Environmental Science and Pollution Research 2019; 26

Soltanian S, Kalogirou SA, Ranjbari M, Amiri H, Mahian O, Khoshnevisan B, et al. Exergetic sustainability analysis of municipal solid waste treatment systems: A systematic critical review. Renewable and Sustainable Energy Reviews 2022; 156: 111975-

Song ZJ, Zhang XW, Tan YJ, Zeng Q, Hua YL, Wu XY, et al. An all-in-one strategy for municipal solid waste incineration fly ash full resource utilization by heat treatment with added kaolin. Journal of Environmental Management 2023; 329 https://doi.org/10.1016/j.jenvman.2022.117074.

Sun Y, Xu C, Yang W, Ma L, Lin A. Evaluation of a mixed chelator as heavy metal stabilizer for municipal solid-waste incineration fly ash: Behaviors and mechanisms. Journal- Chinese Chemical Society Taipei 2018

Tian, Zhipeng, Yinan, Fengting, Zhou, Weixiao, et al. Stabilization/solidification of lead in MSWI fly ash with mercapto functionalized dendrimer Chelator. Waste Management 2016; 50: 105-112

Tian X, Liu KZ, Yang XT, Jiang TY, Chen BH, Tian ZC, et al. Synthesis of metakaolin-based geopolymer foamed materials using municipal solid waste incineration fly ash as a foaming agent. Waste Management 2023; 169: 101-111 https://doi.org/10.1016/j.wasman.2023.07.003.

Tian X, Rao F, Li C, Ge W, Xia L. Solidification of municipal solid waste incineration fly ash and immobilization of heavy metals using waste glass in alkaline activation system. Chemosphere 2021; 283: 131240

Wang S, Xue CH, Zhao QX, Bai YY, Guo WC, Shi YX, et al. A novel binder prepared from municipal solid waste incineration fly ash and phosphogypsum. Journal of Building Engineering 2023; 71 https://doi.org/10.1016/j.jobe.2023.106486.

Wang X, Gao M, Wang M, Wu C, Wang Q, Wang Y. Chloride removal from municipal solid waste incineration fly ash using lactic acid fermentation broth. Waste Manag 2021; 130: 23-29 https://doi.org/10.1016/j.wasman.2021.05.014.

Wang X, Wang M, Zou D, Wu C, Li T, Gao M, et al. Comparative study on inorganic Cl removal of municipal solid waste fly ash using different types and concentrations of organic acids. Chemosphere 2020; 261: 127754 https://doi.org/10.1016/j.chemosphere.2020.127754.

Wei Y, Liu S, Yao R, Chen S, Gao J, Shimaoka T. Removal of harmful components from MSWI fly ash as a pretreatment approach to enhance waste recycling. Waste Management 2022

Yan M, Jiang JH, Zheng RD, Yu CM, Zhou ZH, Hantoko D. Experimental study on the washing characteristics of fly ash from municipal solid waste incineration. Waste Management & Research 2022; 40: 1212-1219 https://doi.org/10.1177/0734242x211068253.

Zhang M, Guo M, Zhang B, Li F, Wang H, Zhang H. Stabilization of heavy metals in MSWI fly ash with a novel dithiocarboxylate-functionalized polyaminoamide dendrimer. Waste Management 2020; 105: 289-298

Zhang Z, Zhao CT, Rao Y, Yu CJ, Luo ZL, Zhao HJ, et al. Solidification/stabilization and risk assessment of heavy metals in municipal solid waste incineration fly ash: A review. Science of the Total Environment 2023; 892 https://doi.org/10.1016/j.scitotenv.2023.164451.

Zhu J, Hao Q, Chen J, Hu M, Jiang C. Distribution characteristics and comparison of chemical stabilization ways of heavy metals from MSW incineration fly ashes. Waste Management 2020; 113: 488-496

Zhu ZH, Guo YY, Zhao YC, Zhou T. A novel waste-recycled chelating agent for the stabilization of lead in municipal solid waste incineration fly ash: Preparation, feasibility, and mechanism analysis. Journal of Hazardous Materials 2022; 427 https://doi.org/10.1016/j.jhazmat.2021.127914.

Genome Analysis of *Aspergillus terreus*-YJ01 for Biodegrading Gossypol

Yao Jiang[#], Xinyue Du, Qianqian Xu, Chunhua Yin, Haiyang Zhang, Yang Liu, Xiaolu Liu, Hai Yan*

School of Chemistry and Biological Engineering, University of Science and Technology Beijing,Beijing 100083, China
* Correspondence: haiyan@ustb.edu.cn (H.Y.)

Abstract: Gossypol, generally found in the roots, stems, leaves, and especially the seeds of cotton plants, is highly toxic to animals and humans, which inhibits the use of cotton stalks as a feed resource. Here, a promising fungal strain for biodegrading gossypol was successfully isolated from the soil of cotton stalk piles in Xinjiang Province, China, and identified as *Aspergillus terreus*-YJ01 with the analysis of ITS. Initial gossypol of 250 mg·L^{-1} could be removed by 97% within 96 h by YJ01, and initial gossypol of 150 mg·L^{-1} could also be catalyzed by 98% or 99% within 36 h by the intracellular or extracellular crude enzymes of YJ01. Sucrose and sodium nitrate were found to be the optimal carbon and nitrogen sources for the growth of YJ01, and the optimal initial pH and inoculum size for the growth of YJ01 were 6.0 and 1%, respectively. To further elucidate the mechanisms of gossypol biodegradation by YJ01, the draft genome of YJ01 was sequenced by Illumina HiSeq, which is 31566870 bp in length, with a GC content of 52.27% and a total of 9737 genes. Eight genes and enzymes were predicted to be involved in gossypol biodegradation. Among them, phosphoglycerate kinase, citrate synthase, and other enzymes are related to energy supply process. With sufficient energy, β-1, 4-endo-xylanase may achieve the purpose for biodegrading gossypol. The findings of this study provide valuable insights into both the basic research and the application of *A. terreus*-YJ01 in the biodegradation of gossypol in cotton stalk.

Keywords: gossypol; *Aspergillus terreus*-YJ01; biodegradation; genomic analysis

1. Introduction

Protein supplies are becoming increasingly limited as animal breeding on a large scale in China[1]. Currently, China's production of widely used soybean meal is woefully inadequate and largely dependent on imports[2]. Cottonseed meal is a reddish or yellow by-product of the cottonseed oil extraction process with high protein content of 40%, which can be used as a high-quality plant protein feed to make up for the shortage of protein feed resources[3,4]. However, the toxic gossypol contained in cottonseed meal is as high as 0.15% ~ 1.80%, which severely limited the use of cottonseed meal in the feed industry[5,6]. Therefore, the removal of gossypol is of great significance to the feed industry.

As a small molecular compound mainly derived from cottonseed, gossypol exists in two forms: bound gossypol and free gossypol (Figure 1)[7,8]. Bound gossypol is formed by combining free gossypol with proteins, amino acids, phospholipids, and other substances[9]. Due to the combination of its active groups, it loses its activity and is not absorbed by the body's digestive system. It can be rapidly excreted in feces, usually with low toxicity[10]. Free gossypol is a major anti-nutritional factor in cottonseed meal that is detrimental to animal growth[11,12]. Gossypol is highly toxic to animals, direct feeding of gossypol can cause acute poisoning, anorexia, weakness, and even death[13,14]. In addition, gossypol can inhibit the production and activity of sperm in male animals, affect the breeding of domestic animals, and directly restrict its application in animal husbandry[15-17].

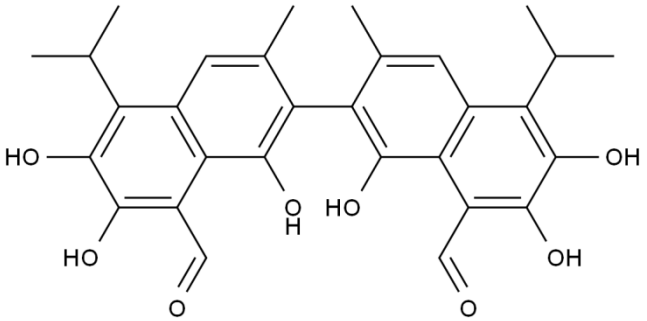

Figure 1. Chemical structure of gossypol (molecular weight: 518.55)

There are many physicochemical and biological approaches to removing gossypol and increasing the use of cottonseed products in animal feed, the most promising of which is biodegradation due to its low cost and low

collateral destruction of native flora and fauna[18,19]. A number of studies have been conducted on the detoxification of gossypol, showing that microbial fermentation can significantly reduce gossypol levels in cottonseed meal[20]. The ability to biodegrade gossypol has been demonstrated in some isolated strains[21]. Some researchers had studied the biodegradation of gossypol, and a few species, including Aspergillus, Penicillium, Saccharomyces, Rhodococcus, Bacillus, and Lactobacillus, were successfully isolated from the environment and found to be capable of degrading gossypol[4,22]. Hou Min et al. identified 32 strains of gossypol-tolerant intestinal endophytes by studying the similarities and differences between the intestinal microorganisms in the normal and cottonseed meal diets. The highest gossypol biodegradation rate was only 90.83%[23]. Rajarathnam reported that an enzyme extract from rice straw colonized by a fungal mycelium (*Pleurotus florida*) had the ability to biodegrade gossypol, which led to the current study on the biodegradation of gossypol by proteins or enzymes[24]. The structure of gossypol is similar to that of naphthalene, and it can be regarded as a derivative of naphthalene[25,26]. At the same time, gossypol is a type of polycyclic aromatic hydrocarbon, and some enzymes involved in the biodegradation of polycyclic aromatic hydrocarbons have been reported[27,28]. Yang et al. have used *Aspergillus niger* AN-1, grown on gossypol as the sole carbon source, for proteomic analysis, using MALDI-TOFMS to identify 20 proteins involved in gossypol biodegradation[29]. At present, although the biodegradation of gossypol has been widely studied, the biodegradation rate of microorganisms reported is generally low. In addition, there is no genome analysis of microorganisms for biodegrading gossypol.

In this study, an efficient fungal strain for the biodegradation of gossypol was isolated and identified as *Aspergillus terreus*-YJ01. Both YJ01 and its intracellular and extracellular crude enzymes showed effective removal of gossypol, indicating in both cellular and enzyme level that YJ01 has a strong ability in the biodegradation of gossypol. Subsequently, the draft genome of YJ01 was sequenced to find genes encoding gossypol biodegradation enzymes, leading to the elucidation of the biodegradation mechanism. These findings were of great significance on the feed industry, and provided an important idea for further study on the mechanism of gossypol biodegradation.

2. Materials and Methods

2.1. Strain and materials

A newly isolated *A. terreus*-YJ01 used in this study was isolated from the soil of cotton straw piling in China using gossypol as the sole carbon source. Standard gossypol with the purity of 98% that used in this study was purchased from Shanghai Ekear Biotechnology Co. All other chemicals used in the experiment were analytical grade.

2.2. Medium and culture conditions

The basal liquid medium for the isolation and culture of YJ01 consisted of 0.5 g of NH_4Cl, 0.5 g of K_2HPO_4, 0.5 g of NaCl, 0.5 g of $MgSO_4$, 0.1 g of peptone, 0.1 g of yeast extract powder, and 1.0 ml of trace element solution in 1000 ml of distilled water. Gossypol was added to the medium at a certain initial concentration as the sole carbon source[30], and the initial pH of medium was adjusted to 7.0 with 1.0 mol·L^{-1} NaOH or HCl.

The Czapek Dox medium for optimal culture of YJ01 consisted of 30.0 g of sucrose, 3.0 g of $NaNO_3$, 0.5 g of $MgSO_4 \cdot 7H_2O$, 0.5 g of KCl, 0.01 g of $FeSO_4 \cdot 4H_2O$, 1.0 g of K_2HPO_4, and 1000 ml of distilled water.

A. terreus-YJ01 was inoculated into the sterilized culture medium and grown in a 100 ml flask containing 20 ml of liquid medium. The culture condition was at 30°C with a shaking rate of 200 r·min^{-1}. Dry cell weight was measured, which represented the growth of YJ01[31]. Both the medium and all experimental apparatus were sterilized at 121°C for 20 min.

Culture broth of 1.0 ml was taken in 1.5 ml centrifuge tube and centrifuged at 148000 r·min^{-1} for 10 min. 1.0 ml of acetonitrile was added to the bottom precipitation, and the gossypol in the precipitation was fully dissolved in acetonitrile by ultrasonic oscillation. The supernatant was diluted and used to determine the concentration of gossypol by high performance liquid chromatography (HPLC)[32,33]. The data presented were the average values derived from three measurements, and their relative standard deviations were less than 10%.

2.3. Isolation and identification of gossypol-biodegrading strain

The cotton straw piling soil sample was inoculated into the liquid culture medium using gossypol of 500 mg·L^{-1} as the sole carbon source, and incubated with a shake rate of 200 r·min^{-1} at 30°C for 3 days. After three consecutive cultures, the mixed bacteria were diluted and spread onto the solid medium containing 2% agar in the presence of 250 mg·L^{-1} gossypol. Single colonies that grew on the plates were picked and inoculated into the liquid medium containing

gossypol of 250 mg·L^{-1} to test its biodegradation ability. The process was repeated several times until a pure fungal strain that had the ability in the biodegradation of gossypol was isolated [34].

A newly isolated strain YJ01 was identified by the morphological, physiological traits and biochemical characteristics, which was further identified by the internal transcribed spacer identification (ITS). The genomic DNA of strain was extracted according to the previous report[35]. The purity of the extracted DNA was measured using nanodrop 2000 and the concentration of DNA was measured using Quantus Fluorometer (Picogreen). The polymerase chain reaction (PCR) was performed on fungal DNA using universal primers ITS1 and ITS4. The PCR conditions were as follows: predenaturation at 95 ℃ for 5 min; Denaturation at 95 ℃ for 30 seconds, annealing at 56 ℃ for 30 seconds, extension at 72 ℃ for 1 min and 30 seconds, 30 cycles; Extend for 10 min at 72 ℃. The upstream primer was 5′- TCC GTA GGT GAA CCT GCG G-3′ and the downstream primer was 5′- TCC TCC GCT TAT TGA TAT GC-3′. After the reaction, the amplified products were observed by 1% agarose gel electrophoresis, which was used to detect DNA integrity. After that, the amplified DNA was sent to the Shanghai Majorbio Bio-Pharm Technology Co., Ltd for sequencing, and the species identification was performed by Sanger sequencing. The nucleotide sequences were compared to the most similar sequences of bacterium on the Gene Bank, which was used to identify this newly isolated fungal strain.

2.4. Preparation of intracellular crude enzyme and extracellular crude enzyme

The fermentation broth of *A. terreus*-YJ01 was obtained by inoculating 1% of the preserved fungal liquid into 50 ml basal medium, cultured at 30℃, 200 r·min^{-1} for 3 days. To obtain the extracellular crude enzyme, the fermentation broth was centrifuged. The filamentous fungal cells were harvested by centrifugation at 12,000 r·min^{-1} for 10 min at 4 °C, followed by washing twice with 0.01 mol·L^{-1} phosphate buffered saline (PBS, pH 7.4). Cells were then resuspended in the phosphate buffer and sonicated at 0 °C in the ice-water mixture with an output power of 300 W for 20 min. The cell debris was removed by centrifugation at 15000 r·min^{-1} for 10 min and the supernate was collected and used as intracellular crude enzyme to catalyze gossypol[36].The protein concentration of intracellular and crude enzyme of *A. terreus*-YJ01 was determined with UV method. Using PBS buffer, 1 g/L bovine serum protein was diluted to 0.2 g/L, 0.4 g/L, 0.6 g/L, 0.8 g/L and 1 g/L, respectively. At 280 nm, the optical density of the series of concentration gradient standard solutions were measured respectively, and the standard curves of protein concentration and absorbance were drawn to calculate the protein concentration of intracellular crude enzyme[34].

2.5. Analysis of gossypol by HPLC

Gossypol content was determined by high-performance liquid chromatography (HPLC, Shimadzu LC-l0ATVP, Shimadzu Co., Japan) with a mobile phase of acetonitrile-0.2% phosphoric acid solution (85∶15) mixture and a flow rate of 1.0 ml·min^{-1}. The detection wavelength was 235 nm using a UV diode array detector coupled to an Agilent SB-C18 column (4.6 mm×250 mm, 5 μm) at 30℃. The calibration curve was established between the peak areas and the concentration of gossypol, which was used to calculate the concentration of gossypol in the experiment[32,37].

2.6. Whole genome sequencing of YJ01

The single colony of *A. terreus*-YJ01 was selected and inoculated into 200 ml of sterilized Czapek Dox medium. After 2 days of culture, microscopic observation was made to ensure that the medium was not contaminated and no mycelium was formed[26,38]. The fungal cell precipitate was collected in 1.5 mL centrifuge tube and sent to Shanghai Majorbio Bio-pharm Technology Co., Ltd. for whole genome sequencing.

Fungal genome denovo sequencing refers to sequencing the fungal genome without relying on a reference sequence and using bioinformatics tools to assemble the genome sequence from scratch[39]. The Illumina second-generation sequencing platform was used to sequence and analyze the fungal genome[40]. Qualified DNA samples were constructed with inserted fragments of 400bp and PE150 pair-end sequencing was performed[41]. Each sample provided original sequencing data with a coverage depth of at least 100× genome[42]. Based on the obtained sequencing data, a series of analyses were performed, including: sequencing data quality control, genome evaluation, genome assembly and prediction, gene annotation, and other analyses[43,44].

3. Results and Discussion

3.1. Isolation and identification of gossypol-biodegrading strain

Using gossypol as the sole carbon source, a fungus YJ01 with gossypol-biodegrading ability was successfully isolated. On solid medium, colonies of this strain were round, with well-developed mycelium, velvety to flocculent texture, thin, slightly raised central part, brown in color, and could produce black spores (Figure 2). Podocytes, conidial heads and conidial stalks can be observed under the microscope. The conidial head is columnar, the apical sac is hemispherical, there are two layers of pedicel, the conidium is almost spherical, and the pedicel is short and smooth. It also showed that YJ01 could be grown on Bengal Red medium, PDA medium and Czapek Dox medium.

Figure 2. Colonies were grown on PDA plate (left) and morphology (1000 X) observed under the microscope (right) of YJ01

ITS of YJ01 was amplified and sequenced to determine its phylogenetic placement. The analysis results of the ITS sequences showed that YJ01 appeared to be closely related to *Aspergillus terreus*(Figure 3). Based on the morphological and physiological characteristics as well as the phylogenetic analysis of ITS sequences, we identified YJ01 as *A. terreus*-YJ01.

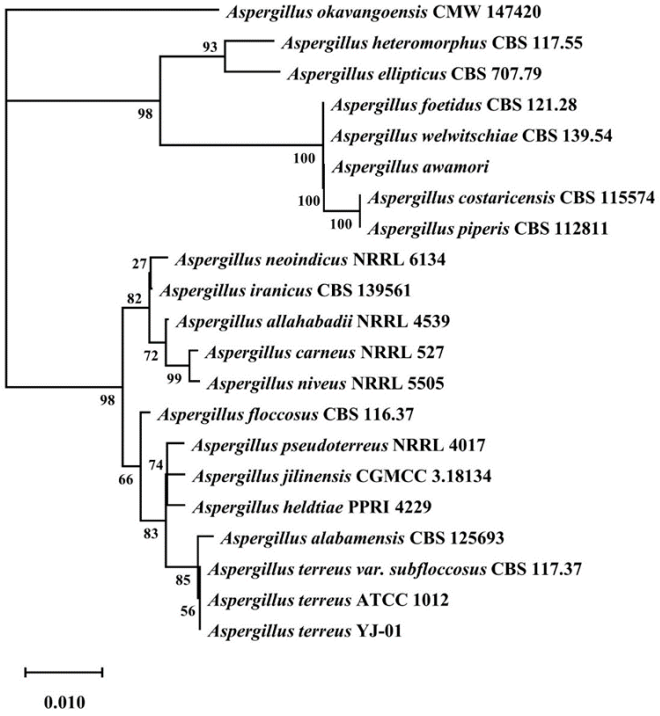

Figure 3. Phylogenetic tree based on ITS sequences of *Aspergillus terreus*-YJ01

3.2. Biodegradation of gossypol by YJ01

Initial gossypol of 250 mg·L^{-1} can be removed by 97% in 96h by *A. terreus*-YJ01 (Figure 4), indicating that this isolated fungal strain has a better ability in the biodegradation of gossypol than any other microorganisms reported[20,29,42]. Different microorganisms have different biodegradability of gossypol[24]. At present, gossypol has been shown to be well biodegradable by fungi such as *Aspergillus niger*, yeast such as *Candida utilis*, *Bacillus subtilis* and

Rhodococcus erythropolis[29,45]. Chen et al. obtained a strain of *Aspergillus terreus* capable of degrading gossypol from soil samples of cotton fields and cottonseed oil extraction plants through several rounds of screening, and its biodegradation rate of gossypol reached only 33.6% within 72 hours[46]. Compared with other gossypol-biodegrading microorganisms reported, YJ01 is a promising fungal strain for the efficient biodegradation of gossypol

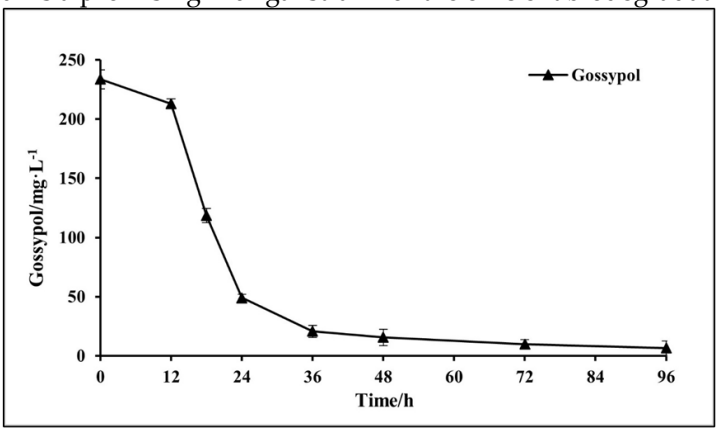

Figure 4. Biodegradation kinetics of gossypol by YJ01.

3.3. Biodegradation of gossypol by intracellular crude enzyme and extracellular crude enzyme

The intracellular crude enzyme of *A. terreus*-YJ01 containing a protein concentration of 2.10 mg·L^{-1} could remove 150 mg·L^{-1} of gossypol by 98% within 36 h. Furthermore, 150 mg·L^{-1} of gossypol could be declined by 99% within 36h by the extracellular crude enzyme with the proteion concentration of 2.13 mg·L^{-1} (Figure 5). Gossypol could be removed by both the cells and the intracellular as well as extracellular crude enzymes of *A. terreus*-YJ01 (Figure 4,5), and compared with the cells of *A. terreus*-YJ01, its intracellular and extracellular crude enzymes show a higher biodegradation rate (Fig. 4 and 5), which is significant on the efficient elimination of gossypol from cottonseed meal.

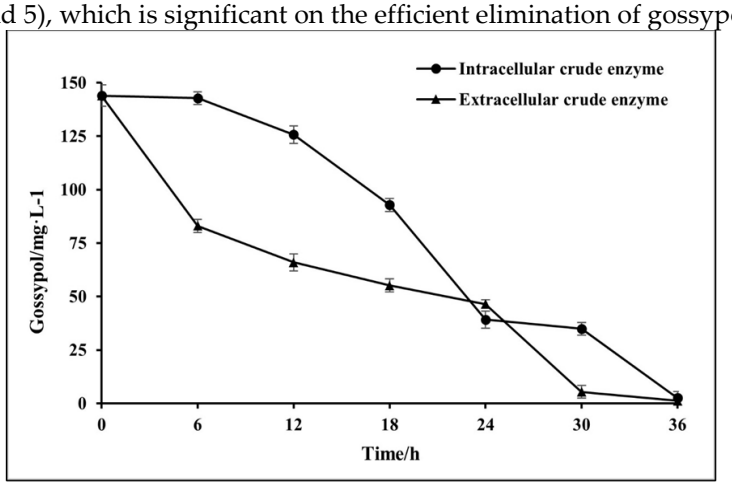

Figure 5. Biodegradation kinetics of gossypol by intracellular crude enzyme and extracellular crude enzyme

3.4. Effects of medium and culture conditions on the growth and gossypol biodegradation of YJ01

The effects of different carbon sources, nitrogen sources, pH and inoculum size on the growth of *A. terreus*-YJ01 and biodegradation of gossypol were studied. As shown in Figure 6(a), compared with glycerol, glucose, sodium lactate, or ethanol as sole carbon source, sucrose was found to be an optimal carbon source to support both the growth and of gossypol biodegradation of *A. terreus*-YJ01e. As shown in Figure 6(b), in the medium with yeast powder, sodium nitrate, urea, peptone and ammonium chloride as sole nitrogen sources, respectively, sodium nitrate was showed to be an optimal nitrogen source to support both the growth and of gossypol biodegradation of *A. terreus*-YJ01.The growth of *A. terreus*-YJ01 and biodegradation of gossypol under the different pH and inoculum size were and 6(d). It showed that both the growth of *A. terreus*-YJ01 and the biodegradation of gossypol were promoted at pH 6.0 from 5.0 to 9.0 as shown in Figure 6(c). It also indicated that the inoculum size of 1% in the range from 0.5% to 2.5% was an optimal inoculum size for both the growth of *A. terreus*-YJ01 and the biodegradation of gossypol as shown in Figure 6(d).

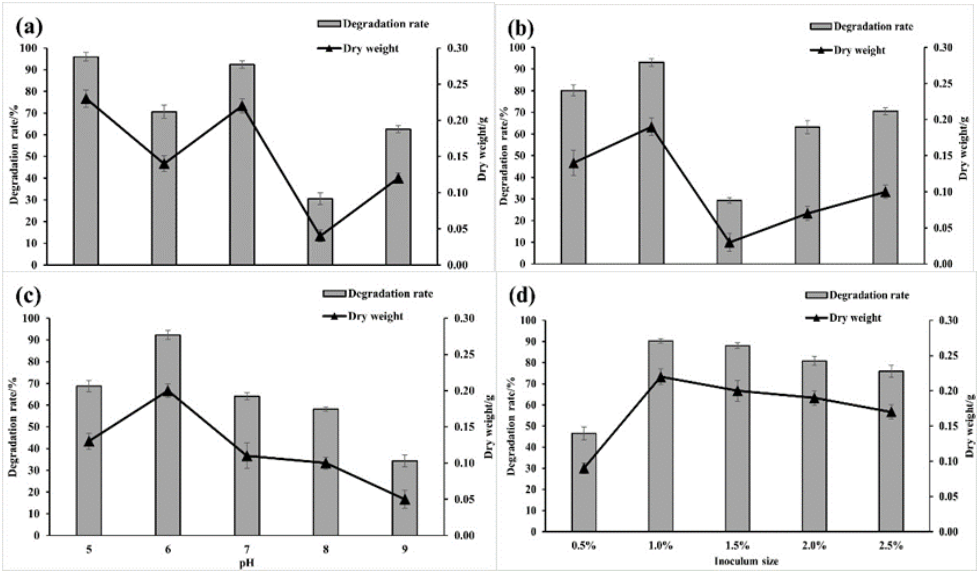

Figure 6. Effects of carbon source (a), nitrogen source (b), initial pH (c), and inoculum size (d) of gossypol on growth and gossypol biodegradation ratio by YJ01 cultured for 72 h.

3.5. Genomic analysis for the biodegradation of gossypol by YJ01

To study the mechanism of gossypol removed by YJ01, DNA from *A. terreus*-YJ01 samples was extracted, purified, and constructed into a library. The draft genome was sequenced, assembled, and checked using the Illumina Hiseq platform with paired-ends sequencing[47]. It revealed a total length of 31566870 bp, with a GC content of 52.27%. The reads were assembled into 275 scaffolds with an N50 of 980104 bp. And 9737 protein-coding genes, 161 tRNA genes, 27 rRNA genes were predicted (Table 1-1).

Table 1-1. Basic information on the genome assembly of YJ01

Attribute	Value
Sample Name	YJ01
Total Scaffolds No.	275
Total Bases in Scaffolds（bp）	31566870
Large Scaffolds No.（＞1000bp）	275
Largest Scaffolds Bases (bp)	31566870
G+C(%)	52.27
Scaf N50(bp)	980104
Scaf N90(bp)	127246

Table 1-2 displays the statistics of the second-generation quality control data. Both the original sequence data (18480614*2) and the post-quality control data (18238868*2) contained a certain number of double-ended reads. 97.45%(Q20) and 93.35%(Q30) of the total bases in the original data were bases with error identification rates less than 0.01 and 0.001, respectively. Following data quality assessments, bases with error identification rates under 0.01 and 0.001 represented, respectively, 97.75%(Q20) and 93.71%(Q30) of the total bases. After quality control, the total base count is 5537387630 bp, compared to the total base count of the original data, which is 5581145428 bp.

Table 1-2. Statistics of quality control data of second-generation sequencing

Attribute	Value
Sample Name	YJ01
Insert Size (bp)	500
Read Len (bp)	150
Raw Pair Reads	18480614*2

Raw Bases (bp)	5581145428
Raw Q20(%)	97.45
Raw Q30(%)	93.35
Clean Pair Reads	18238868*2

Genomic assessments, including GC_depth distribution analysis and K-mer frequency distribution analysis, were performed on the genome sequences generated after assembly to determine whether contamination was present. Figure 7(a) shows the GC_depth distribution with GC content as the horizontal coordinate and the coverage depth of reads as the vertical coordinate. At the same time, the histograms on both sides also reflect the distribution trend of GC content and sequencing depth. From the graph, we can see that most of the spots are distributed in a relatively concentrated area, and the distribution area is narrow, indicating that the sample of YJ01 genome is of high purity and free from contamination. The horizontal coordinate of the K-mer frequency distribution analysis result graph in Figure 7(b) represents the sequencing depth, and the vertical coordinate represents the proportion of the frequency to the total frequency at each sequencing depth. The main peak in the graph is relatively complete and has no heterozygous peak or repeat peak, showing a Poisson distribution, indicating that there are few heterozygotes and repeats in the genome and the quality is good.

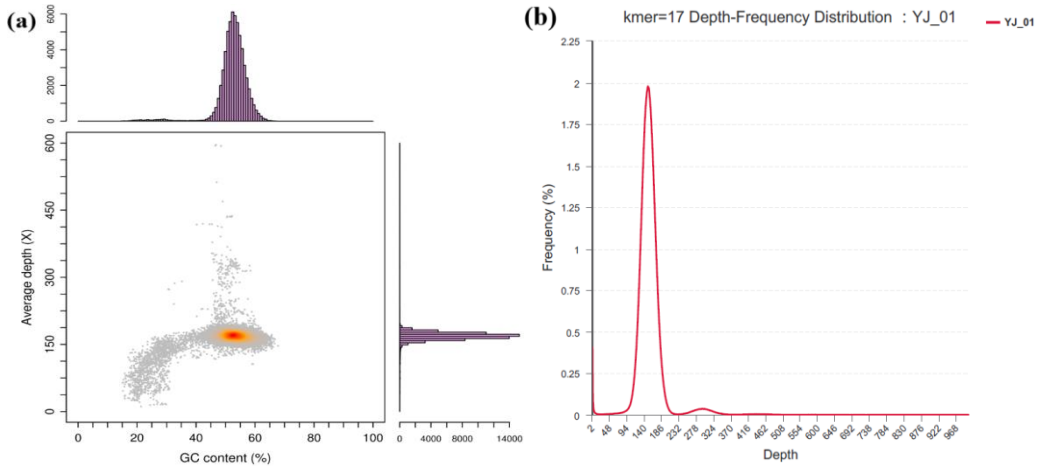

Figure 7. GC_depth distribution(a) and K-mer depth-frequency distribution(b) analysis results

The results of COG annotation revealed that 4079 genes (41.89%) in the genome of YJ01 matched the annotation information in the COG database (Figure 8a) and were involved in 25 metabolic pathways. Notably, there were 693 genes related to carbohydrate transport and metabolism(G), which accounted for the highest proportion (17.0%). The number of genes annotated for general function prediction only(R), lipid transport and metabolism(I), amino acid transport and metabolism(E), energy production and conversion(C), and coenzyme transport(H) was 510, 463, 411, 346, and 334, respectively. Furthermore, in GO functional annotation, 7224 coding genes were annotated to biological processes (3866, 53.5%), cellular components (4449, 61.6%), and molecular functions (5778, 80.0%), respectively (Figure 8b). In biological process, metabolic process (2923), cellular process (2890), localization (556), and biological regulation (526) account for a large proportion of secondary functions, respectively. The cellular anatomical entity (4075) accounts for the largest proportion of genes annotated in the cellular component. The proportion of genes annotating catalytic activity and binding functions in molecular function is high, with 3916 and 3109 genes, respectively. Additionally, 3514 genes in the KEGG database are matched with annotation information and participate in 47 metabolic pathways in six major metabolic hierarchies (Figure 8c). Among them, 1056 genes were associated with the general metabolic pathway, 375 genes with carbohydrate metabolism, 286 genes with amino acid metabolism, and 266 genes with transport and catabolism.

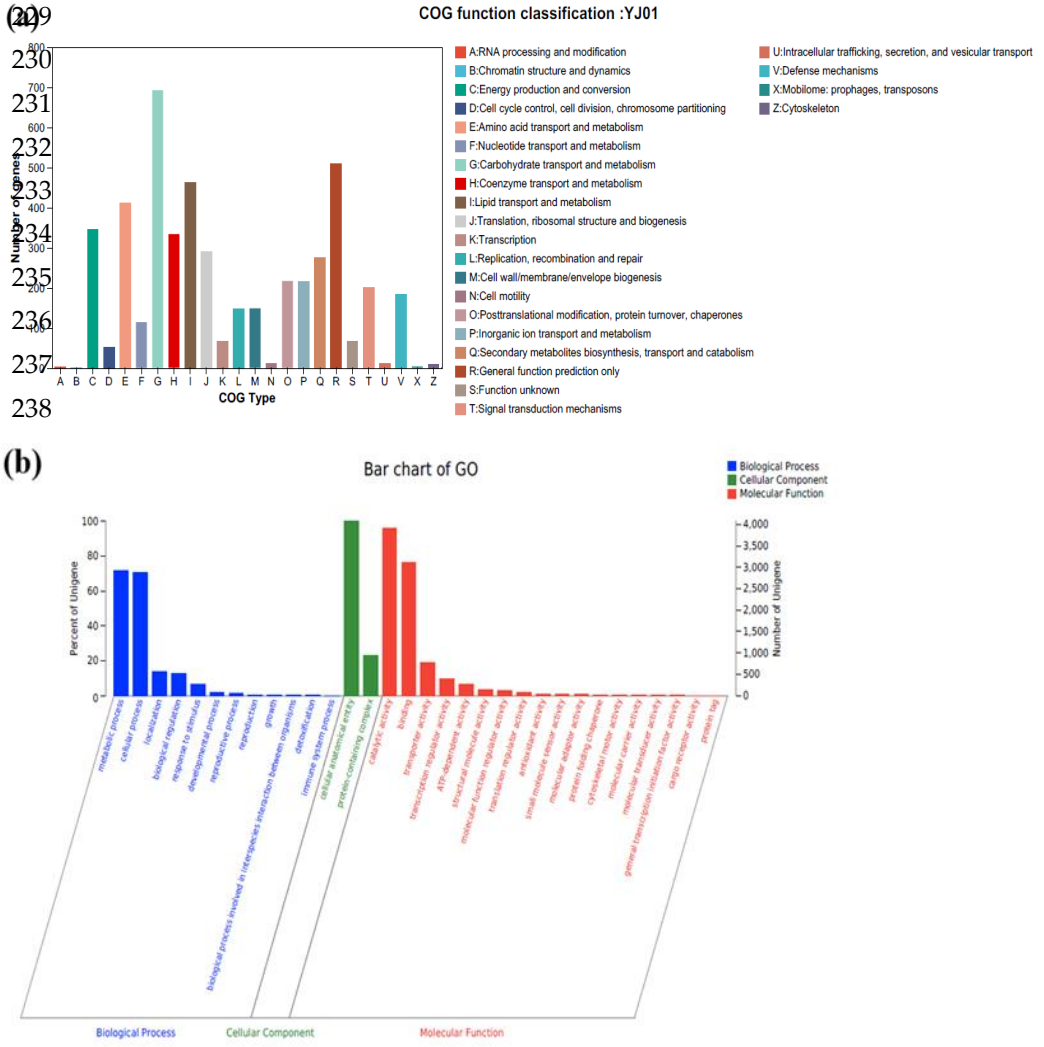
(a)
COG function classification :YJ01
Number of Genes
COG Type
A B C D E F G H I J K L M N O P Q R S T U V X Z
A:RNA processing and modification
B:Chromatin structure and dynamics
C:Energy production and conversion
D:Cell cycle control, cell division, chromosome partitioning
E:Amino acid transport and metabolism
F:Nucleotide transport and metabolism
G:Carbohydrate transport and metabolism
H:Coenzyme transport and metabolism
I:Lipid transport and metabolism
J:Translation, ribosomal structure and biogenesis
K:Transcription
L:Replication, recombination and repair
M:Cell wall/membrane/envelope biogenesis
N:Cell motility
O:Posttranslational modification, protein turnover, chaperones
P:Inorganic ion transport and metabolism
Q:Secondary metabolites biosynthesis, transport and catabolism
R:General function prediction only
S:Function unknown
T:Signal transduction mechanisms
U:Intracellular trafficking, secretion, and vesicular transport
V:Defense mechanisms
X:Mobilome: prophages, transposons
Z:Cytoskeleton
(b)
Bar chart of GO
Biological Process
Cellular Component
Molecular Function
Percent of Unigene
Number of Unigene
metabolic process
cellular process
localization
biological regulation
response to stimulus
developmental process
reproductive process
reproduction
growth
biological process involved in interspecies interaction between organisms
detoxification
immune system process
cellular anatomical entity
protein-containing complex
catalytic activity
binding
transporter activity
transcription regulator activity
ATP-dependent activity
structural molecule activity
molecular function regulator activity
translation regulator activity
antioxidant activity
small molecule sensor activity
molecular adaptor activity
protein binding chaperone
cytoskeletal motor activity
molecular carrier activity
molecular transducer activity
general transcription initiation factor activity
cargo receptor activity
protein tag
Biological Process
Cellular Component
Molecular Function

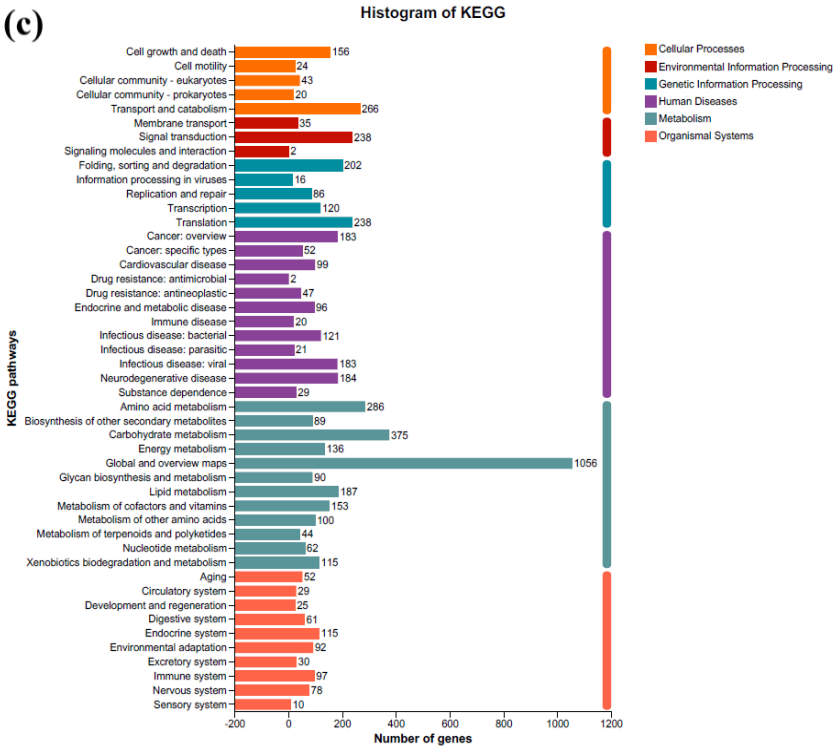

Figure 8. COG (a), GO (b), KEEG (c) annotation classification of YJ01

No metabolic pathway map related to gossypol biodegradation was found in KEGG annotations, but according to previous reports[13,29], 8 enzymes have been speculated to be directly related to the biodegradation of gossypol by *A. terreus*-YJ01, which were glucose-6-phosphate isomerase, phosphoglycerate kinase, glyceraldehyde-3-phosphate dehydrogenase, malate dehydrogenase, citrate synthase, glutamate dehydrogenase, inorganic pyrophosphatase, and β-1,4-endo-xylanase (Table 2). Due to the complex structure of gossypol, more energy is required for biodegradation[48]. Glucose-6-phosphate isomerase, phosphoglycerate kinase, and glyceraldehyde-3-phosphate dehydrogenase play important roles in glycolysis to produce energy. In addition, malate dehydrogenase and citrate synthetase produce additional energy through the TCA cycle. Glutamate dehydrogenase and inorganic pyrophosphatase can further regulate body energy. Under the condition of sufficient energy, *Aspergillus terreus* can further participate in the biodegradation of gossypol through β-1, 4-endoxylanase to achieve the purpose of degrading gossypol. This provided the biological basis for the identification of functional genes involved in gossypol biodegradation and clarified the biodegradation process.

Gossypol is a derivative of naphthalene and its biodegradation pathway may be related to the naphthalene metabolic pathway. Naphthalene is an aromatic compound. Its biodegradation process is much more complex than that of glucose and requires more energy[49]. We speculate that a considerable amount of energy is also required to degrade this complex molecule in the process of gossypol biodegradation, so these proteins may play an important role in gossypol biodegradation. In addition, extracellular xylanase and β-1,4-endo-xylanase have also been identified. A large number of studies have shown that xylanase has some ability to remove crude lignin and can indirectly degrade lignin[26]. It plays an important role in lignin biodegradation. There are phenol hydroxyl groups, alcohol hydroxyl groups, and other active groups in the molecular structure of lignin[25]. Gossypol is one of the polyphenolic hydroxyl groups[27,28]. We speculate that xylanase and β-1, 4-endo-xylanase may be involved in the biodegradation of gossypol through specific pathways.

Table 2. Genes and corresponding enzymes related to gossypol biodegradation by YJ01

Gene ID	Database	Gene Name
gene5756, gene8925	KEGG	xynA
gene0733	KEGG	pgk
gene2649, gene7420	KEGG	-

gene4148	KEGG	ppa
gene2257	KEGG	-
gene1802	KEGG	pgi
gene8994	KEGG	gapA
gene3004, gene7660, gene7979	KEGG	gltA

4. Conclusions

A. terreus-YJ01, an efficient fungal strain for biodegrading gossypol, was successfully isolated from the soil of cotton stalk piles in Xinjiang Province, China. Sucrose and sodium nitrate were proved to be the best carbon and nitrogen sources for the growth of YJ01, and the optimal pH and inoculum size for the growth of YJ01 were 6.0 and 1%, respectively. Under the optimal culture conditions, initial gossypol of 250 mg·L^{-1} could be removed by 97% within 96 h by YJ01. Moreover, initial gossypol of 150 mg·L^{-1} could also be catalyzed by 98% or 99% within 36 h by the intracellular or extracellular crude enzymes of YJ01. These findings clearly demonstrate YJ01's remarkable capacity for gossypol biodegradation. Eight proteins of interest were found to be associated with the biodegradation of gossypol. Notably, phosphoglycerate kinase and malate dehydrogenase produce energy for the biodegradation process through glycolysis and TCA cycle, respectively. Glutamate dehydrogenase and inorganic pyrophosphatase can further regulate energy supply. In case of sufficient energy, *Aspergillus terreus* can further participate in the biodegradation of gossypol through xylanase and β-1, 4-endo-xylanase to achieve the purpose of gossypol biodegradation. The findings of this study provide valuable insights into the metabolism pathway of gossypol biodegradation by *A. terreus*-YJ01. The products of gossypol biodegradation by YJ01 is being investigated in order to to fully understand the mechanisms of gossypol biodegradation.

References

1. Ye, G.; Dong, X.; Yang, Q.; Chi, S.; Liu, H.; Zhang, H.; Tan, B.; Zhang, S. Low-gossypol cottonseed protein concentrate used as a replacement of fish meal for juvenile hybrid grouper (*epinephelus fuscoguttatus* ♀ × *epinephelus lanceolatus* ♂): Effects on growth performance, immune responses and intestinal microbiota. *Aquaculture* **2020**, *524*, 735309.
2. Lordelo, M.M.; Davis, A.J.; Calhoun, M.C.; Dowd, M.K.; Dale, N.M. Relative toxicity of gossypol enantiomers in broilers. *Poultry science* **2005**, *84*, 1376-1382.
3. Wang, W.K.; Wang, Y.L.; Li, W.J.; Wu, Q.C.; Yang, K.L.; Li, S.L.; Yang, H.J. In situ rumen degradation characteristics and bacterial colonization of whole cottonseed, cottonseed hull and cottonseed meal with different gossypol content. *AMB Express* **2021**, *11*, 91.
4. Zhang, Z.; Yang, D.; Liu, L.; Chang, Z.; Peng, N. Effective gossypol removal from cottonseed meal through optimized solid-state fermentation by *bacillus coagulans*. *Microbial cell factories* **2022**, *21*, 252.
5. Wang, W.K.; Wang, Y.L.; Li, W.J.; Wu, Q.C.; Li, S.L.; Yang, H.J. Gossypol exhibited higher detrimental effect on ruminal fermentation characteristics of low-forage in comparison with high-forage mixed feeds. *Toxics* **2021**, *9*.
6. Du, G.; Zhou, Y.; Zhang, J.; Han, S.; Liu, X.; Yuan, C.; Ndayisenga, F.; Shi, J.; Zhang, B. Optimized strategy valorizing unautoclaved cottonseed hull as ruminant alternative feeds via solid-state fermentation: Detoxifying polyphenols, restraining hazardous microflora and antibiotic-resistance gene hosts. *Environmental Technology & Innovation* **2022**, *28*, 102937.
7. Villasenor, M.; Coscioni, A.C.; Galvao, K.N.; Chebel, R.C.; Santos, J.E. Gossypol disrupts embryo development in heifers. *Journal of dairy science* **2008**, *91*, 3015-3024.
8. Zhao, T.; Xie, Q.; Li, C.; Li, C.; Mei, L.; Yu, J.Z.; Chen, J.; Zhu, S. Cotton roots are the major source of gossypol biosynthesis and accumulation. *BMC plant biology* **2020**, *20*, 88.
9. Christopher A. Bailey, R.D.S., Michael S. Ziehr, Akram U. Haq, Minawar Sattar, Leon F. Kubena, Hyeong L. Kim, Robson de M. Vieira. Cottonseed with a high (+)- to (-)-gossypol enantiomer ratio favorable to broiler production. *JOURNAL OF AGRICULTURAL AND FOOD CHEMISTRY* **2000**, *48*, 5692-5695.
10. Wang, C.; Li, Y.; MaiTiSaiYiDi, T.; Yang, H.; Yang, K. Effect of dietary gossypol supplement on fermentation characteristics and bacterial diversity in the rumen of sheep. *PLoS One* **2020**, *15*, e0234378.
11. Chain, E.P.o.C.i.t.F.; Knutsen, H.K.; Barregard, L.; Bignami, M.; Bruschweiler, B.; Ceccatelli, S.; Dinovi, M.; Edler, L.; Grasl-Kraupp, B.; Hogstrand, C., *et al.* Presence of free gossypol in whole cottonseed. *EFSA journal. European Food Safety Authority* **2017**, *15*, e04850.
12. Tang, C.-h.; Liu, J.; Zhao, Q.-y.; Zhang, J.-m. Pharmacokinetic comparison of gossypol isomers in cattle: Transfer from diet to plasma and degradation by rumen microbes. *Journal of Zhejiang University-SCIENCE B* **2018**, *19*, 471-480.
13. Tian, X.; Ruan, J.; Huang, J.; Fang, X.; Mao, Y.; Wang, L.; Chen, X.; Yang, C. Gossypol: Phytoalexin of cotton. *Science China. Life sciences* **2016**, *59*, 122-129.
14. Farthing, A.L.; Schwertner, T.W.; Gasper, D.J.; Mathewson, H.A.; Guay, K.A. Acute toxicity of gossypol in northern bobwhites. *Journal of Applied Animal Research* **2019**, *47*, 326-332.
15. Porat, O. Effects of gossypol on the motility of mammalian sperm. *Molecular reproduction and development* **1990**, *25*, 400-408.
16. C. Brocas, R.M.R., F.F. Paula-Lopes, L.R. McDowell, M.C. Calhoun, C.R. Staples, N.S.Wilkinson, A.J. Boning, P.J. Chenoweth, P.J. Hansen. Deleterious actions of gossypol on bovine spermatozoa, oocytes, and embryos. *BIOLOGY OF REPRODUCTION* **1997**, *57*, 901-907.
17. Zhu, X.; Wu, Y.; Li, C.; Yan, W.; Pan, J.; Wang, S.; Zhao, S. Prenatal exposure to gossypol impairs corticogenesis of mouse. *Front Neurosci* **2020**, *14*, 318.

18. Soares Neto, C.B.; Conceição, A.A.; Gomes, T.G.; de Aquino Ribeiro, J.A.; Campanha, R.B.; Barroso, P.A.V.; Machado, A.E.V.; Mendonça, S.; De Siqueira, F.G.; Miller, R.N.G. A comparison of physical, chemical, biological and combined treatments for detoxification of free gossypol in crushed whole cottonseed. *Waste and Biomass Valorization* **2020**, *12*, 3965-3975.
19. Wang, W.-K.; Yang, H.-J.; Wang, Y.-L.; Yang, K.-L.; Jiang, L.-S.; Li, S.-L. Gossypol detoxification in the rumen and *helicoverpa armigera* larvae: A review. *Animal Nutrition* **2021**, *7*, 967-972.
20. Weng, X.-Y.; Sun, J.-Y. Kinetics of biodegradation of free gossypol by *candida tropicalis* in solid-state fermentation. *Biochemical Engineering Journal* **2006**, *32*, 226-232.
21. Zhang, Y.; Zhang, Z.; Dai, L.; Liu, Y.; Cheng, M.; Chen, L. Isolation and characterization of a novel gossypol-degrading bacteria *bacillus subtilis* strain rumen bacillus subtilis. *Asian-Australasian journal of animal sciences* **2018**, *31*, 63-70.
22. Yusuf, H.A.; Piao, M.; Ma, T.; Huo, R.; Tu, Y. Effect of lactic acid bacteria and yeast supplementation on anti-nutritional factors and chemical composition of fermented total mixed ration containing cottonseed meal or rapeseed meal. *Animal bioscience* **2022**, *35*, 556-566.
23. Hou, M., Bao, H.F, Wang, N, Zhan, F.Q, Yang, R, Long, X.Q, Cui, W.D. Screening of efficient gossypol degrading strains and study on their detoxification conditions. *Xinjiang Agricultural Sciences* **2016**, *53*, 1114-1121.
24. S. Rajarathnam, M.N.S., Zakia Bano. Biodegradation of gossypol by the white oyster mushroom, *pleurotus florida*, during culturing on rice straw growth substrate, supplemented with cottonseed powder. *World journal of microbiology & biotechnology* **2001**, *17*, 221-227.
25. C. DAVID BOYLE, B.R.K., IAN D. REID. Solubilization and mineralization of lignin by white rot fungi. *APPLIED AND ENVIRONMENTAL MICROBIOLOGY* **1992**, *58*, 3217-3224.
26. Pedraza-Zapata, D.C.; Sanchez-Garibello, A.M.; Quevedo-Hidalgo, B.; Moreno-Sarmiento, N.; Gutierrez-Rojas, I. Promising cellulolytic fungi isolates for rice straw degradation. *Journal of microbiology* **2017**, *55*, 711-719.
27. Gennadios, H.A.; Gonzalez, V.; Di Costanzo, L.; Li, A.; Yu, F.; Miller, D.J.; Allemann, R.K.; Christianson, D.W. Crystal structure of (+)-delta-cadinene synthase from gossypium arboreum and evolutionary divergence of metal binding motifs for catalysis. *Biochemistry* **2009**, *48*, 6175-6183.
28. Krempl, C.; Sporer, T.; Reichelt, M.; Ahn, S.J.; Heidel-Fischer, H.; Vogel, H.; Heckel, D.G.; Joussen, N. Potential detoxification of gossypol by udp-glycosyltransferases in the two heliothine moth species *helicoverpa armigera* and *heliothis virescens*. *Insect biochemistry and molecular biology* **2016**, *71*, 49-57.
29. Yang, X.; Sun, J.Y.; Guo, J.L.; Weng, X.Y. Identification and proteomic analysis of a novel gossypol-degrading fungal strain. *Journal of the Science of Food and Agriculture* **2012**, *92*, 943-951.
30. Mageshwaran, V.; Sharma, V.; Chinnkar, M.; Parvez, N.; Krishnan, V. Biodegradation of gossypol by mixed fungal cultures in minimal medium. *Applied Biochemistry and Microbiology* **2018**, *54*, 301-308.
31. Yang, H.; Feng, S.; Ma, Q.; Ming, Z.; Bai, Y.; Chen, L.; Yang, S.T. Influence of reduced graphene oxide on the growth, structure and decomposition activity of white-rot fungus *phanerochaete chrysosporium*. *RSC advances* **2018**, *8*, 5026-5033.
32. de Cássia Romero, A.; Abdalla, A.L.; dos Santos Dias, C.T.; Soltan, Y.A. Assessment of uncertainty sources of free gossypol measurement in cottonseed by high-performance liquid chromatography. *SN Applied Sciences* **2020**, *2*.
33. Aparecido Almeida Conceição, C.B.S.N., José Antônio de Aquino Ribeiro, Felix Gonçalves de Siqueira, Robert Neil Gerard Miller, Simone Mendonça. Development of an rp-uhplc-pda method for quantification of free gossypol in cottonseed cake and fungal-treated cottonseed cake. *PLOS ONE* **2018**, *13*, e0196164.
34. Sh. Ya. Mirzaakhmedov, Z.F.Z., Z. R. Akhmedova, A. B. Saliev,1 D. T. Ruzmetova, Kh. B. Ashurov, Dimitrios Fessas, Stefania Iametti. Isolation, purification, and enzymatic activity of cellulase components of the fungus *aspergillus terreus*. *Chemistry of Natural Compounds* **2007**, *43*, 594-597.

35. Boruta, T.; Bizukojc, M. Culture-based and sequence-based insights into biosynthesis of secondary metabolites by *aspergillus terreus* atcc 20542. *Journal of biotechnology* **2014**, *175*, 53-62.
36. WANG Junfeng, W.P., CHEN Jian, YAN Hai. Biodegradation of microcystin-rr by a new isolated *sphingopyxis* sp. *BIOTECHNOLOGY AND BIOENGINEERING* **2010**, *18*, 1-5.
37. Cheng, C.; Cun-Xi, N.; Jing, L.; Yong-Qiang, W.; Yan-Feng, L.; Wen-Xia, G.; Wen-Ju, Z. Validated method to determine (±)-gossypol in *candida tropicalis* culture by high-performance liquid chromatography. *Acta Chromatographica* **2018**, *30*, 269-273.
38. Revin, V.V.; Liyas'kina, E.V.; Sapunova, N.B.; Bogatyreva, A.O. Isolation and characterization of the strains producing bacterial cellulose. *Microbiology* **2020**, *89*, 86-95.
39. Wu, H.Y.; Mortensen, U.H.; Chang, F.R.; Tsai, H. Whole genome sequence characterization of *aspergillus terreus* atcc 20541 and genome comparison of the fungi a. Terreus. *Scientific reports* **2023**, *13*, 194.
40. Palanivel, M.; Mac Aogain, M.; Purbojati, R.W.; Uchida, A.; Aung, N.W.; Lim, S.B.Y.; Putra, A.; Drautz-Moses, D.I.; Seaton, S.; Rogers, T.R., *et al.* Whole-genome sequencing of *aspergillus terreus* species complex. *Mycopathologia* **2020**, *185*, 405-408.
41. Liu, C.; Zhao, Z.; Xu, Q.; Zhang, H.; Liu, X.; Yin, C.; Yan, H.; Liu, Y. Comparative genomic analysis of *sphingomonas morindae* sp. Nbd5 and *sphingopyxis* sp. Ustb-05 for producing macular pigment. *Microorganisms* **2023**, *11*.
42. Wang, W.K.; Li, W.J.; Wu, Q.C.; Wang, Y.L.; Li, S.L.; Yang, H.J. Isolation and identification of a rumen *lactobacillus* bacteria and its degradation potential of gossypol in cottonseed meal during solid-state fermentation. *Microorganisms* **2021**, *9*.
43. Han, X.; Chakrabortti, A.; Zhu, J.; Liang, Z.X.; Li, J. Sequencing and functional annotation of the whole genome of the filamentous fungus *aspergillus westerdijkiae*. *BMC genomics* **2016**, *17*, 633.
44. Xiu Tian, X.F., Jin-Quan Huang, Ling-Jian Wang, Ying-Bo Mao and Xiao-Ya Chen. A gossypol biosynthetic intermediate disturbs plant defence response. *PHILOSOPHICAL TRANSACTIONS OF THE ROYAL SOCIETY B-BIOLOGICAL SCIENCES* **2019**, *374*.
45. Weng, X.-Y.; Sun, J.-Y. Biodegradation of free gossypol by a new strain of *candida tropicalis* under solid state fermentation: Effects of fermentation parameters. *Process Biochemistry* **2006**, *41*, 1663-1668.
46. Chen, J.J., Zhao, J, Li, B.H, Cao, X.N, Liu, L.T, Wu, S.S. Isolation, identification, and optimization of fermentation conditions of highly efficient cotton phenol degradation strains. *Feed Research* **2016**, *09*, 37-42+46.
47. Yin, W.B.; Grundmann, A.; Cheng, J.; Li, S.M. Acetylaszonalenin biosynthesis in neosartorya fischeri. Identification of the biosynthetic gene cluster by genomic mining and functional proof of the genes by biochemical investigation. *The Journal of biological chemistry* **2009**, *284*, 100-109.
48. Xiu Tian, J.-X.R., Jin-Quan Huang, Chang-Qing Yang, Xin Fang, Zhi-Wen Chen, Hui Hong, Ling-Jian Wang, Ying-Bo Mao, Shan Lu, Tian-Zhen Zhang, Xiao-Ya Chen. Characterization of gossypol biosynthetic pathway. *The Proceedings of the National Academy of Sciences* **2018**, *115*, E5410–E5418.
49. Yu, L.; Zhan, X.; Liu, Q.; Sun, Y.; Li, M.; Zhao, Y.; An, X.; Tian, Y.; He, L.; Zhao, J. Identifying the naphthalene-based compound 3,5-dihydroxy 2-napthoic acid as a novel lead compound for designing lactate dehydrogenase-specific antibabesial drug. *Front Pharmacol* **2019**, *10*, 1663.

Study on the solidification of heavy metals in municipal solid waste incineration fly ash by metallurgical slag-based and cement-based cemented backfill materials

Jia Li[1]， Wen Ni[1*], Chuanfu Wu[2], Qunhui Wang[2]

1 School of Civil and Resource Engineering, University of Science and Technology Beijing, Beijing, 100083, China.

2 School of Civil and Resource Engineering, University of Science and Technology Beijing, Beijing, 100083, China.

* Corresponding author: Wen Ni, E-mail address: niwen@ces.ustb.edu.cn

Abstract

In this paper, the physicochemical characteristics of MSWI fly ash from two different types of incineration processes, including grate furnace（GF）fly ash and circulating fluidized bed（CFB） fly ash. The mechanical properties and leaching toxicity characteristics of cemented materials containing two types MSWI fly ash were studied, as well as, compared with cement-based backfill materials. It is found that the MSWI fly ash creates a high alkalinity reaction environment for the hydration system and promotes the dissolution of activity [SiO_4] and [AlO_4] in the blast furnace slag. The compressive strength of A2 and B2 can reach 3.61MPa and 28.81Mpa at 28d, respectively, which meet the strength requirements of mining backfill bodies of different grades.

Instruction

MSWI fly ash is classified as HW18 hazardous waste, because it contains Cd, As, Cr, Pb, Hg, Zn, Cu, Sb and other heavy metals, as well as dioxins and other organic pollutants[1]. According to statistics, the disposal volume of MSWI fly ash for China has reached 14,607.6 $\times 10^4$ tons, and output has reached 758×10^4 tons in 2020[2]. Stabilization/Solidification is the main treatment methods of MSWI fly ash by using cement[3]. However, there are many problems: (1)The volume of cement-based solidified body will increase during hydration and hardening; (2)the relatively dispersed particle size and high content of soluble salt of MSWI fly ash will also have negative effects on the long-term curing process[4-6]. In addition, cement is not the best binders for S/S MSWI fly ash from the environmental and economic costs[7]. Therefore, the application of industrial solid waste instead of cement to treat hazardous waste has become a new development trend.

In this paper, two incineration technology (GF and CFB)of MSWI fly ash were mixed with metallurgical slag-based cemented materials and ordinary Portland cement, respectively. The effects of the GF fly ash and CFB fly ash on the mechanical properties and leaching concentration of different backfill materials were systematically compared, which can lay the theoretical foundation of environmental mineralogy for the application of metallurgical slag and MSWI fly ash in mine backfill. Moreover, it has important strategic significance for the development and application of low-carbon cemented materials.

2 Materials and methods

The BFS, steel slag, FGDG and tailings used in this experiment were all taken from Hebei province. GF MSWI fly ash was provided by Beijing waste incineration power plant, and CFB fly ash was provided by Tangshan waste incineration Power Plant. It can be found from the results that the main components of

steel slag are CaO, Fe_2O_3, SiO_2, MgO, Al_2O_3 and MnO. The main chemical composition of granulated blast furnace slag powder is CaO, SiO_2 and Al_2O_3. The GF fly ash and CFB fly ash were mixed with metallurgical waste slag, P·O 42.5 cement and tailings in the proportion, and then the filling slurry with different compositions was prepared.

3. Results and discussion

3.1 Compressive strength analysis of different types of backfill materials

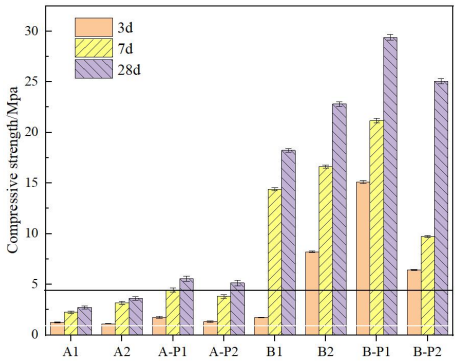

Fig.2 The compressive strength of different samples (black and white line at 1 MPa and 4Mpa: different required strength for backfill materials)

The compressive strength requirement of backfill is about 1~2MPa in foreign. The Mining Engineer Manual of China puts forward the selection range of backfill strength of different mining methods, among which the higher strength requirement is 4~5MPa, and the lower strength requirement is 1~2MPa. Fig. 2 shows the test results of the compressive strength of backfill sample at different ages. The test blocks in group A all meet the lower strength requirements of filling body (> 1 MPa), and the group B meet the higher strength requirements of filling body (> 4 MPa). It can be found from Fig.5 that the compressive strength of cement-fly ash-based backfill samples (A-P2, B-P2) decreases with the increase of MSWI fly ash content in the backfill materials. Therefore, the addition of MSWI fly ash is not conducive to the growth of compressive strength of cement-fly ash-based backfill test blocks.

3.2 Analysis of leaching concentration for backfill materials

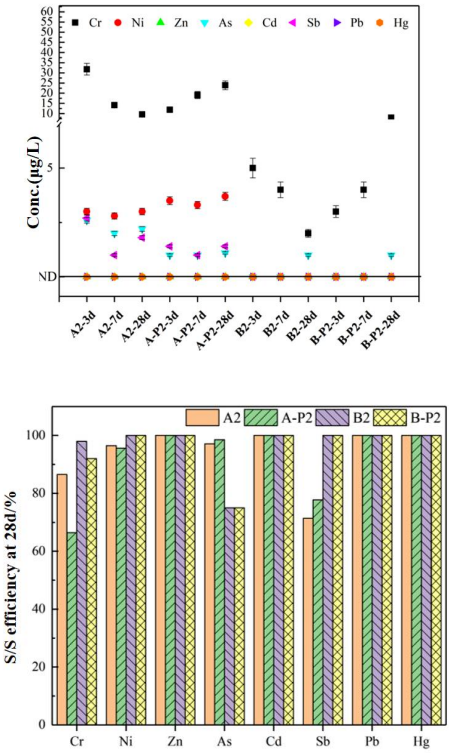

Fig.3 S/S efficiencies (%) after curing at 28 days.（The black line shows the method detection limit (0.01 μg/L))

The leaching concentration of target heavy metals for MSWI fly ash from two types of incineration technology appear beyond the limit standard of the underground class III water quality. It can be found from the leaching results that the leaching toxicity of the backfill materials containing CFB fly ash is obviously lower than that of the backfill materials containing GF fly ash. The low content of hazardous components lays a foundation for the recycling and harmless utilization of CFB fly ash. It is obvious that the leaching concentration of Cr in A-P2 reached 23.9μg/ L after hydration at 28d, while the leaching level of A2 was only 9.6μg/ L at that time. For group B, the leaching concentration of Cr of B-P2 was twice that of B2. In addition, according to the S/S efficiency of Cr of each system at 28d, the metallurgical slag-based

solidified matrix (A2, B2) is significantly higher than that of cement-based system (A-P2, B-P2), especially the A-P2, the S/S efficiency of Cr is only 68.7%. Therefore, compared with metallurgical slag-based backfill materials, there is a greater risk of Cr leaching in cement-based backfill materials, Cr migration should be carefully considered to ensure that the leaching risk is within a controllable range when using cement clinker binder.

4 Conclusion

（1）The GF fly ash has an obvious promoting effect on the late compressive strength, while the CFB fly ash has an obvious promoting effect on the metallurgical slag-based cementing system.

（2） The leaching concentration of target metal meets the requirements of the standard limit of class III groundwater for the metallurgical slag-based cemented system.

Acknowlegement

This work was supported by the National Key R&D Program of China (Grant NO. 2021YFE0112100).

Reference

[1] Tsiliyannis, C.A., 2018. Control of dioxin emissions from alternative fuels via regulated activated carbon injection and flue gas recirculation. Journal of Hazardous Materials. 358, 405-415.

[2] She K. L., 2022. Potential of carbonization for collaborative disposal of pollution and carbon reduction of incineration fly ash. Research of Environmental Science. (in Chinese)

[3] Singh, D., et al., 2017. Geo-environment application of municipal of municipal solid waste incinerator ash stabilized with cement. Journal of Rock Mechanics and Geotechnical Engineering. 9, 370–375.

[4] Wang L., 2003. Recycling of municipal solid waste incineration fly ash for ordinary Portland cement production：A real-scale test [J]. Journal of Hazardous Materials. 96(2-3)：201-216.

[5] Pan J. R., 2008. Recycling MSWI bottom and fly ash as a raw materials for Portland cement[J]. Waste Management. 21(8)：1113-1118.

[6] Aubert J.E., 2004. Use of municipal solid waste incineration fly ash in concrete[J]. Cement and Concrete Research. 6(34): 957-963.

[7] Liu W. T., 2021. CO2 mineral carbonation using industrial solid wastes: A review of recent developments[J]. Chemical Engineering Journal, 129093.

Integrated technology for selectively controlled carbonization and resource utilization of steel slag

Wei Su*, Jiajie Li, Yongkang Cui, Wentao Guo, Jinglei Tian, Fangzhou Sun, Yujia Sun, Yi Xing, Wen Ni

School of Energy and Environmental, USTB, China

HBIS Group Co., Ltd, China

1.Introduction

In 2022, the carbon emissions of my country's steel industry will be approximately 1.8 billion tons, accounting for approximately 65.11% of the global steel industry's carbon emissions. At the same time, my country's annual steel slag production reaches hundreds of millions of tons, but the utilization rate is less than 30%. Steel slag is rich in alkaline elements calcium and magnesium, which can fix the acidic gas CO2, solving the problem of steel slag stacking and disposal while reducing CO2 emissions. This study uses steel slag selective control and carbon fixation technology and based on the carbonization-resource integration process to prepare diversified products suitable for different application scenarios, solves the problem of steel slag resource utilization, and collaboratively achieves the reduction of CO2 emissions in the steel industry.

2.Challenges

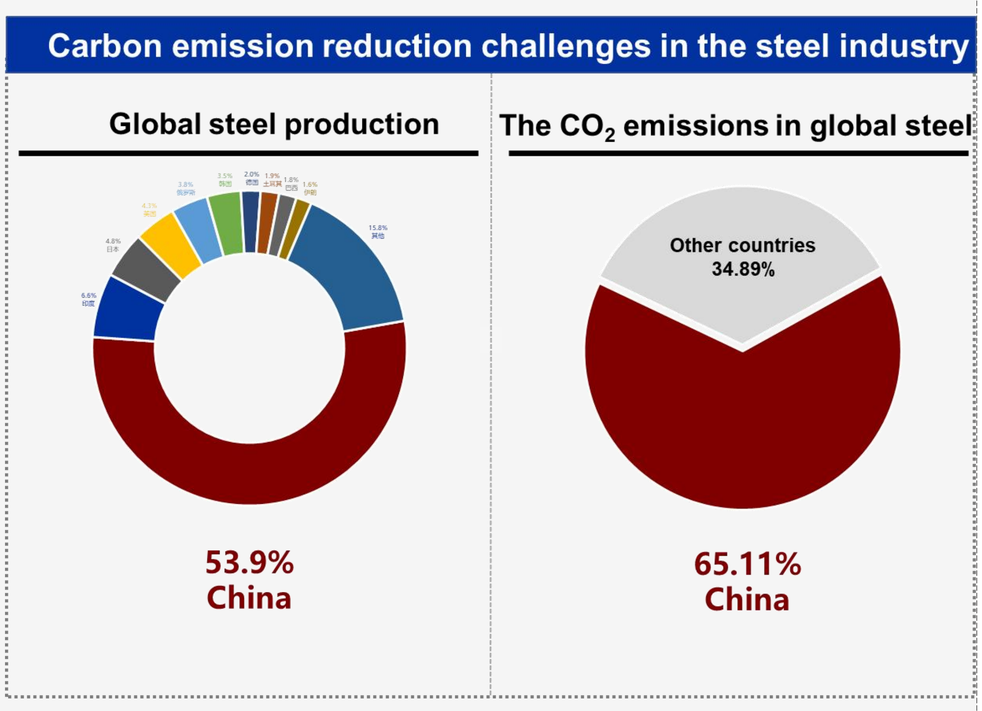

Fig. 1. Global steel production distribution and proportion of CO2 emissions from the steel industry in each country

3.Method

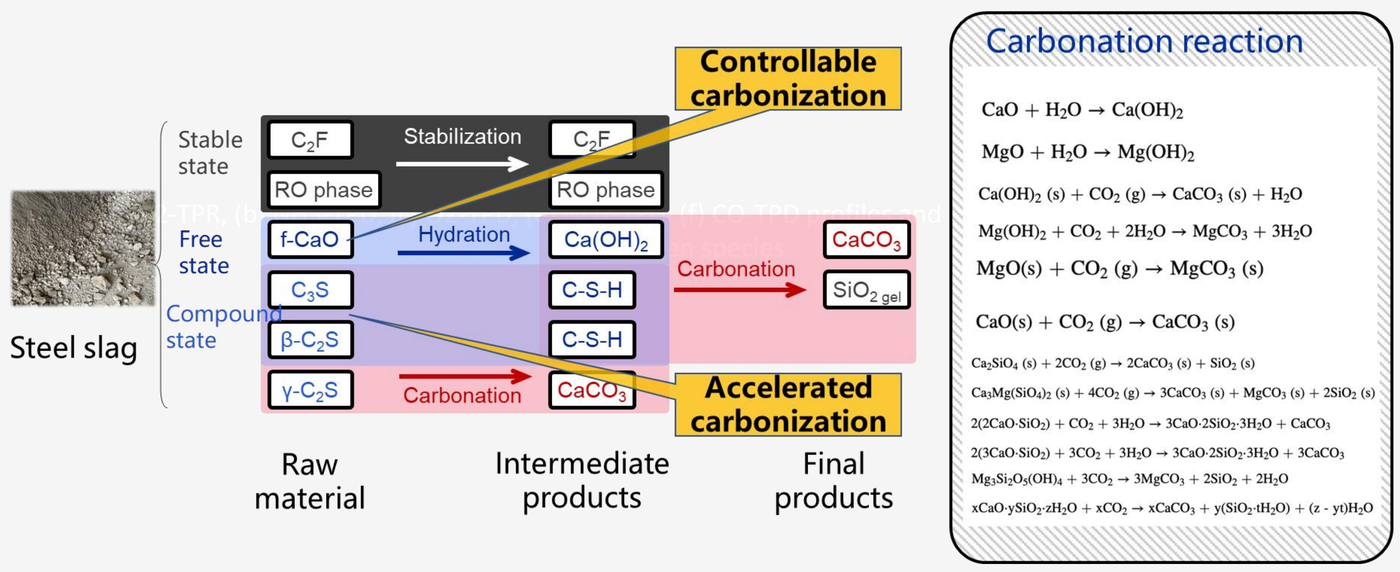

Fig. 2. Schematic diagram of the phase composition and selective carbonization mechanism of steel slag

4.Carbon2Rock

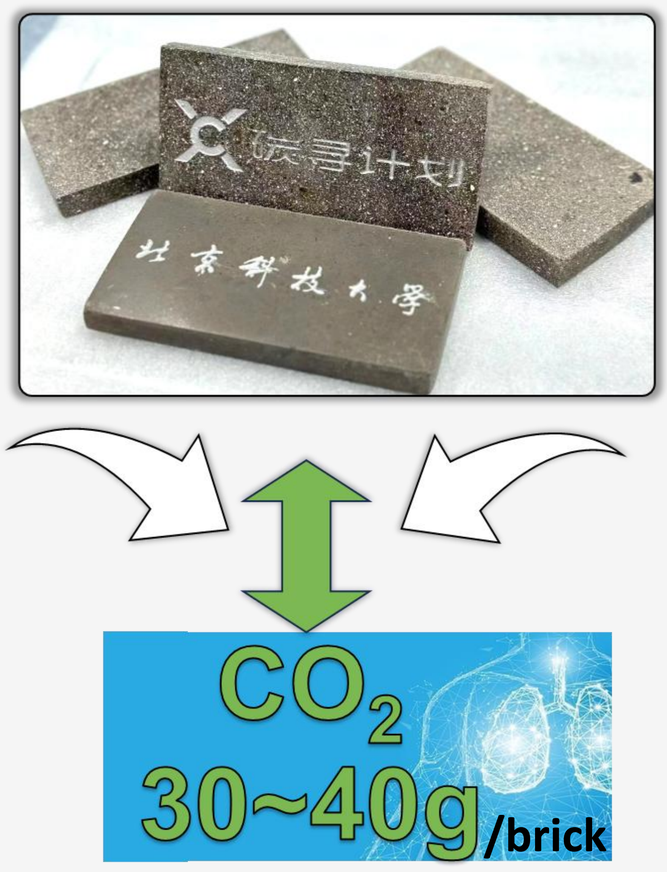

Fig. 3. Cultural and creative products

Fig. 4. building products

5.Low carbon benefits

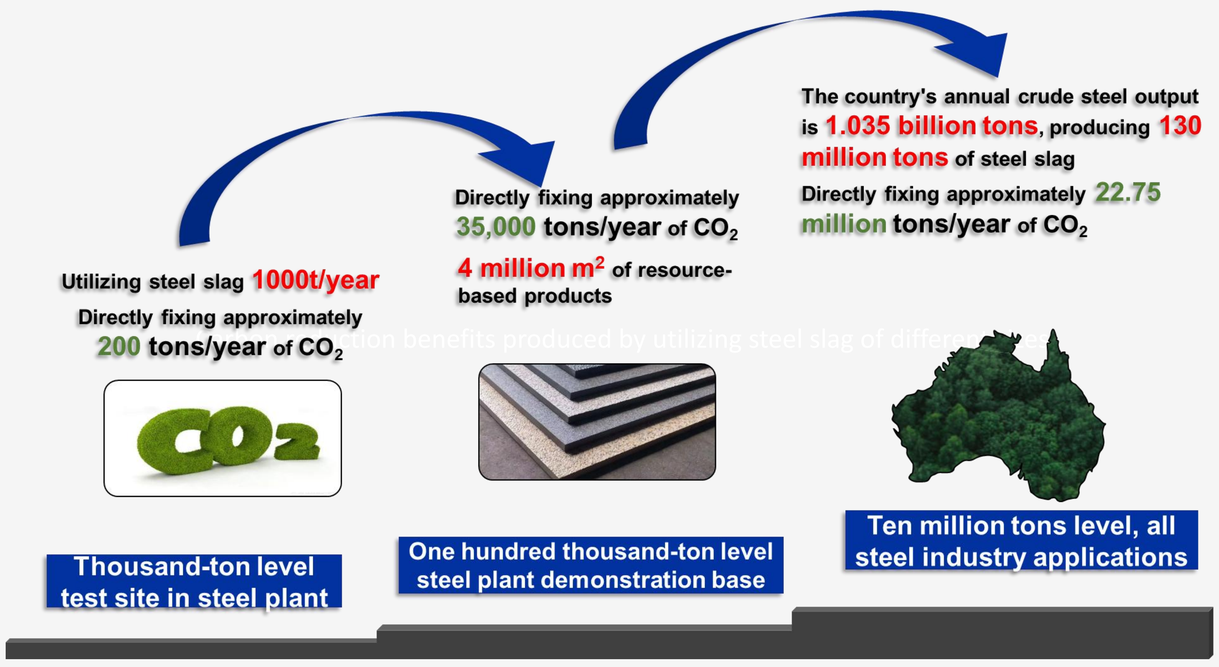

Fig. 5. Carbon reduction benefits produced by utilizing steel slag of different sizes

6.Conclusion

This technology is based on the principle of natural rock weathering reaction and develops a steel slag carbon fixation technology suitable for the direct utilization of low-concentration CO2 in the steel industry. The high-performance thin plate products produced by this project have performance and economic value comparable to that of natural marble. The amount of direct carbon reduction this technology can achieve can contribute approximately 10% of the load of the CCUS path in the steel industry.

Carbon cloth coupled riboflavin aids the anaerobic digestion of dairy manure by promoting direct interspecies electron transfer

Yiwei Zeng[1], Wenwen Chen[1], Huanying Liu[1], Dezhi Sun[1] and Yan Dang[1*]
1 Beijing Key Laboratory for Source Control Technology of Water Pollution, Engineering Research Center for Water Pollution Source Control and Eco-remediation, College of Environmental Science and Engineering, Beijing Forestry University, Haidian Distrct, Beijing, 100083, China

ABSTRACT

Dairy manure generates globally due to increased beef and milk consumption, but its treatment efficiency remains low. Previous studies have shown that riboflavin-loaded conductive materials can improve anaerobic digestion through enhance direct interspecies electron transfer (DIET). However, its effect on the practical anaerobic digestion of dairy manure remained unclear. In this study, carbon cloth loaded with riboflavin (carbon cloth-riboflavin) was added into an anaerobic digester treating dairy manure. The carbon cloth-riboflavin reactor showed a better performance than other two reactors. The metagenomic analysis revealed that *Methanothrix* on the surface of the carbon cloth predominantly utilized the CO_2 reduction for methane production, further enhanced after riboflavin addition, while *Methanothrix* in bulk sludge were using the acetate decarboxylation pathway. Furthermore, the carbon cloth-riboflavin enriched various major methanogenic pathways and activated a large number of enzymes associated with DIET. Riboflavin's presence altered the microbial communities and the abundance of functional genes relate to DIET, ultimately leading to a better performance of anaerobic digestion for dairy manure.

INTRODUCTION

Intensive animal husbandry has experienced rapid development in recent decades in order to meet the increasing demand for food. Globally, there are approximately 1.5 billion cows, and these cows produce around 15 billion tons of dairy manure (DM). If this amount of DM is not managed effectively, it can result in various issues such as odors, water pollution, and the proliferation of harmful bacteria, as well as the release of methane. Therefore, it is crucial to promptly treat DM to prevent its release into the atmosphere.

Anaerobic digestion (AD) can simultaneously treat organic waste disposal and produce biogas, making it an ideal method for treating livestock manure (Scarlat et al., 2018), including DM. However, treating DM with conventional AD may lead to a low methane rate and yield due to its high composition of non-biodegradable materials (Frear et al., 2011). What's more, in reactors with high organic loads, fermentative bacteria produce high levels of volatile acids (VFAs) leading to reactor acidification (Jia et al., 2022; Lei et al., 2016), and the reaction process also encounters challenges in degrading complex organics. Therefore, there is an urgent need to find a new treatment method to improve the efficiency of DM anaerobic digestion.

Direct interspecies electron transfer (DIET) can enhance AD by promoting the flow of extracellular electrons secreted by electrogenic bacteria from intermediate by-products into the methane pathways, thereby reducing the accumulation of VFAs (Cruz Viggi et al., 2014; Li et al., 2015). In general, DIET requires the transfer of electrons through electrically conductive pili and outer membrane c-type cytochromes in direct contact on the cell surface (Lovley, 2017b). However, the addition of carbon-based conductive materials, such as granular activated carbon (Lei et al., 2019; Rotaru et al., 2014b), carbon cloth (Chen et al., 2014a; Jia et al., 2022), and biochar (Chen et al., 2014b; Zhao et al., 2016), to the anaerobic digestion reactors can enhance DIET without the need for direct intercellular contact, significantly improving the performance and stability of digesters (Dang et al., 2017; Huang et al., 2022). The main potential reason for this is that, with the addition of carbon-based conductive materials, cells no longer need to generate large amounts of extracellular substrates for electron transfer, and they can attach to the surface of the materials for fast and remote electron transfer (Zhao et al., 2015; Zhao et al., 2016). Thus, the addition of conductive materials not only saves the cell's energy but also provides an ideal living space (Sasaki et al., 2010). However, there is little research on promoting anaerobic digestion of dairy manure through the addition of conductive materials.

Riboflavin not only serves as a coenzyme precursor involved in fermentation, acetogenesis and methanogenesis (Buckel & Thauer, 2018; Prakash et al.,

2019; Vanoni, 2021), but also acts as a precursor for some important endogenous extracellular electron shuttles in anaerobic digestion systems (Marsili 2008). As a precursor for these substances, riboflavin possesses dual functions as both an accessory factor and electron shuttle (Huang et al., 2020). Unlike other electron transfer shuttles, the addition of riboflavin can specifically enhance the electron shuttles for methane production via DIET, thereby accelerating the methanogenic process. Previous studies have demonstrated that the addition of riboflavin-loaded carbon-based conductive materials can enhance DIET in complex microbial hybrid systems (Huang et al., 2022; Li et al., 2023). However, the effects of riboflavin addition on the microbial genome and metabolic pathways have not been investigated.

The objective of this research was to assess the potential enhancement in the performance of anaerobic digesters treating CD through the incorporation of riboflavin-loaded. Additionally, metagenomic studies were conducted to gain insight into how the addition of differently treated conductive materials affects the dominant metabolic processes occurring in the reactors and their impact on the organisms involved in DIET. Furthermore, we expect to propose a potential biochemical pathway for the involvement of methane formation via DIET, thus expanding the knowledge of community metabolomics in the area.

MATERIALS AND METHODS

Cow dung, inoculated sludge and carbon cloth loaded with riboflavin

Fresh DM in this study was collected from a large cow farm located in Shanxi, China; anaerobic sludge obtained from an anaerobic digester in a municipal wastewater treatment plant (Beijing, China), and stored at 4℃ until use as an inoculum. Carbon cloth (HCP330N, the density is 155 g/cm^3 and the conductivity is about 833 S/m), and riboflavin purchased from Shanghai Macklin Biochemical Co., Ltd. Prior to riboflavin loading, carbon cloth was soaked in acetone for 3 h and sonicated for 15 min, repeated the above operation with anhydrous ethanol, and washed with deionized water until odorless, dried and prepared. The above carbon cloth was soaked in saturated riboflavin solution for 3 d and incubated in an oven at 60℃ for 12 h. The loading process was operated without light to avoid riboflavin decomposition.

Reactor set-up and operation conditions

Three semi-continuous digesters were built from 2 L serum bottles with a working volume of 1 L and sealed with rubber stopper. Each reactor had an influent/effluent port, and a gas outlet port connected to gas collection bag. All reactors were inoculated with 400 ml anaerobic sludge and deionized water was added in each reactor to reach working volume. All reactors were incubated in the dark at 35℃ in a water bath shaker, which the rotation speed was set to 115 rpm.

The three reactors are operated as follows: (1) six pieces of riboflavin-loaded carbon cloth (10×10×0.03 cm3; the volume of 18 cm^3) were added to one of the reactors (experimental group, Carbon cloth-Riboflavin reactor); six pieces of non-loaded carbon cloth (10×10×0.03 cm^3; the volume of 18 cm^3) were added to another reactor (experimental group, Carbon cloth reactor); (3) no carbon cloth amendments were made to the third reactor (control group, Only sludge reactor). The CD added to the reactors was increased gradually and accounts for the increase in OLR, and all reactors were fed once a day.

RESULT AND DISCUSSION

Performance of carbon cloth-riboflavin amended reactor

To investigate the performance of carbon cloth-riboflavin reactor, the methane production, COD concentration, methane content, and pH of each reactor were monitored over the course of 60 days as OLR of three digesters was increased from 2 kgCOD/(m^3·d) to 5 kgCOD/(m^3·d) (Fig. 1). During the first two phases (HRT:25 days and HRT: 16.7 days, phase 1 and phase 2) when OLRs were increased from 2 kgCOD/(m^3·d) to 3 kgCOD/(m^3·d), all digesters were in stable operation, and pH fluctuated between 7.8 and 7.1, gradually decreasing. Carbon cloth and carbon cloth-riboflavin reactors performed similarly with an average COD removal rate >95%, which was higher than the 90% of the only sludge reactor (p<0.05). The first remarkable difference between the experimental groups (carbon cloth reactor and carbon cloth-riboflavin reactor) and control group (only sludge reactor) appears at day 22. As shown in Fig. 1, the COD concentrations of control group fluctuated between 3200 mg/L and 3800 mg/L when OLR was 3 kgCOD/(m^3·d), whereas the experimental groups remained relatively stable at 2400 mg/L when exposed to the same OLR. Methane production rates were also significantly higher (p<0.05) in the experimental groups. Once the OLR in the control group was increased to 4 kgCOD/(m3·d) (HRT: 12.5 day, phase 3), COD concentrations significantly increased to >5600 mg/L, which was much higher than that in the experimental groups (p<0.05). What's more, the average COD removal rate and methane production rate both declined to 80±2.7% and 200 ml(stp)/d. Although the COD in the experimental groups increased sharply in the early days of the phase, it operated stably in the following days, and the carbon cloth-riboflavin reactor was stable earlier compare to the carbon cloth reactor.

The most significant differences between carbon cloth and carbon cloth-riboflavin reactors were observed at phase 4 (p<0.05), when the OLR was increased to 5 kgCOD/(m^3·d) (HRT: 11 day, phase 4). The carbon cloth reactor operated at this phase had the average COD removal rate of only 85±4.5%, and methane production rates dropped to 300 ml(stp)/d, while COD concentrations increased to > 6000 mg/L. On the other hand, the COD in carbon cloth-riboflavin reactor increased slightly during the first 5 days of phase 4 but dropped back down to 5781±432 mg/L, and it operated stably. It maintained a COD removal rate above 90%, methane production rate above 600 ml(stp)/d, and its pH stayed between 7.0-7.2.

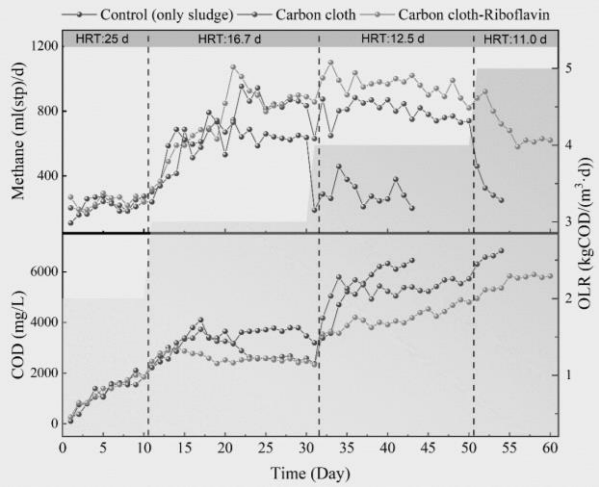

Fig. 1 Methane production and effluent COD concentrations from the three reactors at different stages of the experiment.

Microbial community

The relative abundance of the archaea communities at the genus level in three AD systems were depicted in Fig. 2A. The archaea communities were mainly composed of *Methanothrix* and *Methanobacterium*. Both genera are significant components of the anaerobic digestion community with enhanced DIET using conductive materials (Dang et al., 2016; Zhao et al., 2016). *Methanothrix* is a typical acetoiclastic methanogen, which can also reduce carbon dioxide to methane by accepting electrons from syntrophic bacteria via DIET (Rotaru et al., 2014a). The addition of carbon cloth and riboflavin contributed to the higher relative abundance of *Methanothrix* (CC: 52.86%, CR:62.22%, CRS:49.55%), corresponding to an increase by 42.94%, 68.26% and 33.99%, respectively, compared to OS. The addition of riboflavin increased the proportion of *Methanothrix* and decreased the proportion of *Methanobacterium*. These results indicate that *Methanothrix* was significantly enriched on the carbon cloth surface, and riboflavin loading favored *Methanothrix* enrichment. This suggests that the anaerobic digestion methanogenic systems of the CC and CR groups have the potential to increase methane production via DIET. The ability of *Methanothrix* to participate in DIET (Rotaru et al., 2014a) and the ability of *Methanobacterium* to accept electrons from conductive materials (Salvador et al., 2017; Yuan et al., 2023) suggest that both genera may be involved in the uptake of extracellular electrons from carbon cloth surfaces or other microorganisms. These results indicate that the methanogenic process of the AD systems in this study was probably dominated by carbon cloth through the DIET pathway, interestingly, the presence of riboflavin further promotes this pathway.

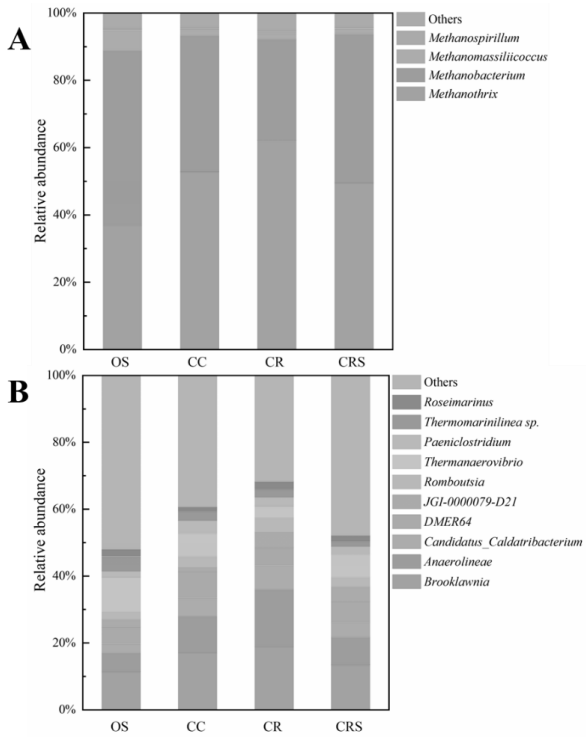

Fig. 2. (A) archaeal and (B) bacterial community structures associated with sludge from only sludge reactor (OS), carbon cloth surfaces (CC), carbon cloth-riboflavin surfaces (CR) and sludge from carbon cloth-riboflavin reactor (CRS).

The main dominant genera are *Brooklawnia*, *Anaerolinea*, *DMER64* and *JGI-0000079-D21*. *Brooklawnia* is capable of producing VFAs as the main fermentation product and plays a crucial role in hydrolysis and acidogenesis during anaerobic digestion (Kim et al., 2017). It is also the dominant genus in various reactors, with a significantly higher abundance of *Brooklawnia* on the surface of carbon cloth (CC and

CR) compared to the suspended sludge (OS: 11.49%, CC: 17.22%; CR: 19.00%; CRS: 13.54%), which is consistent with previous study (Qi et al., 2022). Additionally, *Brooklawnia* has been confirmed to be an electroactive microbe and could be enriched in the presence if conductive materials alongside *Methanothrix* (Qi et al., 2022), thus, the DIET process may be accomplished by the interaction between *Brooklawnia* and *Methanothrix*, the existence of carbon cloth and riboflavin there further made sure that process. *Anaerolinea* can perform mixed acid fermentation metabolism or acetogenic metabolism (Yamada et al., 2006), and current research has shown that they can enhance more complete oxidation of substrates and methane production in fermentation reactors (Miceli et al., 2016). Notably, some species of *Anaerolinea* are iron-reducing bacteria (Kawaichi et al., 2013), indicating their capability of extracellular electron transfer and participation in DIET. *DMER64* is a functional microbe capable of inter-species hydrogen electron transfer, enabling it to establish magnetite-mediated DIET with methanogens (Lee et al., 2019). *DMER64* was found to have higher abundances in CC and CR than in OS and CRS, indicating that the carbon cloth has significantly promoted the growth of *DMER64*, and these abundances are closely related to the interspecies electron transfer of microorganisms (Guo et al., 2020). *JGI-0000079-D21* is a functional bacterium associated with hydrolysis and acidification, and it has the potential to degrade inhibitory compounds (Tian et al., 2020), accounting for 4.75% and 4.52% of CR and CRS, respectively, which is higher than OS and CC, suggesting that riboflavin promotes the degradation of certain recalcitrant organic compounds. Additionally, *JGI-0000079-D21* belongs to Synergistaceae, and research has shown that IET may occur between Synergistaceae and methanogens (Huang et al., 2021; Zhao et al., 2017). The above results indicate that the addition of carbon cloth has enriched a large number of acid-producing bacteria, and riboflavin has promoted the functional microorganisms that degrade complex organic matter. The mechanism may be related to the establishment of DIET pathways with the surface of the carbon cloth.

Methane metabolism and related enzyme activities

In order to investigate the impact of methane metabolism on organic degradation and methane production, the KEGG database was utilized to identify functional modules. The methane metabolism pathways and relative gene abundances of enzymes in the AD system under study are illustrated in Fig. 3. The prevalence of the acetate to methane (M00357) and CO_2 to methane (M00567) conversion modules indicates that acetoclastic and hydrogenotrophic are the primary pathways of methanogenesis. The abundance of M00357 and M00567 did not show significant differences between OS and CRS, but their abundance on the surfaces of the carbon cloths (CC and CR) were higher than those of OS, M00567 increased by 21.93% and 41.67% in CC and CR, while M00357 increased by 12.06% and 21.61%, respectively. Moreover, the abundance of M00567 was significantly higher in CR than in CC.

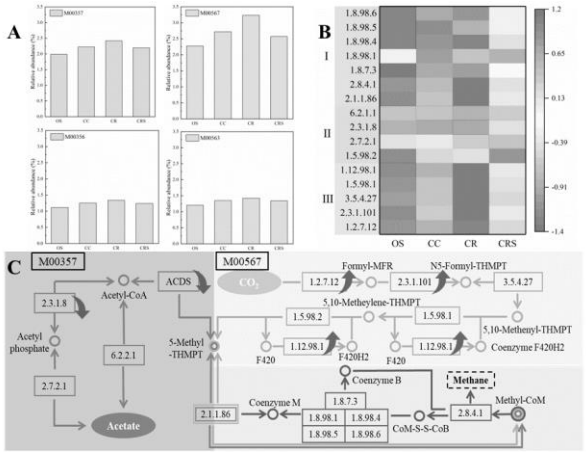

Fig. 3 (A) The relative abundance of modules involved in methanogenesis. (B) The heatmap for the absolute abundance of enzymes in the relevant pathways. (C) The main methane methanogenic pathways based on KEGG.

Meanwhile, the gene abundance of the enzymes associated with M00357 and M00567 exhibited a similar pattern. The first part comprised enzymes present in both M00367 and M00567. Among these enzymes, five tybes of CoM-S-S-CoM reductases catalyse the reduction of CoM-S-S-CoM to Coenzyme B and Coenzyme M (Holmes et al., 2021), Methly-Coenzyme M reductase [EC:2.8.4.1] catalyses the final step of methane production, and tetrahydromethanopterin S-methyltransferase [EC:2.1.1.86] facilitates the conversion of Coenzyme M to Methly-CoM. On the surface of the carbon cloths, most of the enzymes in this part exhibited a higher gene abundance, and the gene abundance of these enzymes in the CR was significantly increased, where riboflavin-loaded carbon cloth was shown to promote methane production more effectively than carbon cloth. The second part includes enzymes exclusively found in M00357. The gene abundance of these enzymes exhibited irregular variations, but generally decreased with the addition of carbon cloth and riboflavin, although carbon cloth and riboflavin increased the abundance of *Methanothrix*, a typical acetoclastic methanogen, *Methanothrix* can also produce methane via the DIET pathway using the CO_2 reduction pathway. The third part contained enzymes only in M00567, hydrogenotrophic methanogenesis was

remarkably enhanced by carbon cloth and riboflavin. Carbon cloth increased the gene abundance of the relevant enzymes compared to OS, and their abundance in CR was significantly increased (p<0.05). The proportion of methane in the biogas increased with the addition of carbon cloth and riboflavin-loaded carbon cloth, which is consistent with stronger hydrogenotrophic methanogenesis in CC and CR. This alignment is
supported by the fact that DIET shares the same pathway as hydrogenotrophic methanogenesis during CO_2 reduction, and that the promotion of hydrogenotrophic methanogenesis may be attributed to DIET enhanced by carbon cloth and riboflavin-loaded carbon cloth. Furthermore, the gene abundance of F420 hydrogenase [EC:1.12.98.1], a key enzyme for electron transfer in the DIET pathway, was significantly increased in CC and CR (p<0.05), compared to OS. These findings indicate that carbon cloth and riboflavin play a role in synthesizing and activating the majority of enzymes associated with methane metabolism, and the promotion of hydrogenotrophic methanogenesis may be attributed to DIET enhanced by carbon cloth and riboflavin-loaded carbon cloth.

Abundance of critical genes in methanogen

Methanothrix uses the acetoclastic pathway for methanogenesis when grown alone, and it also possesses genes related to CO_2 reduction pathway (Holmes et al., 2017). Studies have shown that *Methanothrix* can use the CO_2 reduction pathway for methanogenesis when co-cultured with a bacterial partner, which can only accept electrons directly through the DIET pathway (Holmes et al., 2017; Rotaru et al., 2014a). Therefore, the gene abundances of *Methanothrix* in the CO_2 reduction pathway serve as a reliable indicator of DIET. *Methanothrix* from the surface of carbon cloth (CC and CR) exhibited a significantly higher abundance of genes, *mer* and *mtd*, related to the CO_2 reduction pathway compared to *Methanothrix* from OS and CRS, suggesting that *Methanothrix* from the surface of carbon cloth primarily utilized the CO_2 reduction pathway to produce methane. Furthermore, the abundance of these two genes is 1.28-fold and 1.40-fold higher on CR compared to CC (Fig. 4.), respectively. This is because the intermediate metabolite of the riboflavin metabolic pathway, coenzyme F420, acts as an exchange of electrons in the CO_2 reduction pathway and improves the efficiency of electron transfer, thus the addition of riboflavin enhances CO_2 reduction pathway. To monitor the proportion of *Methanothrix* utilizing acetoclastic methanogenesis, the abundances of acetoclastic genes, *acs* and *cdhA*, was analyzed (Liu et al., 2019). It was observed that both genes were more abundantly expressed in *Methanothrix* from OS and CRS than on the surfaces of carbon cloth. Additionally, their abundance was slightly higher in CC than in CR. Moreover, the abundance of certain genes related to DIET was significantly increased in *Methanothrix* on the carbon cloth surface. Previous study (Holmes et al., 2018) has shown that F420H2 dehydrogenase complex (Fpo) and soluble isodisulfide reductase (HdrA) play crucial roles in methane production through the DIET pathway in *M.barkeri*, a typical acetoclastic methanogen. The abundance of *fpoD* and *hdrA* in *Methanothrix* on the surface of carbon cloth was much higher than that in OS and CRS, and their abundance on CR was 1.4-fold and 6.6-fold higher than that on CC, respectively. In addition, DIET functional proteins require flavin mononucleotide (FMN) as a cofactor to transfer electrons, but methanogens have a limited ability to produce FMN, and as the precursor of FMN, riboflavin can specifically bind to electron transfer proteins and enhance proteolytic activity and function. These results suggest that *Methanothrix* on the surface of the carbon cloth were primarily utilize the CO_2 reduction pathway for methanogenesis, while those in the bulk sludge relied on acetoclastic methanogenesis. Furthermore, it is evident that the loading of riboflavin does not enhance methanogenesis via the acetoclastic methanogenesis pathway but rather through enhanced DIET.

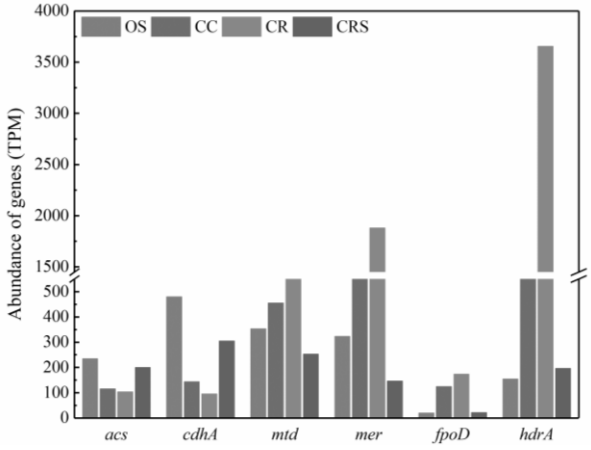

Fig. 5. Abundance of genes involved in DIET or acetoclastic metabolism by *Methanothrix* from OS, CC, CR and CRS.

CONCLUSION

The addition of carbon cloth loaded with riboflavin significantly improved the performance of the anaerobic digestion of dairy manure. Specifically, the carbon cloth-riboflavin reactor, operated stably at an OLR of 5 kgCOD/(m^3·d) with an HRT of 10 days, exhibited superior results compared to the carbon cloth reactor and the only sludge reactor. It demonstrated higher rates of COD removal, methane production, and biogas methane

concentration. The analysis of metagenomics revealed the significant enrichment of *Methanothrix* in the process. *Methanothrix* on the surface of the carbon cloth predominantly utilized the CO_2 reduction pathway for methane production. Following the addition of riboflavin, this proportion was further augmented, indicating the positive influence of riboflavin on this specific metabolic pathway. In contrast, *Methanothrix* in the bulk sludge primarily employed the acetate decarboxylation pathway for methane production. Furthermore, the carbon cloth loaded with riboflavin had a beneficial impact on methanogenesis by enriching various major methanogenic pathways and activating a large number of enzymes associated with methane metabolism. This observation suggests that riboflavin plays a crucial role in promoting methane production during anaerobic digestion. Moreover, the presence of riboflavin significantly altered the microbial communities and the abundance of functional genes relate to the DIET. The knowledge gained from this research contributes to the understanding of the microbial mechanisms underlying anaerobic digestion processes and opens up new possibilities for optimizing biogas production from dairy manure.

REFERANCE

Buckel, W., Thauer, R.K. 2018. Flavin-Based Electron Bifurcation, Ferredoxin, Flavodoxin, and Anaerobic Respiration With Protons (Ech) or NAD(+) (Rnf) as Electron Acceptors: A Historical Review. Front Microbiol. 9, 401.

Chen, S., Rotaru, A.E., Liu, F., Philips, J., Woodard, T.L., Nevin, K.P., Lovley, D.R. 2014a. Carbon cloth stimulates direct interspecies electron transfer in syntrophic co-cultures. Bioresour Technol. 173, 82-86.

Chen, S., Rotaru, A.E., Shrestha, P.M., Malvankar, N.S., Liu, F., Fan, W., Nevin, K.P., Lovley, D.R. 2014b. Promoting interspecies electron transfer with biochar. Sci Rep. 4, 5019.

Cruz Viggi, C., Rossetti, S., Fazi, S., Paiano, P., Majone, M., Aulenta, F. 2014. Magnetite particles triggering a faster and more robust syntrophic pathway of methanogenic propionate degradation. Environ Sci Technol. 48(13), 7536-43.

Dang, Y., Holmes, D.E., Zhao, Z., Woodard, T.L., Zhang, Y., Sun, D., Wang, L.Y., Nevin, K.P., Lovley, D.R. 2016. Enhancing anaerobic digestion of complex organic waste with carbon-based conductive materials. Bioresour Technol. 220, 516-522.

Dang, Y., Sun, D., Woodard, T.L., Wang, L.Y., Nevin, K.P., Holmes, D.E. 2017. Stimulation of the anaerobic digestion of the dry organic fraction of municipal solid waste (OFMSW) with carbon-based conductive materials. Bioresour Technol. 238, 30-38.

Frear, C., Wang, Z.-W., Li, C., Chen, S. 2011. Biogas potential and microbial population distributions in flushed dairy manure and implications on anaerobic digestion technology. Journal of Chemical Technology & Biotechnology. 86(1), 145-152.

Guo, X., Sun, C., Lin, R., Xia, A., Huang, Y., Zhu, X., Show, P.L., Murphy, J.D. 2020. Effects of foam nickel supplementation on anaerobic digestion: Direct interspecies electron transfer. J Hazard Mater. 399, 122830.

Holmes, D.E., Shrestha, P.M., Walker, D.J.F., Dang, Y., Nevin, K.P., Woodard, T.L., Lovley, D.R., Schloss, P.D. 2017. Metatranscriptomic Evidence for Direct Interspecies Electron Transfer between Geobacter and Methanothrix Species in Methanogenic Rice Paddy Soils. Applied and Environmental Microbiology. 83(9).

Holmes, D.E., Rotaru, A.E., Ueki, T., Shrestha, P.M., Ferry, J.G., Lovley, D.R. 2018. Electron and Proton Flux for Carbon Dioxide Reduction in Methanosarcina barkeri During Direct Interspecies Electron Transfer. Front Microbiol. 9, 3109.

Holmes, D.E., Zhou, J., Ueki, T., Woodard, T.L., Lovley, D.R. 2021. Mechanisms for electron uptake by methanosarcina acetivorans during direct interspecies electron transfer. mBio. 83(9).

Huang, L., Liu, X., Ye, Y., Chen, M., Zhou, S. 2020. Evidence for the coexistence of direct and riboflavin-mediated interspecies electron transfer in Geobacter co-culture. Environ Microbiol. 22(1), 243-254.

Huang, S., Shen, M., Ren, Z.J., Wu, H., Yang, H., Si, B., Lin, J., Liu, Z. 2021. Long-term in situ bioelectrochemical monitoring of biohythane process: Metabolic interactions and microbial evolution. Bioresour Technol. 332, 125119.

Huang, Y., Cai, B., Dong, H., Li, H., Yuan, J., Xu, H., Wu, H., Xu, Z., Sun, D., Dang, Y., Holmes, D.E. 2022. Enhancing anaerobic digestion of food waste with granular activated carbon immobilized with riboflavin. Sci Total Environ. 851(Pt 2), 158172.

Rotaru, A.E., Shrestha, P.M., Liu, F., Markovaite, B., Chen, S., Nevin, K.P., Lovley, D.R. 2014b. Direct interspecies electron transfer between Geobacter metallireducens and Methanosarcina barkeri. Appl Environ Microbiol. 80(15), 4599-605.

Salvador, A.F., Martins, G., Melle-Franco, M., Serpa, R., Stams, A.J.M., Cavaleiro, A.J., Pereira, M.A., Alves, M.M. 2017. Carbon nanotubes accelerate methane production in pure cultures of methanogens and in a syntrophic coculture. Environ Microbiol. 19(7), 2727-2739.

Sasaki, K., Morita, M., Hirano, S., Sasaki, D., Ohmura, N., Igarashi, Y. 2010. Efficient degradation of rice straw in the reactors packed by carbon fiber textiles. Appl Microbiol Biotechnol. 87(4), 1579-86.

ENHANCEMENT OF ELECTRON TRANSPORT VIA NANO-MAGNETITE IN A NITRITE-DEPENDENT ANAEROBIC METHANE OXIDATION SYSTEM

Tianjing Shi[1], Xinying Liu[1], Yiting Xue[1], Yan Dang[1], Dezhi Sun[1]
1 College of environmental science and engineering, Beijing Forestry University, 35 Qinghua East Road, Haidian District, Beijing, China

1.INTRODUCTION

Recently, denitrifying anaerobic methane oxidation (DAMO) has attracted mounting attention due to simultaneous nitrogen removal and methane oxidation. In recent studies, addition of magnetite in mere DAMO process can significantly improve the enrichment and growth of DAMO microorganisms. Liang et al. presented that magnetite could shorten the startup of methane-dependent denitrification via mediating an electrically connected community related to DIET (Liang et al., 2022). The stimulation of electron transfer through nano-magnetite enhanced the DAMO process (Chang et al., 2021). However, there are few studies on the mechanism of nano-magnetite promoting electron transfer in DAMO system, and the electron transport system activity and the expression changes of enzymes related to electron transfer are still unclear. In this study, the reactor with nano-magnetite were set up inoculated with DAMO bacteria to investigate the effect of nano-magnetite on the DAMO system and the mechanism of electron transfer.

2.METHODS

Reactor operation. Two identical lab-scale sequencing batch reactors were set up for the experiment, respectively adding nano-magnetite (10 mM of total iron) and control group without adding. The reactors were made up of glass with a total volume of 500 mL including 100 mL headspace and 400 mL liquid. Sludge from a laboratory-scale DAMO enrichment reactor was inoculated in three reactors and sludge and wastewater were mixed completely in a thermostatic gas-bath oscillator. The pH in the reactors was adjusted between 7.0 and 7.5 by adding 1.0 mol/L HCl or NaOH solutions, and temperature was controlled at 35 °C using a thermostatic heater. In the long-term formal experiment, the two reactors were operated under the same manner. Each cycle consisted of five phases: filling phase (10 min), operation phase (47 h), settling phase (30 min), decant phase (10 min), and idle phase (10 min). The ratio of clarified supernatant to operation volume was maintained at 0.5 during the decant phase, and then equal volume of fresh culture medium (Ettwig et al., 2009) was pumped into the reactor during the filling phase. The methane as an electron donor was replaced (resupplied) to keep the pressure in the headspace at normal atmospheric pressure and the methane was sufficient.

3.RESULTS

Concentrations of nitrogen-based compounds (NH_4^+, NO_2^- and NO_3^-) on triplicate samples were monitored throughout the whole experiment while there was no NH_4^+, NO_3^- detected in all samples (Fig. 1). As the nitrite concentrations of influent were incrementally increased, the nitrite concentrations in effluent with nano-magnetite were consistently low (<0.3 mg/L) (Fig. 1a) with >98% nitrite removal efficiency (Fig. 1c). In contrast, the nitrite removal efficiency in control was low as <50%. The nitrite removal rate with nano-magnetite gradually increased and finally plateaued to 17.46 mg $N \cdot L^{-1}d^{-1}$ (Cycle 35), nearly 2.5 times more than that of control.

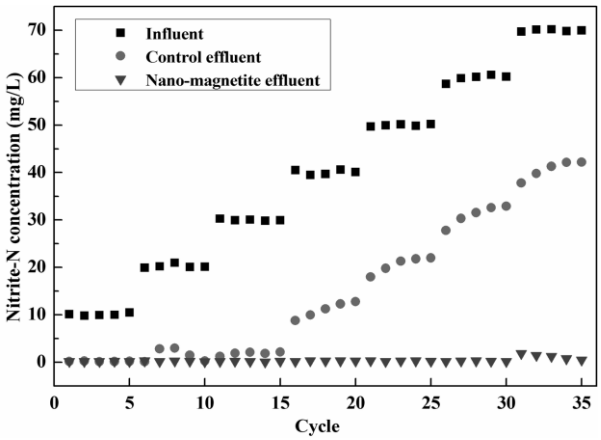

(a)

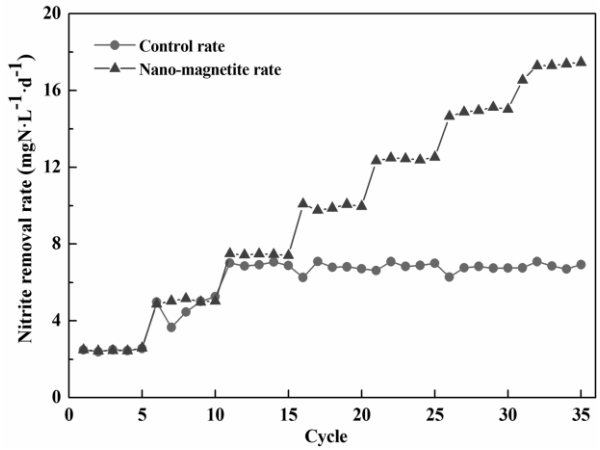

(b)

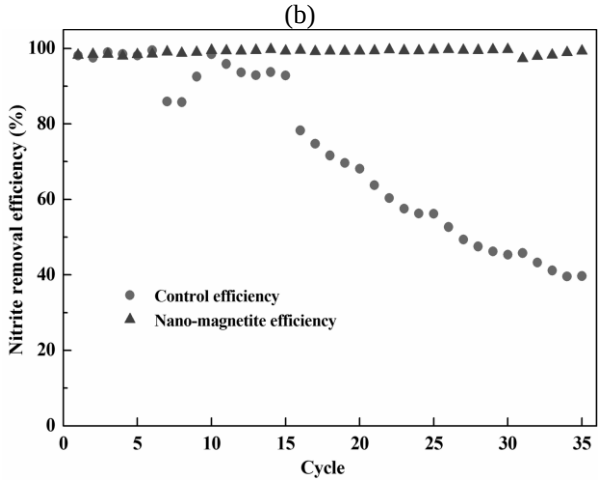

(c)

Figure 1 Nitrite removal performance in nano-magnetite reactor and control during long-term operation of 35 cycles. Influent and effluent of nitrite concentration (a), nitrite removal rate (b) and efficiency (c).

According to the Nyquist plots and fitting results (Figure 2a, b), the solution resistance (R_s), charge transfer resistance (R_{ct}) and the maximum mass transfer resistances (R_{mt}) of nano-magnetite reactor was smaller than that of control. In the nano-magnetite reactor sludge, a more intense featured redox peak was observed at both forward and backward scans (Figure 2c). The electrochemical double-layer capacitance C_{dl} values for nano-magnetite reactor sludge was 11.94 $mF \cdot cm^{-2}$, which was higher than that of the control (10.18 $mF \cdot cm^{-2}$) (Figure 2d).

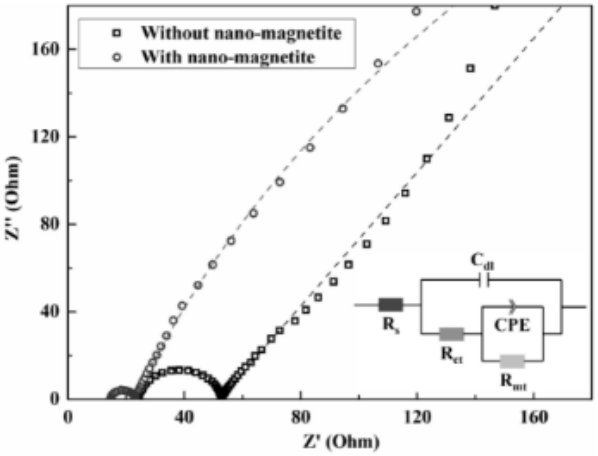

(a)

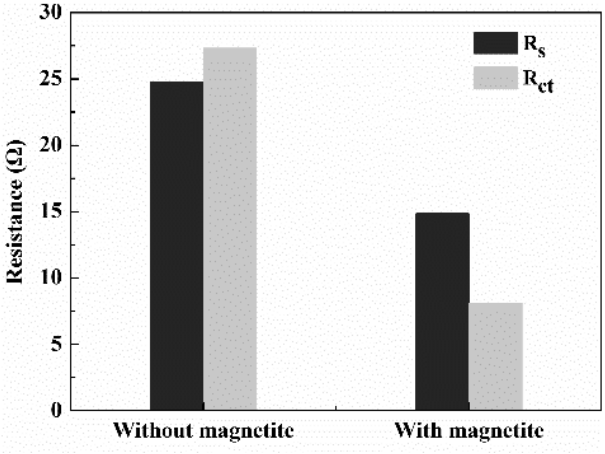

(b)

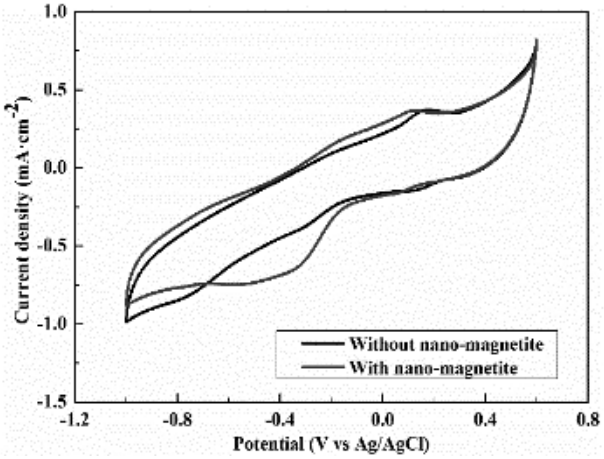

(c)

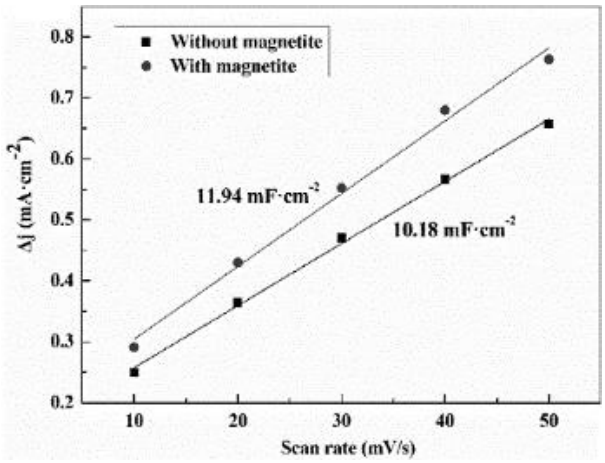

(d)

Figure 2 Nyquist plots, fitted curves, equivalent circuits (a), and impedance components (b) of nano-magnetite reactor sludge. Cyclic voltammograms (c) and charging current density differences Δj plotted against scan rates (d) for the nano-magnetite reactor sludge.

ETS activity (51.3±0.4 μg·(min·g)$^{-1}$) with nano-magnetite was higher than that in control (36.8±0.8 μg·(min·g)$^{-1}$) (Fig. 3a). The concentration of Cyt *C* in the control (27.66 nmol·L^{-1}) was higher than that in nano-magnetite reactor (24.06 nmol·L^{-1}) (Fig. 3a). The enzymatic activities of key enzymes succinate dehydrogenase (SDH), ubiquinol oxidase (UbqO), NADH dehydrogenase (NDH) and ubiquinol cytochrome c reductase (UqCR) (containing cytochrome bc1) activity from nano-magnetite were 1.29, 1.08, 1.31 and 1.09 times higher than those of control (Fig. 3b).

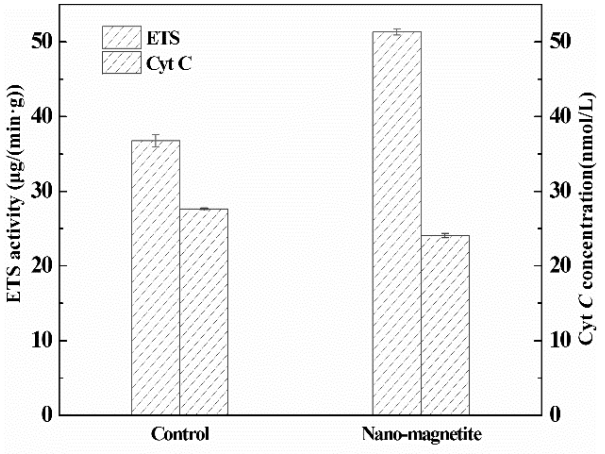

(a)

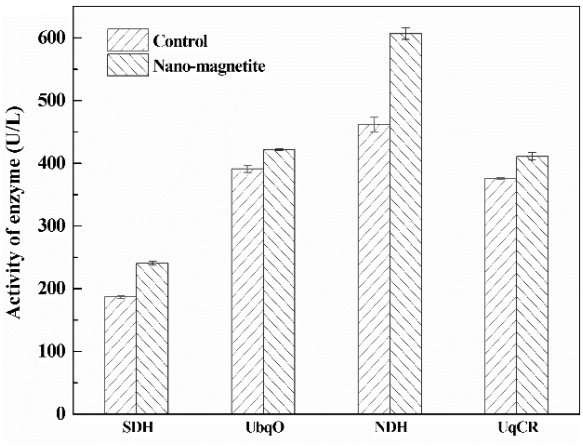

(b)

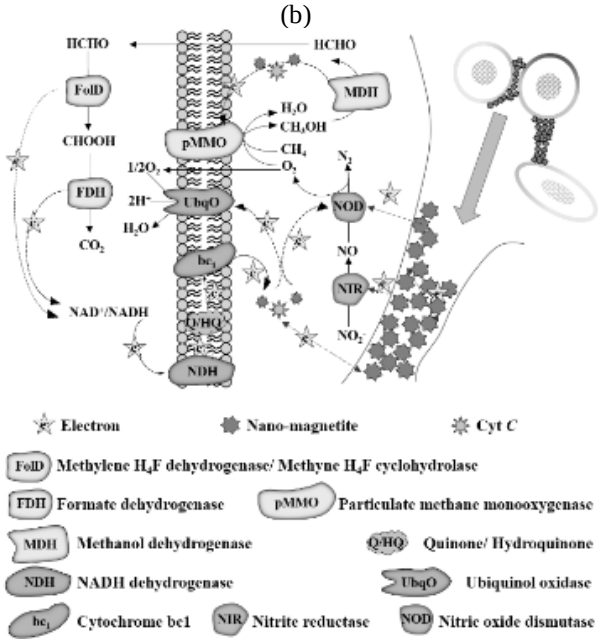

(c)

Figure 3 The ETS activity, Cyt *C* concentration (a), the activity of enzymes related to electron transport chain (b) and mechanism diagram of nano-magnetite involved in electron transfer (c).

The relative taxonomic abundance of microbial communities at genus level (Fig. 4) in samples collected from nano-magnetite reactor and control were analyzed. The majority of DAMO sequences clustered with the genus *Candidatus Methylomirabilis*, which accounted for 31.0% of bacterial sequences in the samples from control compared to only 10.2% in the sludge from nano-magnetite reactor. There were several other genera related to nitrogen and methane metabolism in terms of denitrification were enriched.

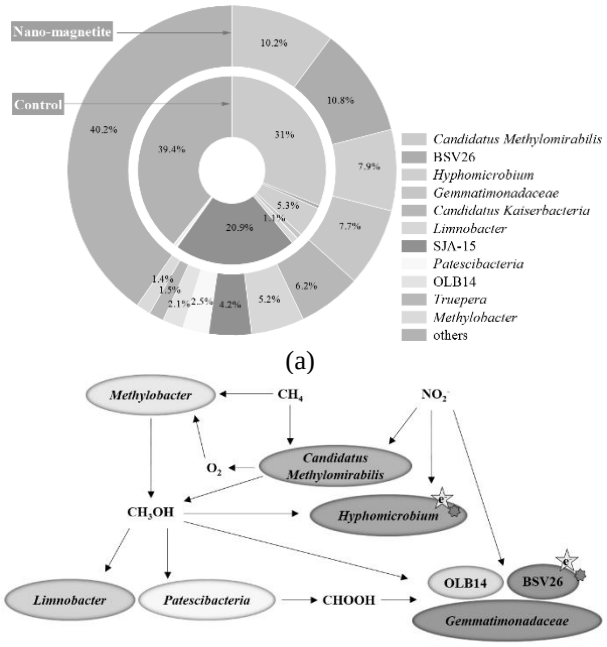

(a)

(b)

Figure 4 Relative abundances of microbial community at genus level in nano-magnetite reactor and the control (a) and potential metabolic pathways between microbial communities in this study (b).

At the end of experiment (Cycle 35), the activities of NIR were 31.38 U/L and 36.62 U/L and the activities of pMMO were 20.84 U/L and 22.59 U/L in the control reactor and nano-magnetite reactor, respectively. Compared with the control, the expressions of denitrification genes and methane oxidation genes in the nano-magnetite reactor were significantly increased.

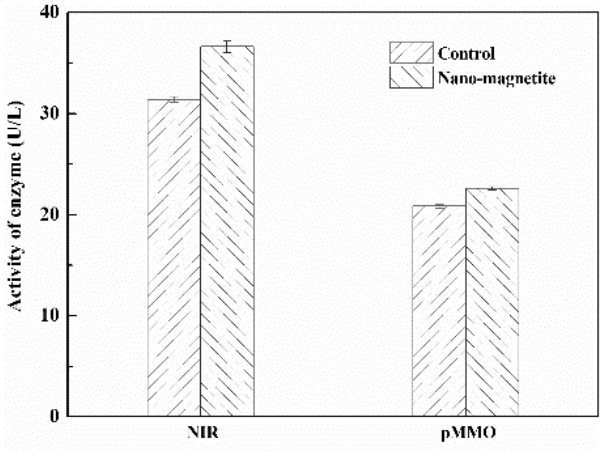

(a)

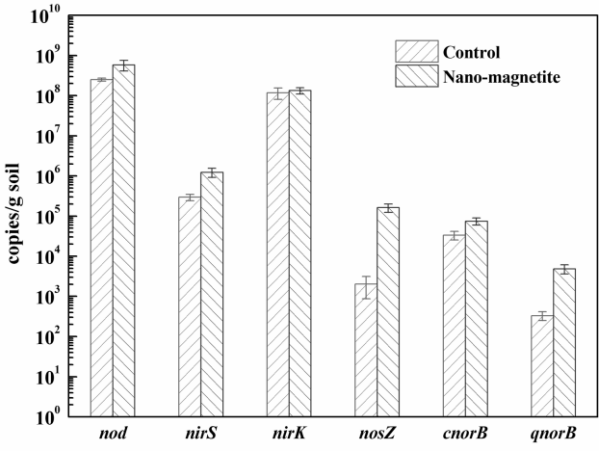

(b)

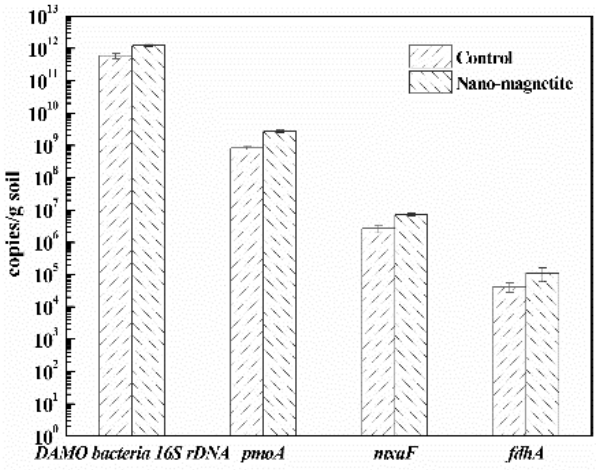

(c)

Figure 5 Comparison of functional enzyme activities (a), nitrogen metabolism genes quantity (b) and methane metabolism genes quantity (c) in nano-magnetite reactor and the control.

4.DISCUSSION

In the long-term reactor experiment, nano-magnetite improved DAMO performance significantly. Generally, R_{ct} characterizes the electron transfer efficiency in the bioelectrochemical system. Smaller R_{ct} with nano-magnetite indicated higher electron transfer efficiency indicating that nano-magnetite acted as electron shuttling mediators and facilitated catalytic efficiency. C_{dl} refers to the capacitance formed by the accumulation of pure electrostatic charge at the electrode/ electrolyte interface. A larger C_{dl} indicates more sufficient contact between the electrode and the solid-liquid interface and the easier the electron transport. The existence of nano-magnetite made the electrode and electrolyte contact more fully, which indicated that nano-magnetite was conducive to the ion exchange between electrode and electrolyte and the transfer of electrons in the system.

In the DAMO system, previous studies suggested

magnetite plausibly facilitated the electron transfer (Chang et al., 2021), which can explain the fact addition of nano-magnetite showed a positive effect on DAMO. Cyt *C* is a hemoglobinase located in the intermembrane spaces of cells and is usually involved in electron transfer process in organisms. Meanwhile, electrically conductive microbial nanowire, which were composed c-type cytochromes, played an important role in facilitating long-range extracellular electron transfer. Additionally, some c-type cytochromes free of microbial nanowires can also participate in electron transfer. Previous studies suggested magnetite substituted for Cyt *C* as the interspecies electrical connection components which reducing the Cyt *C* concentration in DAMO systems (Liang et al., 2022) and anaerobic digestion systems (Wang et al., 2018). Liu et al. proved that magnetite could compensate for the role of c-type cytochromes in extracellular electron exchange using the method of gene knockout (Liu et al., 2015). In this study, it was supported by the decrease of Cyt *C* concentration and the significant increase of ETS activity in the nano-magnetite reactor. The results showed that nano-magnetite facilitated electron transfer in the system, and it alleviated the need for Cyt *C*, promoted the activity of functional enzyme of electron transport chain.

Bacteria associated with nitrogen and methane metabolism were significantly enriched and interact among microbial communities. The activity of NIR enzyme reflected the activity of denitrification, while that of pMMO enzyme reflected the activity of methane oxidation. Improvement in activity of NIR was more significant than pMMO activity, indicating that nano-magnetite was more conducive to strengthening denitrification compared with methane oxidation. The absolute quantity and functional activity of DAMO bacteria in the nano-magnetite reactor were both increased. Recent studies have discovered that nano-magnetite can promote the co-metabolism of nitrite and methane dominated by DAMO microorganisms, methanotrophs and denitrifying bacteria (Chang et al., 2021; Liang et al., 2022). In the DAMO system, nano-magnetite can effectively promote the growth, enrichment and functional activity of DAMO functional microorganisms. In this study, increased gene expression and enzyme activity supported this speculation.

5.CONCLUSIONS

In this study, nano-magnetite was used to enhance electron transfer in DAMO system upon conversion of nitrite to nitrogen using methane as an electron donor. Nano-magnetite improved DAMO performance significantly in the long-term reactor experiment. Nano-magnetite promoted the activity of functional enzyme of electron transport chain and played the function of electron shuttles conducive to electron transfer in the system. Bacteria associated with nitrogen and methane metabolism were significantly enriched and interact among microbial communities. The expression of nitrogen as well as methane oxidation related genes and the activity of functional enzymes had been highly increased.

REFERENCES

Chang, J., Wu, Q., Yan, X., Wang, H., Lee, L.W., Liu, Y., Liang, P., Qiu, Y., Huang, X. 2021. Enhancement of nitrite reduction and enrichment of Methylomonas via conductive materials in a nitrite-dependent anaerobic methane oxidation system. *Environmental Research*, **193**, 110565.

Ettwig, K.F., Van Alen, T., van de Pas-Schoonen, K.T., Jetten, M.S., Strous, M. 2009. Enrichment and molecular detection of denitrifying methanotrophic bacteria of the NC10 phylum. *Applied and environmental microbiology*, **75**(11), 3656-3662.

Liang, L., Sun, C., Jin, Z., Wang, M., Yu, Q., Zhao, Z., Zhang, Y. 2022. Magnetite-mediated electrically connected community for shortening startup of methane-dependent denitrification in a membrane biofilm reactor. *Chemical Engineering Journal*, **428**, 132004.

Liu, F., Rotaru, A.E., Shrestha, P.M., Malvankar, N.S., Nevin, K.P., Lovley, D.R. 2015. Magnetite compensates for the lack of a pilin-associated c-type cytochrome in extracellular electron exchange. *Environmental microbiology*, **17**(3), 648-655.

Wang, T., Zhang, D., Dai, L., Dong, B., Dai, X. 2018. Magnetite triggering enhanced DIET: a scavenger for the blockage of electron transfer in anaerobic digestion of high-solids sewage sludge. *Environ. Sci. Technol.*, **52**(12), 7160-7169.

Contact:Email shitianjingbjfu@163.com, Tel. +86-13521938822, Address 35 Tsinghua East Road, Beijing 100083, China.

Autotrophic direct electron transfer denitrification (DETD) for deep treatment of municipal wastewater treatment plant effluent via *Thiobacillus*

Haoyong Li[1], Yan Dang[1*], Xinying Liu[1], Ruoyu Li[1], Dezhi Sun[1]
1 Beijing Key Laboratory for Source Control Technology of Water Pollution, Engineering Research Center for Water Pollution Source Control and Eco-remediation, College of Environmental Science and Engineering, Beijing Forestry University, 35 Qinghua East Road, Haidian District, Beijing, China

ABSTRACT

The process of denitrification for deep treatment of nitrate requires an electron donor, and biocathode can serve as supplementary electron donors. However, the efficiency and microbial mechanisms of denitrification through microbial electrochemical systems remained unclear. In this study, microbial electrolysis cells (MECs) operated at -500 mV and -800 mV (vs. SHE) were evaluated, with the biocathode serving as the sole electron donor. During stable operation, the removal rate of nitrate was 48.79 ± 8.17 mmol NO_3^-–N L^{-1} day^{-1} m^{-2}, with a maximum nitrate removal rate of 60.17 mmol NO_3^-–N L^{-1} day^{-1} m^{-2}. The biocathode predominantly was covered with *Thiobacillus*, which is a denitrification microbe that can directly accept electrons from the cathode. Further quantitative analysis showed that OmpA and cytochrome c effectively bound to the carbon-based cathode, indicating the potential electron transfer between heme of cytochrome c center and the cathode. Transcriptome analysis indicated that genes related to denitrification pathway were generally upregulated, especially the nitrite reduction gene *nirS* was upregulated 35-fold relative to the -800 mV reactor. These results demonstrated that the direct uptake of electrode electrons by *Thiobacillus* enriched on biocathode had a positive effect on the deep denitrification treatment of wastewater treatment plants effluent.

INTRODUCTION

Municipal wastewater treatment plant tailwater is the effluent of secondary biological treatment. The nutrients contained in WWTP tail water, such as nitrogen, are discharged in large quantities into the surface water causing eutrophication. Therefore, deep treatment of the tailwater is required to remove nitrogen from the tailwater.

In WWTP, low C/N limits denitrification because the low organic carbon content leads to a lack of electron donors limiting the denitrification process. To address the issue of electron acceptor deficiency in effluent from WWTPs, there are currently two approaches. One is to optimize the operation of biological treatment by adopting advanced control methods (e.g., improved A^2/O, step-feed multi-stage A/O) and using new types of bioreactors (e.g., MBRs, MABRs) to further improve the efficiency of electron acceptor denitrification [1]. Although these methods reduce the concentration of nitrate in the tail water, the efficiency in reagent engineering needs to be further improved. The other is to add external electron acceptors, such as organic electron acceptors like acetate, or inorganic electron acceptors like thiosulfate, pyrite, zero-valent iron (ZVI) and hydrogen [2]. However, the addition of organic carbon sources carries the risk of exceeding COD limits and further increases carbon emissions, adding pyrite carries the risk of potential pollution from sulfate ions and color exceedance caused by iron ions, and using hydrogen faces the problem of difficult storage and explosive risk. Alternative carbon sources as electron donors need to be explored to support nitrogen removal in deep tailwater treatment. Microbial electrolysis cells (MESs) offer a promising method for nitrate removal. In MEC, the biocathode can replace organic carbon as an electron donor. The advantages of biocathode electrodes as electron donors are simple and controlled operation, non-risk of secondary contamination and without increase in carbon emissions. Previous studies have shown that *Thiobacillus denitrificans* reduces nitrate to nitrogen in MEC systems.

In this study, a laboratory-scale MEC system applied with a cathodic potential of -500 mV was used to run and study the effect of electron denitrification using biocathodes when the MEC system was inoculated with activated sludge could potentially be enhanced by increasing the DET. The community structure of suspended sludge on and around the cathode surface was studied and *Thiobacillus* was found to be significantly enriched on the cathode surface.

METHODS

Reactor setup and inocula

Two continuous flow laboratory grade H-type dual chamber MECs. The device has a glassy texture and the two chambers are separated by a proton exchange membrane (CEM; CMI-7000) (Membrane International Inc., NJ 07456). The effective volume of both electrode chambers (cathode and anode) was 200 mL, where the anode was a 20 * 25 * 5 mm graphite plate electrode used as the auxiliary electrode and a 40 * 60 mm carbon cloth electrode used as the working electrode. A saturated potassium chloride Ag/AgCl reference electrode (+199 mV vs. SHE) is placed in the cathode chamber to detect the cathodic potential, and a three-electrode system is connected to a multi-channel constant potential rectifier (CHI-1000 C, Shanghai) to maintain a constant cathodic potential in the reactor. The two MEC reactors were operated under conditions of -500 mV vs. SHE (R1) and -800 mV vs. SHE (R2), respectively. The whole experiment was divided into two periods: the starter period (0-35 days), and the energization period (35-80). The nitrate concentration in the starter feed water was set at 6.0 mM (~85 mg-N/L) and the energization period (~20 mg-N/L).

Analytical methods and calculation

Concentrations of various nitrogen compounds were determined in accordance with standard methods. The electrochemical impedance spectroscopy (EIS) and cyclic voltammetry (CV) were performed using an electrochemical workstation (Corrtest, CS2350M) to characterize the electrochemical activity of the biocathode. The coulombic efficiency for the cathodic reaction was evaluated as the ratio of the current flowing through the MEC and the theoretical current estimated assuming total reduction of the nitrate consumed to nitrogen gas as shown in equation (1) [3].

$$\eta_{CE} = \frac{5 \times \Delta NO_3^-}{\int_0^t Idt/F} \qquad (1)$$

where I is the current (mA), is the number of electrons that are transferred during NO_3^- reduction to N_2 (mol-e^- per mol-N), ΔNO_3^- represents the nitrate consumption (mmol), and F is the Faraday constant (96,485 Coulombs per mol-e^-).

DNA extraction and barcoded amplicon sequencing

Sludge samples (1.0 mL) were collected at the end of the experiment (day 43). DNA was extracted with the RNeasy PowerSoil DNA elution kit (QIAGEN) according to the manufacturer's instructions. Amplicons were sequenced on an Illumina Hiseq 2000 platform (Illumia, San Diego, USA) by Major Biotechnology Co., Ltd. (Beijing, China). Sequences were placed into various operational taxonomic units with Pyrosequencing Pipeline software (https://pyro.cme.msu.edu).

RESULTS AND DISCUSSION

Reactor performance

During the phase 1, the concentration of nitrate in the influent water is set to ~80 mg/L in order to quickly attach the biofilm with denitrification function to the cathode surface. The denitrification capacity of reactor R1 with a potential of -500 mV gradually strengthened, reaching a removal rate of ~60% at the end of the start-up period, and the nitrate concentration decreased from ~80 mg/L of the influent to ~34 mg/L (Figure 1). In contrast, the reactor R2 with an applied -800 mV potential showed a decrease of only ~20 mg/L in nitrate concentration.

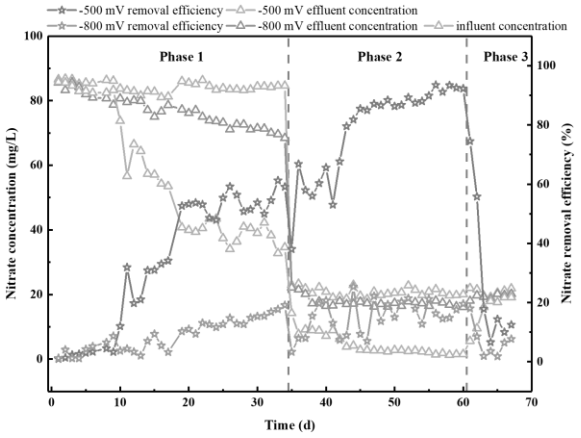

Figure 1 Effluent nitrate concentrations and nitrate removal efficiency

After the denitrification efficiency of the reactor is stable, adjust the concentration of nitrate in the inlet of the reactor to 20 mg/L. The results showed that the concentration of nitrate in the effluent of reactor R1 with a potential of -500 mV gradually decreased from 14.2 mg/L on the 35th day to 4.17 mg/L on the 44th day. Afterwards, the concentration of nitrate in the effluent steadily decreased. From the 45th day to the 60th day, after the reactor stabilized, the average concentration of nitrate in the effluent was 2.25 mg/L, and the nitrate removal rate gradually increased to a maximum of 93%. The reactor R2 with an electric potential of -800 mV was applied, and the nitrate concentration in the effluent was about 17 mg/L, with a nitrate removal rate of only ~15%. At this stage, both reactors did not accumulate nitrite and ammonia.

In order to determine the effect of denitrification, the cathode potential is applied as electron donor, and the cathode potential is stopped at the third stage. When the external potential of the reactor applied with -500 mV and -800 mV potentials stopped, the reactor lost the electron donor for denitrification, and the effluent nitrate concentration gradually increased and finally approached the influent nitrate concentration. At this stage, the nitrate in the influent did not convert, and the concentrations of nitrite and ammonia did not significantly increase.

Electrochemical activity of biofilms

In order to further investigate the reasons for the effect of applying cathodic potential on reactor denitrification, the electrical characteristics of the reactor biofilm were studied (Figure 2).

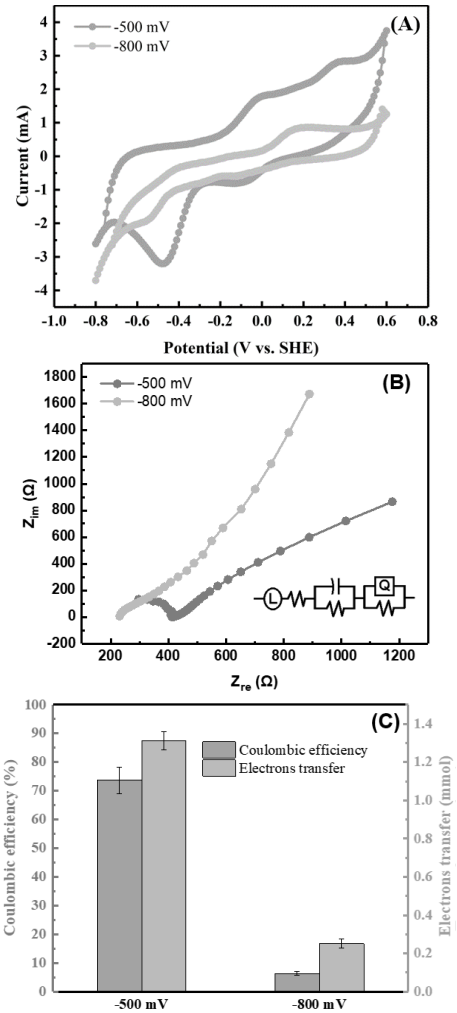

Figure 2 (A) CV, (B) EIS, (C) Coulombic efficiency and electron transfer quantity

Cyclic voltammetry curve was used to investigate the electrochemical characteristics of biofilms. The R1 reactor with a potential of -500 mV showed a reduction peak at -490 mV, which is the reduction peak of nitrite to nitric oxide (Figure 2A). However, the R2 reactor with a potential of -800 mV showed only a very weak peak. The R1 reactor showed a reduction peak at -130 mV, where nitrate was reduced to nitrite, while the R2 reactor did not show a significant reduction peak at this point. Figure 2B shows the Nyquist plots of the cathodic impedance of the R1 and R2 reactors. The charge transfer resistance of the biocathode in the R1 reactor was 1.8 kΩ, while that of the biocathode in the R2 reactor was 14.7 kΩ. The results indicate that the formation of a biofilm capable of directly utilizing electrode electrons for denitrification could reduce the charge transfer resistance between the cathode and microorganisms, thereby promoting electron transfer rate and improving nitrate removal efficiency. Coulomb efficiency analysis shows that 74% of the cathode electrons in the R1 reactor are recovered from the denitrification products (Figure 2C). These differences indicate that the electrochemical behavior of the two systems is different, and the R1 reactor may exhibit higher electrical activity.

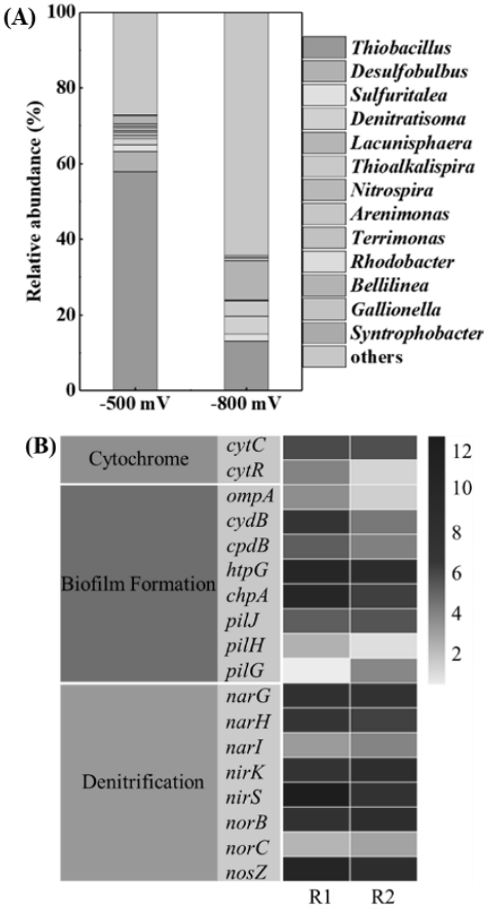

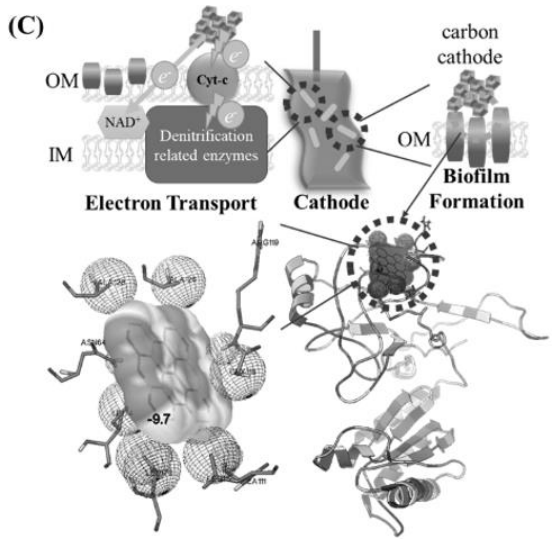

Figure 3 (A) Community structure at the genus level, (B) Gene expression level, (C) Schematic diagram of the interaction between OmpA protein and cathode

In the phase 2 of stable operation and good performance of the reactor, two biofilms on the electrode surface of the reactor were collected. In the bacterial community structure, it could be observed that the R1 reactor with a potential of -500 mV significantly enriched the *Thiobacillus* on the surface of the biological cathode, with a relative abundance of 58% (Figure 3A). However, the relative abundance of *Thiobacillus* in the reactor and R2 under -800 mV was about 10%.

The genes *ompA*, *cydB*, *cypB*, *htpG*, and *chpA*, which are associated with biofilm formation, were upregulated relative to R2 reactor in the R1 reactor (Figure 3B). The OmpA protein has a good affinity with the biological cathode, which contributes to the formation of biofilms (Figure 3C) [4]. The cytochrome genes in the R1 reactor were generally highly expressed, and cytochrome c could transfer electrons to the enzymes used in the denitrification process. Denitrification related genes in R1 reactor were highly expressed, of which *nirS* gene was 35-fold higher than that in R2 reactor.

CONCLUSION

This study demonstrates that *Thiobacillus* can directly utilize MEC biocathode electrons for denitrification of tail water from urban sewage treatment plants at a potential of -500 mV. The concentration of nitrate decreased to 2.25 mg/L, and the removal rate reached 93%. *Thiobacillus* applied -800 mV potential compared with the high expression of denitrification related genes, cytochrome genes related to electron transfer and outer membrane protein genes related to biofilm formation at the biological cathode. The binding between *Thiobacillus* outer membrane protein and carbon biocathode is stable. These results are very important for the deep denitrification of urban sewage treatment plants by directly using the electronic denitrification provided by the electrode, which indicates that the electrode as a electron donor is a more low-carbon and efficient form of electronic supply.

REFERENCE

1. Sun, S.-P.; Nàcher, C. P. i.; Merkey, B.; Zhou, Q.; Xia, S.-Q.; Yang, D.-H.; Sun, J.-H.; Smets, B. F., Effective biological nitrogen removal treatment processes for domestic wastewaters with low C/N ratios: a review. Environmental Engineering Science 2010, 27 (2), 111-126.

2. Zhang, X.-N.; Zhu, L.; Li, Z.-R.; Sun, Y.-L.; Qian, Z.-M.; Li, S.-Y.; Cheng, H.-Y.; Wang, A.-J., Thiosulfate as external electron donor accelerating denitrification at low temperature condition in S0–based autotrophic denitrification biofilter. Environmental Research 2022, 210, 113009.

3. Liu, C.; Sun, D.; Zhao, Z.; Dang, Y.; Holmes, D. E., *Methanothrix* enhances biogas upgrading in microbial electrolysis cell via direct electron transfer. Bioresource technology 2019, 291, 121877.

4. Ma, Q.; Wood, T. K., OmpA influences *Escherichia coli* biofilm formation by repressing cellulose production through the CpxRA two‐component system. Environmental microbiology 2009, 11 (10), 2735-2746.

CAISSON BREAKWATER FOUNDATION RESILIENCE AGAINST SCOURING BY UTILIZING RICE RESINS AND GRAVELS MIXTURE FOR GABIONS

Saatvik Chaturvedi[1], Hemanta Hazarika[2], and Mitsuteru Asai[3]
1 Faculty of Civil Engineering, Kyushu University, Fukuoka, Japan
2 Faculty of Civil Engineering, Kyushu University, Fukuoka, Japan
3 Faculty of Civil Engineering, Kyushu University, Fukuoka, Japan

ABSTRACT

This paper focuses on resilience against tsunami overflow induced scouring on caisson-type breakwater structure foundation. Gabions are steel type caged structures containing gravels which help in prevention of scouring by absorbing the force induced by the waves which results in the erosion of soil from the top of the foundation, and this results in toppling of the caisson structure. This paper analyses the scouring prevention techniques by designing the gabions which contains gravels. The paper also focuses on sustainable development goals and waste reduction by utilizing "rice resins" which is produced from inedible waste left after rice production. The rice resins have been found to be quite effective in reducing liquefaction which makes them a good drainage material. This paper analyses their robustness in terms of preventing overflow water impact.
Additionally, numerical simulation is being performed to analyze the efficacy of gabions in simulating real life tsunami situation as optimal as possible.

Fig. 1. UN SDG 9 Goal

Keywords: Breakwater, caisson, gabion, rice resins.

OBJECTIVE

The research focuses on design of gabions for scouring prevention phenomena by utilizing rice resins mixed with gravels which helps in achieving sustainability goals. The research also focuses on prevention of the displacement of the caisson structure by providing proper solutions for the same. Finally, the research also focuses on providing tenacity to the foundation by preventing seepage of water amongst the gabions. Finally, the aim is getting a sustainable gabion design functioning with actual scenario.

BACKGROUND

This research focuses on Goal 9 of United Nations Sustainable Development Goals which categorizes Industry, Innovation, and Infrastructure as a theme (Fig.1). In previous research, there have been plenty of research going to prevent scouring as a soil failure phenomenon. The gabions, as a scouring prevention structures, have been extensively investigated for their properties. They have been found to be quite effective in scouring prevention but there has been a necessity to improve their design as there have been a few discrepancies regarding their efficacy. For example, the gaps between the steel caged gabions have resulted in seepage of water and ultimately resulting in soil erosion under the gabions thereby resulting in upward force towards gabions and displacement of them from their original position. Additionally, the design of gabions on slope has been a issue due to their design being cubical in shape which leaves space for water to seep at the slope corners. This has been shown in Fig. 2.

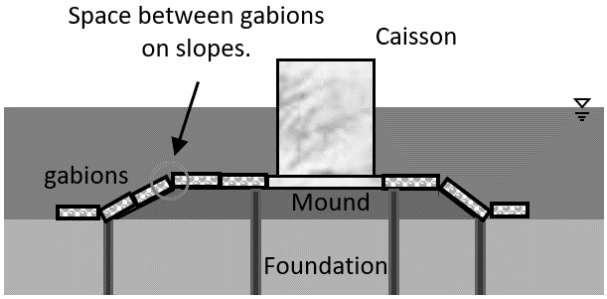

Fig. 2. Space between adjoining gabions at slope

Moreover, the seepage between the caissons also adds up to increase in scouring phenomena. Finally, the major drawback of the design is the material inside the gabions which is purely gravels. The objective of this research is

to address the latter drawback and reduce it as economically as possible. Also, the results shall help in analysis by numerical simulation for the actual situation by comparing with actual set conditions which cannot be achieved in the laboratory.

Previous Research

The design of gabions has been modified to reduce the problems associated with the spaces in between them. To reduce the gaps between the adjoining gabions at slopes, the corners of the gabion's caged structure has been modified to angular shape [1]. Therefore, the linking of adjoining gabions have become more effective.
To reduce the seepage between the caisson and the gabions, impermeable membrane as steel rods have been inserted between the spaces. This has been helped in reduction of seepage of water at the connection point of the caisson and gabions [1]. This has resulted in reduction of scouring phenomena which prevents the toppling of the caisson structure. Although the design of gabions has been able to reduce scouring exponentially, it has also led to increase in pore water pressure inside the foundation. Due to this increase in pressure, the upward forces push rubble mound from beneath and displaces gabions as well as the foundation. Additionally, using impermeable rods have also led to change in pressure levels and using them have also resulted in displacement of the caisson structures.

METHODOLOGY

In this research, hydraulic model experimental apparatus, which has been developed in laboratory, can reproduce steady tsunami overtopping in one direction and can fabricate a moving bed that simulates the seafloor. This apparatus has been shown in Fig. 3. Additionally, since the purpose of this research is to confirm the behavior of breakwaters, including the foundation, during tsunami overtopping, the apparatus has movable weirs on both sides to have the possibility of movement of subsoil as per the requirement of the research.

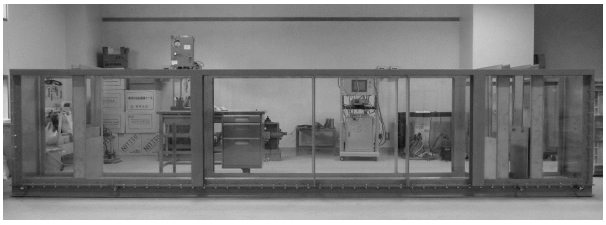

Fig. 3. Tsunami Overflow Flume Equipment

The foundation of the model experiment is utilizing Toyoura sand which is shown in Fig. 3. Regarding the food waste management, we are utilizing inconsumable rice manufacturing by-product. The remaining by-product does not have any nutritional value nor economical value; hence it is first converted to powdered form. Then they are converted to cylindrical shape which as per the scale of gravels being utilized in gravels as well. The rice resins which are being utilized in the research are shown as in Fig. 4. The rice resins are mixed

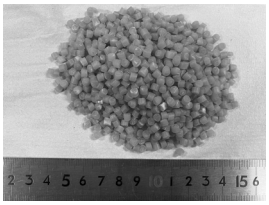

Fig. 4. Rice resins

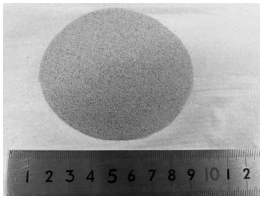

Fig. 3. Toyoura sand

with gravels of size 5 mm to 9.5 mm diameter (average). The model being utilized is shown here in Fig. 5, 6.

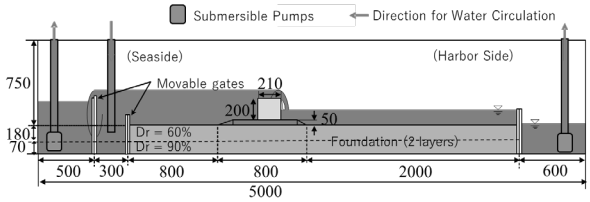

Fig. 5. Side view of model

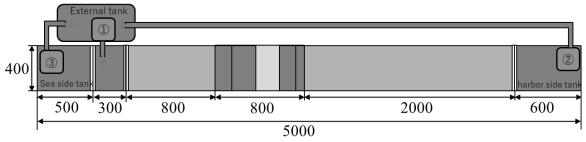

Fig. 6. Planar Side of Model

CONCLUSIONS

1. The rice resins have been found to be equal in density and permeability as the gravels being used in gabions, hence they shall be utilized in gabions for research.
2. The research has shown promise so it is currently in the process of obtaining numerical simulation verification.

REFERENCES

[1] Hazarika, H., Hara, T., Nishimura, K., Yamasaki, N., , Monji, N., Chaudhary, B., Ishikura, R., Kasama, K.: *Fundamental Study on Seismic Resistant Behavior of Caisson Type Breakwater Foundation Reinforced by Steel Sheet Pile and Gabion*, Journal of Japan Association for Earthquake Engineering, 2016, Vol. 16, Issue 1, Pages 1_184 - 1_204, Online ISSN 1884-6246, https://doi.org/10.5610/jaee.16.1_184.

SIMULATION TEST OF NEUTRALIZATION OF INCINERATION ASH LAYER WITH HIGH DISSOLVED CARBON DIOXIDE SOLUTION (BEHAVIOR OF CO_2-UFB WATER IN GLASS BEAD LAYER)

Ayana Matsumoto[1], Kentaro Miyawaki[2]
1 Graduate School of Science and Engineering, Meisei University,
2-1-1 Hodokubo, Hino-city, Tokyo, Japan
2 Department of Interdiciplinary Science and Engineering, Meisei University,
2-1-1 Hodokubo, Hino-city, Tokyo, Japan

Introduction

The main landfill material at municipal solid waste disposal sites is incinerator residue. Therefore, the landfilled layer is always alkaline. At some landfills, leachate pH does not reach the effluent standard of 8.6.
The use of carbon dioxide gas is being considered as a neutralization technology for various high pH countermeasures. In this case, we used ultra fine bubble (UFB). There are examples of studies on the behavior of ultrafine bubbles in porous materials[1)]. However, there are few examples of the use of ultra-fine bubbles using CO_2[2)]. The purpose of this study is to flow CO_2-UFB water into a porous medium simulating incinerator ash and confirm the presence of dissolved carbon dioxide and UFB. Glass beads, which do not react with CO_2, were used as a simulated incinerator ash layer.

TEST PROCEDURE

High dissolved carbon dioxide solution

The test apparatus used was a carbon dioxide high dissolved solution generator (CO_2 dissolution apparatus) with a UFB generation loop type OK nozzle + pump. 2L of pure water was injected with carbon dioxide gas through the diffuser tube at 2.0L/min for 45 minutes. The UFB generating nozzle is pumped at a flow rate of 200mL/min to circulate the solution in the vessel. The operation was performed for 30 minutes to generate bubbles by suctioning the gas phase gas in the vessel from the nozzle side. 11 mL of the highly dissolved carbon dioxide solution produced was placed in a 12mL test tube (17mm diameter, 2.27cm^2 surface area) and a 100mL beaker (50mm diameter, 19.6cm^2 surface area), respectively. IC concentrations over time were examined.

CO_2 dissolved in glass bead layer

The CO_2 dissolved water produced by the apparatus was poured into a glass bead layer. Glass bead packed columns were used, one with a diameter of 42.5 mm and a layer thickness of 150mm and the other with a diameter of 50mm and a layer thickness of 1000mm. The packed glass beads were 1 mm in diameter, and the water flow rate through the column with a layer thickness of 150mm was 284mL/h (200mm/h rainfall equivalent), 142mL/h (100mm/h rainfall equivalent), 71mL/h (50mm/h rainfall equivalent), and 28mL/h (20mm/h rainfall equivalent). In the 1000mm thick column, highly dissolved CO_2 solution was dripped over the glass bead layer at flow rates of 393mL/h (200mm/h rainfall equivalent), 196mL/h (100mm/h rainfall equivalent), and 39mL/h (20mm/h rainfall equivalent) and the IC concentration of the effluent was measured.

Measurement of UFB

I experimented to see how much UFB remained. The sample preparation method is as follows. The flow rate of the UFB generating nozzle is 200mL/min for 2L of pure water, so one loop was created in 10minutes. First, a sample of 3 loops was made, and then 12 more loops were made to make a sample of 15 loops. The 15loop sample was dropped by tube into a glass bead layer with a layer thickness of 1000mm, and the solution after 2 hours of water flow was used as the sample.

RESULTS AND DISCUSSION

High dissolved carbon dioxide solution

Figure 1 shows the results of IC concentration changes in static test tubes and beakers. Static at an IC concentration of 400mg/L resulted in the loss of all CO_2 in the beaker in 4 hours. The reason is that the surface in contact with the atmosphere is large. Figure 2 shows the change in static IC concentration with elapsed time with and without UFB. IC concentrations with UFB were about 20mg/L higher than without, confirming that UFB lasts longer in water. After 48hours, IC concentrations were 250mg/L for the CO_2 high dissolved solution and 280mg/L for the UFB solution. More than 60% of the initial concentration was retained.

CO_2 dissolved in glass bead layer

Figure 3 shows the change in IC concentration ratios by time. ①has a layer thickness of 150mm and rainfall

rates of 200mm/h, 100mm/h, and 50mm/h. ② is 150mm layer thickness, rainfall 200mm/h, 100mm/h, and 20mm/h. ③has a layer thickness of 1000mm and rainfall rates of 200mm/h, 100mm/h, and 20mm/h. The results showed that the higher the flow rate injected into the glass bead layer, the higher the IC concentration ratio. The IC concentration ratio remained almost the same even when the layer thickness was increased by a factor of 7.

Measurement of UFB

Table 1 shows the measurement data for a total of four samples: three samples and blank pure water. Figure 4 summarizes the number concentration for each sample corrected with pure water. The sample ①has 3 loops. S ②has 15 loops. ③was watered through ②for 2hours in a column with a layer thickness of 1,000 mm. ④is pure water. The results showed no significant change in the concentration of UFB counts between the 3 and 15loops. This confirms that 3 loops are sufficient to create a UFB. The number concentration after passing water through the glass bead layer in ③is large. This is thought to indicate the presence of impurities at the nanoparticle level. UFB measurements were performed using a NanoSight NS300.

CONCLUSION

The UFB with CO_2 retained its IC concentration when the surface area was small. Next is the result of CO_2 high dissolved solution in porous media: the CO_2 high dissolved solution retained 40% of the incoming IC concentration in a 1000mm glass bead layer at a rainfall rate of 200mm/h. Finally, the number concentration of UFBs could be measured, confirming that sufficient bubbles were generated in the three loops. etc. We are currently considering conditions for accurate measurements.

REFERENCES

1)Shoichiro Hamamoto. ［Understanding the migration characteristics of fine bubbles in porous media for use in soil remediation］.Multiphase Flow, Vol. 32, No. 1 (2018).in Japanese.

2)Shogo Sakita et al. ［Desalination of Municipal Solid Waste Incineration Ash Using Ultra Fine Bubble Water］. 32nd Annual Meeting of the Japan Society of Material Cycles and Waste Management. (2021).in Japanese.

ACKNOWLEDGEMENTS

This research was supported by JSPS Grant-in-Aid for Scientific Research JP20K12227.

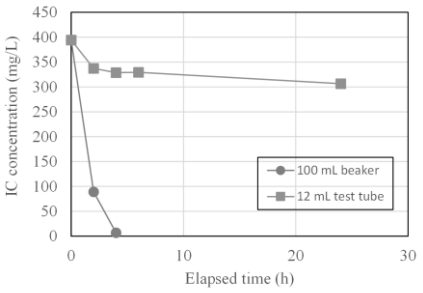

Figure 1: Change in static IC concentration

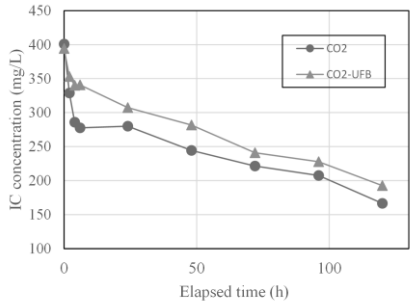

Figure 2: Static IC concentration of elapsed time with and without UFB

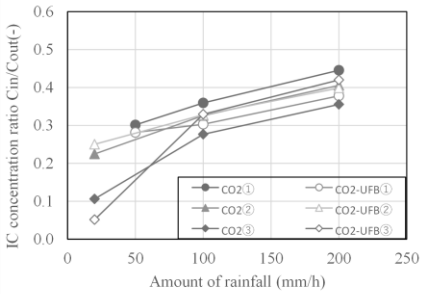

Figure 3. IC Concentration Ratio Change

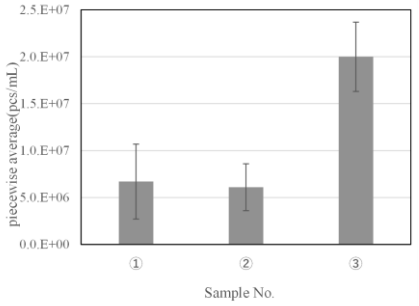

Figure 4: Number concentration of samples after pure water correction

Table 1.UFB measurement results

No.	Sample	Piece density (pcs/mL)	Piecewise average(pcs/mL) (After pure water correction)	Average particle diameter(nm)	Peak particle size(nm)	Median grain size(nm)
①	3 loops	1.5E+07 ± 3.6E+06	6.7E+06 ± 4.0E+06	111.8	101.4	122.0
②	15 loops	1.5E+07 ± 1.7E+06	6.1E+06 ± 2.5E+06	135.8	101.0	155.3
③	②→GB layer	2.8E+07 ± 3.3E+06	2.0E+07 ± 3.7E+06	133.7	104.7	115.5
④	pure water	8.8E+06 ± 1.7E06	—	129.5	113.3	115.2

(GB stands for glass bead layer)

Development and Evaluation of Landfill IoT System Utilizing Battery using landfill leachate as an electrolyte

Nagare Kameno[1], Takayuki Shimaoka[2], Nakayama Hirofumi[2] and Haruichi Kanaya[3]
1 Graduate school of Engineering, Kyushu University, Motooka744, Fukuoka City, JAPAN
2 Faculty of Engineering, Kyushu University, Motooka744, Fukuoka City, JAPAN
3 Faculty of Information Science and Electrical Engineering, Kyushu University, Motooka744, Fukuoka City, JAPAN

1. INTRODUCTION

In waste landfill sites, environmental monitoring is essential to understand the characteristics of landfill waste and variations in the surrounding environment, serving as crucial elements in environmental protection and waste management. Within landfill waste layers, physical, chemical, and biological reactions are unevenly distributed, necessitating a system that can automatically observe numerous points over an extended period for proper monitoring. Therefore, advanced environmental monitoring utilizing IoT technology, which has seen significant advancements in recent years, is expected. However, there are several challenges associated with monitoring using IoT technology.

The first challenge is wireless communication underground. Constructing a sensor network using wireless communication is effective for achieving multi-point automatic observation, but there are few research cases in this area. Wireless communication technology allows easy sensor installation as it can transmit data without using cables. Furthermore, different frequency bands exhibit distinct characteristics, and low-frequency electromagnetic waves have minimal attenuation in underground, bedrock, and underwater environments, as revealed by Tazoe and others[1] (2022).

The second challenge is the power supply for sensor units, with power line installation being difficult in the landfill waste layers. To address this issue, energy harvesting technology has garnered attention, and the concept of "waste batteries," utilizing rainwater in landfill waste layers to form a battery circuit, has been proposed. Murakami and others[2] (2022) have conducted a proof-of-concept demonstration of the "waste battery," utilizing landfill leachate as an electrolyte to recover generated energy. In this study, an evaluation of an IoT system combining the power recovery technology of "waste batteries" and the technology of "low-frequency communication" was attempted, focusing on the waste battery in the experiment.

2. RESEARCH METHODS

2.1 Communication System

In this study, the goal is to construct the wireless communication system shown in Figure 1. Data measured by sensors installed in waterproof sheets and landfill waste layers are transmitted to a relay station on the surface using low-frequency electromagnetic waves.

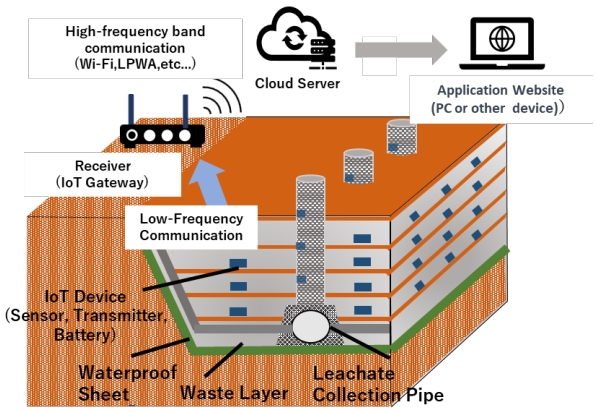

Figure 1: Conceptual Diagram of Wireless Communication System

From the surface relay station, the data is transmitted to a cloud server or the receiver's PC via mobile networks, LPWA, Wi-Fi, etc., forming an IoT system.

2.2 Wireless Communication Device Using Low-Frequency Electromagnetic Waves

Communication devices used in the construction of the IoT system are presented in Table 1. The compact transmitter consists of a data logger, transmission circuit, transmission coil (antenna), and battery. By connecting various sensors to the transmitter, measurement data can be transmitted using low-frequency electromagnetic waves. The receiver is composed of a receiving coil (antenna), receiver main unit, and computer to collect measurement data. Table 1 provides specifications for the communication device using low-frequency electromagnetic waves.

Table 1: Operating Voltage, Communication Speed, Frequency, and Current Consumption of Compact Low-Frequency Transmitter

low-frequency transmitter	
operating voltage	3.6V
data rate	75bps
frequency	8500Hz
current consumption	1.7A (during data transmission)

2.3 Principle of Waste Battery

It is a general term for batteries that utilize a mechanism to recover electrical energy by acting on the retained water within the landfill waste layer as an electrolyte. When the retained water passing through the waste layer of the landfill comes into contact with the power generation device, it acts as an electrolyte, generating electricity by creating a potential difference between two metal electrodes with different electrode potentials. In the prototype waste battery produced, a copper plate is used as the positive electrode, and a magnesium plate (vertical 45 mm × horizontal 15 mm × thickness 0.5 mm) is used as the negative electrode. A mixture of highly absorbent and retentive gypsum and diatomaceous earth is used as the water-retaining material. The mass ratio and water addition of gypsum to diatomaceous earth are based on references by Hagiwara et al. (2019)[3] and Li et al. (1991)[4] with a mass ratio of gypsum to diatomaceous earth as 10:3 and a water addition of 90% of the solid mass. Distilled water was mixed with diatomaceous earth to form a paste, poured into an acrylic case assembled in a rectangular shape, and allowed to cure by leaving it in a 60°C drying oven for one day. Additionally, to prevent short-circuiting, a sealing treatment with silicone sealant was applied between the positive and negative electrodes. The prototype waste battery is shown in Figure 2, and Table 2 presents the electromotive force, internal resistance, and maximum power obtained from the waste battery in the experiments by Murakami et al. (2022). The waste battery has a three-layer structure with an electromotive force of 3.37V, enabling the recovery of a voltage sufficient to operate a low-frequency communication device. However, due to high internal resistance and resulting voltage losses, there is an issue preventing the operation of the low-frequency communication device. To address this problem, consideration is given to a method of driving sensors and microcontrollers through a capacitor.

Table 2: Electromotive Force, Internal Resistance, and Maximum Power of Waste Battery

	1 Layer	2 Layers	3 Layers	4 Layers
Electromotive Force(V)	1.29	2.59	3.37	4.55
Internal Resistance(Ω)	510	1120	1860	2350

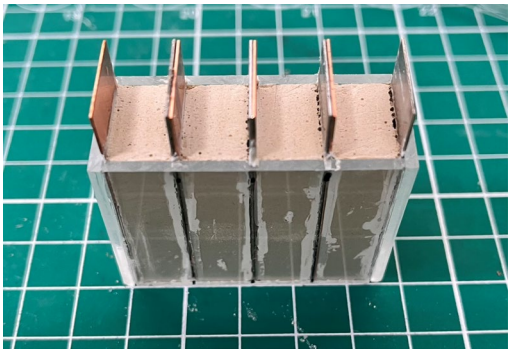

Figure 2: Experimental Setup Diagram

2.4 Relationship between Burial Depth and Power Generation Performance of Waste Battery

To investigate the impact of the depth of burying waste batteries on their power generation performance, a disposal site model layer was created using columns, and the performance of the waste batteries under burial conditions was evaluated. Experiments were conducted using small columns with a height of 50 cm and a diameter of 10 cm, burying only the waste batteries. To prevent poor contact of the conductors, the electrodes were wrapped with conductors and waterproofed. The columns were filled with incineration residue, and by watering, the experiment aimed to replicate the environment in which waste batteries generate electricity through rainwater. Experiment conditions are presented in Table 3, and the experimental setup diagram is shown in Figure 3.

The waste batteries used in this study were constructed with a four-layer structure. The samples used were incineration residues mixed in a ratio of 3:1 of incineration ash to fly ash. The watering conditions were determined based on precipitation data from Fukuoka City, and watering was carried out using a drip device. Additionally, the filling density was adjusted to approximately 1.0 t/m³ to simulate an actual landfill site. The measured data included elapsed time from the start of watering, voltage of the waste batteries, moisture content of the samples (at a depth of 125 mm), and the pH and electrical conductivity (EC) of the leachate. Moisture content was measured using an IoT device, the ESP32, and the data were uploaded to the cloud to establish a monitoring system.

Table 3: Experimental Conditions

Experimental Conditions	Each Value	Notes
Watering Amount	400ml	Watering at the beginning of the experiment. Watering was conducted at a rate of 14ml/min for 29 minutes.
Fill Density	1.0t/m³	
Fill Depth	125㎜, 450㎜	

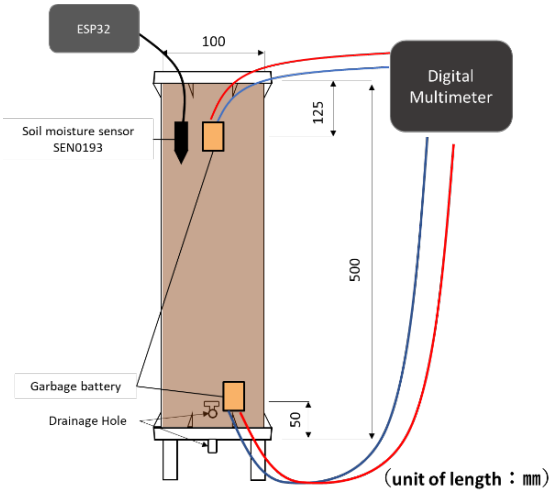

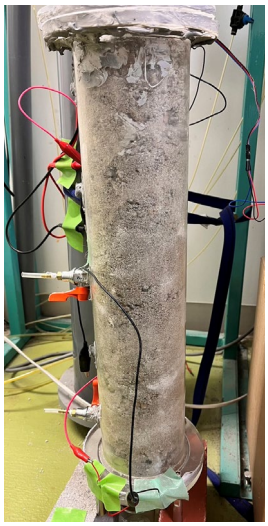

Figure 3: Experimental Setup Diagram and picture

3. RESULTS

The electromotive force of the waste batteries used in this experiment is presented in Table 4. Additionally, Figures 4-5 and Table 5 display the experimental results. Upon examining Figure 4, it is observed that the voltage of the waste battery at the 150mm point reached its maximum value around 3000 minutes and then began to decline. In contrast, the waste battery at the 450mm point showed a gradual increase. This phenomenon is believed to be caused by the gradual infiltration of retained water containing components of incineration ash to the lower layers. Furthermore, the early processing of the waste battery in the upper layer (150mm point) compared to the lower layer (450mm point) is attributed to the significant impact of surface water evaporation. The lower layer, having retained gradually infiltrated water, is likely responsible for the gradual increase in voltage.The measured results of the moisture content at the 125mm point are illustrated in Figure 5. The moisture content variation in this measurement occurred only during watering, remaining constant thereafter. Despite the consistent moisture content, two reasons are considered for the decrease in voltage of the waste battery in the upper layer. First, it could be attributed to the precision issue of the sensor. The soil moisture sensor used in this experiment adopts the capacitive method, which is susceptible to the influence of electrical conductivity (EC) in the soil, making it potentially unsuitable for measuring the output in incineration ash. Second, the reduction in moisture content of the water-retaining body of the waste battery is a possibility. The insufficient voltage in the upper layer's waste battery, not reaching 3V, may be due to a lower concentration of incineration ash in the retained water or potential issues such as poor conductor contact. These factors impact the battery's power generation performance, and future experiments are planned to modify conditions, including increasing burial depth and adjusting watering amounts, to further investigate these influences.

Table 4: Electromotive force of the used waste batteries in this experiment

depth(mm)	450mm	125mm
Electromotive Force(V)	3.284	3.37

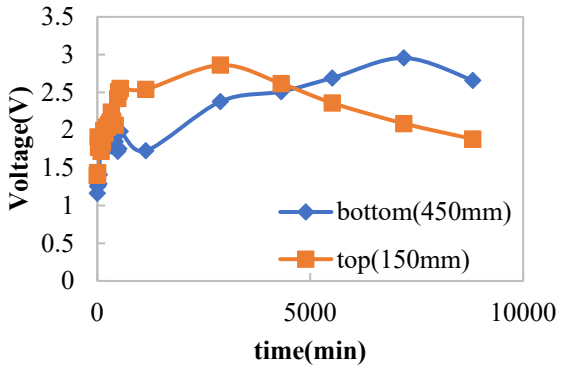

Figure 4: Relationship between Voltage and Time

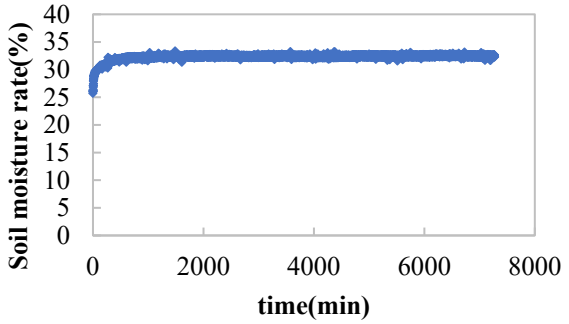

Figure 5: Relationship between Moisture Content and Time (Depth: 150mm)

Table 5: Water Quality of Leachate from the Column

	pH	EC[mS/cm]
Simulated Leachate from Dissolution Test	11.76	170.4
Leachate	11.895	140.5

4. CONCLUSIONS

In this study, a disposal site model layer was created using columns to investigate the impact of burying depth of waste batteries on their power generation performance. The performance evaluation of waste batteries under burial conditions was conducted, and the following insights were obtained:

The study revealed differences in voltage fluctuations at different points where waste batteries were buried at varying depths. Waste batteries buried at a depth of 150mm, closer to the surface, showed a faster rate of reaching maximum voltage compared to those buried at 450mm. The voltage of batteries in the lower layer was observed to rise gradually. This is believed to be due to the evaporation of surface moisture, resulting in a decrease in moisture content.

1)The fact that batteries buried at 450mm continue to show an increase in voltage suggests the potential to detect environmental variations at different depths, considering factors such as water penetration in the deep layers and the concentration of incineration ash components. This result implies the effectiveness of monitoring using IoT technology in tracking the dynamics of water within the landfill waste layer and revealing its impact on battery power generation performance.

2)Waste batteries buried at a depth of 450mm reached a maximum voltage of approximately 3V, meeting the operating conditions of the low-frequency transmitter. It was also revealed that a certain depth is necessary for power supply by waste batteries.

3)It should be noted that the voltage showing values smaller than the electromotive force could be attributed to various factors such as the concentration of electrolyte components and contact of conductors.

Further investigations into the causes are planned for the future.

5. REFERENCES

1)Tazoe:"A Study on Wireless Communication Technology for Environmental Monitoring in Waste Landfill Sites," 2022.
2)Murakami et al.: "Research on Prototype Production of Waste Batteries Using Leachate from Waste Landfills," Proceedings of the 33rd Waste Resource Recycling Society Research Presentation Meeting, 2022, pp. 89-90.
3) Masahide Hanekiri et al : "Absorbent Material Made from Seccou and Diatomaceous Earth," Chemistry and Education, Vol. 67, No. 9, pp. 434-435, 2019.
4)Leng Li et al.: "Pore Characteristics and Absorbency of Gypsum Mold," Journal of the Society of Powder Technology, Vol. 28, No. 11, pp. 684-688, 1999.

PARTICLE SIZE CHARACTERIZATION FOR METAL RECOVERY FROM MUNICIPAL SOLID WASTE INCINERATION ASH

Ryugo Tanaka[1] Teppei Komiya[1] Takayuki Shimaoka[1]

1 Department of Urban and Environmental Engineering, Kyushu University, 744 Motooka, Nishi-ku, Fukuoka, Japan

INTRODUCTION

Japan generates 42 million tons of municipal solid waste incineration (MSWI) annually, about 80% of which is processed at more than 1,200 incineration facilities nationwide, resulting in incinerator bottom ash and fly ash. The advantages of incineration include the mineralization of organic matter, volume reduction, and the use of heat from the incineration process. Incineration bottom ash mainly contains noncombustible materials such as minerals and glass, base metals such as copper and zinc, and precious metals such as gold and silver. If these can be recovered and reused, incinerator ash that would otherwise be disposed of can be given economic value and the burden on the environment can be reduced. However, there are still many aspects of incineration ash that have not yet been elucidated in terms of detailed characteristics and relationships among metal distributions. In this study, we focused on metal recovery from incineration ash and performed inductively coupled plasma mass spectrometry (ICP-MS) and inductively coupled plasma optical emission spectrometer (ICP-OES) on each particle size fraction of classified incineration ash to understand the elemental composition, and based on that, evaluated the efficiency and economic potential of metal recovery.

EXPERIMENTAL METHOD

Information on samples used in the experiment

The samples were bottom ash from incinerators (stoker-type incinerators) at four waste incineration plants: K Plant, S Plant, W Plant, and E Plant. The municipal solid waste incineration bottom ash (MSWI-BA) includes grate sifted and deposited ash (GSDA) (ash that falls through gaps in the stoker in the early to mid-stage of combustion) and main bottom ash (M-BA) (ash produced in the final stage of combustion), and both were sampled separately. Figure 1 shows a schematic diagram of the locations where grate sifted and deposited ash and M-BA were

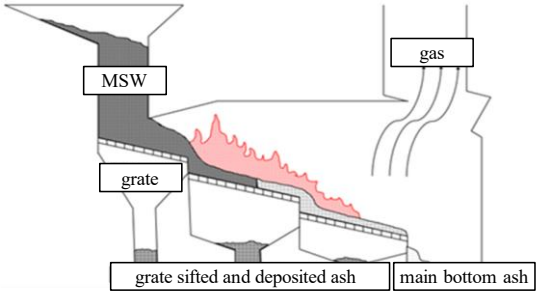

Figure 1 Schematic diagram of a stoker-type incinerator

collected in the stoker furnace. Information on each Plant is shown in Table 1.

Preparation of K and S Plant samples

Noncombustible materials (metals, glass, rocks, etc.) were removed from the sample and divided into five particle size categories using 4mm, 2mm, 1mm, and 0.5mm sieves, and then ground in a vibrating mill for 10 minutes.

Preparation of W and E Plant samples

Noncombustible materials (metals, glass, stones, etc.) were removed from the samples and divided into 12 particle sizes using sieves of 37.5 mm, 26.5 mm, 19 mm, 9.5 mm, 4.75 mm, 2 mm, 0.85 mm, 0.425 mm, 0.25 mm, 0.106 mm and 0.075 mm, then milled for 10 minutes in a vibrating mill. The vibration mill was excluded because it could not grind particles larger than 4.75 mm, and the sample from Plant E was excluded because the amount of particles smaller than 0.075 mm was very small. Thus, seven samples were analyzed at Plant W and six samples at Plant E.

Liquid sample preparation

A total of 33 solid samples obtained by sieving and grinding were treated with aqua regia for ICP-MS analysis and filtered to make liquid samples.

Analysis

Each liquid sample was diluted and analyzed by ICP-MS (subject of analysis: Al, Fe, Cu, Zn, Pb, Pd, Ag, Pt, Au, Li, Be, B, Mg, Si, Ti, V, Cr, Mn, Co, Ni, Ga, Rb, Sr, Zr, Nb, Mo, In, Sb, Te, Cs, Ba, Hf, W, Re, Tl, Bi, Ce) made by Agilent technologies; Agilent 7500ce and ICP-OES (subject of analysis: Al, Fe, Cu, Zn, Pb, Li, B, Mg, Si, Ti, V, Cr, Mn, Co, Ni, Mo, Sb, Ba) made by Agilent technologies; Agilent 700 series ICP-OES.

RESULTS AND CONSIDERATION

Results

Basically, the ICP-MS data with high sensitivity was adopted, while the ICP-OES data was adopted for elements with high content. Figure 2 shows the ICP-MS and ICP-OES analysis results of Pt, Au, Pd, and Ag, which are classified as noble metals among the measured elements (The data for these elements is above the lower limit of quantitation for ICP-MS). In addition to the content of each particle size analyzed in this experiment, the results for the total particle size of the analyzed samples calculated from their respective mass percentages are also shown. Figure 3 shows the content of metals that showed significant differences between GSDA and M-BA by ICP.

Consideration

On the reasons for the major differences between GSDA and M-BA: GSDA is material that falls

Table 1 Information about each plant

Plant	K	S	E	W
Processing system	Stoker-type	Stoker-type	Stoker-type	Stoker-type
Throughput per incinerator	85t/day	114t/day	300t/day	140t/day
Number of incinerators	2	2	2	2
GSDA	○	○	×	×
M-BA	○	○	○	○

through gaps in a moving grate, and since it occurs in the early to mid-stage of combustion, it is likely to have a low melting point or high specific gravity. In addition, elements (e.g., Al) that are not included in GSDA despite their low melting points are thought to exist as oxides or sulfides, but further investigation is needed in this regard.

About evaluating the economics and efficiency of recovering metals[1), 2)]: In examining the economics and efficiency of metal recovery, the grade of the ore from which each metal is derived was used as the basis for comparison. The platinum group is known to be present in ores at about 3 g/t. Although the amount of platinum in incinerator ash is not large, the fact that it is contained in trace amounts in there has a certain value because of its extremely limited location, its small quantity, and its high demand and

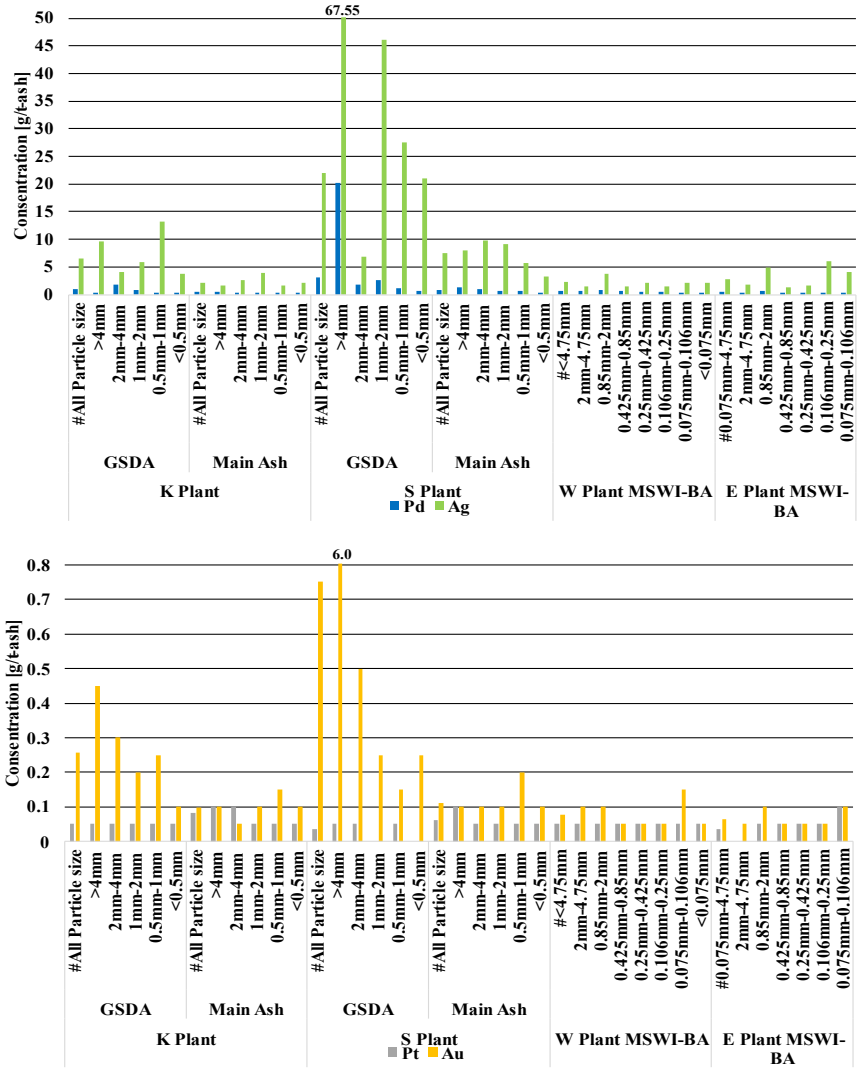

Figure 2 Precious metals content by particle size

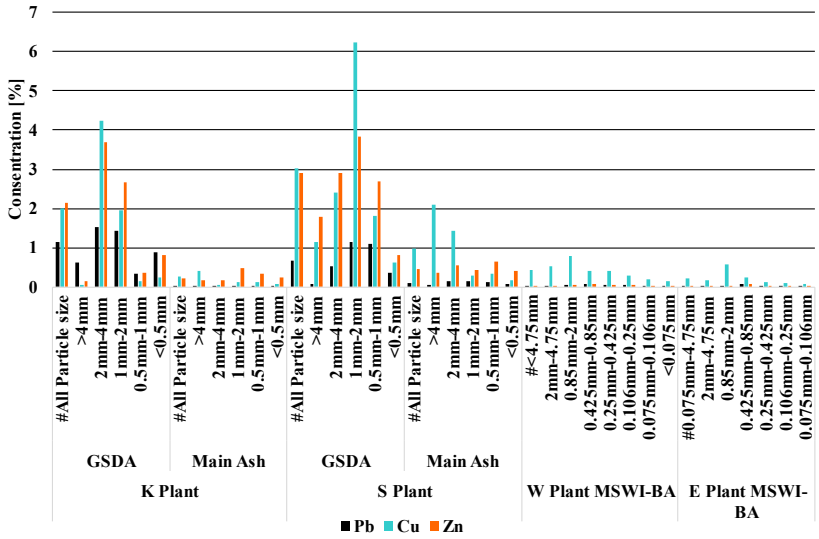

Figure 3 Some metals content by particle size

importance for recycling. Palladium was found to be contained in the incineration ash at a rate of about 3-4 g/t. The content did not show any variation depending on particle size or collection location. The world's major gold mines have grades of 3-5 g/t, and are considered profitable at around 2 g/t. The lowest grade of silver ore is estimated to be around 80 g/t, while the highest grade can be as high as 170 g/t. In this experiment, the highest grade was 67.5 g/t, but most of the others were less than 5 g/t. The properties of incinerated ash vary greatly depending on the plant where it was generated and the date, so there may be room for recovery if the conditions are right, but basically, it would be difficult to recover only silver as a business target. However, the concentration of these elements may be increased by magnetic or density sorting.

The world averages for Pb, Cu, and Zn crude ore grades are 2~2.7%, 0.5~1.2%, and 5.2~5.9%, respectively, and for GSDA, the Pb and Zn content is one step below the average, but the Cu content is much higher. It should be noted, however, that the number of analyses in this experiment was only one.

CONCLUSION

The lead, zinc, and copper content of GSDA was higher than that of M-BA, and it was thought that the separation and recovery of dust from the GSDA would be a good idea in recovering these three metals. As for Pd, it was found that the incinerator ash contained an amount comparable to that of the crude ore. Other precious metals are also present in trace amounts and may be recycled in the future.

REFERENCES

1) Kenji Sawada: Supply-Side Analysis by Mineral Type (1) to (3) - Copper, Zinc, Lead, Metals Resource Report, 2006(in Japanese)

2) JOGMEC Toho-zinc corporation: Joint Study on Pre-FS Evaluation for Recovery of Zinc and Other Metals from Endeavour Mine, Report of Technical Assistance Project for On-Site Needs in 2014 (Public version), 2015(in Japanese)

BASIC STUDY ON DISPERSIBILITY OF MICROPLASTICS IN A FINAL DISPOSAL SITE

Ryo Tanaka[1], Hirofumi Nakayama[2], Takayuki Shimaoka[2]

1 Graduate school of Engineering, Kyushu University 744 Moto-oka, Nishi-ku, Fukuoka 819-0395, JAPAN

2 Faculty of Engineering, Kyushu University 744 Moto-oka, Nishi-ku, Fukuoka 819-0395, JAPAN

1. INTRODUCTIONr

There are concerns about the impact that microplastics (MPs), which are less than 5 mm in size, have on the environment, and there is a need to suppress the generation of MPs and properly manage them. Focusing on the general waste treatment process, waste that has been separated as non-combustibles is sorted into metals such as iron and aluminum, combustible shredding residue, and non-combustible shredding residue through crushing and sorting at a recycling facility. Of these, non-combustible shredding residue is disposed of in landfills at final disposal sites, but it has been revealed that it contains MPs. MPs contained in landfill waste are thought to be scattered during landfill disposal or moved with rainwater after disposal, but the flow is not clear.

Therefore, the purpose of this study was to clarify the material flow of MPs in municipal waste treatment facilities. We conducted a survey of MP contained in the crushed noncombustible residue before landfill and in the covering soil near the landfill at a noncombustible waste crushing facility and final disposal site in Fukuoka City.

2. REVIEW OF SIMILAR PREVIOUS STUDIES

The purpose of this research is to understand the generation status of MPs in intermediate treatment processes such as crushing and sorting of waste containing plastic in general waste treatment. Another purpose is to understand how MPs contained in the treatment residue generated after intermediate treatment moves with scattering and rainwater after being disposed of in a final disposal site, and to clarify the flow of MPs. As a previous study conducted in the past, Fukuda et al. (2022) [1] investigated MPs contained in samples from general waste disposal sites and sewage treatment plants in Japan. As a result, based on the similarities in the typical components of MPs confirmed from the crushed noncombustibles and the intermediate covering soil, it was inferred that the source of MPs at the final waste disposal site was the crushed noncombustibles brought in for landfill. . In addition, many MPs were confirmed in samples collected from various locations at the final waste disposal site. However, MPs were not detected in the sludge and leachate treated water after coagulation and sedimentation at the sewage treatment plant, indicating that MPs were removed during the treatment process and were prevented from flowing outside the disposal site.

On the other hand, Xi et al [2] analyzed agricultural topsoil samples around waste treatment facilities and showed that more MPs were distributed in the leeward area.

Lauriane et al. [3] and Maja et al. [4] pointed out that while large-sized MPs can be treated by removal processes, small MPs can percolate through geological formations and be released as leachate, contaminating groundwater. It is revealed that higher concentrations of various MPs were observed especially after rainfall.

Polyethylene and polypropylene were commonly used as materials for MPs in all studies.

3. METHODOLOGY

3.1. Research targets and sampling methods to understand the scattering status of MPs in landfills

First, we collected non -combustible crushed items from the crushed factory. (hereafter, it is called MPS contained in non -combustible crushed materials). Next, to understand the status of MPS scattering near the landfill, at three points, 20 to 30 meters away from the landfill work, a scoop was collected with a scoop with a scope of 40 cm square and depth of 3 cm using the codrat method, and MPS was extracted from among them. (hereafter, it is called MPS contained in the landing). Finally, a 1m square repair tray was installed about 50 meters away from the landfill, and one week later, the MPS was extracted from the descent in the repair tray (hereinafter, it is called descent MPS).

3.2. Extraction and analysis of MPs from samples

In this study, MPS was extracted from the sample in accordance with the flow of Fig. 1. First, the sample was put in a 24 -hour dryer and dried, and a 5mm sieve and a large particle size and a contaminator were removed. Next, a 70 % yawn sodium solution (specific gravity 1.525) was added to the sample and stirring, then the specific gravity was separated to remove a heavy stone and sand. Furthermore, 30 % hydrogen peroxide and FE (II) solution were added by 20 ml, and organic substance was disassembled by responding for a small period of time. After that, only MPS was taken out of the sample that was filtered and dried.

The MPS taken out of the sample was installed on the ATR device and the FT-IR analysis was performed. The MPS material was identified by comparing the spectrum obtained by the analysis with the high hit rate in the library of the Knowitall software. Next, the MP was observed using an optical entity microscope, and the number was measured and shaped classified. Regarding the shape classification, as a reference, the irregular shape containing a spherical shape is defined as a fragment, a uniform and elongated shape of the diameter is defined as a fiber, and a thin film -shaped one is a film shape, and is classified into three types. Later, using those results was created to create a cross -aggregated table of MPS material and shape.

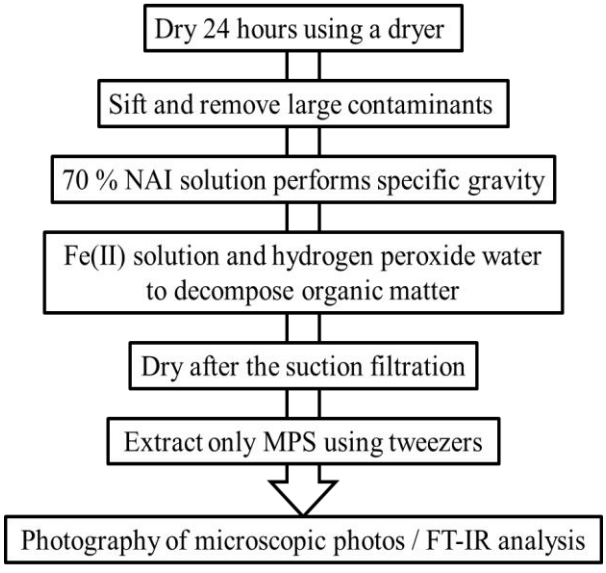

Figure 1 MPs analysis flow

3.3. Result

Fig. 2 shows the results of MPS contained in non -combustible crushed materials, MPS contained in the landing, and descent MPS identification by FT-IR analysis. The largest ratio of MPS contained in non -combustible crushed materials was 35 % for PET, and the second was 32 % for polyethylene. The largest ratio of MPS contained in the landing was 28 % for PET, the second was 24 % for polynosic, and the third was 20 % for polyethylene. The largest ratio of descent MPS was 24 % of polypropylene and polynosic, and the second was 16 % in nylon.

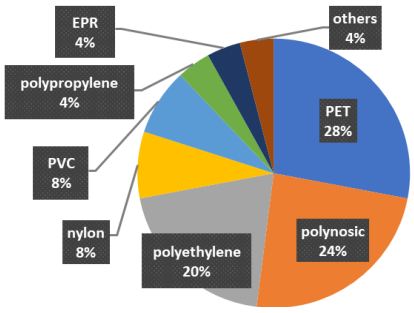

MPS contained in the landing

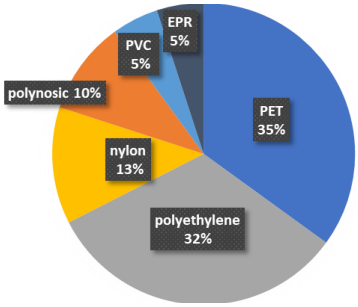

MPS contained in non -combustible crushed materials

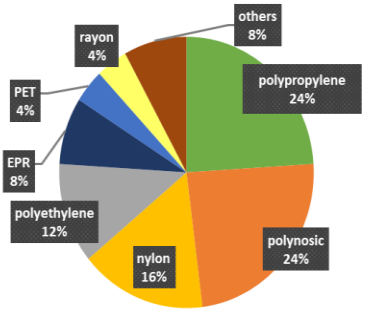

descent MPS

Figure 2 Composition of materials identified through FTIR analysis

Fig. 3 shows the classification result of the shape by microscope observation. In MPS contained in non -combustible crushed materials, the fragment was 16 %, the fiber was 40 %, and the film was 44 %. In MPS contained in the landing, fragment was 21 %, fibers were 60 %, and film was 19 %. In descent MPS, the fragment was 11 %, the fiber was 77 %, and the film was 12 %. Fig. 4 shows the microscopic photo of the MPS obtained by type.

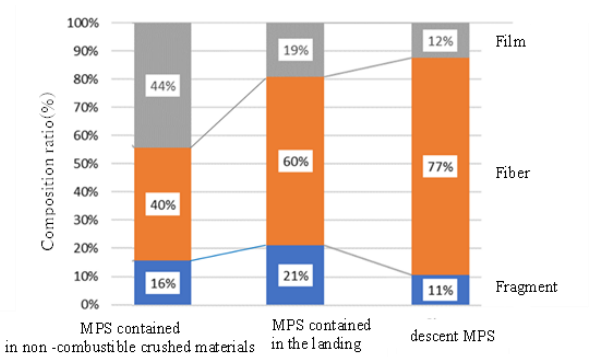

Figure 3 Shape ratio of MPs

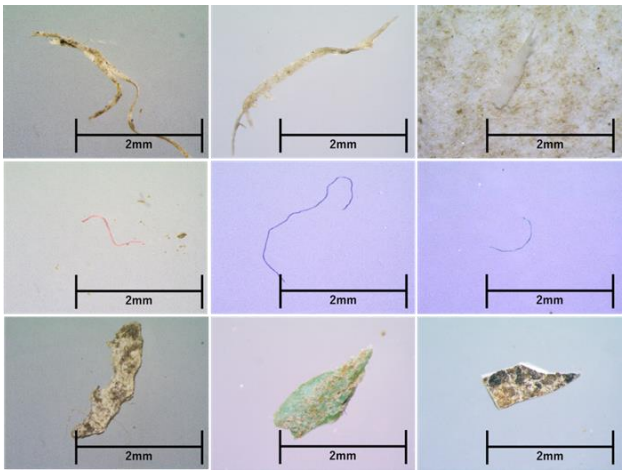

Figure 4 MPS contained in non -combustible crushed materials(left), MPS contained in the landing(center), and descent MPS(right)

Table 5 shows a cross -aggregated table for MPS contained in non -combustible crushed materials and the descent MPS material and shape -by -shape ratio. The

number of MPS obtained from each sample was 191.5piecees/kg with MPS contained in non -combustible crushed materials, 3,003.8pieces/kg with MPS contained in the landing, and 65pieces/week with descent MPS.

Table 5 cross -aggregated table

MPS contained in non -combustible crushed materials

（unit：%）

material and shape	fragment	fiber	film
PET	5.7	20.0	11.4
nylon	2.9	14.3	8.6
polyethylene	17.1	8.6	11.4

descent MPS

（unit：%）

material and shape	fragment	fiber	film
polypropylene	16	12	4
nylon	8	36	8
polyethylene	8	0	8

3.4. Discussion

Comparing the results of the composition ratio by material, there were many PET and poly -chloride in MPS contained in non -combustible crushed materials and MPS contained in the landing, and many polypropylene was found in descent MPS. There were also common things like polynosic and polyethylene.

It was thought that the ratio of fragments and films in the descent MPS was reduced compared to MPS contained in non -combustible crushed materials and MPS contained in the landing, because the heavy fragments and film were harder to scatter than the fiber.

In MPS contained in non -combustible crushed materials and MPS contained in the landing, a dozens of features with similar colors, sizes, and shapes have been confirmed other than those shown in the figure, and these are presumed to be due to the same source.

MPS of material such as nylon is often fiber, and it was considered necessary to prevent occurrence in control from the viewpoint of preventing scattering. Conversely, many MPSs with materials such as polyethylene were considered to be fragmented, and the scattering was not so large.

4. CONCLUSION

Among MPs, PET and PVC with large specific gravity were found to be more abundant in MPS contained in non -combustible crushed materials and MPS contained in the landing, while polypropylene with small specific gravity was found to be more abundant in descent MPs, suggesting that the specific gravity of MPs may affect their susceptibility to scattering.

The results of the cross -aggregated table indicate that nylon and PET have many fibrous materials and that measures to control their generation are necessary from the standpoint of preventing scattering.

References

[1] Atsuki Fukuda, Hirofumi Nakayama, Takayuki Shimaoka : Research on microplastic substance flows in the final disposal site, Civil Engineering Society Western Branch Research Presentation , 2022, 3

[2] Xi Liu, Huirong Lin, Sheng Xu, Yu Yan, Ruilian Yu, Gongren Hu : Occurrence, distribution, and characteristics of microplastics in agricultural soil around a solid waste treatment center in southeast China, Journal of Soils and Sediments (2023)

[3] Lauriane Ledieu, Ngoc-Nam Phuong, Bernard Flahaut, Pauline Radigois, Julya Papin, Cécile Le Guern, Batrice Béchet and Johnny Gasperi : May a Former Municipal Landfill Contaminate Groundwater in Microplastics? First Investigations from the “Prairie de Mauves Site” (Nantes, France), Microplastics 2023, 2

[4] Maja Petrovic, Ivana Mihajlovic, Aleksandra Tubic and Mladenka Novakovic : Microplastics in municipal solid waste landfills, Environmental Toxicology 2023

PREPARATION OF STABILIZED BODIES BY USING COPPER FERROCYANIDE AND EVALUATION OF CESIUM LEACHING CHARACTERISTICS

Hu Yuke[1], Yasumasa Tojo[1], Takayuki Matsuo[1] and In-Hee Hwang[1]
1 Graduate School of Engineering, Hokkaido University
N13W8, Kita-ku, Sapporo, Japan

1. INTRODUCTION

Since Fukushima Daiichi Nuclear Power Plant accident, huge amount of solid waste and soil contaminated by radioactive cesium (hereafter Cs) had been generated. To reduce the volume, various volume reduction treatments are carried out at present. For incineration residue, melting process is applied but it produces fly ash with Cs in high content and high radioactivity. Because Cs in fly ash is highly soluble, fly ash should be solidified for final disposal [1]. Direct solidification by cement, etc. is not promising due to increase of the volume. Thus, extracting Cs in fly ash by water and adsorbing Cs by some adsorbent, then making it solidified body is actively examined. Among them, it was reported that the method using copper ferrocyanide (hereafter CuFeCN) as an adsorbent has extremely high Cs concentration efficiency. Therefore, in this study, first, CuFeCN adsorbing Cs is created, then after thermally decomposing it, solidified body with cement or geopolymer were created. The leaching behavior of Cs from the prepared solidified body was evaluated.

2. METHOD

2.1 Adsorption of Cs on CuFeCN and thermal decomposition of Cs adsorbed body

CuFeCN (Kanto chemical co.) was used as adsorbent. Simulated washing solution of fly ash was adjusted to have CsCl: 0.02 M, KCl: 0.9 M, and NaCl: 3.0 M, based on previous research [2]. To adsorbe Cs in solution, 100 mL of the solution and 2 g of CuFeCN (L/S=50) was shaken at 120 rpm in a 250 mL polyethylene bottle. During this adsorption process, 1 mL of solution was sampled at 0, 30, 60, 90, 120, 180, 240, 300 and 360 min. and Cs concentration in solution was measured by atomic absorption spectrometry (SHIMADZU AA-6800). After this adsorption process, filtration was conducted and the filtration residue (Cs adsorbed CuFeCN) was put into desiccator for 6 days to dry the sample.

For thermal decomposition process, Cs adsorbed CuFeCN was heated at 380°C for 2 hours in a furnace with air flow of 1.6 L/min to thermal decompose. This step aims to decompose Cs adsorbed CuFeCN into cesium carbonate and cesium nitrate. In order to confirm the decomposition was successful or not, leaching test (L/S=10, 200rpm for 6hours) was conducted.

2.2 Solidification of thermal decomposition products with cement/geopolymer

For cement solidification, blast furnace cement type-B was used. The cement and water was mixed in a ratio of 1:0.6 (W/C=0.6). After cement paste was made, thermal decomposition residue was added. The ratio of cement, water and the residue was set at 1:0.6:0.3.

After thoroughly mixing, the mixture was poured into the mold (PVC tube 2cm in diameter, 4cm in height) and workability was confirmed by measuring the diameter of paste after pulling the mold. The cement solidified body was cured in a moist environment for 7 days at room temperature.

As for geopolymer solidification, firstly, 15.04g sodium silicate, 3.85g sodium hydroxide, 10.29g water and 20.82g metakaolin (SOBUECLAY SF-8) were mixed to prepare geopolymer paste. After geopolymer paste was prepared, thermal decomposition residue was added. The ratio of geopolymer and the residue was set to 1:0.65. After thoroughly mixing, the mixture was poured into the mold (PVC tube 2cm in diameter, 4cm in height) and confirmed workability by the method mentioned above. The solidified body was cured in a moist environment for 7 days at room temperature.

2.3 Long-term stirring leaching test

According to ANSI/ANS-16.1-2019, long term leaching characteristics of Cs from solidified body were evaluated. The ratio of the leachant volume to the specimen geometric surface area should be $V_L / S_A = 10 \pm 0.2$(cm) [3]. Here, V_L is the volume (cm^3) of the leachant required for each test interval and S_A is the geometric surface area (cm^2)of the specimen.

Distilled water was used as leachant. Leachant was replaced at 0.25, 1, 3, 5, 7 days and every week after 7 days. After filtration, Cs concentration in solution was measured by Graphite Furnace Atomic Absorption Spectrometry (HITACHI ZA3700).

3. RESULTS

Figure 1 shows Cs concentration during adsorption experiment. The adsorption rate becomes slowly after 240 mins, and the adsorbed Cs in CuFeCN at 240 mins is 71.87 gCs/kg-CuFeCN, which is comparable value to what reported [2].

Table 1 shows Cs leaching ratio from thermal decomposition residue obtained from three different thermal decomposition conditions. In the second experiment and third experiment, the duration is doubled, but the leaching ratio of Cs increases only 5%. This means that there are some Cs still remaining in CuFeCN without transformed to cesium carbonate and cesium nitrate at the end of thermal decomposition.

Figure 2 shows Cs leaching amount in long-term stirring leaching test. At the first 6 hours, the leaching amount of Cs is the largest for both solidified bodies. For the geopolymer solidified body, the leaching amount is initially high but decreases drastically during 7 days, and it becomes quite low after 14 days. For cement solidified body, the leaching amount fluctuates, but it becomes higher than geopolymer solidified body after 7days. Leaching amount of geopolymer solidified body is higher than leaching amount of cement solidified body initially. This is because that the addition of thermal decomposition residue in geopolymer solidified body is much higher than the addition to the cement solidified body. Cs content in geopolymer solidified body is 38.57 gCs/kg, and Cs content of cement solidified body is 15.03 gCs/kg. Cs residual ratio was calculated based on leaching amount and plotted in Fig.3. Cs in geopolymer solidified body leaches out 26.9% into leachant, and Cs in cement solidified body leaches out 35.1% into leachant within 30 days. Compared with cement solidified bodies, geopolymer solidified body has a lower leaching ratio, and few Cs leached out after 14 days. On the other hand, Cs in cement solidified body is still released after 28 days.

4. CONCLUSION

This study aims to find solidified body suitable for final disposal. At present, geopolymer solidification shows better results. However, still approximately 27% of Cs leached out within 30 days. The leaching efficiency of geopolymer depends on combination of each material and curing temperature. Perhaps, changing these parameters will result in much better Cs capturing efficiency

REFERENCES

[1] Ministry of the environment, Radioactive Contaminated Waste Processing Information Site, http://josen.env.go.jp/en/storage/

[2] T Ichikawa, K Yamada, R Iwai, Y Kanazawa, Ion Chromatographic Decontamination of 137Cs-enriched Fly Ash Using Poly (vinyl alcohol)-bound Copper Ferrocyanide as Cs Adsorbent, J. Society for Remediation of Radioactive Contamination in the Environment, 8 (2), 55-66 (2020).

[3] ANSI/ANS-16.1-2019: Measurement of the Leachability of Solidified Low-Level Radioactive Wastes by a Short-Term Test Procedure, American Nuclear Society.

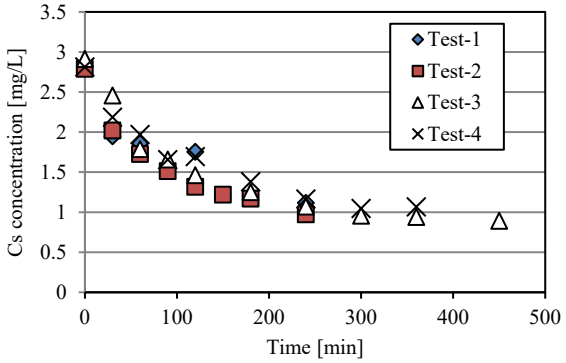

Figure 1 Change of Cs concentration with time during adsorption experiment

Table 1 Leaching ratio of Cs from thermal decomposition residue

Preset temperature	360°C	380°C	380°C
Process duration	0.5hr	1 hr	2hr
Leaching ratio	61%	82%	87%

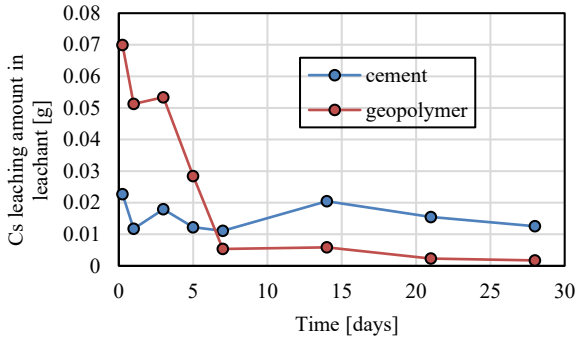

Figure 2 Leaching amount of Cs in long-term stirring leaching test

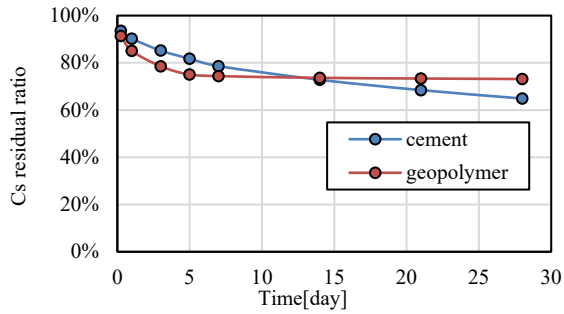

Figure 3 Cs residual ratio during long-term leaching test

Study on treatment and disposal technology of leachate concentrate in Qingdao, China

Huawei Wang [1], Ya-nan Wang [1*], Youxian Fu[2] and Yingjie Sun[1*]

1 School of Environmental and Municipal Engineering, Qingdao University of Technology, Qingdao, China;

2 Qingdao Jieyuan Environment Co. Ltd., Qingdao, China.

Abstract

Landfill leachate reverse osmosis concentrate (LLROC) contains a high amount of refractory organics,antibiotics and antibiotic resistance genes (ARGs), and the improper disposal of LLROC would pose a potential threat to local ecological environment. In this study, a granular activated carbon-catalyzed ozone (GAC/O_3) system was used to simultaneous degrade multiple emerging contaminants from LLROC. The removal efficiency of refractory organics during GAC/O_3 system were optimal when 4 g/L of GAC, 80 mg/min of O_3, and initial pH of 7.65, and 55.7% of COD and 77.3% of UV_{254} were degraded within 30 min reaction. At the optimal conditions, the degradation efficiencies of ofloxacin, enoxacin, azithromycin, and tetracycline were 95.7%, 83.6%, 98.5%, and 100.0%, respectively. Moreover, approximate 80-100% of typical ARGs, including *erm35*, *ermB*, *tetL*, and *dfrA1*, were effectively removed. Hydroxyl radicals ($HO^{\cdot}$) was the dominant reactive oxygen species during GAC/O_3 process, which played an important role in degrading refractory organics and antibiotics and inactivation ARGs. This finding suggests that GAC/O_3 system is a promising technique for cleaning of multiple emerging contaminants from LLROC.

1. Introduction

Antibiotics have been widely used in health care and agricultural industries to treat and prevent human and animal diseases (Shao et al., 2021). It is estimated that the antibiotic annual generation was more than 210,000 tons in China, of which approximately 85% was used for medical care and agriculture (Liu et al., 2017). However, excessive and inappropriate use of antibiotics can induce the spread and transmission of antibiotic resistance genes (ARGs) in diverse environmental matrices (Zhang et al., 2015). It is a global puzzle and hot spot for the contaminations of antibiotics and ARGs. Municipal solid waste (MSW) landfills are important reservoirs of organics, antibiotics and ARGs (Zhang et al., 2022). During landfill, organics, antibiotics and developed ARGs transfer to the leachate. It is inevitable that high concentrations of organics, antibiotics and ARGs have been found in leachate (Chen et al., 2017; You et al., 2018). Sui et al. (2017) reported that fourteen out of eighteen micropollutants were detectable, and their concentrations ranging from 0.39 to 349 μg/L in the landfill leachates. Therefore, stringent control of macro and micro- pollutants in landfill leachate is of critical importance because these contaminants pose severe impact to the environment.

In China, leachate is primarily treated using the "pretreatment-biological treatment-advanced treatment" process. Membrane separation advanced treatment processes, including nanofiltration (NF) and reverse osmosis (RO), are widely used in leachate treatment plants with different treatment scales (Zhang et al., 2020). This method can meet the effluent quality requirements of leachate, but approximately 30% to 45% of concentrate is generated in membrane separation systems (Chen et al., 2021). Landfill leachate RO concentrate (LLROC) harbors many diverse contaminants (i.e., refractory organics, inorganic salts and toxic metals) (Liu et al., 2022). Much research has been conducted on the transformation and degradation of refractory organics during treatment and disposal processes, but few studies have attempted to focus on the coexistence of emerging contaminants such as antibiotics and ARGs (Wang et al., 2021a). For example, Zhao et al. (2018) investigated that 526 ARG subtypes belonging to 21 ARG types were detected in landfill leachate. Wang et al. (2021a) also confirmed that antibiotics and ARGs were excessively accumulated in LLROC. However, the improper disposal of concentrate can lead to the release of multiple contaminants into the environment, causing the spread of antibiotic resistance, which could eventually pose a threat to the local ecosystem and human health. Therefore, the simultaneous removal of these macro and micro-pollutants from LLROC is urgent.

Ozone (O_3) catalytic oxidation technology has been widely investigated for the degradation of refractory organics in LLROC (Wang et al., 2016; 2017a). The O_3 molecule has a strong oxidant redox potential (E_0 = 2.08 V), and directly oxidizes and degrades the molecular structure of refractory organics into lower molecular weight organics (Kurniawan et al., 2006). In addition, catalytic ozonation can promote O_3 decomposition to generate non-selective oxidant, hydroxyl radicals ($HO^{\bullet}$) that enhance the degradation of organic pollutants (Wang et al., 2020). Granular activated carbon (GAC) catalytic ozonation (GAC/O_3) has attracted much attention owing to its high efficiency, easy operation, and simple process. Currently, GAC/O_3 process are commonly used to remove refractory organics from wastewater (He et al., 2017; Nabavi et al., 2022; Vatankhah et al., 2019). Liu et al. (2020) investigated the treatment of refractory organic matters from coal gasification wastewater during GAC/O_3 process, and their experimental results found that the removal efficiency of the total organic carbon (TOC) was 60.1% when the O_3 and the GAC dosages were 30 mg/min and 1.5 g/L, respectively. However, the effectiveness and fundamental reaction mechanisms of GAC/O_3 for antibiotics degradation and the inactivation of ARGs in LLROC is relatively scarce. Moreover, due to the complex composition and characteristics of LLROC, few studies have been conducted on the simultaneous removal of macro and micro- contaminants from LLROC, and more studies are needed to focused on the issue.

In this study, a GAC/O_3 process is used to degrade refractory organics, antibiotics, and ARGs from LLROC. The effects of GAC dosage, ozone concentration and initial pH on the removal of organics and their performance were evaluated and optimized by batch experiments. The degradation of thirty antibiotics, the inactivation of twenty species of ARGs were investigated. To evaluate the fundamental reaction mechanisms of emerging contaminants, electron paramagnetic resonance (EPR) were used to identify the contribution of reactive species during GAC/O_3 process. Additionally, the changes of the number of total bacteria and microbial diversity and community were determined by qPCR. This study provides an experimental basis for the degradation of refractory organics, antibiotics, and ARGs in wastewater. The knowledge acquired from this study is crucial for improving the treatment of multiple emerging contaminants from LLROC. This type of information also can guide the design of full-scale treatment of landfill leachate.

2. Materials and methods

2.1 Materials

The LLROC samples were collected from a landfill leachate treatment plant in Qingdao City, China (Wang et al., 2016). The physicochemical characteristics of the LLROC were the following: pH, 7.68±0.02; chemical oxygen demand (COD), 1680±52 mg/L; biological oxygen demand (BOD_5), 305±24 mg/L; BOD_5/COD, 0.18; UV-radiation at 254 nm (UV_{254}), 12.87±0.45 cm^{-1}; and color (CN), 0.84±0.005 cm^{-1}. Approximately 50 L of the LLROC samples were collected on October 20, 2021 and stored at 4°C for further experimental study.

Granular activated carbon (~3 mm) was purchased from the Sangon Biotech (Shanghai) Co., Ltd. The mixed external standard of sulfonamides, quinolones, tetracyclines, macrolides, and the internal standards of sulfa methoxy pyridazine and ciprofloxacin-D8 were purchased from Sigma Aldrich, USA. The methanol, acetonitrile, and formic acid were chromatographically pure.

2.2 Experimental design

The ozonation experimental device included a pure oxygen cylinder, an ozone generator (CF-G-3-10G), a gas flow meter (LZB-4WB), a 2-L reactor (with aeration by a microporous zeolite at the bottom), and a tail gas absorption bottle (0.1 mol/L KI solution). The pure oxygen flow rate was controlled by adjusting the stabilizer valve, and the inlet gas flow rate was controlled by changing the ozone generator current. Briefly, 1 L of the LLROC sample and desired dosage of GAC and O_3 were added to the reactor. To determine the effect of GAC dosage (1-4 g/L), O_3 concentration (20-100 mg/min) and pH (3-11) on the removal of organics (COD, UV_{254} and CN), three groups of single factor tests were conducted to obtain optimal operational conditions. To investigate the influence of initial pH on organic removal, pH of LLROC were adjusted using HCl and NaOH (0.1 mol/L). At different time intervals (5, 10, 15, 20, 25, and 30 min), 20 mL samples were collected. The water samples were filtered through a 0.45 μm glass fiber membrane for analysis of the water quality parameters (i.e., COD, UV_{254}, and CN) and antibiotics. All the experiments were performed in triplicate.

2.3 Analysis methods

The water quality parameters of pH, COD, BOD_5, and CN were determined according to the standard methods (APHA et al., 1998). The relative content of the aromatic compounds was characterized by the absorbance value of UV_{254}. The characteristics of the fluorescent materials before and after the GAC/O_3 treatment were determined using a three-dimensional fluorescence spectrometer (HORIBA Scientific-Aqualog, USA). The distribution of the molecular weight of organics before and after GAC/O_3 process were detected using a liquid chromatography spectrometer (LC-20AD, Shimadzu, Japan) equipped with a gel column (TSK G4000SW, Tosoh, Japan) and a RID-10A differential refraction detector (Wang et al., 2017b). The generation of free radicals in GAC/O_3 system were detected according to the methods reported

in our previous work (Wang et al., 2021b). The concentration of low molecular weight organic acid was detected by a gas chromatograph (GC9790 plus, Fuli instruments, China).

The concentrations of 30 antibiotics in the LLROC samples before and after the GAC/O_3 process were determined using solid phase extraction (SPE) purification combined with a high performance liquid chromatography equipped with mass spectrometry (HPLC/MS/MS) (Wang et al., 2021a).

The target antibiotics in the LLROC samples were extracted using well-developed SPE protocols. Briefly, 1000 mL of LLROC samples was firstly passed through a pre-conditioned SPE cartridge with a flow rate of 3 mL/min. The SPE cartridges were orderly pre-activated with 6 mL methanol, 6 mL ultrapure water, and 6 mL of a 2 g/L Na_2EDTA solution. The extracts were eluted with 4 mL of a 0.1% formic acid solution and 4 mL of a 3% ammonia water solution. The eluates were blown to near dryness using N_2 gas and reconstituted to 1 mL with methanol for quantification.

The target antibiotics were separated and quantified by using HPLC/MS/MS coupled with a C18 column (Wang et al., 2021a). The mobile phase was 0.1% formic acid and acetonitrile. The target content was quantified using the internal standard method. Quantification of the antibiotics was conducted with a positive ESI mode. The detection and analysis was performed by the selected reaction monitoring mode (MRM). Under the optimized detection conditions, the recoveries ranged from 54.30% to 124.70%. The target concentration was used as the instrumental detection limit at a signal-to-noise ratio ≥3. The detection limit of this method was 0.80–2 ng/L.

3. Results and discussion

3.1 Degradation performance of refractory organics

In order to determine if the GAC/O_3 process was useful in the removal of organics from LLROC, GAC and O_3 were separately applied to treat LLROC, and then their combination experiment. As seen from **Fig. 1a-c**, approximately 20% COD, UV_{254} and CN was removed by GAC within 30 min, and 43.7% of COD and 68.6% of UV_{254} were removed during only O_3 process. However, the removal efficiency of organics in the GAC/O_3 system significantly improved with the combination of GAC and O_3. After 5 min of reaction, the removal efficiencies of COD, UV_{254}, and CN were 32.2%, 55.6%, and 82.2%, respectively, during GAC/O_3 process. With an extension of the reaction time to 30 min, the removal efficiencies of COD, UV_{254}, and CN increased to 55.7%, 77.3%, and 95.5%. In addition, pseudo first-order and zero-order kinetics models were used to analyze the removal kinetics (Jiang et al., 2018). The degradation kinetics of COD and UV_{254} in GAC/O_3 process fitted better with the pseudo first-order model (R^2=0.96-0.99). The rate constant k_0 of COD and UV_{254} removal were 0.016 min^{-1} and 0.03 min^{-1}, respectively. Compared to the results reported by Wang et al. (2016), GAC/O_3 was considered to be a more effective method for organics removal.

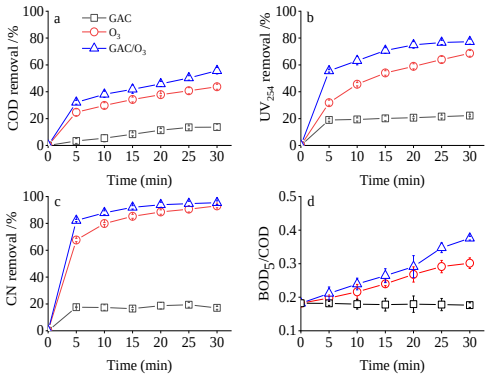

Fig. 1 The removal of organics by GAC, O_3 and GAC/O_3 process: (a)COD; (b)UV_{254}; (c)CN; (d) biodegradability.

Moreover, the GAC/O_3 system had a better influence on improving the biodegradability of the LLROC (**Fig. 1d**). After 30 min of reaction, the value of BOD_5/COD ratio was 0.38 in the GAC/O_3 system, which was higher than of the single GAC (0.17) or O_3 (0.28). These results suggested that the GAC/O_3 system performed better to remove organics in comparison with those of GAC or O_3 alone. In the GAC/O_3 system, the O_3 molecules could directly participate in the oxidation reaction, converting humic substances into low molecular weight organics; meanwhile, GAC can catalyze O_3 to generate $HO^{\cdot}$ to enhance the degradation of organics, improving the degradation of refractory organics in LLROC (Gümüş et al., 2017).

In order to obtain the optimal amount for organic degradation, varying dosage of GAC were tested (**Fig. 2**). Enhanced removal of COD, UV_{254} and CN and the increase of rate constant were observed with the increasing of GAC dosage from 1 g/L to 8 g/L (**Fig. 2a**). However, the removal efficiency and reaction rate of organics were without significant increase when GAC dosage exceeded 4 g/L. Therefore, considering the removal effect and operational cost, 4 g/L of GAC was used for the following studies. In addition, the effect of O_3 dosage on the degradation of organics was investigated during GAC/O_3 process (**Fig. 2b**). The removal efficiencies of COD, UV_{254}, and CN increased with an increasing dosage of O_3. The removal efficiencies of COD, UV_{254}, and CN were 36.3%, 40.2%, and 66.7%, respectively, when O_3 dosage was 20 mg/min within 10 min, and their values reached 42.1%, 63.2%, and 87.9%, respectively, when the O_3 dosage increased to 80 mg/min. However, the removal efficiencies of COD, UV_{254}, and CN increased slightly at high O_3 dosage (100 mg/min). A high dosage of O_3 could cause the emission of O_3 out of the reactor rather than participated in the reaction. Meanwhile, excess O_3 could contribute the generation of $HO^{\cdot}$, which would

result in the accumulation of intermediates such as alcohols and carboxylic acids (Jiang et al., 2019), and thus restricted the degradation of intermediates to CO_2 (Ghuge and Saroha, 2018). Therefore, 80 mg/min of O_3 was used for the following studies.

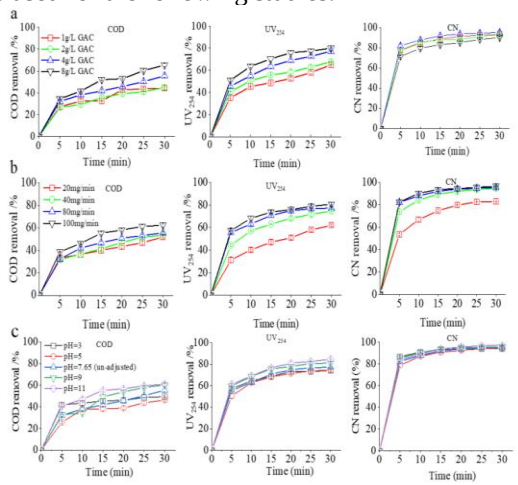

Fig. 2 Effect of GAC dosage (a), O_3 dosage (b), and initial pH (c) on the removal of organics during GAC/O_3 process.

Initial pH of the reaction system is another important factor known to influence the generation of free radicals during GAC/O_3 process. Therefore, the effect of initial pH on the removal of organics in LLROC was performed (**Fig. 2c**). The removal of COD was elevated with increasing of initial pH from 3.0 to 11, and 55.7% of COD and 77.3% of UV_{254} were decomposed during GAC/O_3 process with initial pH of 7.65 (un-adjusted LLROC). The removal efficiencies of COD and UV_{254} increased to 61.0% and 97.4% when the initial pH increased to 11. However, the high pH would lead to the accumulation of high concentrations of OH^-, reducing the concentrations of $HO^{\cdot}$, which resulted in the decrease of organics degradation (Ratpukdi et al., 2010). In addition, due to the presence of high concentrations of Ca^{2+} and Mg^{2+} ions in leachate, it would lead to the generation of $Ca(OH)_2$ and $Mg(OH)_2$ precipitates when the pH was 11. These precipitates inhibited the production of $HO^{\cdot}$ (Jiang et al., 2019). Additionally, the adjusting of pH before LLROC treatment would increase the operational cost. Therefore, an optimal initial pH was 7.65, suggesting that LLROC can be treated directly by GAC/O_3 system.

Taking the efficiency into consideration, the optimum reaction conditions were observed at GAC dosage of 4 g/L, O_3 dosage of 80 mg/min, initial pH of 7.65 in GAC/O_3 system. In addition, some representative techniques for membrane concentrate treatment were shown. It can be confirmed that the GAC/O_3 system was better than the corresponding results reported previously such as O_3 and H_2O_2/O_3. Additionally, the energy consumption and cost were calculated. The calculated energy consumption of GAC/O_3 process was 57.6 kW•h/kg COD with a cost of 7.83 US $/ kg COD, which was economically feasible.

3.2 Degradation of antibiotics during GAC/O3 process

The removal of antibiotics in LLROC by GAC/O_3 was also investigated (**Fig. 3a, b**). It can be seen that the antibiotics in the LLROC samples were primarily quinolones, macrolides, and tetracyclines, while sulfonamides were below the detection limit. The concentrations of ofloxacin, enrofloxacin, and azithromycin were as high as 12416 ng/L, 14591 ng/L, and 13664 ng/L, respectively. These antibiotics are commonly drugs that used to control gram-negative and gram-positive bacterial infections (Myers et al., 2021) and were detected in landfill leachate. You et al. (2018) found that the landfill leachate in Shanghai contained high concentrations of ofloxacin, as high as 23266 ng/L. He et al. (2021) reported that the landfill leachate contained high concentrations of erythromycin, ciprofloxacin, and enrofloxacin, with the concentrations ranging from 8510-252824 ng/L, 0-434740 ng/L, and 0-9074 ng/L, respectively.

The antibiotic concentrations after treatment decreased significantly, indicating that the GAC/O_3 system was effective for antibiotic removal (**Fig. 3b**). The concentrations of ofloxacin, enoxacin, and azithromycin decreased to 528 ng/L, 2391 ng/L, and 208 ng/L, and their removal efficiencies were 95.7%, 83.6%, and 98.5%, respectively, after treated by GAC/O_3. Meanwhile, the removal efficiencies of sarafloxacin, enrofloxacin, and tilmicosin were 86.9%, 100.0%, and 97.5%, respectively. Additionally, the GAC/O_3 system also had a high efficiency for the degradation of tetracyclines. The concentrations of tetracycline, methotrexate, and doxycycline decreased from 101 ng/L, 183 ng/L, and 204 ng/L to 0 ng/L, 78.5 ng/L, and 51 ng/L, respectively, and the removal efficiencies were 100.0%, 55.5%, and 60.0%, respectively. To further prove the removal mechanisms of antibiotics, additional GAC adsorption and ozonation experiments were conducted (data not shown). The results showed that only a small amount of antibiotics were removed by GAC adsorption, which indicated that the antibiotics in LLROC were degraded effectively by the direct oxidation by O_3 and the generation of $HO^{\cdot}$ free radicals. These results were consistent with previous studies (Yang et al., 2021). Wang et al. (2019) also reported that ofloxacin, methoxyprim, miconazole, norfloxacin, and ciprofloxacin from synthetic wastewater were completely removed by ozonation.

3.3 Inactivation of ARGs during GAC/O_3 process

Some previous studies have indicated that the relative abundance of ARGs is closely related to the presence of the antibiotic and antibiotic-resistant bacteria (Li et al., 2019; Sun et al., 2019; Zhang et al., 2018). However, recent studies showed that even though the

antibiotic-resistant bacteria died, the exposed DNA carrying the ARGs still existed for a long time period (Forsberg et al., 2014). Therefore, the degradation and inactivation of ARGs from LLROC by GAC/O_3 also determined. As shown in **Fig. 3c**, six major ARGs, including macrolides, aminoglycosides, chloramphenicols, sulfonamides, trimethoprims, and tetracyclines, were detected, but their relative abundances varied greatly. The abundances of sulfonamides and aminoglycosides ARGs were high in the LLROC, followed by macrolides, chloramphenicols, tetracyclines, and trimethoprims ARGs. Although the concentrations of sulfonamides were not detected in the LLROC, the relative abundances of the *sul1* and *sul2* genes were as a high as 3.83×10^{-2} and 3.71×10^{-2} copies/16S rRNA copies, respectively. Yi et al. (2017) also observed high relative abundances of the *sul1* and *sul2* genes in landfill leachate.

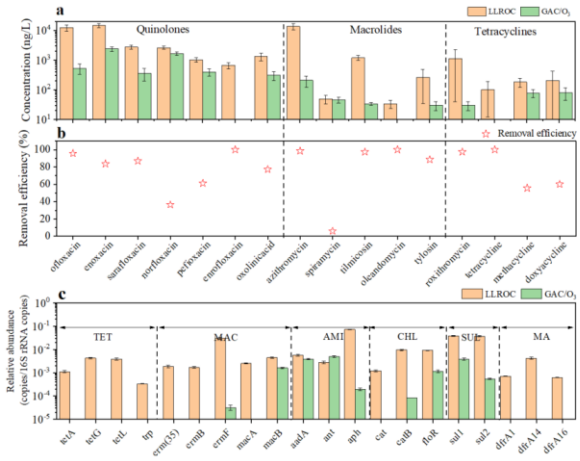

Fig. 3 The concentrations (a) and removal efficiency (b) of antibiotics and the changes in the relative abundance of typical ARGs (c) during GAC/O_3 process. The acronym of TET, MAC, AMI, CHL, SUL and MA represent Tetracyclines, Macrolides, Aminoglycosides, Chloramphenicol, Sulfonamides and Methoxybenzyl aminopyrimidine.

The most ARGs significantly degraded after GAC/O_3 treatment (**Fig. 3c**). The abundances of the *tetA*, *tetG*, *tetL*, and *trp* genes in the tetracyclines and the dfrA1, dfrA14, and dfrA16 genes in the trimethoprims were below the detection limit. The relative abundances of the *ermF* and *macB* genes in the macrolides decreased from 3.01×10^{-2} and 4.45×10^{-3} copies/16S rRNA copies, respectively, to 3.20×10^{-5} and 1.62×10^{-3} copies/16S rRNA copies, respectively, and the other macrolide ARGs (i.e., *erm35*, *ermB*, and *macA* genes) were below the detection limit. The relative abundances of the *cat*, *catB*, and *floR* genes in the chloramphenicols decreased from 1.21×10^{-3}, 9.54×10^{-3}, and 9.03×10^{-3} copies/16S rRNA copies, respectively, to 0, 8.36×10^{-5}, and 1.14×10^{-3} copies/16S rRNA copies, respectively, corresponding to the removal efficiencies of the ARGs of 100.0%, 99.1%, and 87.4%, respectively. The relative abundances of the *sul1* and *sul2* genes in the sulfonamides decreased to 3.86×10^{-3} and 5.47×10^{-4} copies/16S rRNA copies, respectively, and their removal efficiencies were 89.9% and 98.5%, respectively. These results indicated that the major ARGs in LLROC were degraded simultaneously during GAC/O_3 process. The inactivation of ARGs during GAC/O_3 system was mainly owing to direct and indirect oxidation by the generated HO$^{\bullet}$ radicals (Li et al., 2022).

In addition, some ARGs, such as *aadA*, *ant* and *sul*1, with high relative abundance were observed after GAC/O_3 treatment. It might be attributed to that during GAC/O_3 process, the ARGs-carrying bacteria lose membrane integrity and release cytoplasmic contents, resulting in DNA leakage. These free DNA still contains ARGs, which would be resulted in the continuous spread of ARGs to environment (Ahmed et al., 2022; Zhuang et al., 2015). Additionally, although the bacteria are killed, ARGs may still remain independent of the cell, it will enter other cells to show resistance again under specific conditions (Dodd, 2012).

3.4 Removal of total bacteria and changes of bacterial community

The number of the total bacteria and its removal efficiency during GAC/O_3 process were examined. The total bacteria decreased from 6.95-log copies/ml in raw LLROC to 6.61-log copies/ml after GAC/O_3 treatment. The removal efficiency of GAC/O_3 toward total bacteria was 52.8%, which was significantly higher than that in single O_3 system (41.4%). The higher inactivation efficiency of GAC/O_3 system might be due to direct oxidation by generated HO$^{\bullet}$ free radicals. It was worth noting that GAC/O_3 can only kill some of the bacteria but it cannot completely removal them from LLROC. This was related to the mechanism of ozonation killing bacteria. The mechanism of ozonation destroy bacteria is based on its ability to invade the cell membrane, causing cell distortion and death, but a large amount of free DNA still exists in the reaction system with high relative abundance (Ahmed et al., 2022; Dodd, 2012). Moreover, the generation of HO$^{\bullet}$ free radicals was insufficient to completely degrade these bacteria, due to the coexistence of refractory organics and antibiotics that can consume reactive species (Wang et al., 2020).

Moreover, the changes in the microbial diversity in the LLROC during GAC/O_3 treatment are determined. The ACE and Chao1 estimators, reflected the bacterial community richness, were lower in GAC/O_3 system (487344 and 516869, respectively) than those in the untreated LLROC (1066440 and 1052117, respectively). The Shannon and InvSimpson indices reflect the microbial community diversity. The Shannon and InvSimpson values in GAC/O_3 treated samples (8.99

and 3816, respectively) were significantly lower than the values in untreated LLROC (12.57 and 72695, respectively). The changes of these indices indicated that the abundance and diversity of bacteria decreased after treatment.

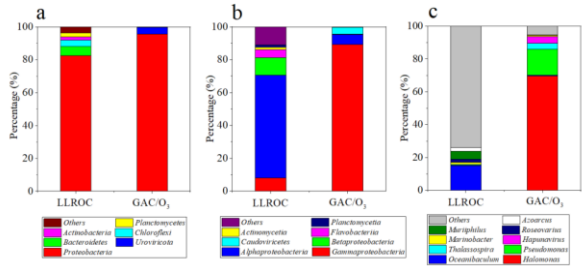

Fig. 4 Changes of microbial community structure after GAC/O_3 treatment at levels of phylum (a), class (b) and genus (c).

The changes of bacterial community after GAC/O_3 treatment were investigated. At the phylum level (**Fig. 4a**), the raw LLROC was predominated by the Proteobacteria with a relative content of 82.4%, followed by Bacteroidetes with a relative content of 5.7%, and the proportion of both accounted for 88.1% of the total bacterial abundance. After treatment, the relative abundance of Proteobacteria and Uroviricota increased to 95.5% and 4.2%, respectively, while the relative abundance of Bacteroidetes, Chloroflexi, Actinobacteria, and Planctomycetes decreased significantly. These results indicated that the GAC/O_3 process can affect the bacterial community, but the dominant phylum of Proteobacteria changed slightly.

At the class level (**Fig. 4b**), the relative content of Gammaproteobacteria and Caudoviricetes increased from 8.0% and 0.07% to 89.2% and 4.2%, respectively, during GAC/O_3 process. On the contrary, the relative abundance of Alphaproteobacteria, Betaproteobacteria, and Flavobacteria decreased significantly, from 62.5%, 10.7%, and 4.8% to 6.0%, 0.3%, and 0.01%, respectively. The Proteobacteria in the raw LLROC primarily included α-, β-, and γ-Proteobacteria. α-Proteobacteria was dominate in untreated LLROC, while γ-Proteobacteria was dominant after GAC/O_3 treatment. Ozonation and $HO^{\cdot}$ have strong bactericidal effect on α- and β-Proteobacteria, and γ-Proteobacteria have a strong antioxidant capacity (Baghal Asghari et al., 2021).

As shown in **Fig. 4c**, at the genus level, the bacterial community of the LLROC changed significantly. *Oceanibaculum* relative abundance decreased from 15.1% to 0.53% after GAC/O_3 treatment. *Halomonas* and *Pseudomonas* became the dominant species, with relative abundances of 69.6% and 15.8%, respectively, and both genera belong to the class γ-Proteobacteria. *Oceanibaculum* and *Pseudomonas* were the common ARGs hosts being found in various environments (Guo et al., 2018; Luo et al., 2021). Among them, *Oceanibaculum*, belonging to Armatimonadetes, poses the positive impacts of GAC/O_3 on the damage of microbial cells, and accounted for the subsequent efficient ARGs degradation. However, the genus of *Pseudomonas*, which was found to commonly carrying multiple ARGs (i.e., *sul*1 and *cml*A) were more resistant to the GAC/O_3 system, leading to the relatively low removal efficiency of ARGs. Additionally, the dominant bacteria *Halomonas* was moderately halotolerant microorganism. The relative abundance of halophilic bacteria remained a large proportion at the genus level in treated LLROC, and this was primarily attributed to their specific salt tolerance mechanisms (Fathepure et al., 2014; Garcia et al., 2004).

3.5 Degradation mechanism during GAC/O_3 process

The GAC/O_3 system exhibited significant improvement for the degradation of refractory organics, antibiotics and ARGs. To clarify the degradation mechanism during GAC/O_3 process, the products and free radicals were identified.

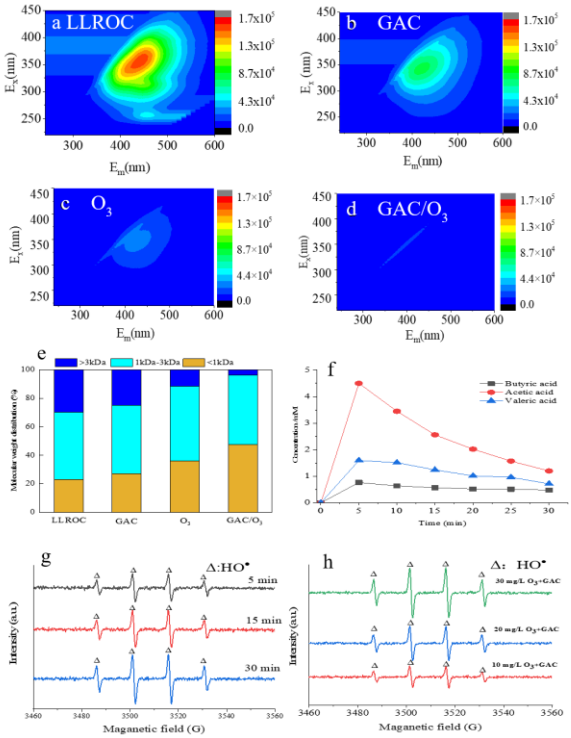

Fig. 5 3D EEM spectra (a-d), molecular weight distribution (e), concentrations of low molecular weight organic acid (f) and EPR spectra of free (g, h) during GAC/O_3 process.

Humic and fulvic substances were detected as the predominated refractory organics in LLROC (Wang et al., 2016). 3D EEM spectra were used to investigate the degradation of refractory matters. As seen from **Fig. 5a**, an intense fluorescence peak located at Ex/Em 340/419 nm was observed, which was associated with a fulvic-like substance (Wu et al., 2003). Similar results with high concentrations of fulvic constituents were

also observed in our previous study (Wang et al., 2020). The fluorescence intensity of the fulvic-like substance decreased significantly. The fluorescence intensity of the characteristic peak decreased 40.2% and 85.5% in GAC and O_3 effluent within 60 min, respectively. However, its peak disappeared after GAC/O_3 treatment (98.8%), indicating that ozonation and free radicals were effectively in the degradation of fulvic substances. Our previous studies indicated that humic substances in concentrates were rapidly degraded and converted to hydrophilic fraction during the ozonation process (Wang et al., 2016, 2017b, 2021b). These results confirmed that refractory organics were degraded during GAC/O_3 process, which was also supported by the results of batch experiments.

To further characterize the generation of intermediates during GAC/O_3 process, the molecular weight distribution of organics was monitored (**Fig. 5b**). The molecular weight proportions of >3 kDa, 1–3 kDa, and <1 kDa in the LLROC were accounted for 30.5%, 47.0%, and 22.5%, respectively. After treatment with GAC/O_3 process for 30 min, the proportion of >3 kDa decreased to 2.4%, while the proportion of <1 kDa increased to 47.2%. This result indicated that refractory organics with high molecular weight converted to compounds with a low molecular weight during GAC/O_3 process. These results were consistent with the previous studies (Chen et al., 2019; Jin et al., 2016). Wang et al. (2016) found that ozonation treatment effectively degraded and converted humic substances into small molecular organics, and the proportion of < 1 kDa increased from 1.1% to 69.5%. In addition, the GAC/O_3 system performed better than single O_3 treatment, which was mainly attributed to the generation of $HO^{\cdot}$ free radicals, contributing to the improvement of organic degradation.

The generation of low molecular weight organic acid during GAC/O_3 process was also investigated. As shown in **Fig. 5c**, high concentrations of low molecular weight organic acid were observed in GAC/O_3 treated samples, but these matters were detected in raw LLROC. In the initial 5 min reaction, the concentrations of acetic acid, butyric acid, and valeric acid were 4.5, 0.77 and 1.59 mM, respectively, and their concentrations decreased to 1.20, 0.48 and 0.72 mM, respectively, at the end of this experiment. This further indicated that refractory organics and antibiotics in LLROC were effectively degraded into organic acid through ozonation and $HO^{\cdot}$ during GAC/O_3 process.

The generation and conversion of free radicals during GAC/O_3 process were identified by EPR. DMPO was used as a scavenger to capture $HO^{\cdot}$ radicals. As shown in **Fig. 5d**, there was no significant signals in DMPO/O_3 system, however, the intense DMPO-OH signals were observed in GAC/O_3 system, which was corresponded to $HO^{\cdot}$ radicals. This result suggest that $HO^{\cdot}$ were the dominant reactive species for the degradation of fulvic-like substances, antibiotics and ARGs during GAC/O_3 process. The generation of radicals in GAC/O_3 system at different reaction time and O_3 concentration were also determined. DMPO-OH signals were detected with 5 min of reaction, and maintained within 30 min of reaction, which indicated contaminants was continuously degraded during GAC/O_3 process. Moreover, a high intensity of DMPO-OH signals were observed at high O_3 conditions, suggesting that the generation of $HO^{\cdot}$ increased with increasing O_3 dosage. These results were consistent with the calculated rate constant in **Fig. 1**. On the basis of the EPR tests, $HO^{\cdot}$ radical plays an important role in eliminating multiple contaminants.

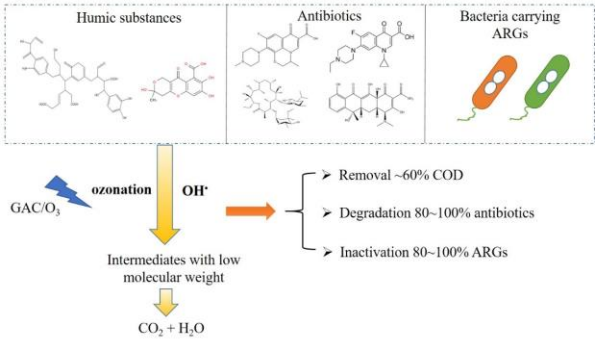

Fig. 6 Proposed degradation mechanism of contaminants in LLROC by GAC/O_3.

According to previous reports and the results of this study, the fundamental mechanisms for GAC/O_3 to degrade organics, antibiotics and ARGs were developed (**Fig. 6**). It is well known that the ozonation process of wastewater includes both direct ozonation, caused by the presence of ozone molecules, and indirect ozonation, caused by the presence of $HO^{\bullet}$ radicals. Firstly, O_3 is rapidly decomposed into the free radical of $OH^{\bullet}$ and other radicals (i.e., $\bullet O_2^-$ and $HO_2\bullet$), and $HO^{\cdot}$ is the dominant reactive oxygen species during GAC/O_3 process. Furthermore, $HO^{\cdot}$ can destroy refractory organics and antibiotics to low molecular weight intermediates, and then these intermediates can be completely mineralized (Wang et al., 2020). Moreover, $HO^{\cdot}$ can nonselectively attack the bacterial cell wall, leading to the leakage of cellular components and even cell death (Foroughi et al., 2022). Subsequently, O_3 and $HO^{\cdot}$ can continue to attack cellular components and free DNA, promoting the degradation of ARGs from LLROC (Zheng et al., 2017). Overall, the GAC/O_3 system can be used as a promising approach for the treatment of various contaminants in LLROC.

3.6 Chemical stability

Long-term reaction for the effectiveness of the catalytic ozonation was evaluated. It was clearly indicated that the GAC/O_3 process has no significant decrease on organics degradation after five cycles. In the first one

cycles, the removal efficiencies of COD and UV_{254} after 30 min of treatment were 55.7% and 77.4%, respectively. The decrease efficiency of organic degradation slightly dropped from the fourth cycle, and the fifth cycle degraded 42.7% of COD and 72.2% of UV_{254}, respectively. The decrease of reactivity might be mainly attributed to the occupancy and reduction of active sites at GAC when its five cycle reaction. Therefore, the GAC/O_3 system has good recyclability and chemical stability.

3.7 Practical implications of this study

There are few literatures on the simultaneous removal of refractory organics, antibiotics and ARGs in LLROC so far. The current study comprehensively investigated the degradation of refractory organics, antibiotics and ARGs in LLROC using GAC/O_3 process. The results confirmed that GAC/O_3 system performed well for the simultaneous removal of refractory organics, antibiotics and ARGs. It can be considered as a potential technique in removing multiple emerging contaminants from LLROC. However, the extent of removal on emerging contaminants liking ARGs need to be improved remarkably during GAC/O_3 process. So, further research need be tested after optimization operation parameters (i.e., ozone concentration, pH, temperature, etc.) in water or wastewater.

4. Conclusions

The results of batch experiments indicated that GAC/O_3 system performed well for the simultaneous removal of refractory organics, antibiotics and ARGs. The removal of refractory organics was optimal when 4 g/L of GAC, 80 mg/min of O_3, and initial pH of 7.65. The dominant antibiotics in the LLROC were ofloxacin, azithromycin, and tetracycline, of which their removal efficiencies were 95.7%, 98.5%, and 100.0%, respectively. Approximate 80-100% ARGs were removed from LLROC by GAC/O_3 system. Among ARGs, the tetracycline ARGs (*tetA*, *tetG*, *tetL*, *trp*) and trimethoprim ARGs (*dfrA1*, *dfrA14*, *dfrA16*) were completely removed. But some ARGs, such as *aadA*, *ant* and *sul*1, with high relative abundance were observed after GAC/O_3 treatment, which might be due to the consumption of $HO^{\cdot}$ by refractory organics and antibiotics. These findings highlight that GAC/O_3 is a promising technique for the removal of emerging contaminants from LLROC.

Competing Interests

The authors declare that they have no competing financial interests or personal relationships that could have appeared to influence the work reported in this paper.

References

Amaral-Silva, N., Martins, R.C., Castro-Silva, S., Quinta-Ferreira, R.M., 2016. Ozonation and perozonation on the biodegradability improvement of a landfill leachate. Journal of Environmental Chemical Engineering 4(1), 527-533.

Ahmed,Y., Zhong, J., Wang, Z., Wang, L., Yuan, Z.G., Guo, J.H., 2022. Simultaneous removal of antibiotic resistant bacteria, antibiotic resistance genes, and micropollutants by FeS_2@GO-based heterogeneous photo-Fenton process. Environmental Science and Technology DOI: 10.1021/acs.est.2c03334.

APHA, AWWA, WEF, 1998. Standard methods for the examination of water and wastewater, 20th ed. American Public Health Association, Washington, DC.

Baghal Asghari, F., Dehghani, M.H., Dehghanzadeh, R., Farajzadeh, D., Shanehbandi, D., Hossein Mahvi, A., Yaghmaeian, K., Rajabi, A., 2021. Performance evaluation of ozonation for removal of antibiotic-resistant *Escherichia coli* and *Pseudomonas aeruginosa* and genes from hospital wastewater. Scientific Reports 11, 24519.

Chen, Q.L., Li, H., Zhou, X.Y., Zhao, Y., Su, J.Q., Zhang, X., Huang, F.Y., 2017. An underappreciated hotspot of antibiotic resistance: The groundwater near the municipal solid waste landfill. Science of the Total Environment 609, 966-973.

Chen, W.M., Gu, Z.P., Ran, G., Li, Q.B., 2021. Application of membrane separation technology in the treatment of leachate in China: A review. Waste Management 121, 127-140.

Chen, W.M., Luo, Y.F., Ran, G., Li, Q.B., 2019. An investigation of refractory organics in membrane bioreactor effluent following the treatment of landfill leachate by the O_3/H_2O_2 and MW/PS processes. Waste Management 97, 1-9.

Dodd, M.C., 2012. Potential impacts of disinfection processes on elimination and deactivation of antibiotic resistance genes during water and wastewater treatment. Journal of Environmental Monitoring14, 1754-1771.

Fathepure, B.Z., 2014. Recent studies in microbial degradation of petroleum hydrocarbons in hypersaline environments. Frontiers in microbiology 5, 173.

Forsberg, K.J., Patel, S., Gibson, M.K., Lauber, C.L., Knight, R., Fierer, N., Dantas, G., 2014. Bacterial phylogeny structures soil resistomes across habitats. Nature 59, 612-616.

Foroughi, M., Khiadani, M., Kakhki, S., Kholghi, V., Naderi, K., Yektay, S., 2022. Effect of ozonation-based disinfection methods on the removal of antibiotic resistant bacteria and resistance genes (ARB/ARGs) in water and wastewater treatment: A systematic review. Science of The Total Environment 811, 151404.

Garcia, M.T., Mellado, E., Ostos, J.C., Ventosa, A., 2004. *Halomonas organivorans* sp. nov., a moderate halophile able to degrade aromatic compounds. International Journal of Systematic and Evolutionary Microbiology 54 (5), 1723-1728.

Ghuge, S.P., Saroha,A.K., 2018. Catalytic ozonation for the treatment of synthetic and industrial effluents – application of mesoporous materials: a review. Journal of Environmental Management 211, 83–102.

Guo, N., Wang, Y., Tong, T., Wang, S., 2018. The fate

of antibiotic resistance genes and their potential hosts during bio-electrochemical treatment of high-salinity pharmaceutical wastewater. Water Research, 133, 79-86.
Gümüş, D., Akbal, F., 2017. A comparative study of ozonation, iron coated zeolite catalyzed ozonation and granular activated carbon catalyzed ozonation of humic acid. Chemosphere 174, 218-231.
He, P.J., Huang, J.H., Yu, Z.F., Xu, X., Raga, R., Lü, F., 2021. Antibiotic resistancecontamination in four Italian municipal solid waste landfills sites spanning34 years. Chemosphere 266, 129182.
He, X.X., Elkouz, M., Inyang, M., Dickenson, E., Wert, E.C., 2017. Ozone regeneration of granular activated c arbon for trihalomethane control. Journal of Hazardous Materials 326, 101-109.
Jiang, F., Qiu, B., Sun, D., 2018. Advanced degradation of refractory pollutants in incineration leachate by UV/Peroxymonosulfate. Chemical Engineering Journal 349, 338-346.
Jiang, F., Qiu, B., Sun, D., 2019. Degradation of refractory organics from biologically treated incineration leachate by VUV/O_3. Chemical Engineering Journal, 370, 346-353.
Jin, P.K., Jin, X., Bjerkelund, V.A., Østerhus, S.W., Wang, X.C., Yang, L., 2016. A study on the reactivity characteristics of dissolved effluent organic matter (EfOM) from municipal wastewater treatment plant during ozonation. Water Research 88, 643-652.
Kurniawan, T.A., Lo, W.H., Chan, G., 2006. Radicals-catalyzed oxidation reactions for degradation of recalcitrant compounds from landfill leachate. Chemical Engineering Journal 125(1), 35-57.
Li, B., Qiu, Y., Song, Y.Q., Lin, H., Yin, H.B., 2019. Dissecting horizontal and vertical gene transfer of antibiotic resistance plasmid in bacterial community using microfluidics. Environment International 131, 105007.
Li, J., Ren, S., Qiu, X., Zhao, S., Wang, R., Wang, Y.K., 2022. Electroactive ultrafiltration membrane for simultaneous removal of antibiotic, antibiotic resistant bacteria, and antibiotic resistance genes from wastewater effluent. Environmental Science and Technology DOI: 10.1021/acs.est.2c00268.
Liu, H., Li, H., Qiu, L., Chen, B., Wang, H., Fang, C., Long, Y., Hu, L., 2022. The panorama of antibiotics and the related antibiotic resistance genes (ARGs) in landfill leachate. Waste Management 144, 19-28.
Liu, Z., Huang, C., Li, J., Yang, J., Qu, B., Yang, S., Cui, Y., Yan, Y., Sun, S., Wu, X., 2020. Activated carbon catalytic ozonation of reverse osmosis concentrate after coagulation pretreatment from coal gasification wastewater reclamation for zero liquid discharge. Journal of Cleaner Production 286, 124951.
Liu, S., Zhao, H., Lehmler, H.J., Cai, X., Chen, J., 2017. Antibiotic pollution in marine food webs in laizhou bay, north china: trophodynamics and human exposure implication. Environmental Science and Technology 51(4), 2392-2400.
Luo, J.Y., Huang, W., Zhang, Q., Wu, Y., Fang, F., Cao, J., Su, Y.L., 2021. Distinct effects of hypochlorite types on the reduction of antibiotic resistance genes during waste activated sludge fermentation: insights of bacterial community, cellular activity, and genetic expression. Journal of Hazardous Materials 403, 124010.
Luu, T.L., 2020. Post treatment of ICEAS-biologically landfill leachate using electrochemical oxidation with Ti/BDD and Ti/RuO_2 anodes. Environmental Technology & Innovation 20, 101099.
Moradian, F., Ramavandi, B., Jaafarzadeh, N., Kouhgardi, E., 2020. Effective treatment of high-salinity landfill leachate using ultraviolet/ultrasonication peroxymonosulfate system. Waste Management 118, 591-599.
Myers, A.G., Clark, R.B., 2021. Discovery of macrolide antibiotics effective against multi-drug resistant Gram-negative pathogens. Accounts of Chemical Research 54, 1635-1645.
Nabavi, E., Sabour, M., Dezvareh, G.A., 2022. Ozone treatment and adsorption with granular activated carbon for the removal of organic compounds from agricultural soil leachates. Journal of Cleaner Production 335, 130312.
Ratpukdi, T., Siripattanakul, S., Khan, E., 2010. Mineralization and biodegradability enhancement of natural organic matter by ozone-VUV in comparison with ozone, VUV, ozone-UV, and UV: effects of pH and ozone dose. Water Research 44, 3531-3543.
Shao, Y., Wang, Y., Yuan, Y., Xie, Y., 2021. A systematic review on antibiotics misuse in livestock and aquaculture and regulation implications in China. Science of The Total Environment 798, 149205.
Sato, Y., Zeng, Q., Meng, L., Chen, G., 2021. Importance of combined electrochemical process sequence and electrode arrangements: a lab-scale trial of real reverse osmosis landfill leachate concentrate. Water Research 192, 116849.
Sun, D.C., Jeannot, K., Xiao, Y.H., Knapp, C.W., 2019. Horizontal gene transfer mediated bacterial antibiotic resistance. Frontiers in microbiology 10, 1933.
Sui, Q., Zhao, W., Cao, X., Lu, S., Qiu, Z., Gu, X., Yu, G., 2017. Pharmaceuticals and personal care products in the leachates from a typical landfill reservoir of municipal solid waste in Shanghai, China: Occurrence and removal by a full-scale membrane bioreactor. Journal of Hazardous Materials 323, 99-108.
Ukundimana, Z., Omwene, P. I., Gengec, E., Can, O.T., Kobya, M., 2018. Electrooxidation as post treatment of ultrafiltration effluent in a landfill leachate MBR treatment plant: effects of BDD, PT and DSA anode types. Electrochimica Acta 286, 252-263.
Vatankhah, H., Riley, S.M., Murray, C., Quiñones, O., Steirer, K.X., Dickenson,E.R., Bellona, C., 2019.

Simultaneous ozone and granular activated carbon for advanced treatment of micropollutants in municipal wastewater effluent. Chemosphere 234, 845-854.
Wang, H.J., Mustafa, M., Yu, G., Östman, M., Cheng, Y., Wang, Y, J., Tysklind,M., 2019. Oxidation of emerging biocides and antibiotics in wastewater by ozonation and the electro-peroxone process. Chemosphere 235:575-585.
Wang, H.W., Wang, Y.N., Li, X.Y., Sun, Y.J., Wu, H., Chen, D.L., 2016. Removal of humic substances from reverse osmosis (RO) and nanofiltration (NF) concentrated leachate using continuously ozone generation-reaction treatment equipment. Waste Management 56, 271-279.
Wang, H.W., Li, X.Y., Hao, Z.P., Sun, Y.J., Wang, Y.N., Li, W.H., Tsang, Y., 2017b. Transformation of dissolved organic matter in concentrated leachate from nanofiltration during ozone-based oxidation processes (O_3, O_3/H_2O_2 and O_3/UV). Journal of Environmental Management 191, 244-251.
Wang, H.W., Xiao, W.S., Zhang, C., Sun, Y.J., Wang, Y.N., Gong, Z.G., Zhan, M., Fu, Y.X., Liu, K.Q. 2021b. Effective removal of refractory organic contaminants from reverse osmosis concentrated leachate using PFS-nZVI/PMS/O_3 process. Waste Management 128, 55-63.
Wang, H., Wang, Y.H., Lou, Z.Y., Zhu, N.W., Yuan, H.P., 2017a. The degradation processes of refractory substances in nanofiltration concentrated leachate using micro-ozonation. Waste Management 69, 274-280.
Wang, K., Reguyal, F., Zhuang, T., 2021a. Risk assessment and investigation of landfill leachate as a source of emerging organic contaminants to the surrounding environment: a case study of the largest landfill in Jinan City, China. Environmental Science and Pollution Research 28(15), 18368-18381.
Wang, Y. N., Wang, H.W., Wu, Y.J., Sun, Y.J., Gong, Z.G., Liu, K.Q., Tsang, Y. F., Zhan, M.L., 2020. Effective removal of contaminants from biotreated leachate by a combined Fe(III)/O_3 process: Efficiency and mechanisms. Journal of Cleaner Production 276, 123397.
Wang, Y. N., Shi, H., Wang, Q.Z., Wang, H.W., Sun, Y.J., Li, W.H., Bian, R.X., 2022a. Insights into the landfill leachate properties and bacterial structure succession resulting from the colandfilling of municipal solid waste and incineration bottom ash. Bioresource Technology 361, 127720.
Wang, Y. Q., Zhang, R., Lei, Y., Song, L.Y., 2022b. Antibiotic resistance genes in landfill leachates from seven municipal solid waste landfills: Seasonal variations, hosts, and risk assessment. Science of The Total Environment 853, 158677.
Wu, F., Evans, R., Dillon, P., 2003. Separation and characterization of NOM by high-performance liquid chromatography and on-line three-dimensional excitation emission matrix fluorescence detection. Environmental Science and Technology 37(16), 3687-3693.
Xue, W.J., Cui, Y.H., Liu, Z.Q., Yang, S.Q., Li, J.Y., Guo, X.L., 2020. Treatment of landfill leachate nanofiltration concentrate after ultrafiltration by electrochemically assisted heat activation of peroxydisulfate. Separation and Purification Technology 231: 115928.
Yang, Y.Y., Liu, Z., Demeestere, K., Hulle, S.V., 2021. Ozonation in view of micropollutant removal from biologically treated landfill leachate: Removal efficiency, • OH exposure, and surrogate-based monitoring. Chemical Engineering Journal 410, 128413.
Yi, X.Z., Tran, N.H., Yin, T.R., He, Y.L., Gin, K, Y.H., 2017. Removal of selected PPCPs, EDCs, and antibiotic resistance genes in landfill leachate by a full-scale constructed wetlands system. Water Research 121, 46-60.
You, X.X., Wu, D., Wei, H.W., Xie, B., Lu, J., 2018. Fluoroquinolones and β-lactam antibiotics and antibiotic resistance genes in autumn leachates of seven major municipal solid waste landfills in China. Environment International 113, 162-169.
Zhao, R., Feng, J., Yin, X., Liu, J., Fu, W., Berendonk, T.U., Zhang, T., Li, X., Li, B., 2018. Antibiotic resistome in landfill leachate from different cities of China deciphered by metagenomic analysis. Water Research 134, 126-139.
Zhang, J., Xiao, K., Huang, X., 2020. Full-scale MBR applications for leachate treatment in China: practical, technical, and economic features. Journal of Hazardous Materials 389, 122138.
Zhang, Q.Q., Ying, G.G., Pan, C.G., Liu, Y.S., Zhao, J.L., 2015. Comprehensive evaluation of antibiotics emission and fate in the river basins of China: source analysis, multimedia modeling, and linkage to bacterial resistance. Environmental Science and Technology 49(11): 6772-6782.
Zhang, R., Yang, S., An, Y., Wang, Y., Lei, Y., Song, L., 2022. Antibiotics and antibiotic resistance genes in landfills: A review. Science of The Total Environment 806, 150647.
Zhang, Y.P., Niu, Z.G., Zhang, Y., Zhang, K., 2018. Occurrence of intracellular and extracellular antibiotic resistance genes in coastal areas of Bohai Bay (China) and the factors affecting them. Environmental Pollution 236: 126-136.
Zheng, J., Su, C., Zhou, J.W., Xu, L.K., Qian, Y.Y., Chen, H., 2017. Effects and mechanisms of ultraviolet, chlorination, and ozone disinfection on antibiotic resistance genes in secondary effluents of municipal wastewater treatment plants. Chemical Engineering Journal 317, 309-316.

ELECTRON SHUTTLE MECHANISM AND ENVIRONMENTAL EFFECTS OF COMPOST HUMUS

Haoyu Chang[1,2,3], Xiaojie Sun[1,2,3*]

1.Guangxi Key Laboratory of Environmental Pollution Control Theory and Technology, Guilin University of Technology, Guilin 541004, China

2.Guangxi Collaborative Innovation Center for Water Pollution Control and Water Safety in Karst Area, Guilin University of Technology, Guilin 541004, China

3. Guangxi Key Laboratory of Environmental Pollution Control Theory and Technology for Science and Education Combined with Science and Technology Innovation Base, Guilin University of Technology, Guilin 541004, China

Abstract: Humus is the core product of compost, which has many functions such as adsorption of complex pollutants, mediating the redox reaction of pollutants, and improving the physical and chemical properties of soil. The soil repair process of compost products is also the soil repair process of humus in essence. The electron transfer ability of compost humus largely determines the remediation effect of compost products on contaminated soil. Therefore, promoting the formation of more highly active humus has become the main research direction to improve the quality of compost. On the basis of introducing the general situation of humus, the electron transfer ability and electron shuttle mechanism of humus are reviewed. We systematically summarized the factors affecting the electron transfer ability of humus in order to better understand the humus formation process and its electron transfer ability during composting. Environmental factors such as microbial activity, pH, temperature, light and oxygen conditions all affect electron transport in humus. In addition, the electron transfer capacity of humus in the environment is mainly reflected in the impact on heavy metals, organic pollutants and the interaction between microorganisms and pollutants.

INTRODUCTION

With the rapid development of Chinese cities, the production of organic waste is increasing. These organic wastes not only occupy a lot of land resources, but also cause serious environmental pollution and waste of resources. Therefore, it is particularly important to find effective treatment methods. Composting is one of the important ways to stabilize, harmless and resource organic waste. Under the action of microorganisms, pathogenic microorganisms and parasites are killed at high temperature, organic pollutants such as antibiotics are degraded, heavy metals are passivated, and unstable organic matter in sludge is gradually transformed into highly active humus.

Humus is the core product of compost, which contains a large number of functional groups of high active sites with electron transfer ability. These site functional groups can be used as electron shuttles to participate in the electron transport process between microorganisms and pollutants. This is essential to accelerate the reduction of high-priced toxic heavy metals and the degradation of organic pollutants in the soil. Therefore, it is particularly important to understand the principle and influencing factors of humus control of environmental pollution.

In this paper, the general situation of humus in compost, the electron transfer ability of humus, the influencing factors of electron shuttles in humus and their environmental effects were systematically reviewed. By further studying the mechanism of

humus control of pollutants, we can promote the rapid development of organic waste resource utilization and provide theoretical basis for its role in environmental pollution control.

HUMUS PROFILE

Humus, the main component of compost organic matter, is a heterogeneous organic polymer compound with complex structure and widely exists in soil, water, sediment, sludge and other environments [1]. The molecular structure of humus contains aromatic ring, heterocyclic ring and polycyclic compound, and also contains a variety of functional groups, including carboxyl group, alcohol hydroxyl group, carbonyl group, quinone group, etc., which also makes humus have many environmental functions.

Humus has the function of improving the physical, chemical and biological conditions of soil. Humus can chelate with a variety of metal cations (such as Ca^{2+} and Mg^{2+}) or form complex forms, affecting the solubility of nutrient elements and promoting the absorption of nutrient elements by plants [3]. Humus itself contains a large number of nutrient elements (such as nitrogen and phosphorus), which can increase soil nutrients. Humus can also have active adsorption, complexation and coordination reactions with heavy metals and organic pollutants in soil, thus affecting the migration, transformation and bioavailability of pollutants [4]. In addition, humus also has redox properties, which can participate in the electron transfer process between microorganisms and pollutants as an electron shuttle, thereby reducing the harm of pollutants to the environment and human health.

Generally speaking, humus can be divided into humic acid (HA), which only dissolves in alkali but does not dissolve in acid, fulvic acid (FA), and humin (HM), which does not dissolve in acid and base [5]. The first two are the main components of humus, also known as humic acid. It usually makes up about 60% of the humus. HA has a high molecular weight, usually 10 kDA-100 kDa, and a high aromatic carbon content. High molecular weight HA is easy to form insoluble complexes with heavy metals, thus passivating and fixing heavy metals in soil. FA is an organic acid with low molecular weight and relatively simple structure, which is easily degraded by microorganisms or converted into more stable humus components [6]. Compared to HA, FA has a lower molecular weight (typically between 600 and 1500 Da) and lower aromaticity, but has a higher carboxyl and phenolic content, and therefore a higher total acidity [7]. FA can also be considered as a small molecular form of HA, and FA can condense to form HA. FA with low humification degree has low molecular weight and is easy to bind to heavy metals as dissolved substances, which may improve the fluidity and bioavailability of heavy metals. However, small molecules of FA can be decomposed and utilized by microorganisms, which can improve soil fertility, provide necessary nutrients for plants, and improve soil structure and reduce soil erosion. FA with a high degree of humification can adsorb complex pollutants and can be used to repair soil polluted by heavy metals or organic pollutants [8]. HM is the most tightly bound component of humus with inorganic minerals, which is very stable in nature and difficult to biodegrade. HM has higher molecular weight and degree of polymerization, more aliphatic structure and aromaticity, and also contains carbonyl carbon, methoxy carbon and phenolic compounds [9]. However, due to the difficult extraction and purification process of HM, there is little information about HM at present, and its properties need to be further studied.

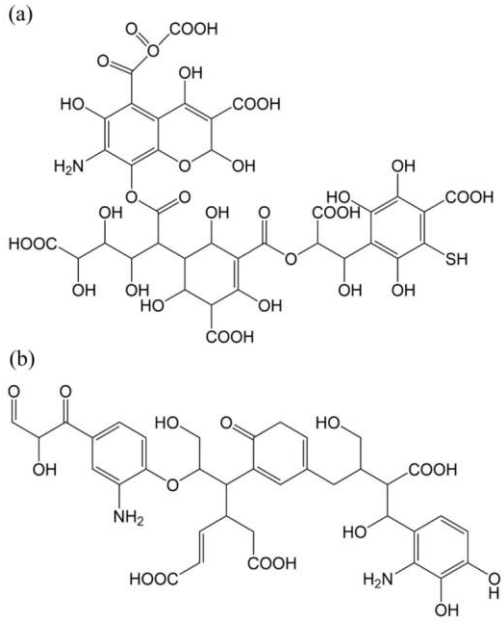

Fig. 1 The structural model of HA basic unit (a) and FA (b)

ELECTRON TRANSFER CAPACITY AND ELECTRON SHUTTLE MECHANISM OF HUMUS

Since Lovley et al. [10] found that humus can mediate extracellular electron transfer of microorganisms, the electron transfer function of humus has been gradually recognized. In an anaerobic environment, the microorganism is able to transfer electrons to humus, which is reduced, and then the humus transfers electrons to electron acceptors, which are reduced, while the humus is oxidized. This transport mechanism is called the electron shuttle mechanism. The structure and properties of humus are relatively stable and are less affected by microorganisms. After being oxidized, humus can once again act as an electron acceptor for microorganisms to continue the next round of electron transfer process [11]. In addition, humus can carry out long-distance electron transfer between microorganisms and electron acceptors, and the energy consumption in the process of electron transfer is less. Moreover, there are more types of microorganisms that can use humus for electron transfer and their distribution is wide, which is an advantage that other extracellular electron transfer mechanisms (such as direct contact mechanism and electrokinetic mechanism, etc.) do not have [12]. Because of this, electron shuttles represented by humus have become the focus of research in recent years.

Electron transfer capacities (ETC) is an important index reflecting the Electron transfer process of humus, which can be divided into Electron-accepting capacities (ETC). EAC) and electron-donating capacities (EDC), where EAC and EDC are humus as Electron acceptors and electron donors, respectively, the number of electrons received or given by organic carbon per unit mass. EAC and EDC can quantify the oxidation and reduction capacity of humus respectively, and the ability of humus to accept and supply electrons sustainably and stably can be expressed by Electron recycling rate (ERR).

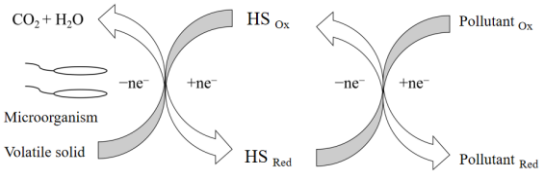

Fig.2 Electron transport mechanism of humic substances

Traditionally, chemical and microbial methods are used to measure the electron transfer capacity of humus. H2S and Zn0 are used as reducing agents to measure the electron acceptance capacity. After reducing organic matter, the amount of oxidation products $S_2O_3^{2-}$ and Zn^{2+} can be calculated to calculate the electron acceptance capacity of organic matter [13, 14]. In the determination of electron supply capacity, Fe3+ is used as oxidant, and then the organic matter transfers electrons to Fe(III), and the electron supply capacity can be calculated by measuring the content of Fe(II) after reduction. However, the experimental process of chemical and microbial methods is complex, and Fe(III) may react with humus, thus affecting the determination accuracy [15].

On this basis. Aeschbacher et al. [16] proposed a new electrochemical test method, namely mediated potentiometry. The mediators ABTS (2, 2-hydrazine bis (3-ethyl-benzothiazole-6-sulfonic acid) diamiammonium salt and DQ (1,1 '-ethyl-2,2' -bipyridine dibromide) were used to determine the electron acceptability and electron supply capacity of organic compounds, which is relatively simple and time-consuming. At present, it is the main method to determine the electron transfer ability of organic matter.

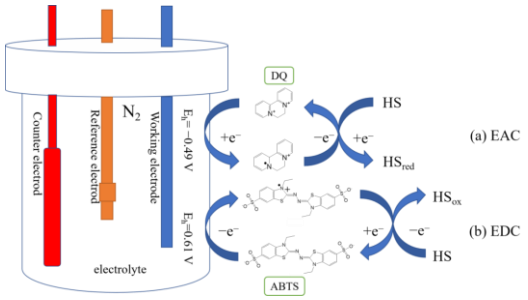

Fig. 3 Method for electrochemical determination of electron transfer capacity of humic substances

The (a) EAC and (b) EDC of humus were obtained by using DQ and ABTS as mediators under hypoxic conditions when the working electrode potentials were set to -0.49V and +0.61 V, respectively.

FACTORS AFFECTING ELECTRON TRANSFER CAPACITY OF HUMUS

Structural factors

The electron transfer ability of humus is mainly affected by the structure of humus. Humus comes from a wide range of sources, and the composition, structure and properties of humus from different sources are very different, which will affect its pollutant degradation and transformation ability. For example, the electron acceptance capacity of humus in soil and sediment is stronger than that of humus in water, because soil and sediment humus contain more aromatic structures. In addition, due to the difference of redox potential (Eh), the electron transfer capacity of humus from different sources cannot be uniformly expressed.

The electron shuttle properties of humus are attributed to various redox active functional groups in the structure of humus, including carboxyl, hydroxyl, quinone, carbonyl, etc., which enable humus to accept electrons and transfer them to electron acceptors, thus participating in the reduction process of some pollutants. For example, humus can act as electron donor and electron acceptor in the reduction of Cr(VI). HA, FA and HM in humus components all have functional groups for reducing Cr(VI), and the reduction effect of HA is better than FA and HM[19, 20]. Quinone functional groups are considered to be the most important redox functional groups [21]. Because humus is rich in quinone groups, quinone template substances have been used to study the electron shuttle mechanism of humus for a long time, such as jughone quinone (JQ) and anthraquinone disulfonate (AQDS). Quinones in humus can cycle between quinones (oxidized state), semi-quinones radicals and hydroquinones (reduced state) when receiving or supplying electrons [22]. The study of Scott et al. [21] showed that quinone group can be converted into semi-quinone radical after accepting electrons, and semi-quinone radical can be converted into hydroquinone group after accepting electrons, and semi-quinone radical is proportional to the electron accepting capacity of humus.

However, a large number of studies have found that quinone groups are not the only redox active groups in humus. Walpen et al. [23] found that non-quinone aromatic structures may also be one of the contributing groups of electron transfer ability. Klupfel et al. [24] found that the electron transfer ability of humus with different chemical properties was positively correlated with its aromatic structure. Compared with FA extracted from the same source, HA tends to have stronger electron acceptance due to its more aromatic structure. Zheng et al. [26] found a significant positive correlation between the electron supplying capacity of humus and the phenolic content

of organic matter, indicating that phenols are one of the main electron donating groups, while carboxyl groups are the main electron producing groups [27]. In addition, sulfur and nitrogen containing components have also been confirmed to be related to the electron transfer capacity of compost DOM [28]. Pham et al. [29] confirmed that S is one of the important redox active elements in HM, which is related to the electron supply capacity of HM in the anaerobic dechlorination reaction of pentachlorophenol.

The humification process of compost organic matter is often more intense than that of soil. The raw materials of compost contain a large number of humus precursor substances, and the composition and structure of these substances will change during the composting process, resulting in changes in its electron transfer ability. Therefore, studying the humification process of compost organic matter is crucial to explain the electron transfer ability of humus.

Environmental Factors

Environmental factors such as microbial activity, pH, temperature, light and oxygen conditions also affect electron transport in humus. Light will cause photolysis and oxidation of humus, which may irreversibly oxidize phenolic groups in humus, thus reducing the electron supply capacity of humus, but having little effect on electron acceptance capacity [30]. The study of Tan et al. [31] showed that the electron acceptance capacity of humus increased with the increase of temperature, but the EDC decreased with the increase of temperature. Humus respiration of microorganisms usually occurs in anaerobic environments because oxygen has a higher REDOX potential than humus and becomes a preferred electron acceptor for microorganisms. However, studies have shown that most humus still has a certain electron transfer ability in the presence of oxygen, although the REDOX functional groups of humus may be protected by oxygen, resulting in a decrease in its electron acceptance capacity [33]. The solubility of humus and the state of redox groups may be affected by pH, thereby altering its ETC. Generally humus has a higher solubility at high pH. The study of Lu et al. [34] showed that the electron transfer capacity of humus increased with the increase of pH. Gu et al. [35] believe that HA can more effectively mediate the biological reduction of Cr(VI) and U(VI) under neutral or weakly alkaline pH conditions. The electron transfer capacity of humus is also affected by the activity and number of humus reducing microorganisms.

ENVIRONMENTAL EFFECTS OF ELECTRON TRANSFERR CAPACITY OF HUMUS

The effect of electron transfer capacity of humus on heavy metals

Humus can directly interact with various kinds of variable valence heavy metal elements, thus affecting the valence state and bioavailability of heavy metals. For example, humus can promote the reduction of U (IV) by microorganisms, and form a humus-U complex that is easily oxidized with the reduced U state [36]. Humus can also be used as electron donor and electron shuttle of dissimilar iron-reducing bacteria to promote the reduction of Fe (III) oxides [37], and can also promote microbial reduction of Ag (I), Cd (II), Hg (II) and Cr (VI), thus changing the toxicity and effectiveness of these heavy metals. Meanwhile, the three components of humus (HA, FA and HM) can promote the reduction of As (V) by microorganisms through electron transfer, thus increasing the environmental risk of As [38].

The effect of electron transfer capacity of humus on organic pollutants

In addition to heavy metals, humus can also promote the degradation and transformation of organic pollutants. For example, Pentachlorophenol (PCP) degradation, pentachlorophenol is a highly toxic persistent organic pollutant, teratogenic and carcinogenic, its toxicity is related to the number of chlorine atoms. Relevant studies have shown that adding humus or humus template to the reaction

system can significantly promote the microbial dechlorination of PCP. Both dissolved humus and solid humus can be used as electron shuttles to accelerate the reduction dechlorination of PCP by MR-1. In addition, humus can also reduce nitrobenzene with high toxicity to aniline with low toxicity that can be degraded by microorganisms [39], and HA in the reduced state can also reduce halogenated aromatics such as hexachloroethane and carbon tetrachloride [40].

The role of electron transfer capacity of humus between microorganisms and pollutants

The study of Zhang et al. [41] showed that solid humus HM also has the ability to transfer electrons between microorganisms and pollutants, such as promoting the dechlorination of pentachlorophenol, and quinone groups also play an important role. Some studies have also shown that HM plays a stronger role in electron transport than humic acid under certain environmental conditions. However, there are few reports on the structural changes and electron transfer ability of HM in the composting process [42], which is worth further research in the future.

CONCLUSION AND PROSPECT

In this paper, the electron shuttle mechanism of compost humus and its environmental effects were reviewed, and the mechanism and influencing factors of electron transfer ability of humus were further explored, as well as the possible environmental effects. Structural factors of humus and environmental factors such as microbial activity, pH, temperature, light and oxygen conditions all affect the electron transfer capacity of humus. Together, these factors determine the function of humus in the environment. The environmental effects of electron transfer capacity of humus are mainly reflected in the interaction between heavy metals, organic pollutants and microorganisms and pollutants. Therefore, the electron transfer ability of humus is closely related to its ability to control environmental pollution. In order to better play its role, we need to pay attention to the factors or processes related to the formation of humus in the composting process, and further strengthen the research of various regulatory means to establish the correlation between them. This will help promote the production of more highly active humus. In addition, it is meaningful to understand the change of electron transfer ability of humus during composting in view of the difference of properties of different organic solid waste materials and composting environment. This will help to better play the environmental effect of electron transfer ability of compost humus. In addition, little is known about the redox properties and structural characteristics of HM extracted from the composting process, and this area needs to be further studied in the future. In conclusion, by exploring the mechanism of humus in environmental remediation, we can provide a more effective method for the utilization of organic waste resources, and provide a theoretical basis for environmental pollution control.

ACKNOWLEDGEMENTS

This work was financially supported by Guangxi innovation research team project (2018GXNSFGA281001) and Guangxi major science and technology projects (GuikeAA18118013).

REFERENCES

[1] Zhang C, Xu Y, Zhao M, et al. Influence of inoculating white-rot fungi on organic matter transformations and mobility of heavy metals in sewage sludge based composting[J]. Journal of Hazardous Materials, 2018,344:163-168.

[2] Maji D, Misra P, Singh S, et al. Humic acid rich vermicompost promotes plant growth by improving microbial community structure of soil

as well as root nodulation and mycorrhizal colonization in the roots of Pisum sativum[J]. Applied Soil Ecology, 2017,110:97-108.

[3] Tang J, Zhuang L, Yu Z, et al. Insight into complexation of Cu(II) to hyperthermophilic compost-derived humic acids by EEM-PARAFAC combined with heterospectral two dimensional correlation analyses[J]. Science of The Total Environment, 2019,656:29-38.

[4] Lipczynska-Kochany E. Humic substances, their microbial interactions and effects on biological transformations of organic pollutants in water and soil: A review[J]. Chemosphere, 2018,202:420-437.

[5] Cheng C, Lehmann J, Thies J E, et al. Oxidation of black carbon by biotic and abiotic processes[J]. Organic Geochemistry, 2006,37(11):1477-1488.

[6] Jindo K, Sonoki T, Matsumoto K, et al. Influence of biochar addition on the humic substances of composting manures[J]. Waste Management, 2016,49:545-552.

[7] Zhao Y, Wei Y, Zhang Y, et al. Roles of composts in soil based on the assessment of humification degree of fulvic acids[J]. Ecological Indicators, 2017,72:473-480.

[8] Yang Y, Shu L, Wang X, et al. Impact of De-Ashing Humic Acid and Humin on Organic Matter Structural Properties and Sorption Mechanisms of Phenanthrene[J]. Environmental Science & Technology, 2011,45(9):3996-4002.

[9] Lovley D R, Coates J D, Blunt-Harris E L, et al. Humic substances as electron acceptors for microbial respiration[J]. Nature, 1996,382(6590):445-448.

[10] Bauer I, Kappler A. Rates and Extent of Reduction of Fe(III) Compounds and O2 by Humic Substances[J]. Environmental Science & Technology, 2009,43(13):4902-4908.

[11] Tang Z, Huang C, GAO R, et al. Application of extracellular respiratory bacteria in the transport and transformation of pollutants [J]. Journal of Agricultural Resources and Environment, 2017,34(04):299-308.

[12] Heitmann T, Blodau C. Oxidation and incorporation of hydrogen sulfide by dissolved organic matter[J]. Chemical Geology, 2006,235(1):12-20.

[13] Blodau C, Bauer M, Regenspurg S, et al. Electron accepting capacity of dissolved organic matter as determined by reaction with metallic zinc[J]. Chemical Geology, 2009,260(3):186-195.

[14] Jiang T, Wei S, Li X, et al. Determination and characterization of mercury reduction capacity by humic acid [J]. Environmental Science, 2012,33(01):286-292.

[15] Aeschbacher M, Vergari D, Schwarzenbach R P, et al. Electrochemical Analysis of Proton and Electron Transfer Equilibria of the Reducible Moieties in Humic Acids[J]. Environmental Science & Technology, 2011,45(19):8385-8394.

[16] Zhang J, Yin H, Wang H, et al. Reduction mechanism of hexavalent chromium by functional groups of undissolved humic acid and humin fractions of typical black soil from Northeast China[J]. Environmental Science and Pollution Research, 2018,25(17):16913-16921.

[17] Mak M S H, Lo I M C. Influences of redox transformation, metal complexation and aggregation of fulvic acid and humic acid on Cr(VI) and As(V) removal by zero-valent iron[J]. Chemosphere, 2011,84(2):234-240.

[18] Scott D T, McKnight D M, Blunt-Harris E L, et al. Quinone Moieties Act as Electron Acceptors in the Reduction of Humic Substances by Humics-Reducing Microorganisms[J]. Environmental Science & Technology, 1998,32(19):2984-2989.

[19] Cory R M, McKnight D M. Fluorescence Spectroscopy Reveals Ubiquitous Presence of Oxidized and Reduced Quinones in Dissolved Organic Matter[J]. Environmental Science & Technology, 2005,39(21):8142-8149.

[20] Walpen N, Getzinger G J, Schroth M H, et al. Electron-Donating Phenolic and

Electron-Accepting Quinone Moieties in Peat Dissolved Organic Matter: Quantities and Redox Transformations in the Context of Peat Biogeochemistry[J]. Environmental Science & Technology, 2018,52(9):5236-5245.

[21] Wolf M, Kappler A, Jiang J, et al. Effects of Humic Substances and Quinones at Low Concentrations on Ferrihydrite Reduction by Geobacter metallireducens[J]. Environmental Science & Technology, 2009,43(15):5679-5685.

[22] Zheng X, Liu Y, Fu H, et al. Comparing electron donating/accepting capacities (EDC/EAC) between crop residue-derived dissolved black carbon and standard humic substances[J]. Science of The Total Environment, 2019,673:29-35.

[23] Zhang X, Ding X, Yang Z, et al. A new method for determination of REDOX functional groups of humus [J]. Environmental Chemistry, 2016,35(10):2106-2116.

[24] He X, Xi B, Cui D, et al. Influence of chemical and structural evolution of dissolved organic matter on electron transfer capacity during composting[J]. Journal of Hazardous Materials, 2014,268:256-263.

[25] Pham D M, Oji H, Yagi S, et al. Sulfur in humin as a redox-active element for extracellular electron transfer[J]. Geoderma, 2022,408:115580.

[26] Sharpless C M, Aeschbacher M, Page S E, et al. Photooxidation-Induced Changes in Optical, Electrochemical, and Photochemical Properties of Humic Substances[J]. Environmental Science & Technology, 2014,48(5):2688-2696.

[27] Tan W, Xi B, Wang G, et al. Increased Electron-Accepting and Decreased Electron-Donating Capacities of Soil Humic Substances in Response to Increasing Temperature[J]. Environmental Science & Technology, 2017,51(6):3176-3186.

[28] Ratasuk N, Nanny M A. Characterization and Quantification of Reversible Redox Sites in Humic Substances[J]. Environmental Science & Technology, 2007,41(22):7844-7850.

[29] Lu Q, Yuan Y, Tao Y, et al. Environmental pH and ionic strength influence the electron-transfer capacity of dissolved organic matter[J]. Journal of Soils and Sediments, 2015,15(11):2257-2264.

[30] Gu B, Chen J. Enhanced microbial reduction of Cr(VI) and U(VI) by different natural organic matter fractions[J]. Geochimica et Cosmochimica Acta, 2003,67(19):3575-3582.

[31] Zhang Y, Chen X, WU Y. Research progress of electron shuttles and their mediated environmental and geochemical processes [J]. Journal of Ecology and Environment, 201,30(01):213-222.

[32] Stern N, Mejia J, He S, et al. Dual Role of Humic Substances As Electron Donor and Shuttle for Dissimilatory Iron Reduction[J]. Environmental Science & Technology, 2018,52(10):5691-5699.

[33] Qiao J, Li X, Li F, et al. Humic Substances Facilitate Arsenic Reduction and Release in Flooded Paddy Soil[J]. Environmental Science & Technology, 2019,53(9):5034-5042.

[34] Yuan Y, Xi B, He X, et al. Compost-derived humic acids as regulators for reductive degradation of nitrobenzene[J]. Journal of Hazardous Materials, 2017,339:378-384.

[35] Kappler A, Haderlein S B. Natural Organic Matter as Reductant for Chlorinated Aliphatic Pollutants[J]. Environmental Science & Technology, 2003,37(12):2714-2719.

[36] Zhang C, Katayama A. Humin as an Electron Mediator for Microbial Reductive Dehalogenation[J]. Environmental Science & Technology, 2012,46(12):6575-6583.

[37] Wei Y, Zhao Y, Zhao X, et al. Roles of different humin and heavy-metal resistant bacteria from composting on heavy metal removal[J]. Bioresource Technology, 2020,296:122375.

RESEARCH PROGRESS OF PHOTOCATALYTIC TREATMENT OF LEACHATE

Muxi Zhang[1,2,3], Xiaojie Sun[1,2,3*]

1.Guangxi Key Laboratory of Environmental Pollution Control Theory and Technology, Guilin University of Technology, Guilin 541004, China

2.Guangxi Collaborative Innovation Center for Water Pollution Control and Water Safety in Karst Area, Guilin University of Technology, Guilin 541004, China

3. Guangxi Key Laboratory of Environmental Pollution Control Theory and Technology for Science and Education Combined with Science and Technology Innovation Base, Guilin University of Technology, Guilin 541004, China

Abstract: In recent years, the environmental pollution caused by landfill leachate has been widely concerned at home and abroad. Landfill leachate is a highly concentrated organic wastewater with complex components produced in the process of garbage stacking and landfill, which causes serious pollution to the environment. But the traditional treatment of leachate has some problems, such as low efficiency, high cost and incomplete treatment. As a new technology to treat landfill leachate, photocatalysis has many advantages, such as high efficiency, environmental protection and economy, and has become a hot spot in current research and application. In this paper, the basic principle and common reaction mechanism of photocatalysis technology are introduced systematically, and the research status of photocatalysis technology in the treatment of landfill leachate is reviewed. At the same time, the existing problems and challenges are discussed, and the direction and development trend of future research are put forward.

INTRODUCTION

With the rapid growth of population and economy, the amount of municipal solid waste is rising, which brings great pressure to the environment. Landfill is one of the main treatment methods of domestic waste [1]. Landfill leachate, as a waste water produced in the process of landfill and other treatment methods, contains a lot of organic matter, nitrogen, phosphorus and other pollutants. Traditional treatment methods are difficult to implement due to their complexity and high cost. The photocatalysis technology is a new treatment technology with high efficiency, environmental protection and low cost, which can degrade the organic matter in the landfill leachate into harmless substances, and at the same time remove the polluting substances to achieve the effective treatment of wastewater. At present, the research on the treatment of landfill leachate by photocatalysis technology is getting deeper and deeper at home and abroad, and the research results on different catalysts, reaction conditions and catalytic mechanism are endless. In this paper, the research progress of photocatalysis in the treatment of landfill leachate in recent years is reviewed, aiming to provide reference for further application of photocatalysis in the field of waste treatment.

COMPOSITION AND TRADITIONAL TREATMENT OF LANDFILL LEACHATE

Formation and composition of landfill leachate

Landfill leachate is a kind of organic polluted water body produced by compaction, fermentation and dewatering in the process of garbage stacking and landfill. The composition of landfill leachate is complex, containing high concentration of organic matter, heavy metal and other pollutants. Among them, organic matter is the main component of landfill leachate, rotten food, peel, paper and other organic matter after the specific conditions in the landfill and the action of

microorganisms will produce a large number of high concentration of organic pollutants, including benzene, phenol, amino acids and acid organic matter. In addition, due to the acidic environment generated by waste degradation, the leachate can also dissolve a large number of heavy metal elements, such as cadmium, chromium, lead and so on. At the same time, pathogenic microorganisms in the garbage will also enter the leachate under the leaching effect of rain.

THE BASIC PRINCIPLE OF PHOTOCATALYSIS TECHNOLOGY

The advantages and disadvantages of traditional treatment of landfill leachate

Traditional landfill leachate treatment methods mainly include physical and chemical methods, biological methods, land treatment and so on. The first is the physical and chemical method, as a more common means of treatment, it needs to treat the leachate according to the physical and chemical characteristics of the garbage itself, which can adsorb, filter, precipitate, REDOX or desalinate the harmful substances contained in the leachate of garbage, so as to better adapt to the subsequent in-depth treatment methods that may be required. The advantages of this method are high processing efficiency, convenient and direct operation, common processing materials required, and strong adaptability to the environment. The disadvantage is that the need to use a certain number of chemical agents may cause secondary pollution of the environment, drug costs and high energy costs. The second is the biological method, which mainly uses microorganisms to degrade organic matter, including aerobic treatment, anaerobic treatment and facultative anaerobic treatment, which has the advantage of low treatment cost and small environmental pollution, but it takes a longer time to process, and is also susceptible to temperature, pH and other factors. Then is the land treatment method, the land treatment method is mainly through the filtration, adsorption and precipitation of soil to remove the suspended matter in the landfill leachate and other related components. There are a large number of microorganisms in the soil that can metabolize and decompose organic pollutants. Its main advantages are relatively low cost and more environmentally friendly, but the disadvantage is that the treatment time is longer and the requirements for the treatment of land soil are more strict [2]. To sum up, the traditional landfill leachate treatment methods have many limitations.

Photocatalytic reaction mechanism

Photocatalysis is a new type of chemical reaction using light, catalyst and solution or gas. Photocatalysis technology excites the catalyst to a high energy state by absorbing light energy, and then chemical reactions occur between the catalyst and organic matter to degrade organic matter, so as to achieve the removal of pollutants. The mechanism of photocatalytic reaction is similar to that of REDOX reaction, and its basic process can be summarized into two steps: (1) photoexcitation stage: the catalyst that absorbs light energy will be excited to a high energy state, and the excited state catalyst is the key to the photocatalytic reaction. (2) The generation and degradation stage of active species: the catalyst in the excited state reacts with water or oxygen to generate active species (such as hydroxyl radicals, hydroxyl radicals, superoxide radicals, etc.) to degrade organic substances and eventually produce harmless substances and water [3].

Types of photocatalytic technologies

Photocatalytic techniques can be classified into several types depending on the reaction system and the type of catalyst. At present, the common photocatalytic technologies mainly include UV/TiO_2 catalytic oxidation, visible photocatalytic oxidation, photo-Fenton oxidation, photoreduction, photodissociation, etc. Among them, UV/TiO_2 catalyzed oxidation is one of the most widely used and effective photocatalytic technologies. It uses titanium dioxide as a catalyst to absorb ultraviolet light energy to stimulate electron pairs,

which can release free radicals from the excited state to the ground state, and decompress and oxidize organic pollutants in the reaction system [4]. With the rapid development of the photocatalytic technology, related studies have advanced, new photocatalytic materials, photocatalytic technology has been widely applied. Researchers have also found that the efficiency of photocatalytic technology can be further improved by changing the composition of the catalyst, the preparation method and the type of support, so the application prospect of photocatalytic technology is very broad.

Treatment of landfill leachate by TiO_2 photocatalyst

Due to the non-toxic, cheap, and strong chemical stability of TiO_2, photocatalytic oxidation technology using TiO_2 as catalyst has become one of the research hotspots in the field of water treatment. TiO_2 photocatalytic oxidation technology is an effective treatment method for landfill leachate. The photocatalytic oxidation process of TiO_2 uses photoactivated electrons to carry out the REDOX reaction of pollutants, accelerate the decomposition and mineralization of organic pollutants, ammonia nitrogen, nitrate and phosphate in landfill leachate, and convert them into harmless substances such as CO_2 and H_2O to achieve the purpose of purifying landfill leachate [5]. In recent years, many scholars of TiO_2 photocatalytic oxidation technology is studied and discussed, found the technology with high efficiency, economy, environmental protection and other advantages. The results of M.V. Bob et al. show that the use of TiO_2 photocatalytic oxidation to treat landfill leachate can achieve the purpose of efficient degradation of organic pollutants. In the experiment, the TiO_2 precipitation solution was added to the landfill leachate of known concentration. After 6 h photocatalytic treatment, the removal rate of organic matter and ammonia nitrogen could reach 63.7% and 57.8%, respectively. At the same time, the study also found that the optimal dosage of TiO_2 is 0.1mg/L. With the same dosage of TiO_2, the COD removal rate of leachate with different stock solution concentrations is basically the same, which is in the range of 73.5% ~ 75.8% [6]. When the amount of TiO_2 was less than 0.1mg/L, the removal rate of organic matter did not change significantly. When the amount of TiO_2 was more than 0.1mg/L, the removal rate of organic matter was slightly improved, but the stability of the system was adversely affected. F. Meng et al. found that combining the Fenton reaction with TiO_2 photocatalysis could significantly improve the efficiency of treating landfill leachate. In the study, TiO_2 nanoparticles were added to landfill leachate together with Fenton reagent, and it was found that TiO_2 photocatalysis could achieve up to 87.2% organic matter removal by degradation of organic matter, while the Fenton reaction could remove 35% of organic matter. When the two are combined, the total removal rate of organic matter can reach 93.6% [7]. C. Li et al. effectively treated landfill leachate by building a system that combines solar-driven direct contact membrane distillation with TiO_2 photocatalytic reaction. In the study, TiO_2 photocatalysis was used to treat landfill leachate. After 120 minutes of treatment, the COD removal rate was 60.1% and the NH_3-N removal rate was 41% [8]. W. Li et al. investigated the effect of TiO_2 nanocomposites on the removal of organic pollutants from landfill leachate. It was found that 88.3% COD removal rate and 38.9% NH_3-N removal rate could be achieved within 60 minutes using nanofiber support for nitride-doped TiO_2 [9]. S. Liang et al. studied UV-assisted TiO_2 photocatalysis and Fenton reaction in landfill leachate. In the study, when the pH is 3 and the amount of TiO_2 is 1.0 g/L, the COD removal rate and NH_3-N removal rate reach 70% and 76% [10]. At the same time, the experimental results show that only TiO_2 photocatalytic oxidation treatment of landfill leachate has certain technical limitations. In the study, it was found that when the initial COD of the leachate was high, the effect of using TiO_2 photocatalytic oxidation to treat the landfill leachate was poor, and the treatment time and dosage needed to be increased. Therefore, it was necessary to optimize the catalyst for photocatalytic oxidation treatment in different scenarios.

Optimization and improvement of TiO_2 photocatalyst

The first is the modification of TiO_2 by ion doping, which is a modification method for TiO_2 catalyst in recent years. The band gap structure of TiO_2 was changed by adding a certain proportion of doped ions (such as N, S, C, etc.) to enhance its photocatalytic activity and selectivity. Ion doping modified TiO_2 has also been widely used in the treatment of landfill leachate. Some studies have shown that ion doping modification TiO_2 can effectively of organic matter and ammonia nitrogen removal of waste leachate, the removal efficiency higher than that of the traditional TiO_2 catalyst. For example, some studies have found that TiO_2 treated by nitrogen doping (N-TiO_2) can significantly improve the removal rate of organic pollutants and ammonia nitrogen. H.L. Qi et al. studied TiO_2 prepared by different doping methods and found that the improvement of COD removal rate and NH_3-N removal rate of S, C and N doped TiO_2 particles exceeded that of traditional undoped TiO_2 particles [11]. G. Guo et al. investigated the removal efficiency of nitrogen-doped TiO_2 (N-TiO_2) treated landfill leachate under different conditions. The results show that under the conditions of light intensity of 300 W/m^2, TiO_2 dosage of 1.5 g/L and pH value of 5.0, the maximum COD removal rate and ammonia nitrogen removal rate of N- TiO_2 reach 70.6% and 64.9% respectively [12]. P. Li et al. investigated the effect of copper doped titanium ferrite nanotubes (Cu-Fe- TiO_2 NTs) on the removal of ammonia nitrogen from landfill leachate. It was found that the maximum removal rate of NH_3-N by Cu-Fe-TiO_2 NTs could reach 80.5% under the conditions of 40 W/m^2 light intensity, 0.5 g/L TiO_2 dosage and pH 7.0. These studies indicate the potential application of ion doping modified TiO_2 in the treatment of landfill leachate. In further studies, the type and proportion of ion doping need to be further explored to improve the catalytic activity and selectivity of the catalyst.

In addition, TiO_2 composites are also widely used in the treatment of landfill leachate, including various nanomaterials composite TiO_2, such as zinc oxide (ZnO) /TiO_2, copper sulfide (CuS) /TiO_2, silicon dioxide (SiO_2) /TiO_2, gold nanoparticles /TiO_2, etc. The introduction of these novel composites can enhance the photocatalytic activity and selectivity of TiO_2, improve the removal efficiency of landfill leachate and reduce the treatment cost. Z. Pang et al. (2018) investigated the removal efficiency of ZnO nanowires /TiO_2 composite nanorods in the treatment of landfill leachate. The results show that landfill leachate can be made using ZnO nanowires /TiO_2 composite nanorods. Z. Li et al. developed a Fe_3O_4-TiO_2 nanocomposite and used it for the treatment of landfill leachate. It was found that compared with the single TiO_2 catalyst, the nanocomposite increased the COD removal efficiency by more than 30% when the light intensity was 100 W/m^2, the catalyst dosage was 1.0 g/L, and the treatment time was 120 min [13].

INFLUENCING FACTORS OF PHOTOCATALYTIC TREATMENT

TiO_2 photocatalytic oxidation technology is widely used in the treatment of landfill leachate, which can accelerate the degradation and mineralization of organic and inorganic substances, and transform pollutants into harmless substances. The successful application of this technology is influenced by a number of factors, the main influencing factors are summarized below.

Illumination intensity

Illumination is required for the photocatalytic oxidation process of TiO_2. Higher light intensity can increase the photo-absorption of the catalyst, accelerate the production of active centers and the reaction speed, and thus improve the catalytic effect. However, with the increase of light intensity, the temperature will rise accordingly, which increases the energy consumption and operation difficulty of the catalytic system. Therefore, it is necessary to find the appropriate light intensity to achieve the best catalytic effect in practical applications.

Type and concentration of catalyst

At present, there are single type, doped type, compound type and supported type photocatalysts. Mono-type photocatalyst is prepared from a single catalyst material, which has the advantages of simplicity, easy preparation, stability and strong photocatalytic activity. Common single photocatalysts include TiO_2, ZnO, CuS, CdS, etc. These catalysts have good activity and high catalytic efficiency, and have their own outstanding advantages in photocatalytic reactions. They all have the ability to degrade organic pollutants in landfill leachate to varying degrees. Titanium dioxide (TiO_2) is one of the most widely used single photocatalysts, and its main advantages include good photocatalytic activity, low cost, and environmental friendliness. Using TiO_2 as a photocatalyst to treat landfill leachate can not only effectively degrade the humic acid and azo compounds, which mainly constitute the color, but also greatly remove the aromatic compounds such as carboxyl and hydroxyl groups and organic pollutants such as alcohols and ketones in the leachate. Especially, the removal of carboxylic acids is more obvious. The doped photocatalyst is prepared by doping other elements on the basis of a single photocatalyst. Doped elements can alter the electronic structure and photophysical properties of photocatalysts, thereby enhancing their photocatalytic activity. Common doping elements include copper (Cu), iron (Fe) and nitrogen (N), among others. For example, nitride-doped TiO_2 (N-TiO_2) photocatalysts have been widely used in the field of visible light (VL) photocatalysis due to their narrow band gap and good VL-responsive performance. Composite photocatalyst is a composite system composed of two or more catalyst materials, which has synergistic effect and excellent photocatalytic performance. Common composite photocatalysts include semiconductor/metal, semiconductor/semiconductor, and metal/metal composite systems. For example, strontium titanate/cuprous oxide ($SrTiO_3/Cu_2O$) composite photocatalyst has strong visible light absorption performance and high photocatalytic activity. The catalytic performance of the composite catalyst is mainly affected by the type of composite material, and the treatment effect of the landfill leachate is generally better than that of the same substance alone. Therefore, when using complex catalysts to treat landfill leachate, the selection of efficient composite materials is the focus of current research. In addition, its excellent performance in treating other pollutants brings many possibilities for landfill leachate treatment. Supported photocatalyst is prepared by loading the photocatalyst on the support with large particle size, which has high stability and reusability. The common carriers are carbon materials, metal oxides and mesoporous materials. For example, the TiO_2/CF composite photocatalyst has good photocatalytic activity and reusability. The supported photocatalyst can catalyze the degradation of landfill leachate, improve its biodegradability and reduce its toxicity. Moreover, the supported photocatalyst itself is regenerative, which can save the treatment cost to a certain extent.

Common catalysts are TiO_2, ZnO, Fe_2O_3 and so on. Among these catalysts, TiO_2 is a more commonly used catalyst, because it has the characteristics of high activity and good stability. However, the activity of TiO_2 also depends on the concentration. When the catalyst concentration is low to a certain extent, the photocatalytic effect of TiO_2 gradually decreases. In order to achieve the best reaction effect, it is necessary to find a balance between the concentration of catalyst and the type of catalyst.

pH

Different leachates have different pH values, so it is necessary to adjust the pH value of the solution according to the actual situation to achieve the best treatment effect. In general, acidic conditions are more favorable for the photocatalytic reaction to proceed. The mechanism by which the pH of the solution affects the

rate and stability of the photocatalytic reaction is achieved by changing the surface charge state of the catalyst, activating the reactants, and regulating the production of intermediates. The photocatalytic oxidation process involves charge transfer reaction, so the pH value of the medium has an important effect on the reaction process. Under neutral or weakly alkaline pH conditions, the catalytic effect is the best. Because in this environment, the fixed OH- ions on the catalyst surface will help to form the active center and the reaction process. However, in an acidic environment, the catalytic effect may be hindered.

Oxygen content

Oxygen is required for photocatalytic oxidation. However, too high or too low oxygen content can affect the catalytic effect. When the oxygen content is below a certain level, the reaction process will be oxygen limited, reducing the reaction speed and catalytic efficiency. However, when the oxygen content is too high, it will increase the cost and affect the OH-ion concentration on the catalyst surface, thus reducing the catalytic effect [14]. To sum up, the above factors are the treatment effect of TiO_2 photocatalytic oxidation technology. In practical applications, researchers need to find a balance between these factors and select appropriate conditions to achieve the optimal catalytic effect.

The applicability of photocatalysis in the treatment of landfill leachate

At present, photocatalytic technology has been widely used in the treatment of landfill leachate. Compared with the traditional physical and chemical methods, the characteristics of the photocatalytic technology has the following several aspects:

(1) Efficiency photocatalytic technology can undertake degradation of pollutants in a short time, high degradation speed and efficiency. However, the choice of different catalysts and light sources has an important impact on the reaction efficiency, and researchers need to choose the optimal treatment scheme according to different situations.

(2) Reaction conditions: photocatalytic technology eliminates the need for high temperature and high pressure conditions, friendly to environment, and the reaction products will not cause secondary pollution to the environment. However, some products generated by the catalytic reaction will accumulate in the reaction system, leading to a decrease in the reaction efficiency. (3) Wide range of treatment: photocatalytic technology for different kinds of organic and inorganic ions have good treatment effect, can be applied to control a variety of environmental pollution problems. However, the expansion of the project scale needs to solve the technical problems such as the construction and operation of the light source, catalyst and reactor, and the design and operation of the reactor also need to be further improved.

(4) Economic feasible: although the price of photocatalytic technology of catalyst is higher, but the processing time is short, reaction product easy to handle, and the comprehensive economic benefit is higher. Therefore, finding a catalyst with relatively low price and good catalytic performance is the key to solve this problem [15].

CONCLUSION

In future study, photocatalytic technology application in waste leachate treatment mainly has the following several directions:

(1) Improve the reaction efficiency and anti-interference ability, photocatalytic technology need further perfect the design and preparation of catalysts, choose suitable reaction conditions and the light source, improve the catalytic efficiency and anti-interference ability.

(2) The optimization of the reactor structure and technological process: photocatalytic technology need combined with the reactor structure and fluid mechanics theory, optimize the structure of reactor fluid field, and the reactor, thus improve the reaction efficiency and

inhibit the accumulation of the problem.

(3) The development of new catalyst, the researchers can explore the use of new materials and new technologies, research the development of catalyst and the preparation, in order to improve the catalytic efficiency and stability of the catalyst. In a word, along with the advance of garbage disposal technology and light catalytic technology constantly improving, photocatalytic technology in waste leachate treatment application prospect is very broad. It is expected that in the future, photocatalysis technology will further integrate new technologies and new materials to achieve large-scale application and provide more efficient and sustainable solutions for landfill leachate and environmental governance.

ACKNOWLEDGEMENTS

This work was financially supported by National Natural Science Foundation of China (No. 52070049).

REFERENCES

[1] Ding, Y.， Zhao, J.， Liu, J.-W., et al. A review of China's municipal solid waste (MSW) and comparison with international regions: Management and technologies in treatment and resource utilization[J]. Journal of Cleaner Production, 2021, 293 (126144).

[2] Zhang W., Zhang G., Wang L., et al. Research progress of landfill leachate treatment technology [J]. Applied Chemical Industry,2022,51(04):1207-1211+1218.

[3] Li, X.Z., Yang, G., and Huan, S.Y. (2019). Heterogeneous photocatalysis: Fundamentals and applications. Progress in Chemistry, 31(3), 285-295.

[4] Shui B., Song X., Fan W.. Research progress a nd challenges of photocatalysis technology in water treatment [J]. Advances in Chemical Industry, 202 1,40(S2):356-363.

[5] Zhang Q., Wang J.. Research on photocatalytic treatment of landfill leachate [J]. Management and Technology of Small and Medium-sized enterprise, 2016(01):214.

[6] He C., Chen C.., Lu Q.. Research progress of titanium dioxide photocatalytic technology for treatment of landfill leachate [J]. Building Materials World,2019,40(02):83-85.

[7] Meng, F., Wang, J., Liang, S., Liu, Y. and Xu, J. (2018). Treatment of landfill leachate by a Fenton-catalyzed oxidation process combined with TiO_2 photocatalysis. Journal of Cleaner Production, 179, 81-87.

[8] Li, C., Dong, J., Sun, H., Chen, X. and Zhao, Y. (2020). Enhanced treatment of landfill leachate using a solar-driven direct-contact membrane distillation integrated with a TiO_2 photocatalytic reactor. Journal of Environmental Sciences, 93, 111-121.

[9] Li, W., Li, X., Zhang, W., Wang, S., Tang, Y., Liu, J. and Li, J. (2019) Photocatalytic performance of nitrogen-doped TiO_2 coated on fiberglass for landfill leachate treatment. Desalination and Water Treatment, 139, 256-264.

[10] Liang, S., Meng, F., Chen, H., Yang, L. and Xu, J. (2019). Treatment of landfill leachate by Fenton's reagent in combination with UV/TiO_2 process. Chemosphere, 216, 216-221.

[11] Qi, H.L., Liu, Y.G., Li, X.Y., Liu, P., and Ma, H.W. (2018). Enhanced photocatalytic activity of TiO_2-based semiconductor catalysts modified by doping with sulfur, carbon, and nitrogen. Journal of Environmental Management, 211, 43-51.

[12] Guo, G., Hu, Q., and Yang, H. (2019). Enhanced photocatalytic removal of landfill leachate with nitrogen-doped TiO_2: optimization

[13] Z. Li, G. Guo, Y. Wang, H. Zhang, X. Zhang, S. Zhu, S. Zhou, Z. Jiang, and T. Li. (2021). Novel Fe_3O_4@TiO_2 nanocomposite for efficient removal of organic pollutants in landfill leachates: synthesis, characterization and photocatalytic performance. Environmental Research, 195, 110855.

[14] Ren, C., Chen, J., Zhang, L., and Li, M. (2012). Effects of pH on the photocatalytic degradation of benzotriazole under UV and visible light irradiation. Journal of Hazardous Materials, 219-220, 98-105.

[15] Xing L Z, Feng L, Chen H H, et al. Research progress of TiO_2 photocatalytic oxidation technology in water treatment [J]. Journal of Shandong Jianzhu University, 2008, 22(6):551-556.

RESEARCH PROGRESS OF SAMPLE PRETREATMENT METHODS IN LANDFILL LEACHATE

Muxi Zhang[1,2,3], Xiaojie Sun[1,2,3*]

1.Guangxi Key Laboratory of Environmental Pollution Control Theory and Technology, Guilin University of Technology, Guilin 541004, China

2.Guangxi Collaborative Innovation Center for Water Pollution Control and Water Safety in Karst Area, Guilin University of Technology, Guilin 541004, China

3. Guangxi Key Laboratory of Environmental Pollution Control Theory and Technology for Science and Education Combined with Science and Technology Innovation Base, Guilin University of Technology, Guilin 541004, China

Abstract: Landfill leachate is a secondary pollutant generated in the landfill treatment process, with large changes in water quality, complex composition, the presence of high levels of chemical pollutants, such as ammonia nitrogen, various types of organic heavy metal molecules and organic substances, there may also be certain highly pathogenic bacteria and carcinogenic, teratogenic and mutagenic chemical substances, posing a great threat to the ecological environment and human health. Therefore, landfill leachate needs to be properly treated to avoid contaminating surface water and groundwater. A more comprehensive understanding of the specific components contained in landfill leachate is necessary to select the appropriate treatment process. In view of the complexity and variability of landfill leachate, the number of interfering substances and the variability of the content of the components to be tested, it is important to obtain accurate information on the content of the components to be tested and to use appropriate sample pretreatment methods during the analysis process to reduce the influence of the sample matrix. This paper presents a comprehensive analysis of four pretreatment methods, namely liquid-liquid extraction, solid-phase extraction, liquid-phase microextraction and solid-phase microextraction, which are commonly used in landfill leachate testing and analysis.

INTRODUCTION

With the improvement of the living standard of modern society, the garbage discharged by People's Daily production and living activities is also increasing, and the disposal of domestic garbage has become an important issue of environmental governance. Sanitary landfill, domestic waste incineration and composting are the three most common domestic waste disposal methods in China at present [1]. According to the China Statistical Yearbook [2], in 2021, China's domestic waste removal volume will reach 248,6921 million tons, and the harmless treatment capacity will reach 248,393,200 tons. Among them, sanitary landfill is still one of the main methods of domestic waste treatment in China, and its harmless treatment capacity reaches 52,085,100 tons, accounting for 20.97% of the total harmless treatment capacity. Sanitary landfill method has the advantages of simple and easy operation and low operating cost, but landfill leachate will be produced in the process of landfill, which will pollute the groundwater environment, atmospheric environment and land near the landfill site. If the landfill leachate is not properly treated, it will cause serious damage to the ecological environment [3]. At present, the contaminant components identified in the landfill leachate are not enough. The comprehensive identification of the contaminant components and their structural characteristics can provide a basis for selecting a suitable treatment process to treat the landfill leachate efficiently. But different landfill leachate contains different pollutants, the concentration of different pollutants is

unknown, the stability is poor. To accurately obtain the content information of the components to be measured, appropriate sample pretreatment technology should be adopted in the analysis process to reduce the influence of the sample matrix [4]. The efficient sample pretreatment technology can not only remove or reduce the matrix interference of the sample, but also achieve the enrichment of the analyte, and improve the accuracy and sensitivity of the analysis.

CHARACTERISTICS OF LANDFILL LEACHATE

Landfill leachate is characterized by high concentration of pollutants, high content of organic pollutants, serious imbalance of microbial nutrient elements, high metal content, large changes in water quality and complex components [5]. According to domestic and foreign studies, more than 200 chemical components have been identified in landfill leachate, and the most commonly detected organic compounds are: alkanes, halogenated hydrocarbons, polycyclic aromatic hydrocarbons, phenols, phthalates, esters, ketones, aldehydes, nitrogen compounds, perfluorinated compounds, sterols, etc. [5]. Liu Jun et al. [6] detected 63 major organic pollutants in landfill leachate, 34 of which were more than 60% reliable, including alkanes, olefins, aromatic hydrocarbons, aldehydes, alcohols, ketones, esters, carboxylic acids, phenols, amides and other organic compounds. There are also a large number of organic compounds in landfill leachate that are difficult to biodegrade, such as phenols, heterocyclic, heterocyclic aromatic and polycyclic aromatic compounds [7]. In addition to toxic organic compounds, landfill leachate also contains a large number of heavy metal elements [8].

PRETREATMENT METHOD

There are many kinds of pollutants in landfill leachate, low concentration and great changes in water quality. It is necessary to achieve the concentration and enrichment of trace pollutants in the sample through pre-treatment to reduce the damage of impurities in the sample to the instrument and the signal interference in the subsequent instrument analysis and data processing [9]. The pre-treatment methods commonly used for the detection and analysis of landfill leachate include liquid-liquid extraction, solid phase extraction, liquid phase microextraction and solid phase microextraction.

LIQUID-LIQUID EXTRACTION (LLE)

Liquid-liquid extraction is one of the common pre-treatment methods, which consists of two phases consisting of two kinds of non-miscible or rarely miscible liquids. The difference in solubility of the components to be tested in the two phases is utilized to make them transfer from one phase to another under certain conditions, so as to realize the separation of the components to be tested [10]. Liquid-liquid extraction method has the characteristics of simplicity, speed and good separation effect, but it needs to use a large number of harmful organic solvents, and the production of a large number of pollutants makes the process time-consuming, expensive, environmentally unfriendly and laborious [11]. Ramirez-Sosa DR Et al. [12] used 50 mL chromatograph-grade CH_2Cl_2 to carry out liquid-liquid extraction, and then determined the components of landfill leachate by gas chromatography and mass spectrometry. The results showed that aniline, methyl-phenol, 2-chlorocyclohexamol and other organic compounds existed in the landfill leachate. Popiel S et al. [13] carried out liquid-liquid extraction with dichloromethane, and determined the organic compound components of the landfill leachate in the main landfill of Merida City, Yucatan State, Mexico by gas chromatography and mass spectrometry. The results showed that 11 main organic compounds, including 3 phenolic compounds and 2 benzene compounds, were detected in the landfill leachate. 2 carboxylic acids, 2 ketones, 1 terpene and 1 alcohol. Xu Xinyan et al. [14] tested the composition of landfill leachate by liquid-liquid extraction and gas chromatography combined with mass spectrometry, and analyzed that there were 103 kinds of organic compounds in the leachate, which contained various oxygen-containing functional groups,

mainly hydroxyl, phenolic hydroxyl, alcohol hydroxyl, methoxyl and carbonyl.

LIQUID PHASE MICROEXTRACTION (LPME)

Liquid phase microextraction is an important sample pretreatment technology, which is developed on the basis of liquid-liquid extraction, overcomes many shortcomings of traditional liquid-liquid extraction technology, and only uses micro-upgraded or even nano-upgraded organic solvents for extraction. The extraction phase of liquid microextraction can be directly analyzed by modern instruments such as gas chromatograph, high performance liquid chromatograph, high performance capillary electrophoresis, chromatography-mass spectrometry or capillary electrophoresis - mass spectrometry. Liquid phase microextraction has been widely used to extract different organic, inorganic and pharmaceutical compounds from different environmental and biological substrates. The advantages of organic solvent such as low consumption, simple, fast, flexible and cheap all promote the development of this technology. In liquid phase microextraction, a small amount of organic solvent that is not miscible with water is used to extract the target analyte from the water-based sample. This miniaturized liquid-liquid extraction provides a more environmentally friendly method to improve extraction efficiency using fewer chemicals in a shorter analysis time [10]. Beldean-Galea et al. [15] analyzed 72 organic compounds in municipal landfill leachate by liquid phase microextraction and full two-dimensional gas chromatography combined with mass spectrometry. In the pre-treatment process, a mixed solution of 100 microliter acetone and 75 microliter chloroform was used for extraction, and 41 organic compounds were quantitatively detected. These include hydrocarbons, monocyclic and polycyclic aromatic hydrocarbons, carbonyl compounds, terpenes, terpenes, phenols, amines, and phthalates.

SOLID PHASE EXTRACTION (SPE)

Solid phase extraction (SPE) is a sample preparation technique developed in the late 1870s. It is developed by the combination of liquid-solid extraction column and liquid chromatography technology, mainly used for sample separation, purification and concentration, compared with the traditional liquid-liquid extraction method can improve the recovery of analyte, more effective separation of analyte and interference components, simple operation, saving time and labor. It is widely used in medicine, food, environment, commodity inspection, chemical industry and other fields [5]. Sun Xianhong [16] established a method for the determination of perfluorooctanoic acid in the landfill leachate of Chongqing Fengsheng Waste Incineration Plant based on solid phase extraction (SPE) and high performance liquid chromatograms (HPLC) - mass spectrometry (MS). The conditions of SPE were optimized, and WAX SPE column was used for sample pre-treatment. The detection limit of the method was 0.17 ng/L. Yan H [17] et al. used solid phase extraction to pre-treat leachate samples, and then used high performance liquid chromatography-tandem mass spectrometer to analyze the purified solid phase extraction leachate. Yang Jiahui et al. [18] used solid phase extraction to process the samples, and used high performance liquid chromatography to determine 16 PAHs in the landfill leachate of Guangzhou Xingfeng domestic waste sanitary landfill.

SOLID PHASE MICROEXTRACTION (SPME)

Solid phase microextraction is based on the principle of "similar phase dissolution" to concentrate and concentrate hydrophobic organic matter and volatile matter in sample solution. After extraction, the tested matter is desorbed (usually thermal desorption or solvent desorption) and entered into gas chromatography or liquid chromatography for detection [19]. The principle of solid-phase microextraction is different from that of solid-phase extraction, which does not extract all the object to be measured, but is based on the balanced distribution of the object to be measured between the

fixed phase and the water phase [20]. The biggest feature of this technology is that it integrates extraction, adsorption, enrichment, elution and sample injection without solvent, and has many advantages such as fast, high efficiency, low cost, high safety, and can be combined with other instruments, making sample processing technology and analytical operation simple and time-saving [13]. Compared with the solid phase extraction technology, the operation of solid phase microextraction is more simple, more convenient to carry, and the operation cost is lower. At the same time, solid-phase microextraction overcomes the shortcomings of low recovery rate of solid-phase extraction and easy blockage of adsorbent pores, so it has become one of the most widely used methods in sample pretreatment at present, and has been successfully applied to the analysis of environmental, food, biological, forensic and drug samples [21]. Wang Kun et al. [22] used a solid phase microextraction device to pre-treat domestic garbage leachate, and then used liquid chromatography and mass spectrometry to detect 11 emerging organic pollutants in the leachate. Mei Ming et al. [23] used headspace solid phase microextraction and gas chromatoc-mass spectrometry to detect the substances present in the landfill leachate, and found that the volatile organic compounds in the landfill leachate mainly included ketones, phenols and alcohols, which accounted for 68.22% of the total detected organic compounds, and a small amount of esters. Table 1 shows the advantages and disadvantages of the four pretreatment methods and their applicable objects.

CONCLUSION

Because the water quality of landfill leachate is complex and changeable, there are many interfering substances, and the content of components to be measured changes greatly, the sample needs to be pre-treated before detection. Sample pretreatment is usually the bottleneck in the measurement process, because sample pretreatment accounts for more than 60% of the entire experiment time, and the error accounts for more than 50% of the entire experiment. At present, solid phase extraction (SPE) is the most commonly used pre-treatment method of landfill leachate reported in the literature, which is developed by the combination of liquid-solid extraction column and liquid chromatography technology, and is also the most commonly used method to extract new pollutants in sewage. However, because the types of new pollutants in landfill leachate are too complex and the selectivity of adsorbents for different structures is different, the recovery rate of some new pollutants by SPE is not ideal. Therefore, SPE is more suitable as a pre-treatment method for targeted analysis, and only when there are clear target compounds can the appropriate type of SPE column be selected. The organic solvents commonly used in liquid-liquid extraction are dichloromethane, n-hexane, ethyl acetate, etc., which are polluted by organic solvents and have high toxicity. However, liquid-liquid extraction does not require complex equipment, is simple to operate, is more economical than solid-phase extraction, and because of the extensiveness of liquid-liquid extraction, through the optimization of organic solvents, can be used as a pre-treatment method for non-targeted analysis. In the last decade, solid - or liquid-phase microextraction techniques have become convenient for sample pretreatment, as these techniques require only small amounts of organic solvents or adsorbents to extract various analytes from different substrates prior to instrumental analysis. Among these methods, liquid phase microextraction has become one of the most commonly used methods for pretreating environmental, food, and pharmaceutical samples. The main advantage of LME is that various analytes can be extracted from complex substrates with only a few microliters of solvent. Under the condition of ensuring the pre-treatment effect, the operation steps of liquid phase microextraction are reasonably simplified, and the technology of liquid phase microextraction will be popularized in the pre-treatment of landfill leachate.

ACKNOWLEDGEMENTS

This work was financially supported by Guangxi innovation research team project (2018GXNSFGA281001) and Guangxi major science and technology projects (GuikeAA18118013).

REFERENCES

[1] Zhang Muxi, Sun Xiaojie, Wang Yabo, et al., Trends and causes of domestic waste treatment in Guangdong Province. Chinese Journal of Environmental Engineering. 2021; 15 (11) : 3651-3659.

[2] The National Bureau of Statistics of the People's Republic of China. China statistical yearbook [M]. Beijing: China statistics press, 2021.

[3] Wang Junping. Current treatment methods of landfill leachate in China. Liaoning Chemical Industry Co., LTD. 2022; 51 (11) : 1580-1582 + 1660.

[4] Li Huimin, Zhou Yuchen, Xiao Yufang, et al., Application of cold-assisted solid phase microextraction in the analysis of complex matrix samples. Analytical Chemistry. 2022; 50 (9) : 1289-1298. (9) : 1289-1298.

[5] Zhang Qian, Xu Hang, Su Lianghu, et al., Research progress of analysis methods for new pollutants in landfill leachate. Environmental Science and Management. 2021; 46 (12) : 104-109.

[6] Liu Jun, Bao Linfa, Wang Ping. Analysis of organic pollutants in landfill leachate by GC-MS combined technology. Environmental pollution control technology and equipment. 2003(08):31-33.

[7] Yuan Z, He C, Shi Q, et al. Molecular Insights into the Transformation of Dissolved Organic Matter in Landfill Leachate Concentrate during Biodegradation and Coagulation Processes Using ESI FT-ICR MS. Environmental Science & Technology: ES&T. 2017;51(14):8110-8118.

[8] Jaradat AQ, Telfah DaB, Ismail R. Heavy metals removal from landfill leachate by coagulation/flocculation process combined with continuous adsorption using eggshell waste materials. Water Science and Technology. 2021.

[9] Qian Yuli, Geng Jinju, Yu Qingmiao, et al., Research progress of non-targeted screening for emerging pollutants in sewage. Industrial water Treatment. 2021; (6) : 41 48-57.

[10] Liew CSM, Li X, Lee HK. Miniscale Liquid–Liquid Extraction Coupled with Full Evaporation Dynamic Headspace Extraction for the Gas Chromatography/Mass Spectrometric Analysis of Polycyclic Aromatic Hydrocarbons with 4000-to-14 000-fold Enrichment. Analytical Chemistry. 2016.

[11] Ramírez-Sosa DR, Castillo-Borges ER, Méndez-Novelo RI, Sauri-Riancho MR, Barceló-Quintal M, Marrufo-Gómez JM. Determination of organic compounds in landfill leachates treated by Fenton–Adsorption. Waste Management. 2013;33(2):390-395.

[12] Banel A, Zygmunt B. Application of gas chromatography-mass spectrometry preceded by solvent extraction to determine volatile fatty acids in wastewater of municipal, animal farm and landfill origin. Water Science and Technology. 2011;63(4):590-597.

[13] Popiel S, Sankowska M. Determination of chemical warfare agents and related compounds in environmental samples by solid-phase microextraction with gas chromatography. Journal of Chromatography A. 2011.

[14] Xu Xinyan, Jia Jinping, Lv Zho et al., Changes of organic components in landfill leachate before and after coagulation. Environmental Chemistry. 2007(01):114-115.

[15] Beldean-Galea MS, Vial J, Thiebaut D, Coman M-V. Analysis of multiclass organic pollutant in municipal landfill leachate by dispersive liquid-liquid microextraction and comprehensive two-dimensional gas chromatography coupled with mass spectrometry. Environmental science and pollution research. 2020;27(9):9535-9546.

[16] Sun Xian-Hong. Study on the removal of perfluorooctanoic acid in the leachate treatment Process of Waste Incineration Plant [Master], Chongqing University; 2018.

[17] Yan H, Cousins IT, Zhang C, Zhou Q. Perfluoroalkyl acids in municipal landfill leachates from China: Occurrence, fate during leachate treatment and potential impact on groundwater. Science of the Total Environment. 2015.

[18] Yang Jiahui, Chen Fei-Long, Hou Jun-Pei, WANG Wei. Determination of polycyclic aromatic hydrocarbons in landfill leachate by solid phase extraction, high performance liquid chromatography-double detector method. Shandong Chemical Industry. 2020; 49 (21) : 86-89.
[19] Wu Z K, Rao X F, Ma X B, et al. Research progress of solid phase microextraction. Yunnan Chemical Industry. 2021; 48 (10) : 9-10.
[20] Mangani F, Cenciarini R. Solid phase microextraction using fused silica fibers coated with graphitized carbon black. Chromatographia. 1995.
[21] Dias AN, Simão V, Merib J, Carasek E. Cork as a new (green) coating for solid-phase microextraction: Determination of polycyclic aromatic hydrocarbons in water samples by gas chromatography–mass spectrometry. Analytica Chimica Acta. 2013.
[22] Wang Kun, Zhao Yujie, Zhuang Tao. Distribution characteristics and environmental risks of 43 emerging organic pollutants in landfill leachate. Environmental pollution and Prevention. 2020; 42 (12) : 1523-1530.
[23] Mei Ming, Liang Yuqian, Zhou Xuan, Zuo Miao. HS-SPME/GC-MS analysis of volatile organic compounds in landfill leachate. Journal of Wuhan Institute of Technology. 2011; 33 (01) : 28-31.
[24] Gu Zhanliang. Research progress of chemical sample pretreatment technology. Metallurgy and Materials. 2022; 42 (4) : 98-99.
[25] Mayira Abduklimu. Application analysis of sample pretreatment in physicochemical inspection of food. Food Safety Guide. 2020(18):188.
[26] Liu Pei, Chen Caihong, WU Yonghua. Discussion on sample pretreatment method in physicochemical inspection of food. Quality Safety and Inspection. 2021; 31 (03) : 104-106.
[27] Liu X. Sample pretreatment technology in pesticide residue detection. Food Safety Guide. 2021(19):89-90.
[28] Zhao Yiting. Analysis and research on pre-treatment and detection technology of cosmetic samples. Quality Safety and Inspection. 2021; 31 (4) : 89-91.

RESEARCH PROGRESS ON THE EFFECT OF BIOCHAR ADDITION ON COMPOSTING OF ORGANIC SOLID WASTE

Yufan Jiang[1,2,3], Xiaojie Sun[1,2,3*]

1.Guangxi Key Laboratory of Environmental Pollution Control Theory and Technology, Guilin University of Technology, Guilin 541004, China

2.Guangxi Collaborative Innovation Center for Water Pollution Control and Water Safety in Karst Area, Guilin University of Technology, Guilin 541004, China

3. Guangxi Key Laboratory of Environmental Pollution Control Theory and Technology for Science and Education Combined with Science and Technology Innovation Base, Guilin University of Technology, Guilin 541004, China

Abstract: In recent years, both the amount of organic solid waste produced and the amount of harmless disposal have been increasing. Aerobic composting technology has been the focus of our research and attention, but there are many shortcomings in traditional aerobic composting technology. In order to improve the composting effect of organic solid waste, studies have shown that the addition of biochar has a significant effect on the composting effect of organic solid waste. This paper reviewed the positive effects of biochar addition on organic solid compost, such as reducing nitrogen loss, improving microbial community, reducing harmful gas emissions, extending the high temperature period of the pile, improving the water retention of the pile, and reducing the mobility of heavy metal ions.

INTRODUCTION

With the rapid development of social economy and the continuous improvement of people's living standard, the production of organic solid waste has increased rapidly. According to the data of China Statistical Yearbook, in 2021, China's domestic waste removal volume will be 248.692 million tons, and the number of harmless treatment plants will be 1,407. Compared with 2010, China's domestic waste removal volume increased by 57.4%, and the number of harmless treatment plants increased by 779.

The residual sludge discharged from kitchen waste and municipal sewage plant is the main component of municipal organic solid waste, which contains a large number of organic N and P pollutants, if not properly treated, it will produce odor under the action of pathogenic microorganisms and anaerobic bacteria, causing serious environmental pollution.In recent years, engineers and technicians have applied aerobic treatment technology to the treatment and disposal of urban wet waste, kitchen waste, sewage plant residual sludge, livestock and poultry feces and other organic wastes, and carried out many in-depth studies in the

aspects of nutrient element balance[1] 、 microbial population diversity[2] 、 and pile temperature change[3].As a kind of aerobic stable treatment process, aerobic composting can effectively utilize organic solid waste through the action of microorganisms and realize the virtuous cycle of resources. However, the traditional aerobic compost has some problems, such as low humification degree, serious loss of carbon and nitrogen, long composting cycle and large greenhouse gas emission[4],adding appropriate additives (biochar, lime and fly ash, etc.) to compost can effectively alleviate the above problems and improve the compost effect[4,5].Biochar is a kind of porous carbon-rich product formed by pyrolysis of biomass at low temperature and hypoxia, which is often used to solve many problems such as energy, environment and food. Biochar, as an additive material with low cost and easy preparation, is expected to be applied to improve the composting effect of organic solid waste on a large scale.

With the development of waste resource utilization, the effect of biochar on physicochemical properties and compost quality in the composting process has become increasingly prominent.According to the Law of the People's Republic of China on the Prevention and Control of Environmental Pollution by Solid Waste, "the principle of fully and reasonably utilizing solid waste and harmless disposal of solid waste, and promoting the development of clean production and circular economy" is the basic principle of solid waste treatment and disposal in China. Biochar is prepared from waste materials and added to the composting system to achieve the purpose of "treating waste with waste".In this paper, various limiting factors such as nitrogen loss, microbial community, harmful gas emission, high temperature period, water holding capacity and heavy metal ion mobility of organic solid waste aerobic compost were reviewed. The feasibility and effectiveness of biochar addition in promoting the efficient degradation of compost system were analyzed, and the future research direction was prospected.

EFFECT OF BIOCHAR ADDITION ON COMPOSTING SYSTEM

Reduce nitrogen loss

According to the statistics of relevant researchers, the nitrogen loss in the composting process ranges from 16% to 76%, and is closely related to the carbon loss in the composting process[6],the loss of nitrogen will lead to the reduction of fertilizer efficiency of compost products, and also cause environmental pollution. Generally, the C/N of the pile is between 25-35, and the appropriate C/N value is the most critical factor for efficient composting, it has an important effect on the growth and reproduction of microorganisms, fermentation cycle and the quality of

organic fertilizer.

The addition of biochar can adjust the C/N ratio of compost appropriately and reduce the nitrogen loss during composting. Studies have shown that adding 9% bamboo charcoal to pig manure compost can increase the total nitrogen content by about 65%[7,8]. M.A.Chowdhury et al.[9]found that adding biochar to livestock manure can increase the NH_4^+-N and NO_3^--N contents after compost is decomposed, effectively retaining nutrients in livestock manure.Li Taikui et al.[10]added 5%, 10% and 15% straw biochar to pig manure compost, and found that biochar could significantly increase the NO_3^--N content of pig manure compost and reduce the NH_4^+-N content, which was conducive to the conversion of NH_4^+-N to NO_3^--N, and the NO_3^--N content of the pile at the end of compost increased by 39.64%, 46.68% and 28.84%, respectively. Among them, 10% straw biochar significantly increased the number of nitrogen-fixing bacteria, significantly reduced the number of denitrifying bacteria, and reduced the cumulative ammonia emissions by 25.35%, thus verifying that the addition of biochar changed the abundance of bacteria related to nitrogen utilization, and effectively reduced the nitrogen loss in the pile.

Improve microbial community

Microorganisms are the main participants in the composting process and interact with the composting environment[11,12],which is related to the degradation and maturation of organic matter. Biochar contains negative charges of different functional groups, which have significant adsorption effects on nitrate and phosphate ions, etc., which can increase the content of nitrogen and phosphorus in soil, enhance fertility, optimize the physical and chemical conditions of the heap[13,14], provide a better growth and development environment for microorganisms, and significantly promote compost decomposition. Biochar also has rich porosity, which can provide a microenvironment conducive to microbial growth[15,14],change the diversity of microbial community, increase the abundance of core microorganisms, and promote microbial reproduction [16].However, excessive addition of biochar may delay the composting process.

The study of Farrell et al.[17]confirmed that the relatively developed specific surface area and morphology of biochar itself can provide a larger living environment for the survival and reproduction of microorganisms, thus regulating the activities of various bacterial groups in the compost process and affecting the changing states of other reactions in the heap.

Reduce harmful gas emissions

Biochar has the characteristics of high specific surface area, porous polyhydroxyl structure and strong adsorption capacity, and has a strong

adsorption and emission reduction effect on odor such as H_2S and greenhouse gases (such as CH_4 and N_2O) produced in the composting process.Wang Yixiang et al.[18]added different biochar ratios (0, 3%, 6% and 9%) to pig manure compost, and found that the cumulative greenhouse gas emissions could be reduced, and the greenhouse gas emission reduction effect increased with the increase of biochar addition ratio. M.A. Chowdhury et al.[9]found that adding biochar to livestock and poultry manure could reduce the emission of NH_3, N_2O, CH_4 and other gases in the composting process. In the study of the impact of biochar on chicken manure compost conducted by Wu Xiaodong et al.[19], it was found that the addition of biochar could reduce 17%-40% of ammonia emissions in the pile, which proved that biochar could effectively reduce ammonia emissions in the pile. Li Taikui et al.[10] added 5%, 10% and 15% straw biochar to pig manure compost, and found that the addition of biochar significantly reduced the ammonia volatilization rate of the compost at high temperature, and the cumulative emissions of ammonia volatilization were reduced by 18.77%, 25.35% and 26.39%, respectively, compared with the control, indicating that the addition of biochar could effectively inhibit ammonia volatilization in the compost process.

Increase the reactor temperature and prolong the high temperature period of the reactor

Biochar has a large specific surface area, which can enhance the water holding and aeration capacity, and increase the number and activity of microorganisms in the pile during composting, thus increasing the temperature of the pile[20].Wu Xiaodong et al.[19]believe that biochar is a kind of material similar to black body, which can release far infrared ray after absorbing energy and produce thermal effect to increase the temperature of the reactor.

Biochar can prolong the high temperature period of the reactor to a certain extent by enhancing the activity of microorganisms. The addition of biochar can increase the pore structure in the reactor, which can provide a larger activity place for microorganisms, thus releasing more heat and increasing the temperature of the reactor. Li Taikui et al.[10]found that adding different proportions of biochar to the aerobic compost of pig manure can significantly increase the compost temperature, accelerate the temperature rise of the pile, and make the composting system enter the high temperature period 3-5 days in advance, shortening the composting cycle. Roig A et al.[21]found that the addition of biochar could advance the high temperature period of sheep manure compost by about one week, and make the high temperature period last longer to achieve better composting effect. The extension of the high temperature period can shorten the overall composting cycle, which can save a lot of human

resources and time resources. Zhang Haibin et al.[22]found in the study of biochar on the physicochemical properties of biogas residue compost that the biogas residue compost added with biochar could reach the high temperature period more quickly and prolong the high temperature period because the microporous structure of biochar could increase the water holding capacity, and the higher water content was conducive to the thermal insulation of the pile.

Improve the water retention of the reactor

The moisture content of the pile has a significant effect on the composting process and the degradation rate of organic matter, and is also related to oxygen transport, fermentation process and microbial activity.The ideal moisture content of aerobic compost is 60%-70%[23], if the water content of the pile is too low, it will affect the growth and reproduction rate of microorganisms, lead to the degradation of organic matter, and delay the process of composting reaction;if the water content of the pile is too high, the nitrogen in the pile will be volatilized in the form of ammonia.

In the process of preparing biochar, due to the removal of volatile organic compounds, a large number of pores formed by them account for 70%-80% of the total volume of biochar, which can increase the ventilation porosity and capillary porosity inside the reactor and enhance the water retention of the reactor. According to the study of Zhu Shijiang et al.[24]on the change trend of soil water content after biochar enters farmland, it is found that the water absorption capacity of soil with biochar added is better than that of soil without biochar, which can increase the water content of soil by 3.7%, thus verifying that the addition of biochar can increase the water content of heap.

Reduce the mobility of heavy metal ions

Long-term treatment of organic solid waste will lead to a significant increase in the content of heavy metals such as Cu, Zn, Pb, Ni and Cd in soil and plants[25].Many studies have shown that the available content of heavy metals in soil is directly proportional to the possibility of heavy metals entering plants through biological chains, so reducing the mobility of heavy metals in compost will effectively reduce the accumulation of heavy metals in plants[26,27].

Biochar shows its remediation effect on contaminated soil by absorbing heavy metals in compost. The peanut shell biochar studied by Jiang Yahui et al.[28]can reduce the copper content in contaminated soil by 49.06%, and the coffee grounds biochar can reduce the available nickel and zinc contents in contaminated soil by 23.73% and 9.72%. Li Hua et al.[16]found that when 9% bamboo charcoal was added to sludge compost, the extractable Cu and Zn contents of diethylenetriamine pentaacetic acid based on compost sludge decreased by 44.4% and 19.3%, respectively, indicating that the addition of bamboo

charcoal reduced the heavy metal migration in sludge compost.Studies have also shown that after biochar is added to the pile, the activity of heavy metals in organic solid waste is passivated, which can effectively reduce its bioavailability. Chen et al.[7]found that adding 9% bamboo charcoal to pig manure compost could reduce the mobility of Cu and Zn by 35% and 39%, respectively, which verified that adding biochar could reduce the mobility of heavy metal ions in the pile.

Decreased abundance of antibiotic resistance genes (ARGs)

Biochar provides the best gas environment and suitable habitat for microorganisms in compost mixture, which can effectively improve the removal effect of ARGs in compost treatment. Bao Canxin et al.[29]studied the effects of different biochar on antibiotics and ARGs in the process of pig manure composting and found that different biochar had a certain removal rate of antibiotics. Zhou G et al.[30]added biochar to chicken manure compost, and the abundance of ARGs in the pile decreased by 95.9%, with a significant effect. Other studies have found that the specific surface area and aromatylation structure of biochar affect the allocation coefficient of antibiotics, PENG et al.[31]found through experiments that the adsorption of antibiotics by different biochar is due to the formation of π-π electron doner-acceptor interaction (π-π EDA) between the π bond on antibiotics and the π bond on the aromatic ring of biochar. CUI et al.[32]showed that biochar prepared from mushroom residue could effectively reduce ARGs in pig manure composting process and products; LI et al.[33]added different proportions of bamboo charcoal to chicken manure compost, which could reduce ARGs in compost products by 21.6%~99.5%; Qian Xun[34]showed that the addition of biochar could reduce the total abundance of ARGs in compost products by 81% compared with the control, and biochar reduced the abundance of host bacteria of ARGs, resulting in the decrease of ARGs.

Increase enzyme activity

Biochar, as a leavening agent, has the effect of increasing the porosity of compost, promoting the growth of microorganisms and improving the activity of related enzymes. Dehydrogenase activity can usually reflect the overall microbial dynamics in the composting process, because this enzyme is mainly involved in the biomineralizing respiration process of raw materials, and the maturity of the final product of composting can be indirectly reflected by measuring this enzyme activity[35]. The porous material structure of biochar can adsorb water molecules to retain water in the pile, which makes the microbial phosphatase activity in the pile easier to be excited[36]. Phosphatase can promote the hydrolysis of macromolecules such as polyphosphates and proteins and release phosphoric

acid, promoting the adsorption load and reuse of nutrients in the compost[37].Xylanase can hydrolyze cellulose to xylose in compost system, which plays an important role in reducing greenhouse gas emissions.

Yin et al.[38]found that adding bamboo charcoal to chicken manure compost could increase the activity of cellulase and urease by 56% and 96%, and the degradation ability of carbohydrate and amino acid was increased by 44% and 52%, respectively, and the degradation rate of refractory cellulose was also increased. Duan.Y. Et al.[39]found that adding biochar to sheep manure compost reduced fungal diversity in the pile, but increased enzyme activity, and found that the interaction between biochar and bacteria was more complex than other interactions with fungi, indicating that biochar regulates the microenvironment of compost by affecting microbial diversity and enzyme activity.

CONCLUSION AND PROSPECT

At present, the limiting factors to improve the aerobic composting process are generally achieved through the inoculation of functional microorganisms or the addition of additives, which can reduce the nitrogen loss of the pile, improve the microbial community, reduce harmful gas emissions, extend the high temperature period of the pile, improve the water retention of the pile, reduce the mobility of heavy metal ions and other positive effects. In the future, biochar is expected to be applied to improve the composting effect of organic solid waste on a large scale.

Low humification efficiency is the main bottleneck of aerobic compost at the present stage. Studies have shown that adding biochar to livestock and poultry manure can also promote compost maturation, increase humic acid content[8,40],and improve humus stability.The reason for the low humification efficiency of compost is that the degradation efficiency of organic matter such as lignin, cellulose and hemicellulose is low, which will cause a large loss of C, N and other elements, thus aggravating the degree of mineralization of compost and reducing the quality of compost products. Therefore, the low humification efficiency of organic solid waste compost needs to be solved. The composting process of organic solid waste involves a series of physical, chemical and biological reaction processes, but the relationship between microorganisms and microenvironment is not clear enough. The main microorganisms contained in different stages of composting are different, and the microenvironment conditions required for their survival are also different. At present, the research on optimizing microenvironment at different stages of composting is still not in-depth, and it can be studied on multi-stage inoculation and multi-stage regulation of microenvironment in the future.

ACKNOWLEDGEMENTS

This work was financially supported by Guangxi innovation research team project (2018GXNSFGA281001) and National Natural Science Foundation regional project (51668014).

REFERENCES

[1] CHEN M, HUANG Y, WANG C, et al. The conversion of organic nitrogen by functional bacteria determines the end-result of ammonia in compost[J/OL]. Bioresource Technology, 2020, 299: 122599. DOI:10.1016/j.biortech.2019.122599.

[2] AWASTHI S K, LIU T, AWASTHI M K, et al. Evaluation of biochar amendment on heavy metal resistant bacteria abundance in biosolids compost[J/OL]. Bioresource Technology, 2020, 306: 123114. DOI:10.1016/j.biortech.2020.123114.

[3] LOPEZ ZAVALA M A, FUNAMIZU N, TAKAKUWA T. Temperature effect on aerobic biodegradation of feces using sawdust as a matrix[J/OL]. Water Research, 2004, 38(9): 2406-2416. DOI:10.1016/j.watres.2004.02.026.

[4] CHEN Y, XU Y, QU F, et al. Effects of different loading rates and types of biochar on passivations of Cu and Zn via swine manure composting[J/OL]. Journal of Arid Land, 2020, 12(6): 1056-1070. DOI:10.1007/s40333-020-0026-5.

[5] DUAN Y, AWASTHI S K, LIU T, et al. Positive impact of biochar alone and combined with bacterial consortium amendment on improvement of bacterial community during cow manure composting[J/OL]. Bioresource Technology, 2019, 280: 79-87. DOI:10.1016/j.biortech.2019.02.026.

[6] BARRINGTON S. Effect of carbon source on compost nitrogen and carbon losses[J/OL]. Bioresource Technology, 2002, 83(3): 189-194. DOI:10.1016/S0960-8524(01)00229-2.

[7] CHEN Y X, HUANG X D, HAN Z Y, et al. Effects of bamboo charcoal and bamboo vinegar on nitrogen conservation and heavy metals immobility during pig manure composting[J/OL]. Chemosphere, 2010, 78(9): 1177-1181. DOI:10.1016/j.chemosphere.2009.12.029.

[8] DIAS B O, SILVA C A, HIGASHIKAWA F S, et al. Use of biochar as bulking agent for the composting of poultry manure: Effect on organic matter degradation and humification[J/OL]. Bioresource Technology, 2010, 101(4): 1239-1246. DOI:10.1016/j.biortech.2009.09.024.

[9] CHOWDHURY M A, DE NEERGAARD A, JENSEN L S. Potential of aeration flow rate and bio-char addition to reduce greenhouse gas and ammonia emissions during manure composting[J/OL]. Chemosphere, 2014, 97: 16-25. DOI:10.1016/j.chemosphere.2013.10.030.

[10] Li Taikui, Wang Xiaofei, Guo Zhanling, et al. Effects of biochar addition on nitrogen conversion and ammonia volatilization in aerobic composting of pig manure [J/OL]. Journal of Ecological environment, 2021, 30(4): 874-879. DOI:10.16258/j.cnki.1674-5906.2021.04.025.

[11] RAUT M, PRINCEWILLIAM S, BHATTACHARYYA J, et al. Microbial dynamics and enzyme activities during rapid composting of municipal solid waste – A compost maturity analysis perspective[J/OL]. Bioresource Technology, 2008, 99(14): 6512-6519. DOI:10.1016/j.biortech.2007.11.030.

[12] SULLIVAN D M, BARY A I, THOMAS D R, et al. Food Waste Compost Effects on Fertilizer Nitrogen Efficiency, Available Nitrogen, and Tall Fescue Yield[J/OL]. Soil Science Society of America Journal, 2002, 66(1): 154-161. DOI:10.2136/sssaj2002.1540a.

[13] GLASER B, LEHMANN J, ZECH W. Ameliorating physical and chemical properties of

highly weathered soils in the tropics with charcoal - a review[J/OL]. Biology and Fertility of Soils, 2002, 35(4): 219-230. DOI:10.1007/s00374-002-0466-4.

[14] PIETIKÄINEN J, KIIKKILÄ O, FRITZE H. Charcoal as a habitat for microbes and its effect on the microbial community of the underlying humus[J/OL]. Oikos, 2000, 89(2): 231-242. DOI:10.1034/j.1600-0706.2000.890203.x.

[15] BERNAL M P, ALBURQUERQUE J A, MORAL R. Composting of animal manures and chemical criteria for compost maturity assessment. A review[J/OL]. Bioresource Technology, 2009, 100(22): 5444-5453. DOI:10.1016/j.biortech.2008.11.027.

[16] HUA L, CHEN Y, WU W. Impacts upon soil quality and plant growth of bamboo charcoal addition to composted sludge[J/OL]. Environmental Technology, 2012, 33(1): 61-68. DOI:10.1080/09593330.2010.549845.

[17] FARRELL M, KUHN T K, MACDONALD L M, et al. Microbial utilisation of biochar-derived carbon[J/OL]. Science of The Total Environment, 2013, 465: 288-297. DOI:10.1016/j.scitotenv.2013.03.090.

[18] Wang Yi-xiang, Ye Jing, Lin Yi, et al. Effects of peanut shell biochar on greenhouse gas and NH_3 emissions from pig manure compost [J]. Journal of China Agricultural University, 2021, 26(6): 114-125.

[19] Wu Xiaodong, Xing ZBing, He Yuanling, et al. Study on nutrient conversion of chicken manure in aerobic composting process by adding biochar [J]. Soil and Fertilizer in China, 2019(5): 141-146.

[20] SANCHEZ-MONEDERO M A, CAYUELA M L, ROIG A, et al. Role of biochar as an additive in organic waste composting[J/OL]. Bioresource Technology, 2018, 247: 1155-1164. DOI:10.1016/j.biortech.2017.09.193.

[21] LÓPEZ-CANO I, ROIG A, CAYUELA M L, et al. Biochar improves N cycling during composting of olive mill wastes and sheep manure[J/OL]. Waste Management, 2016, 49: 553-559. DOI:10.1016/j.wasman.2015.12.031.

[22] Zhang Haibin, Meng Haibo, Shen Yujun, et al. Effects of biochar on physicochemical properties and microbial population changes of biogas residue compost [J]. Plant Nutrition and Fertilizer Science, 2019, 25(2): 245-253.

[23] TIQUIA S M, TAM N F Y, HODGKISS I J. Microbial activities during composting of spent pig-manure sawdust litter at different moisture contents[J/OL]. Bioresource Technology, 1996, 55(3): 201-206. DOI:10.1016/0960-8524(95)00195-6.

[24] Zhu Shijiang, Ye Xiaosi, Wang Bin, et al. Effects of different water regulation and biochar ratio on rice yield and water use efficiency [J]. Water-saving irrigation, 2018(1): 1-5.

[25] MULCHI C L, ADAMU C A, BELL P F, et al. Residual heavy metal concentrations in sludge amended coastal plain soils - II. Predicting metal concentrations in tobacco from soil test information[J/OL]. Communications in Soil Science and Plant Analysis, 1992, 23(9-10): 1053-1069. DOI:10.1080/00103629209368649.

[26] PETRUZZELLI G, LUBRANO L, GUIDI G. Uptake by corn and chemical extractability of heavy metals from a four year compost treated soil[J/OL]. Plant and Soil, 1989, 116(1): 23-27. DOI:10.1007/BF02327253.

[27] BEVACQUA R F, MELLANO V J. Sewage Sludge Compost's Cumulative Effects on Crop Growth and Soil Properties[J/OL]. Compost Science & Utilization, 1993, 1(3): 34-37. DOI:10.1080/1065657X.1993.10757886.

[28] Wang Yahui, Qin Yuhong, Ma Yanrong, et al. Effects of biochar combined with micro-fertilizer on the content of available heavy metals in vegetable soil [J]. Journal of South China Agricultural University, 2018, 39(5): 18-24.

[29] Bao Canxin, ZHANG Yuan, Chen Minglong, et al. Study on the reduction of antibiotic and

antibiotic resistance genes in pig manure composting process by different biochar [J/OL]. Environmental pollution and prevention, 2022, 44(2): 160-164+172. DOI:10.15985/j.cnki.1001-3865.2022.02.003.

[30] ZHOU G, QIU X, WU X, et al. Horizontal gene transfer is a key determinant of antibiotic resistance genes profiles during chicken manure composting with the addition of biochar and zeolite[J/OL]. Journal of Hazardous Materials, 2021, 408: 124883. DOI:10.1016/j.jhazmat.2020.124883.

[31] PENG B, CHEN L, QUE C, et al. Adsorption of Antibiotics on Graphene and Biochar in Aqueous Solutions Induced by π-π Interactions[J/OL]. Scientific Reports, 2016, 6(1): 31920. DOI:10.1038/srep31920.

[32] CUI E, WU Y, ZUO Y, et al. Effect of different biochars on antibiotic resistance genes and bacterial community during chicken manure composting[J/OL]. Bioresource Technology, 2016, 203: 11-17. DOI:10.1016/j.biortech.2015.12.030.

[33] LI Y, WANG H, LIU X, et al. Dissipation kinetics of oxytetracycline, tetracycline, and chlortetracycline residues in soil[J/OL]. Environmental Science and Pollution Research, 2016, 23(14): 13822-13831. DOI:10.1007/s11356-016-6513-8.

[34] Qian X. Study on the conditions and mechanism of reducing antibiotic resistance genes in livestock and poultry manure by aerobic compost [D/OL]. Northwest Agriculture and Forestry University, 2016.

[35] LIU D, ZHANG R, WU H, et al. Changes in biochemical and microbiological parameters during the period of rapid composting of dairy manure with rice chaff[J/OL]. Bioresource Technology, 2011, 102(19): 9040-9049. DOI:10.1016/j.biortech.2011.07.052.

[36] AWASTHI M K, WANG Q, REN X, et al. Role of biochar amendment in mitigation of nitrogen loss and greenhouse gas emission during sewage sludge composting[J/OL]. Bioresource Technology, 2016, 219: 270-280. DOI:10.1016/j.biortech.2016.07.128.

[37] CHU Q, LYU T, XUE L, et al. Hydrothermal carbonization of microalgae for phosphorus recycling from wastewater to crop-soil systems as slow-release fertilizers[J/OL]. Journal of Cleaner Production, 2021, 283: 124627. DOI:10.1016/j.jclepro.2020.124627.

[38] YIN Y, YANG C, TANG J, et al. Bamboo charcoal enhances cellulase and urease activities during chicken manure composting: Roles of the bacterial community and metabolic functions[J/OL]. Journal of Environmental Sciences, 2021, 108: 84-95. DOI:10.1016/j.jes.2021.02.007.

[39] DUAN Y, AWASTHI M K, WU H, et al. Biochar regulates bacterial-fungal diversity and associated enzymatic activity during sheep manure composting[J/OL]. Bioresource Technology, 2022, 346: 126647. DOI:10.1016/j.biortech.2021.126647.

[40] CHENG C H, LEHMANN J, THIES J E, et al. Oxidation of black carbon by biotic and abiotic processes[J/OL]. Organic Geochemistry, 2006, 37(11): 1477-1488. DOI:10.1016/j.orggeochem.2006.06.022.

RESEARCH STATUS AND PROSPECTS OF LEACHATE TREATMENT TECHNOLOGY IN DOMESTIC WASTE LANDFILL SITES

Junwen Zheng[1,2,3], Xiaojie Sun[1,2,3*]

1.Guangxi Key Laboratory of Environmental Pollution Control Theory and Technology, Guilin University of Technology, Guilin 541004, China

2.Guangxi Collaborative Innovation Center for Water Pollution Control and Water Safety in Karst Area, Guilin University of Technology, Guilin 541004, China

3. Guangxi Key Laboratory of Environmental Pollution Control Theory and Technology for Science and Education Combined with Science and Technology Innovation Base, Guilin University of Technology, Guilin 541004, China

Abstract: Every year, approximately 11.8 million tons of waste in China are processed through sanitary landfills, generating a large amount of leachate, inevitably reaching as high as 1170.6 to 2341.2 tons. The leachate of waste mainly comes from the internal water in waste, biochemical reactions in waste, and atmospheric precipitation, which may eventually enter the soil and then be discharged into surface water bodies or directly into groundwater. Due to the complex composition of pollutants in landfill leachate, significant fluctuations in water quality, high concentrations of organic matter, ammonia nitrogen, heavy metal ions, and salts, it is difficult to treat the leachate. This article analyzes the physicochemical, biological, and land treatment methods for treating leachate, as well as the commonly used leachate treatment processes in China. It looks forward to the future direction and prospects of leachate treatment: (1) reducing the generation of membrane concentrate; (2) Collaborative processing with multiple processing technologies; (3) The recycling and reuse of valuable substances.

INTRODUCTION

With the rapid development of the economy and the sharp increase in population, humans have generated more and more types of solid waste. According to statistics from the World Bank, the annual production of urban solid waste is approximately 2 billion tons, which will increase to 3.4 billion tons by 2050. Although high-income countries have relatively small populations (16% of the world), their waste accounts for 34% of the world's total. According to the China Statistical Yearbook, China generated 22.8 million tons of waste in 2018. Therefore, the waste generated by various pollutants poses a threat to the safety of the ecological environment. The most common waste treatment methods are sanitary landfill and incineration[1]. A recent survey found that most developed countries mainly treat solid waste through sanitary landfills[2]. For example, sanitary landfills account for 60-70% of the total amount of waste processed in the United States. In addition, approximately 11.8 million tons of waste in China are disposed of through sanitary landfills each year, resulting in a large amount of leachate, inevitably reaching 1170.6 to 2341.2 tons. The leachate of waste mainly comes from the internal water in waste, biochemical reactions in waste, and atmospheric precipitation, which may eventually enter the soil and then be discharged into surface water bodies or directly into groundwater[3]. Research has shown that landfill leachate consists of four main types of compounds, namely dissolved organic compounds, total organic carbon (TOC), volatile fatty acids (VFA), humic acid and humic acid components, inorganic components (Ca^{2+}, Mg^{2+}, NH^{4+}, Fe^{2+}, Mn^{2+}, Cl^{-}), heavy metals (As, Hg, Cd, Cr, Cu, Pb), and exogenous organic

compounds (XOCs benzene, toluene, phenol, chlorinated aliphatic compounds, phthalates). Considering the time variation of leachate parameters during the degradation process of waste, waste leachate can be divided into two categories: acetic acid producing leachate and methane producing leachate. Research has shown that due to the increase in levels of organic pollutants[4] and the increase in acidity of the leachate caused by acetylacetic acid, the solubility of metals is increased, resulting in an increase in levels of heavy metal pollutants. The generation of leachate from landfill sites may also vary depending on the type of waste, climate, site, and surface conditions, making it difficult to treat to a satisfactory level[5]. Moreover, landfill leachate may cause pollution to surface water, groundwater, and soil through transformation, posing a serious threat to the environment. In order to reduce the risk of pollution, pollutants in landfill leachate should be treated as safely as possible[6]. Therefore, it is urgent to explore efficient technologies for treating landfill leachate.

This article mainly summarizes the relatively efficient leachate treatment technologies that have been studied in China and foreign countries, providing reference for the future development of leachate treatment processes.

PROPERTIES OF LEACHATE

Due to the different types of waste, chemical substances contained, landfilling methods, dissolution rates, and evaporation rates, the composition and concentration of pollutants in landfill leachate vary greatly, and are also affected by rainfall, landfill treatment methods, and process methods. According to the operating time, landfill sites are divided into three types. The first type is a landfill site that has been operating for four to five years, which belongs to the initial stage of landfill, The initial landfill site is in the acid production stage, so during this stage, the leachate is highly acidic, containing a large amount of organic acids, BOD, COD, nutrients, and precious metals. Due to its strong acidity, the content of ammonia nitrogen is relatively low, and its biodegradability is strong. Therefore, the treatment of landfill leachate is relatively easy.

The second type is a landfill that has been operating for five to ten years. This stage is in the mature stage, and as the operation time progresses, the landfill has entered the stage of methane production. The concentration of BOD and COD in the leachate has significantly decreased, the ratio of the two has decreased more significantly, the biodegradability has weakened, the ammonia nitrogen content has increased, and the C/N ratio is not ideal. This stage is more difficult for the treatment of leachate.

landfills with a history of more than ten years belong to the category of elderly landfills. The values of BOD and COD in elderly waste landfills have decreased compared to the mature period, and the content of ammonia nitrogen continues to increase. However, the increase in ammonia nitrogen is significantly lower than that of BOD and COD, and the biodegradability of pollutants continues to decrease. Therefore, the difficulty of treating landfill leachate is greater[7]. Table 1 shows the characteristics of leachate quality in various types of landfills.

Table 1 Changes in Physical and Chemical Composition of Leachate with Landfill Age [8,9]

parameter	Age of landfill leachate (years)			
（$mg \cdot L^{-1}$）	0-5	5-10	10-20	>20
pH	3-6	6-7	7-7.5	7.5
BOD	10000-25000	1000-4000	50-1000	<50
COD	15000-40000	10000-20000	1000-5000	<1000
TN	1500-4250	400-800	75-300	<50
NH_4^+-N	1500-4250	250-700	50-200	<30
Cl^-	1000–3000	500–2000	100–500	< 100
P	100–300	10–100	–	<10
alkalinity	8000–	4500–	–	–

	18000	6000		
conductivity	15000–41500	6000–14000	–	–
SO_4^{2-}	500–2000	200–1000	50–200	< 50
Fe^{2+}	500–1500	500–1000	100–500	< 100
Zn^{2+}	100–200	50–100	10–50	< 10
total dissolved solids	10000–25000	5000–10000	2000–5000	< 1000

(-) Not detected

In summary, the water quality of landfill leachate has the following characteristics: (1) complex pollutant composition and significant water quality fluctuations. Due to the fact that waste is usually treated in a centralized manner, its composition is complex and contains various chemical substances. Therefore, the leachate of waste also contains various organic, nutrient, and inorganic substances. The main pollutants contained in landfill leachate are heavy metals, phenols, soluble fatty acids, dissolved cations, and other organic pollutants. (2) High concentration of organic matter means high concentration of COD and BOD. The concentration of BOD and COD landfill leachate is as high as tens of thousands of milligrams per liter, but it will gradually decrease with the migration of landfill time. Even so, it still meets the requirements of thousands of milligrams per liter, which is relatively higher than other wastewater. (3) The concentration of ammonia nitrogen is high. As the landfill time of household waste increases, under the action of microorganisms, the organic nitrogen in the waste decomposes and releases, leading to an increase in ammonia nitrogen content, which can increase from 800-1500 mg/L to 2000-3000 mg/L. Some landfills may even reach as high as 4000 mg/L, while the BOD_5/COD of leachate decreases from 0.5-0.6 at the beginning of landfill to 0.1-0.2. With the decomposition and utilization of easily degradable organic matter, the proportion of organic carbon sources that can be decomposed and utilized by microorganisms in the late stage leachate is relatively small, coupled with a low C/N ratio, conventional biological treatment methods cannot meet the requirements[10]. (4) The concentration and salt content of heavy metal ions are high. Landfill domestic waste separately, and the heavy metal content in the waste dump is not high. When sludge and industrial wastewater are added to household waste, the content of salt, heavy metals, and other substances in the waste pile will rapidly increase. The commonly used biochemical treatment methods cannot control biochemical toxicity. (5) High chromaticity and foul odor. Leachate has a high chromaticity, usually a tan, dark brown, or black liquid, and its appearance characteristics are related to the age of the leachate. The landfill leachate has a strong odor of waste spoilage.

LEACHATE TREATMENT

There are many influencing factors for landfill leachate, and conventional treatment techniques are often not suitable for the treatment of landfill leachate in a specific landfill or area[11]. In addition, the composition of landfill leachate is complex, with a high content of toxic and harmful substances. The water quality and quantity change greatly, making it difficult to treat. While ensuring the treatment effect, it is also necessary to consider economic rationality. At present, it is difficult to meet the treatment requirements by using a single process, and multiple methods need to be combined and optimized to effectively achieve standard emissions[12]. For the treatment of landfill leachate, physical and chemical methods, biological treatment methods, and land treatment methods are mainly used.

Physical and chemical treatment

The biodegradability of waste leachate is poor (low BOD_5/COD value), the concentration of difficult to degrade organic matter is high, and the biological toxicity is high. It is difficult to achieve the ideal treatment effect solely using biological treatment methods. Therefore, using certain physical and chemical methods combined with biological treatment methods can further improve the treatment effect. The commonly used physicochemical treatment methods in sewage include coagulation[13], adsorption[14],

electrolysis[15], advanced oxidation[16], membrane separation[17].

Coagulation treatment technology

Coagulation/flocculation is one of the most common pre-treatment methods, where chemicals called coagulants or flocculants are used to separate small suspended particles from larger flocs in water through the formation, followed by physical separation or gravity sedimentation[18]. Shang Pingping used polymeric aluminum chloride (PAC) and polymeric iron sulfate (PFS) as coagulants, added coagulant aid polyacrylamide (PAM), and combined with bird droppingstone precipitation method to pre-treat landfill leachate. The removal rate of ammonia nitrogen in the treated effluent reached 95.60% . Coagulation treatment is generally used as a pre-treatment method for landfill leachate, which can settle some difficult to degrade pollutants and effectively reduce the toxicity of landfill leachate to microorganisms. However, its disadvantages are high cost of chemicals, high sludge production, and limited ability to remove pollutants[19].

Adsorption treatment technology

Adsorption method is a common and efficient water treatment method that utilizes different types of adsorbents to achieve sewage purification. It is widely used in the treatment of printing and dyeing wastewater, pharmaceutical wastewater, chemical wastewater, and heavy metal wastewater. The preparation of adsorption materials with stable performance and low cost is an important influencing factor for the application of adsorption treatment in practical wastewater treatment engineering[20]. Due to the presence of a large amount of humic acid substances in the leachate, the molecular weight of humic acid substances is extremely high, ranging from 20000-100000Da, and contains a variety of common active groups. Therefore, the selection and application of adsorbents with larger pore sizes and full of active groups are key to the adsorption and treatment of organic matter in waste leachate. However, the applicability of adsorption treatment technology in waste leachate related applications still needs to be verified[21]. K Erabee I. et al. used coconut shell based activated carbon to remove TSS, ammonia nitrogen, Zn, and Cu from landfill leachate with removal rates of 91%, 99%, 86%, and 100%, respectively. The study found that the pollutant removal rate depends on the bed depth and contact time of the adsorbent[22]. Yang et al. studied the combined treatment technology of ozone oxidation and activated carbon adsorption for the removal of micro pollutants in landfill leachate, and found that ozone oxidation can effectively improve the adsorption efficiency of activated carbon by 1%-41% [23].

Electrolytic treatment technology

Electrolytic treatment is a process in which harmful substances in wastewater undergo oxidation and reduction reactions at the positive and negative poles through electrolysis, transforming them into harmless substances to achieve wastewater purification [24]. Deng Yang et al. used Ti/RuO_2-Fe-Cu/Zn as electrodes to treat landfill leachate and found that under the optimal conditions of current density of 100 mA/cm^2, electrolysis time of 4 hours, chloride ion concentration of 2840 mg/L, and initial pH value of 8.5, the removal rates of COD, ammonia nitrogen, TN, and TOC reached 94.12%, 99.55%, 94.17%, and 61.65%, respectively. Pasalar et al. studied the effects of electrochemical oxidation and low current density electrochemistry on the anaerobic co-digestion system of landfill leachate and sludge. Under conditions of current density of 10-40mA/cm^2, electrode spacing of 0.5-2cm, and contact time of 15-60 minutes, the biodegradability of leachate was significantly improved [25].

Advanced oxidation process

Advanced oxidation method is the process of converting pollutants into stable, low toxicity, or non-toxic substances through oxidation or reduction. It mainly includes ozone oxidation method[26], Fenton oxidation method[27], Fenton like catalytic oxidation method[28], persulfate oxidation method[29], photocatalytic oxidation method[30], and ultrasonic wave oxidation method[31]. Commonly used oxidants include ozone, hydrogen peroxide, hypochlorite,

chlorine gas, chlorine dioxide, potassium permanganate, and Fenton reagent, It can rapidly degrade organic matter and is not prone to secondary pollution. It has a wide range of applications and can also improve the biodegradability of landfill leachate[32]. Shriwan K. Singh et al. used ozone oxidation as a pre-treatment for landfill leachate membrane treatment, using 66.7 g/m^3 ozone and a reaction time of 5-30 minutes. They found that the permeation flux of landfill leachate after ozone oxidation increased compared to before treatment[33]. Caihua Li et al. used (MnO_2-Co_3O_4/AC) supported activated carbon composite materials (MnO_2-Co_3O_4/AC) as catalysts. When the ratio of MnO_2: Co_3O_4: AC was 1:2.49:31.23, the biodegradability of wastewater (BOD_5/COD) was improved from 0.15 to 0.80[34] at 0.4g/L (MnO_2-Co_3O_4/AC) and 6.11 mg/(min · L^{-1}) of ozone catalytic oxidation.

Membrane separation technology

Membrane treatment technology refers to the process of selectively separating liquids through semi permeable membranes with different pore sizes. According to the pore size of the semi-permeable membrane, it can be divided into technologies such as microfiltration, ultrafiltration, nanofiltration, reverse osmosis, etc. When applied to the treatment of landfill leachate, it can greatly save treatment costs and effectively solve the problem of leachate pollution. Membrane treatment technology has the advantages of small footprint and good water permeability, However, a large amount of concentrated solution is generated during the treatment process, and membrane fouling is a serious problem, so it is often combined with other technologies[35]. Magdalena Zieliń Ska et al. studied the removal of COD and chromaticity from landfill leachate by microfiltration, ultrafiltration, and high-efficiency ultrafiltration alone or in combination with powdered activated carbon, and found that they have good treatment effects, with the combination of powdered activated carbon and membrane filtration having the best treatment effect[36]. Vitória Santos et al. used three different combined processes of microfiltration, nanofiltration, and Fenton oxidation to achieve effective treatment of landfill leachate, with COD removal rates reaching 94~96% and chromaticity removal rates reaching 96~99%[37].

Biological treatment

Biological method is a commonly used technology in the treatment of landfill leachate, which can be divided into anaerobic treatment, aerobic treatment, anaerobic aerobic combination, and short range nitrification denitrification anaerobic ammonia oxidation processes. The biological method for treating landfill leachate has the advantages of low investment, high treatment efficiency, and stable operation, and has been widely used at home and abroad .

Anaerobic biological treatment

Anaerobic biological treatment refers to the process in which anaerobic microorganisms convert organic matter into methane (CH_4) and carbon dioxide (CO_2) under anaerobic conditions. It has the advantages of stable performance, low energy consumption, and easy operation, and is suitable for the treatment of high concentration organic wastewater. However, for landfill leachate treated by anaerobic biological treatment, the effluent still contains high COD and ammonia nitrogen, and further treatment is needed[38]. Yao Qian et al. studied the effect of initial ammonia nitrogen mass concentration on anaerobic pretreatment of landfill leachate and found that when the water temperature was at 30 ℃ and the load was 1 kg COD/(m^3 · d), the initial ammonia nitrogen concentration was set from low to high at five levels: 1600 mg/L, 1800 mg/L, 2000 mg/L, 2200 mg/L, and 2500 mg/L. Other experimental conditions were the same, and the final COD removal rates were 85%, 69%, 52%, 51%, 40%, and 41%, respectively. Therefore, it can be concluded that, Different concentrations of ammonia nitrogen content have mild, moderate, and severe inhibition on COD removal, respectively[39].

Aerobic biological treatment

Aerobic biological treatment technology refers to the use of dissolved organic matter in water as a carbon source by microorganisms under aerobic conditions to decompose organic matter into inorganic matter,

achieving stability and harmless treatment. It is divided into activated sludge method and biofilm method[40]. The activated sludge method is economical and efficient, and is widely used. Many studies have shown that traditional activated sludge can effectively remove BOD_5 from landfill leachate[41]. Compared with traditional activated sludge, biofilm method has the advantage of resistance to shock loading, and biofilm plays a certain interception role, capable of growing microorganisms with longer generation cycles, such as nitrifying bacteria[42]. In summary, biological methods are widely used in the treatment of landfill leachate, and the biochemical treatment technology of landfill leachate is still one of the hot research topics at home and abroad. But in order to ensure stable treatment effect, combined treatment processes are usually used.

Anaerobic ammonia oxidation technology

Anaerobic ammonia oxidation refers to the conversion of ammonia nitrogen and nitrite nitrogen into N_2 by anaerobic ammonia oxidizing bacteria under anaerobic or anaerobic conditions.This process has the characteristics of low oxygen consumption, fast reaction speed, low residual sludge amount, and no need for additional organic carbon sources. Combined with the short-range nitrification process, it has the advantages of low operating cost, saving reactor volume and reaction time[43]. Zhu et al. used the coupling process of "partial nitrification anaerobic ammonia oxidation soil infiltration" to treat landfill leachate. After 166 days of operation, the average removal rates of TN, NH^{4+}- N, and COD reached 87%, 97%, and 89%, respectively[44].Lina Wu et al. used partial nitrification coupled anaerobic ammonia oxidation to synergistically treat municipal wastewater at low temperatures (13 ℃ -21 ℃) to treat landfill leachate. After mixing municipal wastewater with landfill leachate in a 1:1 ratio and incubating for 100 days, the final removal rates of COD, NH^{4+}- N, and TN remained stable at 87.10%,97.40-97.70%,and 93.30-94.70%,with the contribution rate of ammonia nitrogen removal in the anaerobic ammonia oxidation stage being 11.40% -29.30%[45].

Land treatment technology

Land treatment method is a relatively primitive treatment method that utilizes vegetation soil as the main treatment facility, with functions such as adsorption and filtration, in order to achieve purification[46]. Land treatment methods include irrigation and artificial wetlands, among which artificial wetlands are widely used. The removal of organic matter in wetlands mainly relies on microorganisms. Due to the large specific surface area of artificial substrates, microorganisms are easily able to form a dense biofilm on the substrate surface. When landfill leachate flows through the substrate surface, large particles of organic matter are trapped on the biofilm surface due to sedimentation and filtration, providing energy for microbial growth, Soluble organic matter is removed through membrane adsorption and biodegradation[47].

FUTURE PROSPECT

The characteristics of COD, BOD/COD ratio, and landfill age of landfill leachate are necessary conditions for determining the appropriate treatment technology selection. However, the chemical composition of leachate from different landfills varies significantly, and even if they have the same COD value, it can lead to performance differences during the treatment process. Therefore, it is necessary to understand the treatment processes of different landfills in order to choose the most cost-effective treatment technology

Although there are various methods for treating landfill leachate, none of them are effective and cost-effective enough to meet the requirements of effluent standards. Given the application and development of landfill leachate treatment technology, the future direction and prospects are discussed.

(1) Reduce the production of membrane concentrate. Due to the fact that biological treatment and membrane filtration are the main technologies used worldwide for the treatment of landfill leachate, reducing the generation of membrane concentrate can

be directly carried out for subsequent treatment and avoiding secondary pollution. The key to solving this problem is how to improve the permeability of the membrane and how to reduce membrane fouling. The membrane flux is determined by external driving forces and membrane resistance. The changes in membrane fouling mainly depend on the characteristics of membrane components, operating conditions, and the composition of landfill leachate, as the fouling process is controlled by the interaction between fluid dynamics and solution chemistry. In order to strengthen the membrane process and reduce membrane concentration, some requirements and challenges should be considered: designing new membrane materials with high filtration and anti fouling performance; Application of pre-treatment, such as reducing salt content before membrane filtration; Research on the mechanism of membrane fouling, such as the impact of the main components in landfill leachate on the membrane filtration process.

(2) Collaborative processing with multiple processing technologies. Each technology has its unique advantages, disadvantages, and applicability. The synergy of different treatment methods for landfill leachate can not only synergize the advantages of a single treatment method, but also overcome their respective shortcomings, which has been proven to have higher efficiency and lower costs. For example, AOP has high efficiency in removing organic pollutants from landfill leachate, but the cost of reagents and/or operations may be high. Therefore, they can be used as pre-treatment or post-processing steps to improve removal efficiency and reduce costs. Alternatively, graded treatment may be a worthwhile research direction, as in single stage reaction processes, reaction efficiency may be reduced/suppressed due to changes in reaction conditions, such as ineffective decomposition of H_2O_2 and changes in solution pH. By combining multiple levels, a thorough reaction can be achieved to the maximum extent possible.

(3) The recycling and reuse of valuable substances. waste leachate contains rich metal elements and humic substances, and recycling it as secondary resources such as fertilizer is a promising method. Therefore, efforts should be made to develop effective methods for separating (such as resin separation) and enriching valuable substances in landfill leachate. In addition, the added solid chemical reagents can be recycled and reused multiple times, while the added ionic chemical reagents can be separated and extracted as raw materials for other applications. It is necessary to fully utilize the large amount of resources in landfill leachate and reduce the use of expensive synthetic substances.

ACKNOWLEDGEMENTS

This work was financially supported by Guangxi innovation research team project (2018GXNSFGA281001) and Guangxi major science and technology projects (GuikeAA18118013).

REFERENCES

[1] Bolyard, S.C., Reinhart, D.R., 2016. Application of landfill treatment approaches for stabilization of municipal solid waste. Waste Manag. 55, 22–30.

[2] Das, S., Lee, S.H., Kumar, P., Kim, K.-H., Lee, S.S., Bhattacharya, S.S., 2019. Solid waste management: scope and the challenge of sustainability. J. Clean. Prod. 228, 658–678.

[3] Fan, H., Shu, H.-Y., Yang, H.-S., Chen, W.-C., 2006. Characteristics of landfill leachates in central Taiwan. Sci. Total Environ. 361, 25–37.

[4] Robinson, H., 2007. The composition of leachates from very large landfills: an international review. Commun. Waste Resour. Manag. 8, 19–32.

[5] Bhalla, B., Saini, M.S., Jha, M.K., 2012. Characterization of leachate from municipal solid waste (MSW) landfilling sites of Ludhiana, India: a comparative study. Int. J. Eng. Res. Appl. 2, 732–745.

[6] Abdulhussain, A.A., Guo, J., Liu Zhi, P., Pan Ying, Y., Wisaam, S.A.-R., 2009. Review on landfill leachate treatments. Am. J. Appl. Sci. 6 (4), 672–684.

[7] Yanping Liu,Xiujin Li,Baozhen Wang,et all. Performance of landfill leachate treatment system with disc-tube reverse osmosis units[J]. Frontiers of Environmental Science &Engineering in China,2008,21(03):123-128.
[8] Farquhar, G.J., 1989. Leachate: production and characterization. Can. J. Civ. Eng. 16,317–325.
[9] Ziyang, L., Youcai, Z., Tao, Y., Yu, S., Huili, C., Nanwen, Z., Renhua, H., 2009. Natural attenuation and characterization of contaminants composition in landfill leachate under different disposing ages. Sci. Total Environ. 407, 3385–3391.
[10] Mojiri A, Zhou J L, Ratnaweera H, Ohashi A, Ozaki N, Kindaichi T, Asakura H. Treatment Of Landfill Leachate With Different Techniques: An Overview[J]. Journal Of Water Reuse And Desalination, 2021,11(1).
[11] Fang D, Wang J, Cui D, Dong X, Tang C, Zhang L, Yue D. Recent Advances Of Landfill Leachate Treatment[J]. Journal Of The Indian Institute Of Science, 2021,101(4).
[12] Wijekoon P, Koliyabandara P A, Cooray A T, Lam S S, Athapattu B C L, Vithanage M. Progress And Prospects In Mitigation Of Landfill Leachate Pollution: Risk, Pollution Potential, Treatment And Challenges[J]. Journal Of Hazardous Materials, 2022,421.
[13] Mehdi G L, Mohammad R S, Elnaz G, Allahyar A. Energy Consumption And Relative Efficiency Improvement Of Photo-Fenton – Optimization By Rsm For Landfill Leachate Treatment, A Case Study[J]. Waste Management, 2018,79.
[14] Binay K T, Mathava K. Suitability Of Microwave And Microwave-Coupled Systems For Landfill Leachate Treatment: An Overview[J]. Journal Of Environmental Chemical Engineering, 2017,5(6).
[15] Pubali M, Brajesh K D, Ashok K G. Review On Landfill Leachate Treatment By Electrochemical Oxidation: Drawbacks, Challenges And Future Scope[J]. Waste Management, 2017,69.
[16] Yao P. Perspectives On Technology For Landfill Leachate Treatment[J]. Arabian Journal Of Chemistry, 2013,10(S2).
[17] Archa B, R. G, S. T R, P. V N. Combined Heterogeneous Electro-Fenton And Biological Process For The Treatment Of Stabilized Landfill Leachate[J]. Journal Of Environmental Management, 2018,210.
[18] Wang H, Xiao W, Zhang C, Sun Y, Wang Y, Gong Z, Zhan M, Fu Y, Liu K. Effective Removal Of Refractory Organic Contaminants From Reverse Osmosis Concentrated Leachate Using Pfs-Nzvi/Pms/O_3 Process[J]. Waste Management, 2021,128.
[19] Xuefei T, T. H P N, Shih H H, Tau C L, Joon C J, Preeti P, Pau L S, Kuan S K. Treatment For Landfill Leachate Via Physicochemical Approaches: An Overview[J]. Chemical And Biochemical Engineering Quarterly, 2020,34(1).
[20] Hashmi Z, Jatoi A S, Nadeem S, Anjum A, Imam S M, Jangda H. Comparative Analysis Of Conventional To Biomass-Derived Adsorbent For Wastewater Treatment: A Review[J]. Biomass Conversion And Biorefinery, 2022(Prepublish).
[21] Wenjie S, Dongbei Y, Jiangang S, Yongfeng N. Adsorption Removal Of Refractory Organic Matter In Bio-Treated Municipal Solid Waste Landfill Leachate By Anion Exchange Resins[J]. Waste Management, 2018,81.
[22] K Erabee I., Ahsan A., Jose Bipin, Manniruzzaman A Aziz M., W M Ng A., Idrus S., N N Daud N. Adsorptive Treatment Of Landfill Leachate Using Activated Carbon Modified With Three Different Methods[J]. Ksce Journal Of Civil Engineering, 2018,22(4).
[23] Yang K, Liu M, Weng X, Owens G, Chen Z. Fenton-Like Oxidation For The Simultaneous Removal Of Estrone And B-Estradiol From Wastewater Using Biosynthesized Silver Nanoparticles[J]. Separation And Purification Technology, 2022,285.
[24] Garcia R O, Mousset E, Olvera V H, Lefebvre O. Electrochemical Treatment Of Highly Concentrated Wastewater: A Review Of Experimental And Modeling Approaches From Lab- To Full-Scale[J]. Critical Reviews In Environmental Science And Technology, 2022,52(2).

[25] Pasalari H, Esrafili A, Rezaee A, Gholami M, Farzadkia M. Electrochemical Oxidation Pretreatment For Enhanced Methane Potential From Landfill Leachate In Anaerobic Co-Digestion Process: Performance, Gompertz Model, And Energy Assessment[J]. Chemical Engineering Journal, 2021,422.

[26] Phan L T, Schaar H, Saracevic E, Krampe J, Kreuzinger N. Effect Of Ozonation On The Biodegradability Of Urban Wastewater Treatment Plant Effluent.[J]. The Science Of The Total Environment, 2021,812.

[27] Chen L, Yan B, Lu H. An Experimental Study On The Pretreatment Of Lignite Upgrading Wastewater Using The Fenton Oxidation Method[J]. Chemical Papers, 2021(Prepublish).

[28] Reza S M, Tari K, Shabanloo A, Salari M, Zolghadr N H. Synergistic Degradation Of Acid Blue 113 Dye In A Thermally Activated Persulfate (Tap)/Zno-Gac Oxidation System: Degradation Pathway And Application For Real Textile Wastewater[J]. Separation And Purification Technology, 2020,247(C).

[29] Pan Y, Zhang Y, Huang Y, Jia Y, Chen L, Cui H. Synergistic Effect Of Adsorptive Photocatalytic Oxidation And Degradation Mechanism Of Cyanides And Cu/Zn Complexes Over Tio2/Zsm-5 In Real Wastewater[J]. Journal Of Hazardous Materials, 2021,416.

[30] Ping Z, Jijun D, Yonghui S, Yongqiang L, Ruixia L, Panyue Z, Shuhu X. Efficiency Comparison For Treatment Of Amantadine Pharmaceutical Wastewater By Fenton, Ultrasonic, And Fenton/Ultrasonic Processes[J]. Environmental Earth Sciences, 2015,73(9).

[31] Nuno A, Rui C M, SÉRgio C, Rosa M Q. Ozonation And Perozonation On The Biodegradability Improvement Of A Landfill Leachate[J]. Journal Of Environmental Chemical Engineering, 2016,4(1).

[32] Shrawan K S, Chris M M, Timothy G T. Ozonation Pretreatment For Stabilized Landfill Leachate Anammox Plant Combining Activated Sludge And High-Pressure Membrane Treatment[J]. Desalination, 2014,344.

[33] Caihua L, Feng J, Dezhi S, Bin Q. Catalytic Ozonation For Advanced Treatment Of Incineration Leachate Using (MnO_2-Co_3O_4)/Ac As A Catalyst[J]. Chemical Engineering Journal, 2017,325.

[34] Bilal A, Jinwoo C, Hyun S S, Jin H. Using Eem-Parafac To Probe Nf Membrane Fouling Potential Of Stabilized Landfill Leachate Pretreated By Various Options[J]. Waste Management, 2020,102(C).

[35] Magdalena Z, Dorota K, Marcin S. Adsorption – Membrane Process For Treatment Of Stabilized Municipal Landfill Leachate[J]. Waste Management, 2020,114.

[36] Santos A V, Andrade L H D, Amaral M C S, Lange L C. Integration Of Membrane Separation And Fenton Processes For Sanitary Landfill Leachate Treatment.[J]. Environmental Technology, 2019,40(22).

[37] Tabish N, Ashiqur R, Shanglei P, Kyleigh D, Burgandy P, Thinesh S. A Review Of Landfill Leachate Treatment By Microalgae: Current Status And Future Directions[J]. Processes, 2020a,8(4).

[38] To-Hung T, Hao W, Bing S, Shuang-Shuang L, Anuja B, Jonathan W C W. Food Waste Leachate Treatment Using An Upflow Anaerobic Sludge Bed (UASB): Effect Of Conductive Material Dosage Under Low And High Organic Loads[J]. Bioresource Technology, 2020,304(C).

[39] Tabish N, Ashiqur R, Shanglei P, Kyleigh D, Burgandy P, Thinesh S. A Review Of Landfill Leachate Treatment By Microalgae: Current Status And Future Directions[J]. Processes, 2020b,8(4).

[40] Zhenguo C, Xiaojun W, Yongyuan Y, Markus W M, Yanlei Y. Partial Nitrification And Denitrification Of Mature Landfill Leachate Using A Pilot-Scale Continuous Activated Sludge Process At Low Dissolved Oxygen[J]. Bioresource Technology, 2016,218.

[41] Mohammad A, Uwe W, Volker R, Ji-Dong G, Martin D. More Than A Decade Of Experience Of Landfill Leachate Treatment With A Full-Scale Activated Carbon Biofilm[J]. Chemosphere, 2017,174.

[42] Deng W, Wang L, Cheng L, Yang W, Gao D. Nitrogen Removal From Mature Landfill Leachate Via Anammox Based Processes: A Review[J]. Sustainability, 2022,14(2).
[43] Zhu L, Junxin L. Landfill Leachate Treatment With A Novel Process: Anaerobic Ammonium Oxidation (Anammox) Combined With Soil Infiltration System[J]. Journal Of Hazardous Materials, 2007,151(1).
[44] Wu L, Yan Z, Huang S, Li J, Su B, Wang C, Peng Y. Rapid Start-Up And Stable Maintenance Of Partial Nitrification–Anaerobic Ammonium Oxidation Treatment Of Landfill Leachate At Low Temperatures[J]. Environmental Research, 2020,191:110131.
[45] Pazoki M, Abdoli M A, Karbassi A, Mehrdadi N, Yaghmaeian K. Attenuation Of Municipal Landfill Leachate Through Land Treatment.[J]. Journal Of Environmental Health Science & Engineering, 2014,12(1).
[46] Madera-Parra C A, Peña M R, Peña E J, Lens P N L. Cr(Vi) And Cod Removal From Landfill Leachate By Polyculture Constructed Wetland At A Pilot Scale.[J]. Environmental Science And Pollution Research International, 2015,22(17).
[47] Yang C, Fu T, Wang H, Chen R, Wang B, He T, Pi Y, Zhou J, Liang T, Chen M. Removal Of Organic Pollutants By Effluent Recirculation Constructed Wetlands System Treating Landfill Leachate[J]. Environmental Technology & Innovation, 2021,24.

Sponsor Companies of CJJC2023

株式会社イッコウ

Hitz 日立造船
Hitachi Zosen

JFE エンジニアリング 株式会社

TAKUMA

EBARA

三ツ星ベルト

前田建設

鹿島
KAJIMA CORPORATION

日鉄エンジニアリング
NIPPON STEEL ENGINEERING

安藤ハザマ

Kubota

五洋建設株式会社

人と自然を、技術でむすぶ。
奥村組
OKUMURA CORPORATION

GeoWaste Tech.

ESRG

協賛口数順、申込受付順で記載しております。